Chaotic Neural Circuit Dynamics

Dissertation

for the award of the degree
"Doctor rerum naturalium"
Division of Mathematics and Natural Sciences
of the Georg-August-University Göttingen

within the doctoral program
Theoretical and Computational Neuroscience
of the Georg-August University School of Science (GAUSS)

submitted by
Rainer Engelken

from Schorndorf
Göttingen 2017

Thesis Committee:

- Prof. Dr. Fred Wolf (Reviewer)
  Department of Nonlinear Dynamics,
  Max Planck Institute for Dynamics and Self-Organization

- Prof. Dr. Jörg Enderlein (Reviewer)
  Third Institute of Physics,
  Georg-August-University Göttingen

- Prof. Dr. Siegrid Löwel
  Department of Systems Neuroscience,
  Georg-August-University Göttingen

Further members of the Examination Board:

- Dr. Robert Gütig
  Theoretical Neuroscience Group,
  Max Planck Institute for Experimental Medicine

- Prof. Dr. Ulrich Parlitz
  Biomedical Physics Group,
  Max Planck Institute for Dynamics and Self-Organization

- Prof. Dr. Reiner Kree
  Institute for Theoretical Physics,
  Georg-August-University Göttingen

Date of oral examination: 13th February 2017

Dedicated to Janni

Contents

1 Introduction **1**

2 Fundamentals **3**

2.1 Biophysics of neuronal activity 3

2.2 Action potential onset: a bottleneck for information transmission 4

2.3 Balanced state: A generic mechanism for asynchronous irregular activity 7

2.4 Chaotic dynamics in spiking neural networks 11

2.5 Chaotic dynamics in firing-rate networks 12

2.6 Ergodic theory of dynamical systems 13

2.7 Random dynamical systems: merging stochastic and dynamical systems 19

2.8 Controlling chaos and variability in neural circuits receiving input spike trains . . . 21

2.9 Overview 23

3 Lyapunov exponents of spiking balanced networks **25**

3.1 Summary 25

3.2 Manuscript 26

4 Action potential onset rapidness and spontaneous collective dynamics **51**

4.1 Summary 51

4.2 Manuscript 52

4.3 Supplemental Material 59

5 The transition to control in spiking networks **97**

5.1 Summary 97

5.2 Manuscript 98

5.3 Supplemental Material 102

6 Reanalysis of “Two types of asynchronous activity” **117**

6.1 Summary 117

6.2 Manuscript 118

7 Dimensionality and entropy of spontaneous and evoked rate activity 129

7.1 Summary 129

7.2 Manuscript 130

8 Dynamical models of cortical circuits 161

8.1 Summary 161

8.2 Manuscript 162

9 Discussion 171

9.1 Summary of results 171

9.2 Relation to previous work 174

9.3 Outlook 179

References 189

List of Symbols 213

List of Symbols 213

1 Introduction

The brain is wider than the sky,
For, put them side by side,
The one the other will include
With ease, and you beside.

Emily Dickinson [1]

Information is processed in the brain by the coordinated activity of large neural circuits. Yet, we are still only starting to understand how this high-dimensional complex system gives rise to functions such as processing sensory information, making decisions and controlling behavior. Technological advances such as optogenetics and cellular resolution imaging provide tools to measure and manipulate the activity of many neurons simultaneously. These developments open novel avenues for the interplay of theory and experiment in neuroscience and foster the development of mathematical approaches for the systematic dissection and understanding of cortical information processing. This will undoubtedly allow more systematic and comprehensive insights into the brain's structure, function, dynamics, and plasticity. But given the complexity of neural network dynamics, it is not yet clear to what extent this will also give rise to a better conceptual and quantitative understanding of principles underlying neural circuit information processing.

Depending on the specific question, we might need a diversity of theoretical concepts and perspectives. Among these are both *mechanistic bottom-up* approaches which assemble simplified well-understood units into circuits giving rise to less-understood network dynamics and *normative top-down* approaches, starting for example from information theoretic, geometric or evolutionary constraints to infer how computations should be performed [2].

How information is encoded, processed and transmitted by neural circuits is intimately related to their collective network dynamics. Therefore, it is desirable to better understand how different factors shape the patterns of activity across neural populations. Prominent factors that shape circuit dynamics include single-cell properties, synaptic features, network topology and external input statistics.

In this thesis, we develop novel numerical and analytical techniques from dynamical systems, stochastic processes and information theory to characterize the evoked and spontaneous dynamics and phase space organization of large neural circuit models. Our target is to determine how biophysical properties of neurons and network parameters influence information transmission. We investigate the role and relevance of single-cell properties in the collective network dynamics and study how the statistics of external input spike trains affect the chaoticity and reliability of balanced target circuits. By varying the statistics of the streams of input spike trains and investigating the scaling of properties of the collective dynamics with different network parameters, we identify key parameters that regulate information transmission and the ability to control the activity states in a driven network.

In **Chapter 2**, we present the biological and mathematical foundations of this thesis. We review previous work on chaos, both in spiking and in rate networks. Finally, we motivate the scientific questions addressed in the subsequent chapters.

In **Chapter 3**, we introduce a novel efficient method for numerically exact simulations of large sparse networks of model neurons and the calculation of their Lyapunov exponents. Our algorithm reduces the computational cost from $\mathscr{O}(N)$ to $\mathscr{O}(\log(N))$ operations per network spike for a fixed number of synapses per neuron and Lyapunov exponents. This allows for numerically exact simulations of large networks ($N = 10^9$ neurons) and the characterization of their chaoticity.

In **Chapter 4**, we study the role of action potential (AP) onset rapidness both for information transmission in a feedforward architecture and for the collective dynamics in recurrent networks. We quantify the bandwidth of information transmission in the feedforward architecture. Using the novel approach introduced in Chapter 3, we investigate in large random recurrent networks how AP onset rapidness affects the attractor dimensionality and the pairwise spike count correlations. Our results demonstrate that AP onset has a drastic effect on the microscopic phase space structure, which is not detectable by the pairwise statistics. We corroborate our results in simulations of more realistic circuits having second-order motif statistics and a multilayered cortical column structure.

In **Chapter 5**, the role of the statistics of spiking input for the recurrent network dynamics and its reliability across trials is analyzed. Our results show that structured streams of input spike trains generally reduce dynamical entropy rate and attractor dimensionality of the dynamics of the driven target circuit. Strong external input tames the chaos in the recurrent target circuit. For sufficiently strong input, we find a transition towards network state control, which occurs for stronger input than the transition to stability. We describe under which conditions streams of incoming spike trains completely control the spike patterns in the target circuit. Intriguingly, we find that rapid AP onset facilitates both suppressing chaos and controlling the network state.

In **Chapter 6**, we reanalyze a recent study on the dynamics of balanced spiking networks and their relationship to rate networks [3]. The reexamined study considered spiking networks of leaky integrate-and-fire (LIF) neurons and proposed that for strong coupling they would exhibit a chaotic instability mathematically analogous to the well-known transition to chaos in rate networks [4]. We revisited the behavior of the spiking LIF networks and the matched rate networks and found hallmarks of a chaotic instability in the rate network, but not in the spiking network. Changes of network parameters revealed further differences between the mean-field theory for rate networks and simulations of spiking networks. Thus, our reanalysis demonstrates fundamental differences between the behavior of networks of pulse-coupled LIF neurons and matched rate networks. In particular, there is no indication of a corresponding chaotic instability in the spiking networks.

In **Chapter 7**, for the first time to our knowledge, we calculate full Lyapunov spectra of random rate networks. The dynamics of such networks and their transition from a stable state for small couplings to a chaotic state for strong couplings has been studied extensively [5]. Our study allows measuring the dynamical entropy rate and attractor dimensionality for such networks of rate units. The mean Lyapunov exponent is calculated analytically. For several limiting cases analytical random matrix approximations of the Lyapunov spectrum are presented. The Lyapunov spectrum is also obtained for rate networks driven by frozen white noise, extending earlier studies, which examined the behavior of the largest Lyapunov exponent upon time-varying external input [6–8].

In **Chapter 8**, we review recent advances in modeling the dynamics of cortical circuits [9]. Both theoretical and experimental evidence for an inhibition-dominated operating regime of cortical circuits is discussed. Furthermore, we revisit progress in the theoretical understanding of microstate dynamics, stimulus selectivity, response heterogeneity and spike count correlation.

2 Fundamentals

2.1 Biophysics of neuronal activity

Neurons are specialized cells that have excitable membranes which allow them to communicate electrochemically with other connected neurons. Excitability of neurons arises from ion-selective voltage-sensitive channels that use the ion gradients across the semi-permeable membrane to change the transmembrane voltage. The concentration gradients are maintained by various transmembrane ion transporters acting as solute pumps. If a threshold potential is crossed, fast sodium channels open causing an inward current of Na^+, followed by the slower opening potassium channels that cause an outward K^+ current. The interplay of voltage-gated ion channels gives rise to stereotypical all-or-nothing membrane depolarizations, called *action potentials* (APs), or simply *spikes*, that travel as unattenuated self-supporting waves along the axon. A mathematical description of this interplay was first presented for the squid giant axon in a seminal study by Hodgkin and Huxley in 1952 [11]. Four coupled differential equations for voltage and two hypothesized activation variables for potassium and sodium and an inactivation variable for sodium captured remarkably accurately a series of voltage-clamp experiments performed by Hodgkin, Huxley, and Katz [12–14].

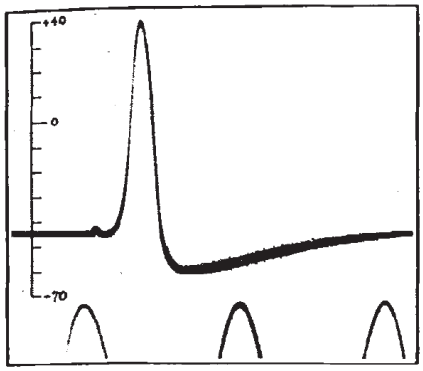

Figure 2.1 – First intracellular recording of an action potential in the squid giant axon by Hodgkin and Huxley in 1939 [10].

From a dynamical systems perspective, excitability of neurons means that the voltage-gated ion channels position their dynamics close to a bifurcation from a resting state to spiking activity [15]. APs are elicited at the axon initial segment (AIS) which is in the proximal part of the axon. The AIS has a high density of sodium channels [16–21] with specialized kinetics with heightened sensitivity that might facilitate spike onset. For example, the half-activation voltage and half-inactivation voltage of sodium channels in the AIS was reported to be 10 to 15 mV lower compared to the soma [22].

Different levels of detail in mathematical modeling Mathematical descriptions for neural activity exist on different levels of detail. On the nanoscopic scale, single channels and the stochastic switching between their different states is described by Markov chain models and stochastic processes [23]. At a coarser scale are models that describe the dynamics of ions by reaction-diffusion systems [24]. In multi-compartment models, several often cylindrical compartments are modeled by finite-element methods which allow spatiotemporally detailed descriptions of spatially extended neurons while usually ignoring the underlying stochasticity [25]. Such models can also

describe subcellular computations, e.g., dendritic computation [26, 27]. More simplified are zero-dimensional models of cells, called *point neurons*, where the membrane potential and optionally several latent variables – e.g., slow potassium currents or synaptic input currents – are modeled as coupled differential equations [11, 28]. Spiking neuron models often ignore internal degrees of freedom and provide an effective description of the internal dynamics [29, 30]. Even more abstract are rate models and neural field models where the compound activity of many neurons is subsumed in a single activity variable that can vary in time and optionally in space [5, 31]. Depending on the specific scientific question, different levels of description can yield complementary insights. As we are only beginning to understand neural information processing, for many questions it is not clear which biophysical details can be left out and which details are necessary to capture the core features of cortical information processing.

Which biophysical details matter? How strongly do the collective dynamics depend on biophysical details of single neurons? One might expect that population dynamics are insensitive to cellular details as in many instances the effect of single-cell properties can become negligible at the macroscopic circuit level. This would be similar to statistical physics where the macroscopic description of fluids and gases is often independent of the microscopic features of its elements. For example, asynchronous irregular activity in idealized cortex models emerges robustly in inhibition-dominated circuits and can be described by a mean-field theory whose mean rate at dynamical equilibrium is insensitive to details of the neuron model [32, 33]. Collective dynamics rather are expected to be strongly shaped by the wiring diagram – known as the connectome – and most learning algorithms, in fact, operate at this level [34–36]. Can cellular properties have a similarly strong effect on the collective dynamics? Could it be that single-cell properties are even amplified by the network? An example where single element input-output functions determine the critical properties of the collective dynamics are rate networks [5, 37]. A promising single-cell feature for investigating the dependence of the collective dynamics on cellular details is the rapidness of the onset of action potentials discussed next.

2.2 Action potential onset: a bottleneck for information transmission

Action potential initiation is an important bottleneck for cortical information transmission. Only the information a neuron encodes in its spike train can be used by its local network, by subsequent processing stages and, ultimately, to guide behavior. Experimental studies estimated that the spiking output of a cortical neuron contains twenty- to one hundred fold less information about the synaptic input than its membrane potential [38]. This might not come as a surprise because the membrane potential carries more information about the dense stream of incoming postsynaptic potentials than the temporally sparse sequence of outgoing action potentials. However, the finding highlights the gatekeeping function of the action potential generation mechanism for the information transmission: it decides which aspects of the membrane potential are reflected in the outgoing spike train.

Experimental findings revealed a surprisingly broad encoding bandwidth of cortical neurons: high-frequency input components of a stimulus immersed in noise are reliably encoded in the outgoing spike trains up to frequencies of several hundred Hertz. This has been first reported in acute slice preparations of regular-spiking layer 5 pyramidal cells of the rat somatosensory cortex for

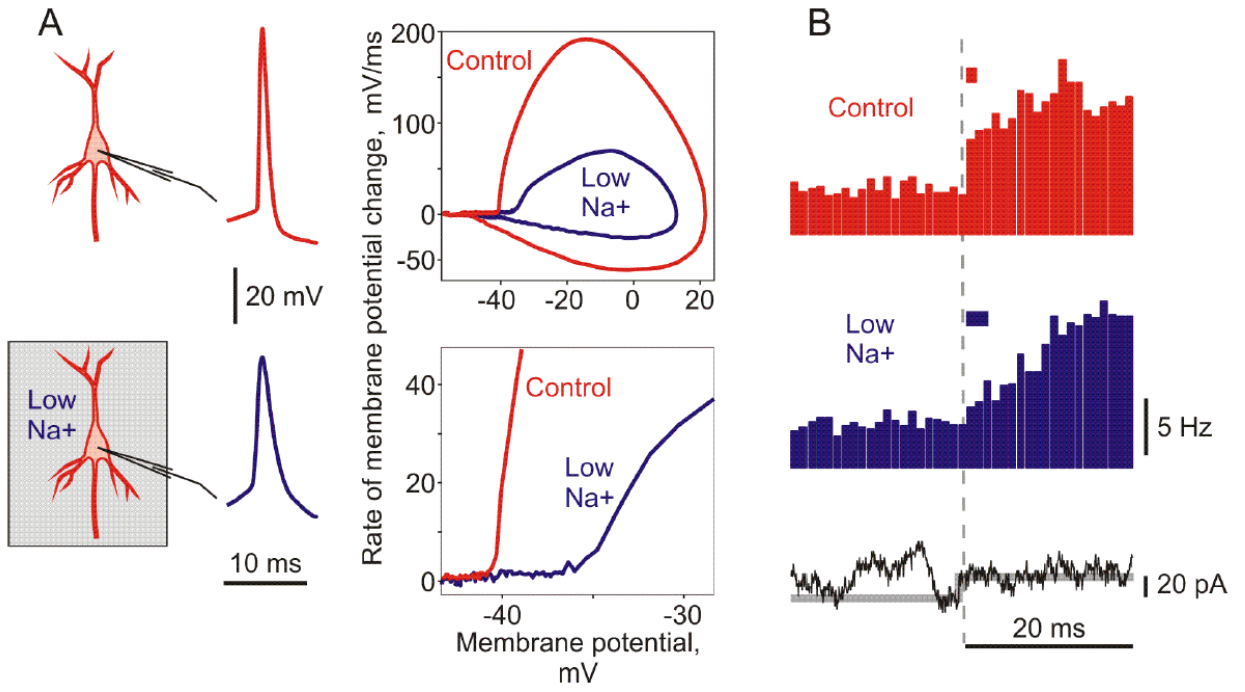

Figure 2.2 – Rapid action potential onset is necessary for broad encoding bandwidth (Figures adapted from Ref. [44]). **A** Cortical neurons have a rapid action potential (AP) onset (red) with a characteristic kink at AP onset (arrow). In the phase plot (middle column), the rate of membrane potential change $\frac{dV}{dt}$ takes off almost vertically. **B** The ensemble rate of neurons receiving an external current step embedded in fluctuations responds ultrafast, indicating a broad encoding bandwidth, (red peristimulus time histogram (PSTH)). Lowering the extracellular sodium concentration decreases the AP onset rapidness (blue lines). Decreasing the AP onset reduces the ability to respond quickly to an external stimulus change (**B**, blue PSTH).

mean-modulated fluctuations [39] and was also later found for variance-modulated fluctuations later [40]. Independent studies confirmed the broad bandwidth using a protocol with weaker stimulation strength both in the time and frequency domain [41–44].

Theoretical predictions Theoretical studies predict that a rapid spike onset is necessary for the ultra-fast response in a feedforward architecture. Ensembles of neurons with instantaneous spike onset, such as leaky integrate-and-fire neurons [29], can transmit signals in the variance channel unattenuated for arbitrarily high frequencies [45, 46]. For the mean-modulation channel, however, the output amplitude declines $\propto \frac{1}{\sqrt{f}}$ [45]. More generally, high spike onset rapidness increases the population encoding bandwidth. This relationship between broad encoding bandwidth and high action potential (AP) onset rapidness was first directly demonstrated in the exponential integrate-and-fire model, whose AP onset rapidness is changeable [30]. A strong influence of spike onset on high-frequency encoding was also predicted by Naundorf and colleagues [47, 48]. Wei and Wolf confirmed this analytically using a mathematically tractable piecewise linear neuron model, which allows an analytical calculation of the frequency response for different AP onset rapidness [49]. In numerical simulations of multi-compartment conductance-based models, which reproduce the initiation of spikes in the axon initial segment, fast AP onset at the initiation site was necessary for encoding high frequencies [44].

Experimental confirmations These theoretical predictions on the importance of rapid AP onset for high-frequency encoding were confirmed in several experiments. In a recent study, different ways of decreasing the AP onset rapidness all impaired the ability to encode high-frequency stimulus components into the spike train [44]. In this experiment, the AP onset rapidness was decreased in slices of rat visual cortex first by decreasing extracellular sodium concentration by partially substituting NaCl by choline chloride in the extracellular solution (See Fig. 2.2). Secondly, the effective density of voltage-gated sodium channels (Na_V) was reduced by blocking voltage-gated sodium channels using small concentrations of tetrodotoxin (TTX) locally at the site of the axon initial segment (AIS). Both manipulations had the effect of impairing the high-frequency encoding. A similar impaired high-frequency encoding was observed in neurons from juvenile animals (P9 - P13), which naturally have a slower AP onset [44]. Complementing these experiments, a recent experimental study investigated the effect of a reduced Na_V channel density in the AIS caused by the genetic mutation qv3J on the frequency response [50]. The genetic knockout selectively slowed down the action potential onset without altering other somatic characteristics (peak potential, peak rate of voltage rise) and impaired high-frequency encoding of mature hippocampal neurons [50] was observed. In addition, a recent experimental study in cultured maturing hippocampal neurons showed that the AP onset rapidness is strongly correlated with the density of Na_V channels in the AIS [51].

Biophysics of rapid AP onset The biophysics underlying the rapid action potential onset is a topic of ongoing investigation in electrophysiology and biophysical modeling. Cooperative gating between sodium channels in the AIS was suggested to account for both rapid AP onset and broad encoding bandwidth [48, 52]. Although there exists evidence for such cooperative gating in other tissues [53–55] and in $Ca_V1.3$ channels of rat hippocampal neurons [56], there is no direct evidence for cooperative gating in Na_V channels in the central nervous system yet. Opposing this view, it was proposed that the sharp rise of AP onset in the soma is an epiphenomenal effect resulting solely from backpropagation of AP. Accordingly, spikes would have a slow onset at the AIS but become sharper while invading the soma [57]. To test this backpropagation hypothesis, experimentally measuring the high-frequency response of cortical neurons was proposed [58]. The experimental results suggest that the backpropagation hypothesis fails to explain the broad encoding bandwidth and the impaired high-frequency response resulting from experimentally manipulating the slowed down AP onsets [44]. As an alternative, it was proposed that fast spike onset could be caused by a loss of voltage control [59]. However, this model cannot account for the experimentally observed high-frequency response [60]. Another study proposed that a large dendritic arbor causes a larger impedance load and hence increases the AP onset rapidness and the cutoff frequency [61]. In conclusion, the underlying mechanism of the rapid spike onset is still a largely open question of interest for both biophysical modeling and electrophysiological experiments.

AP onset and recurrent dynamics While the role of broad encoding bandwidth and rapid spike onset in a feedforward architecture sparked an intense debate, its role and relevance for the dynamics of recurrently connected neuronal circuits is not well understood and has not yet been studied systematically. Extending the analysis of an analytically solvable neuron model [62], we will ask in Chapter 4: How can the role of spike onset rapidness for information transmission in a feedforward architecture be quantified in information-theoretic quantities, i.e., the mutual information rate between a stimulus embedded in fluctuations and the spiking response? What is the effect of changing the AP onset rapidness on the organization of the phase space of recur-

rently connected neurons? We study these questions in sparse random networks of spiking neuron models in the balanced state. The balanced state is a generic mechanism to generate experimentally observed asynchronous irregular activity in cortical circuits where individual neurons are in a fluctuation-driven regime.

2.3 Balanced state: A generic mechanism for asynchronous irregular activity

Origin of asynchronous irregular cortical activity Many neural circuits in the cortex exhibit asynchronous, irregular activity whose origin has been puzzling theoreticians and experimentalists for a long time. Neurons in the cortex emit sequences of action potentials in an irregular, Poisson-like fashion in contrast to more peripheral afferent and efferent neurons that often display tonic or bursty firing [63]. One hypothesis on the origin of such aperiodic, seemingly erratic activity was that neurons are intrinsically unreliable devices whose activity can be described by a random walk towards an absorbing barrier [64]. Although different intrinsic sources of membrane potential fluctuations exist, for example, stochasticity of synaptic release, ion channel shot noise and thermal noise [65]. Experiments showed that individual neuron's spike times can respond reliably to a time-varying external stimulus [66–69]. It thus appears somewhat implausible that these or other internal noise contributions can account for the irregular spiking of cortical neurons. If intrinsic variability cannot explain the observed irregular activity, it might be caused by input fluctuations [70]. From a simple perspective of the central limit theorem, if K independent identical quantities are summed up, their mean is $\sqrt{K}$ times larger than their standard deviation. As experimental data suggest that the *average number of synapses per cortical neuron* K is approximately 1000 to 10000 [71], one might expect that for such a large number of incoming synapses per neuron the mean current is much larger than its fluctuations. This would result in tonic firing for excess excitation or silence for excess inhibition [72, 73]. At a first glance, this seems to contradict the hypothesis that input fluctuations are the source of the asynchronous irregular activity.

The balance hypothesis Shadlen and Newsome proposed that an approximate balance of excitatory and inhibitory incoming synaptic currents could resolve this riddle: in that case, mean excitation and inhibition would approximately cancel and only the residual fluctuations would drive the cells to fire [74,75]. Despite explaining the origin of irregular activity, this solution raised another question: How can excitatory and inhibitory synaptic currents be approximately balanced for all cells? This balance should be kept in different brain activity states and with different external input without rewiring or fine-tuning all synaptic strengths. In a seminal study, van Vreeswijk and Sompolinsky showed that in a broad parameter regime, such a balance of excitatory and inhibitory currents emerges robustly self-organized for strong synapses, sparse large networks and sufficiently strong inhibition [33, 76, 77].

The balanced state theory The core mechanism of the balanced state is a fast strong negative feedback loop (Fig. 2.3). If there is an excess excitatory input current, the inhibitory network increases its firing rate. As a consequence, the recurrent inhibitory currents grow until the excess excitation is canceled. Conversely, if there is an excess inhibitory input current, the inhibitory network decreases its firing rate until it is sufficiently low and balance is restored. If the synaptic strength is scaled with $J = \frac{J_0}{\sqrt{K}}$, where K is the number of synapses per neuron, the residual

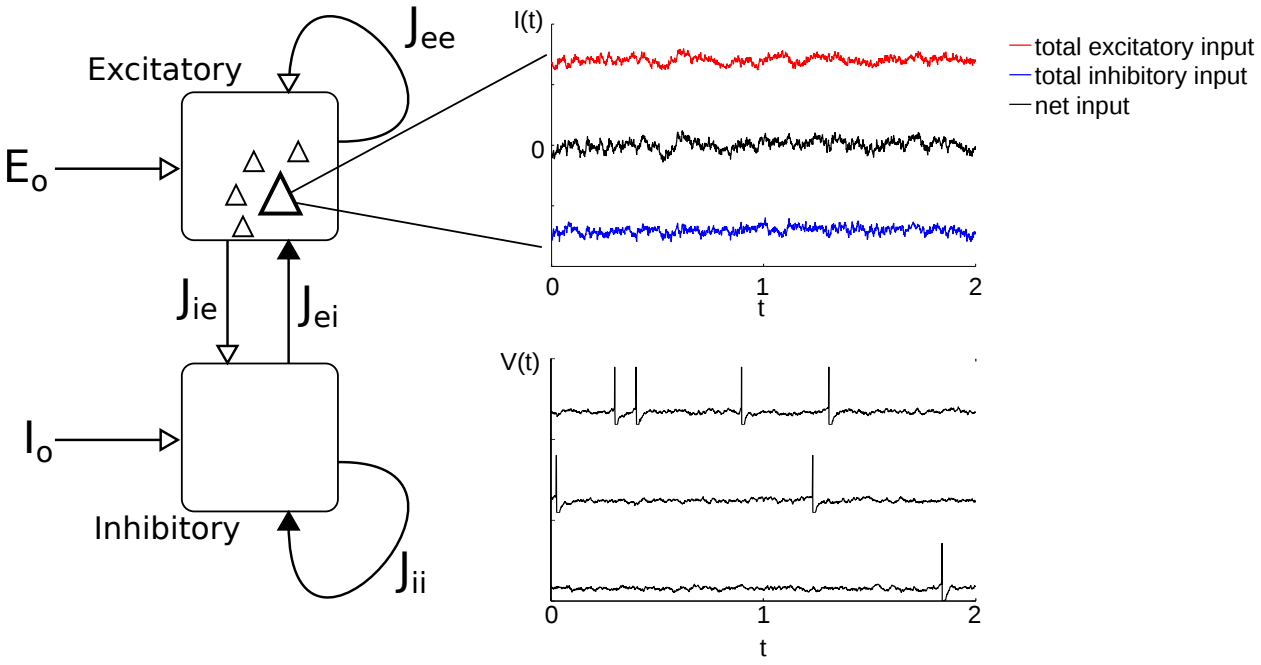

Figure 2.3 – The balanced states robustly emerge in local circuits of inhibitory and excitatory neurons. Neurons in balanced networks are driven by residual input fluctuations that result from the mutual cancellation of excitatory and inhibitory inputs (upper right). The balance of excitatory and inhibitory inputs is a collective phenomenon and emerges from fast recurrent inhibition in the network. The balanced state was first described in sparse random networks. Recent studies demonstrated that a balanced state also emerges in structured and densely connected circuits where correlations are actively suppressed by a dynamic cancellation of correlations. Networks in the balanced state robustly exhibit irregular and asynchronous activity patterns over a large parameter regime without any fine-tuning (lower right).

fluctuations of large excitatory and inhibitory input currents neither vanish nor diverge in the large network size limit $N \to \infty$ [33, 76]. The negative recurrent feedback loop therefore acts like an operational amplifier and linearizes the system's overall rate-current relation. Even if single units have nonlinear input-output functions, the recurrent inhibitory interactions lead to an overall linear stationary rate-current relation

$$\bar{\nu} = \frac{I_0}{J_0 \tau_{\mathrm{m}}}$$

for large K [33, 76], where $\bar{\nu}$ is the mean population firing, I_0 is the external input strength, J_0 is the coupling strength and τ_{m} is the membrane time constant. The derivation of this relation and the generalization to excitatory-inhibitory mixed networks can be found in chapter 3. In case of mixed networks an inequality involving the different inter- and intrapopulation coupling strengths, external input strengths, and population firing rates has to be fulfilled to achieve a balanced state. Similar to the purely inhibitory case, the mixed balanced state also requires no fine-tuning; it is achieved over a large parameter regime. Purely inhibitory networks can also be balanced. In that case, the recurrent inhibition balances the excitatory external input. The mean-field theory of the original work required large sparse networks i.e., $\log(N) \gg K \gg 1$, to guarantee that the input current correlations arising from the shared input are negligible [78, 79]. Thus, in the mean-field theory first N is sent to infinity, and in a second step, $K \to \infty$.

Balanced state in dense networks It was later shown that even in *dense* networks, where the connection probability $p = \frac{K}{N-1}$ is fixed independent of network size N, asynchronous irregular activity emerges self-organized because the recurrent inhibition actively decorrelates any input correlation [32, 80]. Correlations generated by shared input and population-rate fluctuations are canceled by negative correlations of the recurrent inhibition. The mean-field theory for dense networks of binary neurons sends K and N to infinity simultaneously and predicts that mean pairwise spike count correlations decay $\bar{\rho} \propto 1/K$, while their standard deviation decays much slower $\bar{\sigma} \propto 1/\sqrt{K}$. This implies a wide distribution of pairwise spike count correlations with a mean close to zero [32]. This is consistent with the experimental finding that the mean pairwise spike count correlations of cortical circuits can be low, especially in awake behaving animals [32,81,82]. Such low pairwise correlations were surprising because excitatory neurons in the same local circuit share on average approximately 10% of their input [83–88], which by itself would result in strong pairwise spike count correlations [32]. The balanced state theory provides a natural explanation for this observation.

Balanced state with different neuron models Balanced state networks were studied in different classes of neuron models. The initial mean-field theory considered networks of binary neurons [33, 76]. Later, for networks of leaky integrate-and-fire neurons the transition from the balanced state to other network states, for example to synchronous irregular activity (oscillations), synchronous regular (network synchrony) and asynchronous regular (splay state) were studied analytically [45, 89]. These studies also included an analysis of the role of external input spike trains and synaptic delays. Balanced networks were also investigated with conductance-based neuron models, where the effective time constant of the voltage dynamics decreases as a function of the number of synapses per neuron [90, 91]. Firing-rate networks can also be in the balanced regime if the balance inequality is fulfilled [37, 92].

Experimental evidence Several theoretical predictions for the balanced state were later tested and confirmed experimentally. More refined recordings corroborated the hypothesis that irregular spiking activity seems to originate from a fluctuation-driven high-conductance state [93]. Unfortunately, directly measuring excitatory and inhibitory currents into the same neuron is currently not possible. However, inhibitory and excitatory conductance (g_I, g_E) can be measured by clamping the membrane voltage of neighboring neurons at the respective reversal potential of Na^+ and K^+ channels. Several experiments found that the average ratio g_E/g_I remains constant across different stimuli and behavioral states [94–97]. Balanced networks can be seen as a subset of inhibition stabilized networks (ISN) [98, 99] for which several, experimentally-testable predictions were made. In ISNs the recurrent excitation is so strong that runaway excitation would occur for fixed inhibition but is dynamically stabilized by inhibitory feedback [9]. If recurrent excitation and inhibition is sufficiently strong, a *paradoxical* response to an external drive of the inhibitory population is predicted in ISNs [99]: Intuitively, one might expect that increased excitatory input into the inhibitory population would increase the inhibitory population firing rate and indirectly decrease the excitatory firing rate by disynaptic inhibition. The opposite is the case for the inhibitory rate: in ISNs with sufficiently strong recurrent excitation and inhibition, increasing excitatory input to the inhibitory population paradoxically causes a decrease of the mean activity of both populations because of the strong recurrent connections [100, 101]. Such a paradoxical response was observed experimentally in hippocampal CA1 recordings in rats [102] and in cat V1 when studying surround suppression [98]. These findings provide evidence for an inhibition-stabilized operating

regime, but comparable surround suppression experiments in the rodent visual system gave less clear evidence: while the firing rate of inhibitory Parvalbumin-expressing (PV+) interneurons was decreased by an increasing stimulus size that suppresses excitatory neuron activity, mean firing rates of Somatostatin-expressing (SOM+) interneurons showed ambiguous responses: they either decreased [103], which would be consistent with ISNs, or they increased [104], which is inconclusive. Optogenetic perturbation experiments of cortical interneuron activity in mice provide a promising avenue for testing ISN predictions, but they have resulted so far in a variety of different effects without clear evidence for a paradoxical effect [105, 106].

Functional role of the balanced state "Why should the cortex simultaneously push on the accelerator and on the brake [107]?" From an evolutionary perspective [108, 109], the prevalence of an asynchronous irregular regime of cortical activity suggests that it endows advantages which justify the high metabolic costs [110] of such a seemingly wasteful cancellation of large excitatory and inhibitory currents: Are there potential functional advantages of a balanced state as a cortical operating regime? Firstly, a potential benefit of a balanced state is that it drives neurons robustly into a fluctuation-driven regime which enables faster response to an external stimulus change than populations in a mean-driven regime [111]. At any moment, a fraction of neurons in the population has voltages close to threshold and therefore will respond quickly to an external input change through the delay or advance of that the next spike. Secondly, balanced circuits are able to quickly track an external time-varying input due to the strong mean input that scales $\propto \sqrt{K}$, while the recurrent response keeps the network in the balanced regime as long as the speed of input changes do not pass a limit [33]. Thirdly, the recurrent balance of an external large excitation might be useful for certain cortical computations, e.g., adaptively subtracting a large untuned input component from a weakly tuned signal. Such a mechanism was proposed to account for tuned responses in rodent visual cortical neurons that receive only weakly tuned input due to their dispersed *salt-and-pepper* layout of orientation selectivity [112, 113]. While there is clear evidence for feature-selective input into rodent visual cortical neurons, such an adaptive mean-subtracting *iceberg-effect* might account for tuned responses in juvenile rodents where no feature-selective wiring has been found [114, 115]. Fourthly, it was recently proposed that asynchronous, irregular activity of dense balanced networks could represent a high-dimensional population rate code, which performs efficiently when assuming a linear readout [116, 117]. In this perspective, which requires a tight balance, the voltage is interpreted as prediction error about a population signal. The prediction error is kept small in the balanced state. Such a rate code would also be robust to deletion of synapses or neurons.

Beyond balance The initial riddle about the origin of asynchronous irregular activity relied on the assumption of many weak uncorrelated synaptic inputs whose fluctuations are much smaller than their mean. Recently, it was pointed out that spiking of cortical neurons might predominantly be driven by few, stronger synapses. In consequence, a balance of excitation by recurrent inhibition might not be necessary to achieve irregular activity [118]. From such a perspective, inhibition-stabilization might be sufficient to generate irregular activity even in large neural circuits. However, different to the balanced state regime, it is not clear how in an inhibition-stabilized regime low pairwise correlations can be explained, potentially another decorrelation mechanism would be necessary for unbalanced inhibition-stabilized networks.

Another important extension to the balanced state theory is to include networks with nonrandom wiring, e.g., distance-dependent connection probabilities [119, 120], heterogeneity in inde-

gree [121], inhomogeneous coupling [122] and feature-dependent wiring [112, 113].

In the following chapters on spiking network dynamics, we will consider balanced networks, although the concepts and tools we develop for an ergodic theory of spiking neural circuits are more generally applicable also for neural circuits beyond and out of the balanced regime.

The insensitivity of the balance equation to details of the neuron model might suggest that biophysical details are negligible for understanding the collective circuit dynamics. However, previous work suggests that depending on the neuron model, the dynamical nature of balanced networks can be chaotic [33, 123] or stable [124–126]. In the following sections, we will describe previous results on chaos in spiking and rate neurons in more details and discuss potential implications for information processing in cortical circuits.

2.4 Chaotic dynamics in spiking neural networks

Chaotic dynamics and neural information processing The dynamic stability of spiking neural circuits constrains the capability of information processing. In chaotic systems, a sensitive dependence on initial conditions makes predictions of future states impossible if the initial condition is known only with finite precision. This corresponds to a dynamical entropy rate because nearby states, which could not be distinguished by a finite precision readout initially, are pulled apart by the chaotic network dynamics and are distinguishable later on. Therefore, the dynamical entropy rate quantifies the rate by which information about a microscopic perturbation becomes accessible to the macroscopic state [127]. Its interpretation depends on the neural coding: If the microscopic initial state contains a relevant signal, the dynamical entropy rate measures the rate by which this information becomes accessible. If the microscopic initial state encodes merely noise, the dynamical entropy rate measures the rate with which information in the macroscopic state is overwritten by microscopic noise. Chaotic dynamics might be useful for computation to amplify small differences of initial conditions. If such a mechanism is used by cortical circuits, it would be important to find out how different factors regulate this. Certainly, dynamical entropy rate contributes to noise entropy and can thereby impair encoding capacity. Because of this, it is a challenge to understand how different factors affect this deterministic contribution to noise entropy. It was argued that sensitivity to perturbations suggests rate coding in the cortex [128]. While this conclusion remains controversial, probing the stability of cortical dynamics by external perturbations is a promising approach to constrain models on cortical information processing both for experiments and theory.

Chaos in the balanced state? Previous work found seemingly contradictory results on the stability of the balanced state. While balanced networks of binary neurons were shown to be extremely chaotic ($\lambda_{max} = \infty$ for $N \to \infty$) [33], balanced networks of inhibitory pulse-coupled leaky integrate-and-fire neurons exhibit stable dynamics ($\lambda_{max} = 0$) but interestingly still asynchronous irregular activity [124, 125]. This phenomenon of aperiodic irregular activity despite stability with respect to infinitesimal perturbations was – potentially misleading – called *stable chaos* [129]. In small networks with fixed in-degree, the aperiodic activity was shown to be a transient towards a periodic orbit [125]. The transient time until the periodic orbit is reached was shown to grow exponentially with network size N. Consequently, one might expect a diverging transient time in the large network limit $N \to \infty$.

Dynamical flux tubes Stability to infinitesimal perturbations accompanied by instability to sufficiently large perturbations yields an exotic phase space structure in pulse-coupled networks of leaky integrate-and-fire (LIF) neurons [130]. Sufficiently strong state perturbations diverge with an exponential rate $\lambda_{\mathrm{p}} \sim K\bar{\nu}$, where K is the mean number of synapses per neuron and $\bar{\nu}$ is the mean population firing rate, while small perturbations converge to the unperturbed trajectory with $\exp\left(-\frac{t}{\tau_{\mathrm{m}}}\right)$ [130]. The average diameter of the basins of attraction, called *flux tubes*, was numerically found to scale $\varepsilon_{\mathrm{ft}} \propto \frac{1}{\sqrt{NK\bar{\nu}\tau_{\mathrm{m}}}}$, where N is the network size and τ_m is the membrane time constant [130]. As a consequence, the flux tube radius $\varepsilon_{\mathrm{ft}}$ becomes tiny for large networks which results in high sensitivity even to microscopic state perturbations. Later, the scaling of the flux tube radius was derived analytically [126]. Initially, flux tubes were found in random inhibitory randomly-coupled networks of pulse-coupled leaky integrate-and-fire neurons driven with constant external input. It is an interesting question how relaxing these different constraints (*(i)* random network architecture, *(ii)* purely inhibitory interactions *(iii)* pulse-coupled synapses *(v)* LIF neurons *(vi)* constant external input) of the initial finding will affect diameter, shape and fate of the flux tubes. Hence, related questions addressed in this thesis are: does this phenomenon survive in more detailed neuron models with an active spike generation mechanism? How are flux tubes affected by external time-varying input and different single-cell properties?

2.5 Chaotic dynamics in firing-rate networks

Rate chaos The cerebral cortex displays temporally irregular activity and heterogeneous response properties. A seminal study showed that randomly connected rate units display a transition from an inactive state to a highly heterogeneous, chaotic state with evanescent patterns of activity for sufficiently strong couplings [5]. In this class of models, each rate unit maps its synaptic input h_i smoothly into a firing rate by a sigmoid input-output transfer function ϕ. Coupling strengths are drawn from a Gaussian distribution with zero mean and standard deviation $g/\sqrt{N}$. When increasing g, large networks exhibit a phase transition from stable to chaotic dynamics at a critical coupling $g_{\mathrm{crit}} = 1$. Recently, the classical study has been extended and the transition has been studied for different input-output functions [37], sparse and balanced network architectures [37] and heterogeneous networks with different subpopulations [131]. The chaotic, heterogeneous state of these rate networks possess high computational capabilities because rich internal dynamics provide a substrate for complex nonlinear computations e.g. learning input-output relations [35].

Rate chaos in spiking networks Neurons in the brain, however, communicate via spikes and it is a theoretical challenge to obtain similar rate fluctuations in networks of spiking neuron models. It was proposed that in the limit of slow synaptic time constants ($\tau_s \gg \bar{\nu}^{-1}$), spiking neurons behave like rate units and simply integrate the synaptic input [132]. Later, it was shown that networks of spiking neurons with slow synaptic time constant can be treated using dynamical mean-field theory developed for rate networks [92]. A different approach to obtain rate fluctuations in networks of spiking neurons would be to group N/k spiking neurons together into k subpopulations. In the large N limit, the subpopulations behave as rate units and their population averaged firing rate can be interpreted as the output firing rate of the unit.

Rate chaos in pulse-coupled LIF networks? Recently the dynamics of a spiking balanced network of pulse-coupled leaky integrate-and-fire (LIF) neurons was compared to a matched rate

network with identical topology. The input-output transfer functions of the matched rate units were chosen from isolated LIF neurons receiving Gaussian white noise input. A mathematical analogy between the chaotic instability of the matched rate networks and spiking network dynamics was proposed [4]. Finding a transition to chaotic slow-varying rate dynamics in spiking networks in such a simple model would fill a gap in the current understanding of network dynamics. Moreover, it would potentially pave the road for harnessing the rich internal dynamics of the chaotic heterogeneous state for computations in spiking networks [133].

We reexamine the behavior of LIF networks and ask [3]: Can we find fingerprints of a phase transition mathematically analogous to the instability found in rate networks also in spiking networks? How generic is the described phenomenon? Do the predictions of the proposed mean-field theory match numeric simulations if parameters are slightly changed? How sensitive is the phenomenon to features of single neuron dynamics, e.g. the synaptic delay, the refractory period and neuron models?

2.6 Ergodic theory of dynamical systems

Lyapunov exponents An autonomous dynamical system is usually defined by a set of ordinary differential equations $\frac{d\mathbf{x}}{dt} = \mathbf{F}(\mathbf{x})$, $\mathbf{x} \in \Omega$ in the case of continuous dynamics or as a map $\mathbf{x}_{s+1} = \mathbf{f}(\mathbf{x}_s)$ in the case of discrete dynamics. Ω is the phase space where every possible state $\mathbf{x}$ of the system corresponds to one unique point. We focus here on discrete dynamical systems as the spiking neural network dynamics studied in this work can be exactly solved between spike times and can therefore be treated as iterated maps but it can directly be extended to continuous systems [134]. An initial condition $\mathbf{x}_0$ forms an orbit. As a natural extension of linear stability analysis, one can ask, how an infinitesimal perturbation $\mathbf{x}_0' = \mathbf{x}_0 + \varepsilon\mathbf{u}_0$ evolves in time. Chaotic systems are sensitive to initial conditions, hence almost all infinitesimal perturbations $\varepsilon\mathbf{u}_0$ of the initial condition grow exponentially. Finite size perturbations therefore may lead to a drastically different future behavior. The largest Lyapunov exponent measures the average rate of exponential divergence or convergence of nearby initial conditions.

$$\lambda_{\max}(\mathbf{x}_0) = \lim_{t\to\infty} \frac{1}{t} \lim_{\varepsilon\to 0} \log \frac{||\varepsilon\mathbf{u}_t||}{||\varepsilon\mathbf{u}_0||} \tag{2.1}$$

It is crucial to first take the limit $\varepsilon \to 0$ and then $t \to \infty$, as $\lambda_{\max}(\mathbf{x}_0)$ would be trivially zero for a bounded attractor if the limits are exchanged because $\lim_{t\to\infty} \log \frac{||\varepsilon\mathbf{u}_t||}{||\varepsilon\mathbf{u}_0||}$ is finite for finite-size perturbations even if the system is chaotic. To measure N Lyapunov exponents, one has to study the temporal evolution of N independent infinitesimal perturbations spanning the tangent space:

$$\mathbf{u}_{s+1} = \mathbf{D}_s\mathbf{u}_s \tag{2.2}$$

where the Jacobian $\mathbf{D}_s(\mathbf{x_s}) = \frac{d\mathbf{f}(\mathbf{x_s})}{d\mathbf{x}}$ characterizes the evolution of generic infinitesimal perturbations during one step. As we are interested in the asymptotic behavior, we have to study the long-term Jacobian:

$$\mathbf{T}_t(\mathbf{x}_0) = \mathbf{D}_{t-1}(\mathbf{x}_{t-1}) \dots \mathbf{D}_1(\mathbf{x}_1)\mathbf{D}_0(\mathbf{x}_0) \tag{2.3}$$

Note that $\mathbf{T}_t(\mathbf{x}_0)$ is a product of generally noncommuting matrices.

The Lyapunov exponents $\lambda_1 \geq \lambda_2 \cdots \geq \lambda_N$ are defined by the logarithms of the eigenvalues of

the positive-semidefinite symmetric Oseledets matrix

$$\Lambda(\mathbf{x}_0) = \lim_{t\to\infty}[\mathbf{T}_t(\mathbf{x}_0)^\top \mathbf{T}_t(\mathbf{x}_0)]^{\frac{1}{2t}}, \tag{2.4}$$

where $\top$ denotes the transpose operator. The expression inside the brackets is the Gram matrix of the long-term Jacobian $\mathbf{T}_t(\mathbf{x}_0)$. When the Gramian $\mathbf{T}_t(\mathbf{x}_0)^\top \mathbf{T}_t(\mathbf{x}_0)$ is multiplied by a perturbation vector $\mathbf{u}_0$ of unit length from right and its transpose $\mathbf{u}_0^\top$ from left and the log is taken, the first Lyapunov exponent (Eq. 2.1) is obtained. Geometrically, the determinant of the Gram matrix is the squared volume of the parallelotope spanned by the columns of $\mathbf{T}_t(\mathbf{x}_0)$ [135, 136]. Oseledets' multiplicative ergodic theorem guarantees the existence of the Oseledets matrix $\Lambda(\mathbf{x}_0)$ for μ-almost all initial conditions $\mathbf{x}_0$ [135]. In ergodic systems, the Lyapunov exponents λ_i do not depend on the initial condition $\mathbf{x}_0$. However, for numerically calculating the Lyapunov spectrum, Eq. 2.4 cannot be used directly to calculate the Lyapunov spectrum because the long-term Jacobian $\mathbf{T}_t(\mathbf{x}_0)$ quickly becomes ill-conditioned, i.e., the ratio between its largest and smallest singular value diverges exponentially with time.

Algorithm for calculating Lyapunov spectrum For calculating the full Lyapunov spectrum, we can instead exploit the fact that the growth rate of an m-dimensional infinitesimal volume element is given by $\lambda^{(m)} = \sum_{i=1}^{m} \lambda_i$ [137, 138], therefore $\lambda_1 = \lambda^{(1)}$, $\lambda_2 = \lambda^{(2)} - \lambda_1$, $\lambda_3 = \lambda^{(3)} - \lambda_1 - \lambda_2$, etc. The volume growth rates can be obtained via QR-decomposition. First one needs to evolve an orthonormal basis $\mathbf{Q}_s = [\mathbf{q}_s^1, \mathbf{q}_s^2, \dots \mathbf{q}_s^m]$ in time using the Jacobian:

$$\widetilde{\mathbf{Q}}_{s+1} = \mathbf{D}_s \mathbf{Q}_s \tag{2.5}$$

Secondly, one performs the QR-decomposition

$$\widetilde{\mathbf{Q}}_{s+1} = \mathbf{Q}_{s+1}\mathbf{R}^{s+1} \tag{2.6}$$

Hereby the non-orthonormal matrix $\widetilde{\mathbf{Q}}_{s+1}$ is uniquely decomposed into an orthonormal matrix $\mathbf{Q}_{s+1}$ of size $N \times m$ so $\mathbf{Q}_{s+1}^\top \mathbf{Q}_{s+1} = \mathbb{1}$ and an upper triangular matrix $\mathbf{R}^{s+1}$ of size $m \times m$ with positive diagonal elements.

Geometrically, $\mathbf{Q}_{s+1}$ describes the rotation of $\mathbf{Q}_s$ caused by $\mathbf{D}_s$ and the diagonal entries of $\mathbf{R}^{s+1}$ describes the stretching and/or shrinking of $\mathbf{Q}_s$, while the off-diagonal elements describe the shearing. Figures 2.4 visualizes $\mathbf{D}_s$ and the QR-decomposition for $m = 2$. The Lyapunov exponents are obtained from the diagonal elements of $\mathbf{R}^s$:

$$\lambda_i = \lim_{t\to\infty} \frac{1}{t} \log \prod_{s=1}^{t} \mathbf{R}_{ii}^s = \lim_{t\to\infty} \frac{1}{t} \sum_{s=1}^{t} \log \mathbf{R}_{ii}^s$$

Note that the QR-decomposition does not need to be performed in every step, just sufficiently often such that $\widetilde{\mathbf{Q}}_{s+w} = \mathbf{D}_{s+w-1} \cdot \mathbf{D}_{s+w-2} \dots \mathbf{D}_s \cdot \mathbf{Q}_s$ is well-conditioned. An appropriate reorthonormalization interval w_{ONS} thus depends on the condition number, given by the ratio of the smallest and largest singular value:

$$\kappa_2(\widetilde{\mathbf{Q}}_{s+w}) = \kappa_2(\mathbf{R}^{s+w}) = \frac{\sigma_1(\mathbf{R}^{s+w})}{\sigma_m(\mathbf{R}^{s+w})} = \frac{\mathbf{R}_{11}^{s+w}}{\mathbf{R}_{mm}^{s+w}}.$$

The condition number can therefore be estimated based on the ratio of the largest and smallest Lya-

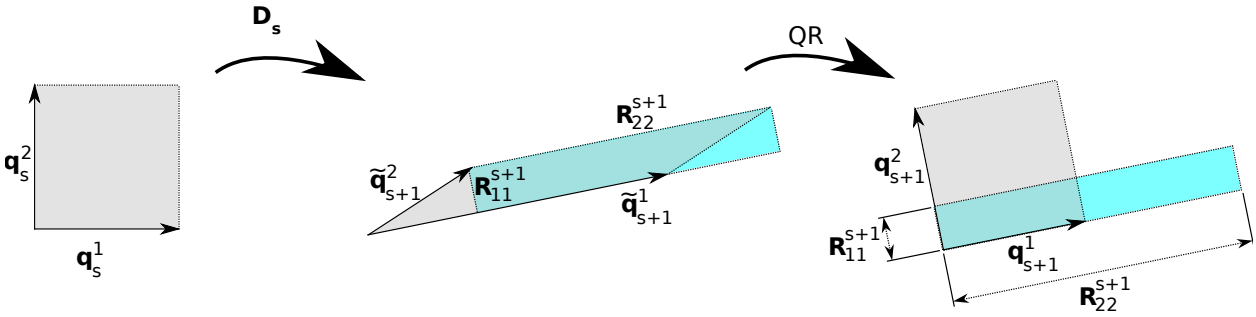

Figure 2.4 – Geometric illustration of calculation of Lyapunov spectrum. An orthonormal matrix $\mathbf{Q}_s = [\mathbf{q}_s^1, \mathbf{q}_s^2, \dots \mathbf{q}_s^m]$, whose columns are the axes of an m-dimensional cube, is rotated and distorted by the Jacobian $\mathbf{D}_s$ into an m-dimensional parallelotope $\widetilde{\mathbf{Q}}_{s+1} = \mathbf{D}_s\mathbf{Q}_s$ embedded in $\mathbb{R}^{\mathbf{N}}$. The figure illustrates this for $m = 2$, in this case the columns of $\widetilde{\mathbf{Q}}_{s+1}$ span a parallelogram. It can be divided into a right triangle and a trapezoid, and rearranged into a rectangle. This means that the area of the gray parallelogram is the same as that of the cyan rectangle. The QR-decomposition reorthonormalizes $\widetilde{\mathbf{Q}}_{s+1}$ by decomposing it into the product of an orthonormal matrix $\mathbf{Q}_{s+1} = [\mathbf{q}_{s+1}^1, \mathbf{q}_{s+1}^2, \dots \mathbf{q}_{s+1}^m]$ and the upper-triangular matrix $\mathbf{R}^{s+1}$. $\mathbf{Q}_{s+1}$ describes the rotation of $\mathbf{Q}_s$ caused by $\mathbf{D}_s$. The diagonal entries of $\mathbf{R}^{s+1}$ give the stretching/shrinking along the columns of $\mathbf{Q}_{s+1}$, thus the volume of the parallelotope formed by the first m columns of $\widetilde{\mathbf{Q}}_{s+1}$ is given by $V_m = \sum_{i=1}^m \mathbf{R}_{ii}^{s+1}$. The time-normalized logarithms of the diagonal elements of $\mathbf{R}^s$ give the Lyapunov spectrum: $\lambda_i = \lim_{t\to\infty} \frac{1}{t} \log \prod_{s=1}^t \mathbf{R}_{ii}^s = \lim_{t\to\infty} \frac{1}{t} \sum_{s=1}^t \log \mathbf{R}_{ii}^s$.

punov exponent that are calculated: $\kappa_2(\widetilde{\mathbf{Q}}_{s+w}) \approx \exp(\lambda_1 - \lambda_m)$. Thus, an appropriate reorthonormalization interval is given by $s_{\text{ONS}} = \mathscr{O}\left(\frac{\log(\hat{\kappa}_2)}{\lambda_1 - \lambda_m}\right)$, where $\hat{\kappa}_2$ is some acceptable condition number. The acceptable condition number depends on the desired accuracy of the entries of $\mathbf{R}^{s+w}$. Here a minimal example of this algorithm in pseudocode:

general algorithm for Lyapunov exponents (Benettin)

```
initialize x, Q
warmup of x
warmup of Q
for s = 1 → t do
    x ← f(x)
    D ← df(x)/dx
    Q ← D · Q
    if s % w_ONS = 0 then
        Q, R ← qr(Q)
        γ_i += log(R_ii)
    end if
end for
λ_i = γ_i / t
```

Covariant Lyapunov vectors Covariant Lyapunov vectors describe the local orientation of stable and unstable manifolds of a dynamical system. In contrast to the Gram-Schmidt vectors, which are the orthonormal basis evolved during the standard calculation of the Lyapunov spectrum [137, 138], the covariant Lyapunov vectors are covariant with the dynamics, $D_s\mathbf{v}_s^i = \gamma_i \mathbf{v}_{s+1}^i$

and invariant under time-reversal $\mathbf{v}^i_{s-} = \mathbf{v}^{-i+N+1}_{s+}$ with $\lambda_i^+ = -\lambda^-_{-i+N+1}$. Their time-average exponential expansion and contraction rates are the Lyapunov exponents. Thus, they characterize how a small volume element evolves locally in time.

Although Lyapunov vectors were already introduced by Oseledets (1968) and more formally described by Ruelle as tangent directions of invariant manifolds in 1979, they received little attention because there was no efficient algorithm to determine them. Only recently, efficient methods have been introduced [139–141].

To obtain the covariant Lyapunov vectors using the dynamic algorithm [139], one iterates an orthonormal basis $\mathbf{Q}_s = [\mathbf{q}^1_s, \mathbf{q}^2_s, \ldots \mathbf{q}^m_s]$ forward in time, performs the *QR* decomposition and stores the upper diagonal $\mathbf{R}^s$ matrices [139]. By backward iteration of a random vector in the subspace of the first k columns of $\mathbf{Q}_s$, one can obtain the k^{th} Lyapunov vector. The reason is that almost any infinitesimal perturbation will asymptotically shrink with the largest Lyapunov exponent and align along the fastest expanding direction, which is given by the largest Lyapunov vector, when evolved forward. Similarly, if the system is backward iterated, almost any infinitesimal perturbation will grow exponentially with $-\lambda_N$ and align along the last Lyapunov vectors. To obtain the other Lyapunov vectors, one can evolve a random perturbation contained in the subspace spanned by the first k Gram-Schmidt vectors, which will converge along the k^{th} Lyapunov vector.

Lyapunov vectors provide additional information about the local geometric structure of an attractor, which is not contained in the Lyapunov spectrum. The direction of the first covariant Lyapunov vector or more generally the orientation of the unstable manifolds can be used to assess how localized the chaos is: Are there only a few degrees of freedom contributing to the exponential expansion? Or is the chaos rather distributed in many directions? How fast are the unstable directions changing over time? Can they be related to other quantities of the dynamics? Furthermore, the angles between unstable and stable manifolds can be used to numerically test whether a system is hyperbolic. If a dynamical system is hyperbolic, there is always a finite angle between stable and unstable manifolds. In this case, the existence of a SRB measure is guaranteed [142–144].

Entropy of a dynamical system Chaos of a dynamical system is always associated with a dynamical entropy rate because nearby states, which could not be distinguished by a finite precision readout, are pulled apart by the sensitive dependence on initial conditions [127]. This concept was formalized by Kolmogorov and Sinai in 1959 and termed metric entropy (also called Kolmogorov-Sinai entropy or dynamical entropy rate). Let (Ω, Σ, μ) be a probability space, where Ω is the N-dimensional phase space, Σ is a σ-algebra of subsets of Ω and μ is a probability measure on (Ω, Σ) following conventional notation [135,145–147]. Let $f\colon\ \Omega \to \Omega$ be a measure-preserving transformation, which means for all subsets $A \in \Sigma$, the following holds: $\mu(f^{-1}A) = \mu(A)$. Let $\mathscr{A} = \{A_1, A_2, \ldots, A_k\}$ be a finite measurable partition of Ω, i.e. $A_i \in \Omega$, $A_i \cap A_j = \emptyset$ for $i \neq j$ and $\bigcup_i A_i = \Omega$. In each iteration, the initial partition is refined $\mathscr{A}^n = f^{-n}\mathscr{A} \vee f^{-n+1}\mathscr{A} \ldots \vee f^{-1}\mathscr{A} \vee \mathscr{A}$, where $\vee$ denotes the join $\mathscr{A} \vee \mathscr{B} = \{A \cap B | A \in \mathscr{A}, B \in \mathscr{B}\}$. We use the preimage $f^{-1}A$, as fA is not a partition if f is not injective. A block entropy of the partition $\mathscr{A}$ of Ω with respect to the measure μ is defined by

$$H(\mathscr{A}) := -\sum_i \mu(A_i)\log(\mu(A_i))$$

j is called the $\mathscr{A}$-address of each $x \in A_j$. For any trajectory, the associated symbolic dynamics can be defined by tracking the sequence of $\mathscr{A}$-addresses visited. The entropy of f with respect to $\mathscr{A}$ is

$$h(f, \mathscr{A}) := h_\mu(f, \mathscr{A}) := H(\mathscr{A}^n) = \lim_{n\to\infty} \frac{1}{n} H(f^{-n}\mathscr{A} \vee f^{-n+1}\mathscr{A} \ldots \vee f^{-1}\mathscr{A} \vee \mathscr{A})$$

The entropy of the generated symbolic dynamics measures the dynamic complexity of the system with respect to $\mathscr{A}$. For fixed points or limit cycles, the entropy is trivially zero as the future symbolic dynamics can be perfectly predicted based on a sufficiently long past trajectory. In contrast, in chaotic systems, the stream of symbols can't be predicted based on the past as the sensitivity on initial conditions constantly separates trajectories. If a partition $\mathscr{A}$ indefinitely refines itself under the effect of the dynamics, such that $\bigvee_{n=0}^{\infty} f^{-n}\mathscr{A}$ consists only of points, then an infinite symbolic string uniquely identifies the initial condition and the partition is called a *generating partition*. In some systems, such a generating partition was found, although for generic dynamical systems finding a generating partition is believed to be difficult [145].

The Kolmogorov-Sinai entropy of f, written $h_\mu(f)$ is defined as:

$$h_\mu(f) := \sup_{\mathscr{A}} h(f, \mathscr{A}).$$

It is the supremum over all finite partitions and therefore does not depend on $\mathscr{A}$. This means, $h_\mu(f)$ is the average amount of uncertainty as one attempts to predict the next $\mathscr{A}$-address of a random point. In conclusion, the KS entropy quantifies the average dynamic complexity of a typical trajectory. Measuring the KS entropy of a high-dimensional system is difficult if no generating partition is known. A brute force ansatz of partitioning the phase space into small boxes is doomed to fail as the number of partitions grows exponentially with the degrees of freedom [148]. Fortunately, the KS entropy can be related to the Lyapunov spectrum which is accessible even in high-dimensional systems. This is the only known general way of accessing the entropy of a high-dimensional differentiable dynamical system [145].

Relating entropy and Lyapunov exponents Ruelle showed that the sum of the positive Lyapunov exponents give an upper bound to the Kolmogorov-Sinai entropy [144]:

$$h_\mu(f) \leqslant \sum_{\lambda_i > 0} \lambda_i$$

Equality holds if and only if the system is endowed with an SRB (Sinai-Ruelle-Bowen) measure (Pesin entropy formula) [149]. An f-invariant Borel probability measure μ is an SRB measure if the conditional probability of μ on smooth manifolds is absolutely continuous [150]. The interpretation is that uncertainty in the prediction of future states comes from positive Lyapunov exponents, or more precisely from the expanding manifolds with smooth densities [147]. In several classes of dynamical systems, the existence of an SRB measure was proved [151].

Measuring the attractor dimensionality of a dynamical system The trajectory of an N-dimensional dissipative chaotic system does not cover the whole phase space. After a transient period, it relaxes onto a strange attractor, which has a dimensionality $D \leq N$. This can be a zero-dimensional fixed point, a one-dimensional periodic orbit, a higher-dimensional quasi-periodic orbit or a chaotic strange attractor with typically non-integer dimensionality. Such an attractor is a special case of a fractal set and one classical approach to measuring its dimensionality is box counting: the idea is to count the number M of N-dimensional boxes of side length a that are necessary to cover the attractor (Fig. 2.5). The box-counting dimension is then defined as $D = -\lim_{a\to 0} \frac{\log(M(a))}{\log(a)}$. Thus, the box-counting dimension is the exponent, by which the number of covering boxes M is scaling up as one decreases the box size. By the same token the number of

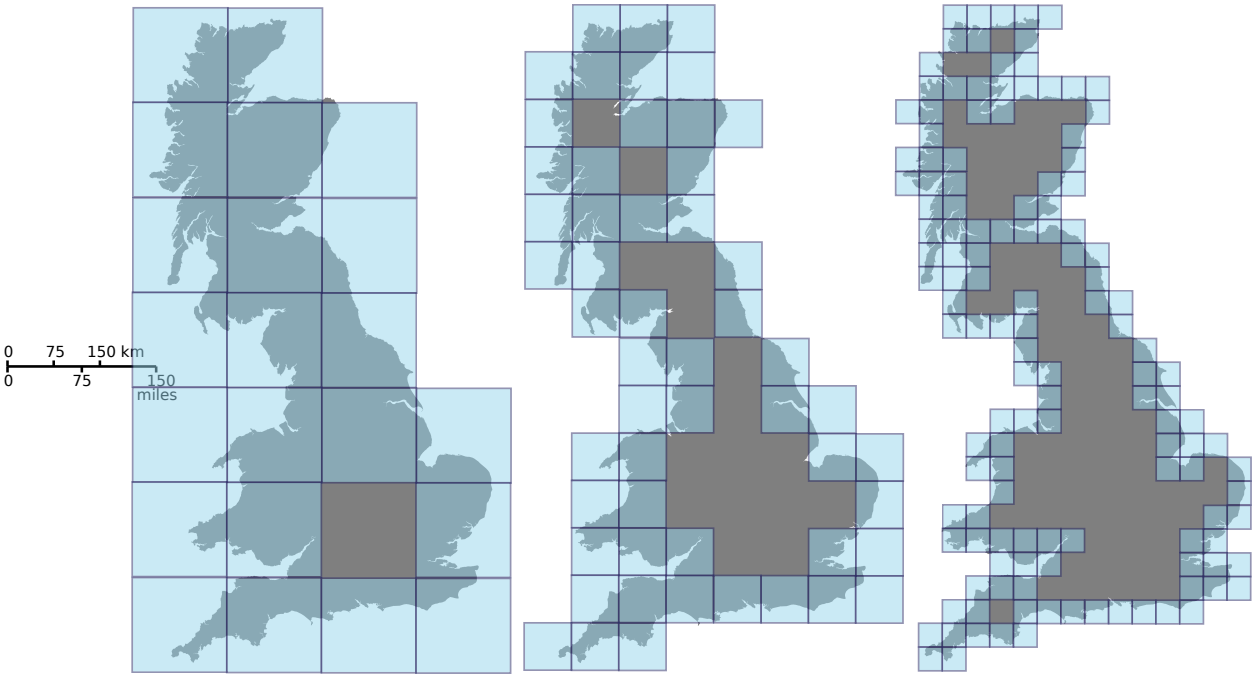

Figure 2.5 – Box counting dimension and the curse of dimensionality. The dimensionality D of a geometric object can be measured by evaluating the scaling of the number of boxes M of size a required to cover the object when decreasing the box size: $D = -\lim_{a\to 0} \frac{\log(M(a))}{\log(a)}$. For increasing number of dimensions, the number of boxes grows exponentially with the dimensionality. Therefore, this and similar sampling-based methods are not suitable to characterize high-dimensional strange attractors (Figures modified from [152]).

boxes needed to cover the set scales exponential with its dimensionality. To sample the attractor, the data necessary for the box counting therefore also scales exponentially with the dimensionality. For increasing dimension, one runs into the curse of dimensionality. There are other related techniques, e.g. the Grassberger-Procaccia algorithm [153, 154], which estimates the correlation dimension D_2. Similar to the case of box counting, a strict lower bound on the data required to estimate the attractor dimensionality with a fixed desired accuracy scales exponentially in the degrees of freedom N [155, 156]. Therefore, the computational complexity of this calculation is exponential in N. It is well understood in nonlinear dynamics that such direct approaches of measuring dimensionality are inappropriate for high-dimensional dynamical systems. In contrast, the attractor dimensionality can be calculated in polynomial time based on the Lyapunov spectrum of a dynamical system [135].

The Lyapunov dimension D_L relates the attractor dimensionality to the Lyapunov spectrum. It is given by the interpolated number of Lyapunov exponents that sum to zero:

$$D_\mathrm{L} = k + \frac{\sum_{i=1}^{k} \lambda_i}{\lambda_{k+1}} \quad \text{with} \quad k = \max_n \left\{ \sum_{i=1}^{n} \lambda_i \geq 0 \right\}$$

It was conjectured that "in general", if μ is an SRB (Sinai-Ruelle-Bowen) measure, D_L is equivalent to the information dimension [157–159]:

$$D_1 = D_\mathrm{L}$$

This Kaplan-Yorke conjecture is believed to be true for many systems, but it has been rigorously proved only for certain classes of dynamical systems; there exists no general proof [160]. Geometrically, one can think of k as the dimensionality of the highest dimensional hypersphere whose volume does not shrink by the dissipative system dynamics. A different perspective is that all points on the attractor are mapped back on the attractor by f. Expansion along unstable manifolds and contraction along stable manifold need to be balanced on the attractor because of its invariance.

2.7 Random dynamical systems: merging stochastic and dynamical systems

The dynamics of many systems is shaped by an interplay of deterministic and stochastic contributions. While dynamical systems theory often assumes purely deterministic equations of motion, the theory of *random dynamical systems* (RDS) allows uniting these two perspectives. RDS studies how an ensemble of initial conditions evolves in time under the influence of a frozen noise realization. This allows extending concepts from ergodic theory like Lyapunov spectra, Kolmogorov-Sinai entropy and attractor dimensionality to systems with a stochastic external input.

Random dynamical systems and neural reliability Random dynamical systems provide a mathematical framework to study the reliability of a system and more specifically trial-to-trial variability in neuroscience [161–164]. In this perspective, the stochastic external input is interpreted as a signal and one asks how reliably different initial states respond to this external signal. A system is considered reliable if different initial conditions converge to the same trajectory. Conversely, if the system is unreliable, different initial conditions remain separated despite the same external input [147, 161].

Random dynamical systems Consider a stochastic differential equation of the form:

$$dx_t = a(x_t) + \sum_{i=1}^{N} b_i(x_t) \circ dW_t^i$$

where dW_t^i represent independent Brownian motions (following the notation of [147, 161, 162, 165]). An associated *stochastic flow map* is a solution for the dynamics, i.e. $F_{t_1,t_2;\zeta}(x_{t_1}) = x_{t_2}$. Instead of studying the temporal evolution of some initial measure μ, where each initial condition receives *private* noise, as it is usually done in a Fokker-Planck ansatz, the theory of random dynamical systems studies the evolution of a *sample measure* μ_ζ^t, defined as

$$\mu_\zeta^t = \lim_{s\to\infty} (F_{-s,t;\zeta})_* \mu$$

where the push-forward $(F_{-s,t;\zeta})_*$ transports the initial measure μ for some fixed white noise realization $\zeta(t)$ defined for all $t \in (-\infty, \infty)$ along the flow $F_{-s,t;\zeta}$. In other words, the sample measure μ_ζ^t is the conditional measure at time t given the infinite past history of $\zeta(t)$. Note that in general, while μ_ζ^t depends both on time t and the noise realization ζ, it possesses invariant properties, characterizing its structure. For example, the Lyapunov exponents $\lambda_1 \geqslant \lambda_2 \geqslant \ldots \geqslant \lambda_N$ are independent of the input realization ζ [166].

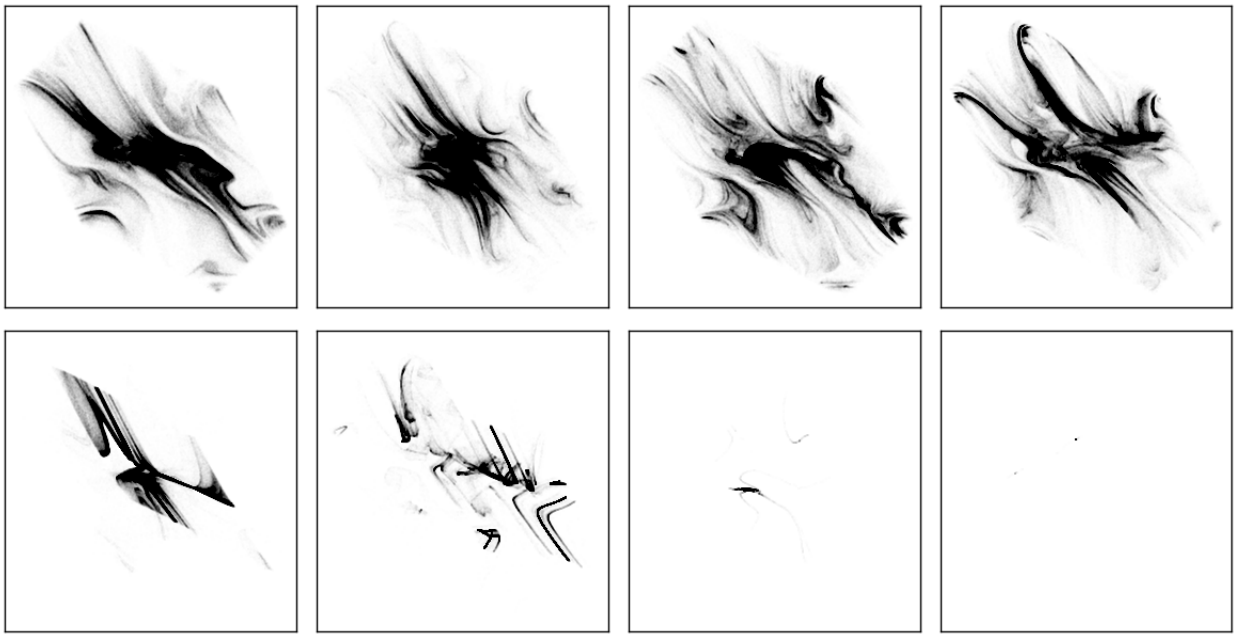

Figure 2.6 – Random dynamical systems: random strange attractor and random sink. A two-dimensional projection perpendicular to the flow of a chaotic network of three neurons driven by a fixed realization of random stream of incoming spike trains. **Top panels:** For weak input, uniformly distributed independent initial conditions driven by the same frozen input realization converge to a time-dependent random strange attractor (shown from left to right for $t = 1, 2, 6, 10$ s). **Bottom panels:** For sufficiently strong input, the uniform initial conditions collapse into one single trajectory (shown from left to right for $t = 1, 2, 6, 10$ s). In this example, the uniformly distributed initial conditions coalesce into a wandering time-dependent sink after approximately 10 s.

Chaos and Reliability Two theorems from random dynamical systems link sample measure μ_ζ^t and Lyapunov spectrum in chaotic and stable systems respectively.

Firstly, Ledrappier and Young proved that if $\lambda_1 > 0$, then μ_ζ^t is a random SRB (Sinai-Ruelle-Bowen) measure [167].

As a consequence, in contrast to autonomous systems, for random dynamical systems the Pesin identity $h_\mu(f) \leqslant \sum_{\lambda_i>0} \lambda_i$ is guaranteed to hold. Note that in contrast to SRB measures of autonomous systems, random SRB measures are time-dependent. However, they have a similar meaning: dynamical systems with SRB measure have smooth conditional measures along the unstable manifolds.

Secondly, Baxendale and Le Jan showed that if $\lambda_1 < 0$ and the stationary measure is ergodic and some nondegeneracy conditions on the measure are fulfilled [168], then μ_ζ^t is a random sink, which means $\mu_\zeta^t(\mathbf{x}) = \delta(\mathbf{x} - \mathbf{x}_t)$, where $\mathbf{x}_t$ is a solution of the stochastic dynamics for a given noise realization ζ [168, 169].

This means that any trajectory of a stable random dynamical system will at some time be absorbed into one single trajectory, which is independent of the initial condition but depends only the noise realization. Equally, any smooth initial measure will asymptotically coalesce into a wandering time-dependent sink. Note that the theorems by Baxendale and Le Jan do not say when the random sink will be reached. Its asymptotic existence might in the case of long transients therefore have no practical relevance at the timescale of interest [170].

2.8 Controlling chaos and variability in neural circuits receiving input spike trains

Controlling recurrent circuits by streams of input spike trains Understanding the interaction of recurrent dynamics and external input is relevant for understanding information transmission between neural circuits. The brain can be seen as a network of different networks driving

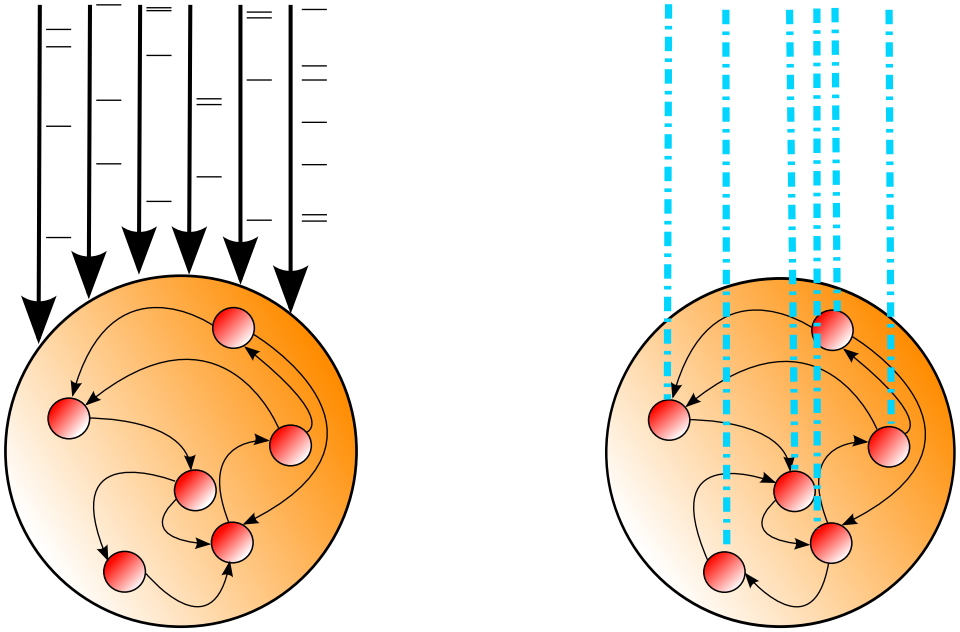

Figure 2.7 – Controlling spiking neural network by spatiotemporally structured external input. A It is essential to understand how streams of incoming spike trains control the recurrent activity of a local circuit. To obtain a better understanding of the functioning of cortical projections between different microcircuits, it is vital to clarify how different features of the projection regulate the extent to which the input is able to control the recurrent chaotic activity of recurrent target circuits. **B** Another neuroscientific application, where a better understanding of the interaction of recurrent dynamics and external input is needed, is the design of future optogenetic experiments. Novel tools and bidirectional neural circuit interfaces for the first time allow selectively manipulating and monitoring the activity of vast numbers of neurons in behaving animals. These technological advancements promote the perturbation of neural activity with millisecond and single-cell precision and allow new approaches to fundamental questions. To fully harness the potential of such tools and approaches, it is vital to build better theoretical models for the interaction of recurrent circuit dynamics and artificial perturbations.

each other with streams of spike trains. Therefore, it is essential to understand how external input controls the recurrent activity of a local circuit. If the driving circuit's activity does not exert control over the recurrent activity, the target network is independent of the input. Consequently, no information from the input to the recurrent system can be transmitted. In contrast, if the dynamics of the target circuit is strongly controlled by the input, then information is transmitted along the set of projections [171]. To obtain a better understanding of the functioning of cortical projections between different microcircuits, it is therefore important to clarify how different features of the projection regulate the extent to which the input is able to control the recurrent chaotic activity of recurrent target circuits. What is the optimal projection design in terms of connection strength, spike time irregularity and correlations to control activity in a subsequent circuit? What can we

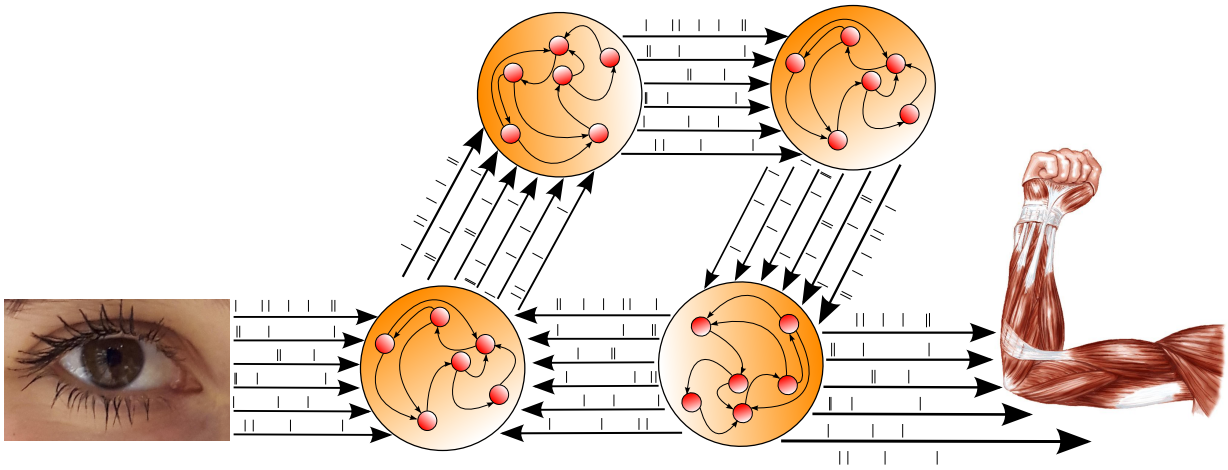

Figure 2.8 – The brain as a network of networks driving each other with streams of spike trains. Different neural circuits in the brain communicate with streams of spike trains. Understanding what aspects of a stream of incoming spike trains control the recurrent activity is relevant to understand information transmission and the reliability of neural circuits.

learn about important projections in the brain, e.g. the hippocampal projection from dentate gyrus to CA3, which is believed to be crucial for encoding and retrieval of memories [172, 173]? Such questions can also be asked for sensory input from thalamus to the cortex, e.g. projections from the lateral geniculate nucleus to layer 4 of the primary visual cortex [174].

Controlling cortical circuits optogenetically Another neuroscientific application, where a better understanding of the interaction of recurrent dynamics and external input is needed, is the design of future optogenetic experiments. Emerging techniques allow controlling and measuring the activity of many of cortical neurons at the same time in an intact organism that performs tasks [175]. Different optogenetic tools allow selectively activating and deactivating different subpopulations or even single neurons [176]. Until now, optogenetic tools have mostly been used for reversibly silencing or activating subpopulation. However, a potential application, which still waits to be fully harnessed, are time-dependent optical stimulation protocols and closed-loop experiments [176]. It is vital for hypothesis-driven research to build better theoretical models of the interaction of recurrent circuit dynamics and external time-dependent artificial stimulation. Such models would allow for the deduction of predictions that are testable in experiments. Scientific questions that can be addressed in this way are, e.g.: Which optogenetic stimulation protocols are most promising to obtain complete control of the recurrent cortical dynamics? Can such a control also be obtained if only a fraction of the circuit is externally driven? How does the spatiotemporal stimulus structure affect controllability of the recurrent activity? Which optogenetic stimuli can shed light on the input-output function of a cortical circuit? How are single-cell features expected to affect the controllability of neural circuits?

Reliability of neural activity It has been a longstanding question in neuroscience how reliable neurons can respond to an external stimulus. This has been studied experimentally in single neurons. *In vitro* experiments found that isolated neurons can under many experimental conditions respond reliably across trials to an external time-varying input [66–69]. In these studies, more structured input tended to increase the response reliability. Technological advances bring experi-

mental circuit-level investigation of reliability into reach. Theoretical studies in single neurons also found that identical external stochastic forcing tends to synchronize unconnected copies of identical model neurons that were initialized with different states [68, 177–183] even if the dynamics of the single neuron model was chaotic when driven by a constant external input. However, there are interesting exceptions [177]. It is a challenge to extend this analysis to large recurrent neural networks. The high dimensional and often chaotic dynamics of large recurrent networks requires a type of analysis that can systematically assess the role of recurrent interactions and characterize the networks' collective dynamics. Studies in rate chaotic networks suggest a suppression of chaos by structured input [6–8] but in spiking networks, this has not yet been thoroughly analyzed. Earlier studies of chaos in spiking networks used constant external input [9, 33, 76, 123–125, 184] or white noise drive [162, 163]. The main finding of the latter was that even in chaotic systems, individual neurons can respond surprisingly reliably to an external (white noise) stimulus when the input variance is strong enough [162].

Our approach To address this challenge, we develop an approach to calculate the full Lyapunov spectra of balanced networks driven by input streams of spike trains, thus yielding the dynamical entropy rate in numerically exact event-based simulations. To explore how features of input streams affect information transmission, we vary correlations, irregularity, coupling strength and spike rate of the input, the number of externally driven cells and action potential onset rapidness of recurrent neurons. Furthermore, we investigate how single neuron properties shape the target circuits' reliability.

2.9 Overview

This thesis aims to elucidate how the collective dynamics of neural circuits depend on both the statistics of an external time-varying input and on biophysical properties of single cells. We will investigate this with concepts from dynamical systems, stochastic processes and information theory applied to large circuits of spiking model neurons.

To study the dynamics of such large circuits with high precision and reasonable computational effort, we will first develop a novel algorithm for numerically exact event-based simulations of large spiking circuits and the calculation of their Lyapunov exponents in Chapter 3.

We then investigate the role and relevance of action potential (AP) onset rapidness for the spontaneous collective dynamics of balanced recurrent circuits. While in a feedforward architecture AP onset rapidness has a great impact on the bandwidth of information encoding both in theoretical predictions and experimental observations [30, 44, 47–49, 58, 185, 186], the role and relevance of a broad encoding bandwidth and a rapid spike onset in the dynamics of recurrent networks has not yet been studied systematically. We will analyze the effect of changing the AP onset rapidness on the organization of the phase space of recurrently connected neurons with a constant external input current in Chapter 4. Based on the Lyapunov spectrum of the network dynamics, we shall find a drastic reduction of the attractor dimension for rapid AP onset, which is not detected by a pairwise dimensionality estimate. This will be corroborated by simulations of more realistic circuits having experimentally measured second order motif statistics and a multilayered cortical column structure. Furthermore, we present a systematic analysis how key features of the collective dynamics scale with network parameters.

Based on the strong effect of AP onset rapidness in the spontaneous dynamics of balanced cir-

cuits, we will investigate the effect of AP onset rapidness on information encoding into a recurrent network driven by incoming streams of action potentials in Chapter 5. We will study what rate and coupling strength of incoming streams of spike trains is sufficient to control the driven target circuit and to suppress chaotic dynamics. Furthermore, we will investigate how the complete network state control depends on network parameters and single-cell features. We shall find that rapid AP onset facilitates the transition to complete network state control and the transition from chaos to stability in driven balanced circuits.

In Chapter 6, a recent study that compared the dynamics of spiking balanced networks of pulse-coupled leaky integrate-and-fire (LIF) neurons and matched networks of rate neurons will be re-examined [3]. The reexamined study proposed an intriguing mathematical analogy between the chaotic instability of the matched rate networks and the spiking network dynamics [4]. We will ask for the spiking LIF network: Can we find fingerprints of a phase transition mathematically analogous to the instability found in rate networks? How generic is the described phenomenon? Do the predictions of the proposed mean-field theory match numeric simulations if parameters are slightly changed? How sensitive is the phenomenon to details of single neuron dynamics, e.g. the synaptic delay, the refractory period and neuron models?

In Chapter 7, for the first time to our knowledge, we will calculate full Lyapunov spectra of random firing-rate networks. The dynamics of such networks and their transition from a stable state for small couplings to a chaotic state for strong couplings has been studied extensively [3–7, 37, 92, 131, 187–194]. Our study allows for the measuring of dynamical entropy rate and attractor dimensionality for such networks of firing-rate units. This approach provides a toolkit from dynamical systems theory to analyze how these different factors shape the complex rate dynamics. We will compare the Lyapunov dimension with a dimensionality estimate based on principal component analysis (PCA), which is commonly used in neuroscience [7, 188, 195–197]. The Lyapunov spectrum is also obtained for rate networks driven by frozen white noise, extending earlier studies, which examined the behavior of the largest Lyapunov exponent upon time-varying external input [6–8].

In Chapter 8, we will review recent advances in modeling the dynamics of cortical circuits [9]. Both theoretical and experimental evidence for an inhibition-dominated operating regime of cortical circuits will be discussed. Furthermore, we will revisit progress in the theoretical understanding of microstate dynamics, stimulus selectivity, response heterogeneity and spike count correlation.

Finally, in Chapter 9, we will summarize our key findings, discuss their relation to previous theoretical and experimental studies and propose several potential future research directions building on our results.

3 Lyapunov exponents of spiking balanced networks

3.1 Summary

The ergodic theory of chaotic dynamical systems allows to characterize the dynamics and complex phase space structure of large-scale neural network models. Here, a brief introduction to the mathematical theory of chaos and strange attractors will be given. This is followed by two example calculation of the full Lyapunov spectrum of a spiking neural network of leaky and quadratic integrate-and-fire neurons. Finally, we provide checks of the numerical implementation and introduce a novel algorithm for an efficient numerical implementation of large sparse spiking networks. Our new algorithm reduces the computational cost from $\mathscr{O}(N)$ to $\mathscr{O}(\log(N))$ operations per network spike for a fixed number of synapses per neuron and Lyapunov exponents. This allows numerically exact simulations of large spiking networks ($N = 10^9$ neurons) and the characterization of their phase space structure. For example, calculating the largest Lyapunov exponent of a spiking neural network with one million neurons is sped up by more than four orders of magnitude.

Efficient numerically exact calculation of Lyapunov exponents in spiking neural networks

Rainer Engelken[1,2,3,4*],Fred Wolf[1,2,3,4]

1 Max Planck Institute for Dynamics and Self-Organization, Göttingen, Germany
2 Bernstein Center for Computational Neuroscience, Göttingen, Germany
3 Bernstein Focus for Neurotechnology, Göttingen, Germany
4 Faculty of Physics, University of Göttingen, Göttingen, Germany

* rainer@nld.ds.mpg.de

Abstract

The ergodic theory of chaotic dynamical systems allows us to characterize the dynamics and complex phase space structure of large-scale neural network models, including the attractor dimensionality and dynamical entropy rate. Here, a brief introduction to the mathematical theory of chaos and strange attractors will be given. This is followed by example calculations of the full Lyapunov spectrum of spiking neural networks of both leaky integrate-and-fire neurons and quadratic integrate-and-fire neurons. Finally, we provide checks of the numerical implementation and introduce a novel algorithm for an efficient numerically exact event-based implementation of large sparse spiking networks. Our new algorithm reduces the computational cost from $\mathcal{O}(N)$ to $\mathcal{O}(\log(N))$ operations per network spike for a fixed number of synapses per neuron and Lyapunov exponents. This allows numerically exact simulations of large spiking networks ($N = 10^9$ neurons) and the characterization of their phase space structure. For example, calculating the largest Lyapunov exponent of a spiking neural network with one million neurons is sped up by more than four orders of magnitude compared to earlier implementations.

Introduction

Motivation

How information is encoded, processed and transmitted by neural circuits is intimately related to their collective network dynamics. Therefore, it is desirable to better understand how different factors shape the patterns of activity across neural populations. Prominent factors that shape circuit dynamics include single cell properties, synaptic features, network topology and external input statistics.

Using concepts from dynamical systems theory, we calculate the attractor dimensionality and dynamical entropy rate for spiking networks. The attractor dimension measures the diversity of activity states. Dynamical entropy quantifies the uncertainty amplification due to sensitivity to initial conditions. We obtain these two canonical measures of the collective network dynamics from the full set of Lyapunov exponents which measure the exponential sensitivity to small perturbations in the tangent space along a trajectory.

Our new algorithm, which applies to arbitrary network topologies and many neuron models, reduces the computational cost from $\mathcal{O}(N)$ to $\mathcal{O}(\log(N))$ operations per network spike for a fixed number of synapses per neuron and Lyapunov exponents. We

achieved this by changing the frame of reference of the neurons' phase-representation and by employing a data structure that avoids iterating through all neurons at every network spike time to find the next spiking neuron. This allows numerically exact simulations of large spiking networks ($N = 10^9$ neurons) and the characterization of their phase space structure. This facilitates investigating the chaotic dynamics of simplified cortical microcircuit models (e.g. [1]), which usually require a supercomputer for simulations [2–4]. Efficient simulation of large networks might also be useful when gradually experimentally obtained wiring diagrams known as connectomes become available by novel circuit reconstruction methods [5, 6].

Our approach opens a novel avenue to determine how biophysical properties of neurons and network parameters influence the collective dynamics of large networks and shape the geometric structure of the corresponding high-dimensional chaotic attractor.

Overview

We will first briefly introduce the dynamical entropy rate and attractor dimensionality of dynamical systems and then show how they can be estimated based on the Lyapunov spectrum. Next, we introduce Lyapunov exponents and how they can be calculated in numerically exact event-based simulations in spiking neural networks using a novel algorithm. We then show two example calculations of the Lyapunov spectrum for networks of both leaky and quadratic integrate-and-fire neurons in the balanced state. Finally, we discuss numerically efficient implementations and several checks of the semi-analytic calculation.

Entropy and attractor dimensionality of dynamical systems

The dynamical stability of network activity constrains the capability of information processing: In chaotic systems, a sensitive dependence on initial conditions makes predictions of future states impossible, if the initial state is known only with finite precision. This corresponds to a dynamical entropy rate because nearby states, which could not be distinguished by a finite precision readout initially, are pulled apart by the chaotic dynamics and are distinguishable later on [7]. Therefore, the dynamical entropy rate quantifies the speed by which microscopic perturbations such as ion channel noise affect global firing patterns. The concept of an entropy rate associated to the amplification of uncertainty in a dynamical system was formalized by Kolmogorov and Sinai in 1959 and termed metric entropy (also called Kolmogorov-Sinai entropy rate or dynamical entropy rate). A rigorous introduction to Kolmogorov-Sinai entropy rate is beyond our scope here, we refer instead to the literature [8–14].

Measuring the Kolmogorov-Sinai (KS) entropy of a high-dimensional system is difficult if no generating partition is known. A brute force ansatz of partitioning the phase space into small boxes is doomed to fail as the number of partitions grows exponentially with the number of degrees of freedom. Fortunately, the KS entropy can be related to the Lyapunov spectrum which is accessible even in high-dimensional systems. This is the only known general way of accessing the entropy of a high-dimensional differentiable dynamical system [13].

Ruelle showed that the sum of the positive Lyapunov exponents gives an upper bound to the KS entropy [15]:

$$H \leqslant \sum_{\lambda_i > 0} \lambda_i$$

Equality holds if and only if the system is endowed with an SRB (Sinai Ruelle Bowen) measure (Pesin entropy formula) [16]. An f-invariant Borel probability measure μ is an SRB measure if the conditional probability of μ on smooth manifolds is absolutely

continuous. The interpretation is that uncertainty in the prediction of future states comes from positive Lyapunov exponents, or more precisely from the expanding manifolds with smooth densities [14]. In several classes of dynamical systems, the existence of an SRB measure has been proven [17].

Furthermore, the Lyapunov spectrum gives an estimate of the attractor dimension [9, 16, 18]. The trajectory of an N-dimensional dissipative chaotic system does not cover the whole phase space. After a transient period, it relaxes onto a strange attractor, which has a dimensionality $D \leq N$. The Lyapunov dimension is given by the interpolated number of Lyapunov exponents that sum to zero [19–21]:

$$D_L = k + \frac{\sum_{i=1}^{k} \lambda_i}{|\lambda_{k+1}|} \quad \text{with} \quad k = \max_n \left\{ \sum_{i=1}^{n} \lambda_i \geq 0 \right\}.$$

It was conjectured that "in general", if μ is an SRB (Sinai-Ruelle-Bowen) measure, D_L is equivalent to the information dimension [19–21]: $D_1 = D_L$. This Kaplan-Yorke conjecture is believed to be true for many systems, but it has been rigorously proved only for certain classes of dynamical systems; there exists no general proof [22].One can think of it as the highest dimensional hypersphere, whose volume neither shrinks nor expands by the dissipative system dynamics. A lower bound on the attractor dimension is given by the number of positive Lyapunov exponents [23].

Lyapunov spectrum of dynamical systems

An autonomous dynamical system is usually defined by a set of ordinary differential equations $\frac{d\mathbf{x}}{dt} = \mathbf{F}(\mathbf{x})$, $\mathbf{x} \in \mathbb{R}^N$ in the case of continuous dynamics or as a map $\mathbf{x}_{s+1} = \mathbf{f}(\mathbf{x}_s)$ in the case of discrete dynamics. For pedagogic reasons, we focus here on discrete dynamical systems, but everything can directly be extended to continuous systems [24]. An initial condition $\mathbf{x}_0$ forms an orbit. As a natural extension of linear stability analysis, one can ask how an infinitesimal perturbation $\mathbf{x}_0' = \mathbf{x}_0 + \epsilon\mathbf{u}_0$ evolves in time. Chaotic systems are sensitive to initial conditions, therefore almost all infinitesimal perturbations $\epsilon\mathbf{u}_0$ of the initial condition grows exponentially and may lead to a drastically different future behavior. The largest Lyapunov exponent measures the average rate of exponential divergence or convergence of nearby initial conditions.

$$\lambda_{\max}(\mathbf{x}_0) = \lim_{t\to\infty} \frac{1}{t} \lim_{\epsilon\to 0} \log \frac{||\epsilon\mathbf{u}_t||}{||\epsilon\mathbf{u}_0||} \tag{1}$$

It is crucial to first take the limit $\epsilon \to 0$ and then $t \to \infty$, as $\lambda_{\max}(\mathbf{x}_0)$ would be trivially zero for a bounded attractor if the limits are exchanged, as $\lim_{t\to\infty} \log \frac{||\epsilon\mathbf{u}_t||}{||\epsilon\mathbf{u}_0||}$ is bounded for finite perturbations even if the system is chaotic. To measure m Lyapunov exponents, one has to study the evolution of m independent infinitesimal perturbations spanning the tangent space:

$$\mathbf{u}_{s+1} = \mathbf{D}_s\mathbf{u}_s \tag{2}$$

where the Jacobian $\mathbf{D}_s(\mathbf{x_s}) = \frac{d\mathbf{f}(\mathbf{x_s})}{d\mathbf{x}}$ characterizes the evolution of generic infinitesimal perturbations during one step. Again, we are interested in the asymptotic behavior, therefore we have to study the long-term Jacobian:

$$\mathbf{T}_t(\mathbf{x}_0) = \mathbf{D}_{t-1}(\mathbf{x}_{t-1}) \dots \mathbf{D}_1(\mathbf{x}_1)\mathbf{D}_0(\mathbf{x}_0) \tag{3}$$

Note that $\mathbf{T}_t(\mathbf{x}_0)$ is a product of generally noncommuting matrices.

The Lyapunov exponents $\lambda_1 \geq \lambda_2 \cdots \geq \lambda_N$ are defined by the logarithms of the eigenvalues of the positive-semidefinite symmetric Oseledets matrix

$$\mathbf{\Lambda}(\mathbf{x}_0) = \lim_{t\to\infty} [\mathbf{T}_\mathrm{t}(\mathbf{x}_0)^\top \mathbf{T}_\mathrm{t}(\mathbf{x}_0)]^{\frac{1}{2t}}, \tag{4}$$

where $\top$ denotes the transpose operator. The expression inside the brackets is the Gram matrix of the long-term Jacobian $\mathbf{T}_t(\mathbf{x}_0)$. Geometrically, the determinant of the Gram matrix is the squared volume of the parallelotope spanned by the columns of $\mathbf{T}_\mathrm{t}(\mathbf{x}_0)$. Oseledets' multiplicative ergodic theorem guarantees the existence of the Oseledets matrix $\mathbf{\Lambda}(\mathbf{x}_0)$ for μ-almost all initial conditions $\mathbf{x}_0$. Here μ-almost all initial conditions means that it applies to all conditions except from a set of measure zero with respect to μ. In ergodic systems, λ_i does not depend on the initial condition $\mathbf{x}_0$. However, for numerically calculating the Lyapunov spectrum, Eq. 4 can not be used directly because the long-term Jacobian $T_t(\mathbf{x}_0)$ quickly becomes ill-conditioned, i.e., the ratio between its largest and smallest singular value diverges exponentially with time.

Algorithm to calculate the Lyapunov spectrum

To calculate the full Lyapunov spectrum, we can instead exploit the fact that the growth rate of an m-dimensional infinitesimal volume element is given by $\lambda^{(m)} = \sum_{i=1}^{m} \lambda_i$ therefore $\lambda_1 = \lambda^{(1)}$, $\lambda_2 = \lambda^{(2)} - \lambda_1$, $\lambda_3 = \lambda^{(3)} - \lambda_1 - \lambda_2$, etc. The volume growth rates can be obtained via QR-decomposition as illustrated in Fig. 1 [9, 12, 25]. First, one needs to evolve an orthonormal basis $\mathbf{Q}_s = [\mathbf{q}_s^1, \mathbf{q}_s^2, \dots \mathbf{q}_s^m]$ in time using the Jacobian:

$$\widetilde{\mathbf{Q}}_{s+1} = \mathbf{D}_s \mathbf{Q}_s \tag{5}$$

then one performs the QR-decomposition

$$\widetilde{\mathbf{Q}}_{s+1} = \mathbf{Q}_{s+1} \mathbf{R}^{s+1} \tag{6}$$

Hereby the non-orthonormal matrix $\widetilde{\mathbf{Q}}_{s+1}$ is uniquely decomposed into an orthonormal matrix $\mathbf{Q}_{s+1}$ of size $N \times m$ so ${\mathbf{Q}^\top}_{s+1}\mathbf{Q}_{s+1} = \mathbb{1}_{m\times m}$ and an upper triangular matrix $\mathbf{R}^{s+1}$ of size $m \times m$ with positive diagonal elements.

Geometrically, $\mathbf{Q}_{s+1}$ describes the rotation of $\mathbf{Q}_s$ caused by $\mathbf{D}_s$ and the diagonal entries of $\mathbf{R}^{s+1}$ describes the stretching and/or shrinking of $\mathbf{Q}_s$, while the off-diagonal elements describe the shearing. Fig. 1 visualizes $\mathbf{D}_s$ and the QR-decomposition for $m = 2$. The Lyapunov exponents are given by time-normalized logarithms of the diagonal elements of $\mathbf{R}^s$:

$$\lambda_i = \lim_{t\to\infty} \frac{1}{t} \log \prod_{s=1}^{t} \mathbf{R}_{ii}^s = \lim_{t\to\infty} \frac{1}{t} \sum_{s=1}^{t} \log \mathbf{R}_{ii}^s \tag{7}$$

Note that the QR-decomposition does not need to be performed in every simulation step, just sufficiently often such that $\widetilde{\mathbf{Q}}_{s+w} = \mathbf{D}_{s+w-1} \cdot \mathbf{D}_{s+w-2} \dots \mathbf{D}_s \cdot \mathbf{Q}_s$ is well-conditioned [25]. An appropriate reorthonormalization interval $w_\mathrm{ONS} = t_\mathrm{ONS}/\Delta t$ thus depends on the condition number, given by the ratio of the smallest and largest singular value:

$$\kappa_2(\widetilde{\mathbf{Q}}_{s+w}) = \kappa_2(\mathbf{R}^{s+w}) = \frac{\sigma_1(\mathbf{R}^{s+w})}{\sigma_m(\mathbf{R}^{s+w})} = \frac{\mathbf{R}_{11}^{s+w}}{\mathbf{R}_{mm}^{s+w}}. \tag{8}$$

The condition number can therefore be estimated based on the ratio of the largest and smallest Lyapunov exponent that are calculated: $\kappa_2(\widetilde{\mathbf{Q}}_{s+w}) \approx \exp(\lambda_1 - \lambda_m)$. Thus, an appropriate reorthonormalization interval is given by $t_\mathrm{ONS} = \mathcal{O}\left(\frac{\log(\hat{\kappa}_2)}{\lambda_1 - \lambda_m}\right)$, where $\hat{\kappa}_2$ is some acceptable condition number. The acceptable condition number depends on the desired accuracy of the entries of $\mathbf{R}^{s+w}$. Here we show a minimal example of this algorithm in pseudocode:

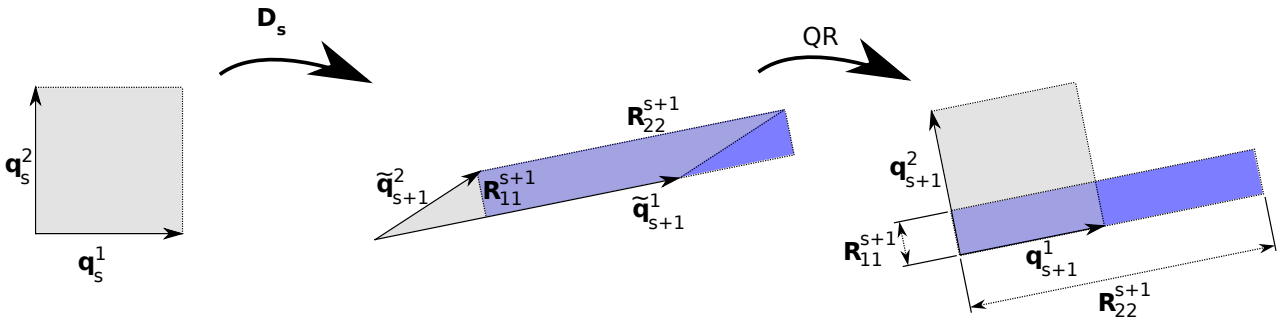

Fig 1. Geometric illustration of Lyapunov spectrum calculation. An orthonormal matrix $\mathbf{Q}_s = [\mathbf{q}_s^1, \mathbf{q}_s^2, \dots \mathbf{q}_s^m]$, whose columns are the axes of an m-dimensional cube, is rotated and distorted by the Jacobian $\mathbf{D}_s$ into an m-dimensional parallelotope $\widetilde{\mathbf{Q}}_{s+1} = \mathbf{D}_s\mathbf{Q}_s$ embedded in $\mathbb{R}^{\mathbf{N}}$. The figure illustrates this for $m = 2$, in this case the columns of $\widetilde{\mathbf{Q}}_{s+1}$ span a parallelogram. It can be divided into a right triangle and a trapezoid, which can be rearranged into a rectangle. Thus, the area of the gray parallelogram is the same as that of the purple rectangle. The QR-decomposition reorthonormalizes $\widetilde{\mathbf{Q}}_{s+1}$ by decomposing it into the product of an orthonormal matrix $\mathbf{Q}_{s+1} = [\mathbf{q}_{s+1}^1, \mathbf{q}_{s+1}^2, \dots \mathbf{q}_{s+1}^m]$ and the upper-triangular matrix $\mathbf{R}^{s+1}$. $\mathbf{Q}_{s+1}$ describes the rotation of $\mathbf{Q}_s$ caused by $\mathbf{D}_s$. The diagonal entries of $\mathbf{R}^{s+1}$ gives the stretching/shrinking along the columns of $\mathbf{Q}_{s+1}$, thus volume of the parallelotope formed by the first m columns of $\widetilde{\mathbf{Q}}_{s+1}$ is given by $V_m = \sum_{i=1}^{m} \mathbf{R}_{ii}^{s+1}$. The time-normalized logarithms of the diagonal elements of $\mathbf{R}^s$ give the Lyapunov spectrum: $\lambda_i = \lim_{t\to\infty} \frac{1}{t} \log \prod_{s=1}^{t} \mathbf{R}_{ii}^s = \lim_{t\to\infty} \frac{1}{t} \sum_{s=1}^{t} \log \mathbf{R}_{ii}^s$.

General algorithm for Lyapunov exponents (Benettin)

initialize $\mathbf{h}$, $\mathbf{Q}$
warm-up of $\mathbf{h}$
warm-up of $\mathbf{Q}$
for $t = 1 \to t_{\text{sim}}/\Delta t$ **do**
  $\mathbf{h} \leftarrow \mathbf{f}(\mathbf{h})$
  $\mathbf{D} \leftarrow \frac{d\mathbf{f}}{d\mathbf{h}}$
  $\mathbf{Q} \leftarrow \mathbf{D} \cdot \mathbf{Q}$
  if $t \,\%\, t_{\text{ONS}} = 0$ **then**
    $\mathbf{Q}, \mathbf{R} \leftarrow qr(\mathbf{Q})$
    $\gamma_i \mathrel{+}= \log(R_{ii})$
  end if
end for
$\lambda_i = \gamma_i / t_{\text{sim}}$

0.0.1 Calculating the Lyapunov spectrum of a spiking neural network

The dynamics of a spiking recurrent neural network is usually described by a system of coupled differential equations:

$$\tau_{\text{m}} \frac{\mathrm{d}V_i}{\mathrm{d}t} = F(V_i) + I_i^{\text{ext}} + \sum_{j,s} J_{ij}\, g(t - t_j^{(s)}), \tag{9}$$

thus, the rate of change of the membrane potential V_i depends on the internal dynamics of membrane potential $F(V_i)$, on some external input I_i^{ext} and on the recurrent input

$\sum_{j,s} J_{ij}\, g(t - t_j^{(s)})$. Thus, when neuron j spikes at time $t_j^{(s)}$, the resulting membrane potential change of the i^{th} neuron is described by some temporal kernel $g(\tau)$ and coupling strength J_{ij}. The Lyapunov spectrum of a spiking neural network can be calculated precisely, by choosing a single neuron model $\frac{dV}{dt} = F(V)$ with an analytically solvable solution between spikes. In this case, a map that evolves the network state numerically exact from one spike to the next can be obtained [26–28], allowing an event-based simulation with machine precision. This is possible for a variety of different neuron models, also for some with temporally extended synapses (e.g. LIF [29–31] and QIF [32]). In the following, we discuss the calculation of the Lyapunov spectrum for networks of neurons that can be mapped to pulse-coupled phase oscillators. In this case, the dynamics can be solved particularly simply and efficiently (See Fig. 3). For phase oscillators, the network dynamics can be written as

$$f\big(\phi_i^+(t_s)\big) = \begin{cases} d\big(\phi_i^+(t_s) + \omega(t_{s+1} - t_s)\big) & \text{for } i \in \text{post}(j^*) \\ \phi_i^+(t_s) + \omega(t_{s+1} - t_s) & \text{else} \end{cases} \tag{10}$$

where ω is the phase velocity and $d(\phi)$ is the phase transition curve evaluated on the neurons that are postsynaptic to the spiking neuron j^* just before the next network spike. The ϕ^+ (ϕ^-) denotes the phase of a neuron just after (before) evaluation of the phase transition curve. The phase transition curve (PTC) tells each spike-receiving neuron, how much their phase changes depending on their phase just before the next network spike. Therefore, for an event-based simulation, just four simple steps have to be performed iteratively: Finding the neuron that fires next, evolving all phases to the next spike time, updating postsynaptic neurons using the PTC and finally resetting the spiking neuron. All entries of the Jacobian $\mathbf{D}_s = \frac{d\mathbf{f}}{d\mathbf{x}}$ follow immediately from Eq. 10. Its elements are:

$$D_{ij}(t_s) = \begin{cases} d'_{i^*}(t_{s+1}^-) & \text{for } i = j = i^* \\ 1 - d'_{i^*}(t_{s+1}^-) & \text{for } i = i^* \text{ and } j = j^* \\ \delta_{ij} & \text{else,} \end{cases} \tag{11}$$

Again t_{s+1}^- denotes the state before evaluation of the PTC. The first case denotes diagonal elements for all spike-receiving neurons, this corresponds to the effect of a perturbation on a spike-receiving neuron on its own state at the next spike time, which is given by the derivative of the PTC. The second case denotes off-diagonal entries in the $j^{*\text{th}}$ column of all spike-receiving neurons corresponding to the effect of a perturbation of the spiking neuron and its spike time on the postsynaptic neurons. Finally, the third case denotes all other trivial entries, where the Jacobian has zeros in off-diagonal entries and ones in diagonal entries.

Algorithm 1 Lyapunov spectrum for spiking network

initialize $\phi(t_0)$, $\mathbf{Q}$
warm-up of $\phi(t_0)$
warm-up of $\mathbf{Q}$
for $s = 1 \to t$ **do**
    find index of next spiking neuron: $j = \max_i \phi_i(t_s)$
    calculate time to next spike: $t_{s+1} = t_s + \dfrac{\phi^{\mathrm{th}} - \phi_j(t_s)}{\omega}$
    evolve network states: $\phi_i^-(t_{s+1}) = \phi_i^+(t_s) + \omega(t_{s+1} - t_s)$
    evaluate PTC: $\phi_{i^*}^+(t_s) = d\big(\phi_{i^*}^-(t_s)\big)$
    reset spiking neuron: $\phi_j^-(t_{s+1}) = \phi^{\mathrm{re}}$
    calculate Jacobian elements $d'_{i^*}(t_{s+1})$
    evolve ONS: $\mathbf{Q} = \mathbf{D} \cdot \mathbf{Q}$
    if $s \,\%\, s_{\mathrm{ONS}} = 0$ **then**
        $\mathbf{Q}, \mathbf{R} \leftarrow qr(\mathbf{Q})$
        $\gamma_i \mathrel{+}= \log(R_{ii})$
    end if
end for
$\lambda_i = \gamma_i / t_{\mathrm{sim}}$

Pseudophase representation of leaky integrate-and-fire neurons

For a network of pulse-coupled leaky integrate-and-fire neurons, Eq. 9 reads in dimensionless notation

$$\tau_{\mathrm{m}} \frac{\mathrm{d}V_i}{\mathrm{d}t} = -V_i + I^{\mathrm{ext}} + \tau_{\mathrm{m}} \sum_{j,s} J_{ij}\, \delta(t - t_j^{(s)}) \tag{12}$$

If a membrane potential V_i reaches threshold V_{th}, it is reset to V_{re}. Without loss of generality we set $V_{\mathrm{th}} = 0$ and $V_{\mathrm{re}} = -1$. Between two network spikes, the solution is given by:

$$V_i(t_{s+1}) = I^{\mathrm{ext}} - (I^{\mathrm{ext}} - V_i(t_s) \exp\left(-\frac{t_{s+1} - t_s}{\tau_{\mathrm{m}}}\right) \tag{13}$$

In this phase representation (slightly different from [31, 33]), the phases $\phi_i \in (-\infty, 0]$ describe the neuron states relative to the unperturbed interspike interval.

To obtain the unperturbed interspike interval T_i, we have to solve Eq. 13 between reset and threshold in the absence of synaptic input.

$$\begin{aligned} T_i^{\mathrm{free}} &= -\tau_{\mathrm{m}} \ln\left(\frac{V_{\mathrm{T}} - I_{\mathrm{c}}}{V_{\mathrm{R}} - I_{\mathrm{c}}}\right) && (14)\\ &= \tau_{\mathrm{m}} \ln\left(\frac{I^{\mathrm{ext}} + 1}{I^{\mathrm{ext}}}\right) && (15)\\ &= \tau_{\mathrm{m}} \ln\left(1 + \frac{1}{\sqrt{K} I_0}\right). && (16) \end{aligned}$$

Its inverse is the phase velocity $\omega = 1/T_i^{\mathrm{free}}$. The phase ϕ_i is thus given by

$$\phi_i = -\omega \ln\left(\frac{I^{\mathrm{ext}}}{I^{\mathrm{ext}} - V_i}\right) \tag{17}$$

The reverse transformation is

$$V_i = I^{\mathrm{ext}} \left(1 - \exp\left(-\phi_i T_i^{\mathrm{free}}/\omega\right)\right). \tag{18}$$

Therefore, the phase transition curve is

$$d\big(\phi_{i^*}(t^-_{s+1})\big) = -\omega \cdot \ln\left(\exp\left(-\phi_{i^*}(t^-_{s+1})/\omega\right) + c\right), \tag{19}$$

where c is the effective coupling strength $c = \frac{J}{I_c}$, where J is the synaptic coupling strength. Usually, as discussed later in on page 9, balanced networks this is scales with $J = \frac{J_0}{\sqrt{K}}$, where K is the number of synapses per neuron. The derivative of the phase transition curve is given by [34]:

$$d'(\phi_{i^*}(t^-_{s+1})) = \frac{\Psi^-_{s+1}}{\Psi^-_{s+1} + c} = 1 - \frac{c}{\Psi^-_{s+1} + c}. \tag{20}$$

where $\Psi^-_{s+1} = \mathrm{e}^{-\phi_{i^*}(t^-_{s+1})/\omega}$. In the last expression, Ψ^-_{s+1} needs only to be evaluated once and allows in-place evaluation.

Phase representation of quadratic integrate-and-fire neurons

The quadratic integrate-and-fire neuron has – in contrast to the LIF neuron – a dynamic spike generation mechanisms and still allows to be solved exactly between network spikes.

For a network of QIF neurons Eq. 9 reads in dimensionless voltage representation:

$$\tau_{\mathrm{m}} \frac{\mathrm{d}V_i}{\mathrm{d}t} = V_i^2 + I_i^{\mathrm{ext}} + \tau_{\mathrm{m}} \sum_{j,s} J_{ij}\, \delta(t - t_j^{(s)}) \tag{21}$$

The quadratic integrate-and-fire model can be mapped via a change of variables $V = \tan(\theta/2)$ to the theta model with a phase variable $\phi \in (-\pi, \pi]$ [35–37].

The dynamical equation between incoming spikes is the topological normal form for the saddle-node on a limit cycle bifurcation (SNIC) and allows a closed form solution of the next network spike thanks to the exact derivation of the phase response curve [38]. Therefore, the quadratic integrate-and-fire neuron is commonly used to analyze networks of spiking neurons [34, 39–42].

When $I_i^{\mathrm{ext}} > 0 \; \forall \; i$, the right-hand side of the dynamics is strictly positive and all neurons would spike periodically in the absence of incoming postsynaptic potentials. In this case, we can choose another particularly tractable phase representation, called phi-representation with $V_i(t) = (K^{\frac{1}{2}} I_i^{\mathrm{ext}})^{\frac{1}{2}} \tan(\phi_i(t)/2)$, where the neuron has a constant phase velocity [34]. Again K is the mean number of synapses per neuron using the balanced scaling. This transformation directly yields the phase transition curve

$$g(\phi_i) = 2 \arctan\left(\tan\frac{\phi_i}{2} + c\right) \tag{22}$$

with the effective coupling strength $c = \frac{-J_0}{\sqrt{K}\sqrt{I_0\sqrt{K}}}$. With $I^{\mathrm{ext}} = -I_0 \cdot \sqrt{K}$, the phase velocity is given by

$$\omega = 2\sqrt{I_0 \cdot \sqrt{K}}.$$

The derivative of the phase transition curve is given by [34]:

$$d'(\phi_{i^*}(t^-_{s+1})) = \frac{\left(\tan\left(\phi_{i^*}(t^-_{s+1})/2\right)\right)^2 + 1}{\left(\tan\left(\phi_{i^*}(t^-_{s+1})/2\right) + J_{i^*j^*}/\left(K^{\frac{3}{2}} I_{i^*}^{\mathrm{ext}}\right)^{\frac{1}{2}}\right)^2 + 1} \tag{23}$$

Spiking networks in the balanced state

The pattern of action potentials in cortical tissue is asynchronous and irregular [43, 44], although single neurons can respond reliably [45–48]. This is commonly explained by a balance of excitatory and inhibitory synaptic currents [49, 50], which cancels large mean synaptic inputs on average. A dynamically self-organized balance can be achieved without the fine-tuning of synaptic coupling strength in heterogeneous networks, if the connectivity is inhibition-dominated and the couplings are strong, meaning that a small active fraction of incoming synapses can elicit an action potential [51]. The statistics of this state is described by a mean-field theory, which is largely insensitive to the neuron model [52].

We studied large sparse networks of N leaky or quadratic integrate-and-fire neurons arranged on a directed Erdős–Rényi random graph of mean degree K. All neurons $i = 1, \ldots, N$ received constant external currents I^{ext} and non-delayed δ-pulses from the presynaptic neurons $j \in \text{pre}\,(i)$. The external currents were chosen to obtain a certain average network firing rate $\bar{\nu}$ using a bisection method.

Setup of the balanced network

The coupling strengths were chosen such that the magnitudes of the input current fluctuations were identical in all studied networks. Assuming that inputs from different presynaptic neurons are only weakly correlated, the compound input spike train received by neuron i can be modeled by a Poisson process with rate $\Omega_i = \sum_{j\in\text{pre}(i)} \nu_j \approx K\bar{\nu} \equiv \Omega$, where $\bar{\nu}$ is the network-averaged firing rate and K the average number of presynaptic neurons. Under the assumption that the compound input spike train is a Poisson process, the input current auto-correlation function reads

$$\begin{aligned} C(\tau) &= \langle \delta I(t)\delta I(t+\tau)\rangle_t && (24)\\ &\approx \left(\frac{J_0}{\sqrt{K}}\right)^2 \Omega \int \delta(t-s)\delta(t+\tau-s)\mathrm{d}s && (25)\\ &= \frac{J_0^2}{K}\Omega\delta(\tau) && (26)\\ &\approx J_0^2\bar{\nu}\delta(\tau) && (27)\end{aligned}$$

Thus, the fluctuations in the input currents can be described as delta-correlated white noise of magnitude

$$\sigma^2 = J_0^2\bar{\nu}. \quad (28)$$

Note that due to the scaling of the coupling strengths $J = -\frac{J_0}{\sqrt{K}}$ with the square root of the number of synapses K the magnitude of the fluctuations σ^2 is independent of the number of synapses. Therefore, the input fluctuations do not vanish in the thermodynamic limit and the balanced state in sparse networks emerges robustly [51, 52].

The existence of a balanced state fixed point in the large K-limit follows from the equation of the network-averaged mean current

$$\bar{I} \approx \sqrt{K}(I_0 - J_0\bar{\nu}). \quad (29)$$

In the large K-limit, self-consistency requires the balance of excitation and inhibition $I_0 = J_0\bar{\nu}$: If $\lim_{K\to\infty}(I_0 - J_0\bar{\nu}) > 0$ the mean current $\bar{I}$ would diverge to ∞ and the neurons would fire at their maximal rate. The resulting strong inhibition would break the inequality, leading to a contradiction. If $\lim_{K\to\infty}(I_0 - J_0\bar{\nu}) < 0$ the mean current $\bar{I}$

would diverge to $-\infty$ and the neurons would be silent. The resulting lack of inhibition again breaks the inequality. The large K-limit is self-consistent only if

$$I_0 - J_0\bar{\nu} = \mathcal{O}\left(\frac{1}{\sqrt{K}}\right),$$

such that excitatory external drive and mean recurrent inhibitory current cancel each other. Note that since $I_0 - J_0\bar{\nu} = \mathcal{O}(1/\sqrt{K})$ the network mean current has a finite large K-limit. The average firing rate in units of the membrane time constant τ_{m}^{-1} is approximately

$$\bar{\nu} = \frac{I_0}{J_0} + \mathcal{O}\left(\frac{1}{\sqrt{K}}\right). \tag{30}$$

This approximation generally becomes exact for large K. For excitatory-inhibitory mixed network, an analogous self-consistency argument can be made which results in a set of inequalities that must be fulfilled to achieve a balanced state [52].

Novel efficient algorithm for large sparse networks

A basic implementation of Algorithm 1 is numerically costly, as for every spike in the network, the matrix multiplication $\widetilde{\mathbf{Q}}_{s+1} = \mathbf{D}_s\mathbf{Q}_s$, which has computational complexity $\mathcal{O}\left(N^3\right)$, has to be performed. However, $\mathbf{D}_s$ is sparse: it can be written as a sparse diagonal matrix plus a matrix which is nonzero at the j^{th} column:

$$\mathbf{D}(t_s) = \begin{pmatrix}
1 & 0 & & & & & & & \dots & 0 \\
0 & 1 & & & & & & & & \vdots \\
 & & d' & & & & 1-d' & & & \\
 & & & & 1 & & 0 & & & \\
 & & & & & d' & 1-d' & & & \\
 & & & & & & 1 & 0 & & \\
 & & & & & & & \ddots & \vdots & \\
 & & & & & & & & 0 & \\
 & & & & & & & & 1 & \\
 & & & & & & & & & \vdots \\
\vdots & & & & & & & & \ddots & 0 \\
0 & \dots & & & & & & & \dots\ 0 & 1
\end{pmatrix} \begin{matrix} \\ \\ \leftarrow \text{postsynaptic } i^* \\ \\ \leftarrow \text{postsynaptic } i^* \\ \\ \\ \\ \\ \\ \\ \end{matrix} \tag{31}$$

$$\uparrow$$

column j^*

Further, only rows corresponding to the indices of the postsynaptic neurons have nontrivial entries. Therefore, the matrix multiplication, which would have a numerical time complexity of $\mathcal{O}\left(N^2 \cdot m\right)$ in a basic implementation, can be reduced to $\mathcal{O}\left(K \cdot m\right)$, where K denotes the number of synapses per neuron and m the number of Lyapunov exponents to be calculated.

Another computationally costly step of numerical time complexity of $\mathcal{O}\left(N\right)$ is the propagation of all phases $f\left(\phi_i^+(t_s)\right) = \phi_i^+(t_s) + \omega(t_{s+1} - t_s)$ to the state right before the next network spike. In homogeneous networks, where all neurons have the same phase

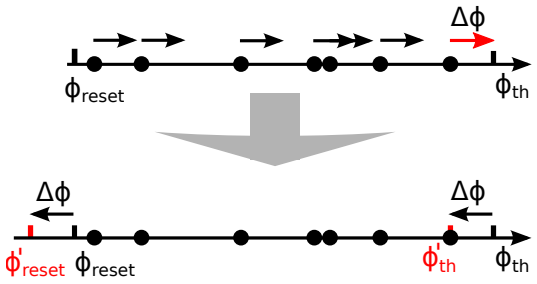

Fig 2. Change of reference frame allows efficient evolution of network state. Conventionally, every phase is shifted by $\Delta\phi_i = \omega_i \Delta t$, where $\Delta t = \min_i \left(\frac{\phi_{\text{th}} - \phi_i}{\omega} \right)$. Instead, we propose just to change threshold and reset by $\Delta\phi = \phi_{\text{th}} - \phi_i$ at every spike. This gives a speedup of $\mathcal{O}(N/K)$, as instead of shifting N phases, one has to consider the global phase shift only for evaluating the phase transition curve of the K postsynaptic neurons (not shown in the figure). Crucially, for long simulations, all phases and the global phase shift have to be reset when the global phase exceeds some threshold to avoid numerical errors resulting from subtractive cancellation due to floating-point arithmetics.

velocity ω this can be avoided, when instead, just threshold and reset are changed by $\Delta_{s+1} = \Delta_s + \omega(t_{s+1} - t_s)$, starting with $\Delta_0(\phi) = 0$. Thus $\phi^{\text{th}}_{s+1} = \phi^{\text{th}} - \Delta_{s+1}$. Similarly, $\phi^{\text{reset}}_{s+1} = \phi^{\text{reset}} - \Delta_{s+1}$. In inhibition dominated networks, the phases $\phi(t_s)$ will thus become increasingly negative. For long simulations, all phases and the global phase should therefore be reset if the global phase exceeds a certain threshold Δ^{th}, to avoid numerical errors resulting from subtractive cancellation due to floating-point arithmetics [53].

Finally, finding the next spiking neuron is also an operation of numerical time complexity of $\mathcal{O}(N)$, which can become the computational bottleneck in very large sparse networks. A numerical efficient implementation to avoid iterating through all neuron's phases ϕ_i to find the maximum at every spike time is the implementation of a priority queue. A priority queue is a data structure whose elements have a priority and efficient operations for returning the elements with the highest priority and insertion of new elements or updating of priorities are available [54]. Priority queues can be implemented as a heap-ordered binary trees. A binary tree is heap-ordered if the value in each node is larger than the values in that nodes two children. Returning the elements with the highest priority has numerical time complexity of $\mathcal{O}(1)$ and insertion of elements has complexity of $\mathcal{O}(\log(N))$ [55]. Thus, only $\mathcal{O}(K \cdot \log(N))$ operations have to be performed per network spike, as for K postsynaptic neurons and for one spiking neuron, a new phase needs to be updated in the priority queue.

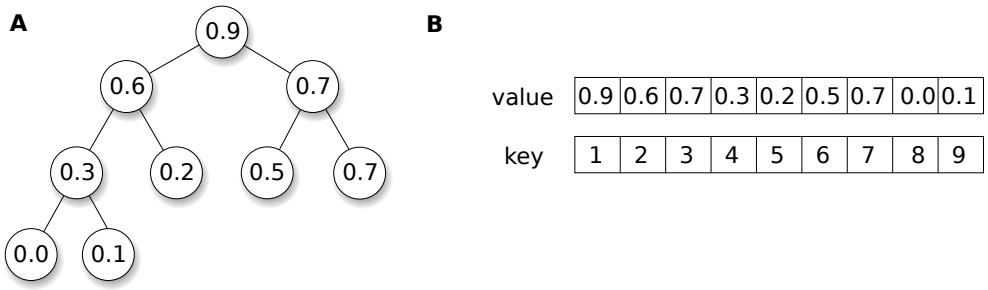

Fig 3. A suitable data structure allows efficient search for next spiking neuron for numerically exact simulation of large spiking networks. A By using a priority queue, the next spiking neuron can be found without iteration through all neurons of the network at every spike time. One implementation of a priority queue is a binary heap, as the example shown. In a max-heap, each child node has a value less or equal to its parent node. If an element is deleted, removed or added, the heap property is restored by swapping parents and children systematically. Finding the node with the highest priority has a numerical complexity of $\mathcal{O}(1)$ and changing the value of any element has an amortized time complexity of $\mathcal{O}(\log(N))$. **B** Array implementation of binary heap shown in **A**. As per spike all postsynaptic neurons and the spiking neuron have to be updated, this requires on average $K+1$ operation, thus an amortized time complexity $\mathcal{O}(K \cdot \log(N))$ [55].

Algorithm 2 Efficient calculation of Lyapunov spectrum for sparse spiking network

initialize $\phi(t_0)$, $\mathbf{Q}$,$\Delta = 0$
heapify $\phi(t_0)$
warm-up of network $\phi(t_0)$
warm up of orthonormal set $\mathbf{Q}$
for $s = 1 \to t$ **do**
    get phase of next spiking neuron: $j, \phi_j = \text{peek}(\phi_i(t_s))$
    calculate phase increment: $d\phi = \phi^{\text{th}} + \Delta - \phi_j(t_s)$
    update global phase shift: $\Delta \mathrel{+}= d\phi$
    evaluate PTC: $\phi_{i^*}^+(t_s) = Z\left(\phi_{i^*}^-(t_s) + \Delta\right) - \Delta$
    reset spiking neuron: $\phi_j(t_{s+1}) = \phi^{\text{re}} - \Delta$
    calculate Jacobian elements $d_{i^*}(t_{s+1})$
    evolve orthonormal set: $\mathbf{Q} = \mathbf{D} \cdot \mathbf{Q}$
    if $s \,\%\, s_{\text{ONS}} = 0$ **then**
        $\mathbf{Q} = \mathbf{Q} \cdot \mathbf{R}$
        $\gamma_i \mathrel{+}= \log(R_{ii})$
    end if
    if $\Delta > \Delta^{\text{th}}$ **then**
        $\phi \mathrel{+}= \Delta$
        $\Delta = 0$
    end if
end for
$\lambda_i = \gamma_i / t_{\text{sim}}$

As the number of network spikes for a given simulation time grows linearly with network size, the overall computational cost for a given simulation time of the proposed efficient numerical implementation scales $\mathcal{O}(K \cdot N \cdot \log(N))$, which for sparse networks is far more efficient compared to a conventional implementation (see Fig. 4).

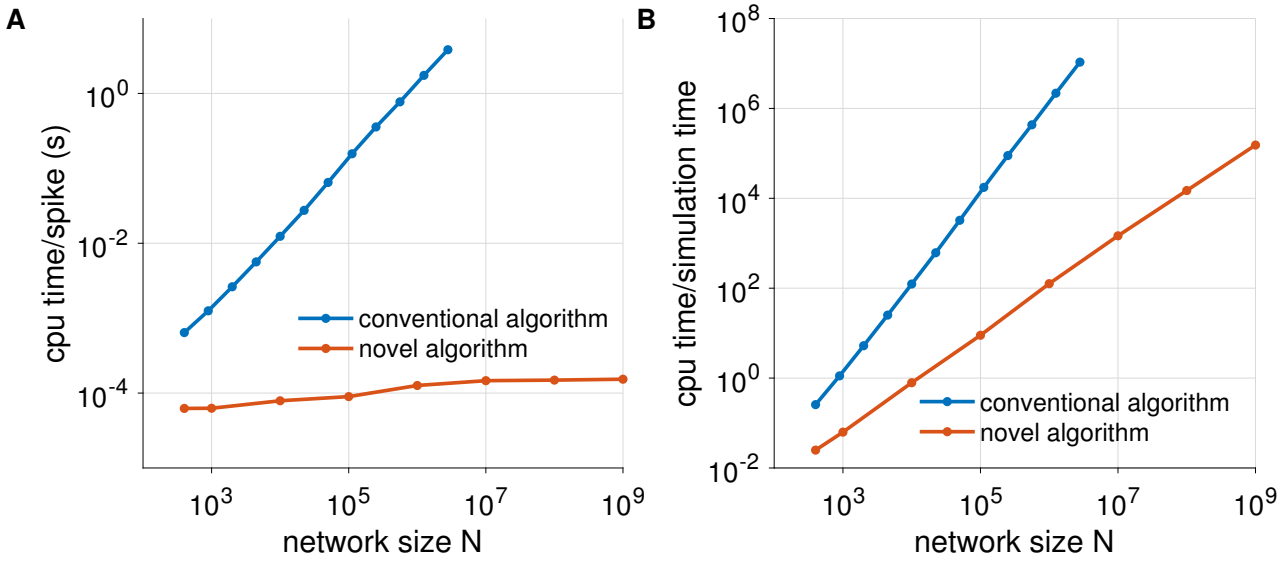

Fig 4. Benchmark of novel vs. conventional algorithm for calculating a fixed number of Lyapunov exponents. The computational cost per network spike scales linear with network size N in a conventional event-based implementation. In the large sparse network limit, the computational bottleneck is to find the next spiking neuron in the network and to propagate all neurons phases to the next network spike. Both operations can be implemented efficiently. Firstly, instead of shifting all neurons phases, instead the threshold and reset values can be shifted. Secondly, by using a binary heap as a data structure for the phases, finding the next phase and keeping the heap-ordering has computational complexity of $\mathcal{O}\left(K \cdot \log(N)\right)$. **A**: CPU time per network spike for an inhibitory network of leaky integrate-and-fire neurons. Benchmark was performed on an Intel® Xeon® CPU E5-4620 v2 @ 2.60 GHz and 512 GB RAM. Parameters: $\bar{\nu} = 1\,\mathrm{Hz}$, $J_0 = 1$, $\tau_\mathrm{m} = 10\,\mathrm{ms}$, $K = 100$, $m = 1$.

Heterogeneous networks and further improvements Note that this can be easily extended to mixed networks of excitatory and inhibitory neurons (or to k population networks with different external input and resulting distinct phase velocities). In that case, each population k needs its own priority queue and a distinct global phase Δ^k_{s+1} as well as ϕ^{th_k} and ϕ^{reset_k}, as different populations can have distinct phase velocities ω^k. At each network spike, for all populations the next spike time has to be calculated by returning the next spiking neuron from all priority queues. Alternatively, for heterogeneous networks or for neuron models that are analytically solvable between spikes but don't allow a mapping to a phase oscillator, one can use a priority queue of all the next unperturbed spike times for all neurons. In this case, the algorithm for network simulation still consists of four steps: First finding the next spiking neuron, then evolving the state of the postsynaptic neurons to the next network spike time, followed by the update of the postsynaptic neurons by the incoming spikes. Finally, resetting the spiking neuron to the reset value. This algorithm has also a numerical complexity of $\mathcal{O}\left(K \cdot \log(N)\right)$ per network spike. Still, in cases where the phase representation is applicable, it should be used because it is faster and numerically more stable. Note that this algorithm can also be used for univariate neuron models where no analytical solution between spike times is known, e.g., the exponential

	basic algorithm	conventional algorithm	novel algorithm
find next spiking neuron	$\min(\phi_{\text{th}} - \phi/\omega)$	$\min(\phi_{\text{th}} - \phi/\omega)$	$\text{peek}(\phi)$
evolve neurons	$\phi \mathrel{+}= \omega \cdot dt$	$\phi \mathrel{+}= \omega \cdot dt$	$\Delta+ = \Delta\phi$
update postsynaptic neurons	K operations	K operations	K operations + K key updates
evaluate Jacobian	K operations	K operations	K operations
evolve ONS	$N^2 \cdot m$	$2K \cdot m$	$2K \cdot m$
QR decomposition	$N \cdot m^2$ every N^{th} step	$N \cdot m^2$ every N^{th} step	$N \cdot m^2$ every N^{th} step
reset spiking neuron	one array operation	one array operation	$\mathcal{O}(\log(N))$
total amortized costs per network spike	$\mathcal{O}\left(N^2 \cdot m\right)$	$\mathcal{O}\left(N + K \cdot m + m^2\right)$	$\mathcal{O}\left(K \cdot \log(N) + m^2\right)$
total amortized costs for fixed simulation time	$\mathcal{O}\left(N^3 \cdot m\right)$	$\mathcal{O}\left(N^2 + N \cdot K \cdot m + N \cdot m^2\right)$	$\mathcal{O}\left(K \cdot N \cdot \log(N) + N \cdot m^2\right)$

Table 1. Comparison computational cost for calculating Lyapunov spectrum of spiking network different algorithms N denotes number of neurons, K is the average number of synapses per neuron, m is the number of Lyapunov exponents to be calculated. For large sparse networks ($K \ll N$) and a fixed number of Lyapunov exponents to be calculated, the dominant term grows cubic with N for the basic algorithm (also for Refs. [61–63]), quadratic for the conventional algorithm [31, 33, 33, 34, 64, 65] and linearithmic ($\mathcal{O}(\log(N))$) for our novel algorithm.

integrate-and-fire model. In this case, the phase transition curve can be calculated numerically before the network simulation. During run time, the phase transition curve and its derivative can be interpolated from the precomputed lookup tables.

For dense networks, where the number of synapses scales proportional to the number of neurons [56], a priority queue implemented by a binary heap is unfavorable compared to a conventional array in the large network limit, as every network spike involves changing the priority of $\mathcal{O}(N)$ neurons, thus $\mathcal{O}((N+1) \cdot \log(N))$ flops per network spike which corresponds to $\mathcal{O}((N+1) \cdot N \cdot \log(N))$ flops for a fixed simulation time. A batch-update of all postsynaptic neurons might be faster for very large networks [57], but is beyond the scope of this work. It would involve $\mathcal{O}(K + \log(K) \cdot \log(N))$ flops corresponding to $\mathcal{O}(N + \log(N) \cdot \log(N))$ in dense networks. In the case of purely excitatory sparse spiking networks, a Fibonacci heap might be a more efficient implementation in the large network limit [58], as the decrease key operation takes constant time $\mathcal{O}(1)$ compared to $\mathcal{O}(\log(N))$ in the case of a binary heap. Note that for practical purposes, the asymptotic scaling of the computational complexity of Fibonacci heaps has an unfavorably large prefactor [59]. Therefore, other heap structure implementations might be faster [60].

Implementation of reorthonormalization Finally, the QR-decomposition is a numerical bottleneck. Although the QR-decomposition is unique when the diagonal elements of the R matrix are chosen to be positive, there exist several ways to implement the QR-decomposition, which have different features concerning accuracy, speed, memory consumption and the availability of a parallel implementation [66]. Three common implementations are the modified Gram-Schmidt procedure, the Givens rotation, and the Householder reflection. The error of the Householder reflection scales only with machine precision, while the error of the modified Gram-Schmidt procedure

scales with machine precision times condition number. Imprecision in reorthonormalization can be quantified by the deviation of the inner product of $\mathbf{Q}_s$ from the identity: $\mathbf{Q}_s^\top \mathbf{Q}_s = \mathbf{I} + \mathbf{E}$, where $\mathbf{I}$ is the identity matrix and $\mathbf{E}$ is the error matrix. For the Householder reflection and the Givens rotation, $\|\mathbf{E}\| \approx \varepsilon$, where ε is machine epsilon, while for the Gram-Schmidt procedure, $\|\mathbf{E}\| \approx \varepsilon\kappa_2(\mathbf{R})$, where $\kappa_2(\mathbf{R})$ is the condition number of the triangular matrix $\mathbf{R}_s$, which is given by the ratio of the largest and the smallest singular value of $\mathbf{R}$: $\kappa_2(\mathbf{R}) = \frac{\sigma_1(\mathbf{R})}{\sigma_m(\mathbf{R})}$. On the other hand, the modified Gram-Schmidt procedure facilitates parallel implementation (e.g. [67]).

The computational cost for the Householder approach involve $2N \cdot m^2 - 2m^3/3$ flops to get $\mathbf{Q}$ in factored form and another $2N \cdot m^2 - 2m^3/3$ to calculate $\mathbf{Q}$. In comparison, the modified Gram Schmidt procedure needs $2N \cdot m^2$ flops in total, thus it is approximately twice as efficient as the Householder approach [66]. The QR-decomposition only needs to be performed sufficiently often, such that $\mathbf{Q}$ does not get ill-conditions. Thus, to keep the error constant with increasing network size, the reorthonormalization interval can be increased linearly. Therefore, the QR step has a numerical complexity of $\mathcal{O}\left(m^2\right)$ per network spike on average. Therefore, for calculating a fixed number of Lyapunov exponents in a large sparse network, the computational bottleneck is not the QR-decomposition but heapifying the priority queue after applying the phase transition curve to the postsynaptic neurons. In contrast, for calculating a fixed finite fraction of Lyapunov exponents in a large sparse network, the QR step has a numerical complexity of $\mathcal{O}\left(N^2\right)$ per network spike and is therefore the computational bottleneck. For a fixed simulation time this corresponds to $\mathcal{O}\left(N^3\right)$ flops. A further extension would be to perform the QR-decomposition on a graphics processing unit (GPU).

Convergence of Lyapunov spectra

Lyapunov exponents measure rates of exponential divergence and convergence in the long-time limit. While Oseledets' multiplicative ergodic theorem guarantees the existence of this limit, it does not say how fast the limit is approached. Heuristically, the trajectory needs to sample a representative portion of the attractor to allow a good estimate of the average rates of exponential divergence and convergence of nearby trajectories. Although subsequent Jacobians can be correlated, in chaotic systems they can generally be assumed to be independent for long times. Therefore, for sufficiently large reorthonormalization intervals the $\mathbf{R}_{ii}^s$ follow a Gaussian distribution according to the central limit theorem. Thus, the sampling error of the Lyapunov exponents estimator $\hat{\lambda}(t)_i = \frac{1}{t}\sum_{s=1}^{t} \log \mathbf{R}_{ii}^s$ converges generally towards zero $\propto 1/\sqrt{t}$. The convergence of some Lyapunov exponents in an event-based simulation of a spiking network of quadratic integrate-and-fire neurons is shown in Fig. 6.

There are two main contributions for the variability of numerically calculated Lyapunov spectra. Firstly, variability arising from the fact that Lyapunov spectra are asymptotic properties of dynamical systems. Secondly, variability arising from the quenched noise of different random topologies. The first contribution vanishes in the limit of infinitely long simulations for ergodic systems because Lyapunov exponents are then independent of initial conditions. The second contribution vanishes in the large networks limit due to self-averaging. Quantities that are self-averaging converge in the limit of large system sizes to the ensemble average. The Lyapunov spectrum of one realization of a large network is thus representative for the whole ensemble. Hence, averaging over different network realizations is not necessary for large networks.

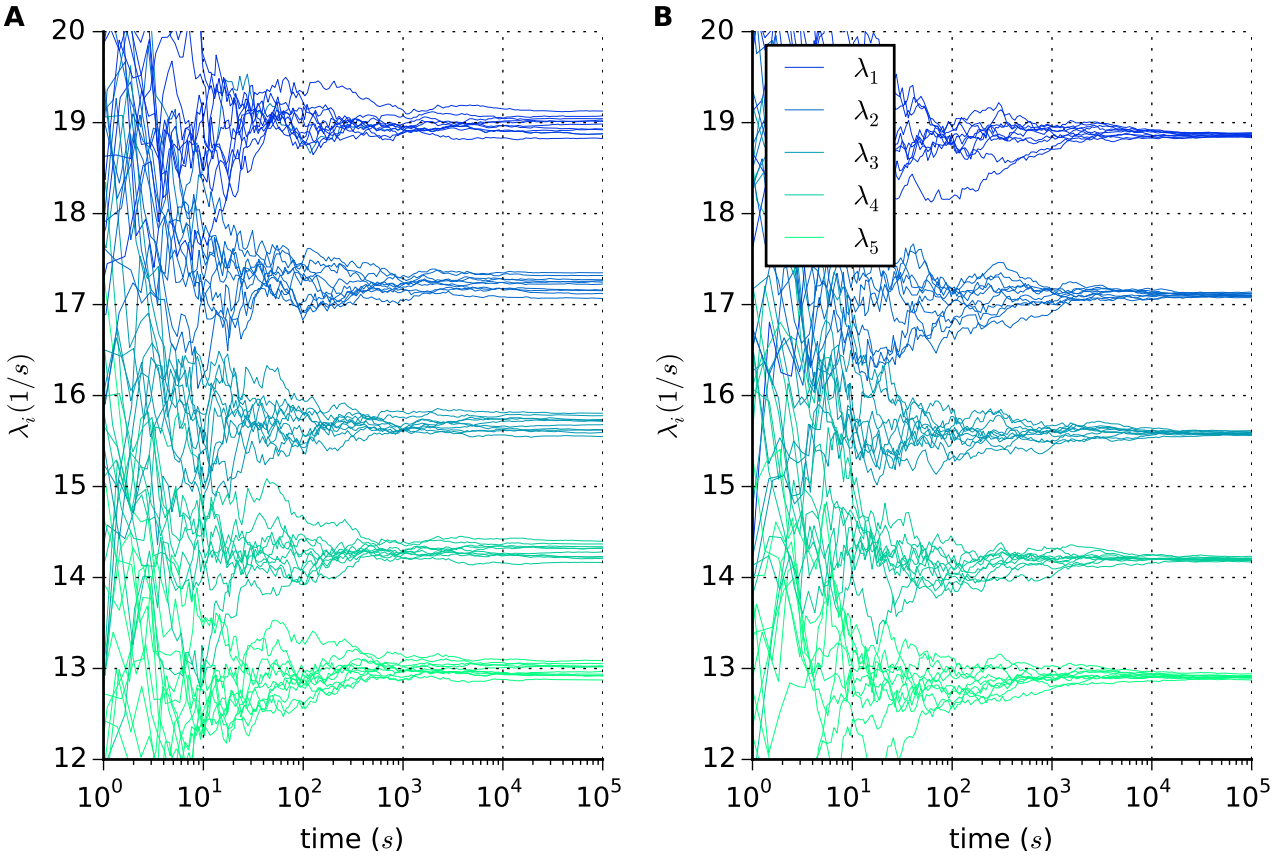

Fig 5. Convergence of Lyapunov spectra versus time in inhibitory networks of quadratic integrate-and-fire neurons. (logarithmic time scale) **A** Convergence of the first five Lyapunov exponents for different network topologies realization. **B** Convergence of the first five Lyapunov exponents for distinct initial conditions but the same network topology. Note that for small networks different topologies have slightly different Lyapunov spectra due to quenched noise. For large N, the Lyapunov spectrum becomes increasingly independent of network realization. Simulations started with different realizations of the orthonormal system quickly converge and are not shown here. (parameters: $N = 200$, $\bar{\nu} = 1\,\mathrm{Hz}$, $K = 10$, $J_0 = 1$, $\tau_\mathrm{m} = 10\,\mathrm{ms}$).

Checks of numerical implementation

It is important to corroborate results with different approaches. Although for high-dimensional systems, it is not possible to estimate the dynamical entropy rate or attractor dimensionality using direct methods, there exist several independent checks for the numerical implementation of the Lyapunov spectrum.

Firstly, the largest Lyapunov exponent can be checked by direct numerical simulations [12]. Two sufficiently close initial states are evolved in time and their rate of exponential separation or convergence is measured. When employing this method, one

has to be careful to avoid arithmetic underflow and overflow. The perturbed trajectory has to be reset after appropriate time intervals, to stay in a linear regime.

Secondly, in autonomous systems, which are not at a fixed point, there exists a zero Lyapunov exponent corresponding to a perturbation in the direction of the flow. Thus, in the Benettin scheme, there has to be one Lyapunov exponent that converges to zero.

Thirdly, the mean Lyapunov exponent $\bar{\lambda} = \frac{1}{N}\sum_{i=1}^{N}\lambda_i$, which quantifies the mean dissipation of a dynamical system, can often be obtained analytically using random matrix theory [33, 34]. For dissipative systems, $\bar{\lambda}$ has to be smaller than zero.

Lastly, while obtaining an analytical expression for the full spectrum of Lyapunov exponents is difficult because of the generally non-commuting product of Jacobians, there exist some cases, where the full spectrum can be obtained from a product of random matrices [12, 68–70].

In the case that the system of interest has a limit, in which the Jacobians commute, this limit can be used to check the numerical results. It is important to stress that all these checks just test necessary conditions for the numerical implementation to be correct.

Poincaré maps of small chaotic network

A Poincaré map is the intersection of the trajectory of an N degree of freedom dynamical system with a $N-1$ dimensional subspace called the Poincaré surface or section. Fig. 6 shows a Poincaré section through the chaotic strange attractor of a three neurons network. Whenever one specific neuron fires an action potential, the values of the other two neurons are stored. This results in a 2D section through the 3D phase space.

Example code for Poincaré maps in Julia

The following code for Julia Version 0.7 demonstrates the event-based simulations in a network of three theta neurons. Saving phases of neuron 2 and 3 whenever neuron 1 spikes yields a Poincaré map as displayed in Fig. 6.

```
function poincare()
        ncalc = 10^7                          # number of spikes in calculation
        a = 0 .<[0 0 0;1 0 1;0 1 0]           # define adjacency matrix
        ϕ = rand(3)                           # initialize neurons
        Φ = Float64[]                         # initialize phase history
        for s = 1:ncalc
                ϕmax,j = findmax(ϕ)           # find next spiking neuron j
                dt = pi/2-ϕmax                # calculate next spike time
                ϕ.+= dt                       # evolve phases till next spike time
                p = a[:,j]                    # postsynaptic neurons
                ϕ[p] = atan.(tan.(ϕ[p]).-1) # update postsynaptic neurons with PTC (QIF)
                ϕ[j] = -π/2                   # reset spiking neuron
                j==1 && append!(Φ,ϕ[2:3])     # save neuron 2 & 3 when neuron 1 spikes
        end
        plot(Φ[1:2:end],Φ[2:2:end],".k",markersize=.01); axis("off")
end
```

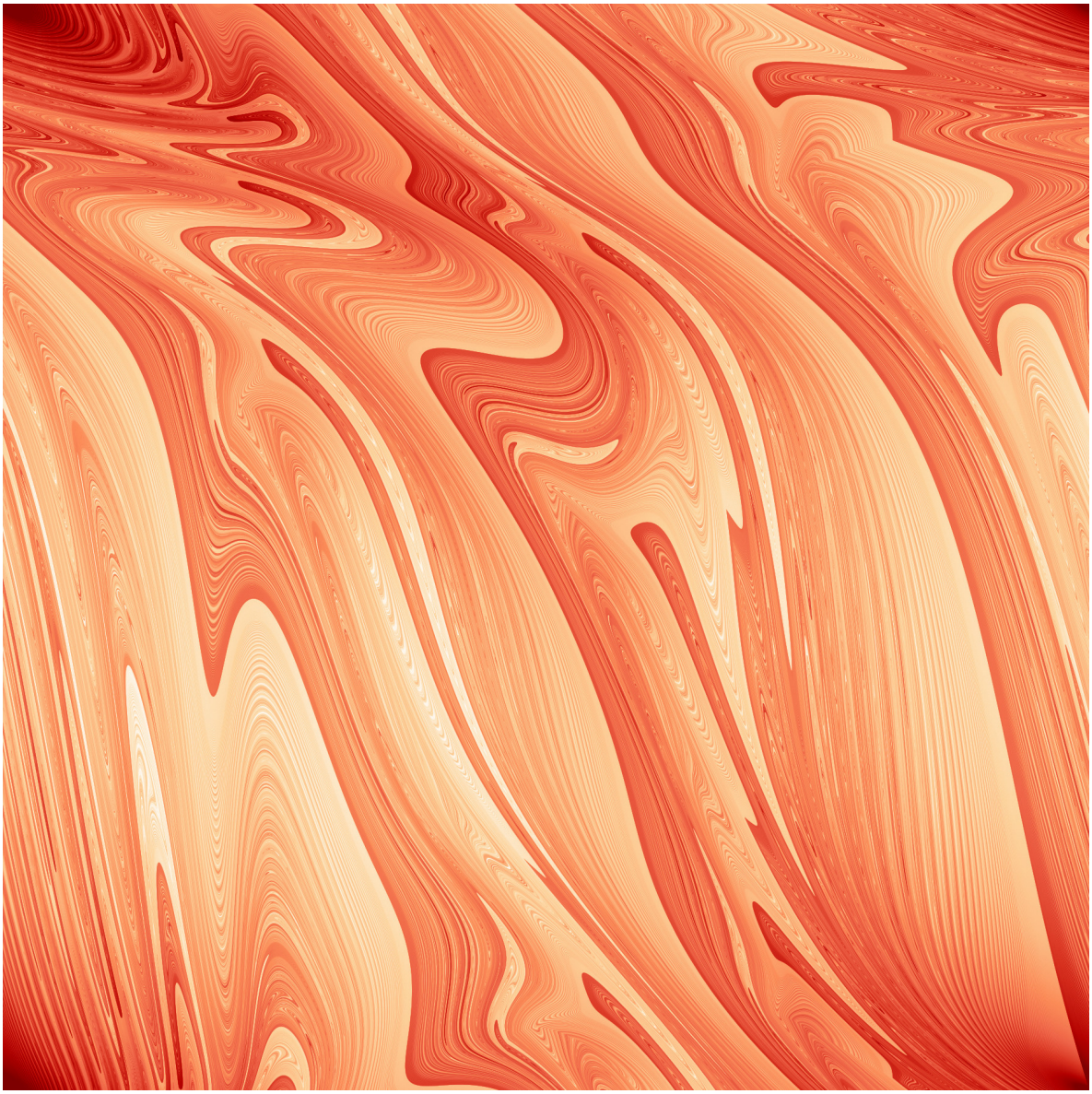

Fig 6. Poincaré section through phase space visualizes the chaotic strange attractor in a small network ($N = 3$): Poincaré section of the phases of neuron 2 and 3 whenever neuron 1 spikes. The relative density of points is represented using a color map, where high densities correspond to higher intensities. The x-axis gives the value of $\phi_2 \in (-\pi, \pi]$ and the y-axis the value of $\phi_3 \in (-\pi, \pi]$ whenever neuron 1 spikes. Axes are omitted for aesthetic reasons (parameters: $\bar{\nu} = 14.5$ Hz, $J_0 = 1$, $\tau_\mathrm{m} = 10$ ms, $N = 3$, $K = 1$)

Minimal code for efficient spiking network simulation in Julia

This code for Julia v0.7 implements the novel algorithm for efficiently simulating a spiking network ($N = 10^5$ LIF neurons).

```
using DataStructures, RandomNumbers. Xorshifts, StatsBase, PyPlot

function lifnet(n,nstep,k,j0,ratewnt,τ,seedic,seedtopo)
        iext = τ*sqrt(k)*j0*ratewnt/1000                # iext given by balance equation
        ω,c = 1/log(1. + 1/iext),j0/sqrt(k)/(1. + iext) # phase velocity LIF
        ϕth, ϕshift = 1., 0.                            # threshold for LIF
        r = Xoroshiro128Star(seedic)                    # init. random number generator
        ϕ = mutable_binary_maxheap(rand(n))             # initialize binary heap
        spikeidx = Int64[]                              #initialize time
        spiketimes = Float64[]                          # spike raster
        postidx = rand(Int,k)
        for s = 1 : nstep                               # main loop
                ϕmax, j = top_with_handle(ϕ)            # get phase of next spiking neuron
                dϕ = ϕth - ϕmax - ϕshift                # calculate next spike time
                ϕshift += dϕ                            # global shift to evolve network state
                srand(r,j+seedtopo)                     # spiking neuron index is seed of rng
                sample!(r,1:n-1,postidx;replace=false)  # get receiving neuron index
                @inbounds for i = 1:k                   # avoid autapses
                postidx[i] >= j && ( postidx[i]+=1 )
                end
                ptc!(ϕ,postidx,ϕshift,ω,c)              # evaluate phase transition curve
                update!(ϕ,j,-ϕshift)                    # reset spiking neuron
                push!(spiketimes,ϕshift)                # store spiketimes
                push!(spikeidx,j)                       # store spiking neuron index
        end
        nstep/ϕshift/n/τ*ω,spikeidx,spiketimes*τ/ω      # output: rate, spike times & indices
end

function ptc!(ϕ, postid, ϕshift, ω, c)                  # phase transition curve of LIF
        for i = postid
                ϕ[i] = - ω*log(exp( - (ϕ[i] + ϕshift)/ω) + c) - ϕshift #(Eq. 19)
        end
end

# set parameters:
#n: # of neurons, k: synapses/neuron, j0: syn. strength, τ: membr. time const.
n,nstep,k,j0,ratewnt,τ,seedic,seedtopo = 10^5,10^5,100,1,1.,.01,1,1
# quick run to compile code
@time lifnet(100, 1, 10, j0, ratewnt, τ, seedic, seedtopo);

# run & benchmark network with specified parameters
gc();@time rate,sidx,stimes = lifnet(n,nstep,k,j0,ratewnt,τ,seedic,seedtopo)

# plot spike raster
plot(stimes,sidx,",k",ms=0.1)
ylabel("Neuron Index",fontsize=20)
xlabel("Time (s)",fontsize=20);tight_layout()
```

Supporting Information

S1 Code Source code for the Lyapunov spectrum of spiking networks of leaky integrate-and-fire neurons in an efficient numerically exact implementation. We provide all necessary code to calculate the full Lyapunov spectrum with code written in Julia [71]. The efficient implementation is parallelized using level-3 matrix-matrix operations from BLAS (Basic Linear Algebra Subprograms) called via LAPACK (Linear Algebra PACKage). Furthermore, the program provides bootstrapped 95 percentile confidence intervals for the first and the last Lyapunov exponent, the KS entropy rate, and the Lyapunov dimensionality. Optionally, also a principal component-based dimensionality estimate can be calculated. Finally, the program provides the convergence of the Lyapunov spectrum in time. Input variables are network size N, number of synapses per neuron K, coupling strength J_0, simulation time t_{sim}, number of Lyapunov exponents to be calculate m, reorthonormalization interval s_{ONS}, seed for initial conditions of recurrent network $seed_{\mathrm{IC}}$, seed for random network topology $seed_{\mathrm{Topo}}$, seed for orthonormal system $seed_{\mathrm{ONS}}$ and finally the subdirectory where the results are stored.

S2 Code Source code for Lyapunov spectrum of spiking networks of quadratic integrate-and-fire neurons in efficient numerically exact implementation. Similar to S1 Code, the full Lyapunov spectrum of a network of quadratic integrate-and-fire neurons is obtained by a reorthonormalization procedure [25], which is done in the tangent space along a semi-analytical solution of the network dynamics obtained in event-based numerically exact simulations.

Acknowledgments

We thank G. Lajoie, J. Liedtke, R.-M. Memmesheimer, M. Monteforte, A. Palmigiano, M. Puelma Touzel, A. Schmidt, M. Schottdorf and F. Wolf for fruitful discussions as well as S. Migirditch and Y. Park for comments on the manuscript.

References

1. Potjans TC, Diesmann M. The Cell-Type Specific Cortical Microcircuit: Relating Structure and Activity in a Full-Scale Spiking Network Model. Cerebral Cortex. 2014;24(3):785–806. doi:10.1093/cercor/bhs358.
2. Potjans TC, Diesmann M. Multi-population Network Models of the Cortical Microcircuit. In: Advances in Cognitive Neurodynamics (III). Springer Netherlands; 2013. p. 91–96. Available from: http://link.springer.com/chapter/10.1007/978-94-007-4792-0_13.
3. Albada SJv, Kunkel S, Morrison A, Diesmann M. Integrating Brain Structure and Dynamics on Supercomputers. In: Brain-Inspired Computing. Springer International Publishing; 2013. p. 22–32. Available from: http://link.springer.com/chapter/10.1007/978-3-319-12084-3_3.
4. Albada SJv, Helias M, Diesmann M. Scalability of Asynchronous Networks Is Limited by One-to-One Mapping between Effective Connectivity and Correlations. PLOS Computational Biology. 2015;11(9):e1004490. doi:10.1371/journal.pcbi.1004490.
5. Mikula S, Denk W. High-resolution whole-brain staining for electron microscopic circuit reconstruction. Nature Methods. 2015;12(6):541–546. doi:10.1038/nmeth.3361.
6. Kasthuri N, Hayworth KJ, Berger DR, Schalek RL, Conchello JA, Knowles-Barley S, et al. Saturated Reconstruction of a Volume of Neocortex. Cell. 2015;162(3):648–661. doi:10.1016/j.cell.2015.06.054.
7. Shaw R. Strange Attractors, Chaotic Behavior, and Information Flow. Zeitschrift Naturforschung Teil A. 1981;36:80–112. doi:10.1515/zna-1981-0115.
8. Schuster HG, Just W. Deterministic Chaos: An Introduction. John Wiley & Sons; 2006.
9. Eckmann JP, Ruelle D. Ergodic theory of chaos and strange attractors. Reviews of Modern Physics. 1985;57(3):617–656. doi:10.1103/RevModPhys.57.617.
10. Ruelle D. Chaotic Evolution and Strange Attractors. Cambridge University Press; 1989.
11. Jost J. Dynamical Systems: Examples of Complex Behaviour. 2005th ed. Berlin ; New York: Springer Berlin Heidelberg; 2008.
12. Pikovsky A, Politi A. Lyapunov Exponents: A Tool to Explore Complex Dynamics. Cambridge: Cambridge University Press; 2016.
13. Vulpiani A, Cecconi F, Cencini M. Chaos: From Simple Models to Complex Systems. Hackensack, NJ: World Scientific Pub Co Inc; 2009.
14. Young LS. Mathematical theory of Lyapunov exponents. Journal of Physics A: Mathematical and Theoretical. 2013;46(25):254001. doi:10.1088/1751-8113/46/25/254001.
15. Ruelle D. An inequality for the entropy of differentiable maps. Bol Soc Bras de Mat. 1978;.

16. Ledrappier F, Young LS. The Metric Entropy of Diffeomorphisms: Part II: Relations between Entropy, Exponents and Dimension. Annals of Mathematics. 1985;122(3):540–574. doi:10.2307/1971329.

17. Young LS. What Are SRB Measures, and Which Dynamical Systems Have Them? Journal of Statistical Physics. 2002;5-6(108):733–754. doi:10.1023/A:1019762724717.

18. Ledrappier F, Young LS. Entropy formula for random transformations. Probability Theory and Related Fields. 1988;80(2):217–240. doi:10.1007/BF00356103.

19. Kaplan JL, Yorke JA. Preturbulence: A regime observed in a fluid flow model of Lorenz. Communications in Mathematical Physics. 1979;67:93–108. doi:10.1007/BF01221359.

20. Frederickson P, Kaplan JL, Yorke ED, Yorke JA. The Liapunov dimension of strange attractors. Journal of differential equations. 1983;49(2):185–207.

21. Alexander JC, Yorke JA. Fat baker's transformations. Ergodic Theory and Dynamical Systems. 1984;4(1):1–23. doi:10.1017/S0143385700002236.

22. Ledrappier F. Some relations between dimension and Lyapounov exponents. Communications in Mathematical Physics. 1981;81(2):229–238. doi:10.1007/BF01208896.

23. Dymnikov VP, Filatov AN. Mathematics of Climate Modeling. Springer Science & Business Media; 2012.

24. Geist K, Parlitz U, Lauterborn W. Comparison of Different Methods for Computing Lyapunov Exponents. Progress of Theoretical Physics. 1990;83(5):875–893. doi:10.1143/PTP.83.875.

25. Benettin G, Galgani L, Giorgilli A, Strelcyn JM. Lyapunov Characteristic Exponents for smooth dynamical systems and for hamiltonian systems; A method for computing all of them. Part 2: Numerical application. Meccanica. 1980;15(1):21–30. doi:10.1007/BF02128237.

26. Tsodyks M, Mitkov I, Sompolinsky H. Pattern of synchrony in inhomogeneous networks of oscillators with pulse interactions. Physical Review Letters. 1993;71(8):1280–1283. doi:10.1103/PhysRevLett.71.1280.

27. Ernst U, Pawelzik K, Geisel T. Synchronization Induced by Temporal Delays in Pulse-Coupled Oscillators. Physical Review Letters. 1995;74(9):1570–1573. doi:10.1103/PhysRevLett.74.1570.

28. Timme M, Wolf F, Geisel T. Unstable attractors induce perpetual synchronization and desynchronization. Chaos (Woodbury, NY). 2003;13(1):377–387.

29. Brette R. Exact Simulation of Integrate-and-Fire Models with Exponential Currents. Neural Computation. 2007;19(10):2604–2609. doi:10.1162/neco.2007.19.10.2604.

30. D'Haene M, Schrauwen B, Van Campenhout J, Stroobandt D. Accelerating Event-Driven Simulation of Spiking Neurons with Multiple Synaptic Time Constants. Neural Computation. 2008;21(4):1068–1099. doi:10.1162/neco.2008.02-08-707.

31. Puelma Touzel M. Cellular dynamics and stable chaos in balanced networks. Georg-August-University Göttingen; 2016. Available from: https://ediss.uni-goettingen.de/handle/11858/00-1735-0000-0028-869D-B.

32. Tonnelier A, Belmabrouk H, Martinez D. Event-Driven Simulations of Nonlinear Integrate-and-Fire Neurons. Neural Computation. 2007;19(12):3226–3238. doi:10.1162/neco.2007.19.12.3226.

33. Monteforte M, Wolf F. Dynamic Flux Tubes Form Reservoirs of Stability in Neuronal Circuits. Physical Review X. 2012;2(4):041007. doi:10.1103/PhysRevX.2.041007.

34. Monteforte M, Wolf F. Dynamical Entropy Production in Spiking Neuron Networks in the Balanced State. Physical Review Letters. 2010;105(26):268104. doi:10.1103/PhysRevLett.105.268104.

35. Ermentrout G, Kopell N. Parabolic Bursting in an Excitable System Coupled with a Slow Oscillation. SIAM Journal on Applied Mathematics. 1986;46(2):233–253. doi:10.1137/0146017.

36. Ermentrout B. Type I Membranes, Phase Resetting Curves, and Synchrony. Neural Computation. 1996;8(5):979–1001. doi:10.1162/neco.1996.8.5.979.

37. Gutkin BS, Ermentrout GB. Dynamics of Membrane Excitability Determine Interspike Interval Variability: A Link Between Spike Generation Mechanisms and Cortical Spike Train Statistics. Neural Computation. 1998;10(5):1047–1065. doi:10.1162/089976698300017331.

38. Izhikevich EM. Dynamical Systems in Neuroscience. MIT Press; 2007.

39. Osan R, Ermentrout B. Two dimensional synaptically generated traveling waves in a theta-neuron neural network. Neurocomputing. 2001;38–40:789–795. doi:10.1016/S0925-2312(01)00390-3.

40. Gutkin BS, Jost J, Tuckwell HC. Transient termination of spiking by noise in coupled neurons. EPL (Europhysics Letters). 2008;81(2):20005. doi:10.1209/0295-5075/81/20005.

41. Hansel D, Mato G. Asynchronous States and the Emergence of Synchrony in Large Networks of Interacting Excitatory and Inhibitory Neurons. Neural Computation. 2003;15(1):1–56. doi:10.1162/089976603321043685.

42. Latham PE, Richmond BJ, Nirenberg S, Nelson PG. Intrinsic Dynamics in Neuronal Networks. II. Experiment. Journal of Neurophysiology. 2000;83(2):828–835.

43. Softky WR, Koch C. Cortical Cells Should Fire Regularly, But Do Not. Neural Computation. 1992;4(5):643–646. doi:10.1162/neco.1992.4.5.643.

44. Softky WR, Koch C. The highly irregular firing of cortical cells is inconsistent with temporal integration of random EPSPs. The Journal of Neuroscience. 1993;13(1):334–350.

45. Calvin WH, Stevens CF. Synaptic noise and other sources of randomness in motoneuron interspike intervals. Journal of Neurophysiology. 1968;31(4):574–587.

46. Bryant HL, Segundo JP. Spike initiation by transmembrane current: a white-noise analysis. The Journal of Physiology. 1976;260(2):279–314.

47. Hunter JD, Milton JG, Thomas PJ, Cowan JD. Resonance Effect for Neural Spike Time Reliability. Journal of Neurophysiology. 1998;80(3):1427–1438.

48. Mainen ZF, Sejnowski TJ. Reliability of spike timing in neocortical neurons. Science. 1995;268(5216):1503–1506. doi:10.1126/science.7770778.

49. Shadlen MN, Newsome WT. Noise, neural codes and cortical organization. Current Opinion in Neurobiology. 1994;4(4):569–579. doi:10.1016/0959-4388(94)90059-0.

50. Shadlen MN, Newsome WT. The Variable Discharge of Cortical Neurons: Implications for Connectivity, Computation, and Information Coding. The Journal of Neuroscience. 1998;18(10):3870–3896.

51. van Vreeswijk C, Sompolinsky H. Chaos in Neuronal Networks with Balanced Excitatory and Inhibitory Activity. Science. 1996;274(5293):1724 –1726. doi:10.1126/science.274.5293.1724.

52. van Vreeswijk C, Sompolinsky H. Chaotic Balanced State in a Model of Cortical Circuits. Neural Computation. 1998;10(6):1321–1371. doi:10.1162/089976698300017214.

53. Goldberg D. What every computer scientist should know about floating-point arithmetic. ACM Computing Surveys (CSUR). 1991;23(1):5–48. doi:10.1145/103162.103163.

54. Cormen TH, Leiserson CE, Rivest RL, Stein C. Introduction to Algorithms, 3rd Edition. 3rd ed. Cambridge, Mass: The MIT Press; 2009.

55. Sedgewick R, Wayne K. Algorithms. 4th ed. Upper Saddle River, NJ: Addison-Wesley Professional; 2011.

56. Renart A, Rocha Jdl, Bartho P, Hollender L, Parga N, Reyes A, et al. The Asynchronous State in Cortical Circuits. Science. 2010;327(5965):587–590. doi:10.1126/science.1179850.

57. Sack JR, Strothotte T. An algorithm for merging meaps. Acta Informatica. 1985;22(2):171–186. doi:10.1007/BF00264229.

58. Fredman ML, Tarjan RE. Fibonacci heaps and their uses in improved network optimization algorithms. Journal of the ACM (JACM). 1987;34(3):596–615. doi:10.1145/28869.28874.

59. Fredman ML, Sedgewick R, Sleator DD, Tarjan RE. The pairing heap: A new form of self-adjusting heap. Algorithmica. 1986;1(1-4):111–129. doi:10.1007/BF01840439.

60. Brodal GS. Worst-case efficient priority queues. Proceedings of the Seventh Annual Acm-siam Symposium on Discrete Algorithms. 1996; p. 52–58.

61. Lajoie G, Lin KK, Shea-Brown E. Chaos and reliability in balanced spiking networks with temporal drive. Physical Review E. 2013;87(5):052901. doi:10.1103/PhysRevE.87.052901.

62. Lajoie G, Thivierge JP, Shea-Brown E. Structured chaos shapes spike-response noise entropy in balanced neural networks. Frontiers in Computational Neuroscience. 2014;8:123. doi:10.3389/fncom.2014.00123.

63. Lajoie G, Lin KK, Thivierge JP, Shea-Brown E. Encoding in Balanced Networks: Revisiting Spike Patterns and Chaos in Stimulus-Driven Systems. PLOS Computational Biology. 2016;12(12):e1005258. doi:10.1371/journal.pcbi.1005258.

64. Festa D. Chaos Characterization of Pulse-Coupled Neural Networks in Balanced State. MPI DS / Università di Pisa. Göttingen/Pisa; 2011.

65. Liedtke J. Geometry and organization of stable and unstable manifold in balanced networks. Georg-August-University. Göttingen; 2013.

66. Golub GH, Loan CFV. Matrix Computations. fourth edition edition ed. Baltimore: Johns Hopkins University Press; 2012.

67. Yokozawa T, Takahashi D, Boku T, Sato M. Efficient parallel implementation of classical Gram-Schmidt orthogonalization using matrix multiplication. In: Proceedings of Fourth International Workshop on Parallel matrix Algorithms and Applications (PMAA'06); 2006. p. 37–38.

68. Newman CM. The distribution of Lyapanov exponents: exact results for random matrices. Communications in mathematical physics. 1986;103(1):121–126.

69. Isopi M, Newman CM. The triangle law for Lyapunov exponents of large random matrices. Communications in mathematical physics. 1992;143(3):591–598.

70. Crisanti A. Products of Random Matrices: in Statistical Physics. Softcover reprint of the original 1st ed. 1993 ed. Berlin; New York: Springer-Verlag; 1993.

71. Bezanson J, Edelman A, Karpinski S, Shah V. Julia: A Fresh Approach to Numerical Computing. SIAM Review. 2017;59(1):65–98. doi:10.1137/141000671.

4 Action potential onset rapidness and spontaneous collective dynamics

4.1 Summary

Spike initiation is a bottleneck for neural information transmission. Recent studies showed that the bandwidth of information encoding is limited by spike onset rapidness. Experiments revealed that neocortical neurons have a surprisingly broad encoding bandwidth. How this impacts the collective network dynamics is not well understood. Here we show that increasing the spike onset rapidness leads to decreasing attractor dimension, chaos and dynamical entropy rate, which vanishes at a critical value. We numerically calculated all Lyapunov exponents and derived exact upper and lower bounds for attractor dimension and dynamical entropy rate of random spiking networks. Analysis of large networks with more realistic structure indicate the generality of these findings. This demonstrates that spike initiation drastically shapes the entropy rate by which information about the initial state is erased by the chaotic recurrent network dynamics. The effect of spike onset on chaotic entropy rate surpasses the effect on the bandwidth of information encoding by orders of magnitude.

Citation

Rainer Engelken, Michael Monteforte, Fred Wolf. **"Spike Initiation Shapes Entropy in Neural Circuits."** *submitted*

Original Contribution

RE performed and analyzed all simulations. RE and FW wrote the main manuscript. RE wrote the supplementary material, but sections I, V and VI are adapted from the PhD thesis of MM [62]. RE and MM performed earlier network simulations. RE derived the random matrix theory of the mean Lyapunov exponent and the analytical approximation of the mutual information rate.

Spike Initiation Shapes Entropy in Neural Circuits

Rainer Engelken,* Michael Monteforte, and Fred Wolf
Max Planck Institute for Dynamics and Self-Organization, Göttingen, Germany,
Faculty of Physics, Georg-August-Universität Göttingen, Göttingen, Germany,
Bernstein Center for Computational Neuroscience, Göttingen, Germany

Spike initiation is a bottleneck for neural information transmission. Recent studies showed that the bandwidth of information encoding is limited by spike onset rapidness. Experiments revealed that neocortical neurons have a surprisingly broad encoding bandwidth. How this impacts the collective network dynamics is not well understood. Here we show that increasing the spike onset rapidness leads to decreasing attractor dimension, chaos and dynamical entropy rate, which vanishes at a critical value. We numerically calculated all Lyapunov exponents and derived exact upper and lower bounds for attractor dimension and dynamical entropy rate of random spiking networks. Analysis of large networks with more realistic structure indicate the generality of these findings. This demonstrates that spike initiation drastically shapes the entropy rate by which information about the initial state is erased by the chaotic recurrent network dynamics. The effect of spike onset on the chaotic entropy rate surpasses the effect on the bandwidth of information encoding by orders of magnitude.

PACS numbers: xx.xx.xx, xx.xx.-x, xx.xx.-x, xx.xx.-x

Information is processed in the brain by the spatio-temporal activity of large spiking neural circuits. Only information that is encoded in the spike train can be used by the local network, subsequent processing stages and to ultimately guide behavior. The spiking output of a cortical neuron contains twenty- to hundredfold less information about the synaptic input than its membrane potential [1]. Thus, spike initiation is an important bottleneck for neural information transmission. Experiments revealed that neocortical neurons have a surprisingly broad encoding bandwidth: the high-frequency input components of a stimulus are reliably encoded in the outgoing spike trains [2–5]. As predicted theoretically and observed experimentally, small changes to the spike onset rapidness can have a great impact on the bandwidth of information encoding in a feedforward architecture [5–11]. The role of broad encoding bandwidth and rapid spike onset in the dynamics of recurrent networks, however, has not yet been studied systematically. One might expect that collective dynamics are insensitive to cellular details, as in many instances the effect of single cell properties can become negligible at the macroscopic circuit level. For example, asynchronous irregular activity in idealized cortex models emerges robustly in inhibition-dominated circuits and can be described by a mean-field theory, which is largely independent of the neuron model [12, 13]. Collective dynamics rather is expected to be strongly shaped by the wiring diagram known as connectome and most learning algorithms in fact operate at this level [14, 15]. An example where single element input-output functions determine the critical properties of the collective dynamics are rate networks [16]. These analytical approaches were recently extended to heterogeneous networks, networks with bistable units and spiking networks with slow synaptic dynamics [17].

Here we use concepts from ergodic theory to analyze how the collective network state of spiking networks is shaped by spike onset rapidness. The dynamics of large scale dissipative systems often evolve towards a low dimensional attractor and it is challenging to characterize the collective modes on this lower dimensional manifold. Ergodic theory provides an estimate of the attractor dimension with exact upper and lower bounds. It also provides access to the dynamical entropy rate associated with the chaotic network dynamics that can contribute to the so-called noise entropy [20]. The dynamical stability of network activity constrains the capability of information processing: In chaotic systems a sensitive dependence on initial conditions makes predictions of future states impossible, if the initial state is known only with finite precision. This corresponds to a dynamical entropy rate, because nearby states, which could not be distinguished by a finite precision readout initially, are pulled apart by the chaotic dynamics and are distinguishable later on. Therefore, the dynamical entropy rate quantifies the speed by which microscopic perturbations such as ion channel noise affect global firing patterns.

Tunable spike onset model neuron.

To study the impact of spike onset rapidness on the collective network dynamics, we constructed a novel analytically solvable neuron model, in which the spike onset rapidness r can be changed, as shown in Figure 1a. (See methods for equations). Increasing r decreases the time constant at the unstable fixed point V_U leading to a larger instability and a sharper spike initiation (Fig. 1b,c). Figure 1d, e illustrates that high rapidness enables the neuron to transmit high frequency information of a time-

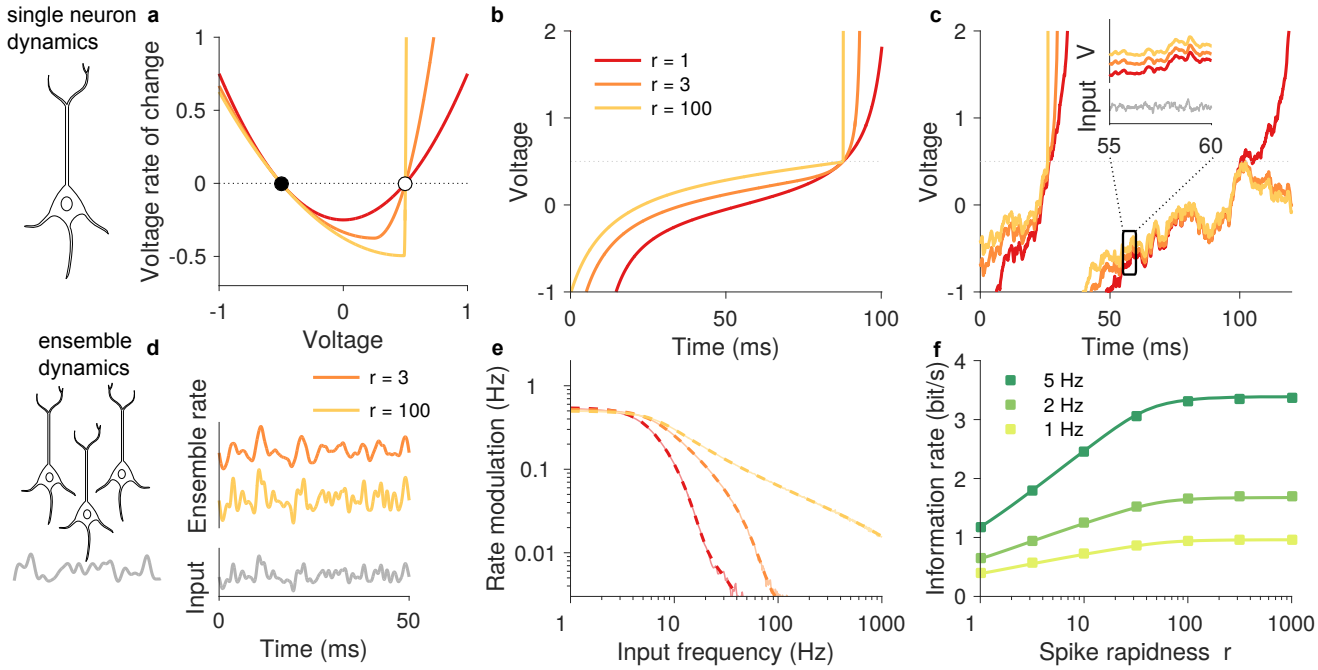

Figure 1: **High spike onset rapidness r increases population encoding bandwidth.** **a** Single neuron dynamics have two fixed points: a stable fixed point (filled circle, resting potential) and unstable fixed point (white circle, spike threshold). Slope at resting potential $-1/\tau_m$, slope at spike threshold r/τ_m. **b** Voltage traces of neuron model with constant input currents varying rapidness r. **c** Same for fluctuating input currents. Note that the spike waveform and initiation depends strongly on r, while the subthreshold dynamics is insensitive to r. The inset shows a magnified window of the voltage traces and the corresponding fluctuating input (gray) **d** Firing rates of an ensemble of rapid theta neurons with low and high rapidness for fluctuating input currents. Note that high rapidness enables the ensemble to accurately track the high frequency components of the input. **e** Linear firing rate response for different values of rapidness, direct numerical simulations (shaded line) and Fokker Planck solution (dashed line) superimposed. ($\nu_0 = 1$ Hz) , **f** mutual information rate in Gaussian channel approximation based on spectral coherence, Fokker Planck solution (full line) and direct numerical simulation (squares) for different mean ensemble firing rates ($\nu_0 = 1$, 2, 5 Hz) (parameters: $\tau_m = 10$ ms).

varying input current in its ensemble-averaged firing rate, while a low rapidness allows only the transmission of low and middle frequencies [4–11]. We find, as expected from earlier studies [5–11], that the ability to transmit information about a presynaptic signal embedded in noise is limited by the rapidness. We obtained the mutual information rate in the Gaussian channel approximation from the spectral coherence of the input and output signal. Moreover, we find that the information rate grows approximately logarithmically with rapidness (Fig. 1f and Supplementary Information for analytical results). The reason for the logarithmic scaling is that the rapidness determines the cutoff frequency, up to which the spectral coherence is proportional to f^{-1}.

In contrast to many neuron models including the exponential integrate and fire model, our model can be solved exactly between spikes, which is a crucial prerequisite for the precise and efficient calculation of the Lyapunov spectrum. To analyze the role of spike initiation for dynamical stability, we calculate the full Lyapunov spectrum of a spiking network of rapid theta neurons. Lyapunov exponents measure the rate of exponential divergence and convergence of nearby trajectories. The Lyapunov spectrum gives a good estimate of the attractor dimension (Kaplan-Yorke conjecture) including exact upper and lower bounds [22–24]. The trajectory of a N-dimensional dissipative chaotic system does not cover the whole phase space. After a transient period, it relaxes onto a strange attractor, which has a dimensionality $D \leq N$. The Kaplan Yorke attractor dimension is given by the number of Lyapunov exponents that sum to zero. One can think of it as the highest dimensional hypersphere, whose volume does not shrink by the dissipative system dynamics. A lower bound on the attractor dimension is given by the number of positive Lyapunov exponents. Another canonical measure for dynamical systems is the dynamic entropy rate, which is bounded from above by the sum of positive Lyapunov exponents. This bound becomes exact for smooth densities of the physical measure along the unstable directions (Pesin identity) [25]. We analytically calculate the Jacobian of the flow of the dynamics, which determines how an infinitesimal perturbation of the network state evolves from one spike time till just after the next spike time in the net-

work. We evaluate the Jacobians in numerically exact event-based simulations. The product of the Jacobians gives the long term Jacobian, which yields the spectrum of all Lyapunov exponents using Oseledets' multiplicative ergodic theorem [26].

Impact on dynamical entropy rate.

We find that rapidness strongly shapes the dynamical stability of recurrent networks in the balanced state (Fig. 2). First, we will discuss results from inhibitory random (Erdős–Rényi) networks, later we discuss mixed excitatory-inhibitory random networks and more structured network topologies. One could expect that for increasing rapidness r the collective chaos becomes stronger as the single neurons become more unstable. This is indeed the case for low rapidness: We find that the largest Lyapunov exponent grows linearly with rapidness (Fig. 2d) up to a peak rapidness. For high rapidness the largest Lyapunov exponent decreases as $1/r$ (Fig. 2d). Numerical simulation reveal the scaling of the peak rapidness $r_{\text{peak}} = \sqrt{K\nu_0\tau_m/J_0}$. It occurs, where the diffusion approximation breaks down and the finite connectivity K and nonvanishing coupling strength J_0 become important. For smaller rapidness r, the largest Lyapunov exponent is independent of the connectivity K , the coupling strength J and the mean firing rate $\bar{\nu}$.

At a critical rapidness, which scales $r_{\text{crit}} \propto N^{0.5}K^{0.4}\bar{\nu}^{0.8}\tau_m^{0.8}J_0^{-0.7}$, the largest Lyapunov exponent turns zero and the network activity becomes dynamically stable. Still, for any finite network size N, the largest Lyapunov exponent can be reduced arbitrary by choosing a sufficiently large r (Supplementary Section X). The dynamical entropy rate decreases monotonically with rapidness reaching zero at r_{crit} (Fig. 2e). The full spectrum reveals that the monotonic reduction can be explained by the drastic reduction in the number of positive Lyapunov exponents, which overcompensates the increase of the first few Lyapunov exponents (Fig. 2c). Despite such a drastic change in the collective dynamics, the statistics of the spike trains are essentially unaffected (Fig. 2a, b). This is very surprising, as for many other physical systems, a transition from chaos to stability is strongly reflected in the autocorrelations of the activity and in its pairwise cross-correlations [16].

The scaling of the entropy rate with network size N reveals that the network chaos is extensive: For sufficiently large N, the entropy rate grows linearly with network size N (Fig. 2f). The convergence of the Lyapunov spectra is demonstrated in the Supplementary Section VIII. Using random matrix theory, we calculated the mean Lyapunov exponent analytically (Supplementary Section IX).

The transition from chaos to stability for increasing rapidness also occurs for random networks with both excitatory and inhibitory coupling. To isolate the effect of excitation, we parametrized the coupling matrix, such that the input variance into each population stays the same for different scaling ϵ of the excitatory couplings. (See Supplementary Information for definition of ϵ). When increasing the scaling ϵ of the excitatory couplings, the dynamical entropy rate increases. If the excitation is strong enough, r_{crit} diverges, so these networks are always chaotic.

Interestingly, while the dynamical stability changes drastically for different values of r, the statistics of the spike trains remains almost unchanged. Both the distribution of firing rates and coefficients of variation are insensitive to changes in r (Fig. 2b). The mean pairwise Pearson correlation $\bar{\rho}$ of the spike count is weak and goes to zero for large networks with $\bar{\rho} \approx 1/N$, while the width of the standard deviation goes to zero as $\bar{\sigma} \approx 1/\sqrt{N}$ (3e, f, g). This confirms theoretical results predicting broadly distributed, but weak pairwise correlations in the balanced state [13].

Attractor dimensionality.

How is the drastic change of the collective dynamics reflected in the attractor dimensional and the structure of pairwise correlations? We find that increasing spike onset rapidness reduces the attractor dimension including its upper and lower bounds by orders of magnitude (Fig. 3a). We found that this reduction is independent of network size and also exists in mixed excitatory-inhibitory networks (Fig. 3b, c). The dimensionality of neural activity is often measured by the number of principal components required to explain a fixed fraction of variance [27–30]. In this case, such a dimensionality estimate based on pairwise statistics vastly overestimates the attractor dimension (dotted lines in 3a and c). This implies the network dynamics have strongly "entangled" statistics which are hidden when inspecting only pairwise correlations (Fig. 3e, f, g). Thus, the twisted low-dimensional strange attractor is interlaced in a high-dimensional phase space [31]. In the extreme case of very high rapidness beyond the critical rapidness r_{crit} the network dynamics become stable and the basins of attraction can be visualized by random cross sections of the phase space along two random N-dimensional vectors (Fig. 3d, h). Adjacent initial conditions that converge to the same trajectories are assigned the same color. When approaching r_{crit}, the basins of attraction get smaller and more curved, at r_{crit} they vanish (Supplementary Information).

Cortical circuit models.

In the previous sections, we studied the dynamics of random (Erdős–Rényi) balanced networks, which are canonical idealized models of neocortical networks. As

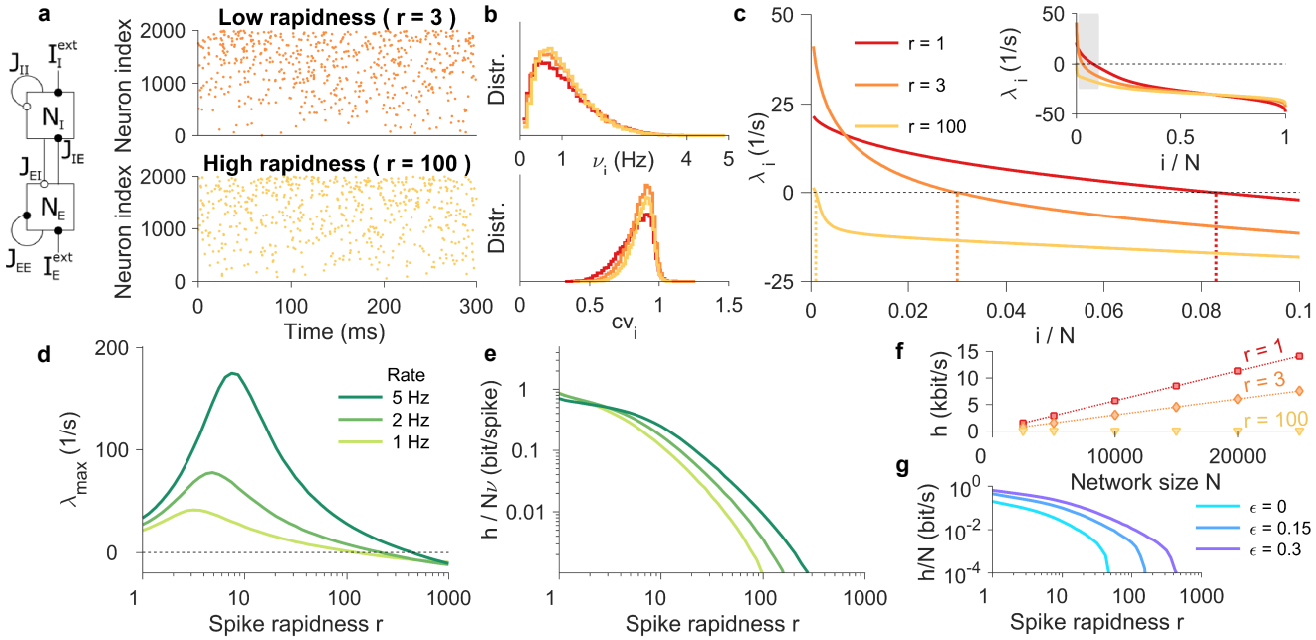

Figure 2: **High spike onset rapidness spike r dramatically reduces chaos and dynamical entropy rate.** **a** Spike trains of 50 random neurons for low (upper panel) and high (lower panel) rapidness. **b** Distribution of firing rates (upper panel) and coefficients of variation (lower panel) for different values of rapidness (ordered by time averaged single neuron firing rate) **c** Lyapunov spectra reorganize with increasing rapidness, (inset: full Lyapunov spectra) **d** Largest Lyapunov exponent and **e** Entropy rate h as a function of rapidness for different mean firing rates ($\bar{\nu} = 1$, 2, 5 Hz), **f** Entropy rate h for different network sizes (upper panel) and **g** different strengths of the scaling ϵ of the excitatory couplings (parameters: $N_I = 2000$, $N_E = 8000$, $K = 100$, $\bar{\nu} = 1$ Hz, $J_0 = 1$, $\tau_m = 10$ ms).

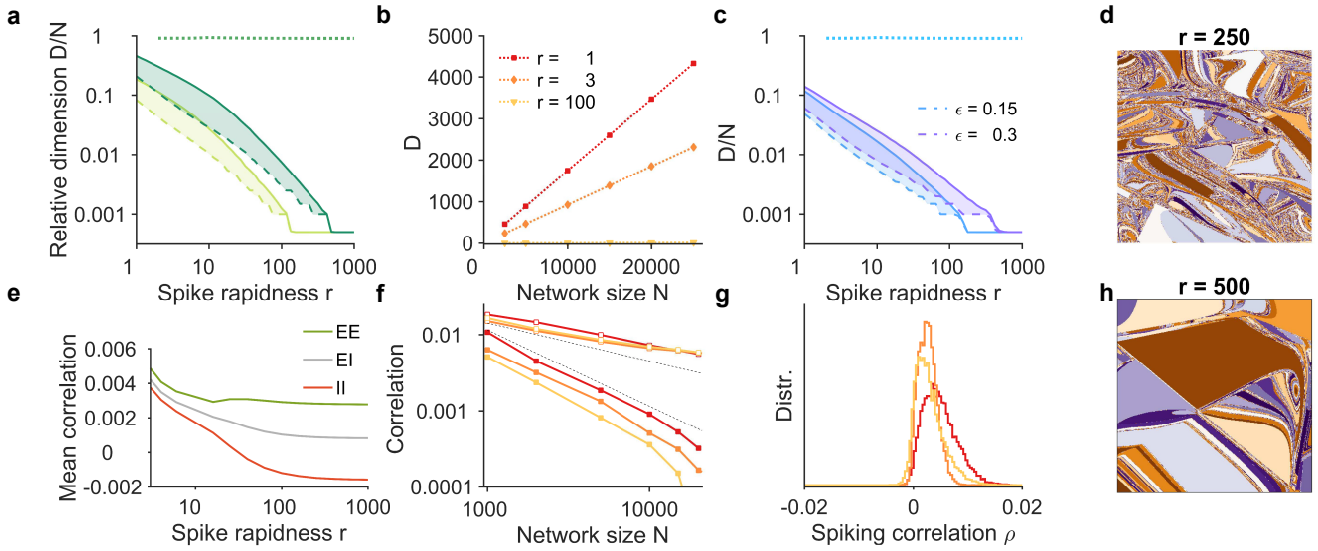

Figure 3: **Reduction of attractor dimensionality in the asynchronous state despite low pairwise spike count correlations.** **a** Attractor dimension for different mean firing rates and varying spike rapidness r, dotted line: dimensionality estimate based on principal components of pairwise spike count correlations matrix (Supplementary Information), full line: Kaplan-Yorke (KY) attractor dimension, dashed line: lower bound on attractor dimension (fraction of positive exponents) **b** KY Attractor dimension grows linearly with network size N **c** same as **a** for different scaling ϵ of the excitatory couplings **d, h** cross sections of basis on attraction in a plane perpendicular to the trajectory for $r = 250$, 500. Colors indicate basins of attraction of different trajectories ($N = 200$, $K = 100$ $r_c \approx 203$) **e** Mean pairwise spike count correlations for different values of rapidness r between excitatory (E) and inhibitory (I) neurons, excitatory-excitatory pairs (EE) in green, inhibitory-inhibitory pairs (II) in red, mixed pairs in yellow **f** Mean pairwise spike count correlations decay $\propto 1/N$, their standard deviations decays $\propto 1/\sqrt{N}$, (color code as in **b**) **g** histograms of spike count correlations for different rapidness r (EE-pairs)(color code as in **b**)(parameters as in Fig. 2, spike count window 20 ms)

cortical tissue has a very distinct architecture with a microscopic motif structure that is far from random and a layered structure where the layers have different wiring probabilities and distinct thalamic input, we investigate in the following, whether the previous findings are robust with respect to a more realistic microscopic and macroscopic structure. To analyze the effect of a multilayered topology, we took experimental data of wiring probability and synapse count from [32] to build a full cortical column with 77,169 neurons, around 285 Million synapses and four layers, each with an excitatory and inhibitory neuron population. We obtained spiking dynamics with layer-specific firing rates (Fig. 4a, b). For the first time, we calculated Lyapunov spectra in more realistic large networks, using an efficient massively parallelized implementation (Fig. 4e). We also constructed large mixed excitatory-inhibitory circuits, which are equipped with experimentally measured motif frequencies (Fig. 4f) [33].

In these more realistic network structures, our findings from idealized random cortex models were confirmed (Fig. 4). In the multilayered network the largest Lyapunov exponent behaves similarly to the one from the random network. It increases first as a function of rapidness and then decreases (Fig. 4c). The entropy rate shows a decline for growing rapidness (Fig. 4d). When comparing a random topology to a network with experimentally measured motif frequencies, we find a similarly strong reduction of dynamical entropy rate for increasing spike onset rapidness (Fig. 4g). Thus, the drastic reduction of chaos and dynamical entropy rate by high spike onset rapidness was independent of network structure. This justifies the analysis of more idealized random networks.

Conclusion and summary

Theoretical and experimental studies showed in recent years that cortical neurons have a surprisingly broad encoding bandwidth which depends on details of the spike initiation mechanism. Here we investigated the effect of this on the collective recurrent dynamics of neocortical spiking circuits. We found that canonical measures of the collective dynamics are not universal and insensitive to single cell properties, but they show a strong dependence on the spike onset rapidness. While slow spike onset leads to strong extensive chaos, rapid spike onset stabilizes the collective dynamics. The stabilization is accompanied by a decrease in dynamical entropy rate and attractor dimension, despite low pairwise correlations. This holds also in more realistic network structures including multilayered and second order motif networks. The effect of spike onset on chaotic entropy rate is orders of magnitude larger than the effect on the bandwidth of information encoding. The importance of single cell dynamics limiting the encoding bandwidth in a feedforward architecture is thus not washed out by the collective network dynamics.

The dimensionality of collective states in neural circuits is a fundamental quantity. Different measures of dimensionality might be necessary to characterize the complex dynamics. Using concepts from ergodic theory, we show that the attractor dimension decreases drastically for increasing spike onset rapidness which is hidden from conventional dimensionality estimates based on the correlations of the activity. This implies that neuron states have strong statistical dependencies. How such dependencies can be used for computations in a neocortical circuit is a question for future research.

As the spike threshold acts as unstable fixed point for the single cell dynamics, one might expect that high single cell instability (i.e. high spike onset rapidness r) increases the network chaos. Surprisingly, we find the opposite: A large single cell instability stabilizes the collective dynamics. Chaotic dynamics might be useful for computation to amplify small differences of initial conditions. If such a mechanism is used by cortical circuits, spike onset rapidness would be an important parameter to regulate this. Certainly, the dynamic entropy rate contributes to noise entropy and can therefore impair coding capacity. Therefore, it is remarkable that cortical neurons seem to be tuned to reduce this deterministic contribution to noise entropy.

Information in the cortex is processed by a deeply layered system of neuronal circuits. How well streams of spikes from one circuit can control spiking dynamics in the subsequent circuit limits its ability to encode information. It is presumably harder to control very chaotic networks by input spike trains. We therefore conjecture that high spike onset rapidness facilitates network state control and information transmission of subsequent circuits.

We are only beginning to use ergodic theory to understand neural computation. By employing these concepts in large scale neural circuits we have laid the foundations for further investigation. Computational ergodic theory of spiking networks has been until now the only way to measure information theoretic quantities of large recurrent circuits. It is an important challenge, to extend this to other quantities like transfer entropy and mutual information rate.

Methods

The governing piecewise differential equation for the single neuron dynamics is

$$\tau_m \dot{V}_i = \begin{cases} a_U (V_i - V_G)^2 + I_i(t) & V > V_G \\ a_S (V_i - V_G)^2 + I_i(t) & V \leq V_G \end{cases} \quad (1)$$

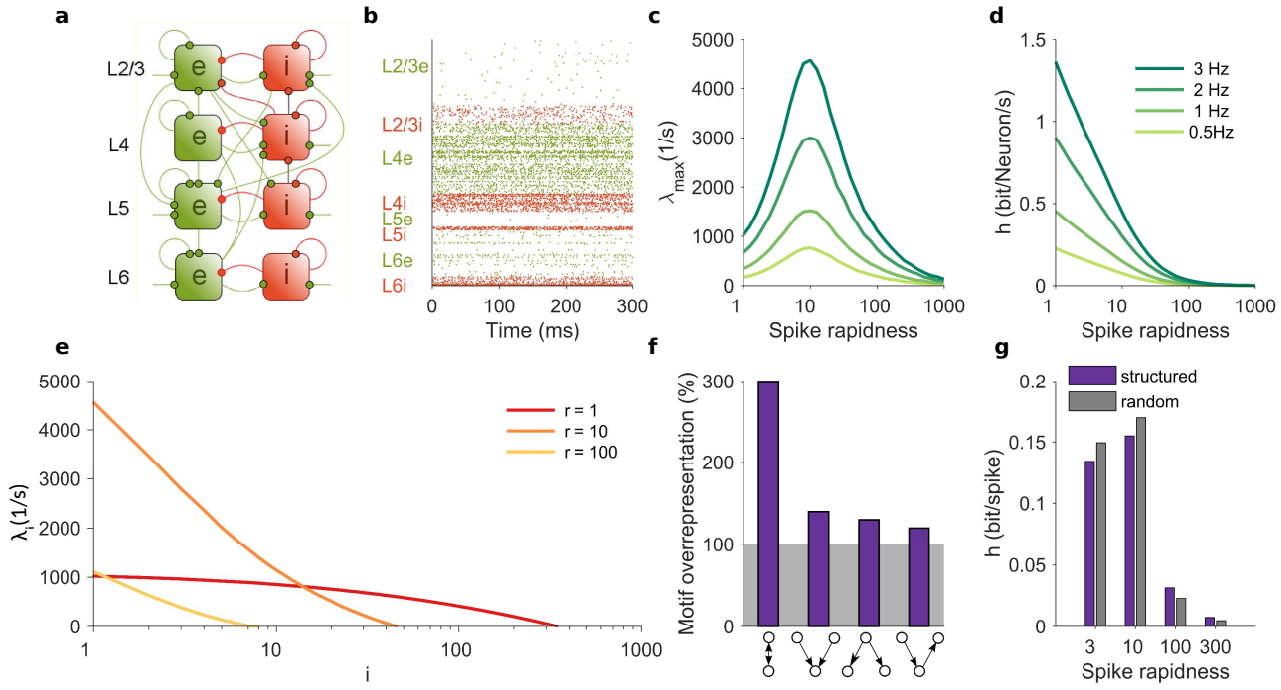

Figure 4: **High spike onset rapidness r reduces chaos and entropy rate in cortical circuit models: a** Multilayered cortical column network model with layer- and cell type specific connection probabilities, 77,169 neurons, ∼285 Million synapses **b** spike raster illustrating layer-specific firing rates **c** largest Lyapunov exponent vs. spike onset rapidness r **d** entropy rate h vs. spike onset rapidness r, **e** positive Lyapunov exponents of multilayered model. **f** Second order network motif overrepresentation estimated from experiments **g** dynamic entropy rate for random and realistic second order motif structure at different values of spike onset rapidness r.

with the membrane time constant τ_m, the glue point $V_G = \frac{1}{2}\frac{r-1}{r+1}$, the curvatures $a_S = \frac{r+1}{2r}$ and $a_U = r^2 a_S$ and the synaptic input current

$$I_i(t) = -I_T + I_{ext} + \tau_m \sum_{j \in \mathrm{pre}(i)} J\delta(t - t_j^{(s)})) \qquad (2)$$

where $I_T = \frac{1}{2}\frac{r}{r+1}$, $J = J_0/\sqrt{K}$. I_{ext} is adapted to obtain a desired target firing rate $\bar{\nu}$. The elements of the Jacobian of the flow of the dynamics are

$$D_{ij}(t_s) = \begin{cases} 1 + Z'(\phi_{i^*}(t_{s+1}^-) & \text{for } i = j \in \mathrm{post}(j^*) \\ -\frac{\omega_{i^*}}{\omega_{j^*}} Z'(\phi_{i^*}(t_{s+1}^-)) & \text{for } i \in \mathrm{post}(j^*) \text{ and } j = j^* \\ \delta_{ij} & \text{otherwise} \end{cases} \qquad (3)$$

where Z is the phase response curve, $\omega = \frac{2}{\tau_m}\sqrt{I_{ext}/a_S}$ is the phase velocity and stars indicate the neuron spiking at t_{s+1}. The Kaplan-Yorke attractor dimension was calculated from the interpolated number of Lyapunov exponents that sum to zero:

$$D = k + \frac{\sum_{i=1}^{k} \lambda_i}{\lambda_{k+1}} \quad \text{with} \quad k = \max_n \left\{ \sum_{i=1}^{n} \lambda_i \geq 0 \right\}.$$

This work was supported by MPG and BMBF.

* Electronic address: rainer@nld.ds.mpg.de

[1] Polavieja, G. G. de, Harsch, A., Kleppe, I., Robinson, H. P. C. & Juusola, M. Stimulus History Reliably Shapes Action Potential Waveforms of Cortical Neurons. J. Neurosci. **25**, 5657–5665 (2005).

[2] Köndgen, H. et al. The Dynamical Response Properties of Neocortical Neurons to Temporally Modulated Noisy Inputs In Vitro. Cereb. Cortex **18**, 2086–2097 (2008).

[3] Higgs, M. H. & Spain, W. J. Conditional Bursting Enhances Resonant Firing in Neocortical Layer 2–3 Pyramidal Neurons. J. Neurosci. **29**, 1285–1299 (2009).

[4] Tchumatchenko, T., Malyshev, A., Wolf, F. & Volgushev, M. Ultrafast Population Encoding by Cortical Neurons. The Journal of Neuroscience **31**, 12171–12179 (2011).

[5] Ilin, V., Malyshev, A., Wolf, F. & Volgushev, M. Fast Computations in Cortical Ensembles Require Rapid Initiation of Action Potentials. J. Neurosci. **33**, 2281–2292 (2013).

[6] Fourcaud-Trocmé, N., Hansel, D., van Vreeswijk, C. & Brunel, N. How Spike Generation Mechanisms Determine the Neuronal Response to Fluctuating Inputs. J. Neurosci. **23**, 11628–11640 (2003).

[7] Fourcaud-Trocmé, N. & Brunel, N. Dynamics of the Instantaneous Firing Rate in Response to Changes in Input

Statistics. J Comput Neurosci **18**, 311–321 (2005).

[8] Naundorf, B., Geisel, T. & Wolf, F. Action Potential Onset Dynamics and the Response Speed of Neuronal Populations. J Comput Neurosci **18**, 297–309 (2005).

[9] Naundorf, B., Wolf, F. & Volgushev, M. Unique features of action potential initiation in cortical neurons. Nature **440**, 1060–1063 (2006).

[10] Naundorf, B., Wolf, F. & Volgushev, M. Neurophysiology: Hodgkin and Huxley model — still standing? (Reply). Nature **445**, E2–E3 (2007).

[11] Wei, W. & Wolf, F. Spike Onset Dynamics and Response Speed in Neuronal Populations. Phys. Rev. Lett. **106**, 088102 (2011).

[12] van Vreeswijk, C. & Sompolinsky, H. Chaos in Neuronal Networks with Balanced Excitatory and Inhibitory Activity. Science **274**, 1724–1726 (1996); van Vreeswijk, C. & Sompolinsky, H. Chaotic Balanced State in a Model of Cortical Circuits. Neural Computation **10**, 1321–1371 (1998).

[13] Renart, A. et al. The Asynchronous State in Cortical Circuits. Science **327**, 587–590 (2010).

[14] Bienenstock, E. L., Cooper, L. N. & Munro, P. W. Theory for the development of neuron selectivity: orientation specificity and binocular interaction in visual cortex. J. Neurosci. **2**, 32–48 (1982).

[15] Sussillo, D. & Abbott, L. F. Generating Coherent Patterns of Activity from Chaotic Neural Networks. Neuron **63**, 544–557 (2009).

[16] Sompolinsky, H., Crisanti, A. & Sommers, H. J. Chaos in Random Neural Networks. Phys. Rev. Lett. **61**, 259–262 (1988).

[17] Stern, M., Sompolinsky, H. & Abbott, L. F. Dynamics of random neural networks with bistable units. Phys. Rev. E **90**, 062710 (2014).

[18] Harish, O. & Hansel, D. Asynchronous Rate Chaos in Spiking Neuronal Circuits. PLoS Comput Biol **11**, e1004266 (2015).

[19] Kadmon, J. & Sompolinsky, H. Transition to Chaos in Random Neuronal Networks. Phys. Rev. X **5**, 041030 (2015).

[20] Lajoie, G., Thivierge, J.-P. & Shea-Brown, E. Structured chaos shapes spike-response noise entropy in balanced neural networks. Front. Comput. Neurosci **8**, 123 (2014).

[21] Bernardi, D. & Lindner, B. A frequency-resolved mutual information rate and its application to neural systems. Journal of Neurophysiology **113**, 1342–1357 (2015).

[22] Frederickson, P., Kaplan, J. L., Yorke, E. D. & Yorke, J. A. The Liapunov dimension of strange attractors. Journal of differential equations **49**, 185–207 (1983).

[23] Ledrappier, F. Some relations between dimension and Lyapounov exponents. Commun.Math. Phys. **81**, 229–238 (1981).

[24] Eckmann, J.-P. & Ruelle, D. Ergodic theory of chaos and strange attractors. Rev. Mod. Phys. **57**, 617–656 (1985).

[25] Ledrappier, F. & Young, L.-S. The Metric Entropy of Diffeomorphisms: Part I: Characterization of Measures Satisfying Pesin's Entropy Formula. Annals of Mathematics **122**, 509–539 (1985).

[26] Benettin, G., Galgani, L., Giorgilli, A. & Strelcyn, J.-M. Lyapunov characteristic exponents for smooth dynamical systems and for Hamiltonian systems - A method for computing all of them. I - Theory. II - Numerical application. Meccanica **15**, 9–30 (1980).

[27] Mazor, O. & Laurent, G. Transient Dynamics versus Fixed Points in Odor Representations by Locust Antennal Lobe Projection Neurons. Neuron **48**, 661–673 (2005).

[28] Machens, C. K., Romo, R. & Brody, C. D. Functional, But Not Anatomical, Separation of 'What' and 'When' in Prefrontal Cortex. J. Neurosci. **30**, 350–360 (2010).

[29] Mante, V., Sussillo, D., Shenoy, K. V. & Newsome, W. T. Context-dependent computation by recurrent dynamics in prefrontal cortex. Nature **503**, 78–84 (2013).

[30] Gao, P. & Ganguli, S. On simplicity and complexity in the brave new world of large-scale neuroscience. Current Opinion in Neurobiology **32**, 148–155 (2015).

[31] Schneidman, E., Berry, M. J., Segev, R. & Bialek, W. Weak pairwise correlations imply strongly correlated network states in a neural population. Nature **440**, 1007–1012 (2006).

[32] Potjans, T. C. & Diesmann, M. The Cell-Type Specific Cortical Microcircuit: Relating Structure and Activity in a Full-Scale Spiking Network Model. Cereb. Cortex **24**, 785–806 (2014).

[33] Song, S., Sjöström, P. J., Reigl, M., Nelson, S. & Chklovskii, D. B. Highly Nonrandom Features of Synaptic Connectivity in Local Cortical Circuits. PLoS Biol **3**, e68 (2005).

[34] Zhao, L., II, B. B., Netoff, T. & Nykamp, D. Q. Synchronization from second order network connectivity statistics. Front. Comput. Neurosci. **5**, 28 (2011).

[35] R. Zillmer, R. Livi, A. Politi, and A. Torcini, Phys. Rev. E **74**, 036203 (2006); S. Jahnke, R. M. Memmesheimer, and M. Timme, Phys. Rev. Lett. **100**, 048102 (2008); R. Zillmer, N. Brunel and D. Hansel, Phys. Rev. E **79**, 031909 (2009).

[36] 1.Politi, A., Livi, R., Oppo, G.-L. & Kapral, R. Unpredictable Behaviour in Stable Systems. EPL **22**, 571 (1993).

[37] P. E. Latham et al., J. Neurophysiol. **83**, 808 (2000); R. Osan and B. Ermentrout, Neurocomputing **38**, 789 (2001); D. Hansel and G. Mato, Neural Comput. **15**, 1 (2003); B. S. Gutkin, J. Jost and H. C. Tuckwell, Europhys. Lett. **81**, 20005 (2008).

[38] G. B. Ermentrout and N. Kopell, SIAM J. Appl. Math. **46**, 233 (1986); B. S. Gutkin and G. B. Ermentrout, Neural Comput. **10**, 1047 (1998); J. C. Brumberg and B. S. Gutkin, Brain Res. **1171**, 122 (2007)

[39] Ruelle, D. Large volume limit of the distribution of characteristic exponents in turbulence. Commun.Math. Phys. **87**, 287–302 (1982).

[40] Takeuchi, K. A., Ginelli, F. & Chaté, H. Lyapunov Analysis Captures the Collective Dynamics of Large Chaotic Systems. Phys. Rev. Lett. **103**, 154103 (2009).

[41] London, M., Roth, A., Beeren, L., Häusser, M. & Latham, P. E. Sensitivity to perturbations in vivo implies high noise and suggests rate coding in cortex. Nature **466**, 123–127 (2010).

[42] Monteforte, M. & Wolf, F. Dynamical Entropy Production in Spiking Neuron Networks in the Balanced State. Phys. Rev. Lett. **105**, 268104 (2010).

[43] Monteforte, M. & Wolf, F. Dynamic Flux Tubes Form Reservoirs of Stability in Neuronal Circuits. Phys. Rev. X **2**, 041007 (2012).

Supplemental Material for "Spike Initiation Shapes Entropy in Neural Circuits"

Rainer Engelken,* Michael Monteforte, and Fred Wolf
Max Planck Institute for Dynamics and Self-Organization, Göttingen, Germany,
Faculty of Physics, Georg-August-Universität Göttingen, Göttingen, Germany,
Bernstein Center for Computational Neuroscience, Göttingen, Germany

Contents

I. The rapid theta neuron model 1

II. Stationary firing rate of the rapid theta neuron 3

III. Linear response of an ensemble of rapid theta neurons 4

IV. Mutual information rate and action potential onset rapidness 7

V. Phase representation of the rapid theta neuron 13

VI. Single spike Jacobian of the rapid theta neuron network 14

VII. Setup of network and event-based simulation 16

VIII. Convergence of the Lyapunov spectra 19

IX. Random matrix theory of the mean Lyapunov exponent 20

X. Scaling of the largest Lyapunov exponent with network parameters 22

XI. Participation ratio and localization of chaos 23

XII. Pairwise correlations in rapid theta networks 25

XIII. Attractor dimension and "entangled" statistics 27

XIV. Flux-tube structure of phase space, stable chaos and single-spike perturbations 29

XV. Poincaré maps of chaotic networks 31

XVI. Local Lyapunov exponents reveal stable and unstable manifolds 32

XVII. Chaos and dynamical entropy rate in structured network topologies 34

XVIII. Minimal example for Julia 37

References 37

I. THE RAPID THETA NEURON MODEL

To examine the impact of the action potential (AP) onset rapidness on the collective dynamics of cortical networks, we constructed a new neuron model with variable AP onset rapidness, called the rapid theta neuron model (**Fig. 1**, main paper). This model is similar to the exponential integrate and fire neuron, but much more tractable for high precision calculations. The rapid theta neuron model combines the advantage of the theta neuron model for the analytical derivation of the phase-response curve with a modifiable AP onset rapidness r. For $r = 1$, the rapid theta

neuron model is equivalent to the theta neuron model. Increasing r decreases the time constant at the unstable fixed point V_{U} (voltage threshold) leading to a larger instability and *sharper* AP initiation. The membrane time constant τ_{m}, the time constant at the stable fixed point V_{S} (resting potential) remains unchanged. This is achieved by gluing two parabolas smoothly together at V_{G}. In the dimensionless voltage representation, the resulting rapid theta neuron model is described by the differential equation

$$\tau_{\mathrm{m}}\frac{\mathrm{d}V}{\mathrm{d}t} = \begin{cases} a_{\mathrm{S}}(V-V_{\mathrm{G}})^2 - I_{\mathrm{T}} + I(t) & V \le V_{\mathrm{G}} \\ a_{\mathrm{U}}(V-V_{\mathrm{G}})^2 - I_{\mathrm{T}} + I(t) & V > V_{\mathrm{G}}. \end{cases} \tag{1}$$

In this equation, I_{T} denotes the rheobase current and $I(t)$ is the synaptic input current. The curvatures $a_{\mathrm{U,S}}$ depend on the AP onset rapidness r and together with V_{G} and I_{T} define the positions of the two branches of the parabolas. The glue point, denoted V_{G}, where the two branches are continuously and smoothly glued together divides the single neuron phase space into two ($V \le V_{\mathrm{G}}$) ($V > V_{\mathrm{G}}$) parts. At the stable fixed point V_{S}, the slope of the subthreshold parabola is set to $-1/\tau_{\mathrm{m}}$ and at the unstable fixed point V_{U} the slope is r/τ_{m}. This leads to the expressions

$$\frac{\partial \dot{V}(V_{\mathrm{S,U}})}{\partial V} = \begin{cases} -1 = 2a_{\mathrm{S}}(V_{\mathrm{S}} - V_{\mathrm{G}}) \\ r = 2a_{\mathrm{U}}(V_{\mathrm{U}} - V_{\mathrm{G}}) \end{cases} \tag{2}$$

$$\begin{aligned} a_{\mathrm{S}} &= \frac{1}{2}\frac{1}{(V_{\mathrm{G}} - V_{\mathrm{S}})} \\ a_{\mathrm{U}} &= \frac{r}{2}\frac{1}{(V_{\mathrm{U}} - V_{\mathrm{G}})}. \end{aligned}$$

The rate of change of the voltage vanishes at the two fixed points V_{S} and V_{U} for zero synaptic inputs ($I(t) \equiv 0$). This defines the gluing point V_{G} and the rheobase current I_{T}:

$$\dot{V}(V_{\mathrm{S,U}}) = 0 = \begin{cases} a_{\mathrm{S}}(V_{\mathrm{S}} - V_{\mathrm{G}})^2 - I_{\mathrm{T}} \\ a_{\mathrm{U}}(V_{\mathrm{U}} - V_{\mathrm{G}})^2 - I_{\mathrm{T}} = \frac{rV_{\mathrm{U}} - V_{\mathrm{G}}(r+1) + V_{\mathrm{S}}}{2} \end{cases} \tag{3}$$

$$\begin{aligned} I_{\mathrm{T}} &= \frac{V_{\mathrm{G}} - V_{\mathrm{S}}}{2} \\ V_{\mathrm{G}} &= \frac{rV_{\mathrm{U}} + V_{\mathrm{S}}}{r+1}. \end{aligned}$$

Without loss of generality, the stable and unstable fixed points are set to $V_{\mathrm{S}} = -0.5$ and $V_{\mathrm{U}} = +0.5$, yielding:

$$V_{\mathrm{G}} = \frac{1}{2}\frac{r-1}{r+1} \tag{4}$$

$$I_{\mathrm{T}} = \frac{1}{2}\frac{r}{r+1} \tag{5}$$

$$a_{\mathrm{S}} = \frac{r+1}{2r} \tag{6}$$

$$a_{\mathrm{U}} = \frac{r(r+1)}{2} = r^2 a_{\mathrm{S}}. \tag{7}$$

With Eq. (4)-(7) the governing equation of the rapid theta neuron model (1) becomes

$$\tau_{\mathrm{m}}\frac{\mathrm{d}V}{\mathrm{d}t} = \begin{cases} \frac{r+1}{2r}\left(V - \frac{1}{2}\frac{r-1}{r+1}\right)^2 - I_T + I(t) & V \le \frac{1}{2}\frac{r-1}{r+1} \\ \frac{r(r+1)}{2}\left(V - \frac{1}{2}\frac{r-1}{r+1}\right)^2 - I_T + I(t) & V > \frac{1}{2}\frac{r-1}{r+1}. \end{cases} \tag{8}$$

II. STATIONARY FIRING RATE OF THE RAPID THETA NEURON

The stationary firing rate of the rapid theta neuron with constant input current follows directly from solving equation 8. The inverse time from reset $V = -\infty$ to threshold $V = \infty$ gives the firing rate:

$$\nu(I^{\mathrm{ext}}) = \frac{\sqrt{I^{\mathrm{ext}}}}{\pi\tau_{\mathrm{m}}}\sqrt{\frac{2r}{r+1}} \tag{9}$$

Cortical neurons are driven by a dense stream of input spikes. The resulting compound spike train can be modeled as a Poisson process, if the input spike trains are uncorrelated and random. Note, however, that the superposition of many uncorrelated non-Poissonian spike trains deviates from a Poisson process in general [22, 23]. When many weak and uncorrelated spikes arrive at a neuron, it is justified to treat the random component of the synaptic currents as Gaussian white noise [24, 25]. In this diffusion approximation, we obtained the mean firing rate by solving the stationary Fokker-Planck equation with additive Gaussian white noise input current. We start by writing a piecewise Langevin equation for the rapid theta model:

$\tau_{\mathrm{m}}$where $\xi(t)$ is Gaussian white noise with unit variance, $\sigma\sqrt{2\tau_{\mathrm{m}}}$ is the noise intensity of the input and μ is a constant input consisting of the constant external input, the rheobase current and the mean recurrent input. This results in a piecewise Fokker-Planck equation:

$$\frac{\partial P(V,\,t)}{\partial t} = \begin{cases} \frac{\sigma^2}{\tau_{\mathrm{m}}}\frac{\partial^2 P}{\partial V^2} + \frac{\partial}{\partial V}\left(\frac{-\mu(t)-a_{\mathrm{S}}(V-V_{\mathrm{G}})^2}{\tau_{\mathrm{m}}}P\right) & V \le V_{\mathrm{G}} \\ \frac{\sigma^2}{\tau_{\mathrm{m}}}\frac{\partial^2 P}{\partial V^2} + \frac{\partial}{\partial V}\left(\frac{-\mu(t)-a_{\mathrm{U}}(V-V_{\mathrm{G}})^2}{\tau_{\mathrm{m}}}P\right) & V > V_{\mathrm{G}} \end{cases} \tag{10}$$

where $P(V,\,t)$ is the time-dependent probability density of finding a neuron at time t at voltage V. The stationary (time-independent) Fokker-Planck equation can be solved numerically using an efficient threshold integration method [14]. Briefly, the Fokker-Planck equation is set to zero and rewritten in two first order equations for probability flux and probability in V:

$$\tau_{\mathrm{m}}\frac{\partial J_0}{\partial V} = \nu_0\delta(V - V_{\mathrm{th}}) - \nu_0\delta(V - V_{\mathrm{re}}) \tag{11}$$

$$-\frac{\partial P_0}{\partial V} = \begin{cases} \frac{\tau_{\mathrm{m}}}{\sigma_0^2}\left(\frac{-\mu_0-a_{\mathrm{S}}(V-V_{\mathrm{G}})^2}{\tau_{\mathrm{m}}}P_0 + J_0\right) & V \le V_{\mathrm{G}} \\ \frac{\tau_{\mathrm{m}}}{\sigma_0^2}\left(\frac{-\mu_0-a_{\mathrm{U}}(V-V_{\mathrm{G}})^2}{\tau_{\mathrm{m}}}P_0 + J_0\right) & V > V_{\mathrm{G}}. \end{cases} \tag{12}$$

Here $P_0(V)$ is the stationary probability distribution of membrane potentials and $J_0(V)$ is the probability flux. As we know the boundary conditions $\lim_{V\to\infty} P_0(V) = 0$ and $\lim_{V\to\infty} J_0(V) = \nu_0$, we can simultaneously integrate P_0 and J_0 from threshold to some lower bound V_{lb} [40]. The rate ν_0 is initially unknown, but can be scaled out $p_0 = P_0/\nu_0$. The normalization $\int_{V_{\mathrm{lb}}}^{V_{\mathrm{th}}} P_0 dV = 1$ then yields the firing rate

$$\nu_0 = \left(\int_{V_{\mathrm{lb}}}^{V_{\mathrm{th}}} p_0 dV\right)^{-1} \tag{13}$$

Convergence of the numerical integration of the Fokker-Planck solution: **Fig. 2c** and **d** displays the steady-state firing rate of the stationary solution of the Fokker-Planck approach. As the rapid theta model has neither finite threshold nor finite reset in the voltage representation, the threshold, reset and lower bound of the numerical threshold integration scheme have to be chosen sufficiently far away from zero such that the results do not change (**Fig. 2c**). The integration step size ΔV has to be chosen sufficiently small (**Fig. 2f**). For higher rapidness, smaller step sizes are necessary to get the same precision. This is because there is a drastic change of the dynamics at V_{G} therefore close to V_{G} the voltage integration steps have to be small. To increase the numerical accuracy at high rapidness, we chose ΔV, such that both V_{re} and V_{G} fall on a lattice point of the integration scheme. Code for Julia and MATLAB®/Octave is available upon request. We found that $V_{\mathrm{th}} = 1000$ and $\Delta V = 10^{-3}$ are sufficient for a relative precision of the firing rate of $\frac{\Delta\nu_0}{\nu_0} < 10^{-2}$.

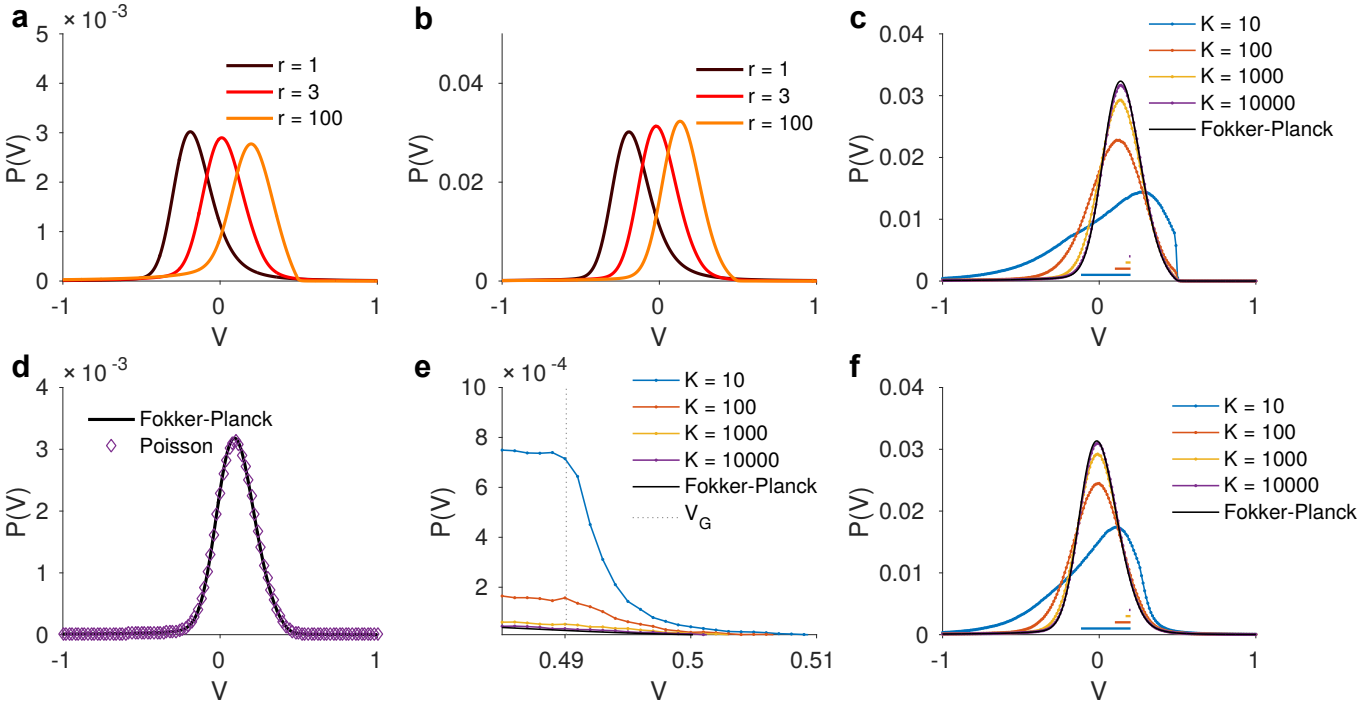

Figure 1: **Action potential onset rapidness r shapes stationary voltage distribution**. **a)** Voltage distribution for different rapidness for fixed external input obtained from the solution of the stationary Fokker Planck equation Eq. 11 and Eq. 12 **b)** same as **a**, but for fixed mean firing rate. **c)** Voltage distribution obtained with inhibitory Poisson input spikes trains. For small K, the shot noise nature of the Poisson input becomes important. ($r = 100$) **d)** Comparison of Poisson input and Fokker Planck solution for $K = 10000$ and $r = 10$. **e)** same as **c)** zoomed in for $r = 10$. The probability density drops at V_{G}. **f)** same as **c)** for $r = 3$ (parameters: $\nu_0 = 1\,\mathrm{Hz}$, $J_0 = 1$, $\tau_{\mathrm{m}} = 10\,\mathrm{ms}$).

Diffusion approximation and shot noise: The Fokker-Planck approach approximates the synaptic input by Gaussian white noise. This is justified in the limit of uncorrelated input and large rate of infinitesimally strong received postsynaptic currents per neurons. To investigate the impact of finite postsynaptic potentials, we replaced the Gaussian white noise with inhibitory Poisson pulses of rate $\nu_{\mathrm{p}} = \nu_0 K$ and strength $J_{\mathrm{p}} = -J_0/\sqrt{K}$. We kept the variance $\sigma_{\mathrm{p}}^2 = \nu_{\mathrm{p}} J_{\mathrm{p}}^2 = \nu_0 J_0^2$ fixed and varied K. The mean firing rate ν_0 was kept constant for different values of rapidness r and K by adapting the constant input current μ. For large K, the diffusion approximation is valid, while for small K, the shot noise nature of the Poisson input becomes relevant (**Fig. 1c+f**). This effect is particularly strong for large rapidness r. For small K, the density just below V_{G} obtained from direct numerical simulation is larger than the probability density obtained from the Fokker-Planck solution. It drops at V_{G} (**Fig. 1e**). This will help later to understand the dependence of the largest Lyapunov exponent on K and r. In principle, a similar analytical investigation of shot noise as in Ref. [15] could also be done but is beyond the scope of this work.

III. LINEAR RESPONSE OF AN ENSEMBLE OF RAPID THETA NEURONS

Figure 1 e of main paper. We calculated the linear response of ensembles of rapid theta neurons using three different approaches: Firstly by solving the time-dependent Fokker-Planck-equation, secondly, by direct numerical simulation using Poisson input and thirdly by direct numerical simulations using band-limited white noise. The same efficient numerical threshold integration method as for the stationary response can be adapted to obtain the linear response to a sinusoidal modulation of the input current. A modulation of the mean input current $\mu(t) = \mu_0 + \mu_1 e^{i\omega t}$ results in a firing rate modulation, which is in linear response $\nu(t) = \nu_0 + \hat{\nu}_\mu e^{i\omega t}$. The absolute value $|\hat{\nu}_\mu(\omega)|$ gives the rate modulation strength and the phase of $\hat{\nu}(\omega)$ gives the phase lag between input and output modulation. The expansion of the flux in first order therefore satisfies:

$$\tau_{\mathrm{m}} \frac{\partial \hat{J}_\mu}{\partial V} = i\omega \hat{P}_\mu + \hat{\nu}_\mu \delta(V - V_{th}) - \hat{\nu}_\mu \delta(V - V_{\mathrm{re}}) \tag{14}$$

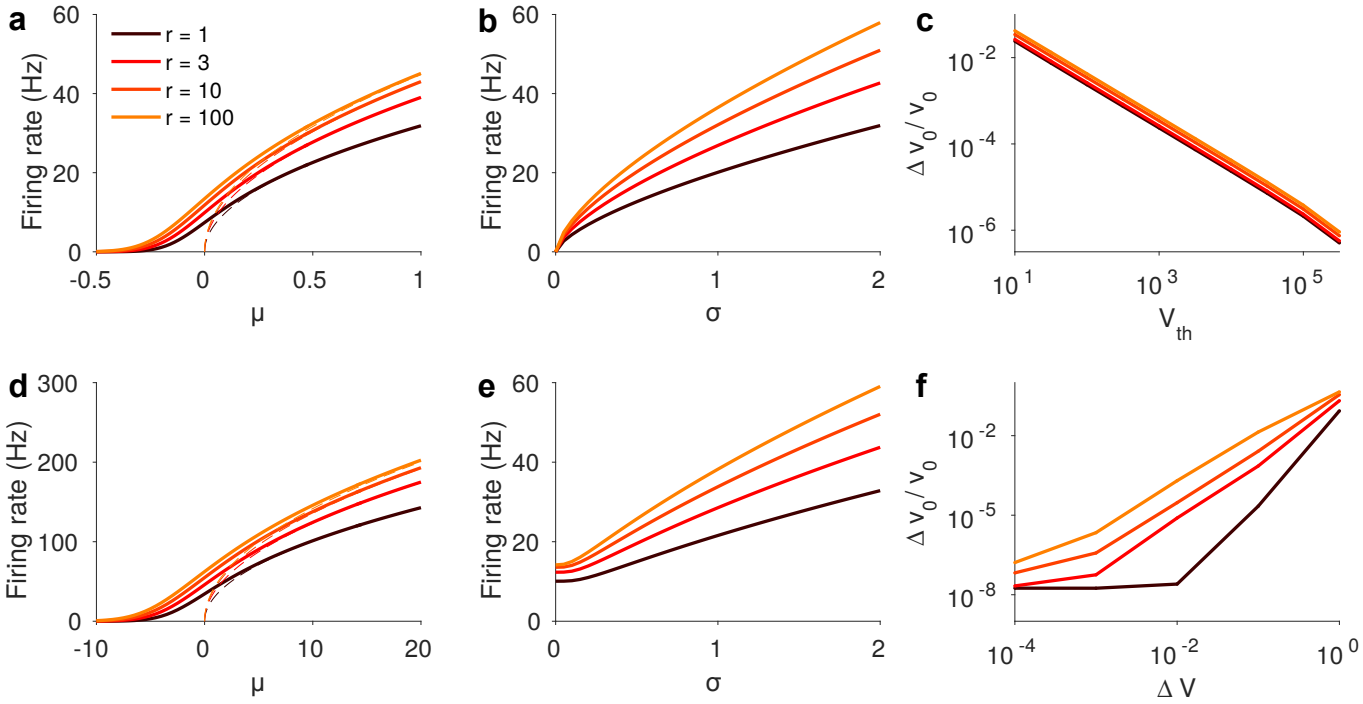

Figure 2: **Spike onset rapidness r mildly affects steady-state firing rate**. **a)** Firing rate as a function of constant input μ for different values of rapidness obtained from stationary Fokker-Planck solution for weak noise ($\sigma = \sqrt{0.05}$). Dashed line is analytical noise-free result (Eq. 9). **b)** same as **a** for varying noise strength σ at $\mu = I_T$. **c)** rate deviation for different threshold levels of numerical integration scheme. **d)** same as **a)** for strong noise ($\sigma = \sqrt{0.5}$) **e)** same as **b)** for strong constant input $\mu = 0.1 + I_T$ **f)** rate deviation for different integration step sizes in the numerical integration scheme (parameters: $\tau_\mathrm{m} = 10\,\mathrm{ms}$, $V_\mathrm{re} = -V_\mathrm{th}$, $\Delta V = 10^{-3}$, $V_\mathrm{th} = 10^3$).

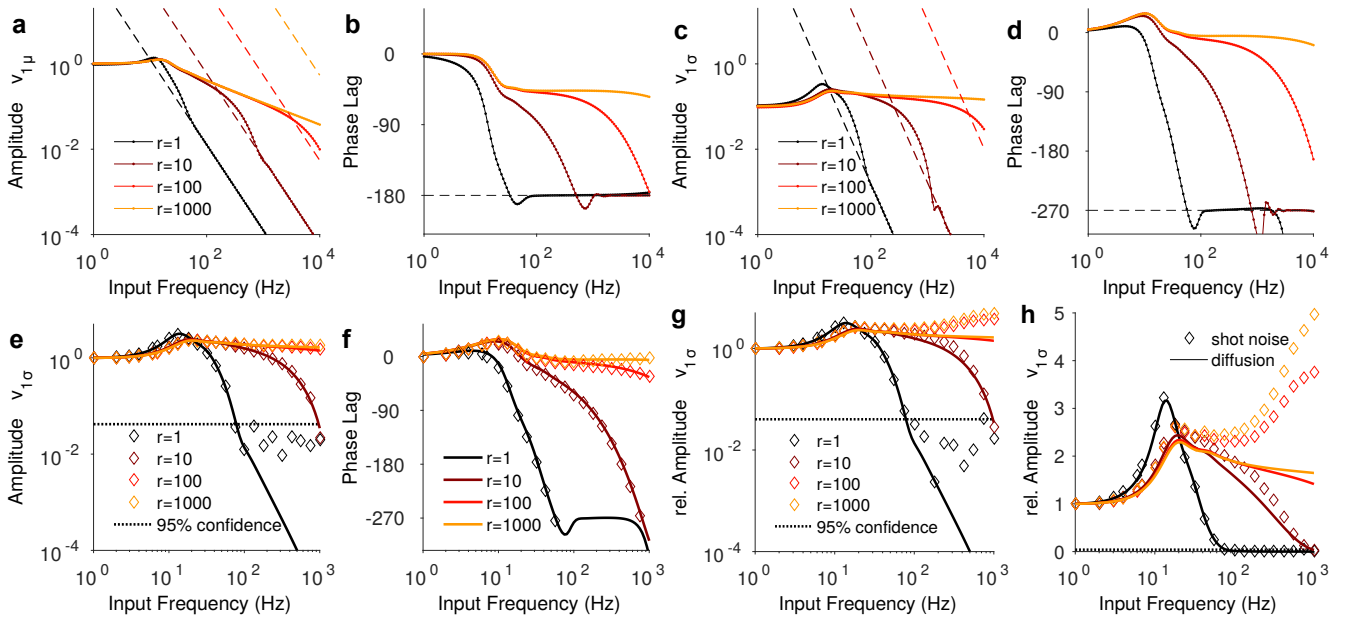

Figure 3: **Action potential onset rapidness r drastically shapes linear firing rate response**: **Fokker-Planck approach (FPA) vs. direct numerical simulations (DNS) vs. high-frequency analytical solution (HFA) a)** Linear response for mean modulation of input current. Increasing rapidness leads to increased cutoff frequency. Full lines are FPA, dashed lines correspond to HFA (Eq. 20). **b)** Phase lag for different input frequencies. **c)+d)** same as **a)+b)** for modulation of variance of the input current. **e)** Comparison of DNS (diamonds) and FPA (full line) for variance modulation with $K = 1000$. Dashed line indicate 95% significance threshold for DNS. **f)** Same for phase lag. **g)** Impact of shot noise: Same as **e)** for $K = 30$. For large values rapidness and large input frequencies, the shot noise gets significant. **h)** Same as **g)** with linear amplitude axis (parameters: $\nu_0 = 10\,\mathrm{Hz}$, $K = 1000$, $\tau_\mathrm{m} = 10\,\mathrm{ms}$.)

$$-\frac{\partial \hat{P}_\mu}{\partial V} = \begin{cases} \frac{\tau_\mathrm{m}}{\sigma_0^2}\left(\frac{-\mu_0 - a_\mathrm{S}(V-V_\mathrm{G})^2}{\tau_\mathrm{m}}\hat{P}_\mu + \hat{J}_\mu + F_\mu\right) & V \le V_\mathrm{G} \\ \frac{\tau_\mathrm{m}}{\sigma_0^2}\left(\frac{-\mu_0 - a_\mathrm{U}(V-V_\mathrm{G})^2}{\tau_\mathrm{m}}\hat{P}_\mu + \hat{J}_\mu + F_\mu\right) & V > V_\mathrm{G}. \end{cases} \tag{15}$$

F_μ describes the inhomogeneous term given by $F_\mu = -\frac{\partial J}{\partial \mu}P_0 = -\frac{\mu_1 P_0}{\tau_\mathrm{m}}$. The boundary conditions are $\lim_{V\to\infty}\hat{P}_\mu(V) = 0$ and $\lim_{V\to\infty}\hat{J}_\mu(V) = \hat{\nu}_\mu$. The solution can be separated into two parts, one proportional to $\hat{\nu}_\mu$ and a second proportional to μ_1.

$$\hat{P}_\mu = \hat{\nu}_\mu\hat{p}_\nu + \mu_1\hat{p}_\mu \text{ and } \hat{J}_\mu = \hat{\nu}_\mu\hat{j}_\nu + \mu_1\hat{j}_\mu \tag{16}$$

The resulting pair of equations can be numerically integrated yielding the linear response rate amplitude and phase lag.

Similarly, for variance-modulations of the input current, the expansion of the flux satisfies in first order:

$$\tau_\mathrm{m}\frac{\partial \hat{J}_{\sigma^2}}{\partial V} = i\omega\hat{P}_{\sigma^2} + \hat{\nu}_{\sigma^2}\delta(V-V_\mathrm{th}) - \hat{\nu}_{\sigma^2}\delta(V-V_\mathrm{re}) \tag{17}$$

$$-\frac{\partial \hat{P}_{\sigma^2}}{\partial V} = \begin{cases} \frac{\tau_\mathrm{m}}{\sigma_0^2}\left(\frac{-\mu_0 - a_\mathrm{S}(V-V_\mathrm{G})^2}{\tau_\mathrm{m}}\hat{P}_{\sigma^2} + \hat{J}_{\sigma^2} + F_{\sigma^2}\right) & V \le V_\mathrm{G} \\ \frac{\tau_\mathrm{m}}{\sigma_0^2}\left(\frac{-\mu_0 - a_\mathrm{U}(V-V_\mathrm{G})^2}{\tau_\mathrm{m}}\hat{P}_{\sigma^2} + \hat{J}_{\sigma^2} + F_{\sigma^2}\right) & V > V_\mathrm{G}. \end{cases} \tag{18}$$

The inhomogeneous term F_{σ^2} is defined by $F_{\sigma^2} = -\frac{\partial J}{\partial \sigma^2}P_0$. It is given by

$$F_{\sigma^2} = \begin{cases} \frac{\sigma_1^2}{\sigma^2}(-\mu - a_\mathrm{S}(V-V_\mathrm{G})^2 - V_\mathrm{T}) & V \le V_\mathrm{G} \\ \frac{\sigma_1^2}{\sigma^2}(-\mu - a_\mathrm{U}(V-V_\mathrm{G})^2 - V_\mathrm{T}) & V > V_\mathrm{G}. \end{cases} \tag{19}$$

The linear response is obtained with the same threshold integration scheme as above.

High-frequency limit: The high-frequency response is obtained by expanding $\hat{P}(t)$ in $\frac{1}{\omega}$ similarly to [14, 16]. The response to modulations of the mean is:

$$\hat{\nu}_\mu(\omega) = \nu_0\mu_1 r(r+1)\frac{1}{(i\omega\tau_\mathrm{m})^2} \tag{20}$$

The high-frequency response for modulations of the variance is:

$$\hat{\nu}_\sigma(\omega) = 3\nu_0\sigma_1^2 r^2(r+1)^2\frac{1}{(i\omega\tau_\mathrm{m})^3} \tag{21}$$

The excellent agreement between analytical high-frequency response and the Fokker-Planck approach is shown in **Fig. 3**. Extending previous work, the functional form of the voltage dependence of the activation variable of fast sodium currents decides how well the spiking of a fluctuation-driven neuron can reflect high frequency input [16–20]. High spike onset rapidness allows neurons to precisely position its spikes in time. For low spike onset rapidness neurons are susceptible to input fluctuations after crossing the unstable fixed point V_U. High frequency components in the input are then washed out and only weakly reflected in the spiking. Therefore, in the presence of noise, the spikes of neurons with high action potential onset rapidness can convey more information about high-frequency input currents. To make this statement quantitative, we calculated a lower bound on the mutual information rate between input current and spike trains (Section IV).

Analytical high-frequency response for high rapidness limit: The high-frequency response in the limit of large rapidness is also obtained by expanding $\hat{P}(t)$ in $\frac{1}{\omega}$ for $r = \infty$. In this case $V_\mathrm{G} = V_\mathrm{U}$ acts as a hard threshold and neurons crossing it spike instantaneously. The high-frequency response to modulations of the mean is, as for the leaky integrate-and-fire neuron:

$$\hat{\nu}_\mu = \frac{\nu_0\mu_1}{\sqrt{i\omega\tau_\mathrm{m}}} \tag{22}$$

IV. MUTUAL INFORMATION RATE AND ACTION POTENTIAL ONSET RAPIDNESS

Figure 1 h of main paper.

Lower bound on mutual information rate: With information theory we can treat a neuron as a noisy communication channel transforming a signal embedded in a noisy current into a spiking response sent to its postsynaptic partners. The mutual information rate measures how much the uncertainty about the input $x(t)$ is reduced given the spiking output $y(t)$ per unit time:

$$R(X,Y) = h(Y) - h(Y|X) = h(X) - h(X|Y) = \lim_{T\to\infty} \frac{1}{T} \int_X \int_Y p(x,y) \log_2 \left(\frac{p(x,y)}{p(x)p(y)} \right) \tag{23}$$

where $p(x,y)$ is the joint probability density function of $x(t)$ and $y(t)$, $h(X)$ and $h(Y)$ are their entropy rates and $h(X|Y)$ is the conditional entropy rate of $x(t)$ given $y(t)$. The continuous Gaussian channel gives a lower bound on the mutual information rate for a Gaussian input signal [26, 27]:

$$R(X,Y) = h(X) - h(X|Y) \geq h(X) - h_{\text{Gaussian}}(X|Y) = R_{\text{lb}}(X,Y) \tag{24}$$

The inequality results from the property that a Gaussian process has the maximum entropy of all processes with fixed variance. Recently it was shown that for moderate input modulation in a fluctuation driven regime this lower bound is very close to the mutual information rate estimated from direct methods [11]. This is convenient, because estimating the mutual information from empirical data is computationally costly, as the sample size has to be much larger than the size of the alphabet [21]. Continuous processes usually have to be discretized resulting in very large alphabets. In our case a Gaussian channel approximation to the mutual information rate between input current and output spike train was estimated based on the spectral coherence between input current and output spike train, which is based purely on second-order statistics.

$$R_{\text{lb}}(X,Y) = -\int_0^{f_{\text{cutoff}}} df \log_2 \left(1 - C_{xy}(f)\right) \tag{25}$$

$C_{xy}(f)$ denotes the magnitude squared spectral coherence. The spectral coherence is the frequency-domain analog of correlation and measures the linear relationship between frequency components of input and output signal. Its magnitude square is

$$C_{xy}(f) = \frac{|S_{xy}(f)|^2}{|S_{xx}(f)||S_{yy}(f)|} \tag{26}$$

$S_{xx}(f)$ is the power spectrum of band-limited Gaussian white noise:

$$S_{xx}(f) = \begin{cases} \sigma^2 & f \leq f_{\text{cutoff}} \\ 0 & \text{else.} \end{cases} \tag{27}$$

$S_{yy}(f)$ is the power spectrum of the spike train. $S_{yy}(f) = \lim_{T\to\infty} \frac{1}{T} \langle \tilde{y}\tilde{y}^* \rangle$, where $\tilde{y}(f)$ is the Fourier transform of the spike train. If and only if $x(t)$ and $y(t)$ are linearly scaled copies of each other, then $C_{xy}(f)$=1. If $x(t)$ and $y(t)$ are independent, then $C_{xy}(f)$=0, the reverse generally does not hold. Nonlinear effects and noise reduce the coherence. We calculated the spectral coherence in two independent ways: Firstly based on the numerical solution of the time-dependent Fokker-Planck equation and secondly based on direct numerical simulations with band-limited white noise. The time-dependent Fokker-Planck solution using the threshold integration scheme above yields a linear response approximation of $S_{xy}(f)$ directly from the linear response. Assuming weak modulations of the input, the stationary power spectrum of the spike train is sufficient, which can be obtained using again threshold integration [14]. The dependence of $S_{yy}(f)$, $S_{xy}(f)$ and $C_{xy}(f)$ on rapidness r and mean rate ν_0 are depicted in **Fig. 4**. At low rates, due to our scaling, neurons are in the fluctuation driven regime, therefore S_{yy} is flat. At high rates, which corresponds to a more mean driven regime, the response amplitude $\nu_{1\mu}$ has a resonance close to ν_0.

Fokker-Planck ansatz and direct numerical simulations with band-limited white noise are in excellent agreement (**Fig. 5**).

The mutual information rate scales approximately logarithmically with r. For large rapidness, the mutual information rate saturates. The saturation level is determined by the band limit of the incoming white noise (**Fig. 6**).

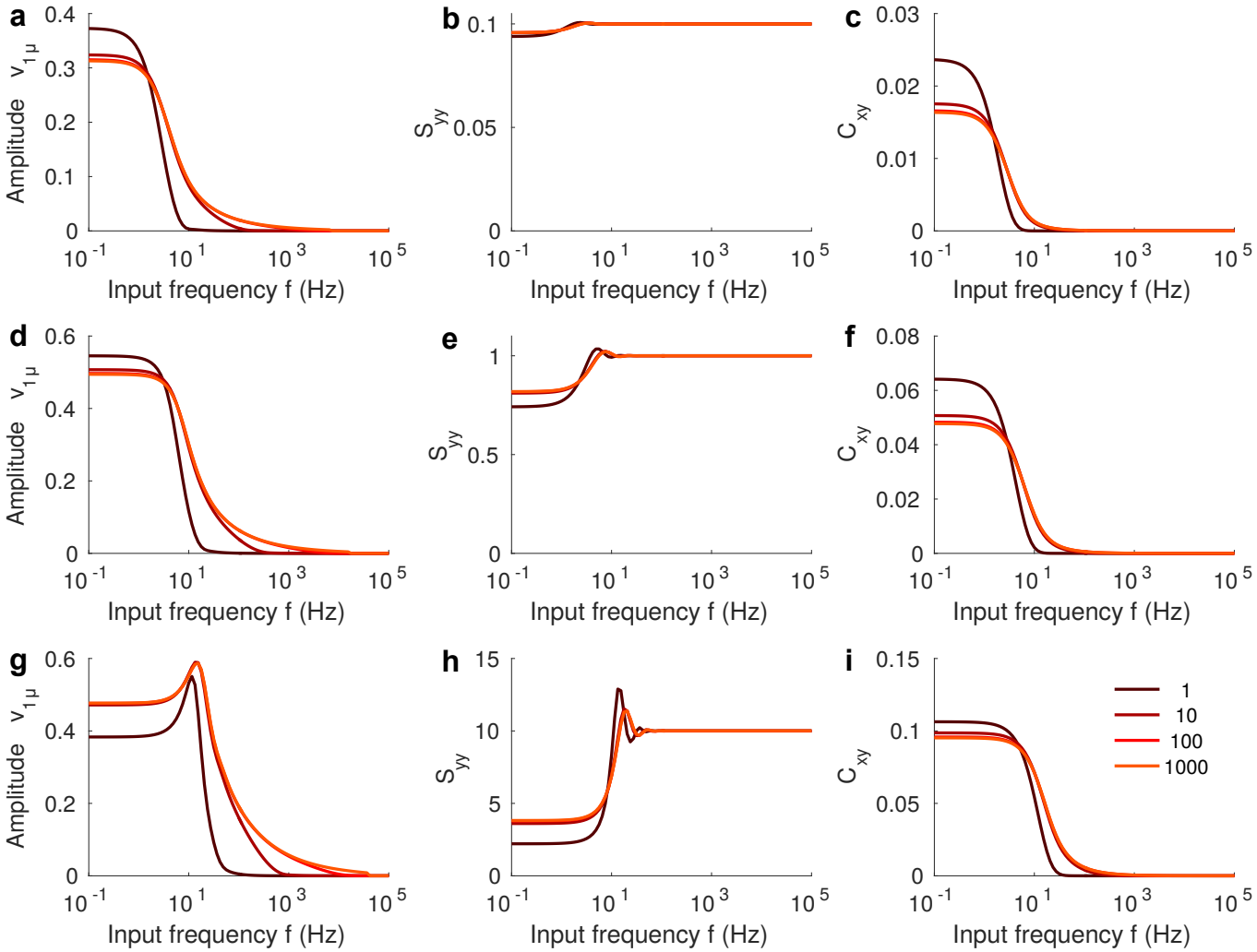

Figure 4: **Action potential onset rapidness r and ν_0 shape frequency-response, spike power spectra and spectral coherence: a)** Linear response for mean modulation of input current for $\nu_0 = 0.1\,\mathrm{Hz}$, **b)** Spike power spectra for different r for $\nu_0 = 0.1\,\mathrm{Hz}$. **c)** spectral coherence for different r for $\nu_0 = 0.1\,\mathrm{Hz}$. **d), e)** and **f)** same as **a**, **b** and **c** for $\nu_0 = 1\,\mathrm{Hz}$. At low rates, neurons are in the fluctuation driven regime, therefore S_{yy} is flat. At high rates (mean driven regime), the response amplitude $\nu_{1\mu}$ has a resonance close to ν_0 (parameters: $\nu_0 = 10\,\mathrm{Hz}$, $\mu_1 = 0.01$, $\tau_\mathrm{m} = 10\,\mathrm{ms}$, $\Delta V = 10^{-4}$, $V_\mathrm{th} = 10^4 = -V_\mathrm{r}$).

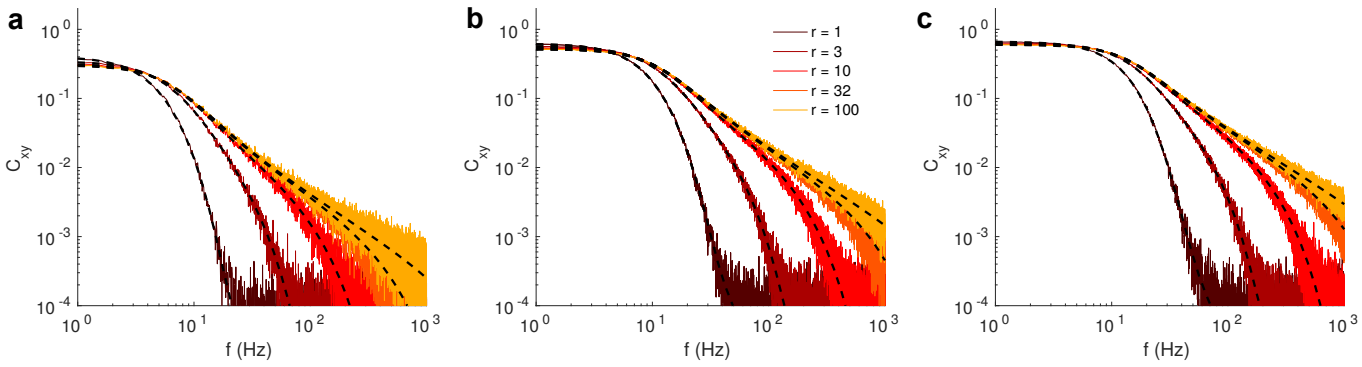

Figure 5: **Action potential onset rapidness r and ν_0 shape spectral coherence: (Fokker-Planck ansatz vs. direct numerical simulations). a)** $\nu_0 = 1\,\mathrm{Hz}$ **b)** $\nu_0 = 5\,\mathrm{Hz}$ **c)** $\nu_0 = 10\,\mathrm{Hz}$. C_{xy} normalized by input modulation μ_1^2 (parameters: $\mu_1 = 0.01$, $\tau_\mathrm{m} = 10\,\mathrm{ms}$, $\Delta V = 10^{-3}$, $V_\mathrm{th} = 10^3 = -V_\mathrm{r}$)

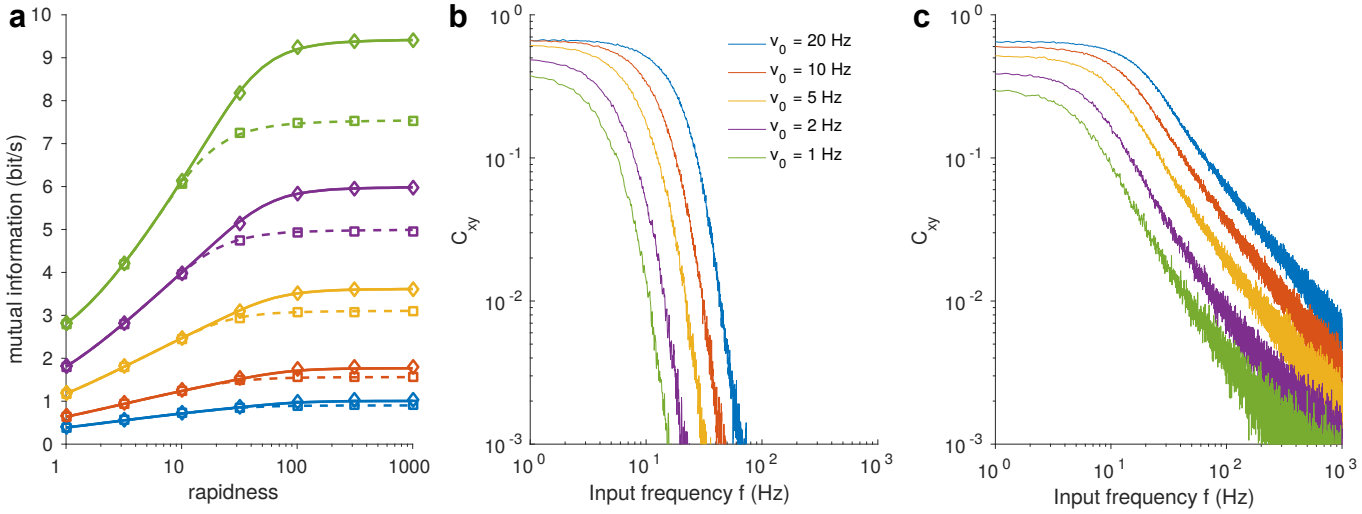

Figure 6: **Action potential onset rapidness r and ν_0 limit mutual information rate and spectral coherence**: **a)** Mutual information rate for two band limits of the incoming white noise: dashed lines for $f_{\text{bandlimit}} = 500\,\text{Hz}$ and full lines for $f_{\text{bandlimit}} = 2000\,\text{Hz}$ both from Fokker-Planck approach. Diamonds and squares are the corresponding direct numerical simulations with band-limited white noise input. **b)** Spectral coherence for different firing rates from direct numerical simulations $r = 1$. **c)** same as **b)** for $r = 1000$ (parameters: $\nu_0 = 10\,\text{Hz}$, $\mu_1 = 0.01$, $\tau_\text{m} = 10\,\text{ms}$, $\Delta V = 10^{-3}$, $V_\text{th} = 10^3 = -V_\text{r}$).

Dependence of mutual information rate on spike rapidness We know $S_{xy}(f)$ both in the high-frequency limit from the analytical high-frequency response and in the low-frequency limit, because for very low frequency input modulations ($f\tau_\text{m} \lll 1$), the spike rate follows adiabatically the input:

$$\lim_{f\to 0} S_{xy}(f) = \mu_1 \frac{\partial \nu_0}{\partial \mu} \tag{28}$$

This is the slope of the $\nu_0 - \mu$ curve depicted in **Fig. 2**. For renewal processes, one can show that for high input frequencies S_{yy} is given by the firing rate

$$\lim_{f\to \infty} S_{yy}(f) = \nu_0 \tag{29}$$

and for low input frequencies

$$\lim_{f\to 0} S_{yy}(f) = \nu_0 c v^2 \tag{30}$$

where cv is the coefficient of variation of the interspike intervals T: $\text{cv} = \sqrt{\langle T^2\rangle - \langle T\rangle^2}/\langle T\rangle$. For intermediate frequencies at intermediate to high onset rapidness, an approximation of the frequency-response of the rapid theta neuron can be obtained from the analytical high-frequency response for high rapidness (Eq. 22). The reason is that for intermediate input frequencies the glue point V_G acts like a hard threshold, if the time from threshold V_U to spike is smaller than the inverse frequency. Plugging these estimates into Eq. 26, we get an analytical approximation of the spectral coherence for different frequency regimes:

$$C_{xy}^{\text{low}}(f) = \frac{|S_{xy}(f)|^2}{|S_{xx}(f)||S_{yy}(f)|} = \frac{|\mu_1 \frac{\partial \nu_0}{\partial \mu}|^2}{\sigma^2 \nu_0 c v^2} = \mu_1^2 \frac{\left(\frac{\partial \nu_0}{\partial \mu}\right)^2}{\sigma^2 \nu_0 c v^2} \tag{31}$$

$$C_{xy}^{\text{mid}}(f) = \frac{|S_{xy}(f)|^2}{|S_{xx}(f)||S_{yy}(f)|} == \frac{|\frac{\nu_0 \mu_1}{\sqrt{i\omega\tau_\text{m}}}|^2 \sigma^4}{\sigma^2 \nu_0} = \frac{\nu_0 \mu_1^2 \sigma^2}{2\pi f \tau_\text{m}} \tag{32}$$

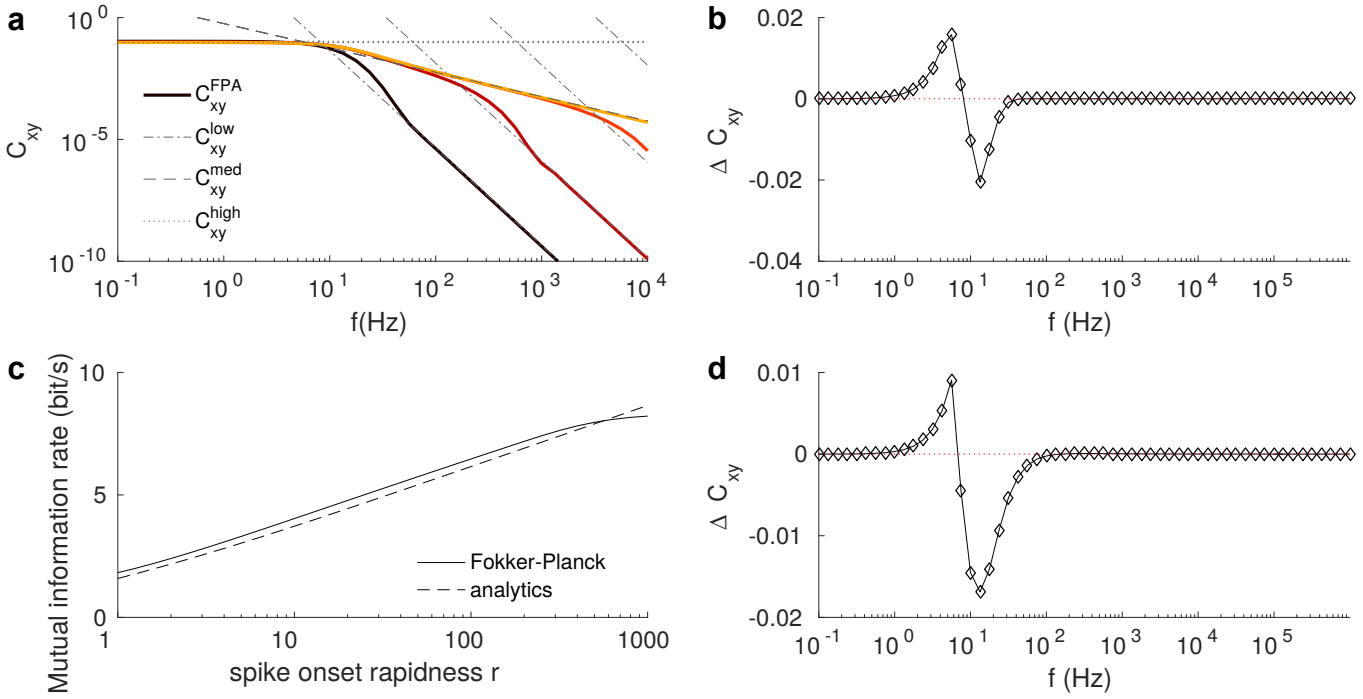

Figure 7: **Analytical estimate of the mutual information rate and spectral coherence explains logarithmic scaling with action potential onset rapidness** r $R_{\mathrm{lb}}(r) \propto \log(r)$**: a)** Spectral coherence obtained from Fokker-Planck ansatz vs analytical estimates for low mid and high frequency regime. Dashed line: high-rapidness scaling, dash-dotted line: high-frequency scaling, dotted line: low frequency estimate. **b)** Deviation between Fokker-Planck ansatz and analytical estimates for $r = 1$. **c)** comparison of mutual information rates obtained from Fokker-Planck ansatz vs. analytical estimate. **d)** Same as **b** for $r = 1000$ (parameters: $\nu_0 = 10\,\mathrm{Hz}$, $\mu_1 = 0.01$, $\tau_{\mathrm{m}} = 10\,\mathrm{ms}$, $\Delta V = 10^{-3}$, $V_{\mathrm{th}} = 10^3 = -V_{\mathrm{r}}$).

$$C_{xy}^{\mathrm{high}}(f) = \frac{|S_{xy}(f)|^2}{|S_{xx}(f)||S_{yy}(f)|} = \frac{|\frac{\nu_0\mu_1 r(r+1)}{(i\omega\tau_{\mathrm{m}})^2}|^2\sigma^4}{\sigma^2\nu_0} = \frac{\nu_0\mu_1^2 r^2(r+1)^2\sigma^2}{(2\pi f\tau_{\mathrm{m}})^4} \tag{33}$$

These estimates are precise in their respective limits of low and high frequencies. In the intermediate transition regimes, deviations occur (**Fig. 7**).

For intermediate mean firing rates the analytical low coherence estimate is overestimating the coherence, while at the transition zone the analytical intermediate estimate is underestimating the coherence. These two errors approximately compensate each other (**Fig. 7b**). For low rates, the overestimation in the analytical low coherence regime is smaller, therefore the analytically obtained approach underestimates the mutual information rate (**Fig. 8**).

For high firing rates, the analytical coherence estimate is strongly underestimating the coherence, therefore the analytical approach overestimates the mutual information rate (**Fig. 9**). The estimation errors are largely insensitive to rapidness, therefore the slopes are still in good agreement with the Fokker Planck approach.

The transition point between the low and intermediate regimes are obtained by calculating the crossings between $C_{xy}^{\mathrm{low}}(f)$ and $C_{xy}^{\mathrm{mid}}(f)$. We obtain:

$$f^{\mathrm{lm}}(r,\nu_0) = \frac{\nu_0^2\sigma^4 cv^2}{\left(\frac{\partial\nu_0}{\partial\mu}\right)^2\tau_{\mathrm{m}}} \tag{34}$$

For weak noise input, we obtain from Eq. 9 $\frac{\partial\nu_0}{\partial\mu} = \frac{1}{\pi\tau_{\mathrm{m}}}\sqrt{\frac{r}{2r(r+1)I_{\mathrm{ext}}}}$. The same is done for the second crossing with $C_{xy}^{\mathrm{mid}}(f)$ and $C_{xy}^{\mathrm{high}}(f)$:

$$f^{\mathrm{mh}}(r,\nu_0) = \left[r(r+1)\sqrt{(\nu_0\tau_{\mathrm{m}}}\right]^{2/3} \tag{35}$$

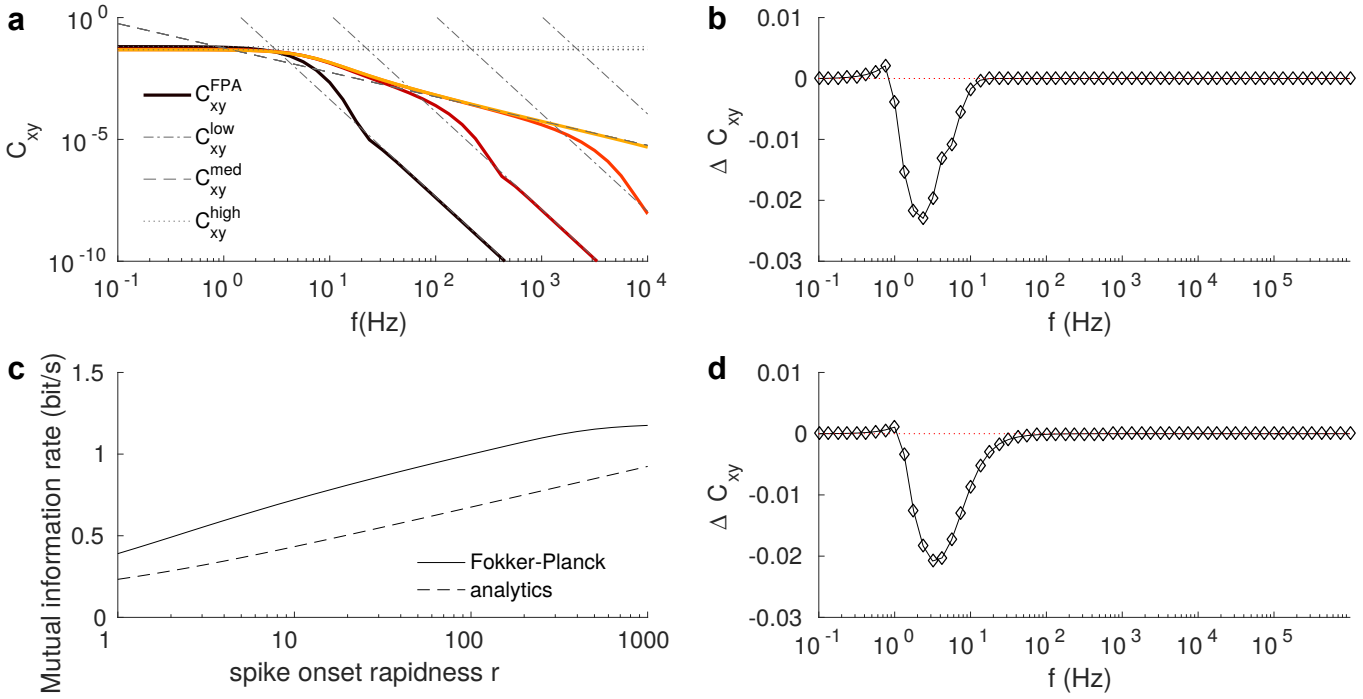

Figure 8: **Analytical estimate of the mutual information rate and spectral coherence with action potential onset rapidness r for low firing rate:** $\nu_0 = 1$ (parameters same as **Fig. 8**).

To obtain an analytical estimate of the mutual information rate, we stitched analytic high-, middle- and low-frequency estimates together at the transition points. Plugging into Eq. 25 gives us:

$$\begin{aligned} R_{\mathrm{lb}} &= R_{\mathrm{lb}} + R_{\mathrm{lb}} + R_{\mathrm{lb}} \\ &\approx -\int_0^{f_{\mathrm{lm}}} df \log_2\left(1 - C_{xy}^{\mathrm{low}}(f)\right) - \int_{f_{\mathrm{lm}}}^{f_{\mathrm{mh}}} df \log_2\left(1 - C_{xy}^{\mathrm{mid}}(f)\right) - \int_{f_{\mathrm{mh}}}^{f_{\mathrm{cutoff}}} df \log_2\left(1 - C_{xy}^{\mathrm{high}}(f)\right) \end{aligned} \tag{36}$$

Only the contribution of the intermediate frequency term changes strongly as a function of rapidness in the relevant parameter regime. To obtain a simple analytical estimate for the dependence on the rapidness, we have to evaluate only the second integral.

$$\begin{aligned} R_{\mathrm{lb}} &\approx -\int_{f_{\mathrm{lm}}}^{f_{\mathrm{mh}}} df \log_2\left(1 - C_{xy}^{\mathrm{mid}}(f)\right) \\ &= -\int_{f_{\mathrm{lm}}}^{f_{\mathrm{mh}}} df \log_2\left(1 - \frac{c_1}{f}\right) \\ &= \left[c_1 \log_2(f - c_1) - f \log_2(1 - \frac{c_1}{f})\right]_{f_{\mathrm{lm}}}^{f_{\mathrm{mh}}} \\ &= c_1 \log_2(f_{\mathrm{mh}} - c_1) - f_{\mathrm{lm}} \log_2(f_{\mathrm{lm}}) + (f_{\mathrm{lm}} - c_1) \log_2(f_{\mathrm{lm}} - c_1) - f_{\mathrm{mh}} \log_2\left(1 - \frac{c_1}{f_{\mathrm{mh}}}\right) \end{aligned} \tag{37}$$

As short-hand notation, we defined $c_1 = \frac{\nu_0 \mu_1^2 \sigma^2}{2\pi\tau_{\mathrm{m}}}$. Only the first term changes strongly as a function of rapidness, therefore

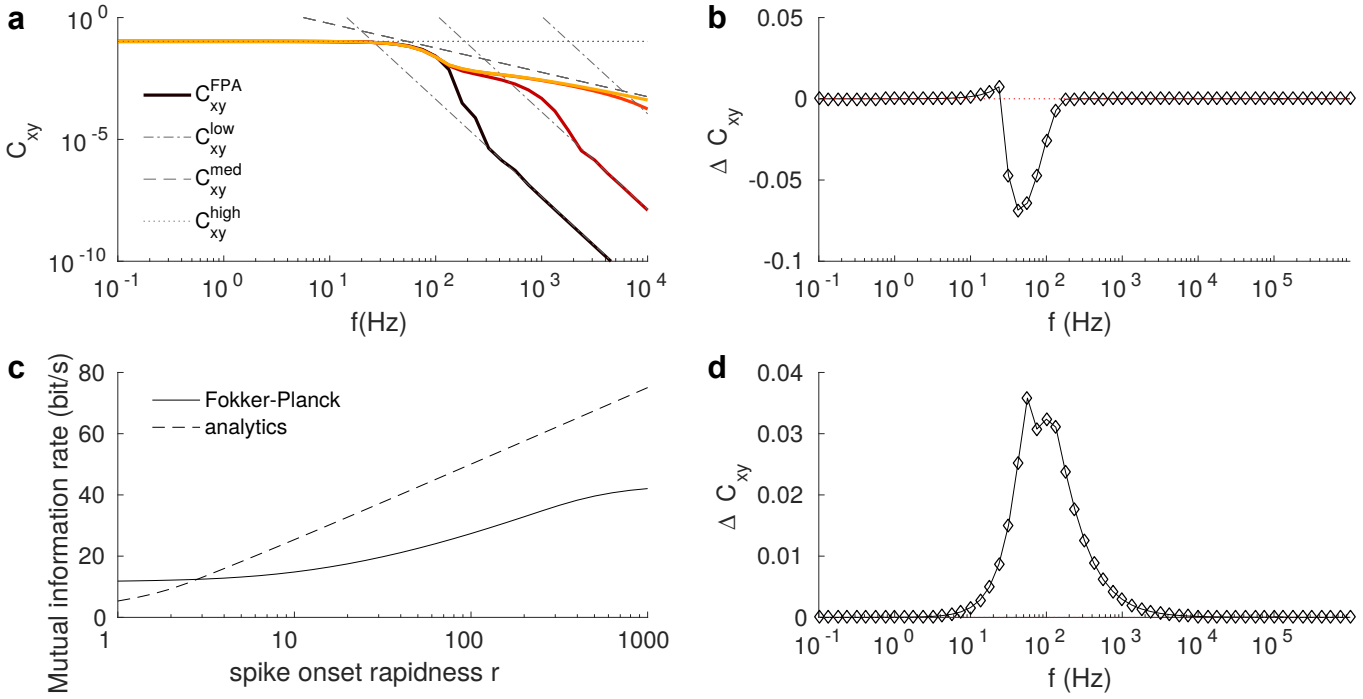

Figure 9: **Analytical estimate of the mutual information rate and spectral coherence for different values of action potential onset rapidness r for high firing rate** ($\nu_0 = 100$, other parameters same as **Fig. 8**).

$$
\begin{aligned}
R_{\mathrm{lb}}(r) &\approx c_1 \log_2(f_{\mathrm{mh}} - c_1) + const \\
&= c_1 \log_2\left(\left[r(r+1)\sqrt{(\nu_0\tau_{\mathrm{m}}}\right]^{2/3} - c_1\right) + const \\
&\overset{r\gg c_1}{\approx} c_1 \log_2\left(\left[r(r+1)\sqrt{(\nu_0\tau_{\mathrm{m}}}\right]^{2/3}\right) + const \\
&= c_1 \frac{2}{3} \log_2\left(r(r+1)\sqrt{(\nu_0\tau_{\mathrm{m}}}\right) + const \\
&= c_1 \frac{2}{3} \log_2\left(r(r+1)\right) + const \\
&\overset{r\gg 1}{\approx} c_1 \frac{4}{3} \log_2(r) + const \\
&= \frac{2\nu_0\mu_1^2\sigma^2}{3\pi\tau_{\mathrm{m}}} \log_2(r) + const
\end{aligned}
\tag{38}
$$

We conclude that the mutual information rate scales approximately logarithmically with action potential onset rapidness for sufficiently large rapidness, weak input and high band limit. Where does the logarithmically scaling of the mutual information rate with rapidness arises from? The reason is that the rapidness determines the cutoff frequency, up to which the rapid theta neuron transmits information approximately like a hard-threshold neuron (e.g. leaky integrate-and-fire neuron). Contributions from frequencies beyond this cutoff are negligible to first order. As a hard threshold always causes an asymptotic linear response $\propto 1/\sqrt{f}$, which becomes proportional to $1/f$ in the squared coherence, the integral that yields the lower bound of the mutual information (Eq. 25) always scales approximately proportional to $\log(f_{\mathrm{cutoff}})$, therefore $R_{\mathrm{lb}}(r) \propto \log(r)$. This conclusion is not restricted to the rapid theta model, a similar line of argumentation holds also e.g. for the exponential integrate and fire model and the rapid-τ model [16, 20]. For the exponential integrate and fire neuron model, the mutual information rate also scales approximately logarithmically with the action potential onset rapidness parameter $1/\Delta_T$ despite the different asymptotic linear response, which scales $\hat{\nu}_\mu \propto \frac{1}{f}$ [16]. In the case of the rapid-τ model the same holds, despite the asymptotic linear response, which scales $\hat{\nu}_\mu \propto \frac{1}{\sqrt{f}} \exp(\frac{\omega}{r})$ [20].

V. PHASE REPRESENTATION OF THE RAPID THETA NEURON

A phase representation of the rapid theta neuron model similar to the classical theta neuron model is obtained with the transformation $\tan\frac{\theta}{2} = V - V_{\mathrm{G}}$ and $\theta \in [-\pi, \pi)$, yielding

$$\tau_{\mathrm{m}}\frac{\mathrm{d}\theta}{\mathrm{d}t} = \begin{cases} \frac{r+1}{2r}\big(1-\cos\theta\big) + \big(I(t)-I_{\mathrm{T}}\big)\big(1+\cos\theta\big) & \theta \le 0 \\ \frac{r(r+1)}{2}\big(1-\cos\theta\big) + \big(I(t)-I_{\mathrm{T}}\big)\big(1+\cos\theta\big) & \theta > 0. \end{cases} \tag{39}$$

For $r = 1$ the theta neuron model is recovered.

The exact solutions of the rapid theta neuron model for constant positive external currents and δ pulse coupling allow us to write down a phase representation with constant phase velocity. Such a phase representation is convenient both for efficient, numerically exact, event-based simulation and also for analytical tractability.

The solution of the governing differential equation in the dimensionless voltage representation (1) for constant input currents $I(t) \equiv I_{\mathrm{T}} + I$ is

$$\begin{aligned} \frac{1}{I}\frac{\mathrm{d}V}{1+\left(\frac{V-V_{\mathrm{G}}}{\sqrt{I/a_{\mathrm{S,U}}}}\right)^2} &= \frac{1}{\tau_{\mathrm{m}}}\mathrm{d}t \\ \frac{1}{I}\sqrt{I/a_{\mathrm{S,U}}}\left[\arctan\left(\frac{V-V_{\mathrm{G}}}{\sqrt{I/a_{\mathrm{S,U}}}}\right)\right]_{V_1}^{V_2} &= \frac{t_2-t_1}{\tau_{\mathrm{m}}} \\ \arctan\left(\frac{V_2-V_{\mathrm{G}}}{\sqrt{I/a_{\mathrm{S,U}}}}\right) &= \arctan\left(\frac{V_1-V_{\mathrm{G}}}{\sqrt{I/a_{\mathrm{S,\,U}}}}\right) + \sqrt{I\,a_{\mathrm{S,U}}}\frac{t_2-t_1}{\tau_{\mathrm{m}}}. \end{aligned} \tag{40}$$

This equation represents the solution for both branches of Eq. (1) separated by V_{G} as before. For the subthreshold part ($V \le V_{\mathrm{G}}$), the curvature is $a_{\mathrm{S}} = \frac{r+1}{2r}$ and for the suprathreshold part ($V > V_{\mathrm{G}}$), the curvature is $_{\mathrm{U}} = \frac{r(r+1)}{2}$. In the phase representation with phase $\phi \in [-\pi, \pi)$ and constant phase velocity, the phase evolution is given by

$$\phi_2 = \phi_1 + \omega\frac{t_2-t_1}{\tau_{\mathrm{m}}}. \tag{41}$$

Identifying Eq. (40) and (41), enables us to derive the constant phase velocity ω and the gluing point ϕ_{G} to define the transformation between the two representations

$$\frac{\phi-\phi_{\mathrm{G}}}{\omega} = \arctan\left(\frac{V-V_{\mathrm{G}}}{\sqrt{I/a_{\mathrm{S,U}}}}\right)\frac{1}{\sqrt{I\,a_{\mathrm{S,U}}}}. \tag{42}$$

During one complete cycle, the time T_{S} spent in the subthreshold part ($V_2 = V_{\mathrm{G}}$ and $V_1 \to -\infty$) and the time T_{U} spent in the suprathreshold part ($V_2 \to \infty$ and $V_1 \to V_{\mathrm{G}}$) was obtained from Eq. (40):

$$T_{\mathrm{S}} = \frac{\pi\tau_{\mathrm{m}}}{\sqrt{2I(r+1)/r}} \quad \text{and} \quad T_{\mathrm{U}} = \frac{\pi\tau_{\mathrm{m}}}{\sqrt{2I(r+1)r}}.$$

The time spent in the subthreshold part is thus $T_{\mathrm{S}}/T_{\mathrm{U}} = r$ times as long as the one in the suprathreshold part. The total cycle length, or unperturbed interspike interval, is thus

$$\begin{aligned} T^{\mathrm{free}} &= (r+1)T_{\mathrm{U}} \\ &= \frac{\pi\tau_{\mathrm{m}}}{\sqrt{I}}\sqrt{\frac{r+1}{2r}}. \end{aligned} \tag{43}$$

Its inverse gives the firing rate for constant external input.

The constant phase velocity is then

$$\begin{aligned} \omega &= \frac{2\pi}{T^{\mathrm{free}}} \\ &= \frac{2\sqrt{I}}{\tau_{\mathrm{m}}}\sqrt{\frac{2r}{r+1}} = \frac{2}{\tau_{\mathrm{m}}}\sqrt{I/a_{\mathrm{S}}} \end{aligned} \tag{44}$$

The phase corresponding to the gluing point is

$$\begin{aligned}\phi_{\mathrm{G}} &= -\pi + \omega T_{\mathrm{S}} \\ &= \pi \frac{r-1}{r+1}.\end{aligned} \tag{45}$$

The constant phase velocity (44) and the gluing point (45) define the transformation (42) between the voltage representation and the phase representation:

$$\phi = \phi_{\mathrm{G}} + \begin{cases} \frac{2}{a_{\mathrm{S}}} \arctan\left(\frac{V-V_{\mathrm{G}}}{\sqrt{I/a_{\mathrm{S}}}}\right) & V \le V_{\mathrm{G}} \\ \frac{2}{ra_{\mathrm{S}}} \arctan\left(r\frac{V-V_{\mathrm{G}}}{\sqrt{I/a_{\mathrm{S}}}}\right) & V > V_{\mathrm{G}} \end{cases} \tag{46}$$

$$V = V_{\mathrm{G}} + \begin{cases} \sqrt{I/a_{\mathrm{S}}} \tan\left(a_{\mathrm{S}}\frac{\phi-\phi_{\mathrm{G}}}{2}\right) & \phi \le \phi_{\mathrm{G}} \\ \sqrt{I/r^2 a_{\mathrm{S}}} \tan\left(ra_{\mathrm{S}}\frac{\phi-\phi_{\mathrm{G}}}{2}\right) & \phi > \phi_{\mathrm{G}}. \end{cases} \tag{47}$$

This transformation between the two equivalent representations is now used to calculate the phase-transition curve $g(\phi)$ and the phase-response curve $Z(\phi)$. Receiving a δ pulse of strength J leads to a step like change of the neuron's voltage $V^+ = V^- + J$. If this change does not lead to a change from the subthreshold to the suprathreshold part or reverse, the calculation of the phase-transition curve is straightforward. Some care needs to be taken, if the δ pulse does lead to such a change.

An inhibitory pulse $J < 0$ can lead to a change from the suprathreshold to the subthreshold part. This happens if the neuron's phase is between ϕ_{G} and ϕ_-. The phase-transition curve for inhibitory δ pulses of strength J and constant external currents I with the effective coupling $C = J/\sqrt{I}$ and $\phi_- = \phi_{\mathrm{G}} + \frac{2}{ra_{\mathrm{S}}} \arctan\left(r(V_{\mathrm{G}} - J - V_{\mathrm{G}})/\sqrt{I/a_{\mathrm{S}}}\right) = \phi_{\mathrm{G}} - \frac{2}{ra_{\mathrm{S}}} \arctan\left(r\sqrt{a_{\mathrm{S}}}C\right)$ is

$$\mathrm{g}_-(\phi) = \phi_{\mathrm{G}} + \begin{cases} \frac{2}{a_{\mathrm{S}}} \arctan\left(\tan\left(a_{\mathrm{S}}\frac{\phi-\phi_{\mathrm{G}}}{2}\right) + \sqrt{a_{\mathrm{S}}}C\right) & -\pi < \phi \le \phi_{\mathrm{G}} \\ \frac{2}{a_{\mathrm{S}}} \arctan\left(\frac{1}{r}\tan\left(ra_{\mathrm{S}}\frac{\phi-\phi_{\mathrm{G}}}{2}\right) + \sqrt{a_{\mathrm{S}}}C\right) & \phi_{\mathrm{G}} < \phi < \phi_- \\ \frac{2}{ra_{\mathrm{S}}} \arctan\left(\tan\left(ra_{\mathrm{S}}\frac{\phi-\phi_{\mathrm{G}}}{2}\right) + r\sqrt{a_{\mathrm{S}}}C\right) & \phi_- \le \phi < \pi. \end{cases} \tag{48}$$

For excitatory δ pulses of strength $J > 0$, the phase can change from the subthreshold to the suprathreshold part if the phase is between ϕ_+ and ϕ_{G}. The phase-transition curve for excitatory δ pulses of strength J and constant external currents I with the effective coupling $C = J/\sqrt{I}$ and $\phi_+ = \phi_{\mathrm{G}} - \frac{2}{a_{\mathrm{S}}} \arctan(\sqrt{a_{\mathrm{S}}}C)$ (displayed in **Fig. 10**) is

$$g_+(\phi) = \phi_{\mathrm{G}} + \begin{cases} \frac{2}{a_{\mathrm{S}}} \arctan\left(\tan\left(a_{\mathrm{S}}\frac{\phi-\phi_{\mathrm{G}}}{2}\right) + \sqrt{a_{\mathrm{S}}}C\right) & -\pi < \phi \le \phi_+ \\ \frac{2}{ra_{\mathrm{S}}} \arctan\left(r\tan\left(a_{\mathrm{S}}\frac{\phi-\phi_{\mathrm{G}}}{2}\right) + r\sqrt{a_{\mathrm{S}}}C\right) & \phi_+ < \phi < \phi_{\mathrm{G}} \\ \frac{2}{ra_{\mathrm{S}}} \arctan\left(\tan\left(ra_{\mathrm{S}}\frac{\phi-\phi_{\mathrm{G}}}{2}\right) + r\sqrt{a_{\mathrm{S}}}C\right) & \phi_{\mathrm{G}} \le \phi < \pi. \end{cases} \tag{49}$$

The phase-response curve is $Z_\pm(\phi) = g_\pm(\phi) - \phi$. Thus, the infinitesimal phase-response curve is the same for both excitatory and inhibitory pulses, since $\phi_\pm \to \phi_{\mathrm{G}}$ for $C \to 0$:

$$Z(\phi) \overset{C\to 0}{\simeq} C \begin{cases} \frac{2\sqrt{a_{\mathrm{S}}}}{a_{\mathrm{S}}} \frac{1}{1+\tan\left(a_{\mathrm{S}}\frac{\phi-\phi_{\mathrm{G}}}{2}\right)^2} = \frac{1+\cos\left(a_{\mathrm{S}}(\phi-\phi_{\mathrm{G}})\right)}{\sqrt{a_{\mathrm{S}}}} & -\pi < \phi \le \phi_{\mathrm{G}} \\ \frac{2r\sqrt{a_{\mathrm{S}}}}{ra_{\mathrm{S}}} \frac{1}{1+\tan\left(ra_{\mathrm{S}}\frac{\phi-\phi_{\mathrm{G}}}{2}\right)^2} = \frac{1+\cos\left(ra_{\mathrm{S}}(\phi-\phi_{\mathrm{G}})\right)}{\sqrt{a_{\mathrm{S}}}} & \phi_{\mathrm{G}} \le \phi < \pi. \end{cases} \tag{50}$$

VI. SINGLE SPIKE JACOBIAN OF THE RAPID THETA NEURON NETWORK

The analytical expression of the derivative of the evolution map, called the single spike Jacobian, is necessary for calculating the full Lyapunov spectrum with high precision. The single spike Jacobian describes the linear evolution of infinitesimal perturbations of the neuron's states and will be used to numerically calculate the Lyapunov spectra. Since infinitesimal perturbations are considered here, the spike-order in the networks is preserved. This is true as long

as there are no exactly synchronous spike events which generally should not occur in the considered asynchronous network states. In a phase representation, the iterative map, which maps the state of the network at one spike time to the state at the next spike in the network, reads

$$\phi_i(t_{s+1}) = \phi_i(t_s) + \omega_i(t_{s+1} - t_s) + Z\big(\phi_i(t_s) + \omega_i(t_{s+1} - t_s)\big)\delta_{i\in\mathrm{post}(j^*)}, \tag{51}$$

where $\delta_{i\in\mathrm{post}(j^*)}$ is one if i is a postsynaptic neuron of the spiking neuron j^* and zero otherwise and $Z(\phi_i)$ is the phase-response curve.

Thus, the single spike Jacobian reads

$$D_{ij}(t_s) = \frac{\mathrm{d}\phi_i(t_{s+1})}{\mathrm{d}\phi_j(t_s)} = \begin{cases} 1 + Z'(\phi_{i^*}(t_{s+1}^-)) & \text{for } i = j = i^* \\ -\frac{\omega_{i^*}}{\omega_{j^*}} Z'(\phi_{i^*}(t_{s+1}^-)) & \text{for } i = i^* \text{ and } j = j^* \\ \delta_{ij} & \text{otherwise,} \end{cases} \tag{52}$$

where j^* denotes the spiking neuron in the considered interval, firing at time t_{s+1}, $i^* \in \mathrm{post}(j^*)$ are the spike receiving neurons and δ_{ij} is the Kronecker delta. The derivatives of the phase-response curves $Z'(\phi)$ are evaluated at the phases of the spike receiving neurons $\phi_{i^*}(t_{s+1}^-) = \phi_{i^*}(t_s) + \omega_{i^*}(t_{s+1} - t_s)$ just before spike reception. To investigate the collective dynamics of networks of rapid theta neurons, the derivative $d(\phi_{i^*}(t_{s+1}^-)) = 1 + Z'(\phi_{i^*}(t_{s+1}^-))$ of the phase-transition curve is needed for the single spike Jacobians. The derivative $d(\phi)$ in case of inhibitory pulses is

$$d_-(\phi) = \begin{cases} \frac{\tan\left(a_\mathrm{S}\frac{\phi-\phi_\mathrm{G}}{2}\right)^2+1}{\left(\tan\left(a_\mathrm{S}\frac{\phi-\phi_\mathrm{G}}{2}\right)+\sqrt{a_\mathrm{S}}C\right)^2+1} & -\pi < \phi \le \phi_\mathrm{G} \\ \frac{\tan\left(ra_\mathrm{S}\frac{\phi-\phi_\mathrm{G}}{2}\right)^2+1}{\left(\frac{1}{r}\tan\left(ra_\mathrm{S}\frac{\phi-\phi_\mathrm{G}}{2}\right)+\sqrt{a_\mathrm{S}}C\right)^2+1} & \phi_\mathrm{G} < \phi < \phi_- \\ \frac{\tan\left(ra_\mathrm{S}\frac{\phi-\phi_\mathrm{G}}{2}\right)^2+1}{\left(\tan\left(ra_\mathrm{S}\frac{\phi-\phi_\mathrm{G}}{2}\right)+r\sqrt{a_\mathrm{S}}C\right)^2+1} & \phi_- \le \phi < \pi. \end{cases} \tag{53}$$

In the voltage representation, this derivative $d(V)$ will be useful for the analytical calculation of the mean Lyapunov exponent in section IX:

$$d_-(V) = \begin{cases} \frac{r^2(V-V_\mathrm{G})^2+\frac{I_0\sqrt{K}}{a_\mathrm{S}}}{\left(V-V_\mathrm{G}+C\sqrt{I}\right)^2+\frac{I_0\sqrt{K}}{a_\mathrm{S}}} & V \le V_\mathrm{G} \\ \frac{r^2(V-V_\mathrm{G})^2+\frac{I_0\sqrt{K}}{a_\mathrm{S}}}{\left(V-V_\mathrm{G}+C\sqrt{I}\right)^2+\frac{I_0\sqrt{K}}{a_\mathrm{S}}} & V_\mathrm{G} < V < V_- \\ \frac{r^2(V-V_\mathrm{G})^2+\frac{I_0\sqrt{K}}{a_\mathrm{S}}}{r^2\left(V-V_\mathrm{G}+C\sqrt{I}\right)^2+\frac{I_0\sqrt{K}}{a_\mathrm{S}}} & V_- \le V. \end{cases} \tag{54}$$

The derivative of the phase-transition curve in the case of excitatory pulses is

$$d_+(\phi) = \begin{cases} \frac{\tan\left(a_\mathrm{S}\frac{\phi-\phi_\mathrm{G}}{2}\right)^2+1}{\left(\tan\left(a_\mathrm{S}\frac{\phi-\phi_\mathrm{G}}{2}\right)+\sqrt{a_\mathrm{S}}C\right)^2+1} - 1 & -\pi < \phi \le \phi_+ \\ \frac{\tan\left(a_\mathrm{S}\frac{\phi-\phi_\mathrm{G}}{2}\right)^2+1}{\left(r\tan\left(a_\mathrm{S}\frac{\phi-\phi_\mathrm{G}}{2}\right)+r\sqrt{a_\mathrm{S}}C\right)^2+1} - 1 & \phi_+ < \phi < \phi_\mathrm{G} \\ \frac{\tan\left(ra_\mathrm{S}\frac{\phi-\phi_\mathrm{G}}{2}\right)^2+1}{\left(\tan\left(ra_\mathrm{S}\frac{\phi-\phi_\mathrm{G}}{2}\right)+r\sqrt{a_\mathrm{S}}C\right)^2+1} - 1 & \phi_\mathrm{G} \le \phi < \pi. \end{cases} \tag{55}$$

The derivative of the phase-response curve is $Z'_\pm(\phi) = d_\pm(\phi) - 1$ and the derivative of the infinitesimal phase-response curve is

$$Z'(\phi) \overset{C\to 0}{\simeq} -C \begin{cases} \sqrt{a_\mathrm{S}}\sin\left(a_\mathrm{S}(\phi-\phi_\mathrm{G})\right) & -\pi < \phi \le \phi_\mathrm{G} \\ r\sqrt{a_\mathrm{S}} - \sin\left(ra_\mathrm{S}(\phi-\phi_\mathrm{G})\right) & \phi_\mathrm{G} \le \phi < \pi. \end{cases} \tag{56}$$

The phase-transition curves (PTC, $g(\phi)$, Eq. (48) and (49)), the phase response curves (PRC, $Z(\phi) = g(\phi) - \phi$) and the infinitesimal phase-response curves (iPRC, Eq. (50)) of the rapid theta neuron model are displayed in **Fig. 10**. The iPRC of the theta neuron ($r = 1$) is fully symmetric, whereas for increasing AP onset rapidness r the iPRC becomes more and more asymmetric. In the limit $r \to \infty$ it becomes monotonically increasing/decreasing and one might expect that this can qualitatively change the collective network dynamics.

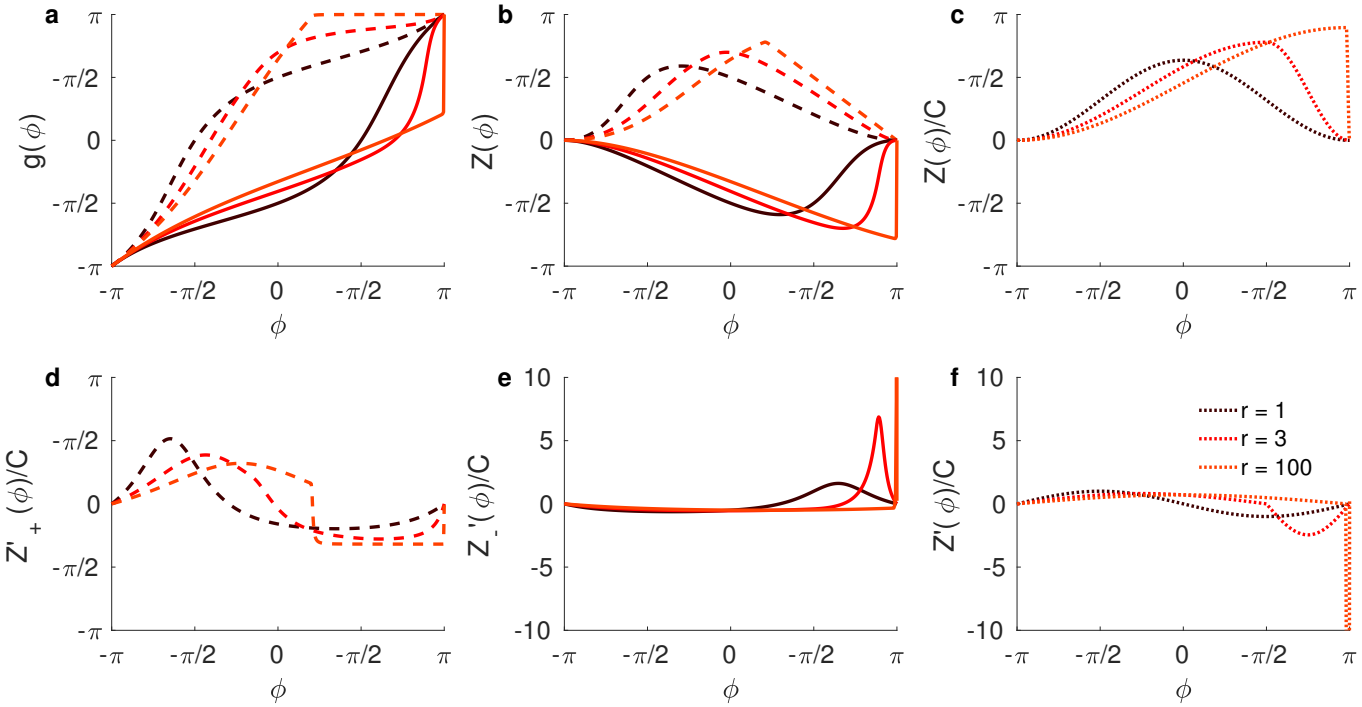

Figure 10: **Phase-transition curve (PTC), phase-response (PRC) and infinitesimal phase-response (iPRC) explain reduction of chaos for high AP onset rapidness** r. **a)** The phase-transition curve (PTC) $g(\phi)$ shown with inhibitory coupling $C = -1$ (full lines, Eq. (48)) and excitatory coupling $C = +1$ (dashed lines, Eq. (49)) for three values of spike onset rapidness $r = 1$, 3, 100. **b)** Same for phase response curve (PRC) $Z(\phi) = g(\phi) - \phi$. **c)** Same for infinitesimal PRC (Eq. (50)). **d)** Derivative of PRC for excitatory coupling. **e)** Derivative of PRC for excitatory coupling. **f)** Derivative of derivative of infinitesimal phase response curve (Eq. (56)). Note that in the limit $r \to \infty$ the iPRC becomes monotonically increasing and its derivative is positive almost everywhere.

VII. SETUP OF NETWORK AND EVENT-BASED SIMULATION

The pattern of action potentials in cortical tissue is asynchronous and irregular [29], despite reliable response of single neurons [30]. This is commonly explained by a balance of excitatory and inhibitory synaptic currents [33], which cancels large mean synaptic inputs. A dynamical self-organized balance can be achieved without fine-tuning of synaptic coupling strength, if the connectivity is inhibition-dominated [1]. The statistics of this state is described by a mean-field theory, which is largely independent of neuron model. We studied large sparse networks of N rapid theta neurons arranged on a directed Erdős–Rényi random graph of mean indegree K. All neurons $i = 1, \ldots, N$ received constant external currents I_{ext} and non-delayed δ-pulses from the presynaptic neurons $j \in \text{pre}\,(i)$. The external currents were chosen to obtain a certain average network firing rate $\bar{\nu}$ using a bisection method in purely inhibitory networks. In purely inhibitory networks the non-zero coupling strengths were set to $J_{ij} = -J_0/\sqrt{K}$ and all neurons received identical external currents. In two-population networks, the intra-population couplings were $J_{EE} = \frac{J_0}{\sqrt{K}}\eta\varepsilon$ and $J_{II} = -\frac{J_0}{\sqrt{K}}\sqrt{1-\varepsilon^2}$ for the excitatory (E) and inhibitory (I) population, respectively. The inter-population couplings were $J_{IE} = \frac{J_0}{\sqrt{K}}\varepsilon$ and $J_{EI} = -\frac{J_0}{\sqrt{K}}\sqrt{1-\eta^2\varepsilon^2}$. At $\varepsilon = 0$, all excitatory neurons are completely passive. They only receive inputs from the inhibitory neurons but do not provide feedback. Increasing $\varepsilon > 0$ activates the excitatory feedback loops in the network. The specific choice of couplings preserves the temporal variance of the input currents $\sigma_I^2 = J_0^2\bar{\nu}$ in the purely inhibitory networks for the two-population networks, as explained below. In mixed networks, the external currents were adapted using two-dimensional Newton-Raphson root-finding, to obtain the desired mean firing rate in the excitatory and inhibitory population.

Setup of balanced network with strong couplings and nonvanishing fluctuations. The coupling strengths in inhibitory and excitatory-inhibitory networks were chosen such that the magnitudes of the input current fluctuations were identical in all studied networks. Assuming that inputs from different presynaptic neurons are only weakly correlated, the compound input spike train received by neuron i can be modeled by a Poisson process with rate $\Omega_i = \sum_{j\in\text{pre}(i)} \nu_j \approx K\bar{\nu} \equiv \Omega$, where $\bar{\nu}$ is the network-averaged firing rate and K the average number of presynaptic

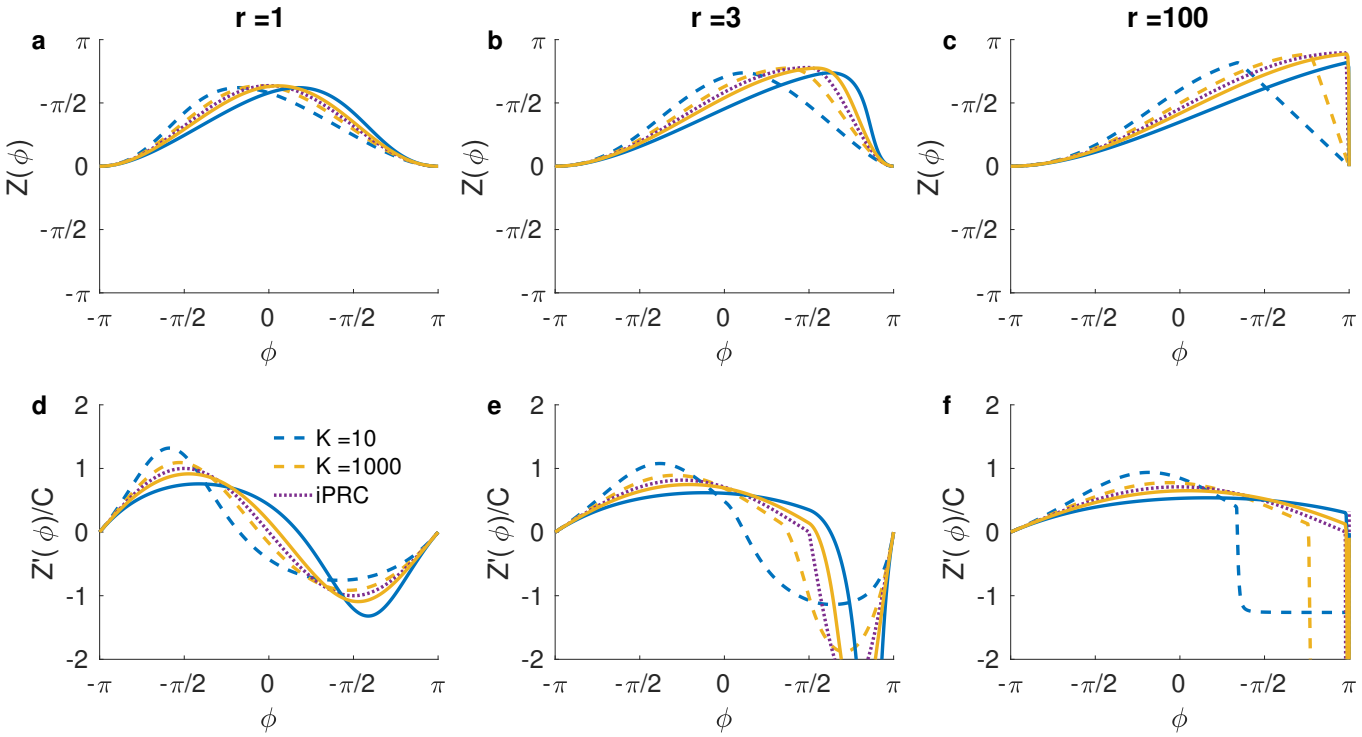

Figure 11: **Phase-response (PRC) and infinitesimal phase-response (iPRC) of the rapid-theta neuron model for different effective coupling strengths**. **a)** The PRC is shown for different K corresponding to different coupling strengths $C = -\frac{J_0}{\sqrt{K}}\sqrt{\frac{a_S}{I}}$ for inhibitory (full lines Eq. (48)) and excitatory couplings (dashed lines, Eq. (49)) for AP onset rapidness $r = 1$. The infinitesimal PRC (Eq. (50)) is also displayed for comparison (dotted lines) **b)** Same as **a** for AP onset rapidness $r = 3$ **c)** Same as **a** for AP onset rapidness $r = 100$. **d)** Derivative of PRC normalized by C for $r = 1$. The derivative of the infinitesimal PRC is shown as dotted line (Eq. (56)). **e)** Same as **d** for $r = 3$. **f)** Same as **d** for $r = 100$ (parameters: $I_0 = 1$, $J_0 = 1$).

neurons. For inhibitory networks the nonzero coupling strengths were $J_{ij} = -\frac{J_0}{\sqrt{K}}$. Under the assumption that the compound input spike train is a Poisson process, the input current auto-correlation function reads

$$\begin{aligned} C(\tau) &= \langle \delta I(t)\delta I(t+\tau)\rangle_t \\ &\approx \left(\frac{J_0}{\sqrt{K}}\right)^2 \Omega \int \delta(t-s)\delta(t+\tau-s)\mathrm{d}s \\ &= \frac{J_0}{K}\Omega\delta(\tau) \\ &\approx J_0^2\bar{\nu}\delta(\tau) \end{aligned} \tag{57}$$

Thus, the fluctuations in the input currents can be described as delta-correlated white noise of magnitude

$$\sigma^2 = J_0^2\bar{\nu}. \tag{58}$$

Note that due to the scaling of the coupling strengths $J = -\frac{J_0}{\sqrt{K}}$ with the square root of the number of synapses K the magnitude of the fluctuations σ^2 is independent of the number of synapses. Therefore, the input fluctuations do not vanish in the thermodynamic limit and the balanced state in sparse networks emerges robustly [1].

The existence of a balanced state fixed point in the large K-limit follows from the equation of the network-averaged mean current

$$\bar{I} \approx \sqrt{K}(I_I - J_0\bar{\nu}).$$

In the large K-limit, self-consistency requires the balance of excitation and inhibition $I_I = J_0\bar{\nu}$: If $\lim_{K\to\infty}(I_I - J_0\bar{\nu}) > 0$ the mean current $\bar{I}$ would diverge to ∞ and the neurons would fire at their maximal rate. The resulting strong

inhibition would break the inequality, leading to a contradiction. If $\lim_{K\to\infty}(I_I - J_0\bar{\nu}) < 0$ the mean current $\bar{I}$ would diverge to $-\infty$ and the neurons would be silent. The resulting lack of inhibition again breaks the inequality. The large K-limit is self-consistent if

$$\lim_{K\to\infty}(I_I - J_0\bar{\nu}) = \mathcal{O}\left(\frac{1}{\sqrt{K}}\right),$$

such that excitatory external drive and mean recurrent inhibitory current cancel each other. Note that since $I_I - J_0\bar{\nu} = \mathcal{O}(1/\sqrt{K})$ the network mean current has a finite large K-limit. The average firing rate in units of the membrane time constant τ_m is approximately

$$\bar{\nu} = \frac{I_I}{J_0} + \mathcal{O}\left(\frac{1}{\sqrt{K}}\right). \tag{59}$$

Setup of mixed network The input current autocorrelations in networks with excitatory (E) and inhibitory (I) populations are derived analogously to Eq. 57. They also display delta-correlated white noise. Assuming the same average indegree K from each population, the magnitudes of the input fluctuations are

$$\begin{aligned}\sigma_I^2 &= J_{II}^2\bar{\nu}_I + J_{IE}^2\bar{\nu}_E \\ \sigma_E^2 &= J_{EE}^2\bar{\nu}_E + J_{EI}^2\bar{\nu}_I.\end{aligned}$$

Choosing the couplings to be

$$\mathbf{J} = \begin{pmatrix} J_{EE} & -J_{EI} \\ J_{IE} & -J_{II} \end{pmatrix} = \frac{J_0}{\sqrt{K}} \begin{pmatrix} \eta\varepsilon & -\sqrt{1-(\eta\varepsilon)^2} \\ \varepsilon & -\sqrt{1-\varepsilon^2} \end{pmatrix}, \tag{60}$$

and the average firing rates in both populations identical $\bar{\nu}_E = \bar{\nu}_I \equiv \bar{\nu}$ leads to

$$\sigma_E^2 = \sigma_I^2 \equiv \sigma^2 = J_0^2\bar{\nu}.$$

Thus, the magnitude of fluctuations is identical in all networks considered independent of the excitatory feedback loop activation ε. Accordingly, the statistical characteristics of the balanced state were preserved when activating the excitatory loops. The dynamical features of the collective activity, however, changed upon activation of the excitatory loops. Increasing the excitatory coupling enhanced chaoticity in the network dynamics. It is important to note that the balanced state arises in an extended portion of parameters space in mixed networks. This region is constrained by the following inequalities, which can be derived by self-consistency arguments similar to those as for the purely inhibitory network:

$$\frac{J_{EE}}{J_{EI}} < \frac{J_{IE}}{J_{II}} < \min\left\{1, \frac{\bar{\nu}_I}{\bar{\nu}_E}\right\} \text{ and } \frac{J_{EE}}{J_{IE}} < \frac{J_{EI}}{J_{II}} < \frac{E_0}{I_0}. \tag{61}$$

The particular parametrization with η and ϵ was just used to keep the input statistics fixed.

All simulations were run event-based following Ref. [3], where an exact map was iterated from spike to spike in the ϕ-representation of the rapid theta neuron model with homogeneous coupling strengths and homogeneous external currents for all neurons in each population. The next spike time occurring in each population is obtained by inverting Eq. 41

$$t_s = t_{s-1} + \min_i\left\{\frac{\pi - \phi_i(t_{s-1})}{\omega}\right\}. \tag{62}$$

The phase map $f(\vec{\phi}(t_{s-1})) = \vec{\phi}(t_s)$, iterating all neuron's phases between two successive spike events t_{s-1} and t_s in the network, is then the concatenation of Eq. 41 and the phase transition curve (Eq. 48 and Eq. 49)

$$f(\phi_i(t_{s-1})) = \begin{cases} \phi_i(t_{s-1}) + \omega(t_s - t_{s-1}) & \text{if } i \notin \mathrm{post}(j^*) \\ g(\phi_i(t_{s-1}) + \omega(t_s - t_{s-1})) & \text{if } i \in \mathrm{post}(j^*), \end{cases} \tag{63}$$

where $\mathrm{post}(j^*)$ denotes the set of neurons postsynaptic to the spiking neuron j^* in the considered interval.

Eq. 63 was used for all network simulations in an iterative event-based procedure [3]. At the beginning of an iteration the next spike time in the network is calculated with Eq. (62). Then all neuron's phases are evolved until the next spike time with Eq. (63). Since the external currents are identical for all neurons of one population, it is sufficient to search for the neuron with the largest phase and then calculate the corresponding next spike time.

The average number of spikes per simulation time gives the firing rate. We used the interspike intervals T_i between subsequent spike times to calculate the coefficients of variation $\mathrm{cv}_i = \sqrt{\langle T_i^2\rangle - \langle T_i\rangle^2}/\langle T_i\rangle$, with $\langle\ldots\rangle$ denoting the temporal average. The neurons' firing rate and coefficient of variation distributions are shown in **Fig. 2** in the main manuscript.

VIII. CONVERGENCE OF THE LYAPUNOV SPECTRA

With the exact phases of the neurons before spike reception, the single spike Jacobians Eq. 52 were evaluated using Eq. 53 and Eq. 55. These were used to numerically calculate all Lyapunov exponents with the standard procedure [4]. Following a warmup of the network dynamics, of typically 100 spikes per neuron on average, we started with a random N-dimensional orthonormal system that was evolved in each iteration with the single spike Jacobian. Subsequently, after a short warmup of the orthonormal system of about one spike per neuron, these norms were used to calculate the N Lyapunov exponents $\lambda_i = \lim_{p\to\infty} \frac{1}{t_p}\sum_{s=1}^{p} \log g_i(t_s)$. The evolved vectors were reorthonormalized with the Gram-Schmidt-orthonormalization procedure every $\mathcal{O}(N/K)$ network spikes yielding the norms of the orthogonalized vectors $g_i(t_s)$ and the orthonormal system to be used in the following iterations.

All full calculations were performed in custom code written in Julia and C++ with double precision. The GNU Scientific Library (GSL) was used for the random number generator (Mersenne-Twister), the Automatically Tuned Linear Algebra Software (ATLAS) for matrix multiplications in the Gram–Schmidt procedure and the Message Passing Interface (MPI) for the parallel implementation of the simulations. The sparseness of the networks was used for the efficiently storage of the coupling matrices, the updates of the postsynaptic neurons and the matrix multiplications of the orthonormal system with the sparse single spike Jacobians. In the case of very large networks ($N > 10^6$), the topology was not stored as a sparse matrix, but generated on the fly during the simulation employing the index of the spiking neuron as a seed for the random number generator used to generate the indices of the postsynaptic neurons [31]. For the reorthonormalization, we chose a parallel recursive blocked version of the Gram–Schmidt procedure [5] and the BLAS (Basic Linear Algebra Subprograms) and LAPACK (Linear Algebra PACKage) routines.

One should note that the non-converged Lyapunov exponents generated during the transient are meaningless (they neither reflect the local nor finite-time Lyapunov exponents). The converged Lyapunov exponents capture the network dynamics on the balanced attractor. **Fig. 12a** displays the convergence towards the full Lyapunov spectrum on logarithmic time scale. This calculation was repeated for different initial phases. **Fig. 12b** shows the results of ten such runs for six of the Lyapunov exponents (gray lines), together with their averages $\lambda_i = \frac{1}{10}\sum_{n=1}^{10}\lambda_{i,n}$ (straight color lines) and confidence intervals (dotted color lines) of the double standard error $2\triangle\lambda_i = 2\sqrt{\frac{1}{10}\sum_{n=1}^{10}(\lambda_{i,n}-\lambda_i)^2}$. The Lyapunov spectrum was independent of the initial phases as well as network realizations. Generally, all calculations of the Lyapunov spectra were repeated ten times with different initial phases and network realizations. Numerical errors were usually smaller than the symbol sizes in the presented figures in the main manuscript.

Fig. 14 shows the double standard error of Lyapunov exponents, dynamical entropy rate and attractor dimension in random inhibitory networks across trials. **Fig. 15** shows the same for mixed networks. There are two main contributions for variability of numerically calculated Lyapunov spectra. Firstly, variability arising from the fact that Lyapunov spectra are asymptotic properties estimated from finite calculations. Secondly variability arising from the quenched disorder in different random network topologies. The first contribution would vanish in the limit of infinitely long simulations for ergodic systems. The second contribution is expected to vanish in the large networks limit due to self-averaging. Therefore, the Lyapunov spectrum of one realization of a large network is representative for the whole ensemble. Hence, averaging over many network realizations is not a necessity in large networks.

We applied three independent checks of this semi-analytic numerically exact calculation of Lyapunov spectra. Firstly, the largest Lyapunov exponent can be calculated numerically by measuring the exponential rate of divergence or convergence of nearby trajectories [4, 32]. Secondly, in autonomous systems, there is always a neutral Lyapunov vector in the direction of the flow with a zero corresponding Lyapunov exponent as the system can be shifted in time. Thirdly, random matrix theory allows for a calculation of the mean Lyapunov exponent as is shown in the next paragraph. All checks confirmed the results obtained from our implementation of the semi-analytic calculation of the full Lyapunov spectrum.

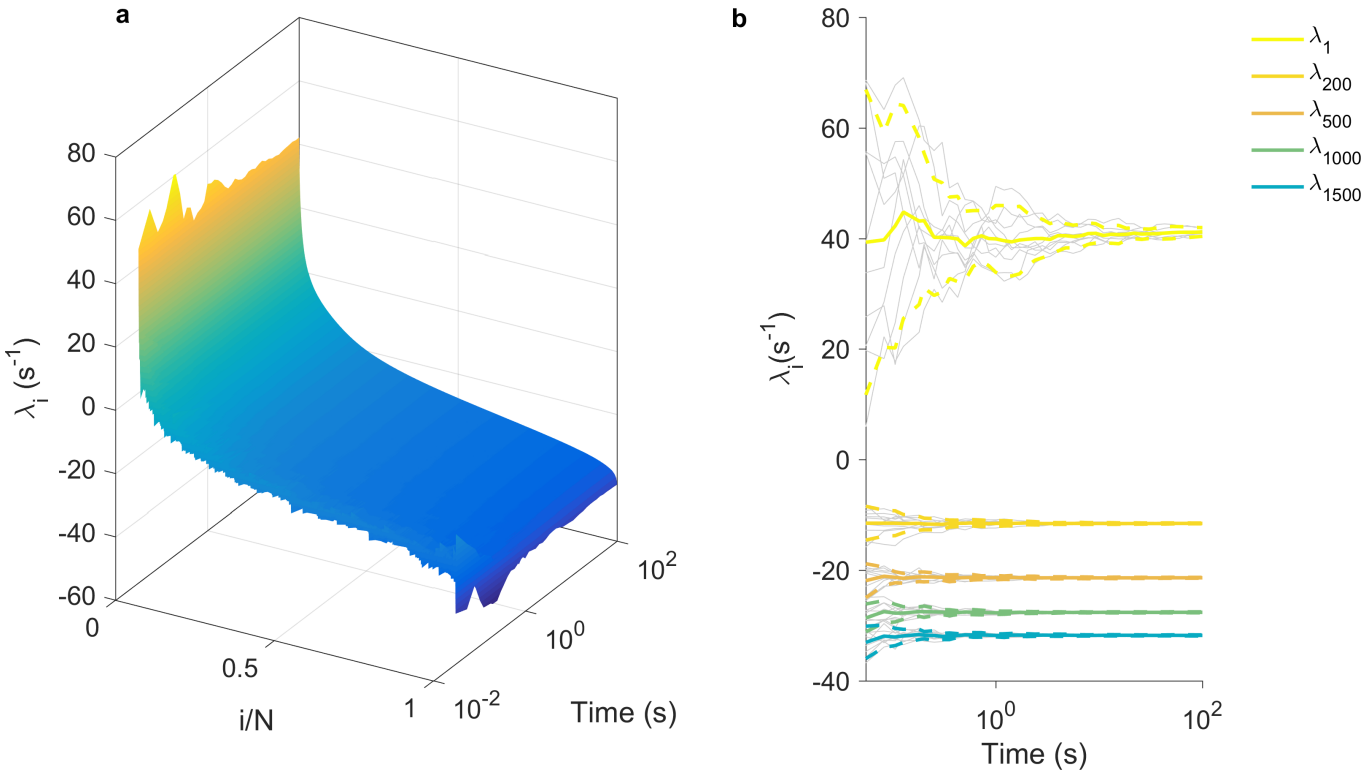

Figure 12: **Convergence of Lyapunov spectra versus time in inhibitory networks for small AP rapidness (r=3).** (logarithmic time scale) **a)** Convergence of Lyapunov spectrum for one initial condition, **b)** gray lines: some Lyapunov exponents for ten different network realizations, straight color lines: averages, dotted color lines: averages ± double standard errors (parameters: $N = 2000$, $\bar{\nu} = 1\,\mathrm{Hz}$, $K = 100$, $J_0 = 1$, $\tau_\mathrm{m} = 10\,\mathrm{ms}$).

IX. RANDOM MATRIX THEORY OF THE MEAN LYAPUNOV EXPONENT

From the single spike Jacobian Eq. 52, we derived a random matrix approximation of the mean Lyapunov exponent $\bar{\lambda} = \frac{1}{N}\sum_{i=1}^{N}\lambda_i$. The mean Lyapunov exponent describes the rate of phase space volume compression, captured by the determinant of the long term Jacobian $\mathbf{T} = \mathbf{D}(t_s)\cdots\mathbf{D}(0)$:

$$\begin{aligned}\bar{\lambda} &= \frac{1}{N}\lim_{s\to\infty}\frac{1}{t_s}\ln\big(\det\mathbf{T}\big)\\ &= \frac{1}{N}\lim_{s\to\infty}\frac{1}{t_s}\sum_{p=1}^{s}\ln\big(\det\mathbf{D}(t_p)\big).\end{aligned}\tag{64}$$

The random matrix approximation is obtained by assuming the single spike Jacobians to be random matrices of the form Eq. 52 with independent and identically distributed random elements obtained from the function $d(V)$, Eq. (54). The probability distribution of the random elements is determined by the stationary membrane potential distribution $P(V)$ in the network.

For inhibitory networks, the determinants of the random matrices can be approximated by $\det\mathbf{D} = \prod_{i^*} d_{i^*} \approx d(V)^K$, since on average there are K diagonal elements d_{i^*}, one for each postsynaptic neuron. We assume homogeneous coupling strengths $J_{ij} \equiv -J_0$ between connected neurons and identical external currents $I_i^{\mathrm{ext}} \equiv I_0$ for all neurons. The number of spike events per unit time is $\lim_{s\to\infty}\frac{1}{t_s}\sum_{p=1}^{s}1 = N\bar{\nu}$. Thus, in the random matrix approximation, the mean Lyapunov exponent for inhibitory networks becomes

$$\begin{aligned}\bar{\lambda} &\approx \frac{1}{N}N\bar{\nu}\int\ln\big(d(V)^K\big)P\big(V\big)\mathrm{d}V\\ &= K\bar{\nu}\int\ln d(V)\,P\big(V\big)\mathrm{d}V.\end{aligned}\tag{65}$$

We obtain $d(V)$ from Eq. (53) using Eq. (47)

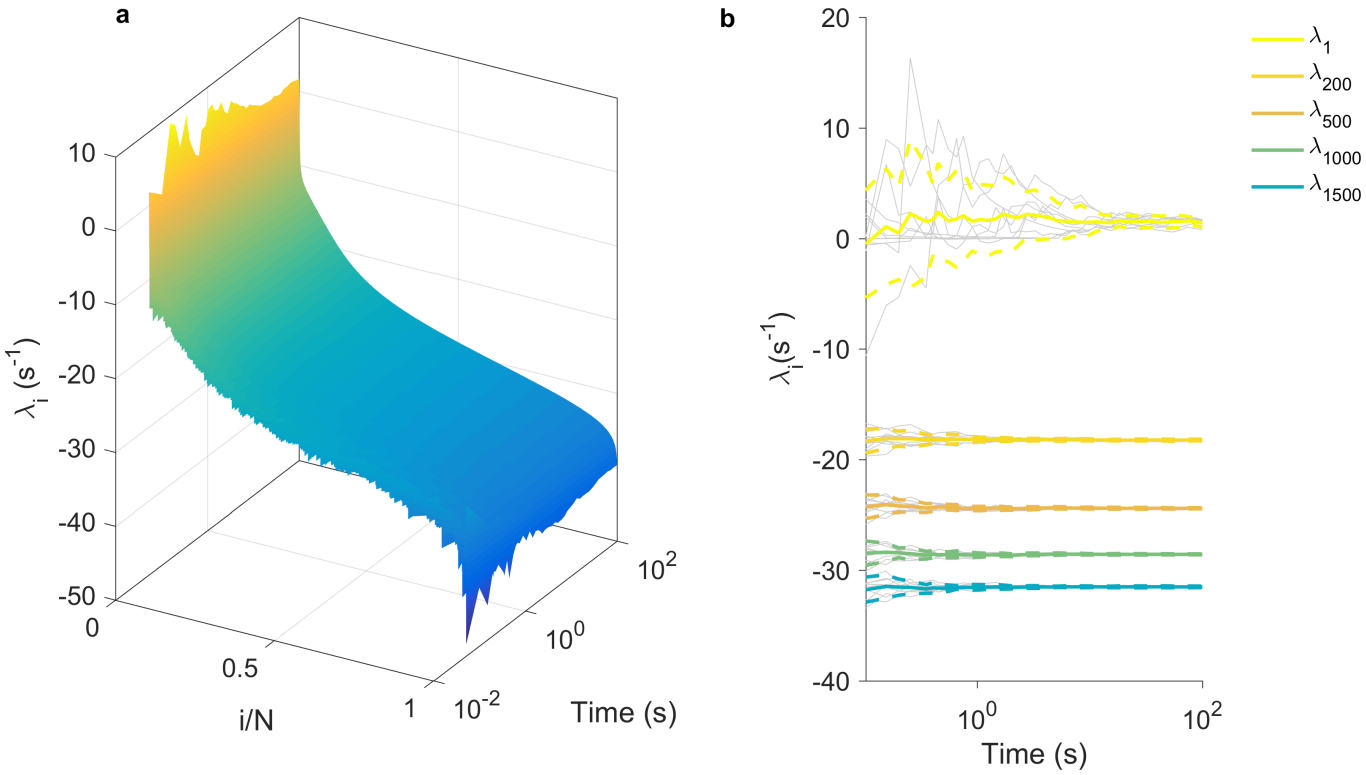

Figure 13: **Convergence of Lyapunov spectra versus time in inhibitory rapid theta networks for large AP rapidness (r=100).** (logarithmic time scale) **a)** Convergence of Lyapunov spectrum for one initial condition, **b)** gray lines: some Lyapunov exponents for ten different network realizations, straight color lines: averages, dotted color lines: averages ± double standard errors (parameters: $N = 2000$, $\bar{\nu} = 1\,\mathrm{Hz}$, $K = 100$, $J_0 = 1$, $\tau_\mathrm{m} = 10\,\mathrm{ms}$).

$$d_-(V) \;=\; \begin{cases} \dfrac{(V-V_\mathrm{G})^2+\frac{I_0\sqrt{K}}{a_\mathrm{S}}}{\left(V-V_\mathrm{G}+C\sqrt{I}\right)^2+\frac{I_0\sqrt{K}}{a_\mathrm{S}}} & V \le V_\mathrm{G} \\ \dfrac{r^2(V-V_\mathrm{G})^2+\frac{I_0\sqrt{K}}{a_\mathrm{S}}}{\left(V-V_\mathrm{G}+C\sqrt{I}\right)^2+\frac{I_0\sqrt{K}}{a_\mathrm{S}}} & V_\mathrm{G} < V < V_- \\ \dfrac{r^2(V-V_\mathrm{G})^2+\frac{I_0\sqrt{K}}{a_\mathrm{S}}}{r^2\left(V-V_\mathrm{G}+C\sqrt{I}\right)^2+\frac{I_0\sqrt{K}}{a_\mathrm{S}}} & V_- \le V. \end{cases} \tag{66}$$

In the large K-limit, $d(V)$ can be approximated by

$$d_-(V) \overset{K\to\infty}{\simeq} \begin{cases} 1+\frac{2a_\mathrm{S}J_0(V-V_\mathrm{G})}{I_0K}+\mathcal{O}\left(K^{3/2}\right) & V \le V_\mathrm{G} \\ 1+\frac{a_\mathrm{S}(r^2-1)(V-V_\mathrm{G})^2}{I_0\sqrt{K}}+\frac{\left(2a_\mathrm{S}J_0-(r^2-1)(V-V_\mathrm{G})^3\right)(V-V_\mathrm{G})}{I_0^2K}+\mathcal{O}\left(K^{3/2}\right) & V_\mathrm{G} < V < V_- \\ 1+\frac{2a_\mathrm{S}r^2J_0(V-V_\mathrm{G})}{I_0K}+\mathcal{O}\left(K^{3/2}\right) & V_- \le V. \end{cases} \tag{67}$$

These approximations and the balance equation (59) lead to

$$\bar{\lambda} \overset{K\to\infty}{\simeq} \frac{2a_\mathrm{S}\langle V_{V\le V_\mathrm{G}}\rangle}{\tau_\mathrm{m}}\alpha+\frac{2_\mathrm{U}\langle V_{V>V_\mathrm{G}}\rangle}{\tau_\mathrm{m}}(1-\alpha)+\mathcal{O}\left(\frac{1}{\sqrt{K}}\right), \tag{68}$$

where $\langle V_{V\le V_\mathrm{G}}\rangle$ ($\langle V_{V>V_\mathrm{G}}\rangle$) denotes the average membrane potential below (above) V_G and α is the fraction of neurons below V_G.

We have compared the derived random matrix approximations of the mean Lyapunov exponent in inhibitory networks Eq. (65) and the large-K limits, Eq. (68), with the results from simulations (**Fig. 16**). They are in very good agreement, indicating the validity of the random matrix approximation. This is probably the case because of the commutativity of the determinants of the Jacobians, a property that generally does not hold for the product of the Jacobians.

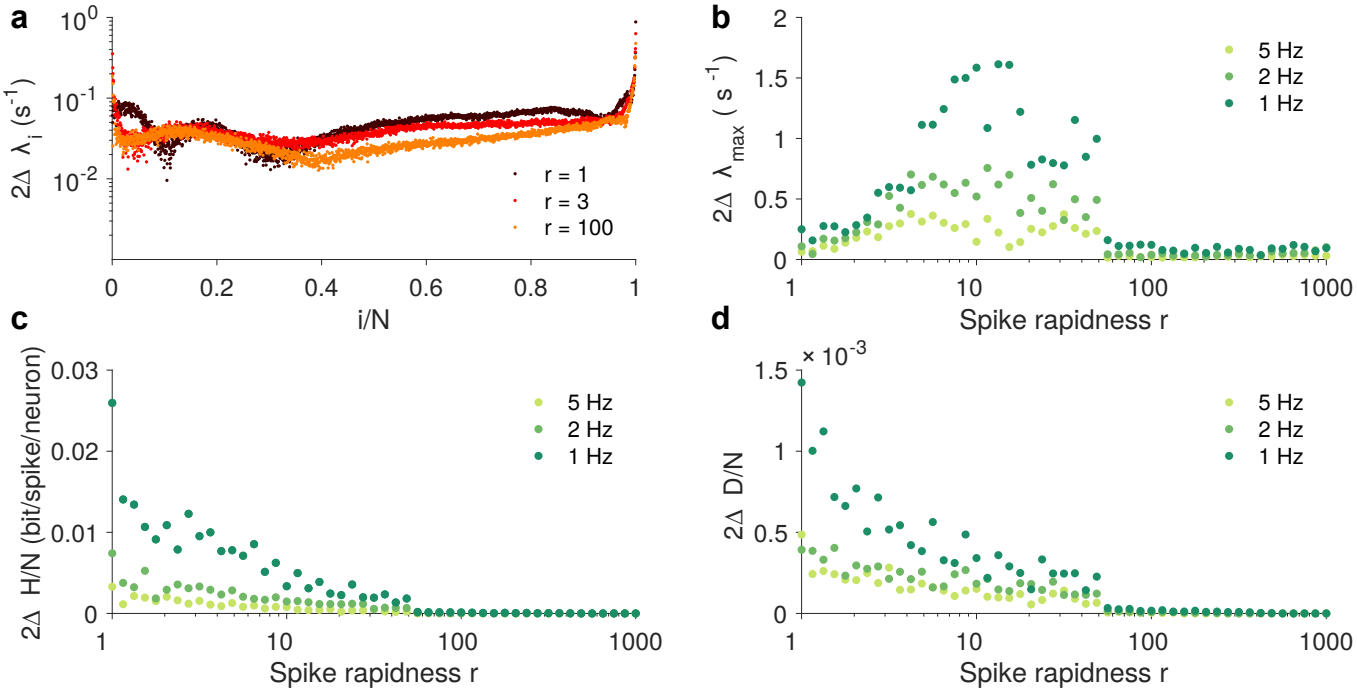

Figure 14: **Small double standard error of Lyapunov exponents, dynamical entropy rate and attractor dimension in random inhibitory network a)** double standard error of Lyapunov exponents across different network realizations for different values of rapidness. **b)** double standard error across network realizations of largest Lyapunov exponent for different values of rapidness. **c)** same as **b** for dynamical entropy rate. **d)** same as **b** for relative attractor dimension. Note that all standard errors are orders of magnitude smaller than the mean values for the respective quantities. ($N = 2000$, $K = 100$, $J_0 = 1$, $\tau_\mathrm{m} = 10\,\mathrm{ms}$).

X. SCALING OF THE LARGEST LYAPUNOV EXPONENT WITH NETWORK PARAMETERS

The largest Lyapunov exponent exhibits a single maximum as a function of action potential onset rapidness. The peak position scales approximately like (**Fig. 17**):

$$r_\mathrm{peak} \propto \sqrt{\frac{K\nu_0\tau_\mathrm{m}}{J_0}} \tag{69}$$

This behavior can be understood as a transition between two qualitatively different scaling regimes for the largest Lyapunov exponent. For small values of K and $\bar{\nu}$ the largest Lyapunov exponent grows, while for large values of K and $\bar{\nu}$ the largest Lyapunov exponent reaches a plateau. In the second regime the diffusion approximation is valid even beyond the glue point V_G during the fastest dynamical process in the neuron's spike initiation. When the diffusion approximation holds, the largest Lyapunov exponent thus becomes independent of K and $\bar{\nu}$ (**Fig. 18a-c**). Consequently, at high values of rapidness, the plateau is reached only at very large values of $\bar{\nu}$ and K. Further, the transition point depends on J_0. For small J_0, the plateau is reached for smaller values of K and $\bar{\nu}$ (**Fig. 18c**). These observations conform with two other findings: Firstly, for large values of rapidness r, the shot-noise nature of spiking input becomes especially relevant for the voltage distribution close to glue point V_G both for the stationary and the linear response solution of the Fokker-Planck equation (**Fig. 1** and **3**). Secondly, both the phase response curve and its derivative show a more pronounced deviation from the infinitesimal PRC and its derivative for large values of spike onset rapidness r (**Fig. 11**). Both these findings mean that for high spike rapidness r higher values of K and $\bar{\nu}$ or smaller values of J_0 are necessary for the diffusion approximation to hold.

The critical spike onset rapidness r_crit separates the chaotic dynamics from the stable dynamics. This transition with network parameters has the following scaling behavior (**Fig. 19**):

$$r_\mathrm{crit} = N^{0.5}K^{0.4}\bar{\nu}^{0.8}\tau_m^{0.8}J_0^{-0.7} \tag{70}$$

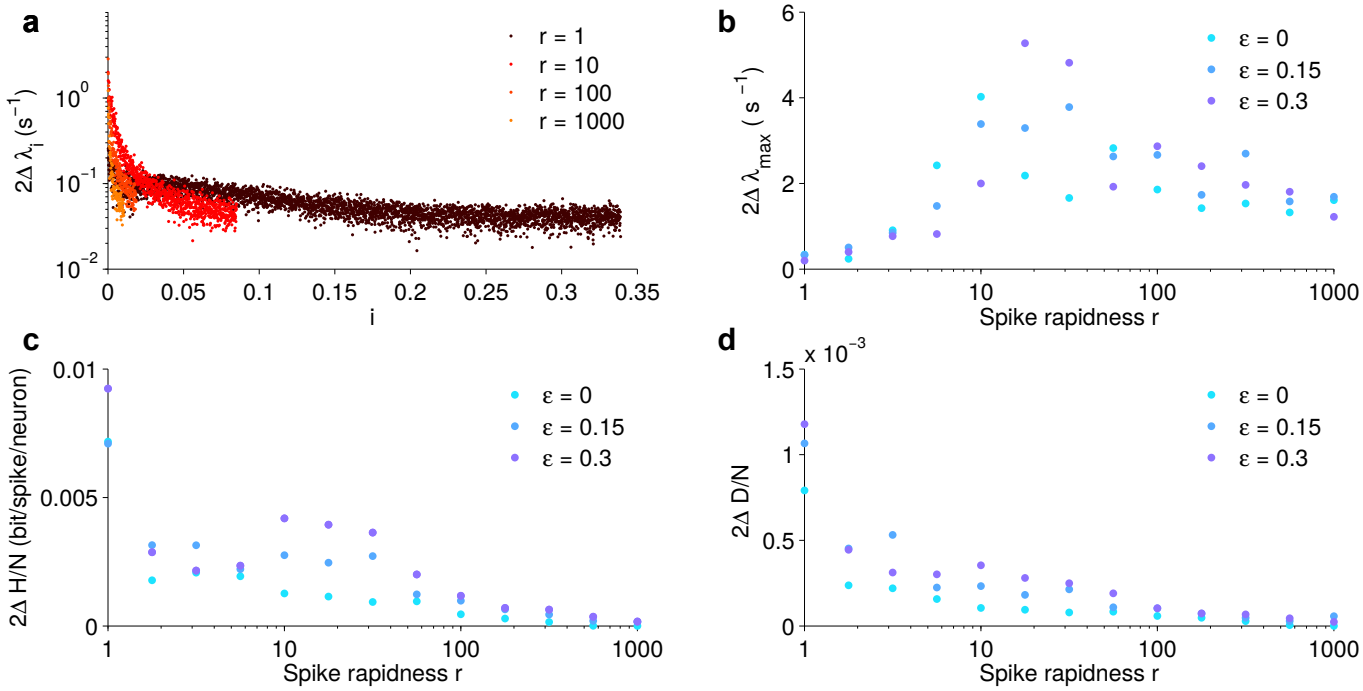

Figure 15: **Small double standard error of Lyapunov exponents, dynamical entropy rate and attractor dimension in random mixed network a)** double standard error of Lyapunov exponents across different initial conditions for different values of rapidness ($\epsilon = 0.3$). **b)** double standard error across network realizations of largest Lyapunov exponent for different values of rapidness. **c)** same as **b** for dynamical entropy rate. **d)** same as **b** for relative attractor dimension. Note that all standard errors are orders of magnitude smaller than the mean values for the respective quantities. ($N_E = 8\,000$, $N_I = 2\,000$, $K = 100$, $J_0 = 1$, $\tau_\mathrm{m} = 10\,\mathrm{ms}$).

This scaling indicates that in the thermodynamic limit of large K and large N, the critical rapidness r_crit diverges and the network is always chaotic. This is in agreement with the scaling of the flux tube radius of networks of leaky integrate and fire neurons, which goes to zero in the limit of large networks. Note however that even in the thermodynamic limit it is possible to bring the largest Lyapunov exponent and thus also the Kolmogorov Sinai entropy rate arbitrarily close to zero by increasing the AP onset rapidness r.

Extensivity of Lyapunov spectrum and asymptotic form: **Figure 2** and **3** of the main paper show that for sufficiently large networks the dynamical entropy rate and Kaplan-Yorke attractor dimension scales linear with network size N indicating extensive deterministic chaos. While the dynamical entropy rate and Kaplan-Yorke attractor dimension converge to a linear scaling with N already for moderate network size, the largest Lyapunov exponent exhibited a slower convergence to its large N limit (**Fig. 20**). While the peak rapidness r_peak is independent of N, $\lambda_\mathrm{max}(N)$ converges exponentially towards its large N limit. This exponential convergence allows an estimate of the asymptotic value $\lim_{N\to\infty} \lambda_\mathrm{max}(N)$, indicated in **Fig. 20b** by a dashed line. Note that the critical rapidness r_crit diverges with N as shown in **Fig. 19**.

XI. PARTICIPATION RATIO AND LOCALIZATION OF CHAOS

To quantify how many neurons contribute to the chaotic dynamics at each and every moment in time, we investigated properties of the covariant Lyapunov vectors $\delta\vec{\phi}^c(t)$. The first Lyapunov vector, which corresponds to the first Gram-Schmidt vector ($\sum_{i=1}^N \delta\phi_i(t)^2 = 1$) gives at any point in time the direction in which almost all initial perturbations grow with asymptotic rate λ_max. The number of neurons contributing to the maximally growing direction at time t can be measure by the participation ratio $P(t) = \left(\sum_{i=1}^N \delta\phi_i(t)^4\right)^{-1}$ [37–39]. If all neurons contribute similarly to the Lyapunov vector $|\delta\phi_i(t)| = 1/\sqrt{N}$ the participation ratio is $P(t) = 1/(N/N^2) = N$. If only one neurons contributes to the Lyapunov vector the participation ratio is $P(t) = 1$. We found that the participation ratio strongly dependent on the spike onset rapidness. Increasing rapidness generally reduced the participation ratio (**Fig. 21**) for

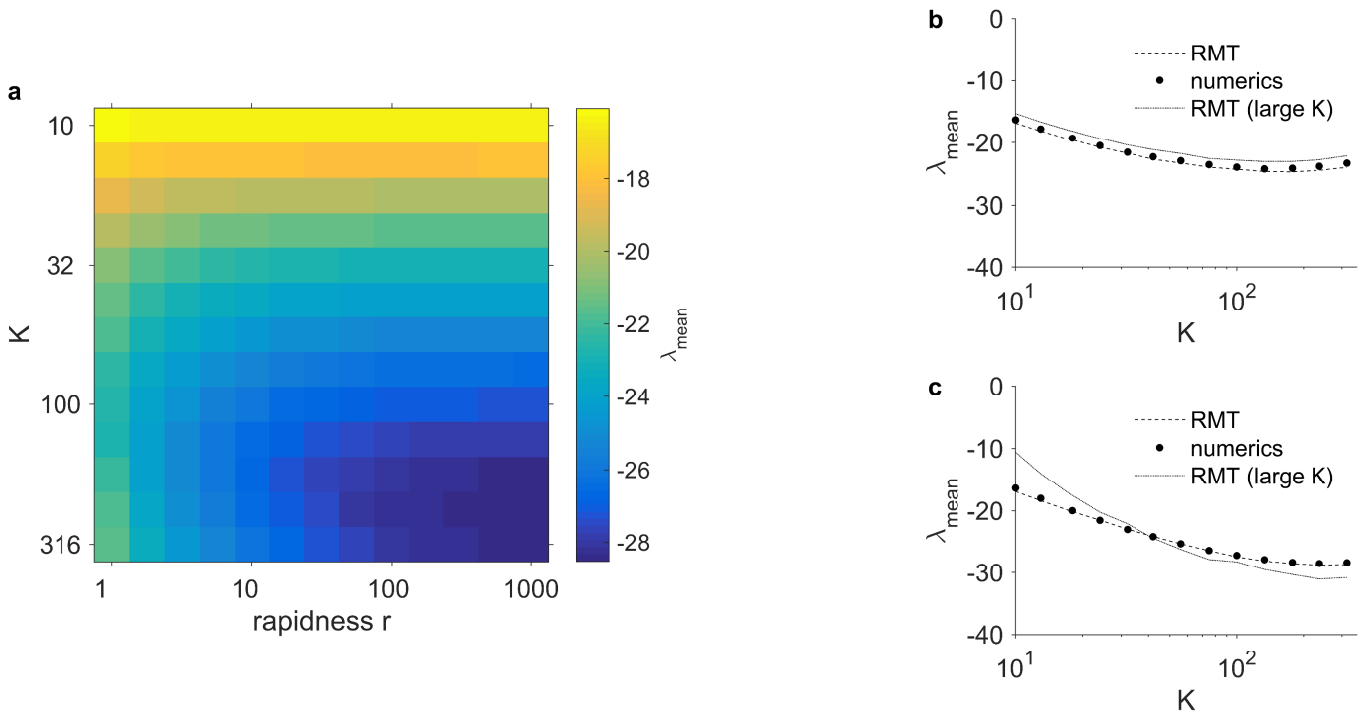

Figure 16: **Good match between mean Lyapunov exponent in random matrix approximations and numerical simulations in balanced theta neuron networks. a)** Mean Lyapunov exponent from numerical simulations for different K and r with $N = 1000$. **b)** K-dependence for $r = 3$. Straight lines: numerical simulations, dashed lines: random matrix approximations with full membrane potential distributions, dotted lines: random matrix approximation in the large K-limit **c)** K-dependence for $r = 100$. Eq. (68) (parameters: $\bar{\nu} = 1\,\mathrm{Hz}$, $J_0 = 1$, $\tau_\mathrm{m} = 10\,\mathrm{ms}$).

large networks. This means that for increasing rapidness fewer neurons contribute to the most unstable direction. On the level of the single neuron dynamics, this can be explained by a decreasing fraction of (postsynaptic) neurons that are in the unstable regime with voltages above the glue point V_G for increasing values of r. Thus, there exist on average fewer entries in the Jacobian with large entries $d(V_i)$. Therefore, the first Lyapunov vector is on average expected to have few entries with large values.

To further characterize the nature of the chaotic collective network state, it is crucial to investigate the scaling of the participation ratio $\bar{P}$ with network size. Whether the Lyapunov vector is called localized or delocalized depends on how $P(t)$ scales as a function of network size N. A delocalized state is indicated by a linear scaling $\bar{P} \sim N$, while in case of a localized state, the participation ratio would be independent of N.

In an earlier study of theta neurons, it was found that the Lyapunov vector was dominated by subsets of neurons that changed over time [12]. The participation ratio exhibited a sublinear scaling $\bar{P} \sim N^\alpha$, with $0 < \alpha < 1$. Here, we found a strong dependence of the participation ratio and localization on the spike onset rapidness r. For increasing spike onset rapidness r, the exponential scaling parameter α deceased approximately logarithmically as function of r and turned zero at a certain value of rapidness that depends on firing rate $\bar{\nu}$, coupling strength J_0, number of synapses per neuron K, and membrane time constant τ_m (**Fig. 22**). For larger values of rapidness, there was on average a fixed number of neurons contributing to the larger Lyapunov vector, which was independent of network size N for large networks. An extensive analysis of the scaling of the onset rapidness with network parameters where the localization occurred coincided with the scaling of the rapidness where the Lyapunov exponents peaks

$$r_\mathrm{localization} \propto \sqrt{\frac{K\nu_0\tau_\mathrm{m}}{J_0}}. \tag{71}$$

This scaling behavior indicates that localization of the first Lyapunov vector occurs when K, ν_0 or τ_m is sufficiently small or when J_0 is sufficiently large. This could be interpreted as localization, when there are few postsynaptic potentials per spike (K small), which occur infrequent (ν_0 or τ_m small), and/or are strong (J_0 large). This is consistent with a breakdown of the diffusion approximation close to the glue point V_G, if the Lyapunov vector is localized.

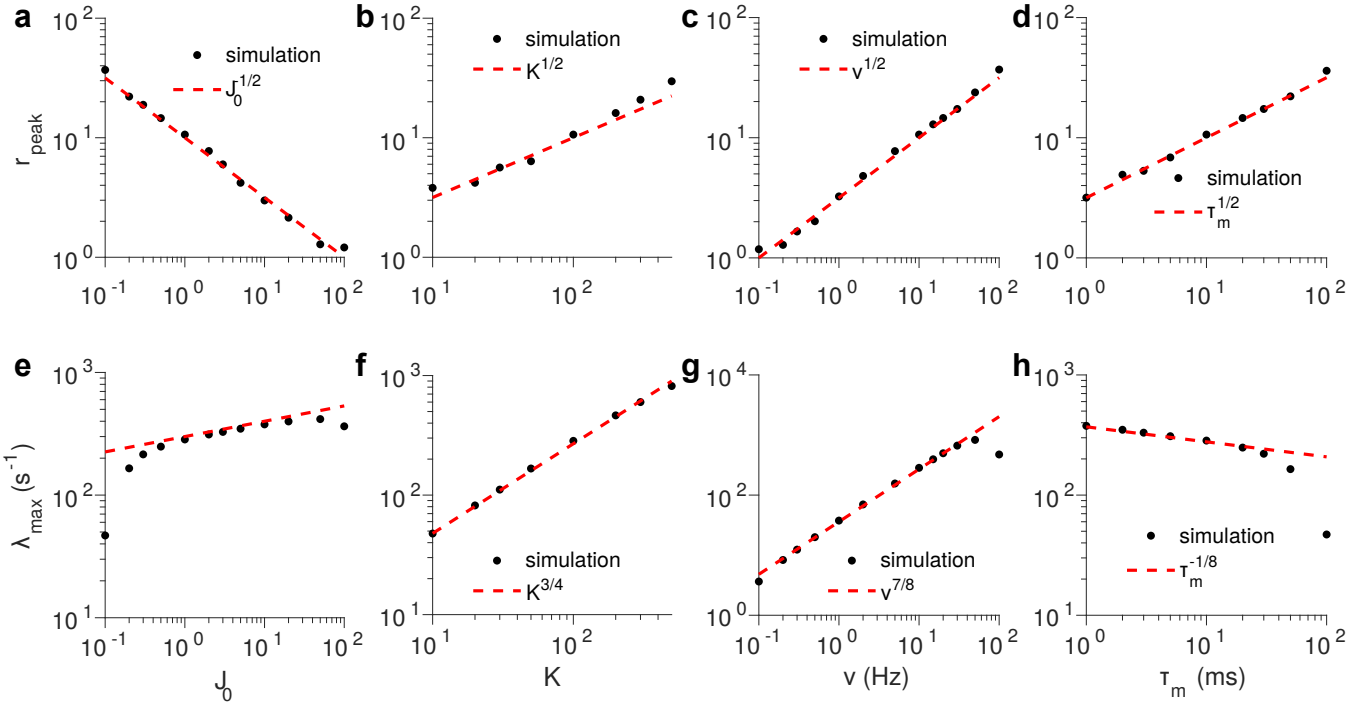

Figure 17: **Scaling of peak AP onset rapidness r_{peak} with network parameters in balanced inhibitory networks** $r_{\text{peak}} \propto \sqrt{K\nu_0\tau_{\text{m}}/J_0}$**.** At the peak onset rapidness r_{peak} the largest Lyapunov exponent has its maximum as a function of rapidness (**Fig. 2** of main paper). **a)** peak onset rapidness r_{peak} vs. J_0, dashed red lines indicate power-law fit using the Levenberg-Marquardt algorithm. **b)** peak onset rapidness r_{peak} vs. K. **c)** peak onset rapidness r_{peak} vs. J_0. **d)** peak onset rapidness r_{peak} vs. J_0. **e)-h)** Second row: corresponding peak onset rapidness $\lambda_{\max}$ (parameters: $\bar{\nu} = 1\,\text{Hz}$, $J_0 = 1$, $\tau_{\text{m}} = 10\,\text{ms}$, $N = 1000$, $K = 100$).

Note that despite the same scaling, localization occurs always at slightly larger values of rapidness than the peak in the largest Lyapunov exponent. So the first Lyapunov vector seems to localize not until the largest Lyapunov exponent is in the regime where it is independent of the number of synapses per neuron K.

For large values of spike onset rapidness r at a fixed network size N, we found that the participation ratio increases with rapidness until it saturates at $\bar{P} = N$ (**Fig. 23a**). This saturation occurred exactly at the critical spike onset rapidness r_{crit}, when the largest Lyapunov exponent becomes zero (**Fig. 23c**).

XII. PAIRWISE CORRELATIONS IN RAPID THETA NETWORKS

Figure 3 e-g of main paper. We measured spiking correlations using zero-lag pairwise Pearson spike count correlations. First we obtained spike counts $n(t)$ by binning the spike train of each neuron i into bins of window size T_{win}. The pairwise Pearson spike count correlation between spike trains of neuron i and j was then calculated using the standard expression [6]:

$$r_{ij} = \frac{\text{cov}(n_i, n_j)}{\sigma_i \sigma_j}, \tag{72}$$

where $\text{cov}(n_i, n_j)$ is the covariance between the spike counts of cells i and j and σ_i,σ_j are the respective standard deviations. By definition, $r_{ij} \in [-1, 1]$. For figure 3 of the main paper, we chose a window size of $T_{\text{win}} = 20$ ms.

To estimate the effect of our limited sampling time, we generated jittered spike trains, where the total number of spikes per neuron was fixed but the spike times drawn uniformly in the interval $[0, T_{\text{total}}]$, where T_{total} is the total simulation time. We calculated the correlation of the shuffled spike trains r_{ij}^{shuffled} using the same binning and definition for the correlation.

To provide a fair comparison of pairwise correlations for networks with different spike onset rapidness r, the mean firing rate $\bar{\nu}$ was fixed by adapting the external current I_{ext}.

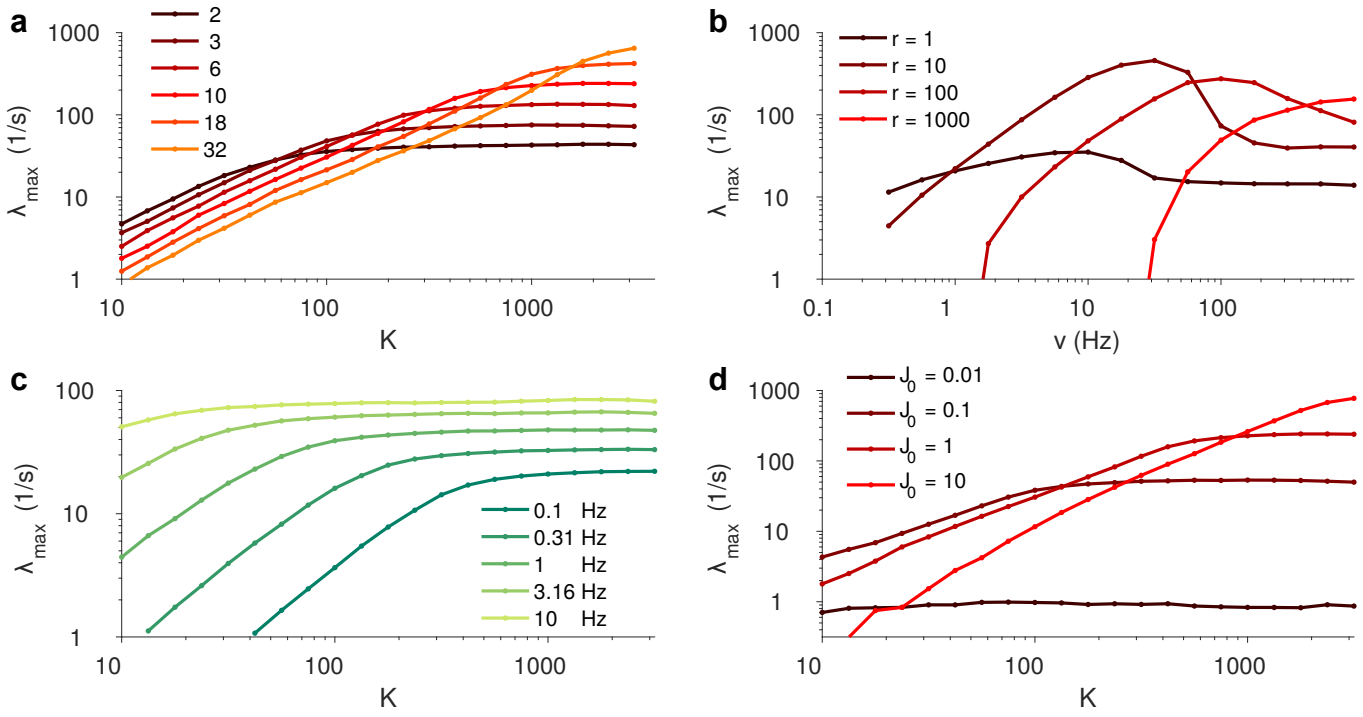

Figure 18: **Different scaling regimes explain peak in the largest Lyapunov exponent $\lambda_{\max}$. a)** K-dependence of largest Lyapunov exponent from for different values of rapidness r with $N = 10000$. **b)** ν-dependence of largest Lyapunov exponent for different rapidness r. **c)** K-dependence of largest Lyapunov exponent for mean firing rate ν_0 with $N = 1000$. **d)** K-dependence of largest Lyapunov exponent for different coupling strength J_0 (parameters: $\bar{\nu} = 10\,\text{Hz}$, $J_0 = 1$, $\tau_\text{m} = 10\,\text{ms}$, $N = 10000$, $K = 100$).

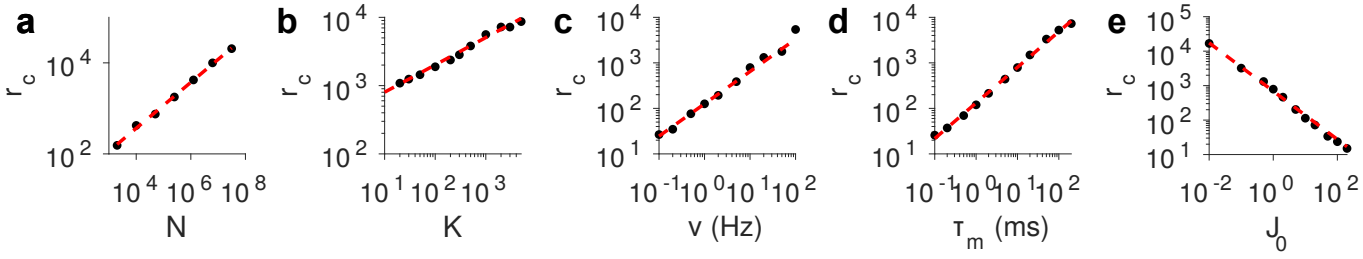

Figure 19: **Scaling of critical AP onset rapidness r_c between stable and chaotic dynamics in balanced inhibitory networks** $r_\text{crit} \propto N^{0.5} K^{0.4} \bar{\nu}^{0.8} \tau_\text{m} J_0^{-0.7}$**.** The critical spike rapidness r_crit separates chaotic dynamics (above) from stable dynamics (below). **a)** r_crit vs. N, **b)** r_crit vs. K, **c)** r_crit vs. $\bar{\nu}$, **d)** r_crit vs. τ_m, **e)**r_crit vs. J_0 Power-law fits done using the Levenberg-Marquardt algorithm (parameters: $\bar{\nu} = 10\,\text{Hz}$, $J_0 = 1$, $\tau_\text{m} = 10\,\text{ms}$, $N = 2000$, $K = 100$).

Additional results: We characterized the effect of different count window sizes T_win on the mean and standard deviation of the pairwise spike count correlation (**Fig. 24**).

At large count window size, the mean pairwise correlations tend to be smaller for large rapidness. This can be explained by the faster inhibitory feedback for large action potential onset rapidness. As for large rapidness, rapid theta neurons are capable of tracking input changes more quickly (**Figure 1d, e** of main paper). Therefore, the dynamic decorrelation of balanced networks, which was described earlier [6], is more effective. For small bin size, the mean pairwise correlations of rapid theta neurons with large rapidness are larger. This is because rapid theta neurons which receive shared excitatory input and are kicked across the unstable fixed point will spike almost instantaneously, which results in moderately increased correlations on very short time scales (**Fig. 24b**).

Cross-correlograms: The cross-correlogram between the pairs of the binned the spike trains $n_i(t)$ and $n_j(t)$ was calculated as:

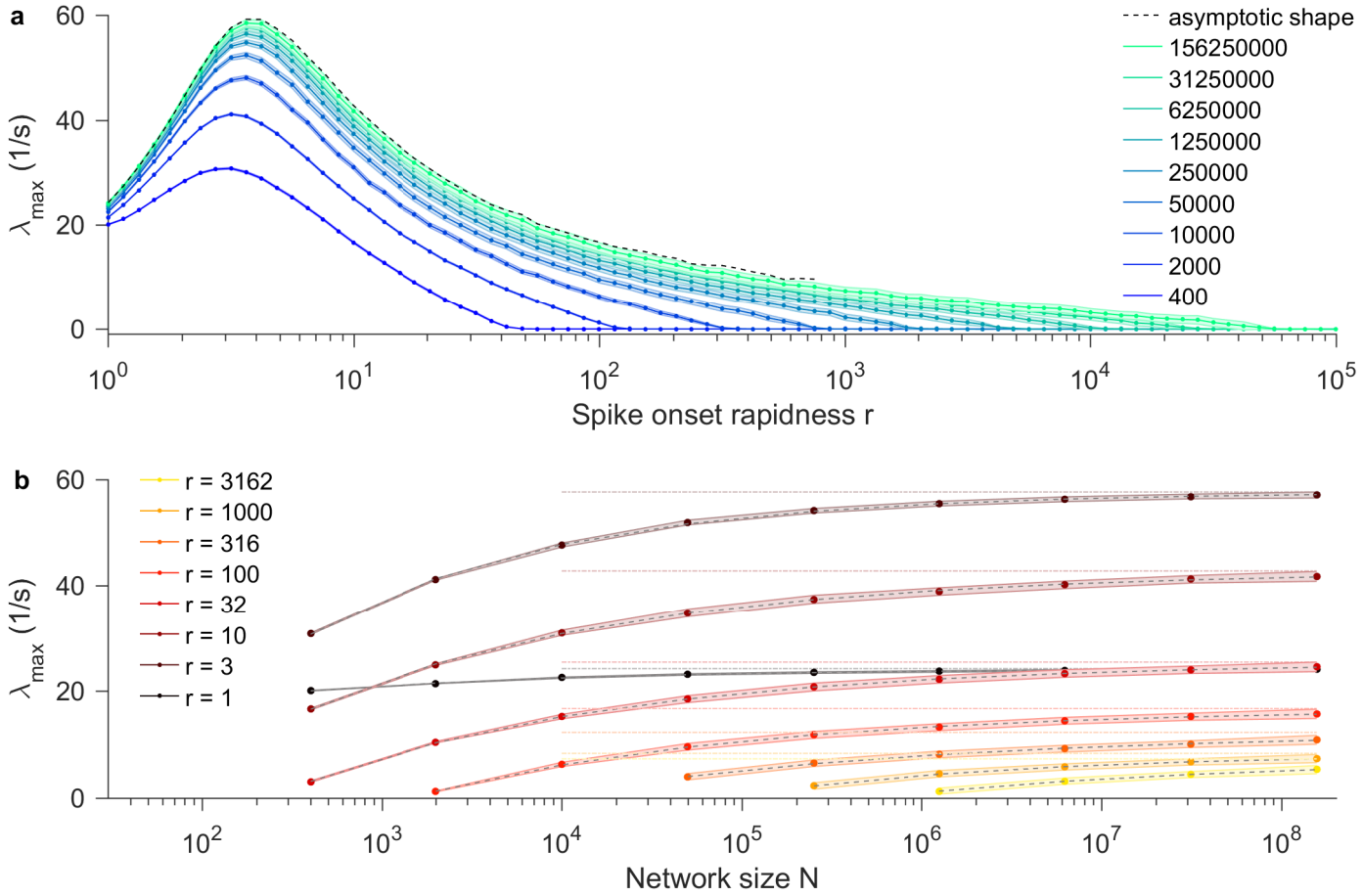

Figure 20: **Largest Lyapunov exponent converges to asymptotic shape for very large network size N: a)** The largest Lyapunov exponent exhibits a slow convergence with network size N ($\bar{\nu} = 1\,\mathrm{Hz}$). **b)** The convergence of $\lambda_{\max}(N)$ can be accurately fitted by $\lambda_{\max}(N) = \lambda_{\max}(\infty) - c \cdot N^{\frac{-1}{\gamma}}$, where $\lambda_{\max}(\infty) = \lim_{N\to\infty} \lambda_{\max}(N)$ (median (dots) across 10 topologies, shaded error shadings indicate median bootstrapped 95% confidence intervals). The estimated $\lambda_{\max}(\infty)$ is indicated by a black dashed line. ($r = 10$, $\bar{\nu} = 10\,\mathrm{Hz}$) (parameters: $J_0 = 1$, $\tau_{\mathrm{m}} = 10\,\mathrm{ms}$, $K = 100$).

$$c_{ij}(\tau) = \frac{\mathrm{cov}(n_i(t), n_j(t+\tau))}{\bar{\nu}_i \bar{\nu}_j} - 1. \tag{73}$$

where $\mathrm{cov}(n_i, n_j)$ is the covariance between the spike counts of cells i and j and $\bar{\nu}_i$, $\bar{\nu}_j$ are the respective mean firing rates. By definition $c_{ij} \in [-\infty, \infty]$, but $\lim_{t\to\infty} c_{ij} = 0$ for shuffled spikes.

XIII. ATTRACTOR DIMENSION AND "ENTANGLED" STATISTICS

In the main paper, we show both an upper and lower bound for the attractor dimension which both strongly depend on the spike onset rapidness (**Fig. 3**). For increasing spike rapidness, the network dynamics has a transition from chaotic to stable dynamics. While chaotic dynamics is accompanied in continuous dynamical systems by a fractal attracting set with dimension $\mathrm{D} > 2$, stable dynamics has an attractor dimension $\mathrm{D} = 1$. Here, we compare this to Gaussian estimates of the dimensionality, based on pairwise correlations, to evaluate higher order correlations. Assuming Gaussian statistics, all dependencies between neurons would be captured by the pairwise correlations. Based on the correlation matrix, an estimate of the dimensionality can be obtained. We use two common estimators of the dimensionality: the number of principle components needed explain 95% of the correlation matrix's variance and a dimensionality based on the participation ratio of the correlation matrix that measures the effective number of degrees of freedom over which power is distributed.

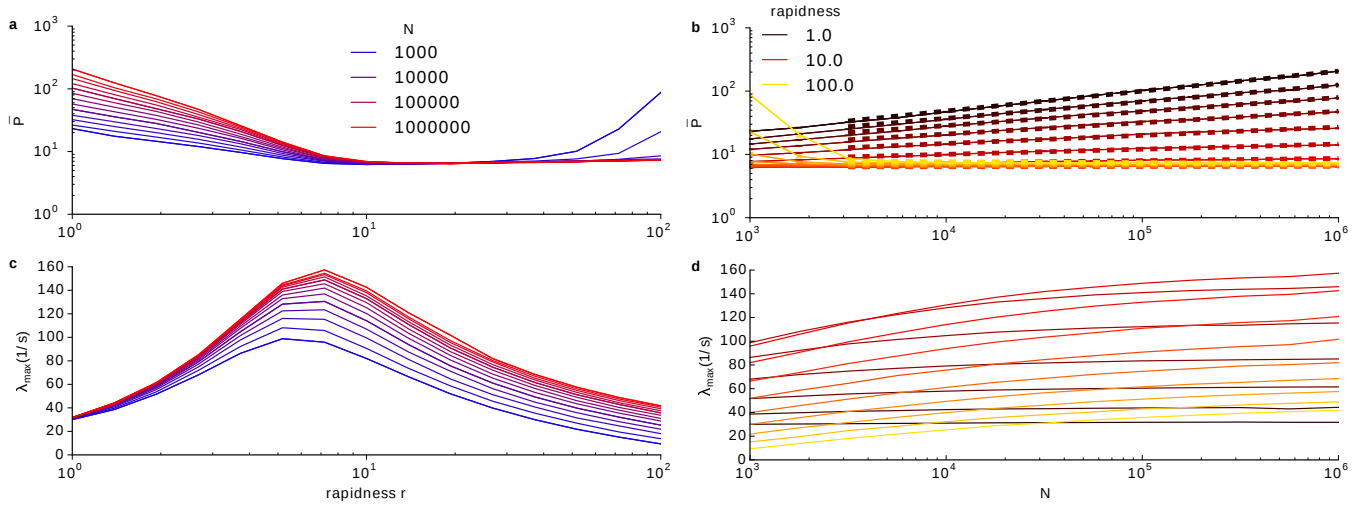

Figure 21: **Average participation vs rapidness r and network size N reveals localization of largest Lyapunov vector at peak rapidness: a)** The mean participation ratio $\bar{P}$ versus rapidness r, colors encode network size N. **b)** $\bar{P}$ versus N, colors encode rapidness r. $\bar{P}$ shows power-law scaling $\bar{P} \sim N^{\alpha}$, where the exponent α decreases as function of rapidness r, dashed lines indicate power-law fits using the Levenberg-Marquardt algorithm (see **Fig. 22** for comprehensive scaling of α). **c)** The largest Lyapunov exponent vs rapidness r exhibits a peak approximately where the participation ratio becomes independent of network size N in **a**. **d)** The largest Lyapunov exponent vs. N converges exponentially to asymptotic limit (parameters: $\bar{\nu} = 3\,\mathrm{Hz}$, $J_0 = 1$, $\tau_\mathrm{m} = 10\,\mathrm{ms}$, $K = 100$).

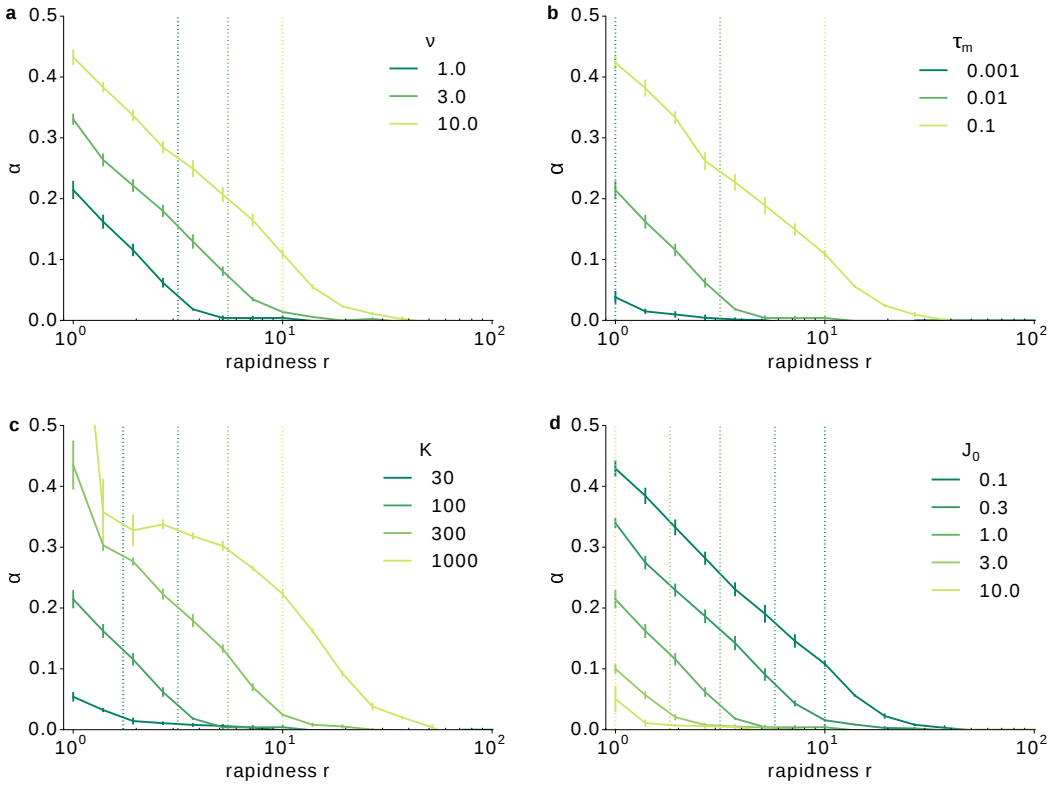

Figure 22: **Scaling of participation ratio with network parameters shows that localization of largest Lyapunov vector has same r-scaling as peak rapidness: a)** power-law scaling exponent α from $\bar{P} \sim N^{\alpha}$ fits mean firing rate $\bar{\nu}$ decreases approximately logarithmically as function of r. Dashed vertical lines indicate corresponding values of peak rapidness r_peak. **b)** Same for different membrane time constants τ_m. **c)** Same for different number of synapses per neuron K. **d)** Same for different coupling strengths J_0 (parameters: $N = 10^3 - 10^6$, $K = 100$, $\bar{\nu} = 1$ Hz, $J_0 = 1$, $\tau_\mathrm{m} = 10$ms, $\varepsilon = 0.3$).

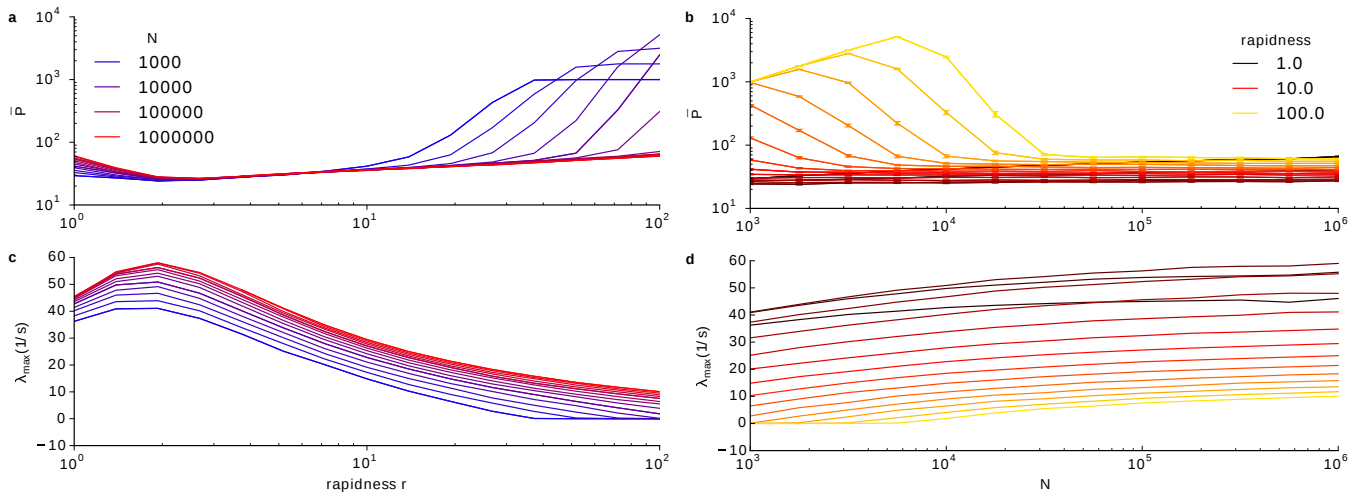

Figure 23: **Average participation vs rapidness r and network size N reveals delocalization of largest Lyapunov vector at critical rapidness:** Same as **Fig. 21** for $\bar{\nu} = 1\,\mathrm{Hz}$, $J_0 = 3$. Note that for large spike onset rapidness r the mean participation $\bar{P}$ increases in small networks and saturates at $\bar{P} = N$, when the largest Lyapunov exponent becomes zero (parameters: $\bar{\nu} = 1\,\mathrm{Hz}$, $J_0 = 3$, $\tau_\mathrm{m} = 10\,\mathrm{ms}$, $K = 100$).

Figure 25a+b shows the correlation matrix for two different values of spike onset rapidness. Principal component analysis (PCA) yields the percentage of the total variance explained by each principal component (**Fig. 25c**). The number of principal components necessary to account for 95% of the total variance gives an estimate of the number of degrees of freedom of the underlying dynamics. If few principal components would explain most of the variance, most of the dynamics is constrained to a hyperellipsoid with few large axes. If many principal components are necessary to explain most of the variance, no such collective structures are detected. This excludes the possibility that the dynamics is explained solely by pairwise correlations. A different estimate of the dimensionality based on the correlation matrix is the inverse participation ratio of the eigenvalue spectrum of the correlation matrix. The inverse participation ratio is defined as the normalized inverse squared sum of eigenvalues of the correlation matrix:

$$D_\mathrm{PR} = \frac{(\sum \lambda_i)^2}{\sum(\lambda_i^2)} \tag{74}$$

where λ_i is the i^th eigenvalue of the correlation matrix. Thus, D_PR is 1 if one eigenvalue is dominating while the others are zero. If all eigenvalues contribute equally $\lambda_\mathrm{i} = \frac{1}{N}$, the dimension is N [12, 13]. The dimensionality estimate based on the participation ratio also shows that the pairwise correlations have very little localized structure independent of spike onset rapidness (**Fig. 26b+d**). Furthermore, we show that this result is largely insensitive to the spike count window of the correlation matrix (**Fig. 26a+c**). To conclude, we find a low attractor dimensionality based on the Kaplan-Yorke dimension and our lower bound estimate coming from the number of positive Lyapunov exponents, despite low and weakly structured pairwise correlations. To obtain a precise estimate of the pairwise spike count correlations, we averaged the correlation matrix over 100 runs with different initial conditions but identical network topology each with $T_\mathrm{total} = 1000$ s.

XIV. FLUX-TUBE STRUCTURE OF PHASE SPACE, STABLE CHAOS AND SINGLE-SPIKE PERTURBATIONS

Figure 3 d,h of main paper: For sufficiently large spike onset rapidness, we find that infinitesimal perturbations decay exponentially but sufficiently strong perturbation lead to an exponential decorrelation of neighboring trajectories. This exotic phase space structure was first described in balanced purely inhibitory networks of pulse-coupled leaky integrate and fire neurons earlier and termed flux tubes [28]. Following Ref. [28], we find the critical perturbation strength ε_ft that is sufficient for an exponential decorrelation of trajectories by fitting the probability that a perturbation of strength ε causes an exponential state separation to the function

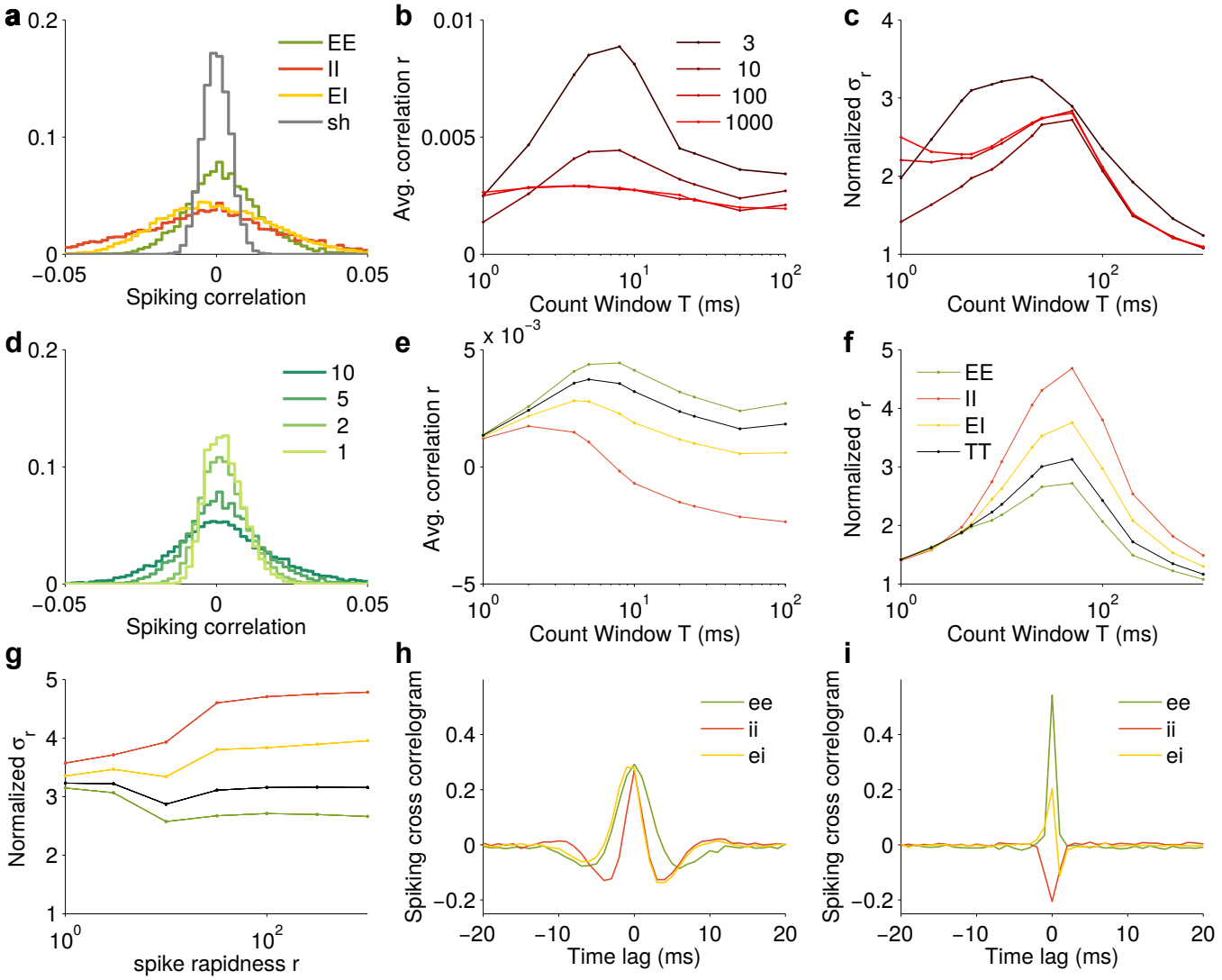

Figure 24: **Pairwise correlations in balanced spiking networks with different values of spike onset rapidness: a)** Histograms of the pairwise count spike correlation r_{ij} for different cell pairs from excitatory and inhibitory populations (count window $T_{\rm win} = 20\,$ms. Jittered spike trains were generated by Poisson process of same rate. **b)** Mean of pairwise spike count correlation vs. count window sizes $T_{\rm win}$ for different values of rapidness. **c)** Standard deviation of spike count correlations vs. $T_{\rm win}$ for different values of rapidness. **d)** Histogram of pairwise correlations for different mean firing rates. **e)** Standard deviation of pairwise spiking correlation as a function of rapidness for $T_{\rm win} = 20\,$ms. **f)** Average spike cross correlogram of different pair types for rapidness $r = 10$ **g)** same as **f** for $r = 1000$. **h)** Spiking cross correlogram of different pair types for rapidness $r = 10$. **i**) same as **h** for $r = 1000$ (parameters as in **Fig. 3** of main paper).

$$P_{\rm s}(\varepsilon) = 1 - \exp(-\varepsilon/\varepsilon_{\rm ft}) \tag{75}$$

$\varepsilon_{\rm ft}$ is the average radius of a basin of attraction, called flux tube radius. We found that this flux tube radius strongly depends on the spike onset rapidness r. For values of r only slightly larger than the critical rapidness $r_{\rm crit}$, the flux tube radius is small, but large r yield larger basins of attraction. This is depicted in **Fig. 24**.

We perturbed initial conditions along two random N-dimensional vectors orthogonal to the flow of the dynamics $\vec{1}$. These two vectors span a two-dimensional cross section of the N-dimensional phase space. Each pixel is a different initial condition for a simulation. Neighboring initial conditions that converge to the same trajectory are assigned same colors. For increasing values of r, the flux tubes radius increases and the boundaries become straighter. In the limit of very large r, the flux tubes are similar to those in the leaky integrate and fire model (compare to **Fig. 7** in [28]). Overall, flux tube radii get smaller with increasing network size N, number of synapses per neuron K, mean

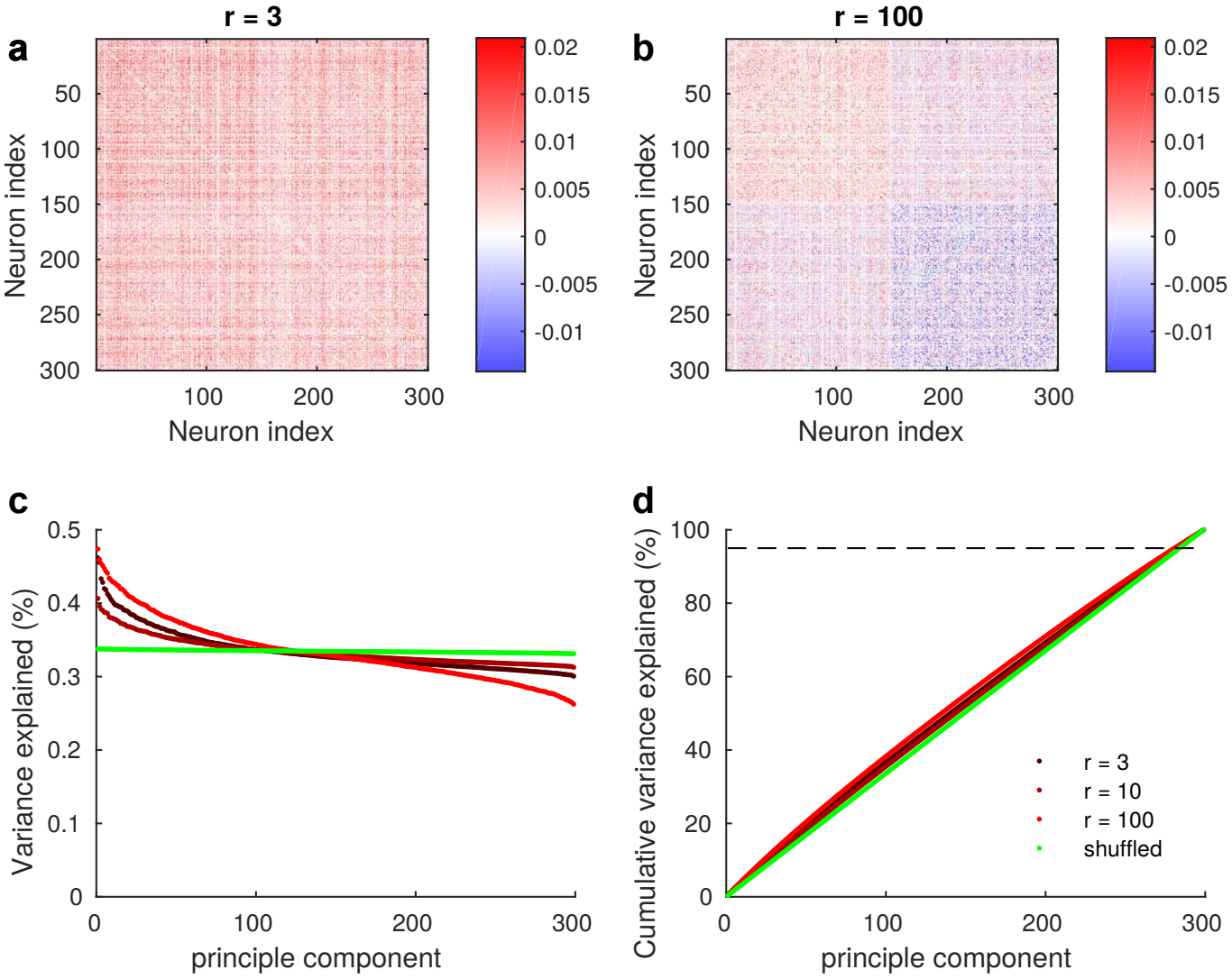

Figure 25: **Weakly structured correlation matrix in balanced spiking networks with different values of spike onset rapidness: a)** Matrix of pairwise spike count correlations r_{ij} for rapidness $r = 3$. First 150 neurons are excitatory, others inhibitory. **b)** same for $r = 100$. **c)** Variance explained per principal component for different rapidness. Jittered spike trains were generated by a Poisson process of the same rate. **d)** Cumulative variance explained for different values of rapidness, (parameters: $T_{\text{win}} = 20$ ms, $T_{\text{total}} = 1000$ s, other parameters as in **Fig. 24**).

firing rate $\bar{\nu}$ and decreasing spike rapidness r. At the critical rapidness r_{crit} the flux tubes vanish.

XV. POINCARÉ MAPS OF CHAOTIC NETWORKS

A Poincaré map is the intersection of the trajectory of a N degree of freedom dynamical system with a $N-1$ dimensional subspace called the Poincaré surface or section.

Increasing the spike rapidness leads to a thinning of stable manifolds (**Fig. 28**). Beyond the critical spike rapidness, the network settles after a transient period into a periodic orbit. Therefore, there is only a finite number of unique points in the Poincare section. For increasing network size, the Poincaré sections did not capture the exotic structure of the phase space. This stresses again that the attractor is a high-dimensional object, which is hard to visualize in two dimensions.

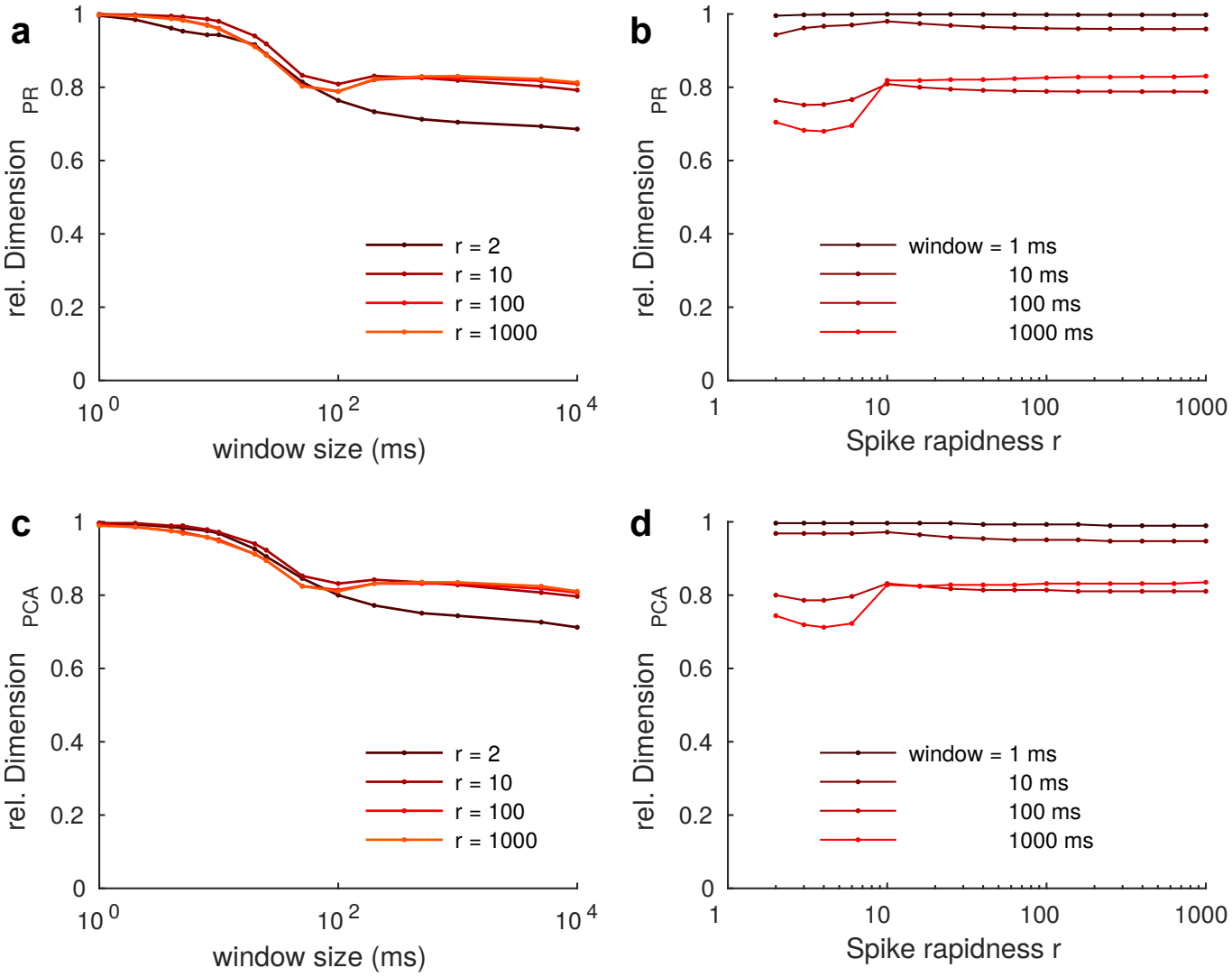

Figure 26: **Correlation based dimensionality estimates of dynamics based on pairwise correlations indicates weakly structured correlations: a)** relative dimension based on participation ratio (Eq. 74) vs. window size T_{win}. **b)** same as **a** as a function of spike rapidness r. **c)+d)** same as **a+b** for relative dimension based on PCA. (parameters as in **Fig. 3**)

XVI. LOCAL LYAPUNOV EXPONENTS REVEAL STABLE AND UNSTABLE MANIFOLDS

In the three-dimensional network, the local Lyapunov exponents (LLEs) can visualize further structural properties of the strange chaotic attractor. In **Fig. 31a**, colors indicate the first local Lyapunov exponent, when neuron 1 spikes, plotted at the location of phases of neuron 2 and 3 for rapidness $r = 1$. Red colors indicate a positive LLE, blue colors indicate a negative LLE. The fine structure of the first LLE is similar to the density (**Fig. 28**), while the third LLE has a fine structure which dissimilar to the density. A possible explanation is that the first LLE is smooth along the unstable manifolds, while the third LLE is smooth along the stable manifolds. The spatial distribution of the LLEs on the Poincaré surface is determined by the topology in combination with the single neuron properties. In the displayed network, neuron 1 is only connected to neuron 2, therefore the LLEs mainly reflect the derivative of the phase response curve evaluated at the respective value of neuron 2. This can also be observed at a higher rapidness (rapidness $r = 1$ **Fig. 32**).

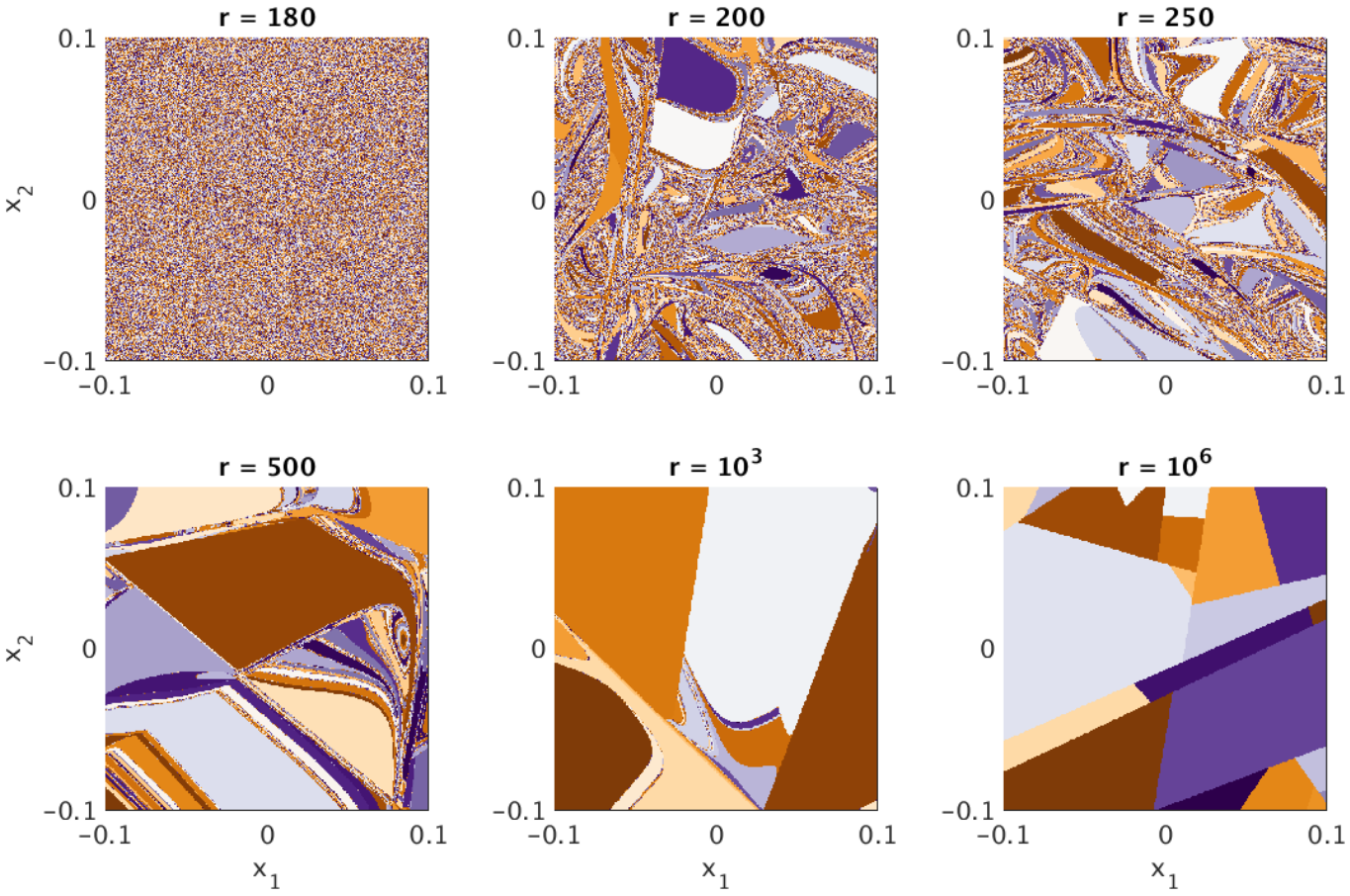

Figure 27: **Random cross section through N-dimensional phase space for different values of spike onset rapidness r:** Phase space cross sections spanned by two random N-dimensional vectors $x_1$and x_2 orthogonal to the trajectory $\vec{1}$ and to each other. Initial conditions that converge to the same trajectory are drawn in the same color (parameters: $\bar{\nu} = 10\,\mathrm{Hz}$, $J_0 = 1$, $\tau_\mathrm{m} = 10\,\mathrm{ms}$, $N = 200$, $K = 100$).

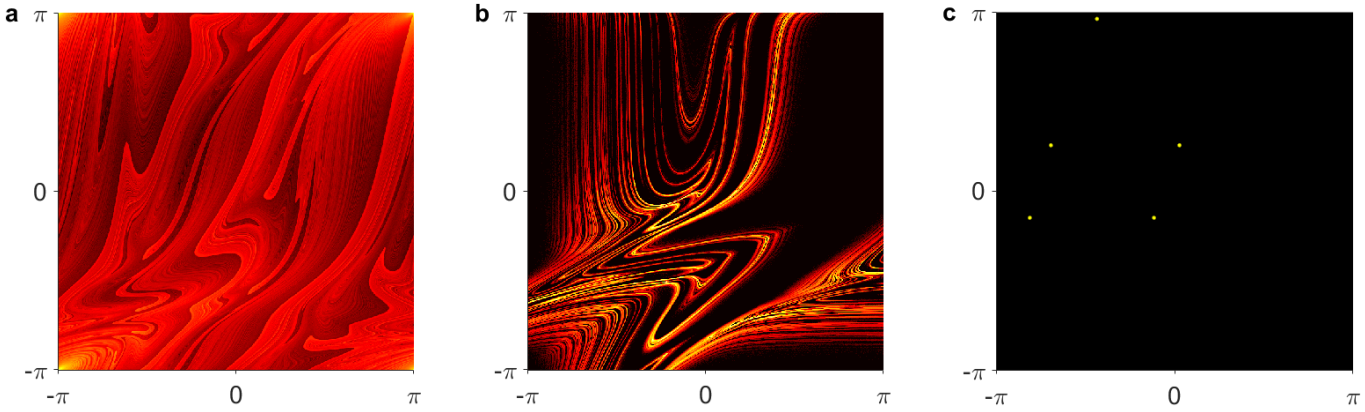

Figure 28: **Poincaré sections through phase space reveal reorganization of chaotic strange attractor by AP onset rapidness r in small networks $N = 3$: a)** Poincare section of the phases of neuron 2 and 3 whenever neuron 1 spikes for low rapidness ($r = 1$). The relative density of points is represented using a heat map, where hot colors indicate high densities. **b)** Same as **a** for $r = 4$. **c)** Same as **a** for $r = 25$ (parameters: $\bar{\nu} = 14.5\,\mathrm{Hz}$, $J_0 = 1$, $\tau_\mathrm{m} = 10\,\mathrm{ms}$, $N = 3$, $K = 1$, $r = 1,\, 4\,, 25$).

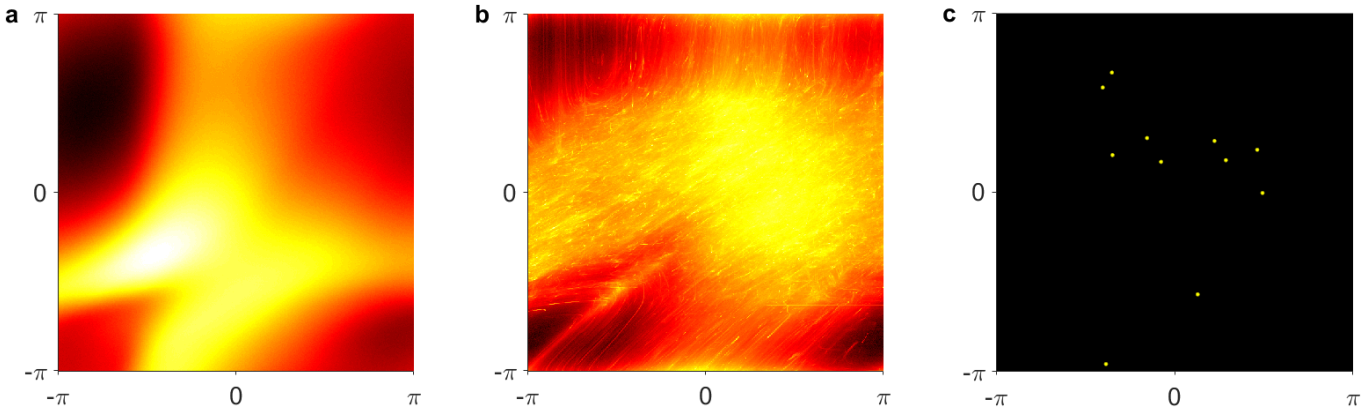

Figure 29: **Two-dimensional sections through phase space for different values of spike onset rapidness r for $N = 20$:** Surface of the phases of neuron 2 and 3 whenever neuron 1 spikes for low rapidness ($r = 1$). The relative density of points is represented using a heat map, where hot colors indicate high densities. **b)** Same as **a** for $r = 10$. **c)** Same as **a** for $r = 25$ (parameters: $\bar{\nu} = 14.5\,\mathrm{Hz}$, $J_0 = 1$, $\tau_\mathrm{m} = 10\,\mathrm{ms}$, $N = 3$, $K = 1$, $r = 1, 10, 25$).

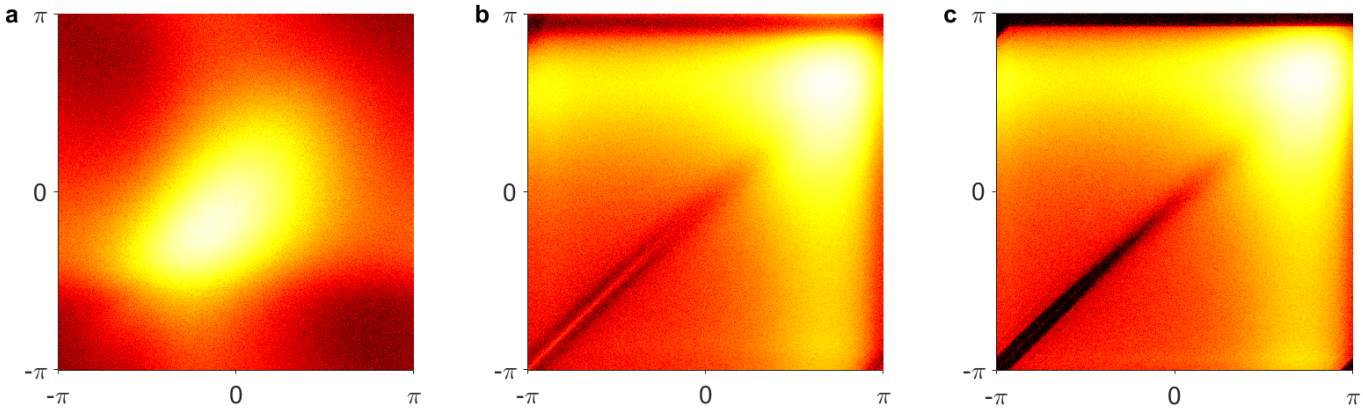

Figure 30: **Two-dimensional sections through phase space for different values of spike onset rapidness r for $N = 200$:** Surface of the phases of neuron 2 and 3 whenever neuron 1 spikes for low rapidness ($r = 1$). The relative density of points is represented using a heat map, where hot colors indicate high densities. **b)** Same as **a** for $r = 25$. **c)** Same as **a** for $r = 250$ (parameters: $\bar{\nu} = 14.5\,\mathrm{Hz}$, $J_0 = 1$, $\tau_\mathrm{m} = 10\,\mathrm{ms}$, $N = 3$, $K = 1$, $r = 1, 25, 250$).

XVII. CHAOS AND DYNAMICAL ENTROPY RATE IN STRUCTURED NETWORK TOPOLOGIES

Figure 4 a-e of main paper: To test whether spike onset also exerts a strong influence on the phase space structure in more realistic network topologies, we used a previously established multilayered model of a cortical column with 77169 neurons and around 285 million synapses [7]. Numbers of neurons per population and inter-layer wiring probabilities were taken from a numerical model of a cortical column based on anatomically measured synapse counts and connection probabilities between different cortical layers [7]. The cortical column model consists of four layers (layers 2/3, 4, 5 and 6) each with an excitatory and an inhibitory population. The number of neurons in each layer and the connection probability between layers are stated in Table 1. According to these numbers, the connectivity for each population and each projection between the populations is generated as a directed sparse Erdős–Rényi random graph (Table I). We calculated also for this large network the Lyapunov spectrum making use of a parallelized implementation of the semi-analytic calculation described in section VIII. The sparseness of the connectivity was utilized for the efficient storage of the coupling matrices, the updates of the postsynaptic neurons and the matrix multiplications of the orthonormal system with the sparse single spike Jacobians implemented in custom code written in Julia and C++ making use of the Automatically Tuned Linear Algebra Software (ATLAS) for matrix multiplications in the Gram–Schmidt procedure and the Message Passing Interface (MPI) for the parallel implementation of the simulations. For the reorthonormalization, we chose a parallel recursive blocked version of the Gram–Schmidt procedure [5]. Constant external input currents were adapted to obtain a desired global firing rate,

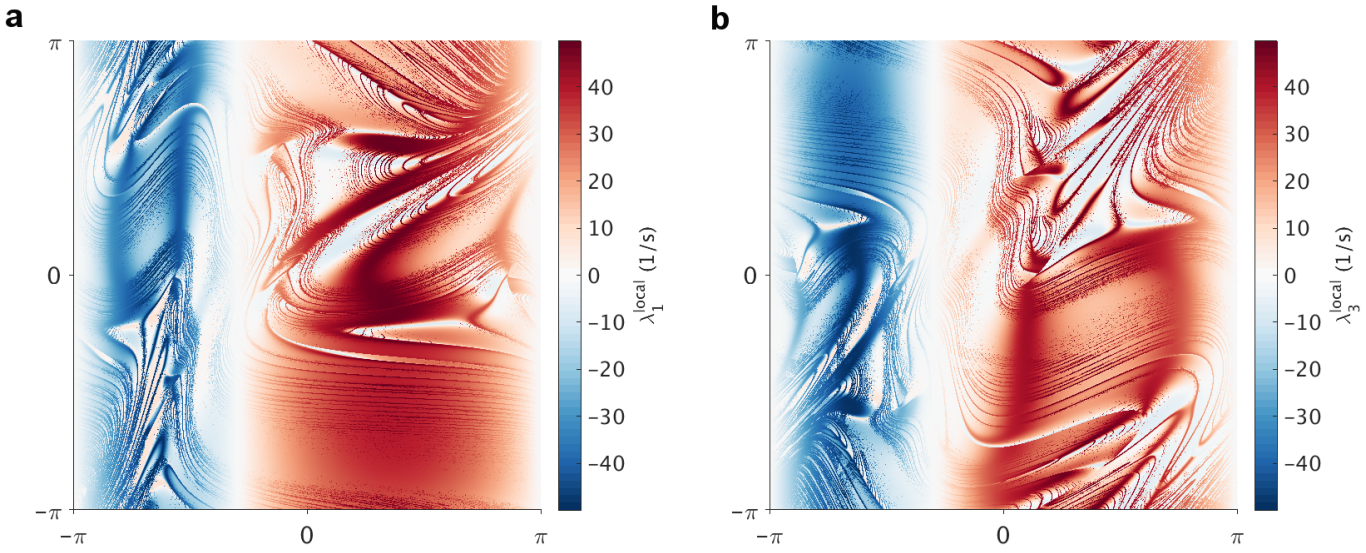

Figure 31: **Local Lyapunov exponent reveal stable and unstable manifolds of chaotic attractor in small networks** $N = 3$, $r = 1$**: a)** Poincaré section of the phases of neuron 2 and 3 whenever neuron 1 spikes. The first local Lyapunov exponents (LLE) at each point is color-coded, red colors indicate local instability, blue indicates local stability. **b)** Same as **a** for third LLE. The second LLE is trivially zero (neutral direction, not shown). The associated density of states is depicted in **Fig. 28a** (parameters: $\bar{\nu} = 14.5\,\text{Hz}$, $J_0 = 1$, $\tau_\text{m} = 10\,\text{ms}$, $K = 1$, $r = 1$).

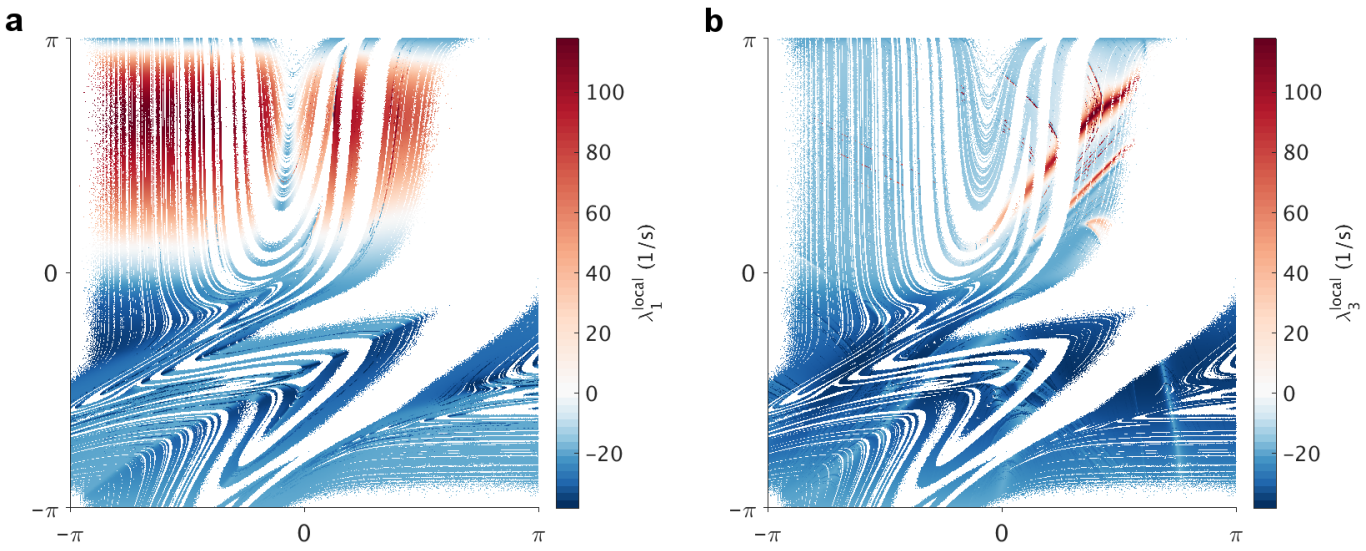

Figure 32: **Local Lyapunov exponent reveal stable and unstable manifolds of chaotic attractor in small networks** $N = 3$, $r = 4$**:** Poincaré section of the phases of neuron 2 and 3 whenever neuron 1 spikes. The first local Lyapunov exponents (LLE) at each point is color-coded, red colors indicate local instability, blue indicates local stability. **b)** Same as **a** for third LLE. The second LLE is trivially zero (neutral direction, not shown). The associated density of states is depicted in **Fig. 28b** (parameters: $\bar{\nu} = 14.5\,\text{Hz}$, $J_0 = 1$, $\tau_\text{m} = 10\,\text{ms}$, $N = 3$, $K = 1$, $r = 4$).

for a fair comparison across different values of AP onset rapidness r. The convergence of the Lyapunov spectrum across different initial conditions is shown in **Fig. 33**. The shaded lines correspond to different initial conditions, dashed lines indicate standard error of the mean. Even for such large networks, the numerically precise event-based implementation fully converges. The neutral Lyapunov exponent converges to zero across multiple orders of magnitude (**Fig. 33b**). The dynamical entropy rate per spike of the multilayered network is considerably smaller than in random networks. A reason for that might be the occurrence of very high firing rate in some neurons with low firing rates in other neurons, possibly because the balance inequality (Eq. 61) is not satisfied. The dynamical entropy rate per spike is known to decrease for high firing rates (See **Fig. 18**).

Probability		from							
		L2/3e	L2/3i	L4e	L4i	L5e	L5i	L6e	L6i
to	L2/3e	0.101	0.169	0.044	0.082	0.032	0	0.008	0
	L2/3i	0.135	0.137	0.032	0.052	0.075	0	0.004	0
	L4e	0.008	0.006	0.050	0.135	0.007	0.0003	0.045	0
	L4i	0.069	0.003	0.079	0.160	0.003	0	0.106	0
	L5e	0.10	0.062	0.051	0.006	0.083	0.373	0.020	0
	L5i	0.055	0.027	0.026	0.002	0.060	0.316	0.009	0
	L6e	0.016	0.007	0.021	0.017	0.057	0.020	0.040	0.225
	L6i	0.036	0.001	0.003	0.001	0.028	0.008	0.066	0.144

	number of neurons	external input
L2/3e	20683	3.6923
L2/3i	5834	12.272
L4e	21915	4.5737 94.0675
L4i	5479	16.5517 106.0455
L5e	4850	19.6825
L5i	1065	85.1521
L6e	14395	9.6156 99.1084
L6i	2948	34.0002 123.491

Table I: Wiring probabilities and number of neurons per population in cortical column model.

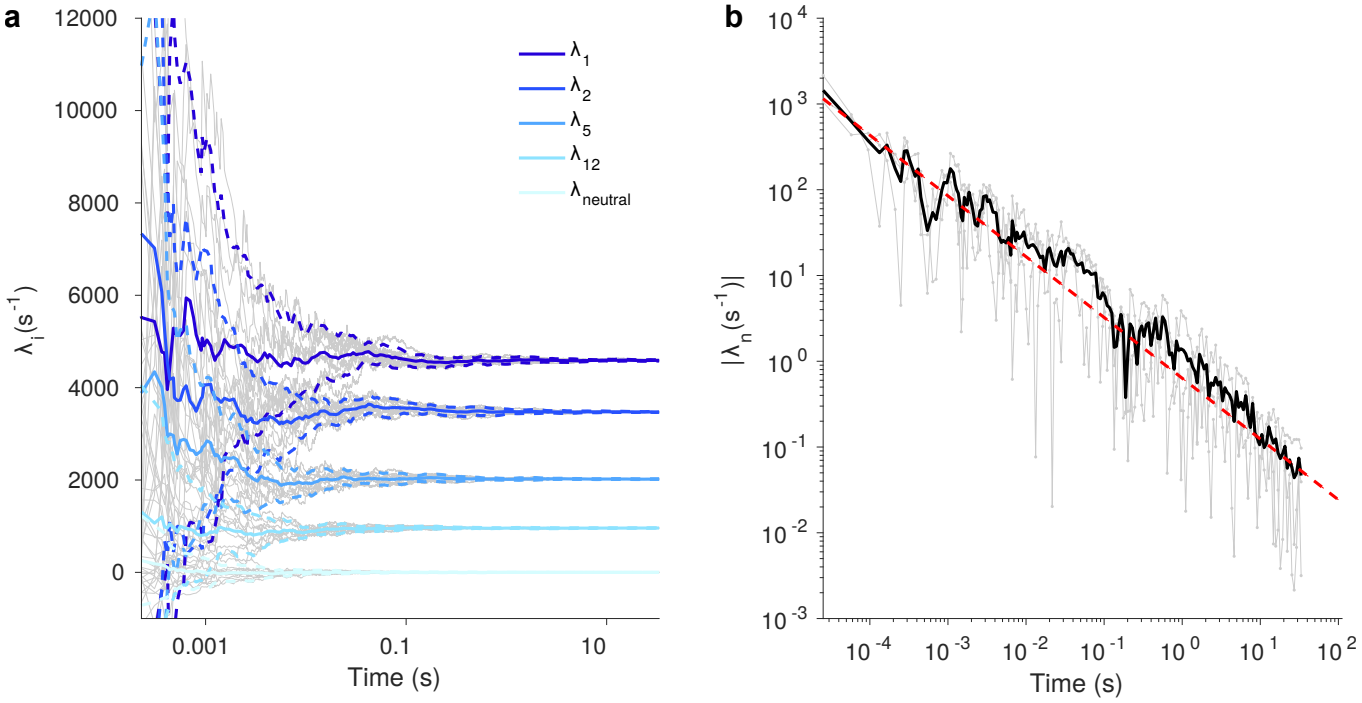

Figure 33: **Lyapunov exponents for cortical column model convergence over orders of magnitude: a)** gray lines: some Lyapunov exponents for ten different initial conditions, straight color lines: averages, dotted color lines: averages ± double standard errors. $r = 10$, where the largest Lyapunov exponent is maximal. **b)** Convergence of the neutral Lyapunov exponent. Grey lines: absolute value of neutral Lyapunov exponent for three initial conditions, black line: average of absolute values of neutral Lyapunov exponents across initial conditions, red line: power law fit using the Levenberg-Marquardt algorithm with exponent -0.7.

Figure 4 f, g of main paper: We also studied the dynamics of networks with a structured microscopic architecture to corroborate our main results. We used second order networks (SONETS), which are random networks where two synapse motifs and connection probabilities are varied, while keeping higher order structures random [9]. This is achieved by using dichotomized Gaussian random variables with a desired covariance structure to generate the topology [10]. In an Erdős–Rényi graph only the connection probability $p = K/(N-1) = P(A_{ij} = 1)$ is fixed, hence for any two synapses, the joint probability of being connected is $P(A_{ij} = 1,\ A_{kl} = 1) = p^2$. In SONETS, also the joint probability of two connections $P(A_{ij} = 1,\ A_{kl} = 1) = p^2(1 + \alpha_x)$ is fixed, where α_x is the respective motif frequency $\alpha_x = \{\alpha_{\text{reciprocal}}, \alpha_{\text{converging}}, \alpha_{\text{diverging}}, \alpha_{\text{chain}}\}$. $\alpha_{\text{converging}}$ is proportional to the variance of the indegree K_{in}, $\alpha_{\text{diverging}}$ is proportional to the variance of the outdegree K_{out} and α_{chain} is proportional to the covariance of the indegree K_{in} and the outdegree K_{out}. Using this approach, we interpolated excitatory-excitatory connectivity from a random graph to a graph with the second order motif structure found experimentally in superficial cortical layers [8]. Again we fixed the average network firing rate by adapting the external current I_{ext}. We used excitatory-inhibitory networks with $N_I = 2000$, $N_E = 8000$, $\eta = 0.9$, $\varepsilon = 0.3$. The excitatory-excitatory adjacency matrix was interpolated between a directed Erdős–Rényi graph and a SONET with the experimentally found motif structure. While varying second

order motifs can generally change the largest Lyapunov exponent, dynamical entropy and the attractor dimensionality by a factor of ≈ 3, we demonstrate that the importance of action potential onset rapidness prevails.

XVIII. MINIMAL EXAMPLE FOR JULIA

The following code for Julia (`www.julialang.org`) Version 0.7 demonstrates the event-based simulations by calculating the Poincaré sections displayed in **Fig. 28a**. Performant code for calculating Lyapunov spectra is available upon request.

```
function poincare()
Ncalc = 10^7                              # number of spikes in calculation
A = 0 .<[0 0 0;1 0 1;0 1 0]               # define connectivity matrix
phi = rand(3)                             # initialize neurons
pAll = Float64[]
    for s = 1:Ncalc
        pMax,j = findmax(phi)             # find next spiking neuron j
        dt = pi/2-pMax                    # calculate next spike time
        phi.+= dt                         # evolve phases till next spike time
        p = A[:,j]                        # postsynaptic neurons
        phi[p] = atan.(tan.(phi[p]).-1)   # update postsynaptic neurons
        phi[j] = -pi/2                    # reset spiking neuron to -π/2
       j==1 && append!(pAll,phi[2:3])     # save neuron 2 & 3 whenever neuron 1 spikes
    end
     plot(2pAll[1:2:end], 2pAll[2:2:end],".k",markersize=0.01); axis("off")
end
```

* Electronic address: rainer@nld.ds.mpg.de

[1] van Vreeswijk, C. & Sompolinsky, H. Chaos in Neuronal Networks with Balanced Excitatory and Inhibitory Activity. Science **274**, 1724–1726 (1996); van Vreeswijk, C. & Sompolinsky, H. Chaotic Balanced State in a Model of Cortical Circuits. Neural Computation **10**, 1321–1371 (1998).

[2] Ermentrout, G. & Kopell, N. Parabolic Bursting in an Excitable System Coupled with a Slow Oscillation. SIAM J. Appl. Math. **46**, 233–253 (1986); Gutkin, B. S. & Ermentrout, G. B. Dynamics of Membrane Excitability Determine Interspike Interval Variability: A Link Between Spike Generation Mechanisms and Cortical Spike Train Statistics. Neural Computation **10**, 1047–1065 (1998); Brumberg, J. C. & Gutkin, B. S. Cortical pyramidal cells as non-linear oscillators: Experiment and spike-generation theory. Brain Research **1171**, 122–137 (2007).

[3] Tsodyks, M., Mitkov, I. & Sompolinsky, H. Pattern of synchrony in inhomogeneous networks of oscillators with pulse interactions. Phys. Rev. Lett. **71**, 1280–1283 (1993); Ernst, U., Pawelzik, K. & Geisel, T. Synchronization Induced by Temporal Delays in Pulse-Coupled Oscillators. Phys. Rev. Lett. **74**, 1570–1573 (1995).

[4] Benettin, G., Galgani, L., Giorgilli, A. & Strelcyn, J.-M. Lyapunov characteristic exponents for smooth dynamical systems and for Hamiltonian systems - A method for computing all of them. I - Theory. II - Numerical application. Meccanica **15**, 9–30 (1980).

[5] Yokozawa, T., Takahashi, D., Boku, T. & Sato, M. Efficient parallel implementation of classical Gram-Schmidt orthogonalization using matrix multiplication. in Proceedings of Fourth International Workshop on Parallel matrix Algorithms and Applications (PMAA'06) 37–38 (2006).

[6] Renart, A. et al. The Asynchronous State in Cortical Circuits. Science **327**, 587–590 (2010).

[7] Potjans, T. C. & Diesmann, M. The Cell-Type Specific Cortical Microcircuit: Relating Structure and Activity in a Full-Scale Spiking Network Model. Cereb. Cortex **24**, 785–806 (2014).

[8] Song, S., Sjöström, P. J., Reigl, M., Nelson, S. & Chklovskii, D. B. Highly Nonrandom Features of Synaptic Connectivity in Local Cortical Circuits. PLoS Biol **3**, e68 (2005).

[9] Zhao, L., II, B. B., Netoff, T. & Nykamp, D. Q. Synchronization from second order network connectivity statistics. Front. Comput. Neurosci. **5**, 28 (2011).

[10] Macke, J. H., Berens, P., Ecker, A. S., Tolias, A. S. & Bethge, M. Generating Spike Trains with Specified Correlation Coefficients. Neural Computation **21**, 397–423 (2008).

[11] Bernardi, D. & Lindner, B. A frequency-resolved mutual information rate and its application to neural systems. Journal of Neurophysiology **113**, 1342–1357 (2015).

[12] Monteforte, M. & Wolf, F. Dynamical Entropy Production in Spiking Neuron Networks in the Balanced State. Phys. Rev. Lett. **105**, 268104 (2010).

[13] Gao, P. & Ganguli, S. On simplicity and complexity in the brave new world of large-scale neuroscience. Current Opinion in Neurobiology **32**, 148–155 (2015).

[14] Richardson, M. J. E. Firing-rate response of linear and nonlinear integrate-and-fire neurons to modulated current-based and conductance-based synaptic drive. Phys. Rev. E **76**, 021919 (2007).

[15] Richardson, M. J. E. & Swarbrick, R. Firing-Rate Response of a Neuron Receiving Excitatory and Inhibitory Synaptic Shot Noise. Phys. Rev. Lett. **105**, 178102 (2010).

[16] Fourcaud-Trocmé, N., Hansel, D., van Vreeswijk, C. & Brunel, N. How Spike Generation Mechanisms Determine the Neuronal Response to Fluctuating Inputs. J. Neurosci. **23**, 11628–11640 (2003).

[17] Fourcaud-Trocmé, N. & Brunel, N. Dynamics of the Instantaneous Firing Rate in Response to Changes in Input Statistics. J Comput Neurosci **18**, 311–321 (2005).

[18] Naundorf, B., Geisel, T. & Wolf, F. Action Potential Onset Dynamics and the Response Speed of Neuronal Populations. J Comput Neurosci **18**, 297–309 (2005).

[19] Naundorf, B., Wolf, F. & Volgushev, M. Unique features of action potential initiation in cortical neurons. Nature **440**, 1060–1063 (2006).

[20] Wei, W. & Wolf, F. Spike Onset Dynamics and Response Speed in Neuronal Populations. Phys. Rev. Lett. **106**, 088102 (2011).

[21] Strong, S. P., Koberle, R., de Ruyter van Steveninck, R. R. & Bialek, W. Entropy and Information in Neural Spike Trains. Phys. Rev. Lett. **80**, 197–200 (1998).

[22] Lindner, B. Superposition of many independent spike trains is generally not a Poisson process. Phys. Rev. E **73**, 022901 (2006).

[23] Câteau, H. & Reyes, A. D. Relation between Single Neuron and Population Spiking Statistics and Effects on Network Activity. Phys. Rev. Lett. **96**, 058101 (2006).

[24] Ricciardi, L. M. & Sacerdote, L. The Ornstein-Uhlenbeck process as a model for neuronal activity. Biol. Cybern. **35**, 1–9 (1979).

[25] Lánský, P. & Lánská, V. Diffusion approximation of the neuronal model with synaptic reversal potentials. Biol. Cybernetics **56**, 19–26 (1987).

[26] Bialek, W., Rieke, F., Steveninck, R. de R. van & Warland, D. Reading a neural code. Science **252**, 1854–1857 (1991).

[27] Rieke, F., Warland, D., Steveninck, R. de R. van & Bialek, W. Spikes: Exploring the Neural Code. (A Bradford Book, 1999).

[28] Monteforte, M. & Wolf, F. Dynamic Flux Tubes Form Reservoirs of Stability in Neuronal Circuits. Phys. Rev. X **2**, 041007 (2012).

[29] Burns, B. D. & Webb, A. C. The Spontaneous Activity of Neurones in the Cat's Cerebral Cortex. Proceedings of the Royal Society of London B: Biological Sciences **194**, 211–223 (1976); J. Neurosci. **13**, 334–350 (1993), 334 (1993); Kara, P., Reinagel, P. & Reid, R. C. Low Response Variability in Simultaneously Recorded Retinal, Thalamic, and Cortical Neurons. Neuron **27**, 635–646 (2000).

[30] Mainen, Z. F. & Sejnowski, T. J. Reliability of spike timing in neocortical neurons. Science **268**, 1503–1506 (1995).

[31] Rosenbaum, R. & Doiron, B. Balanced Networks of Spiking Neurons with Spatially Dependent Recurrent Connections. Phys. Rev. X **4**, 021039 (2014).

[32] Wolf, A., Swift, J. B., Swinney, H. L. & Vastano, J. A. Determining Lyapunov exponents from a time series. Physica D: Nonlinear Phenomena **16**, 285–317 (1985).

[33] Shadlen, M. N. & Newsome, W. T. Noise, neural codes and cortical organization. Current Opinion in Neurobiology **4**, 569–579 (1994).

[34] Shadlen, M. N. & Newsome, W. T. The Variable Discharge of Cortical Neurons: Implications for Connectivity, Computation, and Information Coding. J. Neurosci. **18**, 3870–3896 (1998).

[35] Softky, W. R. & Koch, C. Cortical Cells Should Fire Regularly, But Do Not. Neural Computation **4**, 643–646 (1992).

[36] Softky, W. R. & Koch, C. The highly irregular firing of cortical cells is inconsistent with temporal integration of random EPSPs. J. Neurosci. **13**, 334–350 (1993).

[37] Cross, M. C. & Hohenberg, P. C. Pattern formation outside of equilibrium. Rev. Mod. Phys. **65**, 851–1112 (1993).

[38] Wegner, F. Inverse participation ratio in $2+\epsilon$ dimensions. Z Physik B **36**, 209–214 (1980).

[39] Kaneko, K. Lyapunov analysis and information flow in coupled map lattices. Physica D: Nonlinear Phenomena **23**, 436–447 (1986).

[40] For numerical stability, Eq. 12 is not directly integrated, as $\frac{dV}{dt}$ can take very large values, so the convergence properties would be poor. Instead, we use the numerical scheme proposed in [14]. All code is available upon request.

5 The transition to control in spiking networks

5.1 Summary

We demonstrate that streams of input spike trains suppress chaos in the dynamics of balanced circuits of neurons with adjustable spike mechanism. This analysis is based on an analytical expression for the Jacobian that enables us to calculate the full Lyapunov spectrum. We solved the dynamics in numerically exact event-based simulations and calculated Lyapunov spectra, dynamical entropy rate and attractor dimension. For sufficiently strong input, we find a transition towards complete network control, where the network state is independent of initial conditions. Fast spike onset of single neurons in the target network facilitates both control by external input and suppression of chaos. Our work opens a novel avenue to investigate the role of sensory streams of spike trains in shaping the dynamics of large neural networks.

The Transition to Control in Spiking Networks

Rainer Engelken* and Fred Wolf
Max Planck Institute for Dynamics and Self-Organization, Göttingen, Germany,
Faculty of Physics, Georg-August-Universität Göttingen, Göttingen, Germany,
Bernstein Center for Computational Neuroscience, Göttingen, Germany

How well streams of spikes from one circuit can control spiking dynamics in a subsequent circuit constrains its ability to encode and process information. It is currently not well understood how the statistics of the input and biophysical features of single neurons controls the recurrent dynamics of a target network. We demonstrate that streams of input spike trains suppress chaos in the dynamics of balanced circuits of neurons with adjustable spike mechanism. For sufficiently strong input, we find a transition towards complete network control, where the network state is independent of initial conditions. Fast spike onset of single neurons in the target network facilitates both control by external input and suppression of chaos. Our work opens a novel avenue to investigate the role of sensory streams of spike trains in shaping the dynamics of large neural networks.

PACS numbers: 87.19.lj, 87.10.-e, 05.45.-a, 05.10.-a

Introduction: Information in the cortex is processed by the orchestrated interplay of a deeply layered system of neural circuits. How well streams of spikes from one circuit can control the asynchronous irregular spiking dynamics in a subsequent circuit constrains its ability to encode and process information. In particular noise entropy arising from sensitivity to initial conditions limits the amount of information conveyed about a stimulus [1, 2]. Experiments in single cells revealed that a structured external input enhance reliability of spiking responses [3]. However, it is not well understood how biophysical properties of neurons and the statistics of incoming spike trains regulate information transmission and the ability to control the activity in a driven network.

To address this challenge, we here investigate how streams of input spike trains and AP onset rapidness affects controllability and dynamical entropy rate in balanced networks. Previous studies of the dynamic stability of the asynchronous irregular activity of balanced networks used a constant external input [4, 5] or white noise [1, 2]. We solved the dynamics in numerically exact event-based simulations and calculated Lyapunov spectra, which provide the dynamical entropy rate and attractor dimension. We examined how the target circuit activity changed from constant to structured input by varying the external input coupling strength or input spike rate, while keeping the firing rate of the target population fixed.

Increasing input rate or input coupling aids the control of the driven circuit, reflected both in decreasing dynamical entropy rate and reduced trial-to-trial variability. Intriguingly, the control of spiking activity is facilitated when the driven circuit has a rapid AP onset. For sufficiently strong input, i.e. increased rate or coupling, we observe a suppression of chaos and a transition to complete network control. Surprisingly, suppression of chaos does generally not imply complete network control.

Model We studied the dynamics of large networks of N rapid theta neurons arranged on a directed Erdős-Rényi random graph of mean degree K. Each neuron receives an independent external spike train. The rapid theta neuron model is a phase representation of the quadratic integrate-and-fire model [6] with tunable spike onset rapidness r which was shown to limit the information encoding bandwidth [7]. Neurons have membrane potentials $V_i \in [-\infty, \infty)$ that follow the dynamics:

$$\tau_m \dot{V}_i = \begin{cases} a_{\mathrm{U}}(V_i - V_{\mathrm{G}})^2 - I_{\mathrm{T}} + I_{\mathrm{ext}} + \tau_{\mathrm{m}} I_i(t) & V > V_{\mathrm{G}} \\ a_{\mathrm{S}}(V_i - V_{\mathrm{G}})^2 - I_{\mathrm{T}} + I_{\mathrm{ext}} + \tau_{\mathrm{m}} I_i(t) & V \leq V_{\mathrm{G}} \end{cases} \tag{1}$$

with the membrane time constant τ_{m}, the glue point $V_{\mathrm{G}} = \frac{1}{2}\frac{r-1}{r+1}$, the rheobase current $I_{\mathrm{T}} = \frac{1}{2}\frac{r}{r+1}$, the curvatures $a_{\mathrm{S}} = \frac{r+1}{2r}$, $a_{\mathrm{U}} = r^2 a_{\mathrm{S}}$ and the synaptic currents

$$I_i(t) = \sum_{j \in \mathrm{pre}(i)} \sum_s J_{ij}^{\mathrm{rec}}\, \delta(t - t_j^{(s)}) + \sum_u J^{\mathrm{ext}}\, \delta(t - t^{(u)}). \tag{2}$$

All neurons $i = 1, \ldots, N$ received constant external currents I_{ext}, non-delayed δ-pulses from the presynaptic neurons j and stochastic δ-pulses from independent Poissonian spike trains (Fig. 1a). The recurrent nonzero coupling strengths were set to $J_{ij}^{\mathrm{rec}} = -J_0^{\mathrm{rec}}/\sqrt{K}$ such that the input variance is independent of K [4, 11]. External incoming excitatory pulses of strength $J_{\mathrm{ex}}^{\mathrm{ext}}$ are followed with delay Δ by dominating inhibitory pulses $-J_{\mathrm{in}}^{\mathrm{ext}}$ as observed experimentally in feedforward inhibition [15]. We considered the limit of short delay, s.t. $J^{\mathrm{ext}} = (J_{\mathrm{ex}}^{\mathrm{ext}} - J_{\mathrm{in}}^{\mathrm{ext}})/\sqrt{K} = -J_0^{\mathrm{ext}}/\sqrt{K}$. The constant current I_{ext} was chosen to obtain a desired average recurrent network firing rate $\bar{\nu}$, for a given coupling strength J^{ext} and rate $\nu^{ext} = \nu_0^{ext} \cdot K$ of the Poisson input. From the analytical solutions of Eq. (1) with (2) in a phase representation $\phi_i(V)$, we obtained a map of the neurons' phases between successive spike times in the network $\{t_s\}$ (see supplemental material). This map was

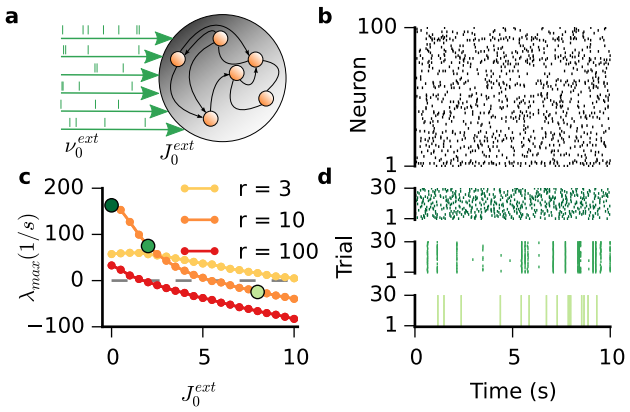

Figure 1: **Streams of input spike trains suppress chaos in balanced target network. a** Each neuron of the target network receives an independent external input Poisson spike train. **b** Asynchronous spike raster of 100 random neurons from balanced target network. **c** Maximal Lyapunov exponent as function of external coupling strength J_0^{ext} for different recurrent spike onset rapidness ($r = 3$, 10, 100). **d** Spike train of one random neuron across different initial conditions for weak (top), intermediate, and strong (bottom) frozen Poisson input realization ($J_0^{\text{ext}} = 0$, 2, 8, $r = 10$) (other parameters: $N = 2000$, $K = 1000$, $\bar{\nu} = 1$ Hz, $\nu_0^{\text{ext}} = 1$ Hz, $J_0 = 1$, $\tau_m = 10$ ms).

used for event-based, numerically exact simulations of the network dynamics and allows us to access the Jacobian $D(t_s) = \frac{\partial \vec{\phi}(t_s)}{\partial \vec{\phi}(t_{s-1})}$, which describes how an infinitesimal network state perturbation evolves from one network spike time until the next:

$$D_{i,j}(t_s) = \begin{cases} d_{i^*}(t_s) & \text{for } i = j = i^* \text{ and } j^* \leq N^* \\ 1 - d_{i^*}(t_s) & \text{for } i = i^* \text{ and } j = j^* \leq N \\ \delta_{ij} & \text{otherwise if j}^* \leq \text{N}, \end{cases} \tag{3}$$

where j^* denotes the neuron spiking at time t_s, $i^* \in \text{post}\,(j^*)$ its postsynaptic neurons, δ_{ij} is the Kronecker symbol and $d_{i^*}(t_s)$ is the derivative of the phase transition curve of ϕ_i. With the Jacobian (3) we can define the long term Jacobian $L(t_p) = \prod_{s=1}^{p} D(t_s)$ and the Oseledets matrix $\Lambda = \lim_{p\to\infty} \left(L^\top(t_p) L(t_p)\right)^{\frac{1}{2t_p}}$ [17]. The logarithms of the eigenvalues of Λ are the Lyapunov exponents, measuring the average exponential sensitivity to small perturbations in the tangent space along a trajectory. As Λ quickly becomes ill-conditioned, the Lyapunov exponents were calculated by the usual reorthonormalization procedure [16] (Code is in the supplemental material). From the ordered Lyapunov exponents $\lambda_1 > \ldots > \lambda_N$, we obtained the attractor dimension via the Kaplan–Yorke conjecture: $D = d + S_d/|\lambda_{d+1}|$ (for maximal d such that $S_d = \sum_{i=1}^{d} \lambda_i \geq 0$ [17]) and the Kolmogorov–Sinai entropy rate via Pesin's formula: $H = \sum_{\lambda_i > 0} \lambda_i$ [10, 17, 22].

Suppression of chaos by spiking input We first investigated the role of the coupling strengths J_0^{ext} of the incoming spike trains on the collective dynamics and controllability of the asynchronous irregular recurrent network dynamics (Fig. 1a+b). Generally, we find a suppression of the chaotic dynamics by input spike trains. Increasing the input coupling strength J_0^{ext} leads to decreasing the largest Lyapunov exponent λ_1 beyond zero, indicating a transition from chaotic to stable dynamics (Fig. 1c). High spike onset rapidness r in the target network facilitates the suppression of chaos, thus weaker external input is sufficient to tame the chaos. The reduction of chaos is accompanied by a reduced variability of spike times across trials with different initial conditions but same frozen input spike trains (Fig. 1d). For sufficiently strong input, even independent initial network states collapse to one time-dependent attractor, if they are driven by a "frozen" realization of input spike trains. This allows a direct interpretation for neural coding: The response of the network becomes reliable across trials, if the time-varying input is sufficiently strong and if the target neurons have a sufficiently rapid AP onset.

Also the dynamical entropy rate H and the attractor dimension D are decreasing for increasing the external input rate ν_0^{ext} and coupling strength J_0^{ext} (Fig. 2b+d, f+g). The critical coupling strength where chaos is suppressed scales numerically approximately $J_{0\,\text{crit}}^{\text{ext}} \propto J_0^{0.75} \nu_0^{\text{ext}\,-0.5} r^{-0.5}$ for large networks in the chaotic regime and saturates with K and N (see supplemental material). This suggests that for large K there is a critical input variance $\sigma_{\text{crit}}^{\text{ext}\,2} = J_0^{\text{ext}\,2} \cdot \nu_0^{\text{ext}}$, where the recurrent chaos is suppressed, which can be either generated by sufficiently frequent or easier by sufficiently strong input spike trains.

Transition towards complete network control: For sufficiently strong input, we observe a transition towards complete network control which is facilitated by rapid AP onset. After a transient, the spike raster of two independent initial conditions becomes identical and their Euclidean distance collapses to machine precision (Fig. 3a+c). Across many initial conditions and network realizations, the probability of convergence over time follows an exponential decay after a transient (Fig. 3b). The characteristic decay constant τ_c reduces as expected for increasing input strength J_0^{ext}, but also for increasing spike onset rapidness r (Fig. 3d). This indicates that networks with rapid spike onset not only require weaker spiking input to suppress chaos, but also that complete network control is obtained faster.

Stability against finite-size perturbations: How does spiking input affect the sensitivity to finite-size perturbations of the recurrent network state? Stability to infinitesimal perturbations accompanied by instability to sufficiently large perturbations was previously described in balanced networks of pulse-coupled leaky integrate-and-fire neurons with constant input [20]. In such non-

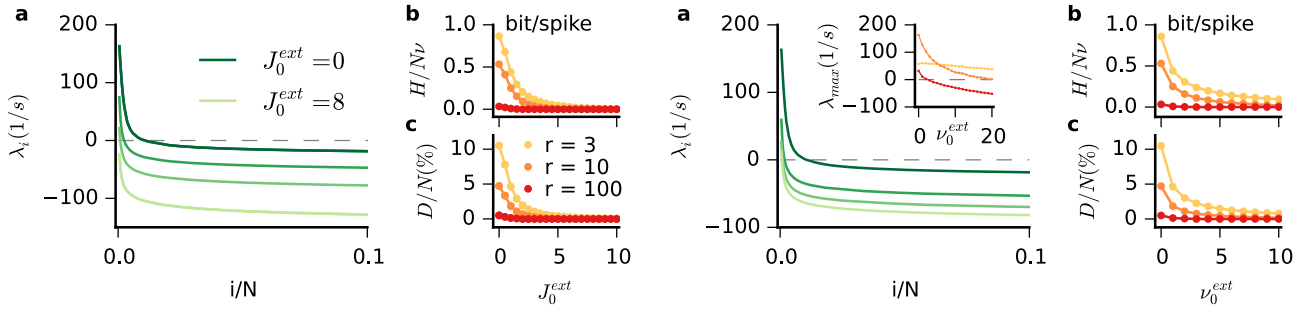

Figure 2: **Increasing input coupling and input rate decreases entropy rate and attractor dimensionality.** **a** Lyapunov spectrum for different input coupling strength ($J_0^{\text{ext}} = 0, 2, 4, 8$, $r = 10$). **b** Dynamical entropy rate H per spike and **c** relative attractor dimension D/N as a function of input coupling strength J_0^{ext}. **d - f** Same as **a-c** for different input firing rate ($\nu_0^{\text{ext}} = 0, 2, 4, 8\,\text{Hz}$). Inset of **d** shows the largest Lyapunov exponent as function of input firing rate ν_0^{ext} for $r = 3, 10, 100$ (other parameters as in Fig. 1).

chaotic networks [13, 20], the probability of separation P_s of perturbed and unperturbed trajectories as function of perturbation strength ε was very well fitted by $P_s(\varepsilon) = 1 - \exp(-\varepsilon/\varepsilon_{\text{ft}})$. The characteristic perturbation size ε_{ft} gives the average diameter of the basins of attraction, called flux tubes. This flux tube radius was numerically and analytically found to scale $\varepsilon_{\text{ft}} \propto \frac{J_0}{\sqrt{NK}\bar{\nu}\tau_{\text{m}}}$[20, 21]. Thus, it becomes very small for large networks, which results in sensitivity even to microscopic perturbations. Here, we investigated the effect of streams of incoming spike trains on flux tubes. We measured the probability of separation P_s as a function of perturbation strength ε for different values of spike onset rapidness r (Fig. 4a) and different values of input coupling strength J_0^{ext} (Fig. 4b) after 10 s of network simulation across different initial conditions and input realizations. Perturbations were applied in the phase representation in random directions perpendicular to the flow of the dynamics. We generally found that external spiking input stabilizes against finite-size perturbations, reflected in an increasing flux tube radius ε_{ft} for increasing the coupling strength of externally incoming streams of spike trains (Fig. 4c). Input spike trains even lead to the emergence of flux tubes in networks that are chaotic without input ($r = 100, 300$). For sufficiently strong input, the flux tube radius diverges, thus the network dynamics becomes insensitive to arbitrarily strong perturbations (Fig. 4c) and no separate flux tubes coexist any more. Intriguingly, this transition to complete network control generally occurs at different values of external input strength than the transition from chaos to stability (Fig. 4c). Crucially, the flux tube radius in strongly driven networks depends on the simulation time (We chose 10 s above). While a sufficiently strong perturbation might lead to a transient decorrelation, the perturbed and the unperturbed trajectory can coalesce later due to the external input.

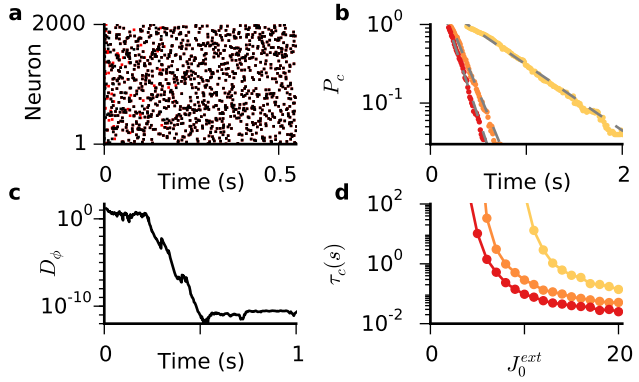

Figure 3: **Transition towards complete network control for strong input.** **a** Example spike raster of two independent initial conditions with same external Poisson input spike trains converge fast. **b** Convergence probability as function of time for different spike onset rapidness r **c** Euclidean distance between network states $\vec{\phi}$ of example **a**. **d** Characteristic convergence time τ_{c} vs. input strength J_0^{ext} for different spike onset rapidness ($r = 3, 10, 100$) (other parameters as in Fig. 1).

Summary: We investigated how the statistics of incoming spike trains and the AP onset rapidness shape chaos and controllability of balanced networks. We find a suppression of chaos and vanishing Kolmogorov–Sinai entropy rate in spiking balanced networks by streams of input spike trains, which is facilitated by a rapid spike onset dynamics. For strong external spiking input, we find a transition to complete network control, which occurs at higher external input coupling strength and rate than the transition from chaos to stability. This is surprising, because earlier studies suggested that a negative largest Lyapunov exponent implies that trajectories formed by different initial conditions collapse on a random sink [1, 2, 22, 23]. While this holds in the limit of large time for random dynamical systems when cer-

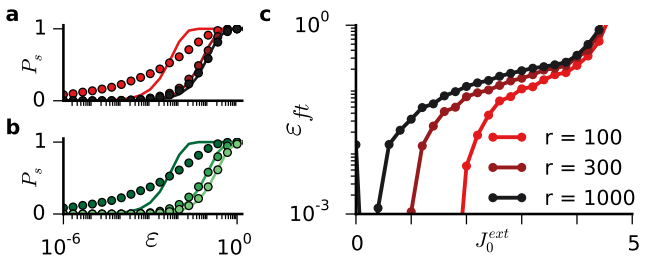

Figure 4: **External spiking input reduces sensitivity to finite-size perturbation in stable networks. a** Probability P_s of separation of trajectories after a perturbation of strength ε for different rapidness r = 100, 300, 1000 in log-linear plot. Full lines: fit to $P_s(\varepsilon) = 1 - \exp(-\varepsilon/\varepsilon_{ft})$. **b** Same as **a** for different input coupling strengths (J_0^{ext} = 2, 3, 4). Note the deviations from the fits in **a**+**b** for small rapidness and strong external input caused by non-exponential separation probabilities. **c** Characteristic perturbation size ε_{ft} as function of input coupling strength J_0^{ext} for different rapidness (r = 100, 300, 1000) (other parameters as in Fig. 1, average of 1000 input realizations and initial conditions with 10 random perturbation directions each).

tain non-degeneracy conditions are satisfied [9], we find that on neurobiologically relevant time scales, streams of input spikes can suppress chaos without collapsing independent initial conditions onto a random sink.

This is for the first time to our knowledge that for recurrent networks a clear link between single cell features and their role in the collective information transmission in a complex system was shown. This study extends earlier works on chaotic networks of rate neurons [25–27] to spiking neurons. Our results suggest that response reliability of neuronal circuits to an external stimulus is increased, the stronger the spatio-temporal input is. Our study predicts that rapid spike onset decreases trial-to-trial variability in a driven target circuit and therefore augments information flow. These results can also be used to understand and optimize emerging optogenetic approaches to achieve network control. We thank G. Lajoie, A. Renart, H. Sompolinsky, C. van Vreeswijk, M. Timme, J. Liedtke, A. Schmidt and M. Puelma Touzel for fruitful discussions. This work was supported by MPG, BMBF and Evangelisches Studienwerk Villigst.

* Electronic address: rainer@nld.ds.mpg.de

[1] G. Lajoie, K. K. Lin, and E. Shea-Brown, Phys. Rev. E **87**, 052901 (2013).
[2] G. Lajoie, J.-P. Thivierge, and E. Shea-Brown, Front. Comput. Neurosci **8**, 123 (2014).
[3] H. L. Bryant and J. P. Segundo, J Physiol **260**, 279 (1976); Z. F. Mainen, T. J. Sejnowski, Science **268**, 1503 (1995).
[4] C. van Vreeswijk and H. Sompolinsky, Science **274**, 1724 (1996); C. van Vreeswijk and H. Sompolinsky, Neural Comput. **10**, 1321 (1998); A. Renart et al., Science **327**, 587 (2010).
[5] M. Monteforte and F. Wolf, Phys. Rev. Lett. **105**, 268104 (2010).
[6] G. B. Ermentrout and N. Kopell, SIAM J. Appl. Math. **46**, 233 (1986); B. S. Gutkin and G. B. Ermentrout, Neural Comput. **10**, 1047 (1998); J. C. Brumberg and B. S. Gutkin, Brain Res. **1171**, 122 (2007).
[7] V. Ilin, A. Malyshev, F. Wolf, and M. Volgushev, J. Neurosci. **33**, 2281 (2013).
[8] M. Monteforte, PhD thesis, Georg-August-University Göttingen (2011).
[9] Y. Le Jan, Annales de l'I.H.P. Probabilités et statistiques **23**, 111 (1987); Baxendale, P. H. in Diffusion Processes and Related Problems in Analysis, Volume II (eds. Pinsky, M. A. & Wihstutz, V.) 3–35 (Birkhäuser Boston, 1992).
[10] F. Ledrappier and L.-S. Young, Probability Theory and Related Fields **80**, 217 (1988).
[11] M. N. Shadlen, W. T. Newsome, Curr. Opin. Neurobiol. **4**, 569 (1994); M. N. Shadlen and W. T. Newsome, J. Neurosci. 18, 3870 (1998); W. R. Softky, Curr. Opin. Neurobiol. **5**, 239 (1995).
[12] M. Tsodyks and T. Sejnowski, Network **6**, 111 (1995); D. J. Amit and N. Brunel, Cereb. Cortex **7**, 237 (1997); D. J. Amit and N. Brunel, Network **8**, 373 (1997); T. W. Troyer, K. D. Miller, Neural Comput. **9**, 971 (1997); N. Brunel, J. Comput. Neurosci. **8** 183 (2000); A. Lerchner et al., Neural Comput. **18**, 634 (2006).
[13] R. Zillmer, R. Livi, A. Politi, and A. Torcini, Phys. Rev. E **74**, 036203 (2006); S. Jahnke, R. M. Memmesheimer, and M. Timme, Phys. Rev. Lett. **100**, 048102 (2008); R. Zillmer, N. Brunel and D. Hansel, Phys. Rev. E **79**, 031909 (2009).
[14] A. Politi et al., Europhys. Lett. **22**, 571 (1993).
[15] J. S. Isaacson and M. Scanziani, Neuron **72**, 231 (2011).
[16] G. Benettin et al., Meccanica **15**, 9 (1980).
[17] J.-P. Eckmann and D. Ruelle, Rev. Mod. Phys. **57**, 617 (1985).
[18] D. Ruelle, Commun. Math. Phys. **87**, 287 (1982).
[19] S. Panzeri et al., Neuron **29**, 769 (2001).
[20] M. Monteforte and F. Wolf, Phys. Rev. X **2**, 041007 (2012).
[21] M. Puelma Touzel, PhD thesis, Georg-August-University Göttingen (2016).
[22] L.-S. Young, Comm. Pure Appl. Math. 66, 1439 (2013).
[23] K. K. Lin, in Nonautonomous Dynamical Systems in the Life Sciences, edited by P. E. Kloeden and C. Pötzsche (Springer International Publishing, 2013), pp. 135–161.
[24] B. D. Burns and A. C. Webb, Proc. R. Soc. B **194**, 211 (1976); W. R. Softky and C. Koch, J. Neurosci. **13**, 334 (1993); P. Kara, P. Reinagel, R. C. Reid, Neuron **27**, 635 (2000).
[25] L. Molgedey, J. Schuchhardt, and H. Schuster, Phys. Rev. Lett. **69**, 3717 (1992).
[26] K. Rajan, L. F. Abbott, and H. Sompolinsky, Phys. Rev. E **82**, 011903 (2010).
[27] S. Goedeke, J. Schuecker, and M. Helias, arXiv:1603.01880 [Nlin, Q-Bio] (2016).
[28] H. Kantz and E. Olbrich, Chaos **7**, 423 (1997).

Supplemental Material for "The Transition to Control in Spiking Networks"

Rainer Engelken* and Fred Wolf
Max Planck Institute for Dynamics and Self-Organization, Göttingen, Germany,
Faculty of Physics, Georg-August-Universität Göttingen, Göttingen, Germany,
Bernstein Center for Computational Neuroscience, Göttingen, Germany

Contents

I. Model: The rapid theta neuron model driven by external and recurrent spike trains 1

II. Phase representation of the rapid theta neuron 2

III. Single spike Jacobian of the rapid theta neuron network with incoming spike train 4

IV. Setup of balanced network and event-based simulation 6

V. Scaling of critical input strength 9

VI. Implementation and convergence of the Lyapunov spectra 9

VII. Bursty input spike trains reduce chaos 11

VIII. Input correlations reduce chaos 12

References 14

I. MODEL: THE RAPID THETA NEURON MODEL DRIVEN BY EXTERNAL AND RECURRENT SPIKE TRAINS

To examine the effect of streams of incoming spike trains on the collective dynamics and reliability of cortical networks with different action potential (AP) onset rapidness, we use a novel neuron model with variable AP onset rapidness, called the rapid theta neuron model [1, 2]. This neuron model is similar to the exponential integrate-and-fire neuron [12], but much more tractable for high precision calculations. The rapid theta neuron model combines the advantage of the theta neuron model for the analytical derivation of the phase-response curve with a modifiable AP onset rapidness r. For $r = 1$, the rapid theta neuron model is equivalent to the theta neuron model [4], which is the phase representation of the quadratic integrate-and-fire neuron. Increasing r decreases the time constant at the unstable fixed point V_{U} (voltage threshold) leading to a larger instability and *sharper* AP initiation. The membrane time constant τ_{m}, the time constant at the stable fixed point V_{S} (resting potential) remains unchanged. This is achieved by gluing two parabolas smoothly together at V_{G}. In the dimensionless voltage representation, the resulting rapid theta neuron model is described by the differential equation

$$\tau_{\mathrm{m}} \frac{\mathrm{d}V}{\mathrm{d}t} = \begin{cases} a_{\mathrm{S}}(V - V_{\mathrm{G}})^2 - I_{\mathrm{T}} + I(t) & V \le V_{\mathrm{G}} \\ a_{\mathrm{U}}(V - V_{\mathrm{G}})^2 - I_{\mathrm{T}} + I(t) & V > V_{\mathrm{G}}. \end{cases} \tag{1}$$

In this equation, I_T denotes the rheobase current and $I(t)$ is the synaptic input current. The curvatures $a_{\mathrm{U,S}}$ depend on the AP onset rapidness r and together with V_G and I_T define the positions of the two branches of the parabolas. The glue point, denoted V_{G}, where the two branches are continuously and smoothly glued together divides the single neuron phase space into two ($V \le V_{\mathrm{G}}$) ($V > V_{\mathrm{G}}$) parts. At the stable fixed point V_{S}, the slope of the subthreshold parabola is set to $-1/\tau_{\mathrm{m}}$ and at the unstable fixed point V_U the slope is r/τ_{m}.

Without loss of generality, the stable and unstable fixed points are set to $V_S = -0.5$ and $V_U = +0.5$, yielding:

$$V_{\mathrm{G}} = \frac{1}{2}\frac{r-1}{r+1} \tag{2}$$

$$I_{\mathrm{T}} = \frac{1}{2}\frac{r}{r+1} \tag{3}$$

$$a_{\mathrm{S}} = \frac{r+1}{2r} \tag{4}$$

$$a_{\mathrm{U}} = \frac{r(r+1)}{2} = r^2 a_{\mathrm{S}}. \tag{5}$$

With Eq. (2)-(5) the governing equation of the rapid theta neuron model (1) becomes

$$\tau_{\mathrm{m}}\frac{\mathrm{d}V}{\mathrm{d}t} = \begin{cases} \frac{r+1}{2r}\left(V - \frac{1}{2}\frac{r-1}{r+1}\right)^2 - \frac{1}{2}\frac{r}{r+1} + I(t) & V \le \frac{1}{2}\frac{r-1}{r+1} \\ \frac{r(r+1)}{2}\left(V - \frac{1}{2}\frac{r-1}{r+1}\right)^2 - \frac{1}{2}\frac{r}{r+1} + I(t) & V > \frac{1}{2}\frac{r-1}{r+1}. \end{cases} \tag{6}$$

II. PHASE REPRESENTATION OF THE RAPID THETA NEURON

A phase representation of the rapid theta neuron model similar to the classical theta neuron model is obtained with the transformation $\tan\frac{\theta}{2} = V - V_G$ and $\theta \in [-\pi, \pi)$, yielding

$$\tau_{\mathrm{m}}\frac{\mathrm{d}\theta}{\mathrm{d}t} = \begin{cases} \frac{r+1}{2r}\big(1-\cos\theta\big) + \big(I(t) - I_{\mathrm{T}}\big)\big(1+\cos\theta\big) & \theta \le 0 \\ \frac{r(r+1)}{2}\big(1-\cos\theta\big) + \big(I(t) - I_{\mathrm{T}}\big)\big(1+\cos\theta\big) & \theta > 0. \end{cases} \tag{7}$$

For $r = 1$ the theta neuron model is recovered [4].

The exact solutions of the dynamics of the rapid theta neuron model between network spikes for constant positive external currents and δ pulse coupling both for the recurrent and external spiking input allow us to write down a phase representation with constant phase velocity. Such a phase representation is convenient both for efficient, numerically exact, event-based simulation and also for analytical tractability. The description of the phase representation, the single spike Jacobian and the setup of the balanced networks are adapted from Ref. [1, 2], taking into account streams of external input spike trains.

The solution of the governing differential equation in the dimensionless voltage representation Eq. (1) for constant input currents between two spikes $I(t) \equiv I_T + I$ is

$$\begin{aligned} \frac{1}{I}\frac{\mathrm{d}V}{1 + \left(\frac{V - V_{\mathrm{G}}}{\sqrt{I/a_{\mathrm{S,U}}}}\right)^2} &= \frac{1}{\tau_{\mathrm{m}}}\mathrm{d}t \\ \frac{1}{I}\sqrt{I/a_{\mathrm{S,U}}}\left[\arctan\left(\frac{V - V_{\mathrm{G}}}{\sqrt{I/a_{\mathrm{S,U}}}}\right)\right]_{V_1}^{V_2} &= \frac{t_2 - t_1}{\tau_{\mathrm{m}}} \\ \arctan\left(\frac{V_2 - V_{\mathrm{G}}}{\sqrt{I/a_{\mathrm{S,U}}}}\right) &= \arctan\left(\frac{V_1 - V_{\mathrm{G}}}{\sqrt{I/a_{\mathrm{S,U}}}}\right) + \sqrt{I\,a_{\mathrm{S,U}}}\frac{t_2 - t_1}{\tau_{\mathrm{m}}}. \end{aligned} \tag{8}$$

This equation represents the solution for both branches of Eq. (1) separated by V_G as before. For the subthreshold part ($V \le V_{\mathrm{G}}$), the curvature is $a_S = \frac{r+1}{2r}$ and for the suprathreshold part ($V > V_{\mathrm{G}}$), the curvature is $a_{\mathrm{U}} = \frac{r(r+1)}{2}$. In the phase representation with phase $\phi \in [-\pi, \pi)$ and constant phase velocity ω, the phase evolution is given by

$$\phi_2 = \phi_1 + \omega\frac{t_2 - t_1}{\tau_{\mathrm{m}}}. \tag{9}$$

Identifying Eq. (8) and (9), enables us to derive the constant phase velocity ω and the glue point ϕ_G to define the transformation between the two representations

$$\frac{\phi - \phi_{\mathrm{G}}}{\omega} = \arctan\left(\frac{V - V_{\mathrm{G}}}{\sqrt{I/a_{\mathrm{S,U}}}}\right)\frac{1}{\sqrt{I\,a_{\mathrm{S,U}}}}. \tag{10}$$

During one complete cycle, the time $T_{\rm S}$ spent in the subthreshold part ($V_2 = V_{\rm G}$ and $V_1 \to -\infty$) and the time $T_{\rm U}$ spent in the suprathreshold part ($V_2 \to \infty$ and $V_1 \to V_{\rm G}$) was obtained from Eq. (8):

$$T_{\rm S} = \frac{\pi\tau_{\rm m}}{\sqrt{2I(r+1)/r}} \quad \text{and} \quad T_{\rm U} = \frac{\pi\tau_{\rm m}}{\sqrt{2I(r+1)r}}.$$

The time spent in the subthreshold part is thus $T_{\rm S}/T_{\rm U} = r$ times as long as the time spent in the suprathreshold part. The total cycle length, or unperturbed interspike interval, is thus

$$\begin{aligned} T^{\rm free} &= (r+1)T_{\rm U} \\ &= \frac{\pi\tau_{\rm m}}{\sqrt{I}}\sqrt{\frac{r+1}{2r}}. \end{aligned} \tag{11}$$

Its inverse gives the firing rate for constant external input.

The constant phase velocity is then

$$\begin{aligned} \omega &= \frac{2\pi}{T^{\rm free}} \\ &= \frac{2\sqrt{I}}{\tau_{\rm m}}\sqrt{\frac{2r}{r+1}} = \frac{2}{\tau_{\rm m}}\sqrt{I/a_{\rm S}} \end{aligned} \tag{12}$$

The phase corresponding to the glue point is

$$\begin{aligned} \phi_{\rm G} &= -\pi + \omega T_{\rm S} \\ &= \pi\frac{r-1}{r+1}. \end{aligned} \tag{13}$$

The constant phase velocity (12) and the glue point (13) define the transformation (10) between the voltage representation and the phase representation:

$$\phi = \phi_{\rm G} + \begin{cases} \frac{2}{a_{\rm S}}\arctan\left(\frac{V-V_{\rm G}}{\sqrt{I/a_{\rm S}}}\right) & V \le V_{\rm G} \\ \frac{2}{ra_{\rm S}}\arctan\left(r\frac{V-V_{\rm G}}{\sqrt{I/a_{\rm S}}}\right) & V > V_{\rm G} \end{cases} \tag{14}$$

$$V = V_{\rm G} + \begin{cases} \sqrt{I/a_{\rm S}}\tan\left(a_{\rm S}\frac{\phi-\phi_{\rm G}}{2}\right) & \phi \le \phi_G \\ \sqrt{I/r^2a_{\rm S}}\tan\left(ra_{\rm S}\frac{\phi-\phi_{\rm G}}{2}\right) & \phi > \phi_G. \end{cases} \tag{15}$$

This transformation between the two equivalent representations is now used to calculate the phase-transition curve $g(\phi)$ and the phase-response curve $Z(\phi)$. Receiving a δ pulse of strength J, irrespective whether it is a recurrently connected neuron $J_{\rm rec}$ or an external input with $J_{\rm in}$ that leads to a step-like change of the neuron's voltage $V^+ = V^- + J$. If this change does not lead to a change from the subthreshold to the suprathreshold part or reverse, the calculation of the phase-transition curve is straightforward. Some care needs to be taken, if the δ pulse does lead to such a change.

An inhibitory pulse $J < 0$ can lead to a change from the suprathreshold to the subthreshold part. This happens if the neuron's phase is between $\phi_{\rm G}$ and ϕ_-. The phase-transition curve for inhibitory δ pulses of strength J and constant external currents I with the effective coupling $C = J/\sqrt{I}$ and $\phi_- = \phi_{\rm G} + \frac{2}{ra_{\rm S}}\arctan\left(r(V_{\rm G}-J-V_{\rm G})/\sqrt{I/a_{\rm S}}\right) = \phi_{\rm G} - \frac{2}{ra_{\rm S}}\arctan\left(r\sqrt{a_{\rm S}}C\right)$ is

$$\mathrm{g}_-(\phi) = \phi_{\rm G} + \begin{cases} \frac{2}{a_{\rm S}}\arctan\left(\tan\left(a_{\rm S}\frac{\phi-\phi_{\rm G}}{2}\right) + \sqrt{a_{\rm S}}C\right) & -\pi < \phi \le \phi_{\rm G} \\ \frac{2}{a_{\rm S}}\arctan\left(\frac{1}{r}\tan\left(ra_{\rm S}\frac{\phi-\phi_{\rm G}}{2}\right) + \sqrt{a_{\rm S}}C\right) & \phi_{\rm G} < \phi < \phi_- \\ \frac{2}{ra_{\rm S}}\arctan\left(\tan\left(ra_{\rm S}\frac{\phi-\phi_{\rm G}}{2}\right) + r\sqrt{a_{\rm S}}C\right) & \phi_- \le \phi < \pi. \end{cases} \tag{16}$$

For excitatory δ pulses of strength $J > 0$, the phase can change from the subthreshold to the suprathreshold part if the phase is between ϕ_+ and $\phi_{\rm G}$. The phase-transition curve for excitatory δ pulses of strength J and constant

external currents I with the effective coupling $C = J/\sqrt{I}$ and $\phi_+ = \phi_G - \frac{2}{a_S}\arctan(\sqrt{a_S}C)$ (displayed in **Fig. 1**) is

$$g_+(\phi) \;=\; \phi_G + \begin{cases} \frac{2}{a_S}\arctan\left(\tan\left(a_S\frac{\phi-\phi_G}{2}\right)+\sqrt{a_S}C\right) & -\pi < \phi \le \phi_+ \\ \frac{2}{ra_S}\arctan\left(r\tan\left(a_S\frac{\phi-\phi_G}{2}\right)+r\sqrt{a_S}C\right) & \phi_+ < \phi < \phi_G \\ \frac{2}{ra_S}\arctan\left(\tan\left(ra_S\frac{\phi-\phi_G}{2}\right)+r\sqrt{a_S}C\right) & \phi_G \le \phi < \pi. \end{cases} \tag{17}$$

The phase-response curve is $Z_\pm(\phi) = g_\pm(\phi) - \phi$. Thus, the infinitesimal phase-response curve is the same for both excitatory and inhibitory pulses, since $\phi_\pm \to \phi_G$ for $C \to 0$:

$$Z(\phi) \overset{C\to 0}{\simeq} C \begin{cases} \frac{2\sqrt{a_S}}{a_S}\frac{1}{1+\tan\left(a_S\frac{\phi-\phi_G}{2}\right)^2} = \frac{1+\cos\left(a_S(\phi-\phi_G)\right)}{\sqrt{a_S}} & -\pi < \phi \le \phi_G \\ \frac{2r\sqrt{a_S}}{ra_S}\frac{1}{1+\tan\left(ra_S\frac{\phi-\phi_G}{2}\right)^2} = \frac{1+\cos\left(ra_S(\phi-\phi_G)\right)}{\sqrt{a_S}} & \phi_G \le \phi < \pi. \end{cases} \tag{18}$$

Note that for $J_0^{\mathrm{rec}} \neq J_0^{\mathrm{ext}}$, the shape of the phase response curve and its derivative can look very differently, depending on whether a recurrent or an external arriving pulse is considered.

III. SINGLE SPIKE JACOBIAN OF THE RAPID THETA NEURON NETWORK WITH INCOMING SPIKE TRAIN

As we drive the rapid theta neuron network with streams of delta-function current pulses, we can solve the dynamics between subsequent network events analytically. The analytical expression of the derivative of the evolution map, called the single spike Jacobian, is necessary for calculating the full Lyapunov spectrum with high precision. The single spike Jacobian describes the linear evolution of infinitesimal perturbations of the recurrent neuron's states and will be used to calculate the Lyapunov spectra numerically. Since infinitesimal perturbations of the recurrent network are considered here, the spike-order in the recurrent network is preserved. This is true as long as there are no exactly synchronous spike events which generally occur with probability zero in the considered asynchronous irregular network states. In a phase representation, the iterative map, which maps the state of the network at one spike time to the state at the next spike in the network, reads

$$\phi_i(t_{s+1}) = \phi_i(t_s) + \omega_i(t_{s+1}-t_s) + Z\big(\phi_i(t_s)+\omega_i(t_{s+1}-t_s)\big)\delta_{i\in\mathrm{post}(j^*)}, \tag{19}$$

where $\delta_{i\in\mathrm{post}(j^*)}$ is one if i is a postsynaptic neuron of the spiking neuron j^* and zero otherwise and $Z(\phi_i)$ is the phase-response curve. Note that j^* is a recurrent neuron if $j^* \le N$. If $j^* > N$, it is a spike of one of the external neurons, which are modeled as Poisson processes.

Thus, the $N \times N$ single spike Jacobian reads

$$D_{ij}(t_s) = \frac{\mathrm{d}\phi_i(t_{s+1})}{\mathrm{d}\phi_j(t_s)} = \begin{cases} 1 + Z'(\phi_{i^*}(t_{s+1}^-)) & \text{for } i=j=i^* \text{ and } j^* \le N \\ -\frac{\omega_{i^*}}{\omega_{j^*}}Z'(\phi_{i^*}(t_{s+1}^-)) & \text{for } i=i^* \text{ and } j=j^* \le N \\ \delta_{ij} & \text{otherwise if } j^* \le N, \end{cases} \tag{20}$$

where j^* denotes the spiking neuron in the considered interval, firing at time t_{s+1}, $i^* \in \mathrm{post}(j^*)$ are the spike receiving neurons and δ_{ij} is the Kronecker delta. The derivatives of the phase-response curves $Z'(\phi)$ are calculated at the phases of the postsynaptic neurons $\phi_{i^*}(t_{s+1}^-) = \phi_{i^*}(t_s) + \omega_{i^*}(t_{s+1}-t_s)$ where Z' is evaluated before they receive the spike, denoted by t_{s+1}^-.

To make the structure of the Jacobian more clear, in case of an externally incoming spike, the full Jacobian takes the following form:

$$\mathbf{D}(t_s) \;=\; \begin{pmatrix} 1 & 0 & & & & \dots & 0 \\ 0 & \ddots & & & & & \vdots \\ & & 1+Z' & & & & \\ & & & 1 & & & \\ & & & & 1+Z' & & \vdots \\ \vdots & & & & & \ddots & 0 \\ 0 & \dots & & & \dots & 0 & 1 \end{pmatrix} \begin{matrix} \\ \\ \leftarrow \text{postsynaptic } i^* \\ \\ \\ \leftarrow \text{postsynaptic } i^* \\ \\ \\ \end{matrix} \tag{21}$$

Thus, in case of external input, the Jacobian is just a scaling of the rows i^* of the orthonormal matrix Q_{ij} corresponding to the postsynaptic neurons by the derivative of the phase transition curve evaluated for the respective postsynaptic neurons. In case of a recurrent incoming spike it takes the following form:

$$\mathbf{D}(t_s) \;=\; \begin{pmatrix} 1 & 0 & & & & & & \dots & 0 \\ 0 & 1 & & & & & & & \vdots \\ & & 1+Z' & & & & -\frac{\omega_{i^*}}{\omega_{j^*}}Z' & & \\ & & & & 1 & & 0 & & \\ & & & & & 1+Z' & -\frac{\omega_{i^*}}{\omega_{j^*}}Z' & & \\ & & & & & 1 & 0 & & \\ & & & & & & \ddots & \vdots & \\ & & & & & & \ddots & 0 & \\ & & & & & & & 1 & \\ & & & & & & & & \vdots \\ \vdots & & & & & & & \ddots & 0 \\ 0 & \dots & & & & & & \dots \; 0 & 1 \end{pmatrix} \begin{matrix} \\ \\ \leftarrow \text{postsynaptic } i^* \\ \\ \leftarrow \text{postsynaptic } i^* \\ \\ \\ \\ \\ \\ \\ \\ \end{matrix} \tag{22}$$

$$\uparrow$$

column j^*

Thus, it can be written as a sum of the identity matrix, a sparse diagonal matrix with diagonal entries Z' and a matrix with one nonzero sparse column j^*. This structure can be used both for efficient storage and for the efficient evolution of the orthonormal basis Q during the calculating of the Lyapunov spectrum. To investigate the collective dynamics of networks of rapid theta neurons, the derivative $d(\phi_{i^*}(t_{s+1}^-)) = 1 + Z'(\phi_{i^*}(t_{s+1}^-))$ of the phase-transition curve is needed for the single spike Jacobians. The derivative $d(\phi)$ in case of inhibitory pulses is

$$d_-(\phi) \;=\; \begin{cases} \frac{\tan\left(a_{\mathrm{S}}\frac{\phi-\phi_{\mathrm{G}}}{2}\right)^2+1}{\left(\tan\left(a_{\mathrm{S}}\frac{\phi-\phi_{\mathrm{G}}}{2}\right)+\sqrt{a_{\mathrm{S}}}C\right)^2+1} & -\pi < \phi \le \phi_{\mathrm{G}} \\ \frac{\tan\left(ra_{\mathrm{S}}\frac{\phi-\phi_{G}}{2}\right)^2+1}{\left(\frac{1}{r}\tan\left(ra_{\mathrm{S}}\frac{\phi-\phi_{\mathrm{G}}}{2}\right)+\sqrt{a_{\mathrm{S}}}C\right)^2+1} & \phi_{\mathrm{G}} < \phi < \phi_- \\ \frac{\tan\left(ra_{\mathrm{S}}\frac{\phi-\phi_{\mathrm{G}}}{2}\right)^2+1}{\left(\tan\left(ra_{\mathrm{S}}\frac{\phi-\phi_{\mathrm{G}}}{2}\right)+r\sqrt{a_{\mathrm{S}}}C\right)^2+1} & \phi_- \le \phi < \pi. \end{cases} \tag{23}$$

The derivative of the phase-transition curve in the case of excitatory pulses is

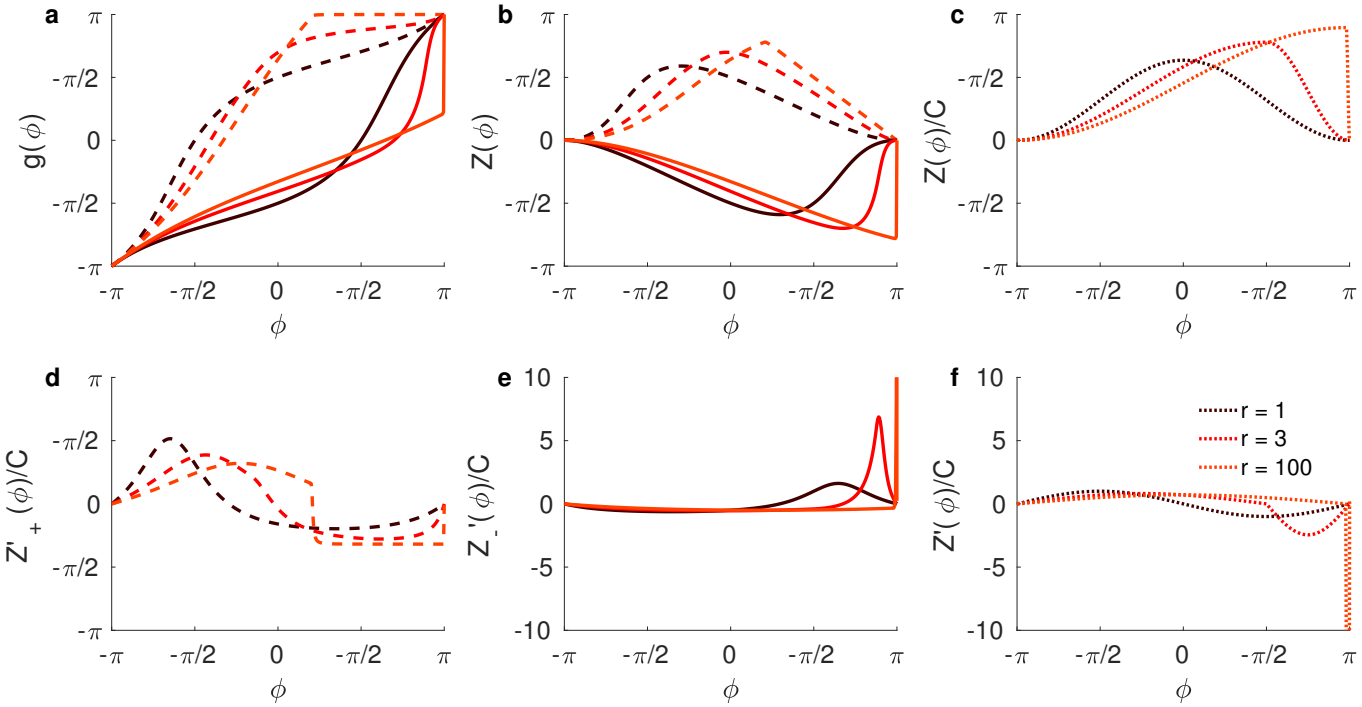

Figure 1: **Phase-transition curve (PTC), phase-response (PRC) and infinitesimal phase-response (iPRC) explain reduction of chaos for high AP onset rapidness** r. **a)** The phase-transition curve (PTC) $g(\phi)$ shown with inhibitory coupling $C = -1$ (full lines, Eq. (16)) and excitatory coupling $C = +1$ (dashed lines, Eq. (17)) for three values of spike onset rapidness $r = 1$, 3, 100. **b)** Same for phase response curve (PRC) $Z(\phi) = g(\phi) - \phi$. **c)** Same for infinitesimal PRC (Eq. (18)). **d)** Derivative of PRC for excitatory coupling. **e)** Derivative of PRC for excitatory coupling. **f)** Derivative of derivative of infinitesimal phase response curve (Eq. (25)). Note that in the limit $r \to \infty$ the iPRC becomes monotonically increasing and its derivative is positive almost everywhere.

$$d_+(\phi) = \begin{cases} \frac{\tan\left(a_S \frac{\phi-\phi_G}{2}\right)^2+1}{\left(\tan\left(a_S \frac{\phi-\phi_G}{2}\right)+\sqrt{a_S}C\right)^2+1} - 1 & -\pi < \phi \le \phi_+ \\ \frac{\tan\left(a_S \frac{\phi-\phi_G}{2}\right)^2+1}{\left(r\tan\left(a_S \frac{\phi-\phi_G}{2}\right)+r\sqrt{a_S}C\right)^2+1} - 1 & \phi_+ < \phi < \phi_G \\ \frac{\tan\left(ra_S \frac{\phi-\phi_G}{2}\right)^2+1}{\left(\tan\left(ra_S \frac{\phi-\phi_G}{2}\right)+r\sqrt{a_S}C\right)^2+1} - 1 & \phi_G \le \phi < \pi. \end{cases} \tag{24}$$

The derivative of the phase-response curve is $Z'_\pm(\phi) = d_\pm(\phi) - 1$ and the derivative of the infinitesimal phase-response curve is

$$Z'(\phi) \overset{C\to 0}{\simeq} -C \begin{cases} \sqrt{a_S}\sin\left(a_S(\phi-\phi_G)\right) & -\pi < \phi \le \phi_G \\ r\sqrt{a_S} - \sin\left(ra_S(\phi-\phi_G)\right) & \phi_G \le \phi < \pi. \end{cases} \tag{25}$$

The phase-transition curves (PTC, $g(\phi)$, Eq. (16) and (17)), the phase response curves (PRC, $Z(\phi) = g(\phi) - \phi$) and the infinitesimal phase-response curves (iPRC, Eq. (18)) of the rapid theta neuron model are displayed in **Fig. 1**. The iPRC of the theta neuron ($r = 1$) is fully symmetric, whereas for increasing AP onset rapidness r the iPRC becomes more and more asymmetric. In the limit $r \to \infty$ it becomes monotonically increasing/decreasing and one might expect that this can qualitatively change the collective network dynamics.

IV. SETUP OF BALANCED NETWORK AND EVENT-BASED SIMULATION

The pattern of action potentials in cortical tissue is asynchronous and irregular [25], despite experimental evidence that single neurons can respond reliably to an injected time-varying external stimulus [26–29].

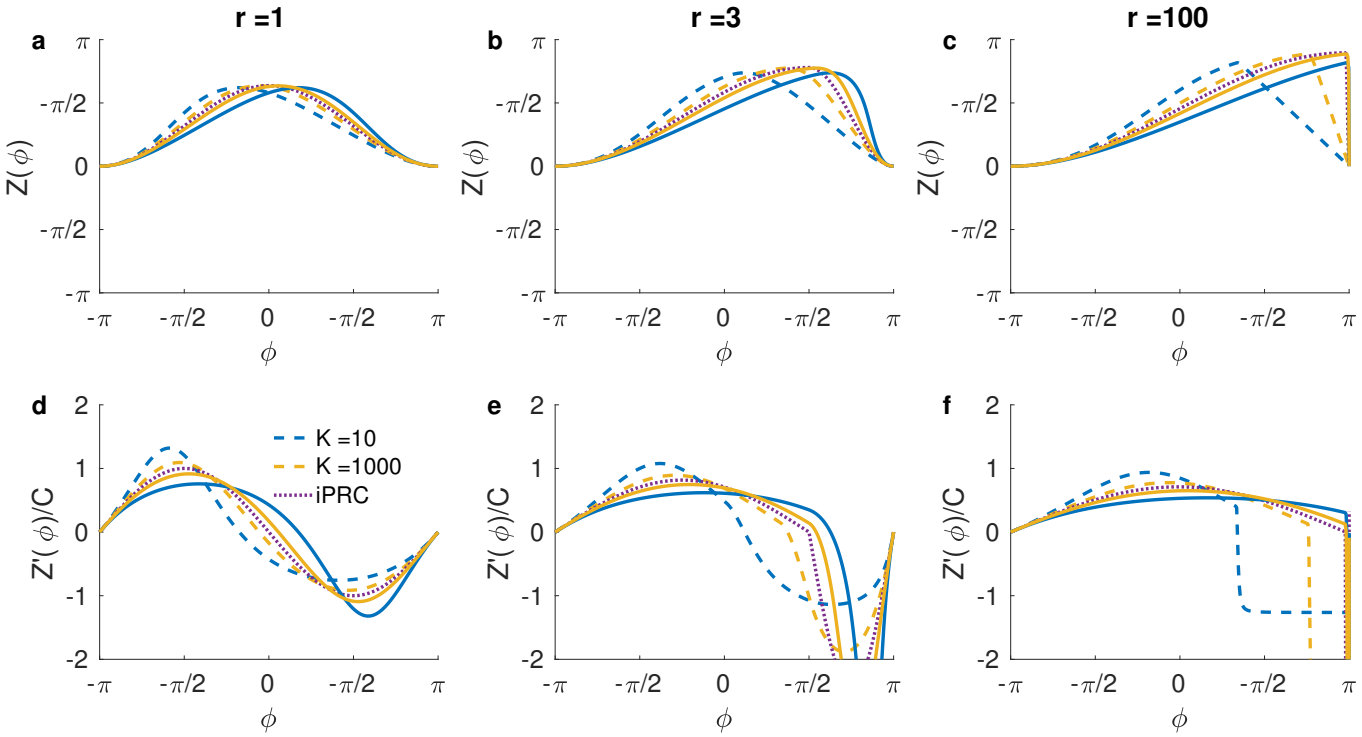

Figure 2: **Phase-response (PRC) and infinitesimal phase-response (iPRC) of the rapid theta neuron model for different effective coupling strengths**. **a)** The PRC is shown for different K corresponding to different coupling strengths $C = -\frac{J_0}{\sqrt{K}}\sqrt{\frac{a_S}{I}}$ for inhibitory (full lines Eq. (16)) and excitatory couplings (dashed lines, Eq. (17)) for AP onset rapidness $r = 1$. The infinitesimal PRC (Eq. (18)) is also displayed for comparison (dotted lines) **b)** Same as **a** for AP onset rapidness $r = 3$ **c)** Same as **a** for AP onset rapidness $r = 100$. **d)** Derivative of PRC normalized by C for $r = 1$. The derivative of the infinitesimal PRC is shown as dotted line (Eq. (25)). **e)** Same as **d** for $r = 3$. **f)** Same as **d** for $r = 100$ (parameters: $I_0 = 1$, $J_0 = 1$).

This is commonly explained by a balance of excitatory and inhibitory synaptic currents [33], which cancels large mean synaptic inputs. A dynamical self-organized balance can be achieved without fine-tuning of synaptic coupling strength, if the connectivity is inhibition-dominated [3]. The statistics of this state is described by a mean-field theory, which is largely independent of neuron model. Originally, the balanced regime was explored in networks of binary neurons, which receive constant external input to demonstrate that incoming variability is not necessary to generate asynchronous irregular activity. Later, this was also studied in networks of leaky-integrate and fire neurons with external Poisson input [8]. We studied large sparse networks of N rapid theta neurons arranged on a directed Erdös-Rényi random graph of mean degree K. All neurons $i = 1, \ldots, N$ received constant external currents I_{ext} and non-delayed δ-pulses from the presynaptic recurrent neurons $j \in \text{pre}\ (i)$ and external spikes with coupling strength $J^{\text{ext}} = -J_0^{\text{ext}}/\sqrt{K}$ from a Poisson process with rate $\nu^{\text{ext}} = \nu_0^{\text{ext}} \cdot K$. The external currents were chosen to obtain a certain average recurrent network firing rate $\bar{\nu}$ using a bisection method. The non-zero recurrent coupling strengths were set to $J_{ij}^{\text{rec}} = -J_0/\sqrt{K}$ and all neurons received identical external currents.

Setup of balanced network with strong couplings and nonvanishing fluctuations. The coupling strengths were chosen such that the magnitudes of the recurrent input current fluctuations were identical in all studied networks. Assuming that inputs from different presynaptic neurons are only weakly correlated, the recurrent compound input spike train received by neuron i can be modeled by a Poisson process with rate $\Omega_i = \sum_{j\in\text{pre}(i)} \nu_j \approx K\bar{\nu} \equiv \Omega$, where $\bar{\nu}$ is the network-averaged firing rate and K the average number of presynaptic neurons. The nonzero coupling strengths were $J_{ij} = -\frac{J_0}{\sqrt{K}}$. Under the assumption that the compound input spike train is a Poisson process, the recurrent input

current auto-correlation function reads

$$\begin{aligned} C(\tau) &= \langle \delta I(t)\delta I(t+\tau)\rangle_t \\ &\approx \left(\frac{J_0}{\sqrt{K}}\right)^2 \Omega \int \delta(t-s)\delta(t+\tau-s)\mathrm{d}s \\ &= \frac{J_0}{K}\Omega\delta(\tau) \\ &\approx J_0^2\bar{\nu}\delta(\tau) \end{aligned} \tag{26}$$

Thus, the fluctuations in the input currents can be described as delta-correlated white noise of magnitude

$$\sigma^2 = J_0^2\bar{\nu}. \tag{27}$$

Note that due to the scaling of the coupling strengths $J = -\frac{J_0}{\sqrt{K}}$ with the square root of the number of synapses K the magnitude of the fluctuations σ^2 is independent of the number of recurrent synapses. Therefore, the input fluctuations do not vanish in the thermodynamic limit and the balanced state in sparse networks emerges robustly [3].

The existence of a balanced state fixed point in the large K-limit follows from the equation of the network-averaged mean current

$$\bar{I} \approx \sqrt{K}(I_0 - J_0\bar{\nu}).$$

In the large K-limit, self-consistency requires the balance of excitation and inhibition $I_0 = J_0\bar{\nu}$: If $\lim_{K\to\infty}(I_0 - J_0\bar{\nu}) > 0$ the mean current $\bar{I}$ would diverge to ∞ and the neurons would fire at their maximal rate. The resulting strong inhibition would break the inequality, leading to a contradiction. If $\lim_{K\to\infty}(I_0 - J_0\bar{\nu}) < 0$ the mean current $\bar{I}$ would diverge to $-\infty$ and the neurons would be silent. The resulting lack of inhibition again breaks the inequality. The large K-limit is self-consistent if

$$\lim_{K\to\infty}(I_0 - J_0\bar{\nu}) = \mathcal{O}\left(\frac{1}{\sqrt{K}}\right),$$

such that excitatory external drive and mean recurrent inhibitory current cancel each other. Note that since $I_0 - J_0\bar{\nu} = \mathcal{O}(1/\sqrt{K})$ the network mean current has a finite large K-limit. The average firing rate in units of the membrane time constant τ_m^{-1} is approximately

$$\bar{\nu} = \frac{I_0}{J_0} + \mathcal{O}\left(\frac{1}{\sqrt{K}}\right). \tag{28}$$

All simulations were run event-based following Ref. [5], where an exact map was iterated from spike to spike in the ϕ-representation of the rapid theta neuron model with homogeneous coupling strengths and homogeneous external currents for all neurons in each population. The next spike time occurring in each population is obtained by inverting Eq. 9

$$t_s = t_{s-1} + \min_i \left\{ \frac{\pi - \phi_i(t_{s-1})}{\omega} \right\}. \tag{29}$$

The phase map $f(\vec{\phi}(t_{s-1})) = \vec{\phi}(t_s)$, iterating all neuron's phases between two successive spike events t_{s-1} and t_s in the network, is then the concatenation of Eq. 9 and the phase transition curve (Eq. 16 and Eq. 17)

$$f(\phi_i(t_{s-1})) = \begin{cases} \phi_i(t_{s-1}) + \omega(t_s - t_{s-1}) & \text{if } i \notin \mathrm{post}(j^*) \\ g(\phi_i(t_{s-1}) + \omega(t_s - t_{s-1})) & \text{if } i \in \mathrm{post}(j^*), \end{cases} \tag{30}$$

where $\mathrm{post}(j^*)$ denotes the set of neurons postsynaptic to the spiking neuron j^* in the considered interval.

Eq. 30 was used for all network simulations in an iterative event-based procedure [5]. At the beginning of an iteration, the next spike time in the network is calculated with Eq. (29). Then all neuron's phases are evolved until the next spike time with Eq. (30). In case external currents are identical for all neurons of one population, it is sufficient to search for the neuron with the largest phase and then calculate the corresponding next spike time. For efficient large network simulations, we changed the frame of reference of the neurons' phase-representation and employed a data structure that avoids iterating through all neurons at every network spike time to find the next spiking neuron.

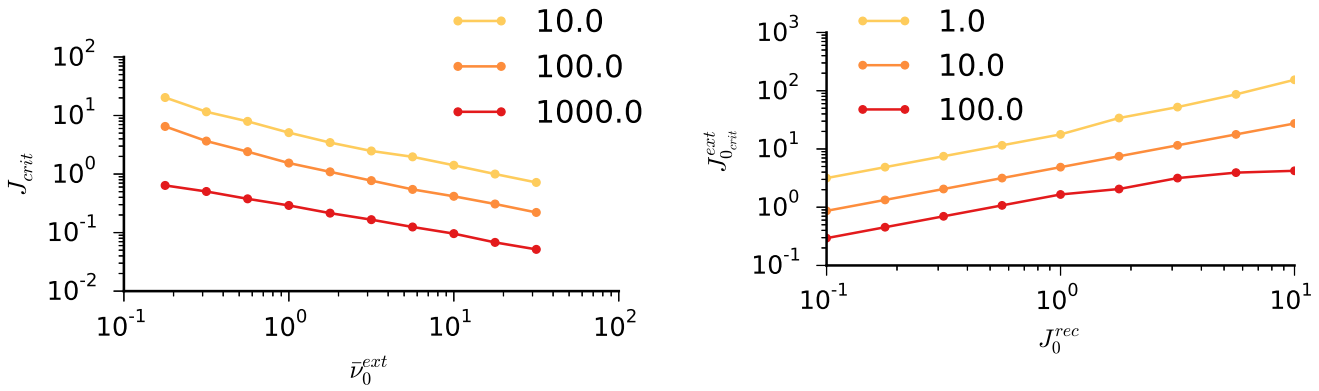

Figure 3: **Scaling of critical input strength with different network parameters:** input rate ν_0^{ext} and J_0^{rec} for $r = 1, 10, 100, 1000$ (other parameters: $N = 2000$, $\bar{\nu} = 1\,\text{Hz}$, $K = 1000$, $\nu_0^{\text{ext}} = 1\,\text{Hz}$, $J_0 = 1$, $\tau_{\text{m}} = 10\,\text{ms}$).

V. SCALING OF CRITICAL INPUT STRENGTH

We found a suppression of chaotic dynamics by streams of input spike trains in a large parameter regime. The critical input coupling strength $J_{0\,\text{crit}}^{\text{ext}}$ separates the chaotic dynamics from the stable dynamics. We investigated the scaling of the critical input coupling strength $J_{0\,\text{crit}}^{\text{ext}}$ with different network parameters by performing a noisy root-finding using a bisection search. This converged towards a critical coupling strength, where the largest Lyapunov exponent changes sign. We then fitted a power law or an exponential to the critical input coupling strength $J_{0\,\text{crit}}^{\text{ext}}$ as a function of the respective parameter using the Levenberg-Marquardt algorithm.

While the critical input coupling strength $J_{0\,\text{crit}}^{\text{ext}}$ exponentially saturated for large N and K (not shown), the dependence on input rate ν_0^{ext}, rapidness r, recurrent coupling J_0^{rec} and membrane time constant τ_{m} follows a power-law over several orders of magnitude.

This transition scales approximately (see **Fig. 3**):

$$J_{0\,\text{crit}}^{\text{ext}} \propto J_0^{0.75} {\nu_0^{\text{ext}}}^{-0.5} r^{-0.5} \tag{31}$$

This scaling behavior indicates that for large K there is a critical input variance $\sigma_{\text{crit}}^{\text{ext}\,2} = J_0^{\text{ext}\,2} \cdot \nu_0^{\text{ext}}$, where the recurrent chaos is suppressed, which can be either generated by sufficiently frequent or easier by sufficiently strong input spike trains.

VI. IMPLEMENTATION AND CONVERGENCE OF THE LYAPUNOV SPECTRA

With the exact phases of the neurons before spike reception, the single spike Jacobians for recurrent and external input spikes Eq. 20 were evaluated using Eq. 23 and Eq. 24. These were used to numerically calculate all Lyapunov exponents with the standard reorthonormalization procedure [6]. After a warmup of the network dynamics, of typically 10^4 network spikes average, we started with a random N-dimensional orthonormal system that was evolved in each iteration with the single spike Jacobian. To determine a suitable reorthonormalization interval, we started with an reorthonormalization interval of $\mathcal{O}\left(\max(\nu_0^{\text{ext}}, \nu_o) \cdot N\right)$ network spike iterations and the adapted it iteratively, such that the evolved orthonormal matrix Q was well-conditioned. The evolved vectors were reorthonormalized, yielding the norms of the orthogonalized vectors $\gamma_i(t_s)$ and the orthonormal system to be used in the following iterations. After a short warmup of the orthonormal system of about one spike per neuron, these norms were used to calculate the N Lyapunov exponents $\lambda_i = \lim_{p\to\infty} \frac{1}{t_p} \sum_{s=1}^{p} \log \gamma_i(t_s)$.

All full calculations were performed in custom code written in Julia with double precision. We used the fastest random number generator of RandomNumbers.jl (Xoroshiro128Star [30]), which is part of a novel class of random number generators based on exclusive or and bit shift. For the evolution of the orthonormal system Q by the Jacobians, we used a custom-written in-place sparse matrix multiplication that reduces cache miss and uses the sparse structure of the Jacobian. Moreover, we used parallelized level-3 matrix-matrix operations from BLAS (Basic Linear Algebra

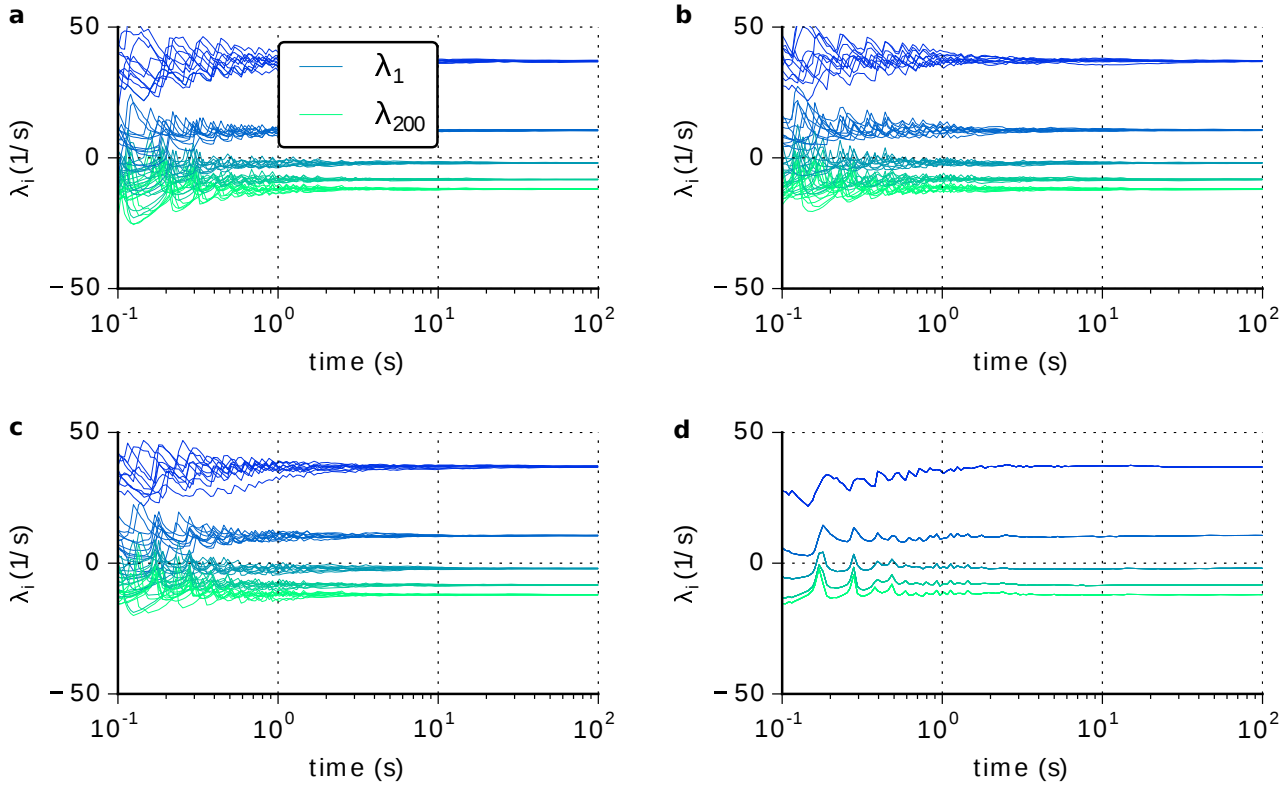

Figure 4: **Convergence of Lyapunov exponents versus time in inhibitory networks for low AP onset rapidness and no external input** ($r = 1$, $J_0^{\text{ext}} = 0$). (logarithmic time scale) **a)** Convergence of selected Lyapunov exponents (λ_1, λ_{50}, λ_{100}, λ_{150}, λ_{200}) across different network topologies, **b)** across different initial conditions of the recurrent network state ϕ_i, **c)** across different realizations of the Poissonian stream of input spike trains, **d)** for different initial realizations of the orthonormal system $\mathbf{Q}$ (parameters: $N = 2000$, $\bar{\nu} = 1\,\text{Hz}$, $K = 1000$, $\nu_0^{\text{ext}} = 1\,\text{Hz}$, $J_0 = 1$, $\tau_{\text{m}} = 10\,\text{ms}$).

Subprograms) called via LAPACK (Linear Algebra PACKage). The sparseness of the networks was used for the efficient storage of the coupling matrices in the Compressed Sparse Column (CSC) Storage format. For very large network topologies, we generated the network topology during the simulation on the fly using the index of the spiking neuron as the seed for the random number generator based on which the postsynaptic neurons are sampled [31].

One should note that the non-converged Lyapunov exponents generated during the transient are meaningless (they neither reflect the local nor finite-time Lyapunov exponents). The converged Lyapunov exponents capture the network dynamics on the balanced attractor, which is time-dependent in case of time-varying input. For different values of rapidness r and external input strength J_0^{ext}, we checked the convergence of the Lyapunov spectra (**Fig. 4-7**). This was done across different network topologies **a**, initial conditions of the recurrent network state **b**, different realizations of the external spiking input **c** and different orthonormal system **d**, to systematically dissect different contributions to variability. Generally, all calculations of the Lyapunov spectra were repeated ten times with different initial phases, input spike train realizations, and network topology realizations. Numerical errors were usually smaller than the symbol sizes in the presented figures in the main manuscript.

There are two main contributions to the variability of numerically calculated Lyapunov spectra. Firstly, variability arising from the fact that Lyapunov spectra are asymptotic properties estimated from finite calculations. Secondly, variability arising from the quenched disorder in different random network topologies. The first contribution would vanish in the limit of infinitely long simulations for ergodic systems. The second contribution is expected to vanish in the large networks limit due to self-averaging. A small deviation of the Lyapunov exponents calculated from different initial conditions can also be inherited from the rate finding procedure which might give slightly different constant external input currents depending on the initial condition. This can also result in small differences of the Lyapunov exponents. As we typically used 10^4 network spikes during the rate finding per iteration, this error is usually $< 0.1\,\%$. Quantities that are self-averaging converge in the limit of large system sizes to the ensemble average. The Lyapunov

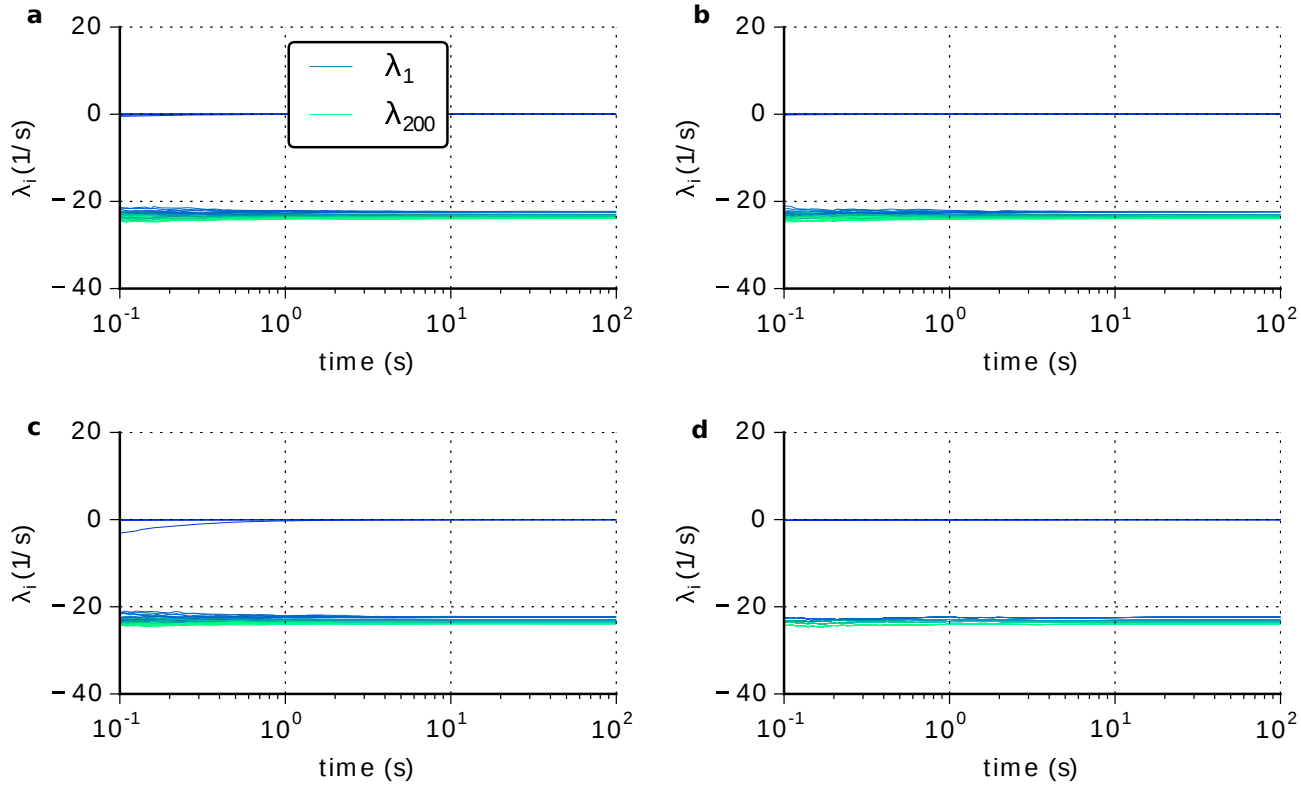

Figure 5: **Convergence of Lyapunov exponents versus time in inhibitory networks for high AP onset rapidness and no external input** ($r = 1000$, $J_0^{\text{ext}} = 0$). (logarithmic time scale) **a)** Convergence of selected Lyapunov exponents (λ_1, λ_4, λ_{14}, λ_{53}, λ_{200}) for across different network topologies, **b)** across different initial conditions of the recurrent network state ϕ_i, **c)** across different realizations of the Poissonian stream of input spike trains, **d)** for different initial realizations of the orthonormal system $\mathbf{Q}$ (parameters: $N = 2000$, $\bar{\nu} = 1\,\text{Hz}$, $K = 1000$, $\nu_0^{\text{ext}} = 1\,\text{Hz}$, $J_0 = 1$, $\tau_{\text{m}} = 10\,\text{ms}$).

spectrum of one realization of a large network is thus representative for the whole ensemble. Hence, averaging over many different network realizations is not a necessity in large networks.

We applied two independent checks of this semi-analytic numerically exact calculation of Lyapunov spectra. Firstly, the largest Lyapunov exponent can be calculated numerically by measuring the exponential rate of divergence or convergence of nearby trajectories [6, 32]. Secondly, in autonomous systems, there is always a neutral Lyapunov vector in the direction of the flow with a zero corresponding Lyapunov exponent as the system can be shifted in time. This neutral Lyapunov exponent vanishes as soon as the network is driven by spiking input. The checks confirmed the results obtained from our implementation of the semi-analytic calculation of the full Lyapunov spectrum.

VII. BURSTY INPUT SPIKE TRAINS REDUCE CHAOS

Role of temporal irregularity of input: To corroborate our results from networks driven by Poissonian input spike trains, we investigated the effect of changing the irregularity of the input. To this end, each rapid theta neuron received external input from an independent gamma process. Thus, the interspike intervals of the external input were drawn from a gamma distribution:

$$f(x;\alpha,\beta) = \frac{\beta^\alpha x^{\alpha-1} e^{-x\beta}}{\Gamma(\alpha)} \qquad \text{for } x \geq 0 \text{ and } \alpha,\, \beta > 0.$$

This allows to adapt the irregularity of the spike trains by changing the shape parameters α of the gamma process, while β allows to regulate the mean firing rate. The temporal irregularity is usually measured by the coefficient of

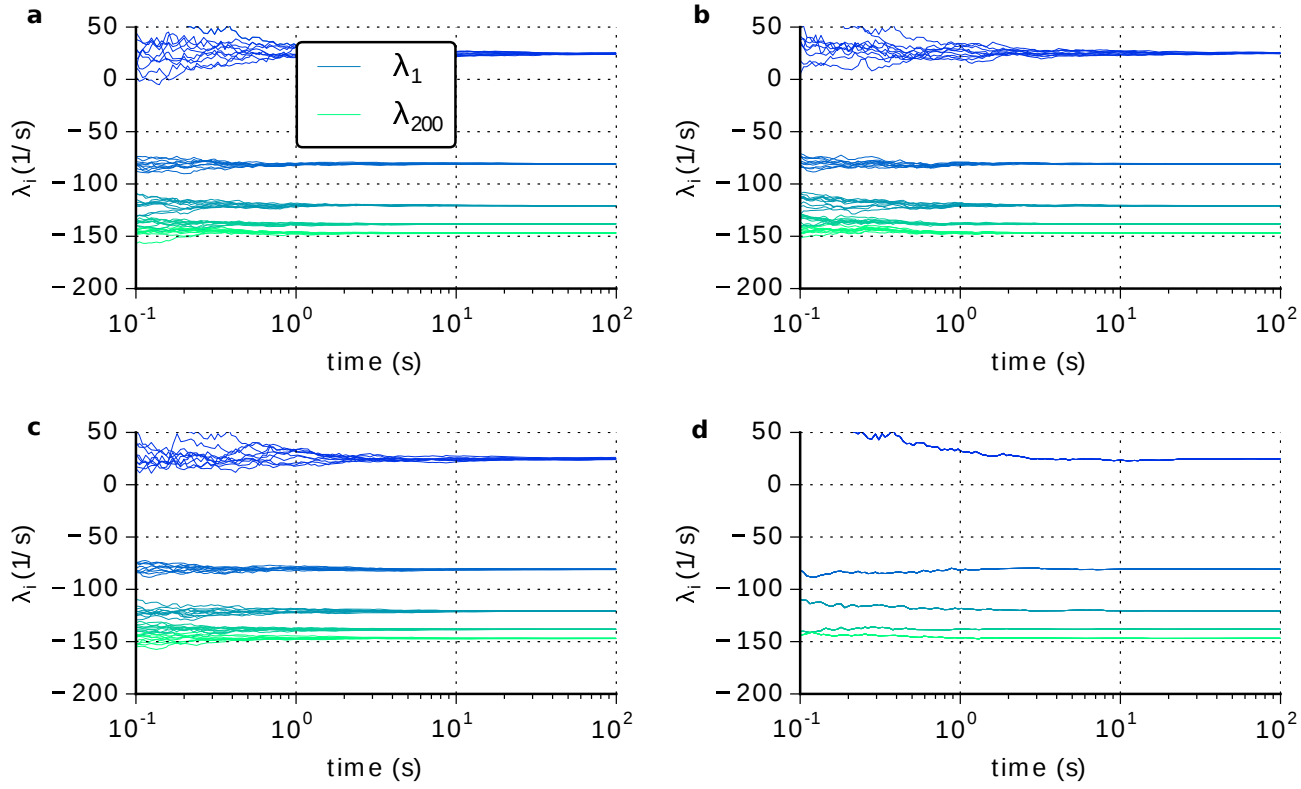

Figure 6: **Convergence of Lyapunov exponents versus time in inhibitory networks for low AP onset rapidness and strong external input** ($r = 1$, $J_0^{\text{ext}} = 10$). (logarithmic time scale) **a)** Convergence of selected Lyapunov exponents (λ_1, λ_{50}, λ_{100}, λ_{150}, λ_{200}) for across different network topologies, **b)** across different initial conditions of the recurrent network state ϕ_i, **c)** across different realizations of the Poissonian stream of input spike trains, **d)** for different initial realizations of the orthonormal system $\mathbf{Q}$ (parameters: $N = 2000$, $\bar{\nu} = 1\,\text{Hz}$, $K = 1000$, $\nu_0^{\text{ext}} = 1\,\text{Hz}$, $J_0 = 1$, $\tau_{\text{m}} = 10\,\text{ms}$).

variation of the interspike interval distribution. For gamma processes it is $cv_i = 1/\sqrt{\alpha_i}$, so for $\alpha_i = 1$, a Poisson process is regained. Despite being a renewal process, for $\beta \neq 1$ the gamma process first has to be aged to start with an equilibrated input to avoid artifacts. This was implemented by a warmup period of usually 10^4 spikes of the external input starting with a random initial offset before the network simulation.

We found that for slightly increasing input irregularity the chaos is suppressed even stronger, while for very regular input ($cv_{\text{in}} \approx 0$) the dynamical entropy rate and largest Lyapunov exponent are close to the case of constant input (**Fig. 8**). If the input spike trains are very irregular ($cv_{\text{in}} \gg 1$), both entropy rate and attractor dimensionality rise again. Note that in this case, the single neuron receives no input for an extended period of time, followed by a barrage of incoming spikes in a short time interval. We further note that the impact of burstiness of the input spike trains also seems to depend on the network size N (not shown).

VIII. INPUT CORRELATIONS REDUCE CHAOS

Role of shared input: How do spatial correlations of the external input spike trains affect chaos and entropy rate in the recurrent network? In our usual scenario, all neurons received either independent Poisson or gamma spike trains. As cortical neurons receive a substantial fraction of shared input, we extended our analysis to investigate the effect of spacial input correlations. To study the role of spatial correlations, each neuron receives input from a random subset of K_{ext} out of N Poisson neurons, each firing with a mean rate of $\nu_{\text{ext}} = \nu_0^{\text{ext}} K/K_{\text{ext}}$, so the rate of incoming Poisson spikes is independent of K_{ext}. Increasing the mean fraction of shared input $p = N/K_{\text{ext}}$ thus lead to an increase of input correlations, similar to the scenario studied in [9].

We found that increasing the input correlations to a moderate level had only a small effect on the Lyapunov

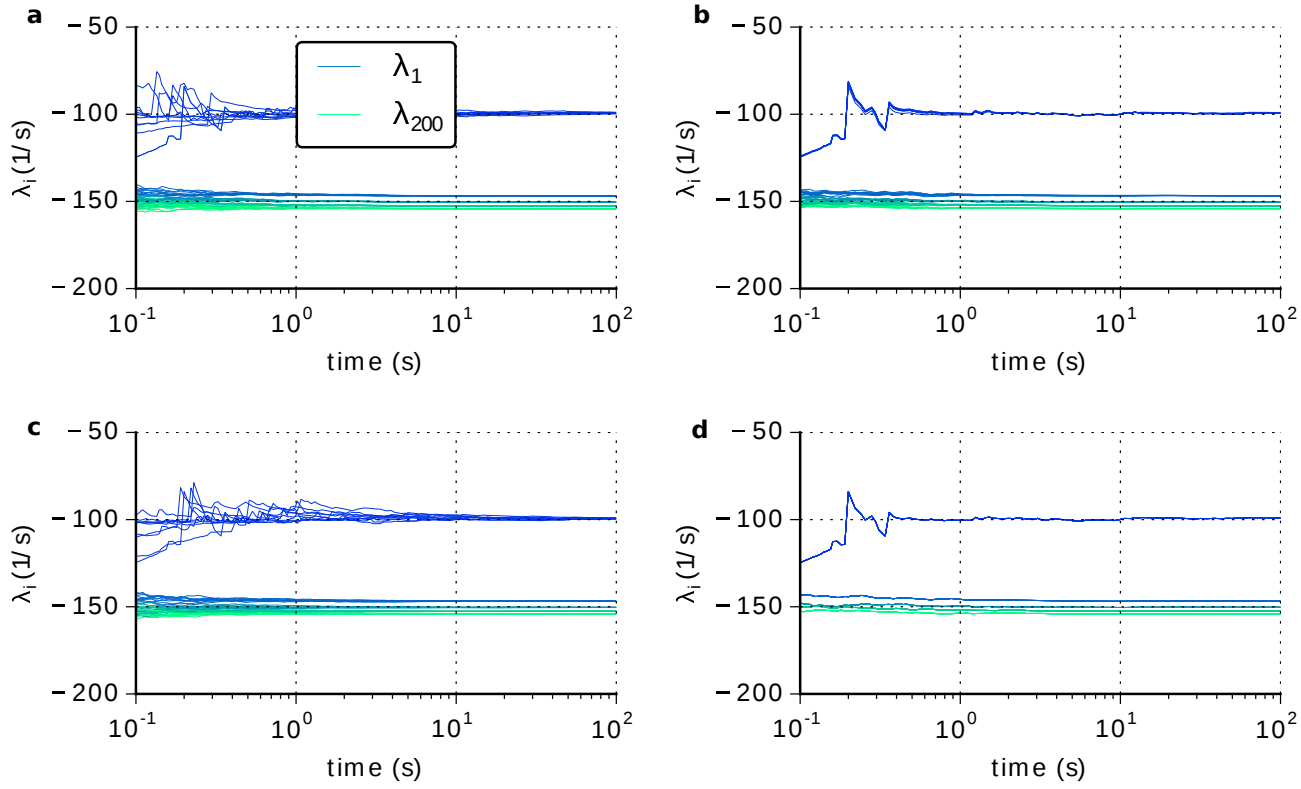

Figure 7: **Convergence of Lyapunov exponents versus time in inhibitory networks for high AP onset rapidness and strong external input** ($r = 1000$, $J_0^{\text{ext}} = 10$). (logarithmic time scale) **a)** Convergence of selected Lyapunov exponents (λ_1, λ_{50}, λ_{100}, λ_{150}, λ_{200}) for across different network topologies, **b)** across different initial conditions of the recurrent network state ϕ_i, **c)** across different realizations of the Poissonian stream of input spike trains, **d)** for different initial realizations of the orthonormal system **Q** (parameters: $N = 2000$, $\bar{\nu} = 1\,\text{Hz}$, $K = 1000$, $\nu_0^{\text{ext}} = 1\,\text{Hz}$, $J_0 = 1$, $\tau_{\text{m}} = 10\,\text{ms}$).

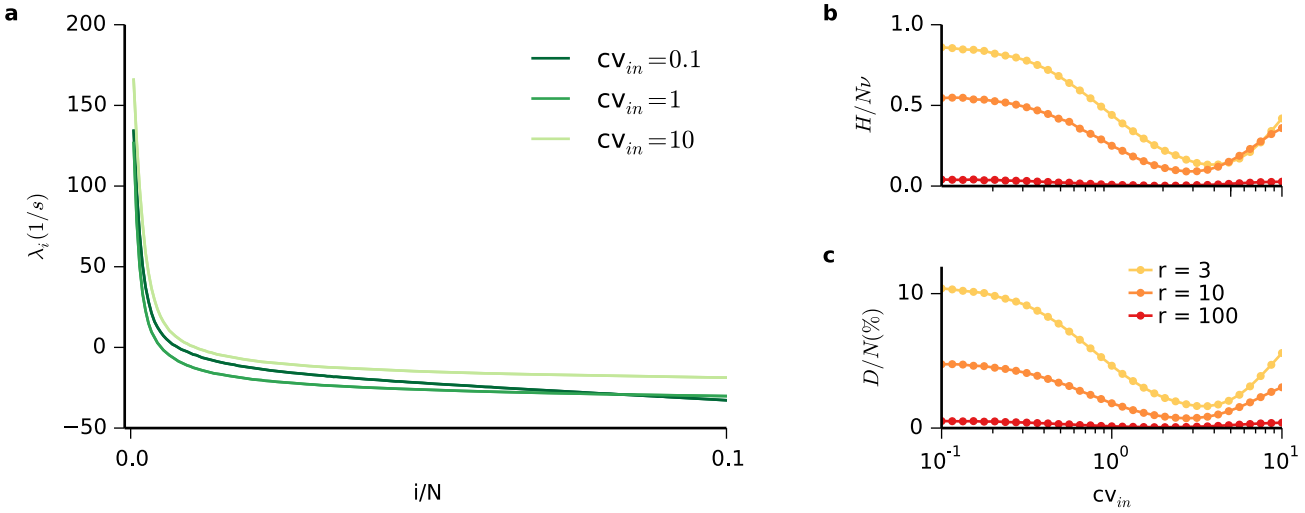

Figure 8: **Bursty input aids the reduction of dynamical entropy rate and attractor dimensionality, while regular and extremely bursty input spike trains have a weaker effect. a** Lyapunov spectrum for different input irregularity cv_{in}(coefficient of variation of interspike interval distribution) **b** dynamical entropy rate H and **c** attractor dimension D as a function of input irregularity cv_{in}(parameters: $N = 2000$, $K = 1000$, $\bar{\nu} = 1$ Hz, $J_0 = 1$, $\tau_m = 10$ ms).

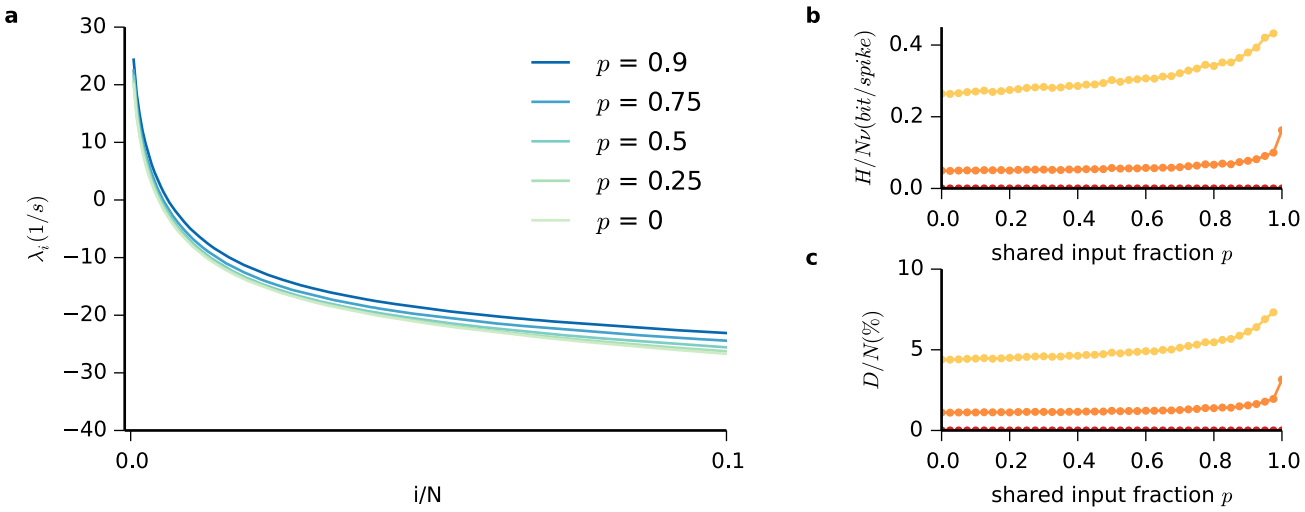

Figure 9: **Shared inputs increase dynamical entropy rate and attractor dimensionality.** **a** Lyapunov spectrum for different of fraction of shared input p. **b** Dynamical entropy rate $H/N\bar{\nu}$ and **c** attractor dimension D as a function of shared input p (parameters: $N = 2000$, $K = 1000$, $\bar{\nu} = 1$ Hz, $J_0 = 1$, $\tau_m = 10$ ms, $\nu_0^{\text{ext}} = 1$ Hz).

spectrum and thus also the dynamical entropy rate and Lyapunov dimensionality. For very large input correlations, we observed that the overall network state tended to synchronize, which interestingly lead first to a slight increase of dynamical entropy rate. A possible explanation for the small effect of input correlations might be that dense balanced networks are very efficient in decorrelation time-varying external inputs, because of fast strong recurrent inhibition that leads to canceling of correlations [9, 34], which results in weak mean pairwise spike count correlations. If in contrast to the scenario studied here, all neurons are externally driven by one external spike train whose strength or rate is gradually increased, the recurrent network dynamics is much less capable of decorrelating the input and network partial synchrony gradually increases while the attractor dimensionality and entropy rate gradually decrease (not shown).

* Electronic address: rainer@nld.ds.mpg.de

[1] R. Engelken, M. Monteforte, and F. Wolf, *to be published*.
[2] M. Monteforte, Chaotic Dynamics in Networks of Spiking Neurons in the Balanced State, 2011.
[3] C. van Vreeswijk and H. Sompolinsky, Science **274**, 1724 (1996); C. van Vreeswijk and H. Sompolinsky, Neural Comput. **10**, 1321 (1998)
[4] G. B. Ermentrout and N. Kopell, SIAM J. Appl. Math. **46**, 233 (1986); B. S. Gutkin and G. B. Ermentrout, Neural Comput. **10**, 1047 (1998); J. C. Brumberg and B. S. Gutkin, Brain Res. **1171**, 122 (2007)
[5] M. Tsodyks, I. Mitkov and H. Sompolinsky, Phys. Rev. Lett. **71**, 1280 (1993); U. Ernst, K. Pawelzik and T. Geisel, Phys. Rev. Lett. **74**, 1570 (1995); M. Timme, F. Wolf, and T. Geisel. Chaos, **13**, 377 (2003);
[6] G. Benettin et al., Meccanica **15**, 9 (1980)
[7] T. Yokozawa, D. Takahashi, T. Boku and M. Sato, Proceedings of the Fourth International Workshop on Parallel Matrix Algorithms and Applications, 37 (2006)
[8] N. Brunel, J Comput Neurosci **8**, 183 (2000)
[9] A. Renart, J. de la Rocha, P. Bartho, L. Hollender, N. Parga, A. Reyes, and K. D. Harris, Science **327**, 587 (2010).
[10] M. Monteforte and F. Wolf, Phys. Rev. Lett. **105**, 268104 (2010).
[11] P. Gao and S. Ganguli, Current Opinion in Neurobiology **32**, 148 (2015).
[12] N. Fourcaud-Trocmé, D. Hansel, C. van Vreeswijk, and N. Brunel, J. Neurosci. **23**, 11628 (2003).
[13] N. Fourcaud-Trocmé and N. Brunel, J Comput Neurosci **18**, 311 (2005).
[14] B. Naundorf, T. Geisel, and F. Wolf, J Comput Neurosci **18**, 297 (2005).
[15] B. Naundorf, F. Wolf, and M. Volgushev, Nature **440**, 1060 (2006).
[16] W. Wei and F. Wolf, Phys. Rev. Lett. **106**, 088102 (2011).
[17] S. P. Strong, R. Koberle, R. R. de Ruyter van Steveninck, and W. Bialek, Phys. Rev. Lett. **80**, 197 (1998).
[18] B. Lindner, Phys. Rev. E **73**, 022901 (2006).

[19] H. Câteau and A. D. Reyes, Phys. Rev. Lett. **96**, 058101 (2006).
[20] L. M. Ricciardi and L. Sacerdote, Biol. Cybern. **35**, 1 (1979).
[21] P. Lánský and V. Lánská, Biol. Cybernetics **56**, 19 (1987).
[22] W. Bialek, F. Rieke, R. de R. van Steveninck, and D. Warland, Science **252**, 1854 (1991).
[23] F. Rieke, D. Warland, R. de R. van Steveninck, and W. Bialek, Spikes: Exploring the Neural Code, Reprint edition (A Bradford Book, 1999).
[24] M. Monteforte and F. Wolf, Phys. Rev. X **2**, 041007 (2012).
[25] B. D. Burns and A. C. Webb, Proceedings of the Royal Society of London B: Biological Sciences **194**, 211 (1976).
[26] W. H. Calvin and C. F. Stevens, Journal of Neurophysiology **31**, 574 (1968).
[27] H. L. Bryant and J. P. Segundo, J Physiol **260**, 279 (1976).
[28] J. D. Hunter, J. G. Milton, P. J. Thomas, and J. D. Cowan, Journal of Neurophysiology **80**, 1427 (1998).
[29] Z. F. Mainen, T. J. Sejnowski, Science **268**, 1503 (1995)
[30] S. Vigna, Journal of Computational and Applied Mathematics **315**, 175 (2017).
[31] R. Rosenbaum and B. Doiron, Phys. Rev. X **4**, 021039 (2014).
[32] A. Wolf, J. B. Swift, H. L. Swinney, and J. A. Vastano, Physica D: Nonlinear Phenomena **16**, 285 (1985).
[33] M. N. Shadlen, W. T. Newsome, Curr. Opin. Neurobiol. **4**, 569 (1994); M. N. Shadlen and W. T. Newsome, J. Neurosci. **18**, 3870 (1998); W. R. Softky, Curr. Opin. Neurobiol. **5**, 239 (1995)
[34] T. Tetzlaff, M. Helias, G. T. Einevoll, and M. Diesmann, PLoS Comput Biol **8**, e1002596 (2012).

6 Reanalysis of "Two types of asynchronous activity in networks of excitatory and inhibitory spiking neurons"

6.1 Summary

We reanalyzed a recent study that investigated networks of leaky integrate-and-fire neurons and suggested that they would exhibit a chaotic instability mathematically analogous to rate networks with matched topology and single unit characteristics for strong synaptic coupling [4]. We found expected hallmarks of a chaotic instability in the rate network. Close to the transition to chaos, we observed critical slowing down in response to small external perturbations. In contrast, in the spiking network rate deviations resulting from small input perturbations rapidly decayed. When approaching the alleged chaotic instability, the decay speeds up contrary to observation in the rate network. We further found a quantitative mismatch between predictions of the mean-field theory and numerical simulations, for a variation of different network parameters, e.g. synaptic delay, fraction of inhibition and number of synapses per neuron K. In conclusion, our reanalysis demonstrates fundamental differences between the behavior of networks of pulse-coupled spiking LIF neurons and rate networks with matched topology and input-output function. In particular, contrary to the reanalyzed study [4], we found no indication of a corresponding chaotic instability in the spiking network [3].

Citation

Rainer Engelken*, Farzad Farkhooi*, David Hansel, Carl van Vreeswijk, and Fred Wolf. **"A Reanalysis of 'Two Types of Asynchronous Activity in Networks of Excitatory and Inhibitory Spiking Neurons.'"** F1000Research 5, 2043 (2016). [*eq. contribution]

Original Contribution

All authors participated in the research design. RE wrote the simulation and analysis code for Figure 1a, d and Figure 2a–d. FF wrote the simulation and analysis code for Figure 1b, c and Figure S1a, b. Earlier simulations were performed by RE, FF, DH. All authors participated in the interpretation of the results and in manuscript writing.

RESEARCH NOTE

A reanalysis of "Two types of asynchronous activity in networks of excitatory and inhibitory spiking neurons" [version 1; referees: 2 approved]

Rainer Engelken[1,2*], Farzad Farkhooi[3*], David Hansel[4], Carl van Vreeswijk[4], Fred Wolf[1,2]

[1]Max Planck Institute for Dynamics and Self-Organization (MPI-DS), Bernstein Center for Computational Neuroscience Göttingen, Faculty of Physics,, University of Göttingen, Göttingen, Germany
[2]Collaborative Research Center 889, University of Göttingen, Göttingen, 37099, Germany
[3]Institut für Mathematik, Technische Universität Berlin and Bernstein Center for Computational Neuroscience, Berlin, Germany
[4]Cerebral Dynamics, Learning and Memory Research Group, Center for Neurophysics, Physiology and Pathology, CNRS UMR8119, Université Paris Descartes, Paris, France

[*] Equal contributors

v1 **First published:** 22 Aug 2016, **5**:2043 (doi: 10.12688/f1000research.9144.1)
Latest published: 22 Aug 2016, **5**:2043 (doi: 10.12688/f1000research.9144.1)

Abstract

Neuronal activity in the central nervous system varies strongly in time and across neuronal populations. It is a longstanding proposal that such fluctuations generically arise from chaotic network dynamics. Various theoretical studies predict that the rich dynamics of rate models operating in the chaotic regime can subserve circuit computation and learning. Neurons in the brain, however, communicate via spikes and it is a theoretical challenge to obtain similar rate fluctuations in networks of spiking neuron models.

A recent study investigated spiking balanced networks of leaky integrate and fire (LIF) neurons and compared their dynamics to a matched rate network with identical topology, where single unit input-output functions were chosen from isolated LIF neurons receiving Gaussian white noise input. A mathematical analogy between the chaotic instability in networks of rate units and the spiking network dynamics was proposed.

Here we revisit the behavior of the spiking LIF networks and these matched rate networks. We find expected hallmarks of a chaotic instability in the rate network: For supercritical coupling strength near the transition point, the autocorrelation time diverges. For subcritical coupling strengths, we observe critical slowing down in response to small external perturbations. In the spiking network, we found in contrast that the timescale of the autocorrelations is insensitive to the coupling strength and that rate deviations resulting from small input perturbations rapidly decay. The decay speed even accelerates for increasing coupling strength.

In conclusion, our reanalysis demonstrates fundamental differences between

Open Peer Review

Referee Status: ✓ ✓

	Invited Referees 1	2
version 1 published 22 Aug 2016	✓ report	✓ report

1 **Jonathan Touboul**, CIRB - Collège de France France

2 **Maoz Shamir**, Ben-Gurion University of the Negev. Israel

Discuss this article

Comments (0)

the behavior of pulse-coupled spiking LIF networks and rate networks with matched topology and input-output function. In particular there is no indication of a corresponding chaotic instability in the spiking network.

This article is included in the Preclinical Reproducibility and Robustness channel.

Corresponding author: David Hansel (david.hansel@parisdescartes.fr)

How to cite this article: Engelken R, Farkhooi F, Hansel D *et al.* **A reanalysis of "Two types of asynchronous activity in networks of excitatory and inhibitory spiking neurons" [version 1; referees: 2 approved]** *F1000Research* 2016, **5**:2043 (doi: 10.12688/f1000research.9144.1)

Grant information: The work of DH and CvV was partially supported by grants ANR-13-BSV4-0014-03 - BALAV1 and ANR-14-NEUC-0001-01-BASCO and performed in the framework of the France-Israel Laboratory of Neuroscience (FILN). FF was supported by the BMBF, FKZ 01GQ 1001B. RE and FW received funding from Evangelisches Studienwerk Villigst, DFG through CRC 889 and Volkswagen Foundation.

Competing interests: No competing interests were disclosed.

First published: 22 Aug 2016, **5**:2043 (doi: 10.12688/f1000research.9144.1)

Introduction

Slow neural dynamics are believed to be important for behavior, learning and memory (Churchland & Shenoy, 2007; Fee & Goldberg, 2011; Murray *et al.*, 2014). Rate models operating in the chaotic regime show rich dynamics at the scale of hundreds of milliseconds and provide remarkable learning capabilities (Barak *et al.*, 2013; Sussillo & Abbott, 2009; Toyoizumi & Abbott, 2011). Understanding the conditions of such a transition to chaos in more detailed network models has recently attracted a lot of interest (Harish & Hansel, 2015; Kadmon & Sompolinsky, 2015). However, neurons in the brain communicate via spikes and it is a challenge in computational neuroscience to obtain similar slow rate dynamics in networks of spiking neuron models.

This question was recently addressed in a paper by Ostojic (2014) published in Nature Neuroscience (Ostojic, 2014). It argues that an "unstructured, sparsely connected network of model spiking neurons can display two fundamentally different types of asynchronous activity". When the synaptic strength is increased, networks of leaky integrate-and-fire (LIF) neurons would undergo a *transition* from the "well-studied asynchronous state, in which individual neurons fire irregularly at constant rates" to another "heterogeneous asynchronous state" in which "the firing rates of individual neurons fluctuate strongly in time and across neurons" (Ostojic, 2014). These two regimes would differ in an essential manner, the rate dynamics being chaotic beyond the phase transition. Finding a transition to chaotic slow-varying rate dynamics in spiking networks in such a simple model would be an important step towards an understanding of the computations underlying behavior and learning and would fill a gap in the current understanding of network dynamics. Here we re-examine the behavior of random LIF networks and demonstrate that there is no such phase transition to chaos in the spiking network analyzed in (Ostojic, 2014). While we confirm the observed deviation from the mean field theory description that assumes uncorrelated Gaussian fluctuations in time and among neurons, we controvert the validity of the presented analysis. We provide a series of tests of dynamical behavior that refute the existence of a chaotic instability and show that the analogy between the spiking network and the rate network is conceptually misleading and mathematically flawed.

The paper (Ostojic, 2014) starts with simulations of a network of LIF neurons for different values of the synaptic strength, J, while all other parameters are fixed to specific values. It is observed that the population mean firing rate of the neurons, ν_0, is well described by a mean field calculation only below a certain coupling strength J*. At this value, the average firing rate starts to deviate from the mean field prediction more than 5%. (Figure 1a in (Ostojic, 2014), denoted Figure P1a; hereafter figures in (Ostojic, 2014) are denoted by their numbers preceded by a "P"). In (Ostojic, 2014), it was claimed that the "classical" asynchronous state exhibits an instability at J=J*. Above J* the dynamics would still be asynchronous, but in a way which would be essentially different from the "classical" asynchronous state. To assess this claim, the author replaced the full dynamics of the spiking LIF network by a rate model of similar connectivity, the "Poisson network". Simulations indicate that as J increases, there is a value, $J=J_c$, at which the dynamics of the latter undergo a phase transition between a state in which the rates are constant in time (fixed point) and a state in which they fluctuate chaotically with long network generated time-scales. The author then derives an equation for a critical value J_c which is in agreement with the simulations of the Poisson model. For the parameters used in Figure P1 and P2 the value of J_c is rather close to J*. Apparently the author felt that this similarity, gives sufficient reason to justify two conclusions: (i) in the LIF network an instability occurs near J* which is of the same nature as the one occurring at J_c in the Poisson network. (ii) The asynchronous states below and above J* are essentially different in the LIF network.

However, as we now show, the reported agreement between the predicted transition at J_c and the spiking network simulation results is coincidental and only valid for the chosen parameters used in the paper (Ostojic, 2014) but not in general. We start by providing two counter-examples to statements (i) and (ii).

Methods and results

Our first counter-example is the LIF model considered in (Ostojic, 2014), we take N=40000 neurons and C=4000 synapses per neuron instead of N=10000 and C=1000 (all other parameters as in Figure P1, except for the network size, keeping the connection probability constant). The population firing rate, ν_0 (J), is plotted in Figure 1a. It deviates from the mean field prediction at $J^* \cong 0.3$ mV by more than 5%. Nonetheless, the critical point in the corresponding Poisson rate network is $J_c \cong 0.96$ mV and thus it is more than three times larger than J*.

Our second counter-example is the LIF network of Figure P1 and P2 with the same parameters except for the delay, Δ. We note that the delay does not affect the existence of the asynchronous state and importantly plays no role in the mathematical considerations of Ostojic (2014). As these yield identical results irrespective of delay we consider the simplest case: $\Delta = 0$ ms. Strikingly, the spiking network shows no longer a large deviation from the mean-field prediction (Figure 1a). However, the proposed analogy with the Poisson rate network still predicts that a deviation should occur at $J^* \cong 0.49$ mV, since the transition to chaos in the Poisson network is independent of the delay. The author seems to be somewhat aware of this discrepancy. Indeed, it is stated in the Online Methods that delays must be larger than the refractory period, because "if the delays are shorter, spikes that reach a neuron while it is refractory do not have an effect and the overall coupling is effectively reduced" (Ostojic, 2014). If this was correct, this effective reduction should be reflected in the formula for predicting J_c (Equation 16). This is not the case: the latter does not depend on Δ. In addition, the spiking network for $\Delta = 0$ ms in fact exhibits no increased level of network synchrony measured by the common synchrony measure χ (Figure 2a) (Hansel & Mato, 2003).

It is also argued in the paper (Ostojic, 2014) that the results plotted in Figure P3a and b support the analogy between the rate dynamics of the Poisson model and the dynamics of the LIF network. However, the comparison made in this figure is conceptually misleading. In the Poisson model, the rate as a function of time is an *unequivocally* defined quantity. It is *the dynamical variable* of the model and the time scale over which the rate fluctuates for strong enough coupling is fully determined by these dynamics.

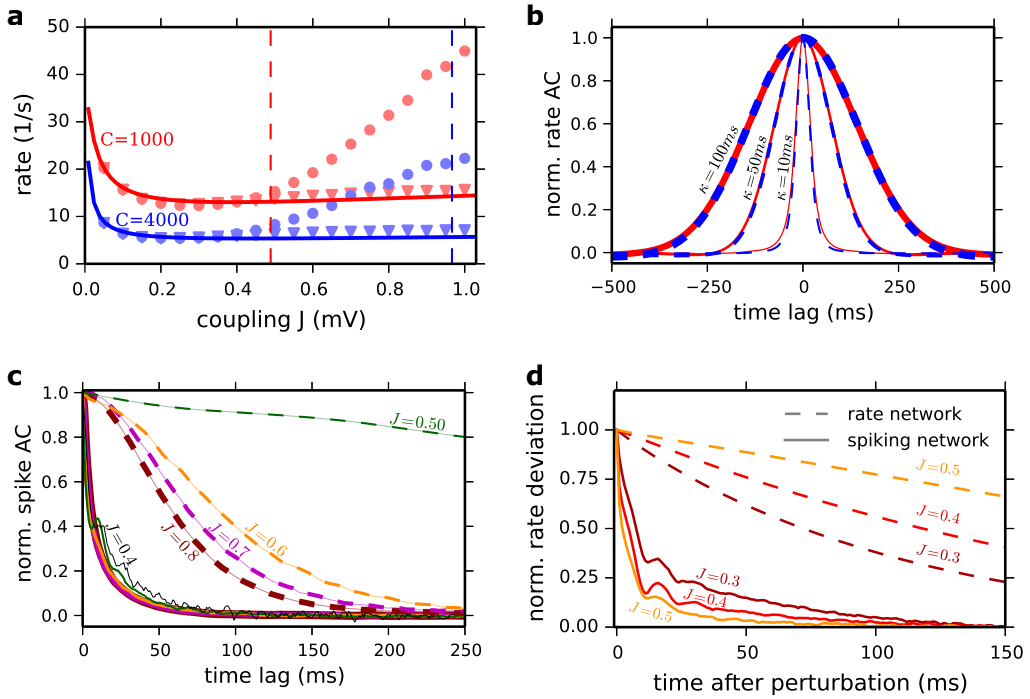

Figure 1. (**a**) Population averaged firing rate in the network vs. coupling strength J. Solid lines: Ricciardi mean field for C=1000 (red) and C=4000 (blue). Predictions for J_c (Equation 16) are indicated by the corresponding dashed vertical lines. Simulation results (event-based simulation implemented in Julia programing language) are also plotted. Dots: Δ=0.55 ms synaptic delay. Triangles: Δ=0.0 ms. Results for C=1000, N=10000 (red marker) and C=4000 and N=40000 (blue marker). (**b**) Averaged normalized AC of neuronal rate functions for J= 0.8 mV and C=1000 (red) and C=4000 (dashed blue) LIF networks. The rate functions were computed by filtering the spike trains of the neurons (1 ms time bin) with a Gaussian filter with 10 ms (the thinnest lines), 50 ms (moderated lines) and 100 ms (the thickest lines) standard deviation. (**c**) Autocorrelation function of the spike trains (no filtering) normalized to the second pick. Solid lines: LIF network. Dashed lines: Poisson network. The results are shown for J = 0.5 mV (dark green), J=0.6 mV (dark orange), J = 0.7 mV (magenta) and J=0.8 mV (dark red). For the LIF the AC is also shown for J=0.4 mV (solid black). To compute the ACs for the Poisson network we simulated a network for 100 s (time step 1 ms) and averaged the results over 40 realizations of the initial conditions. The network size is N=100000 for 0.5≤J≤0.6mV and N=10000 for J>0.6 mV. For the LIF network we averaged spike autocorrelation of 3000 randomly chosen neurons with a 1 ms bin following Equation 23 in the paper. All parameters are as in Figure P3. (**d**) Subcritical behavior of the systems. Rate network and spiking network are both perturbed in the constant feed-forward input current μ_0 in the least stable direction of the linearized rate dynamics (Equation 16) for different coupling strengths J. The resulting rate deviation is projected onto the perturbation direction. Dashed lines reflect the normalized decay of this perturbation in the rate network and the solid lines those of the spiking network (averaged over 1.42 million perturbations). The perturbation was applied to the constant feed-forward input μ_0 for 2 ms where the standard deviation of the perturbation vector was 1 mV. Longer perturbation durations (10 ms) and weaker perturbation strengths (standard deviation 0.1 mV) gave very similar results (not shown). Perturbation direction, strength, duration and network realization were exactly the same for rate and spiking network. Other parameters as in (Ostojic, 2014).

This is not the case in the LIF model where the "rate" and its "dynamics" depend on the temporal width over which the spiking activity is filtered. The width of the Gaussian filter used in (Ostojic, 2014) is 50 ms. This choice is arbitrary and is the reason for the similarity observed in the rate autocorrelations (ACs) plotted in the upper and lower panels in Figure P3b which depends on this choice (Figure 1b). The rate functions were computed by filtering the spike trains of the neurons (1 ms time bin) with a Gaussian filter with 10 ms (the thinnest lines), 50 ms (moderated lines) and 100 ms (the thickest lines) standard deviation. Moreover, the spike ACs plotted in Figure P3c for the two models exhibit essential differences as we now show.

For J=0.2 and 0.4 mV, the spike AC in the Poisson rate model (Figure P3c, upper panel) is close to a Dirac function reflecting that the dynamics are at fixed point - that is the rate variable from which the Poisson process of the spikes is generated is constant. For J=0.6 mV the spike AC is very different: a broad component has now appeared. It is flat at zero time lag and has a negative curvature at short time lags (Figure 1c and Figure P3c). A detailed analysis reveals that this change has all the characteristics of a true phase transition. It shows that close to the phase transition, the amplitude vanishes proportionally to $J-J_c$ and the decorrelation time diverges as $1/\sqrt{J-J_c}$ (Figure S1a). To compute the ACs for the Poisson network we simulated a network for 100 s (time step 1 ms) and

averaged the results over 40 realizations of the initial conditions. The network size is N=100000 for 0.5≤J≤0.6mV and N=10000 for J>0.6 mV. For the LIF network we averaged spike autocorrelation of 3000 randomly chosen neurons with a 1 ms bin following Equation 23 in the paper. All parameters are as in Figure P3.

The spike AC behaves very differently in the LIF network. For J=0.2 mV it exhibits at zero time lag a sharp peak flanked by a trough which reflects the refractoriness (absolute and relative) of the single neuron dynamics. As J increases, there is a progressive change in the AC shape. Eventually, the trough disappears. The flanks of the zero peak are now decreasing exponentially (Figure 1c, solid lines). A careful analysis reveals that the typical time constant of this decrease depends only weakly on J (Figure 1c, solid lines). It is always on the order of the membrane time constant of the neurons (20 ms). Note also that by contrast with what is observed in the Poisson network, for J=0.5 to 0.8 mV, the spike AC curvature is always positive and peaked around zero time lag (Figure 1c, dashed lines).

How do the "strong fluctuations" in the "heterogeneous regime" emerge? For increasing J, the spiking activity of single neurons becomes increasingly irregular, quantified by the mean coefficient of variation (cv) of the interspike interval distribution (Figure 2b). At the same time, the distribution of membrane potentials develops a very long tail towards negative voltages (Figure 2c). For strong coupling (J=0.8 mV), voltage traces of individual neurons show long very negative voltage excursions, followed by short bursts of action potentials (Figure 2d). This explains the super-Poissonian irregularity (CV>1). The super-Poissonian nature of spiking irregularity and the unphysiological negative voltage deviations are properties related to the linear $\dot{V}$-V-relationship of the LIF model. A mean-field description of this phenomenon requires self-consistent spike train autocorrelations (Lerchner *et al.*, 2006; Wieland *et al.*, 2015). For other integrate-and-fire neurons e.g. the quadratic-integrate-and-fire model, even for very strong coupling J, e.g. J = 20 mV, the mean coefficient of variation does not increase beyond one and no strongly negative voltage excursions are observed. All parameters are as in Figure P1.

Additionally, in order to compare the behavior of spiking and rate models below the postulated phase transition, we perturbed rate and spiking networks of identical topology in the least stable direction of the linearized rate dynamics, predicted by Equation 16 in the paper (Ostojic, 2014). The resulting rate deviation is projected onto the perturbation direction. The perturbation was applied to the constant feed-forward input μ_0 for 2 ms where the standard deviation of the perturbation vector was 1 mV. Figure 1d shows that the decay of the perturbation in the rate network slows down near the transition, indicating a critical slowing down (Figure 1d, dashed

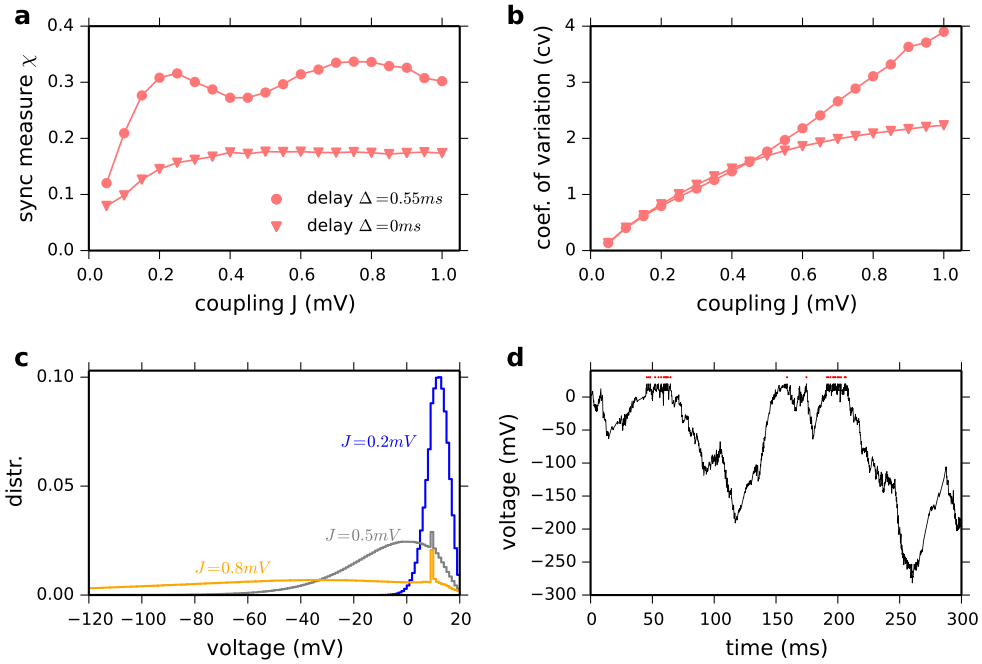

Figure 2. (**a**) Synchrony measure X vs. coupling strength J. Dots: Δ=0.55 ms. Triangles: Δ=0.0 ms for N=10000, C=1000. X is defined as in (Hansel & Mato, 2003) on the phases of neurons. Note that zero delay does not increase network synchrony. (**b**) Coefficient of variation of the interspike intervals vs. coupling strength J. (**c**) Distribution of membrane potentials for different coupling strength J (in mV). (**d**) Example voltage trace for J=0.8 mV shows very negative excursions followed by short bursts of action potentials. Red dots indicate spike times. Numerically exact event-based simulation were implemented in Julia programing language. Other parameters are chosen as in (Ostojic, 2014).

lines). If there were a "mathematically analogous" transition in the spiking network, also its perturbation should decay slower as the transition is approached. Our result (Figure 1d, solid lines) shows that the decay time-scales of the perturbation (averaged over 1.42 million perturbations) is insensitive to J and it stays close to the membrane time constant (similar to solid lines in Figure 1c). Longer perturbation durations (10 ms) and weaker perturbation strengths (standard deviation 0.1 mV) gave very similar results (not shown). All other parameters are chosen as in (Ostojic, 2014).

Conclusion

We therefore conclude that, contrary to what was argued by the author, the spiking LIF network studied in (Ostojic, 2014) does not exhibit a phase transition to a chaotic state similar to the one occurring in the studied rate model. The reported mismatch between the average firing rate in this LIF network simulations and the mean-field calculation is unrelated to such a transition.

Data and software availability

Zenodo: Reanalysis of "Two types of asynchronous activity in networks of excitatory and inhibitory spiking neurons", 10.5281/zenodo.59624 (Engelken & Farkhooi, 2016).

The data for this article are also available on the Open Science Framework at: https://osf.io/q3vt4/

Author contributions

All authors participated in the research design. RE wrote the simulation and analysis code for Figure 1a,d and Figure 2a–d. FF wrote the simulation and analysis code for Figure 1b,c and Figure S1a,b. Earlier simulations were performed by RE, FF, DH. All authors participated in the interpretation of the results and in manuscript writing. DH, CvW and FW share joint first authorship of this article.

Competing interests

No competing interests were disclosed.

Grant information

The work of DH and CvV was partially supported by grants ANR-13-BSV4-0014-03-BALAV1 and ANR-14-NEUC-0001-01-BASCO and performed in the framework of the France-Israel Laboratory of Neuroscience (FILN). FF was supported by the BMBF, FKZ 01GQ 1001B. RE and FW received funding from Evangelisches Studienwerk Villigst, DFG through CRC 889 and Volkswagen Foundation.

Acknowledgments

We thank Ran Darshan, Omri Harish and Gianluigi Mongillo for fruitful discussions.

Supplement material

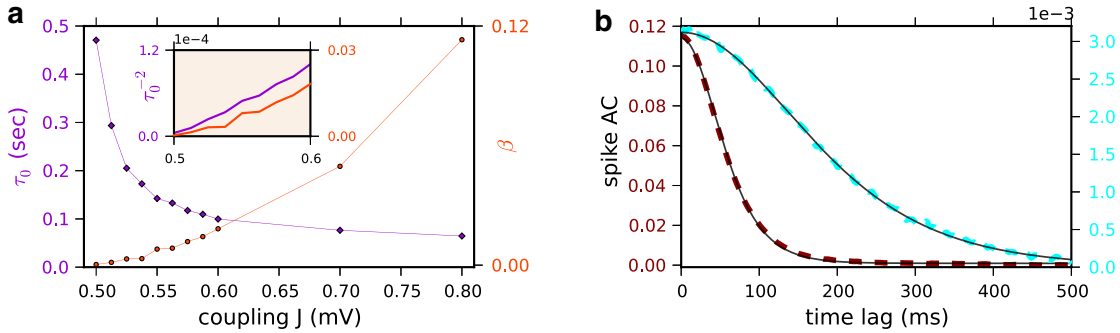

Figure S1. (**a**) The decorrelation time (τ_0, violet diamond, left y-axis) and amplitude at zero time lag (beta, orange circles, right y-axis) of the baseline-subtracted population averaged spike AC are plotted vs. J for the Poisson network. These parameters were obtained by fitting the spike AC with $ACF(\tau) = \beta/cosh(\tau/\tau_0)^2$ (see Figure S1b). Inset: the rescaled estimated τ_0^{-2} (left axis, violet) and β values (orange, right axis) for J=0.5, 0.5125, 0.525, 0.5375, 0.55, 0.5625, 0.575, 0.5875 and 0.6 mV, to show that they vanish linearly near the phase transition. (**b**) The non-normalized spike AC can be very well fitted by $ACF(\tau) = \beta/cosh(\tau/\tau_0)^2$. Dashed lines: Simulation results; J=0.525 mV (cyan, right y-axis) and J=0.8 mV (dark red, left y-axis): Black solid line: The fits.

References

Barak O, Sussillo D, Romo R, *et al.*: **From fixed points to chaos: three models of delayed discrimination.** *Prog Neurobiol.* 2013; **103**: 214–222.
PubMed Abstract | Publisher Full Text | Free Full Text

Churchland MM, Shenoy KV: **Temporal complexity and heterogeneity of single-neuron activity in premotor and motor cortex.** *J Neurophysiol.* 2007; **97**(6): 4235–4257.
PubMed Abstract | Publisher Full Text

Engelken R, Farkhooi F: **reanalysis of "Two types of asynchronous activity in networks of excitatory and inhibitory spiking neurons".** *Zenodo.* 2016.
Data Source

Fee MS, Goldberg JH: **A hypothesis for basal ganglia-dependent reinforcement learning in the songbird.** *Neuroscience.* 2011; **198**: 152–70.
PubMed Abstract | Publisher Full Text | Free Full Text

Hansel D, Mato G: **Asynchronous states and the emergence of synchrony in large networks of interacting excitatory and inhibitory neurons.** *Neural Comput.* 2003; **15**(1): 1–56.
PubMed Abstract | Publisher Full Text

Harish O, Hansel D: **Asynchronous Rate Chaos in Spiking Neuronal Circuits.** *PLoS Comput Biol.* 2015; **11**(7): e1004266.
PubMed Abstract | Publisher Full Text | Free Full Text

Kadmon J, Sompolinsky H: **Transition to chaos in random neuronal networks.** *Phys Rev X.* 2015; **5**(4): 041030.
Publisher Full Text

Lerchner A, Ursta C, Hertz J, *et al.*: **Response variability in balanced cortical networks.** *Neural Comput.* 2006; **18**(3): 634–659.
PubMed Abstract | Publisher Full Text

Murray JD, Bernacchia A, Freedman DJ, *et al.*: **A hierarchy of intrinsic timescales across primate cortex.** *Nat Neurosci.* 2014; **17**(12): 1661–1663.
PubMed Abstract | Publisher Full Text | Free Full Text

Ostojic S: **Two types of asynchronous activity in networks of excitatory and inhibitory spiking neurons.** *Nat Neurosci.* 2014; **17**(4): 594–600.
PubMed Abstract | Publisher Full Text

Sussillo D, Abbott LF: **Generating coherent patterns of activity from chaotic neural networks.** *Neuron.* 2009; **63**(4): 544–557.
PubMed Abstract | Publisher Full Text | Free Full Text

Toyoizumi T, Abbott LF: **Beyond the edge of chaos: amplification and temporal integration by recurrent networks in the chaotic regime.** *Phys Rev E Stat Nonlin Soft Matter Phys.* 2011; **84**(5 Pt 1): 051908.
PubMed Abstract | Publisher Full Text

Wieland S, Bernardi D, Schwalger T, *et al.*: **Slow fluctuations in recurrent networks of spiking neurons.** *Phys Rev E Stat Nonlin Soft Matter Phys.* 2015; **92**(4): 040901.
PubMed Abstract | Publisher Full Text

Open Peer Review

Current Referee Status: ✓ ✓

Version 1

Referee Report 27 September 2016

doi:10.5256/f1000research.9839.r16565

Maoz Shamir
Department of Physiology and Cell Biology, Ben-Gurion University of the Negev., Be'er-Sheva, Israel

The origin and possible computational role of neuronal noise has been the focus of considerable scientific effort during the past decades. In particular, the transition to chaos has been extensively studied using simplified rate-models and much is known about this transition.
A recent work studied the dynamics of a sparsely connected network of excitatory and inhibitory spiking neurons in the balance regime and a compelling mapping between spiking neural network and rate model was proposed. Following analysis and numerical simulations it was suggested that a novel type of asynchronous state exists and it was further hypothesized that this novel state is useful for complex information processing in the central nervous system.
Here the authors reevaluate this claim. Several counter examples are provided to prove that the claim of a transition to a second type of asynchronous state does not hold. Furthermore, the origin of 'strong fluctuation' super-Poisson irregular firing is studied and is found to be related to extremely negative voltage fluctuations that are beyond the typical physiological range.
The work is timely. The results are solid and well presented. I also find the effort devoted to reproduce and re-evaluate results refreshing. I believe this paper will contribute to the scientific debate.

I have read this submission. I believe that I have an appropriate level of expertise to confirm that it is of an acceptable scientific standard.

Competing Interests: No competing interests were disclosed.

Referee Report 07 September 2016

doi:10.5256/f1000research.9839.r15814

Jonathan Touboul
Mathematical Neuroscience Team, CIRB - Collège de France, Oaris, France

Characterizing the dynamics of spiking neural networks and their transitions is currently a prominent issue in computational neuroscience. The question is largely non-trivial and riddled with subtleties: numerical simulations are often delicate to interpret, and theoretical tools to analyze these dynamics are still being developed.

The theoretical community have devoted important effort to address this question. Indeed, progresses on

this question would advance our understanding of the brain and its computations. A question of particular interest is to characterize phase transitions to chaotic regimes in spiking networks. Indeed, since the seminal work of Sompolinsky, Crisanti and Sommers[1] on rate networks, chaotic regime were shown to have rich dynamics able to support efficient computations and learning (see e.g. Sussillo & Abbott 2009[2]). Whether spiking networks do show a similar transition and thus share similar properties as rate networks has recently been the focus of several researches and is an important endeavor in computational neuroscience[3].

The present paper addresses a few important questions on the interpretations and conceptual approach of a theoretical article appeared in Nature Neuroscience in 2014[4] dealing precisely with dynamics and transitions in spiking networks. That paper argued for the existence a transition in a balanced spiking network, between an asynchronous and a "new highly fluctuating regime", using in particular transitions of an associated rate model. The present article comes back to this comparison between spiking and rate network, and argues that, in contrast with the approach of Ostojic (2014)[4], it is not possible to extract accurate information on the spiking network from an analysis of the particular rate network studied, by showing a mismatch between their qualitative dynamics. Moreover, using relevant numerical quantities to identify phase transitions (synchrony measure and effect of perturbations), the authors establish the absence of phase transition in the spiking network, while the rate network does present the hallmarks of phase transitions.

The present paper thus contributes to an important scientific debate on the characterization of the dynamical regimes of spiking networks. This question has been the topic of very recent important works that advance our understanding of spiking networks and the associated mean-field limits (to cite a few, see Kadmon & Sompolinsky 2015[5], Harrish & Hansel 2015[6], Goedeke, Schuecker & Helias 2016[7]).

For its contribution to the scientific debate on a timely and important topic in theoretical neuroscience, this paper shall be helpful to the readers interested in the existence and nature of transitions in spiking networks.

References

1. Sompolinsky H, Crisanti A, Sommers HJ: Chaos in random neural networks.*Phys Rev Lett*. 1988; **61** (3): 259-262 PubMed Abstract | Publisher Full Text
2. Sussillo D, Abbott LF: Generating coherent patterns of activity from chaotic neural networks.*Neuron*. 2009; **63** (4): 544-57 PubMed Abstract | Publisher Full Text
3. Abbott LF, DePasquale B, Memmesheimer RM: Building functional networks of spiking model neurons. *Nat Neurosci*. 2016; **19** (3): 350-5 PubMed Abstract | Publisher Full Text
4. Ostojic S: Two types of asynchronous activity in networks of excitatory and inhibitory spiking neurons. *Nat Neurosci*. 2014; **17** (4): 594-600 PubMed Abstract | Publisher Full Text
5. Kadmon J, Sompolinsky H: Transition to Chaos in Random Neuronal Networks. *Physical Review X*. 2015; **5** (4). Publisher Full Text
6. Harish O, Hansel D: Asynchronous Rate Chaos in Spiking Neuronal Circuits.*PLoS Comput Biol*. 2015; **11** (7): e1004266 PubMed Abstract | Publisher Full Text
7. Goedeke S, Schuecker J, Helias M: Noise dynamically suppresses chaos in random neural networks. *arXiv:1603.01880 [q-bio.NC]*. 2016. Reference Source

I have read this submission. I believe that I have an appropriate level of expertise to confirm that it is of an acceptable scientific standard.

Competing Interests: No competing interests were disclosed.

7 Dimensionality and entropy of spontaneous and evoked rate activity

7.1 Summary

Cortical circuits exhibit complex activity patterns both spontaneously and evoked by external stimuli. Finding low-dimensional structure in this high-dimensional population activity is a challenge both for experiments and theory. What is the diversity of the collective neural activity and how is it affected by an external stimulus?

We present a novel approach to answer these long-standing questions in firing-rate networks. Using concepts from dynamical systems theory, we calculate the attractor dimensionality and dynamical entropy rate for these networks. The dimensionality measures the diversity of collective activity states. Dynamical entropy quantifies the uncertainty amplification due to sensitivity to initial conditions. We obtain these two canonical measures of the collective network dynamics from the full set of Lyapunov exponents which measure the exponential sensitivity to small perturbations in the tangent space along a trajectory. Our approach is applicable for arbitrary network topology and firing-rate dynamics.

For concreteness, we consider a randomly-wired firing-rate network that exhibits chaotic rate fluctuations for sufficiently strong synaptic weights. We show that dynamical entropy scales logarithmically with synaptic coupling strength, while the attractor dimensionality exponentially saturates. Thus, despite the increasing dynamic uncertainty, the diversity of collective activity saturates for strong coupling. We find that a time-varying external stimulus *drastically* reduces both entropy and dimensionality. Finally, we analytically approximate the full Lyapunov spectrum in several limiting cases by random matrix theory. This reveals how coupling strength, autocorrelations and noise affect the chaotic network dynamics.

Our study opens a novel avenue to characterize the complex dynamics of rate networks and the geometric structure of the corresponding high-dimensional chaotic attractor. This not only gives a deeper understanding of the dynamics but also helps to harness its computational capacities, e.g. for plasticity and learning of stable trajectories.

Dimensionality and entropy of spontaneous and evoked neural rate dynamics

Rainer Engelken[1,2,3,4*],Fred Wolf[1,2,3,4]

1 Max Planck Institute for Dynamics and Self-Organization, Göttingen, Germany
2 Bernstein Center for Computational Neuroscience, Göttingen, Germany
3 Bernstein Focus for Neurotechnology, Göttingen, Germany
4 Faculty of Physics, University of Göttingen, Göttingen, Germany,

* rainer@nld.ds.mpg.de

Abstract

Cortical circuits exhibit complex activity patterns both spontaneously and evoked by external stimuli. Finding low-dimensional structure in this high-dimensional population activity is a challenge both for experiments and theory. What is the diversity of the collective neural activity and how is it affected by an external stimulus?

We present a new approach to answer these long-standing questions in firing-rate networks. Using concepts from dynamical systems theory, we calculate the attractor dimensionality and dynamical entropy rate for these networks. The dimensionality measures the diversity of collective activity states. Dynamical entropy quantifies the uncertainty amplification due to sensitivity to initial conditions. We obtain these two canonical measures of the collective network dynamics from the full set of Lyapunov exponents, which measure the exponential sensitivity to small perturbations in the tangent space along a trajectory. Our approach is applicable for arbitrary network topology and firing-rate dynamics.

For concreteness, we consider a randomly-wired firing-rate network that exhibits chaotic rate fluctuations for sufficiently strong synaptic weights. We show that dynamical entropy scales logarithmically with synaptic coupling strength, while the attractor dimensionality exponentially saturates. Thus, despite the increasing dynamic uncertainty, the diversity of collective activity saturates for strong coupling. We find that a time-varying external stimulus *drastically* reduces both entropy and dimensionality. Finally, we analytically approximate the full Lyapunov spectrum in several limiting cases by random matrix theory. This reveals how coupling strength, autocorrelations and noise affect the chaotic network dynamics.

Our study opens a novel avenue to characterize the complex dynamics of rate networks and the geometric structure of the corresponding high-dimensional chaotic attractor. This not only gives a deeper understanding of the dynamics but also helps to harness its computational capacities, e.g. for plasticity and learning of stable trajectories.

Author Summary for Kids

When you dream, think or read this sentence, in your brain gazillions of tiny cells called neurons are active and talk to each other. These neurons process the messages coming from your five senses by sending patterns of tiny electric pulses to each other or to your

big toe if you need to run. Neuroscientist try to make sense out of this complex chatter and want to understand the language the neurons speak. I am using math to build a super simplified model of this chatter. I connected thousands of neurons randomly in my boss' computers into a network, which looks like a giant cobweb of a drunken spider. Each neuron has a very simple rule, by which it turns incoming signals of other neurons into an activity. The neuron then sends the activity to thousands of other neurons it is connected to. The rule looks like a snake, crawling up a step or like a slightly crooked S like this: $\curvearrowleft$. Other scientists found out using pen and paper instead of computers that such networks are quiet as a mouse when the connections are weak, but they start a tumult of chatter, when the connections between the neurons are strong enough.

I discovered (using my boss' computers ;-)) that although the activity of the whole network looks like a complete mess, there is a hidden pattern. I reveal this using tools from chaos theory, which people came up with to describe complex systems with many interacting small things, like for example turbulences of gazillions of water drops in clouds on a rainy day. Such a system is called chaotic if a tiny poke is enough to make it do something very different than it would have done without.

Lyapunov exponents – named after a Russian mathematician – measure, how fast things fly apart in a chaotic system after tiny poking or tickling. There is an almost magic link between these Lyapunov exponents and the universe of all imaginable gibberish the neurons could possibly ever talk about. I use this link and show that although the activity of a chaotic network looks like a random jumble of gibberish, there is a lot more structure than what you would expect when only listening to the neurons one by one. In the space of all imaginable network activity states, there are lots of holes, like in old socks. Actually, in the model I studied, this space is almost empty, it is made up mostly of "thin air". This means that certain network activity states can never occur. But the neurons didn't secretly agreed never to chatter together about certain topics. It's rather that the wiring of the random network (the giant cobweb of the drunken spider) and the neuron rule (the snake on the step) somehow don't allow them to chat about certain things. In the following pages, I propose some ideas how to find out more about this hidden activity structure using other cool tricks and tools from chaos theory. If you want to learn more, just write me an email :-)

Introduction

Cortical circuits display temporally irregular asynchronous activity patterns even in the absence of external input [1]. The time-scale of associated cortical rate fluctuations are often slow compared to the typical time-scale of individual neurons' membrane dynamics [2, 3]. Mean pairwise spike-count correlations can be very low indicating an active decorrelation of local microcircuit activity [4–6].

Behavioral responses to nanostimulation of single cell spiking indicate that behaving animals can be sensitive to single neurons' activity [7] and even to the structure of their spike trains [8, 9]. It has also been proposed that adding a single spike produces a cascade of extra spikes in the local circuits [10]. While the conclusions of such experiments for cortical information coding strategies remain controversial, they suggest a high sensitivity of the circuit dynamics with respect to small perturbations and raise questions about network mechanisms underlying dynamic activity amplification.

It is a major challenge to develop mathematical concepts to characterize high-dimensional circuit activity, find collective degrees of freedom and information representations on the population level. Theoretical work suggested that asynchronous rate activity originates from chaotic dynamics in recurrent networks. A seminal study showed that randomly connected firing-rate units display a transition from an inactive state to a heterogeneous, chaotic state [11] (Fig. 1). In this class of models, each rate

unit maps its synaptic input h_i smoothly into a firing rate by a sigmoidal input-output transfer function ϕ. Coupling strengths are drawn independently from a Gaussian distribution with zero mean and standard deviation $g/\sqrt{N}$. A self-consistent mean-field theory (MFT) was developed for the large network limit where the number of neuron $N \to \infty$. For small coupling $g < 1$ the trivial fixed point $h_i = 0 \; \forall \; i$ is the only stable solution to the MFT (Fig. 1A+B). For increasing coupling strength the trivial fixed point looses stability and chaos emerges from the nonlinear interaction of unstable activity modes (Fig. 1C+D). Using dynamical mean-field theory, Sompolinsky, Crisanti and Sommers showed that above a critical strength $g_{\text{crit}} = 1$, the only stable self-consistent solution to the MFT has chaotic dynamics [11]. The transition to chaos occurs, when the largest real part of the eigenvalues $\hat{\lambda}_{max}$ of the stability matrix obtained from the linearized rate dynamics crosses unity (Fig. 1A+C).

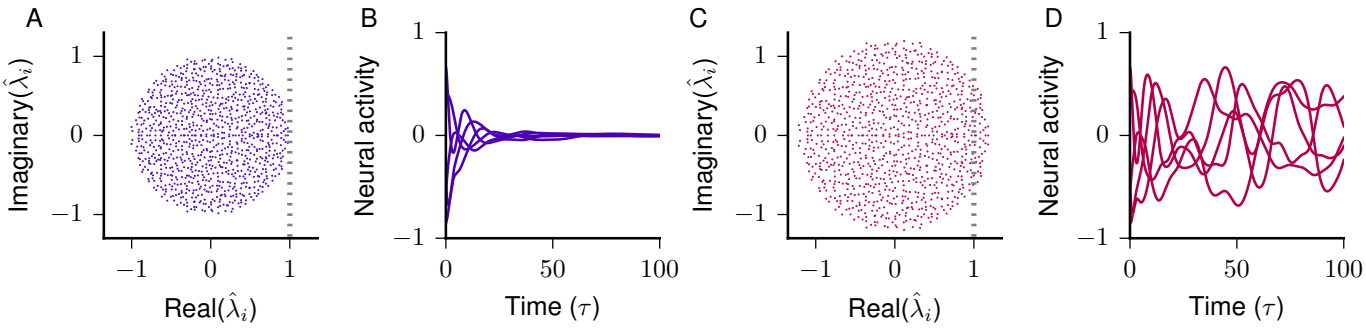

Fig 1. Transition to chaos for sufficiently strong coupling g in rate networks. A Linear stability of rate dynamics around fixed point. Real vs imaginary part of eigenvalues $\hat{\lambda}_i$ of the stability matrix for $g = 0.99$. **B** For subcritical couplings ($g = 0.99$) the trivial fixed point of the neuron states $h_i = 0$ is the only stable solution. **C** The trivial fixed point looses stability at $g_{\text{crit}} = 1$ and chaos emerges from the nonlinear interaction of rate units. In large networks this occurs when the eigenvalues $\hat{\lambda}_{max}$ with the largest real part cross unity. **D** Rate chaos for $g = 1.2$ (other parameters: Network size $N = 1000$, integration step $\Delta t = 10^{-2}\tau$).

Recently, this classical work has been extended and the transition has been studied for heterogeneous networks with different subpopulations [12, 13], various input-output transfer functions [12], bistable units [14], sparse balanced network architectures [12, 15, 16] and external stimuli [17–20]. For networks of spiking model neurons, a quantitative agreement with a corresponding chaotic rate network in the limit of slow synaptic dynamics was found [15, 16] (see also [21]).

The chaotic, heterogeneous state of these rate networks possess high computational capabilities. These arise from the rich internal dynamics that can provide a substrate for complex nonlinear computations, e.g. implementing input/output maps [22–24] and learning temporal sequences [25]. It is a challenge to extend this to spiking neural network [26–29]. Some studies proposed that computational features are favorable closely above the so-called *edge of chaos* [24, 30–34]. Recent developments in machine learning including the renaissance of deep networks also sparked new interests into principles of information processing in recurrent rate networks [35, 36].

Here we use concepts from the ergodic theory of dynamical systems to characterizing the complex collective network dynamics of rate networks. Often large-scale dissipative systems evolve towards a low-dimensional attractor and it is a challenge to find collective modes on this lower dimensional manifold. Ergodic theory provides an

estimate of the attractor dimensionality, which characterizes the diversity of collective network activity states [37]. It also provides access to the dynamical entropy rate measuring the dynamical uncertainty amplification due to sensitivity to initial conditions. The dynamical entropy rate constrains the capability of information processing: In chaotic systems a sensitive dependence on initial conditions makes predictions of future states impossible, if the initial state is known only with finite precision [38, 39]. This corresponds to a dynamical entropy rate, because nearby states, which could not be distinguished by a finite precision readout initially, are pulled apart by the chaotic dynamics and are distinguishable later on. Therefore, the dynamical entropy rate quantifies the speed by which microscopic perturbations affect macroscopic rate fluctuations [38]. Both of these topological invariants of dynamical systems can be obtained from the set of Lyapunov exponents, which measure the evolution of small perturbations in the tangent space along a trajectory [40].This is the only known general way of accessing the entropy of a high-dimensional differentiable dynamical system [37]. Sampling-based estimates of entropy and dimensionality, e.g. the Grassberger-Procaccia algorithm [41–43], which estimates the correlation dimension D_2 are intractable for systems with many degrees of freedom. A strict lower bound on the data required for such sampling-based estimates of the attractor dimensionality with a fixed desired accuracy scales exponentially in the degrees of freedom N [44, 45].

From a neural coding perspective, the dynamical entropy rate can contribute to the so-called noise entropy [46], because the dynamic amplification of microscopic noise by chaotic dynamics can impair coding capacity.

For the first time, we calculate the full Lyapunov spectrum of rate networks. Our approach holds for arbitrary network topology and smooth transfer functions ϕ. We show that dynamical entropy scales logarithmically with synaptic gain g, while the attractor dimensionality saturates exponentially. Thus, despite the increasing uncertainty gain due to sensitivity to initial conditions, the diversity of network activity states saturates for strong coupling. We analytically approximate the full Lyapunov spectrum in several limiting cases using random matrix theory. Finally, we find that time-varying input reduces both entropy and dimensionality.

Results

We study the dynamics of a randomly-wired network of nonlinear firing-rate units. The dynamics of the state of each firing-unit h_i follows [11, 12, 23]:

$$\tau \frac{dh_i}{dt} = f(h_i) = -h_i + \sum_{j=i}^{N} J_{ij}\phi(h_j). \tag{1}$$

Here h_i is the total synaptic current received by neuron i and τ is the characteristic time constant, which we set to 1 in the following without loss of generality. We draw independent identical entries of the coupling matrix J_{ij} from a Gaussian distribution $J_{ij} \sim \mathcal{N}(0, g^2/N)$ and choose the transfer function $\phi(h) = \tanh(x)$ [11].

To calculate the Lyapunov spectrum, we evaluate the Jacobian of the flow of the dynamics. It measures, how infinitesimal perturbations of the network state evolve in the tangent space along the trajectory h_i. The Jacobian is given by

$$D_{ij}(t_s) = \frac{\partial f(h_i)}{\partial h_j}\Big|_{t=t_s} = -\delta_{ij} + J_{ij}\phi'(h_j(t_s)). \tag{2}$$

Thus, in our case the Jacobian is a negative identity matrix plus the coupling matrix with rows scaled by the squared hyperbolic secant $\phi'(x) = \mathrm{sech}^2(x)$ of the network

activity states h_i. In case of strong g, $\mathrm{sech}^2(h_i) \approx 0$ for most i and hence most rows of $D_{ij}(t_s)$ are close to zero. We can make use of this simple structure for several analytical approximations. The full Lyapunov spectrum is obtained by a reorthonormalization procedure [47], which is described in detail in the Materials and Methods section including a detailed analysis of the convergence of the Lyapunov spectra.

Strong coupling intensifies chaos

We first investigate the role of the scaling of the synaptic coupling strength g (Fig. 2).

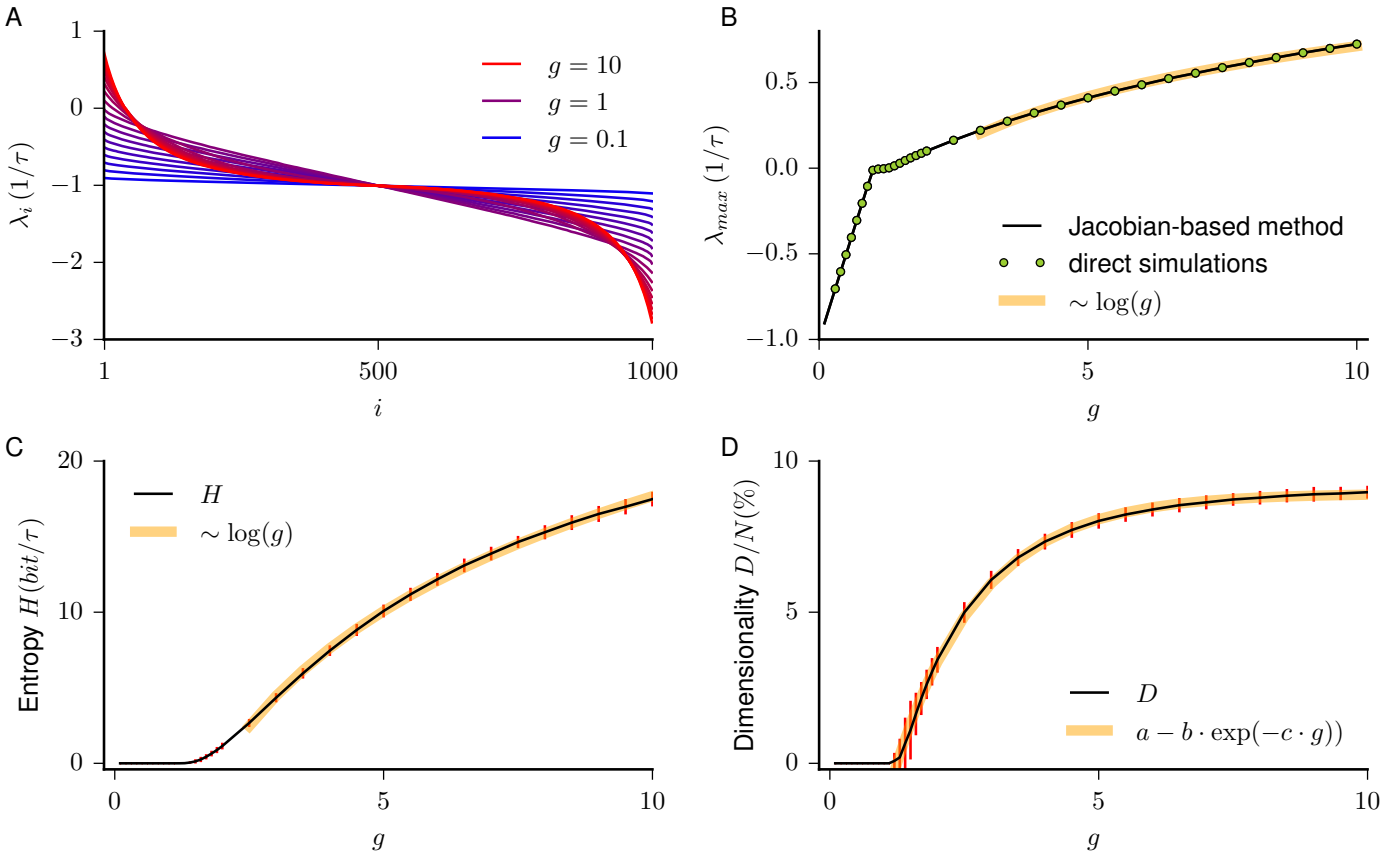

Fig 2. Entropy rate and dimensionality of firing-rate dynamics. **A** Full Lyapunov spectra of rate networks for different coupling strengths g, where g is color coded from blue (small g) to red (large g). The Lyapunov spectrum is point-symmetric around the mean Lyapunov exponent $\bar{\lambda} = -1/\tau$ (See derivation in Materials and Methods). **B** The largest Lyapunov exponent shows the theoretically predicted linear scaling for $g < 1$ and first quadratic and then logarithmic scaling for $g \gg 1$ as function of g [11]. (Green dots: direct numerical simulations, black line: Jacobian-based method, orange: log fit.) **C** The dynamical entropy rate H grows logarithmically with coupling g. **D** Relative attractor dimensionality D/N scales as $a - b \cdot \exp(-c \cdot g)$ and saturates at $\sim 10\%$. (Averages over 20 network realizations, red error bars indicate double std across 20 network realizations, orange fits, parameters: $N = 1000$, $\Delta t = 10^{-2}\tau$, $t_{\mathrm{sim}} = 10^4\tau$, $t_{\mathrm{ONS}} = \tau$).

The full Lyapunov spectrum, which is calculated here for the first time, shows an

interesting dependence on g (Fig. 2A). For increasing g, the first half of the Lyapunov spectrum is increasingly bent upwards (Fig. 2A). The Lyapunov spectrum is symmetric around its constant mean value $-1/\tau$ for all g.

The largest Lyapunov exponent shows the theoretically predicted linear scaling in the stable regime $g < 1$ (Fig. 2B). In the chaotic regime $g > 1$ it scales first quadratic and then logarithmically with g in agreement with previous work [11]. This is confirmed both by tracking the amplitude of a small perturbation in direct numerical simulations and by using the Jacobian-based method [47] (Fig. 2B).

This means that while the exponential separation rate of nearby trajectories increases for growing g, the overall dissipation of the system, measured by the mean Lyapunov exponent $\bar{\lambda}$ stays the same independent of g. We will later gives reasons for this and first focus on the entropy rate and attractor dimensionality.

Entropy rate growths logarithmically with coupling strength

The entropy rate gives the dynamical uncertainty amplification by the chaotic dynamics. It can be estimated by the sum of the positive Lyapunov exponents (Pesin identity). A rigorous upper bound on the Kolmogorov-Sinai entropy rate is given by the sum of the positive Lyapunov exponents [48], which becomes an equality if the system has smooth densities along the unstable manifolds [49–51]:

$$H \leqslant \sum_{\lambda_i > 0} \lambda_i$$

The dynamical entropy rate is zero for $g \leq 1$ and grows monotonically for increasing values of g (Fig. 2C). Our results indicate that for large g, the dynamical entropy rate grows approximately logarithmically with g (See fit in Fig. 2C). While the number of positive Lyapunov exponents decreases for large g, their growth overcompensates the decreasing number, thus the entropy rate does not saturate. The logarithmically increasing entropy rate can be considered as contribution to the noise entropy, if the microscopic network state does not encode relevant information [46].

Attractor dimensionality saturates for strong synaptic gain

The Lyapunov dimension relates the attractor dimensionality to the Lyapunov spectrum. It is given by the number of Lyapunov exponents that sum to zero:

$$D = k + \frac{\sum_{i=1}^{k} \lambda_i}{|\lambda_{k+1}|} \quad \text{with} \quad k = \max_n \left\{ \sum_{i=1}^{n} \lambda_i \geq 0 \right\}.$$

The Lyapunov dimension was conjectured to be in general equivalent to the information dimension D_1 [40, 52–54]. One can think of it as the highest dimensional hypersphere, whose volume does not shrink by the dissipative system dynamics.

We found that the dimensionality of the strange chaotic attractor also increases monotonically with g (Fig. 2D). Surprisingly, in contrast to the entropy rate, the relative attractor dimensionality appears to exponentially saturate as a function of g at around 10% of the number of phase space dimensions N (Fig. 2D, orange fit). This means that although with increasing g the dynamic uncertainty amplification increases, the diversity of network states quantified by the dimensionality saturates.

Comparison of Attractor dimensionality and PCA dimension

We compared the Lyapunov dimension with a dimensionality estimate based on second order statistics of the activity h_i and $\tanh(h_i)$ (See the Materials and Methods section

for details). Such dimensionality estimates based on Principal Component Analysis (PCA) are commonly used in experimental and theoretical neuroscience [18, 19, 55, 56], e.g. to quantify the spatiotemporal complexity of a data set.

We found that a PCA-based dimension strongly differs depending on whether it is estimated based on the statistics of the "firing rates" $\tanh(h_i)$ or based on h_i (Fig. 3). Generally, we find a quantitatively different but qualitatively similar scaling of the PCA-based dimensionality and the Lyapunov dimension: Both exponentially saturate with synaptic scaling for $g > 1$ but they saturate at a different level and with distinct exponents (Fig. 3A). The PCA-based dimensionality seems to grow extensive in network size N (Fig. 3B).

Note that covariance-based dimensionality estimates are generally not invariant with respect to changes of variables and can be misleading if applied to a limited data sets. Also, they obviously miss low-dimensional structured hidden in higher-order correlations.

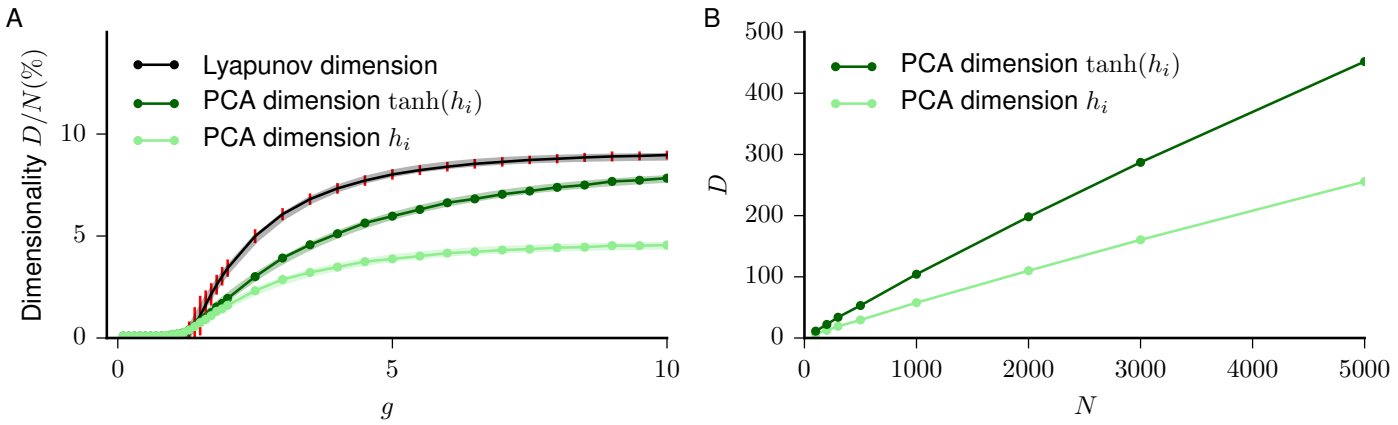

Fig 3. Comparison of PCA dimension and Lyapunov dimension A Principal Component Analysis (PCA)-based dimensionality estimate (green) and attractor dimension based on Lyapunov spectrum (black) for different values of g. With synaptic scaling g both PCA dimension exponentially saturate for $g > 1$ but they saturate at a different level and with distinct exponents (shaded lines are fits to $a - b \cdot \exp(-c \cdot g)$, red errors are double std across 20 network realizations). PCA dimension measured by localization of eigenvectors of covariance matrix of activity C^h_{ij} and $C^{\tanh h}_{ij}$ (See definition in Materials and Methods). PCA dimension estimate of dynamics depends on whether $\tanh(h_i)$ or h_i is considered. **B** Both PCA-based dimensionality estimates seem to be extensive as indicated by the approximately linear growth with N (other parameters: $N = 1000$, $g = 10$, $\Delta t = 0.1\tau$, $t_{\mathrm{ONS}} = \tau$, $t_{\mathrm{sim}} = 10^4\tau$).

Extensive spatiotemporal network chaos

The firing-rate network exhibits extensive deterministic chaos, indicated by the invariance of the Lyapunov spectrum with respect to network size N (Fig. 4A). The largest Lyapunov exponent quickly saturates as a function of network size (Fig. 4B) and both dynamical entropy rate and attractor dimensionality grow linear with network size N over two orders of magnitude (Fig. 4C+D).

The extensivity of the Lyapunov spectrum for rate networks was already conjectured earlier [11], but for the first time demonstrated here. Extensive chaos is often found in extended systems that are decomposable into weakly interacting subsystems, whose

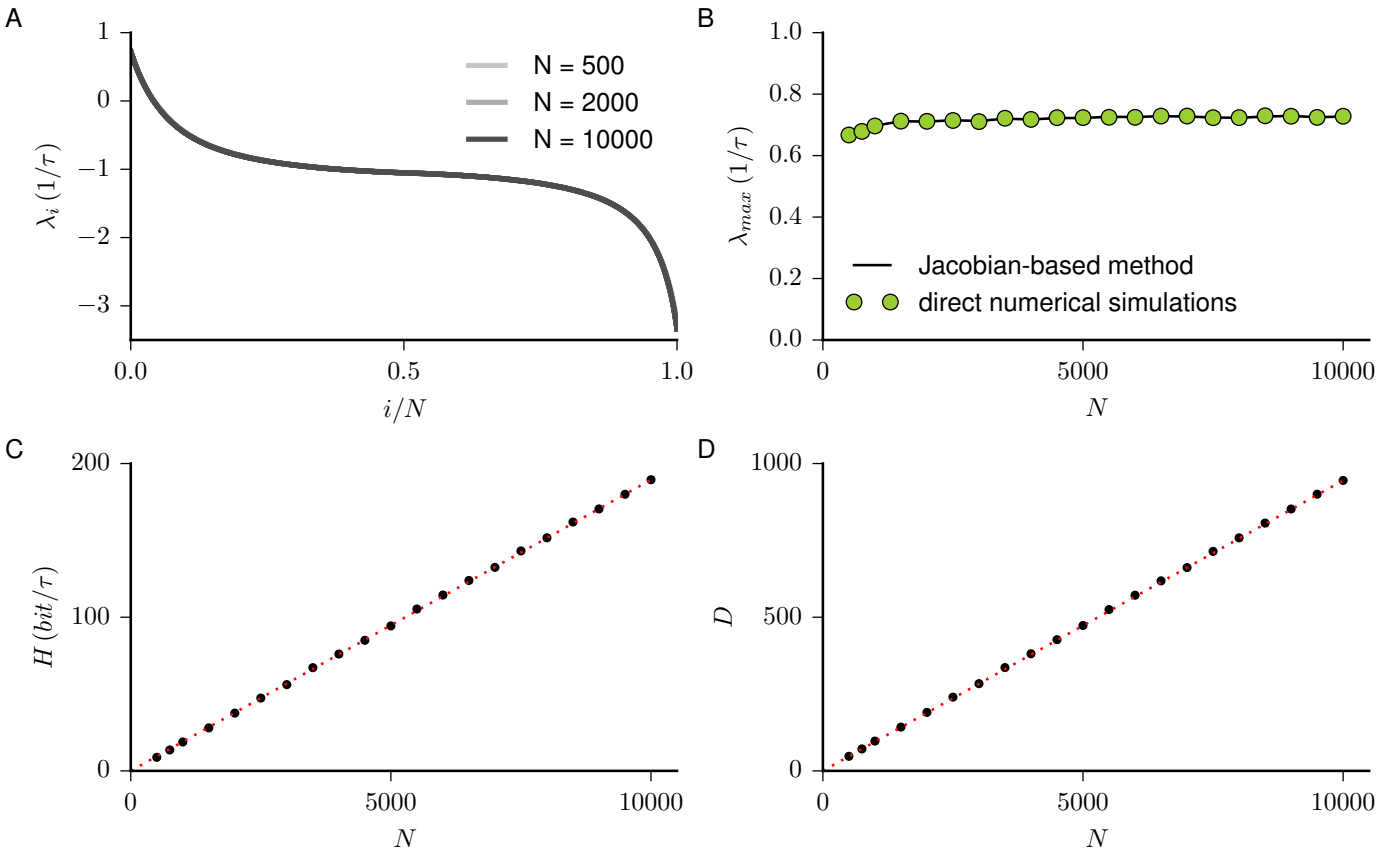

Fig 4. Extensive chaos revealed by size-invariance of Lyapunov spectrum **A** Full Lyapunov spectra for different network size N are on top of each other indicating a same shape. **B** The largest Lyapunov exponent quickly saturates with network size. **C** Kolmogorov-Sinai entropy rate H grows linear with N over two orders of magnitude. **D** The same holds for the Lyapunov attractor D dimensionality (other parameters: $g = 10$, $\Delta t = 0.1\tau$, $t_{\mathrm{ONS}} = \tau$, $t_{\mathrm{sim}} = 10^3\tau$).

number grows linearly with system size [57]. As this is not fulfilled for this fully randomly connected rate network, extensive chaos in our networks is not a trivial property. Globally coupled networks for instance can in fact exhibit nonextensive chaos [58].

Lyapunov spectrum of externally driven firing-rate network

Until now, we analyzed the autonomous dynamics of a deterministic firing-rate network. It is of great interest to extend this to a nonautonomous system driven by time-varying input [17, 19, 20, 59, 60]. The external drive can represent e.g. an artificial optogenetic stimulus, streams of neural activity coming from a cortical projection or the effect of a sensory stimulus. The dynamics of each firing-rate unit now follows:

$$\frac{dh_i}{dt} = f(h_i) = -h_i + \sum_{j=i}^{N} J_{ij}\phi(h_j) + \xi_i(t) \qquad (3)$$

where ξ_i are fixed realizations of independent Gaussian white noise processes with autocorrelation function $\langle \xi_i(t)\xi_i(t+t')\rangle = \sigma^2\delta(t')$. Again, despite the generality of our approach for arbitrary network topology J_{ij} and any differentiable transfer functions $\phi(h)$, we choose for concreteness a Gaussian connectivity with $J_{ij} \sim \mathcal{N}(0, g^2/N)$ and the transfer function $\phi(h) = \tanh(x)$.

To assess the dynamic stability of the stochastic differential equation we employ the theory of random dynamical systems (RDS), where for a frozen input realization, one studies how reliable different initial states respond to this external signal. A system is considered reliable, if different initial conditions converge to the same trajectory and unreliable, if different initial conditions remain separate despite the same external input [61]. More formally, the evolution of a *sample measure* μ_ξ^t is studied for a frozen noise realization $\xi(t)$ with $t \in (-\infty, \infty)$. This is described in more detail in the Materials and Methods section.

The mathematical expression of the Jacobian of the flow of the dynamics is the same as in the autonomous case:

$$D_{ij}(t_s) = \frac{\partial f(h_i)}{\partial h_j}\Big|_{t=t_s} = -\delta_{ij} + J_{ij}\,\mathrm{sech}^2(h_j). \tag{4}$$

While the mathematical expression is the same as in the autonomous case, noise can have a strong effect both on the distribution of h_i and on their autocorrelations $\Delta_i(\tau) = \langle \delta h_i(t)\delta h_i(t+\tau)\rangle$. The full Lyapunov spectrum, which is independent of input realization ξ [62], is again obtained by a reorthonormalization procedure of the Jacobians along a numerical solution of the stochastic differential equation integrated with the Euler-Maruyama method [47]. For details see the Materials and Methods section.

Time-varying input reduces chaoticity

We explored the effect of increasing noise strength σ on the Lyapunov spectrum (Fig. 5). By increasing input noise strength σ, the Lyapunov spectrum is increasingly pushed towards the mean Lyapunov exponent $-1/\tau$ (Fig. 5A). Increasing the input noise strength σ monotonously reduces the largest Lyapunov exponent of the network dynamics as previously observed in discrete [17, 60] and continuous time [20] (Fig. 5B). A similar effect has been observed in rate networks driven by periodic input [18, 19].

Input fluctuations reduce dynamical entropy rate

The conditional entropy rate, which is calculated from the sum of the positive Lyapunov exponents, decreases for increasing external noise strength σ. Thus, time-varying input impedes the flow of information from the microscopic state to the macroscopic network state. If the information in the microscopic state is considered to be noise, one can conclude that stronger external input fluctuations reduces the noise entropy arising from sensitivity to initial conditions. For strong input, the entropy rate is suppressed (Fig. 5C).

Input fluctuations reduce the attractor dimensionality

The attractor dimensionality also decreases for increasing input fluctuation strength σ (Fig. 5D). For sufficiently strong input σ, there is a suppression of chaos, which means that the sample measure collapses on a random sink of conditional dimension zero [63, 64]. Thus, while the network dynamics with strong input noise still might seem very high-dimensional, the conditional attractor dimensionality can shrink drastically by a time-varying external input. Such a transition is important for information processing,

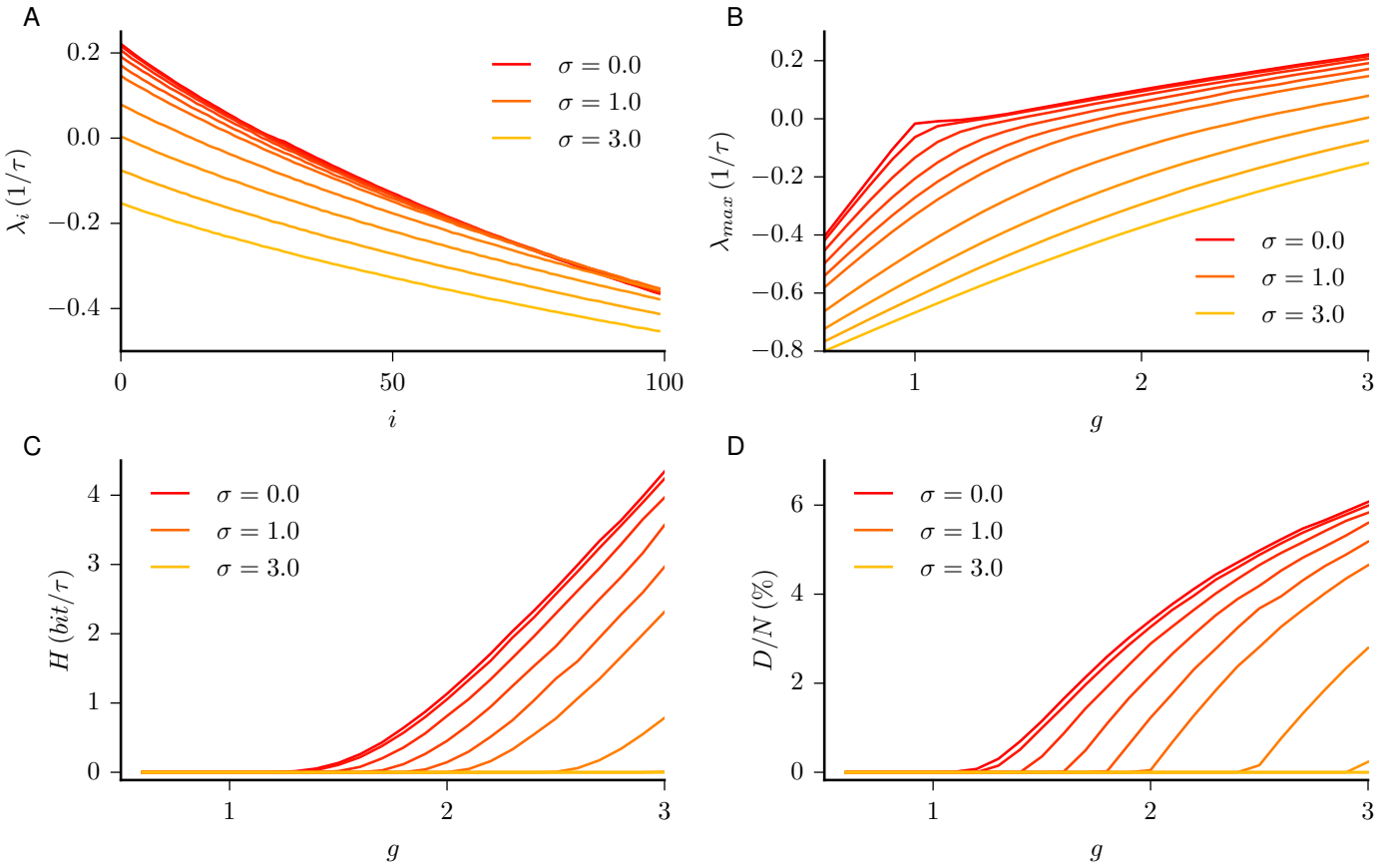

Fig 5. Time-varying stimuli reduce both dynamical entropy rate and attractor dimensionality. A By increasing input noise strength σ, the Lyapunov spectrum is increasingly pushed towards the mean Lyapunov exponent $-1/\tau$. **B** The largest Lyapunov exponent decreases and the transition is smoothed consistent with [12, 20]. **C** The dynamical entropy rate H is reduced. **D** The relative attractor dimensionality D/N is decreasing for increasing σ. (Parameters: $N = 1000$, $\Delta t = 10^{-2}\tau$, $t_{\mathrm{ONS}} = \tau$, $t_{\mathrm{sim}} = 10^3\tau$, averages across 10 network realizations).

because the network looses its dependence on initial conditions, which might be a desirable feature, if the network should generate reliably controlled output trajectories for certain input patterns after learning [23–25].

Lyapunov spectrum of discrete-time firing-rate network

Finally, we assess the effect of introducing a finite temporal discretization. The dynamics of discrete-time rate networks has attracted much attention in the past, because it is mathematically more tractable [17, 60, 65–67]. Here we want to understand the effect of time-discretization on the chaotic dynamics. We study the evolution of the map

$$h_i(t + \Delta t) = f(h_i(t)) = (1 - \Delta t) \cdot h_i(t) + \Delta t \cdot \sum_{j=i}^{N} J_{ij}\phi(h_j(t)) + \xi_i\sqrt{\Delta t} \qquad (5)$$

where ξ is Gaussian white noise with $\langle \xi_i(t)\xi_j(t+\tau)\rangle = \sigma^2\delta_{t\tau}\delta_{ij}$. In the limit $\Delta t \to 0$ the continuous-time dynamics [11, 12, 20] is recovered. For $\Delta t = 1$, the discrete-time network [17, 17, 60, 67] is obtained.

The Jacobian for the discrete-time case is

$$D_{ij}(t_s) = \frac{\partial f(h_i(t))}{\partial h_j(t)}\Big|_{t=t_s} = (1-\Delta t)\delta_{ij} + \Delta t \cdot J_{ij}\,\mathrm{sech}^2(h_j(t_s)). \tag{6}$$

The full Lyapunov spectrum is again obtained by a reorthonormalization procedure of the Jacobians along a numerical solution of the stochastic map [47]. For details see the Materials and Methods section.

Time discretization breaks the spectral symmetry

We found a drastic effect on the Lyapunov spectrum coming from the time-discretization (Fig. 6). For finite Δt, the Lyapunov spectrum looses it central symmetry (Fig. 6A). While the largest Lyapunov exponent changes only moderately by larger step size, the dynamical entropy rate and attractor dimensionality both grow for large Δt. This growth of entropy rate and dimensionality is caused by an increasing number of positive Lyapunov exponents (6C+D). At the same time, the other end of the Lyapunov spectrum decreases drastically (6A). This also strongly lowers the mean Lyapunov exponent (Fig. 6A and Fig. 7B). The mean Lyapunov exponents $\bar{\lambda}$ converges for small Δt towards $-1/\tau$. For finite Δt, the mean Lyapunov exponent can be approximated using random matrix theory by

$$\bar{\lambda}(\Delta t) = \frac{\log(1-\Delta t)}{\tau \Delta t} \tag{7}$$

This analytical result agrees well with numerical simulations (Fig. 7B). The derivation can be found in the Materials and Methods section.

For $\Delta t = 1$ and small g the Jacobians become close to independent Gaussian matrices and the full Lyapunov spectrum can be approximated by the triangle law for products of random matrices [68, 69] (See Materials and Methods section).

Discussion

Cortical circuits exhibit spatiotemporally complex rate dynamics whose origin and computational properties have puzzled both theoreticians and experimentalists for decades.

Here we used canonical measures from ergodic theory of strange attractors to characterize the chaotic dynamics of randomly-wired networks of firing-rate units. This is to our knowledge the first time the full Lyapunov spectrum of a continuous-time random rate network was calculated and used to obtain the dynamical entropy rate and attractor dimensionality.

We show that dynamical entropy scales logarithmically with synaptic coupling strength, while the relative attractor dimensionality saturates exponentially for strong coupling. Thus, despite the increasing uncertainty gain due to sensitivity to initial conditions, the diversity of network activity states saturates for strong coupling. We analytically approximate the full Lyapunov spectrum in several limiting cases using random matrix theory. Finally, we find that time-varying input reduces both entropy and dimensionality.

We demonstrate that the shape of the Lyapunov spectrum is size invariant and exhibits a linear growth of attractor dimensionality and entropy rate with network size N. This is clear evidence of extensive chaos, which was already conjectured in the

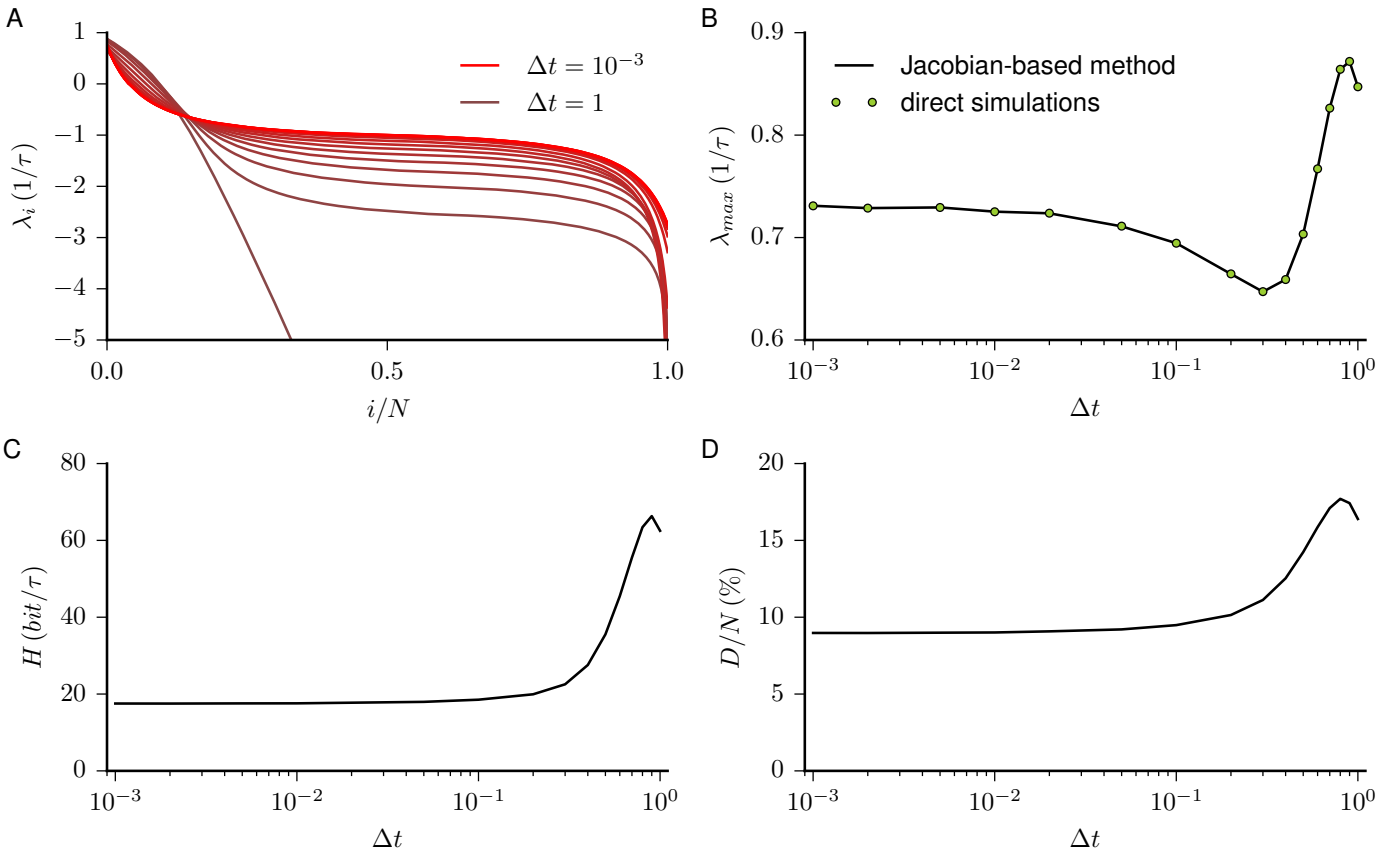

Fig 6. Full Lyapunov spectrum for different time-discretisation Δt. **A** The full Lyapunov spectrum reveals a drastic change for increasing Δt. For finite Δt, the Lyapunov spectrum looses its symmetry (See also Fig. 7). While the majority of Lyapunov exponents decrease for increasing Δt, the number of positive exponents increases. For $\Delta t = \tau$ and small g, the distribution of Lyapunov exponents follows a shape close to the triangular distribution, obtained from products of random matrices [68, 69] (see Materials and Methods section). **B** The largest Lyapunov exponent saturates for small Δt. For increasing Δt, it first decreases and then increases moderately. **C** The dynamical entropy rate saturates for small Δt and increases for large Δt. **D** The Attractor dimensionality behaves similar to the dynamical entropy rate, (other parameters: $N = 1000$, $g = 10$, $t_{\mathrm{ONS}} = \tau$, $t_{\mathrm{sim}} = 10^4\tau$, $\sigma = 0$ averages across 10 network realizations).

seminal initial work [11]. We further found the Lyapunov spectrum to be symmetric around the mean Lyapunov exponent $-1/\tau_m$, which we derived analytically using Random Matrix Theory. Symmetry of Lyapunov spectra around zero are usually found in dynamical systems with a symplectic structure [70, 71]. Symmetry around a negative value were previously described in a class of dissipative dynamical systems with viscous damping [70]. They were shown to be symmetric with respect to a constant determined by the dissipation of the system.

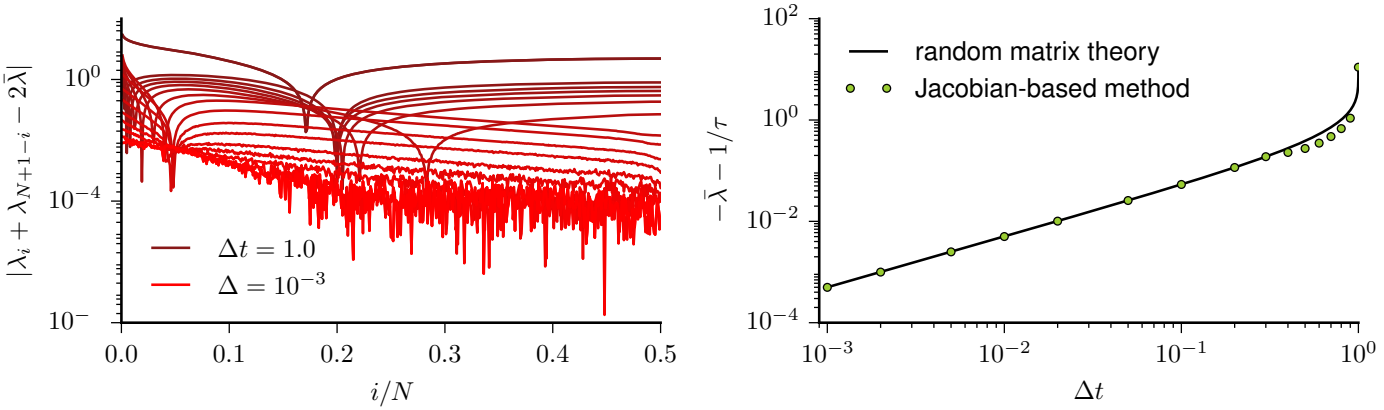

Fig 7. Point-symmetry of Lyapunov spectrum in continuous-time limit $\Delta t \to 0$ and mean Lyapunov exponent $\bar{\lambda}$. Left: For $\Delta t \to 0$, the Lyapunov spectrum approaches point-symmetry, shown by the convergence of $|\lambda_i - \bar{\lambda} + \lambda_{N+1-i} - \bar{\lambda}|$ towards zero. Note that even for very small Δt, there exist a small asymmetry because of the neutral Lyapunov exponent. Removing the neutral Lyapunov exponent improves the point-symmetry of the Lyapunov spectrum. Thus, the Lyapunov spectrum is only symmetry in the limits $N \to \infty$ and $\Delta t \to 0$. Right: The mean Lyapunov exponents $\bar{\lambda}$ converges for small Δt towards $-1/\tau$. For finite Δt, the mean Lyapunov exponent can be approximated using random matrix theory (See Materials and Methods section), (other parameters: $N = 1000$, $g = 10$, $t_{\mathrm{ONS}} = \tau$, $t_{\mathrm{sim}} = 10^4\tau$, $\sigma = 0$ averages across 10 network realizations).

Relation to previous work

Firing-rate networks can generate spontaneous rate-fluctuations by recurrent chaotic dynamics [11]. Mechanisms underlying rate chaos recently attracted substantial attention in studies of network heterogeneity [13], bistability [14], external stimuli [17–20] and the role of single unit transfer function [12] and slow synaptic dynamics [15, 16] for the collective network state. See also e.g. [60, 67, 72–76].

Our approach provides a toolkit from dynamical systems theory to analyze how these different factors shape the complex rate dynamics.

We compared the Lyapunov dimension with a dimensionality estimate based on Principal Component Analysis, which is commonly used in neuroscience [18, 19, 55, 56, 77]. Generally, we find a quantitatively different but qualitatively similar scaling of the PCA-based dimensionality and the Lyapunov dimension: Both exponentially saturate with synaptic scaling for $g > 1$ but they saturate at a different level and with distinct exponential rates. Note that Lyapunov exponents and thus also the Lyapunov dimension is invariant under diffeomorphisms on the phase space [78], while covariance-based dimensionality estimates are generally not invariant with respect to changes of variables and can be misleading if applied to a limited data sets [79].

Further, our approach also allows interpolating from continuous-time to discrete dynamics. Discrete-time dynamics of rate networks has previously been studied in random diluted network topologies [67], noise-driven networks [17] and on a ring topology.

It is also increasingly appreciated that chaotic rate dynamics provide a substrate for complex nonlinear computations, e.g. learning input-output

relations [22, 24, 26, 34, 80, 81], and learning temporal sequences [25]. Intriguingly, transient rate chaos yields exponential expressivity in deep networks [36]. Our tools allow to quantify the reorganization of the collective network dynamics during learning and to dissect underlying mechanisms of different reservoir computing strategies.

A suppression of chaos by time-dependent input was studied earlier both with white noise input in discrete-time [17] and continuous-time networks [20] and with sinusoidal input [19]. Such a transition has relevance for information processing, because the network looses its dependence on initial conditions, which might be a desirable feature, if the network should generate reliably controlled output trajectories for certain input patterns after learning [23–25]. The transition to complete control by an external stimulus and the associated independence from recurrent initial conditions was earlier studied in rate networks in the context of echo state networks for reservoir computing and termed echo state property [82–85].

Outlook

We are only beginning to use ergodic theory to understand neural computation. By employing these concepts in large scale rate networks we have laid the foundation for further investigation. Computational ergodic theory of firing-rate networks has been until now the only way to measure information theoretic quantities of large recurrent circuits. It is an important challenge to obtain a more comprehensive understanding how different factors shape the collective network dynamics.

To this end, our analysis of dimensionality and dynamical entropy rate should be extended to other input-output transfer functions ϕ and other network topologies. One should e.g. study the role of excess of bidirectional connections [86], other second order motifs [87]and strong self-coupling [14]. The analysis should also be extended to circuits in a balanced state, where large excitatory and inhibitory currents dynamically cancel each other. This has been investigated both in spiking [88–91], and rate networks [12, 15, 72] (But see also [92]).

The existence of a transition to rate chaos and its critical properties strongly depend on the onset of the nonlinear transfer function $\phi(h)$ [12]. A similar important role of the transfer function is expected both for the attractor dimensionality and the dynamical entropy rate.

The link between firing-rate networks and spiking neural networks was recently studied by investigating networks in the limit of very slow synaptic dynamics. In this limit the synaptic input current integrates over a long time and the network dynamics is analogous to a rate network [16] with quantitatively similar activity fluctuations. An interpolation from spiking to rate dynamics with increasing τ_s and a comparison of the associated Lyapunov spectra of rate and spiking networks might improve our understanding of chaos both in spiking and rate networks.

Recent work suggested a link between dynamical and topological complexity [73]. One should explore the attractor dimensionality and dynamical entropy rate to investigate this suggested link.

It is also important to investigate how different features of a time-dependent external stimulus shape dimensionality and dynamical entropy [17–19, 60, 67]. (See also [46, 93–95] for driven spiking networks).

Which features of the input statistics facilitate complete network state control and govern a transition from chaos to stability? How do spatial and temporal correlations in the input affect entropy rate and attractor dimensionality? Answering such questions does not only deepen our understanding of driven network dynamics, but also helps to harness the computational capabilities of cortical circuit models [22, 24, 25, 34, 80, 81, 96]. This applies both to rate networks and to learning in spiking networks [26–29].

Earlier studies investigated learning capabilities of rate networks by linearizing the rate dynamics e.g. around fixed points [80, 96]. Our approach would allow to study the dynamics in the tangent space along a trajectory. For tracking the orientations of stable and unstable manifolds and the associated instantaneous exponential rates of expansion and contraction time, one should calculate the Lyapunov vectors and the local Lyapunov exponents [97–99]. How does the Lyapunov spectrum change from before to after learning for different task types? What does the Lyapunov spectra reveal about why some network topologies are better at learning than others? Is it – for example– desirable to have many Lyapunov exponents close to zero? How is learning performance reflected in the Lyapunov spectrum? Is there some optimal chaotic reservoir to learn many or long patterns? How are transient stable periods reflected in the Lyapunov spectrum?

Answering such questions would provide a deeper understanding of the reorganization of the phase space underlying different learning strategies in recurrent circuits.

Materials and Methods

We first give a brief summary of the mathematical foundations of Lyapunov spectra and our concrete implementation for rate networks. We then check the convergence of the Lyapunov spectra with various system parameters. Afterwards, we extend the approach to random dynamical systems and the implementation of Lyapunov spectra for nonautonomous networks with time-dependent input. Finally, we calculate the mean Lyapunov exponent analytically and give analytical approximations of the Lyapunov spectra in several limit cases.

Lyapunov spectrum of a dynamical system

An autonomous dynamical system is usually defined by a set of ordinary differential equations $\frac{d\mathbf{x}}{dt} = \mathbf{F}(\mathbf{x})$, $\mathbf{x} \in \mathbb{R}^N$ in the case of continuous dynamics or as a map $\mathbf{x}_{s+1} = \mathbf{f}(\mathbf{x}_s)$ in the case of discrete dynamics. We focus here on discrete dynamical systems, which are numerically studied in the limit of small time steps, but everything directly extends to continuous systems [100]. In our specific case, we study the discrete network dynamics in the limit of small Δt. This corresponds to the usual Euler method in the autonomous case or to the Euler-Maruyama method [101] in the nonautonomous case. More generally, the dynamics could also be solved using e.g. a fourth order Runge-Kutta method, but their stochastic counterparts become increasingly complex. An initial condition $\mathbf{x}_0$ forms an orbit. As a natural extension of linear stability analysis, one can ask, how an infinitesimal perturbation $\mathbf{x}_0' = \mathbf{x}_0 + \epsilon\mathbf{u}_0$ evolves in time. Chaotic systems are sensitive to initial conditions, therefore almost all infinitesimal perturbations $\epsilon\mathbf{u}_0$ of the initial condition grow exponentially. Finite size perturbations therefore may lead to a drastically different future behavior. The largest Lyapunov exponent measures the average rate of exponential divergence or convergence of nearby initial conditions.

$$\lambda_{\max}(\mathbf{x}_0) = \lim_{t\to\infty} \frac{1}{t} \lim_{\epsilon\to 0} \log \frac{||\epsilon\mathbf{u}_t||}{||\epsilon\mathbf{u}_0||} \tag{8}$$

It is crucial to first take the limit $\epsilon \to 0$ and then $t \to \infty$, as $\lambda_{\max}(\mathbf{x}_0)$ would be trivially zero for a bounded attractor, if the limits are exchanged, as $\lim_{t\to\infty} \log \frac{||\epsilon\mathbf{u}_t||}{||\epsilon\mathbf{u}_0||}$ is bounded for finite perturbations even if the system is chaotic. To measure N Lyapunov exponents, one has to study the evolution of N independent infinitesimal perturbations spanning the tangent space:

$$\mathbf{u}_{s+1} = \mathbf{D}_s \mathbf{u}_s \tag{9}$$

where the $N \times N$ Jacobian $\mathbf{D}_s(\mathbf{x_s}) = \frac{d\mathbf{f}(\mathbf{x_s})}{d\mathbf{x}}$ characterizes the evolution of generic infinitesimal perturbations during one step. Again, we are interested into the asymptotic behavior, therefore we have to study the long-term Jacobian:

$$\mathbf{T}_t(\mathbf{x}_0) = \mathbf{D}_{t-1}(\mathbf{x}_{t-1}) \dots \mathbf{D}_1(\mathbf{x}_1)\mathbf{D}_0(\mathbf{x}_0) \tag{10}$$

Note that $\mathbf{T}_t(\mathbf{x}_0)$ is a product of generally noncommuting matrices. The Lyapunov exponents $\lambda_1 \geq \lambda_2 \cdots \geq \lambda_N$ are defined by the logarithms of the eigenvalues of the positive-semidefinite symmetric Oseledets matrix

$$\mathbf{\Lambda}(\mathbf{x}_0) = \lim_{t\to\infty} [\mathbf{T}_\mathrm{t}(\mathbf{x}_0)^\top \mathbf{T}_\mathrm{t}(\mathbf{x}_0)]^{\frac{1}{2t}}, \tag{11}$$

where $\top$ denotes the transpose operator. The expression inside the brackets is the Gram matrix of the long-term Jacobian $\mathbf{T}_t(\mathbf{x}_0)$. Geometrically, the determinant of the Gram matrix is the squared volume of the parallelotope spanned by the columns of $\mathbf{T}_\mathrm{t}(\mathbf{x}_0)$. Oseledets' multiplicative ergodic theorem guarantees the existence of the Oseledets matrix $\mathbf{\Lambda}(\mathbf{x}_0)$ for μ-almost all initial conditions $\mathbf{x}_0$. In ergodic systems, the Lyapunov exponents λ_i do not depend on the initial condition $\mathbf{x}_0$. However, for numerically calculation of the Lyapunov spectrum, Eq. (11) can not directly be used, because the long-term Jacobian $T_t(\mathbf{x}_0)$ quickly becomes ill-conditioned, i.e. the ratio between its largest and smallest singular value diverges exponentially with time.

Algorithm for calculating Lyapunov spectrum of rate networks

For calculating the first m Lyapunov exponents, we instead exploit the fact that the growth rate of an m-dimensional infinitesimal volume element is given by $\lambda^{(m)} = \sum_{i=1}^{m} \lambda_i$. Therefore, $\lambda_1 = \lambda^{(1)}$, $\lambda_2 = \lambda^{(2)} - \lambda_1$, $\lambda_3 = \lambda^{(3)} - \lambda_1 - \lambda_2$, etc [47]. The volume growth rates can be obtained via QR-decomposition. Firstly, one needs to evolve an orthonormal basis $\mathbf{Q}_s = [\mathbf{q}_s^1, \mathbf{q}_s^2, \dots \mathbf{q}_s^m]$ in time using the Jacobian:

$$\widetilde{\mathbf{Q}}_{s+1} = \mathbf{D}_s \mathbf{Q}_s \tag{12}$$

Secondly, one performs the QR-decomposition

$$\widetilde{\mathbf{Q}}_{s+1} = \mathbf{Q}_{s+1}\mathbf{R}^{s+1} \tag{13}$$

Hereby the non-orthonormal matrix $\widetilde{\mathbf{Q}}_{s+1}$ is uniquely decomposed into an orthonormal matrix $\mathbf{Q}_{s+1}$ of size $N \times m$ so $\mathbf{Q}_{s+1}^\top \mathbf{Q}_{s+1} = \mathbb{1}_{m\times m}$ and an upper triangular matrix $\mathbf{R}^{s+1}$ of size $m \times m$ with positive diagonal elements.

Geometrically, $\mathbf{Q}_{s+1}$ describes the rotation of $\mathbf{Q}_s$ caused by $\mathbf{D}_s$ and the diagonal entries of $\mathbf{R}^{s+1}$ describes the stretching and/or shrinking of $\mathbf{Q}_s$, while the off-diagonal elements describe the shearing. Fig. 8 visualizes $\mathbf{D}_s$ and the QR-decomposition for $m = 2$. The Lyapunov exponents are obtained from the diagonal elements of $\mathbf{R}^s$:

$$\lambda_i = \lim_{t\to\infty} \frac{1}{t} \log \prod_{s=1}^{t} \mathbf{R}_{ii}^s = \lim_{t\to\infty} \frac{1}{t} \sum_{s=1}^{t} \log \mathbf{R}_{ii}^s \tag{14}$$

Note that the QR-decomposition does not need to be performed in every simulation step, just sufficiently often such that $\widetilde{\mathbf{Q}}_{s+w} = \mathbf{D}_{s+w-1} \cdot \mathbf{D}_{s+w-2} \dots \mathbf{D}_s \cdot \mathbf{Q}_s$ is well-conditioned. An appropriate reorthonormalization interval $w_\mathrm{ONS} = t_\mathrm{ONS}/\Delta t$ thus

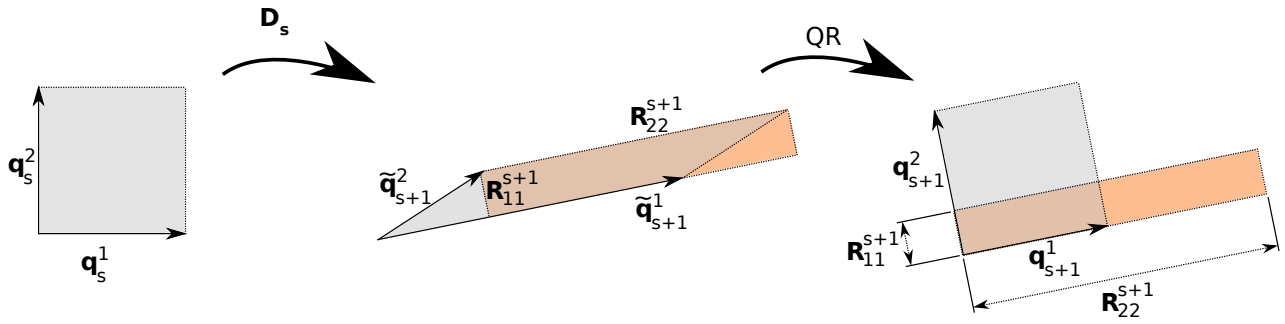

Fig 8. Geometric illustration of Lyapunov spectrum calculation. An orthonormal matrix $\mathbf{Q}_s = [\mathbf{q}_s^1, \mathbf{q}_s^2, \dots \mathbf{q}_s^m]$, whose columns are the axes of an m-dimensional cube, is rotated and distorted by the Jacobian $\mathbf{D}_s$ into an m-dimensional parallelotope $\widetilde{\mathbf{Q}}_{s+1} = \mathbf{D}_s\mathbf{Q}_s$ embedded in $\mathbb{R}^{\mathbf{N}}$. The figure illustrates this for $m = 2$, in this case the columns of $\widetilde{\mathbf{Q}}_{s+1}$ span a parallelogram. It can be divided into a right triangle and a trapezoid, and rearranged into a rectangle. Thus, the area of the gray parallelogram is the same as that of the orange rectangle. The QR-decomposition reorthonormalizes $\widetilde{\mathbf{Q}}_{s+1}$ by decomposing it into the product of an orthonormal matrix $\mathbf{Q}_{s+1} = [\mathbf{q}_{s+1}^1, \mathbf{q}_{s+1}^2, \dots \mathbf{q}_{s+1}^m]$ and the upper-triangular matrix $\mathbf{R}^{s+1}$. $\mathbf{Q}_{s+1}$ describes the rotation of $\mathbf{Q}_s$ caused by $\mathbf{D}_s$. The diagonal entries of $\mathbf{R}^{s+1}$ gives the stretching/shrinking along the columns of $\mathbf{Q}_{s+1}$, thus volume of the parallelotope formed by the first m columns of $\widetilde{\mathbf{Q}}_{s+1}$ is given by $V_m = \sum_{i=1}^m \mathbf{R}_{ii}^{s+1}$. The time-normalized logarithms of the diagonal elements of $\mathbf{R}^s$ give the Lyapunov spectrum: $\lambda_i = \lim_{t\to\infty} \frac{1}{t} \log \prod_{s=1}^t \mathbf{R}_{ii}^s = \lim_{t\to\infty} \frac{1}{t} \sum_{s=1}^t \log \mathbf{R}_{ii}^s$.

depends on the condition number, given by the ratio of the smallest and largest singular value:

$$\kappa_2(\widetilde{\mathbf{Q}}_{s+w}) = \kappa_2(\mathbf{R}^{s+w}) = \frac{\sigma_1(\mathbf{R}^{s+w})}{\sigma_m(\mathbf{R}^{s+w})} = \frac{\mathbf{R}_{11}^{s+w}}{\mathbf{R}_{mm}^{s+w}}. \tag{15}$$

The condition number can therefore be estimated based on the ratio of the largest and smallest Lyapunov exponent that are calculated: $\kappa_2(\widetilde{\mathbf{Q}}_{s+w}) \approx \exp(\lambda_1 - \lambda_m)$. Thus, an appropriate reorthonormalization interval is given by $t_{\mathrm{ONS}} = \mathcal{O}\left(\frac{\log(\hat{\kappa}_2)}{\lambda_1 - \lambda_m}\right)$, where $\hat{\kappa}_2$ is some acceptable condition number. The acceptable condition number depends on the desired accuracy of the entries of $\mathbf{R}^{s+w}$. Here we show a minimal example of this algorithm in pseudocode:

Jacobian-based algorithm (Benettin)

initialize $\mathbf{h}$, $\mathbf{Q}$
warm-up of $\mathbf{h}$
warm up of $\mathbf{Q}$
for $t = 1 \rightarrow t_{\mathrm{sim}}/\Delta t$ **do**
  $\mathbf{h} \leftarrow \mathbf{f}(\mathbf{h})$
  $\mathbf{D} \leftarrow \frac{d\mathbf{f}}{d\mathbf{h}}$
  $\mathbf{Q} \leftarrow \mathbf{D} \cdot \mathbf{Q}$
  if $t \,\%\, t_{\mathrm{ONS}} = 0$ **then**
    $\mathbf{Q}, \mathbf{R} \leftarrow qr(\mathbf{Q})$
    $\gamma_i \mathrel{+}= \log(R_{ii})$
  end if
end for
$\lambda_i = \gamma_i / t_{\mathrm{sim}}$

Convergence of the Lyapunov spectrum

We checked the convergence of the Lyapunov spectrum as a function of different simulation parameters. Firstly, the Lyapunov exponents were checked to be converged with simulation time t_{sim} (Fig. 9). Figure 9 shows the temporal convergence of selected Lyapunov exponents for ten network topologies for different values of g and σ. The Lyapunov spectra were independent of initial conditions, but showed some variability across different network topology realizations. There are two main contributions for variability of numerically calculated Lyapunov spectra, finite-time sampling noise and quenched fluctuations: Lyapunov exponents are asymptotic properties numerically estimated from finite time calculations.

In addition, variability is arising from the quenched disorder in different random topologies. The first contribution would vanish in the limit of long simulations for ergodic systems. The second contribution is expected to vanish in the large network limit due to self-averaging. Quantities that are self-averaging converge in the limit of large system size to the ensemble average. Secondly, we confirmed that the orthonormalization interval was chosen sufficiently small (Fig. 10a). If the reorthonormalization is not carried out sufficiently often, the long-term Jacobian $\mathbf{T}_t(\mathbf{x}_0)$ becomes ill-conditioned. As a consequence, the orthonormalization becomes numerically instable beginning from the end of the Lyapunov spectrum and errors start to accumulate (Fig. 10d). As described, a suitable orthonormalization interval inversely scales with the difference between smallest and largest Lyapunov exponent to be calculated $|\lambda_1 - \lambda_k|$. Therefore, it is no surprise that for large Δt, the errors in the Lyapunov spectrum grow faster with t_{ONS} (Fig. 10d), because the difference $|\lambda_1 - \lambda_k|$ is larger (Fig. 7).

Thirdly, we checked convergence with integration time step Δt (Fig. 6A). For large g, the integration time step Δt has to be chosen smaller, because the autocorrelations of the Jacobians become very short ($\tau_{AC} \ll \tau$), although the autocorrelations of the dynamics variables h_i stays finite even for $g \rightarrow \infty$ [11].

Fourthly, we confirmed the convergence of the shape of the Lyapunov spectrum with network size N (Fig. 4B). Note that even for very small Δt, there exist a small asymmetry in the Lyapunov spectrum because of the neutral Lyapunov exponent. Thus, the Lyapunov spectrum is only symmetric in the limits $N \rightarrow \infty$ and $\Delta t \rightarrow 0$.

Fifthly, we confirmed numerically that the neutral Lyapunov exponent associated to a perturbation in the direction of the flow converges towards zero in the limit of small Δt (not shown).

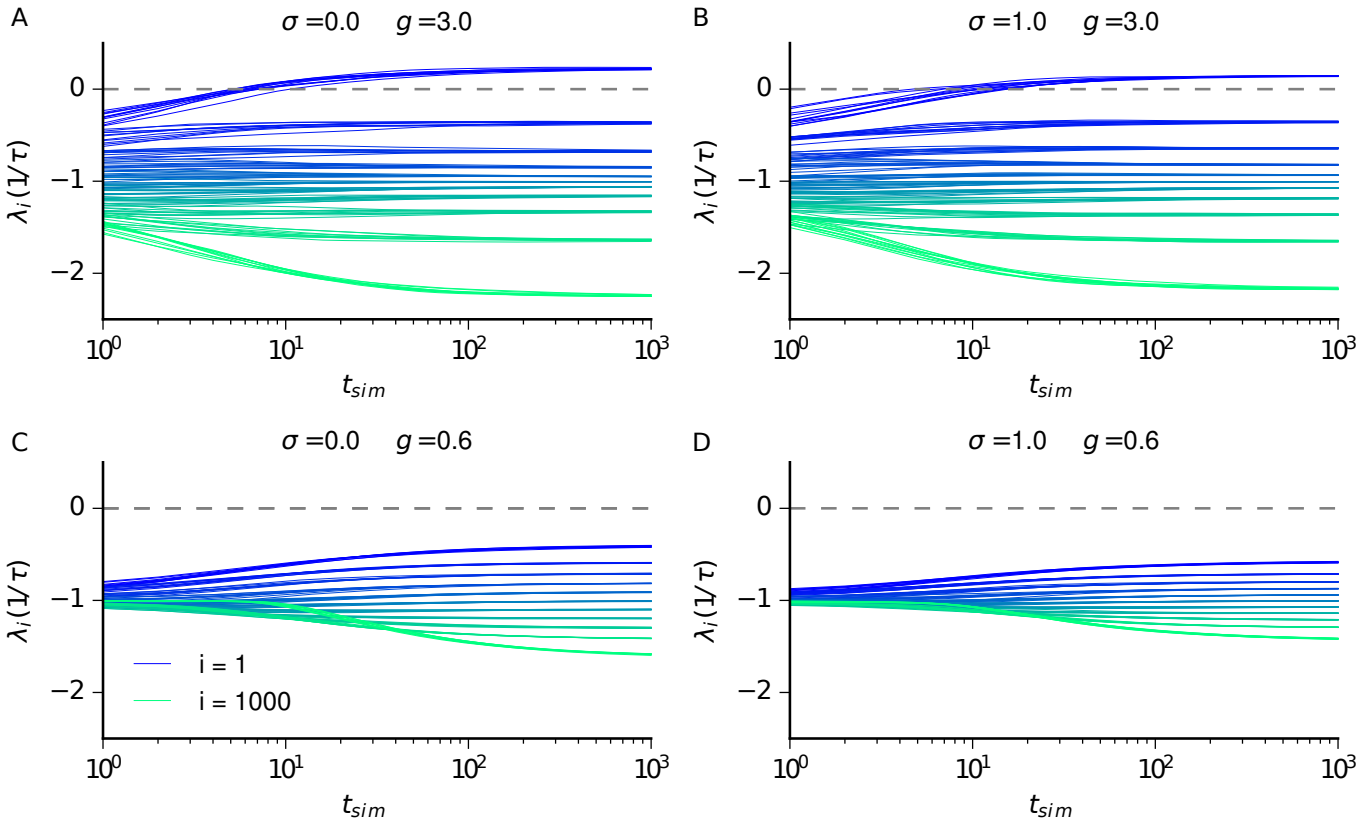

Fig 9. Convergence of Lyapunov spectrum with simulation time $t_{\rm sim}$. **A**: Convergence of selected Lyapunov exponents λ_i for ten different network realizations with simulation time (in units of τ)($i = 1, 100, 200, \ldots 1000$) for $\sigma = 0$ and $g = 3$. **B** same as top left, but for $\sigma = 1$ and $g = 3$. **C** $\sigma = 0$ and $g = 0.6$. **D** $\sigma = 1$ and $g = 0.6$. (Other parameters: $N = 1000$, $\Delta t = 0.01\tau$, $t_{\rm sim} = 10^4\tau$, $t_{\rm ONS} = \tau$).

Random Dynamical Systems and trial-to-trial variability

Consider a stochastic differential equation of the form:

$$dx_t = a(x_t)dt + \sum_{i=1}^{N} b_i(x_t) \circ dW_t^i$$

where dW_t^i are independent Brownian motions. An associated *stochastic flow map* is a solution for the dynamics, i.e. $F_{t_1,\,t_2;\zeta}(\mathbf{x}_{t_1}) = \mathbf{x}_{t_2}$. Instead of studying the temporal evolution of some initial measure μ, where each initial condition receives "private" noise, as it is usually done in a Fokker-Planck approach, the theory of random dynamical systems studies the evolution of a *sample measure* μ_ζ^t, defined as

$$\mu_\zeta^t = \lim_{s\to\infty} (F_{-s,\,t;\zeta})_* \mu$$

where the propagator $(F_{-s,\,t;\zeta})_*$ transports the initial measure μ for some fixed white noise realization $\zeta(t)$ defined for all $t \in (-\infty, \infty)$ along the flow $F_{-s,\,t;\zeta}$. In other words, the sample measure μ_ζ^t is the conditional measure at time t given the infinite past history of $\zeta(t)$. Note that in general, while μ_ζ^t depends both on time t and the noise

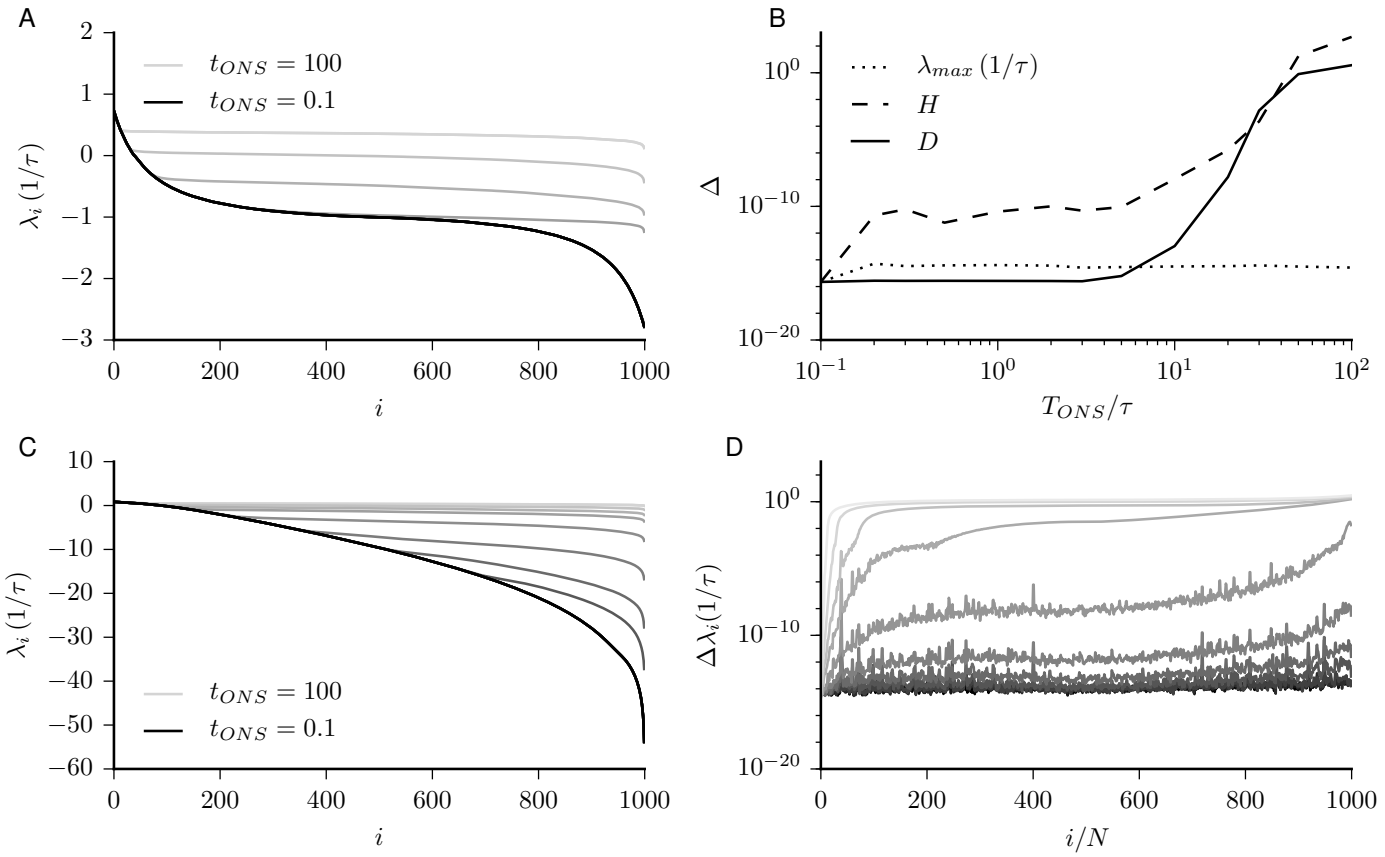

Fig 10. Convergence of Lyapunov spectrum with reorthonormalization interval t_{ONS}. The reorthonormalization does not need to be carried out in every simulation step. One has to reorthonormalize sufficiently often such that $\tilde{\mathbf{Q}}_{s+w} = \mathbf{D}_{s+w-1} \cdot \mathbf{D}_{s+w-2} \ldots \mathbf{D}_s \cdot \mathbf{Q}_s$ is well-conditioned. If the reorthonormalization is not performed sufficiently often, the error of the Lyapunov exponents grow. This is reflected in a flattening of the Lyapunov spectrum for too large t_{ONS}. **A** Lyapunov spectra for $t_{\mathrm{ONS}} \in \{0.1, 0.2, 0.3, 0.5, 1, 2, 5, 10, 20, 50, 100\}\tau$ for $\Delta t = 0.01$. **B** $\Delta\lambda_{max}$ shows the deviation of the largest Lyapunov exponent for different t_{ONS} from the smallest $t_{\mathrm{ONS}} = 0.1\tau$. Same is shown for H and D. For our typical parameter sets an orthonormalization interval of $t_{\mathrm{ONS}} = 1\tau$ is sufficient to keep errors in H and D orders of magnitudes smaller than the deviations across topologies due to quenched fluctuations. **C** Same as **A** for $\Delta t = 1$. **D** Deviations of full Lyapunov spectra for different t_{ONS} from the smallest $t_{\mathrm{ONS}} = 0.1$ for $\Delta t = 0.01$. (Other parameters: $N = 1000$, $\Delta t = 0.01\tau$, $g = 10$, $t_{\mathrm{sim}} = 10^4\tau$, averages across 10 network realizations).

realization ζ, it posses invariant properties, characterizing its structure. For example, the Lyapunov exponents $\lambda_1 \geqslant \lambda_2 \geqslant \ldots \geqslant \lambda_N$ are independent of the input realization ζ [62].

Two theorems for random dynamical systems link sample measure μ_ζ^t and Lyapunov spectrum in chaotic and stable systems respectively.

Firstly, Ledrappier and Young proved that if $\lambda_1 > 0$, then μ_ζ^t is a random SRB (Sinai-Ruelle-Bowen) measure [50].

As a consequence, in contrast to autonomous systems, for random dynamical

systems the Pesin identity $H = \sum_{\lambda_i>0} \lambda_i$ is guaranteed to hold. Note that in contrast to SRB measures of autonomous systems, random SRB measures are time-dependent. However, they have a similar meaning: Systems with SRB measure have smooth conditional measures along the unstable manifolds.

Secondly, Baxendale and Le Jan showed that if $\lambda_1 < 0$ and the stationary measure is ergodic and some nondegeneracy conditions on the measure are fulfilled [63], then μ_ζ^t is a random sink, which means $\mu_\zeta^t(\mathbf{x}) = \delta(\mathbf{x} - \mathbf{x}_t)$, where $\mathbf{x}_t$ is a solution of the stochastic dynamics for a given noise realization ζ [63, 64].

This means that any trajectory of a stable rate network driven by white noise will at some time be absorbed into one single trajectories, which is independent of the initial condition but depends only the noise realization. Equally, any smooth initial measure will asymptotically coalesce into a wandering time-dependent sink.

Note that the theorems by Baxendale and Le Jan do not say, when the globally attracting random sink will be reached, which means in case of very long transients, its asymptotic existence might have no practical relevance on the timescale of interest [39].

Principal component-based dimensionality estimate

We compared the Lyapunov dimension to a principal component-based dimensionality estimate. Principal component analysis (PCA) has been widely used as dimensionality reduction technique both in experimental and theoretical neuroscience [18, 19, 55, 56].

PCA provides for a data set the succeeding orthogonal directions that account for most of the variance in the data and the associated fraction of variance explained. Mathematically, PCA is given by the eigenvalue decomposition of the covariance matrix. From the eigenvalues one can obtain the percentage of the total variance explained by each principal component. The number of principal components necessary to account for the majority of the total variance gives an estimate of the number of degrees of freedom of the underlying dynamics. If few principal components explain most of the variance, the dynamics is mostly constrained to a hyperellipsoid with few large axes. If many principal components are necessary to explain most of the variance, no such localized structures in the second order statistics of the collective dynamics are detected. To avoid choosing an arbitrary threshold of variance, one can use a participation ratio, commonly used in physics to quantify e.g. localization of collective activity modes [102], Anderson localization of waves in a disordered medium [103] or localized Lyapunov vectors [91, 97]. We calculated PCA-based dimensionality estimates both based on the covariance of the total synaptic currents h_i and of the "rates" $r_i = \tanh(h_i)$:

$$C_{ij}^h = \langle (h_i - \langle h_i \rangle)(h_j - \langle h_j \rangle) \rangle \tag{16}$$

A covariance-based dimensionality estimate is then given by the inverse participation ratio

$$D_{\mathrm{PCA}}^h = \frac{(\sum_{n=1}^N \mu_n^h)^2}{\sum_{n=1}^N \mu_n^{h2}} \tag{17}$$

where μ_n^h is the n^{th} eigenvalue of the covariance matrix C_{ij}^h. If all eigenvalues contribute equally (i.e. $\frac{\mu_n^h}{\sum_i \mu_n^h} = 1/N$), the dimension estimate is $D_{\mathrm{PCA}}^h = N$. Conversely, if only one eigenvalue contributes then $D_{\mathrm{PCA}}^h = 1$ [18, 55, 91]. $D_{\mathrm{PCA}}^{\tanh h}$ was calculated the same way, but for the covariance matrix $C^{\tanh h}$.

Random matrix theory of Lyapunov exponents

We first derive the mean Lyapunov exponent both in the continuous-time and discrete-time case. We then give approximations of the full Lyapunov spectrum in several limiting cases.

Random matrix theory of mean Lyapunov exponent

From the Jacobian, we derive a random matrix approximation of the mean Lyapunov exponent $\bar{\lambda} = \frac{1}{N}\sum_{i=1}^{N}\lambda_i$. The mean Lyapunov exponent describes the average dissipation rate of phase space compression, captured by the determinant of the long term Jacobian $\mathbf{T}_t = \mathbf{D}_t \cdots \mathbf{D}_0$: First, we calculate the distribution of entries of the Jacobian analytically. In the discrete-time case the Jacobian is given by:

$$D_{ij}(t_s) = \frac{\partial f(h_i(t))}{\partial h_j(t)}\Big|_{t=t_s} = (1-\Delta t)\delta_{ij} + \Delta t \cdot J_{ij}\,\mathrm{sech}^2(h_j(t_s)). \tag{18}$$

Thus, the Jacobian is a negative scaled identity matrix plus the coupling matrix with rows scaled by the squared hyperbolic secant of the network activity states h_i. It is known that in the chaotic regime, the activity variables h_i follow for large N approximately a Gaussian distribution both in discrete and continuous time $h \sim \mathcal{N}(0, \Delta_0)$, where for large N, Δ_0 solely depends on g [11,12,17,20]. The variance of h_i grows with g, thus the squared hyperbolic secant of h_i is close to zero for most i. For this reason, in case of strong g, most rows of $D_{ij}(t_s)$ are close to zero and D_{ij} becomes sparse.

The long-term Jacobian $\mathbf{T}_t(\mathbf{h}_0)$ is

$$\begin{aligned}
\mathbf{T}_t(\mathbf{h}_0) &= \mathbf{D}_{t-1}(\mathbf{h}_{t-1})\ldots\mathbf{D}_1(\mathbf{h}_1)\mathbf{D}_0(\mathbf{h}_0) && (19)\\
&= \prod_{s=0}^{t-1}\mathbf{D}_s && (20)\\
&= \prod_{s=0}^{t-1}\left[(1-\Delta t)\mathbb{1} + \Delta t\cdot\mathbf{J}\cdot\mathrm{sech}^2(\mathbf{h}(t_s))\right] && (21)\\
& && (22)
\end{aligned}$$

Thus, the mean Lyapunov exponent is

$$\begin{aligned}
\bar{\lambda} &= \frac{1}{N\tau}\lim_{t_{\mathrm{sim}}\to\infty}\frac{1}{t_{\mathrm{sim}}}\ln\left(\det\mathbf{T}_t\right) && (23)\\
&= \frac{1}{N\tau}\lim_{t\to\infty}\frac{1}{t\Delta t}\ln\left(\det\mathbf{T}_t\right) && (24)\\
&= \frac{1}{N\tau}\lim_{t\Delta t\to\infty}\frac{1}{t\Delta t}\ln\left(\det\left[\prod_{s=0}^{t-1}(1-\Delta t)\mathbb{1} + \Delta t\cdot\mathbf{J}\cdot\mathrm{sech}^2(\mathbf{h}(t_s))\right]\right) && (25)\\
&= \frac{1}{N\tau}\lim_{t\Delta t\to\infty}\frac{1}{t\Delta t}\ln\left(\prod_{s=0}^{t-1}\det\left[(1-\Delta t)\mathbb{1} + \Delta t\cdot\mathbf{J}\cdot\mathrm{sech}^2(\mathbf{h}(t_s))\right]\right) && (26)\\
&\approx \frac{1}{N\tau}\lim_{t\Delta t\to\infty}\frac{1}{t\Delta t}\ln\left(\det\left[(1-\Delta t)\mathbb{1} + \Delta t\cdot\mathbf{J}\cdot\mathbf{y}\right]^t\right) && (27)\\
&\approx \frac{1}{\tau}\lim_{\tau\Delta t}\frac{1}{t\Delta t}\ln\left((1-\Delta t)^t\right) && (28)\\
&= \frac{1}{\tau\Delta t}\ln(1-\Delta t) && (29)\\
& && (30)
\end{aligned}$$

In the limit $\Delta t \to 0$, the mean Lyapunov exponent thus becomes $-\frac{1}{\tau}$.

Random matrix approximations of full Lyapunov spectrum

The full Lyapunov spectrum is given by the eigenvalues of the Oseledets matrix

$$\mathbf{\Lambda} = \lim_{t\to\infty} [\mathbf{T}_\mathrm{t}{}^\top \mathbf{T}_\mathrm{t}]^{\frac{1}{2t}}. \tag{31}$$

As the long term Jacobian $\mathbf{T}_t(\mathbf{h}_0)$ is a product of generally noncommuting matrices, it is considered to be difficult to calculate the full Lyapunov spectrum analytically [104]. However, we identified several limits, where correlations between subsequent Jacobians vanish and random matrix approximations are justified [104]. The autocorrelations

$$\Delta_i(\tau) = \langle \delta h_i(t) \delta h_i(t+\tau) \rangle \tag{32}$$

can be solved self-consistently [11]. In the limit of large g, expanding the self-consistency equation near $t = 0$ yields

$$\Delta(\tau) = g \cdot \Delta_0 + g \cdot (\Delta_0 - 1) \frac{t^2}{2} + \dots \tag{33}$$

with $\Delta_0 = 2(1 - 2/\pi)$ [11]. Close to the chaotic instability $g \to 1^+$, the autocorrelations are approximately [11]

$$\Delta(\tau) \approxeq \frac{g^2-1}{2} \operatorname{sech}\left(\frac{t\cdot(g^2-1)}{2\sqrt{3}}\right). \tag{34}$$

As h_i follows a Gaussian distribution $h \sim \mathcal{N}(0, \Delta_0)$, we can calculate the distribution of the off-diagonal entries y of the Jacobians analytically:

$$p(y) = \int dh\ \delta(y - \operatorname{sech}^2(h)) \frac{e^{-\frac{h^2}{2\Delta_0}}}{\sqrt{2\pi\Delta_0}} = \frac{\exp\left(-\frac{\ln\left(1/y \pm \sqrt{1/y-1}\right)}{2\Delta_0}\right)}{\sqrt{2\pi\Delta_0^2}|2y\sqrt{1-y}|} \tag{35}$$

We can thus write the Jacobian as

$$D_{ij}(t_s) = (1 - \Delta t)\delta_{ij} + \Delta t \cdot J_{ij} y_j. \tag{36}$$

where y_i are drawn from $p(y)$. But how can we deal with correlations between subsequent Jacobians? Firstly, we note that the autocorrelations of the Jacobians become arbitrary short in the limit of large g, although the autocorrelations of the activity variables h approach Eq. (33). For large g, the model behaves like the fully asymmetric Ising spin glas model [105]. Substituting $\Delta(t) = \Delta_0 \exp(-t/\tau_h)$ into the self-consistency equation and taking the large t limit yield a relaxation of the autocorrelation of $\tau_h^{-1} = \sqrt{1 - 2/\pi}$ [11]. Thus, the autocorrelation of D_{ij} relax approximately like $\tau_D \sim \frac{1}{g}$. We numerically confirmed that for large g the Jacobians approximately commute and the Lyapunov spectrum obtained after shuffling the sequence of Jacobians is almost the same. Thus, the long-term Jacobian can be approximated by a product of random matrices of the form of Eq. (36).

In the continuous-time limit $g \to 1^+$, the timescale of the autocorrelations of h_i diverges with $\tau_h = (g^2 - 1)/(2\sqrt{3})$ [11]. Because $\lim_{g\to 1^+} \Delta_0 = g - 1$, the autocorrelations of D_{ij} diverge with the same time constant $\tau_D = (g^2 - 1)/(2\sqrt{3})$. Numerical simulations also showed that in the limit $g \to 1^+$ the Jacobian approximately commute and the Lyapunov spectrum obtained after shuffling the sequence of Jacobians is almost the same. Thus, the Lyapunov spectrum is given by the logarithms of the eigenvalues of a product of almost identical random matrices, which follows the celebrated Wigner semicircle distribution [104, 106].

In the discrete-time limit $g \to 1^+$ and $\Delta t = 1$ subsequent Jacobians are close to uncorrelated. The Lyapunov spectrum can thus be obtained from a product of uncorrelated Gaussian matrices, whose eigenvalue distribution follow a triangle law [68, 69]. The full Lyapunov spectrum in this limit can thus be approximated by

$$\lambda_i = \log\left(\exp(\lambda_1)\cdot\sqrt{1-\frac{i}{N}}\right) = \lambda_1 + \frac{1}{2}\log\left(1-\frac{i}{N}\right) \tag{37}$$

where the largest Lyapunov exponent λ_1 can be obtained analytically as described earlier both in the discrete and continuous-time case with constant input and frozen white noise drive [11, 12, 17, 20].

Supporting Information

S1 Code Source code for Lyapunov spectrum of rate networks. We provide all necessary code to calculate the full Lyapunov spectrum with code written in Julia [107]. The efficient implementation is parallelized using level-3 matrix-matrix operations from BLAS (Basic Linear Algebra Subprograms) called via LAPACK (Linear Algebra PACKage). The code also provides an alternative estimate of the largest Lyapunov exponents by tracking the evolution of a small but finite initial perturbation and resizing it iteratively [40]. Furthermore, the program provides bootstrapped 95 percentile confidence intervals for the first and the last Lyapunov exponent, the Kolmogorov-Sinai entropy rate and the Lyapunov dimensionality. Optionally, also a principal component-based dimensionality estimate can be calculated. Finally, the program provides the convergence of the Lyapunov spectrum in time. Input variables are network size N, coupling strength g, time discretization Δt, simulation time t_{sim}, number of Lyapunov exponents to be calculate nLE, orthonormalization time interval t_{ONS}, seed for initial conditions $seed_{IC}$, seed for random network topology $seed_{Topo}$, seed for orthonormal system $seed_{ONS}$ and finally the subdirectory where the results are stored. Code written in MATLAB®/Octave is available upon request.

S2 Code Source code for Lyapunov spectrum of noise-driven rate networks. Similar to S1 Code, the full Lyapunov spectrum of a noise driven rate network is obtained by a reorthonormalization procedure [47], which is done along a numerical solution of the stochastic differential equation obtained with the Euler-Maruyama method [101]. The noise strength σ is now an additional input parameter. Code written in MATLAB®/Octave is available upon request.

Acknowledgments

We thank A. Crisanti, S. Goedeke, J. Kadmon, G. Lajoie, J. Liedtke, U. Parlitz, M. Schottdorf, M. Stern, H. Sompolinsky and M. Timme for fruitful discussions.

References

1. Arieli A, Sterkin A, Grinvald A, Aertsen A. Dynamics of Ongoing Activity: Explanation of the Large Variability in Evoked Cortical Responses. Science. 1996;273(5283):1868–1871. doi:10.1126/science.273.5283.1868.
2. Goris RLT, Movshon JA, Simoncelli EP. Partitioning neuronal variability. Nature Neuroscience. 2014;17(6):858–865. doi:10.1038/nn.3711.
3. Murray JD, Bernacchia A, Freedman DJ, Romo R, Wallis JD, Cai X, et al. A hierarchy of intrinsic timescales across primate cortex. Nat Neurosci. 2014;17(12):1661–1663.
4. Ecker AS, Berens P, Keliris GA, Bethge M, Logothetis NK, Tolias AS. Decorrelated Neuronal Firing in Cortical Microcircuits. Science. 2010;327(5965):584–587. doi:10.1126/science.1179867.
5. Renart A, Rocha Jdl, Bartho P, Hollender L, Parga N, Reyes A, et al. The Asynchronous State in Cortical Circuits. Science. 2010;327(5965):587–590. doi:10.1126/science.1179850.
6. Ecker A, Berens P, Cotton RJ, Subramaniyan M, Denfield G, Cadwell C, et al. State Dependence of Noise Correlations in Macaque Primary Visual Cortex. Neuron. 2014;82(1):235–248. doi:10.1016/j.neuron.2014.02.006.
7. Houweling AR, Brecht M. Behavioural report of single neuron stimulation in somatosensory cortex. Nature. 2008;451(7174):65–68. doi:10.1038/nature06447.
8. Doron G, von Heimendahl M, Schlattmann P, Houweling A, Brecht M. Spiking Irregularity and Frequency Modulate the Behavioral Report of Single-Neuron Stimulation. Neuron. 2014;81(3):653–663. doi:10.1016/j.neuron.2013.11.032.
9. Doron G, Brecht M. What single-cell stimulation has told us about neural coding. Phil Trans R Soc B. 2015;370(1677):20140204. doi:10.1098/rstb.2014.0204.
10. London M, Roth A, Beeren L, Häusser M, Latham PE. Sensitivity to perturbations in vivo implies high noise and suggests rate coding in cortex. Nature. 2010;466(7302):123–127. doi:10.1038/nature09086.
11. Sompolinsky H, Crisanti A, Sommers HJ. Chaos in Random Neural Networks. Physical Review Letters. 1988;61(3):259–262. doi:10.1103/PhysRevLett.61.259.
12. Kadmon J, Sompolinsky H. Transition to Chaos in Random Neuronal Networks. Physical Review X. 2015;5(4):041030. doi:10.1103/PhysRevX.5.041030.
13. Aljadeff J, Stern M, Sharpee T. Transition to Chaos in Random Networks with Cell-Type-Specific Connectivity. Physical Review Letters. 2015;114(8):088101. doi:10.1103/PhysRevLett.114.088101.
14. Stern M, Sompolinsky H, Abbott LF. Dynamics of random neural networks with bistable units. Physical Review E. 2014;90(6):062710. doi:10.1103/PhysRevE.90.062710.
15. Harish O, Hansel D. Asynchronous Rate Chaos in Spiking Neuronal Circuits. PLoS Comput Biol. 2015;11(7):e1004266. doi:10.1371/journal.pcbi.1004266.

16. Harish O. Network mechanisms of working memory : from persistent dynamics to chaos. Paris 5; 2013.

17. Molgedey L, Schuchhardt J, Schuster H. Suppressing chaos in neural networks by noise. Physical Review Letters. 1992;69(26):3717–3719. doi:10.1103/PhysRevLett.69.3717.

18. Rajan K, Abbott L, Sompolinsky H. Inferring Stimulus Selectivity from the Spatial Structure of Neural Network Dynamics. In: Lafferty JD, Williams CKI, Shawe-Taylor J, Zemel RS, Culotta A, editors. Advances in Neural Information Processing Systems 23. Curran Associates, Inc.; 2010. p. 1975–1983.

19. Rajan K, Abbott LF, Sompolinsky H. Stimulus-dependent suppression of chaos in recurrent neural networks. Physical Review E. 2010;82(1):011903. doi:10.1103/PhysRevE.82.011903.

20. Goedeke S, Schuecker J, Helias M. Noise dynamically suppresses chaos in neural networks. arXiv:160301880 [nlin, q-bio]. 2016;.

21. Shriki O, Hansel D, Sompolinsky H. Rate Models for Conductance-Based Cortical Neuronal Networks. Neural Computation. 2003;15(8):1809–1841. doi:10.1162/08997660360675053.

22. Maass W, Natschläger T, Markram H. Real-Time Computing Without Stable States: A New Framework for Neural Computation Based on Perturbations. Neural Computation. 2002;14(11):2531–2560. doi:10.1162/089976602760407955.

23. Jaeger H, Haas H. Harnessing Nonlinearity: Predicting Chaotic Systems and Saving Energy in Wireless Communication. Science. 2004;304(5667):78–80. doi:10.1126/science.1091277.

24. Sussillo D, Abbott LF. Generating Coherent Patterns of Activity from Chaotic Neural Networks. Neuron. 2009;63(4):544–557. doi:10.1016/j.neuron.2009.07.018.

25. Laje R, Buonomano DV. Robust timing and motor patterns by taming chaos in recurrent neural networks. Nature Neuroscience. 2013;16(7):925–933. doi:10.1038/nn.3405.

26. Abbott LF, DePasquale B, Memmesheimer RM. Building functional networks of spiking model neurons. Nature Neuroscience. 2016;19(3):350–355. doi:10.1038/nn.4241.

27. DePasquale B, Churchland MM, Abbott LF. Using Firing-Rate Dynamics to Train Recurrent Networks of Spiking Model Neurons. arXiv:160107620 [q-bio]. 2016;.

28. Thalmeier D, Uhlmann M, Kappen HJ, Memmesheimer RM. Learning Universal Computations with Spikes. PLOS Comput Biol. 2016;12(6):e1004895. doi:10.1371/journal.pcbi.1004895.

29. Nicola W, Clopath C. Supervised learning in spiking neural networks with FORCE training. Nature Communications. 2017;8(1):2208. doi:10.1038/s41467-017-01827-3.

30. Bertschinger N, Natschläger T. Real-Time Computation at the Edge of Chaos in Recurrent Neural Networks. Neural Computation. 2004;16(7):1413–1436. doi:10.1162/089976604323057443.

31. Schweighofer N, Doya K, Fukai H, Chiron JV, Furukawa T, Kawato M. Chaos may enhance information transmission in the inferior olive. Proceedings of the National Academy of Sciences of the United States of America. 2004;101(13):4655–4660. doi:10.1073/pnas.0305966101.

32. Legenstein R, Maass W. Edge of chaos and prediction of computational performance for neural circuit models. Neural Networks. 2007;20(3):323–334. doi:10.1016/j.neunet.2007.04.017.

33. Büsing L, Schrauwen B, Legenstein R. Connectivity, Dynamics, and Memory in Reservoir Computing with Binary and Analog Neurons. Neural Computation. 2009;22(5):1272–1311. doi:10.1162/neco.2009.01-09-947.

34. Toyoizumi T, Abbott LF. Beyond the edge of chaos: Amplification and temporal integration by recurrent networks in the chaotic regime. Physical Review E. 2011;84(5):051908. doi:10.1103/PhysRevE.84.051908.

35. Saxe AM, McClelland JL, Ganguli S. Exact solutions to the nonlinear dynamics of learning in deep linear neural networks. arXiv:13126120 [cond-mat, q-bio, stat]. 2013;.

36. Raghu M, Poole B, Kleinberg J, Ganguli S, Sohl-Dickstein J. On the Expressive Power of Deep Neural Networks. In: PMLR; 2017. p. 2847–2854. Available from: `http://proceedings.mlr.press/v70/raghu17a.html`.

37. Vulpiani A, Cecconi F, Cencini M. Chaos: From Simple Models to Complex Systems. Hackensack, NJ: World Scientific Pub Co Inc; 2009.

38. Shaw R. Strange Attractors, Chaotic Behavior, and Information Flow. Zeitschrift Naturforschung Teil A. 1981;36:80–112. doi:10.1515/zna-1981-0115.

39. Young LS. Mathematical theory of Lyapunov exponents. Journal of Physics A: Mathematical and Theoretical. 2013;46(25):254001. doi:10.1088/1751-8113/46/25/254001.

40. Eckmann JP, Ruelle D. Ergodic theory of chaos and strange attractors. Reviews of Modern Physics. 1985;57(3):617–656. doi:10.1103/RevModPhys.57.617.

41. Grassberger P, Procaccia I. Characterization of Strange Attractors. Physical Review Letters. 1983;50(5):346–349. doi:10.1103/PhysRevLett.50.346.

42. Grassberger P, Procaccia I. Estimation of the Kolmogorov entropy from a chaotic signal. Physical Review A. 1983;28(4):2591–2593. doi:10.1103/PhysRevA.28.2591.

43. Grassberger P. Generalized dimensions of strange attractors. Physics Letters A. 1983;97(6):227–230. doi:10.1016/0375-9601(83)90753-3.

44. Eckmann JP, Ruelle D. Fundamental limitations for estimating dimensions and Lyapunov exponents in dynamical systems. Physica D: Nonlinear Phenomena. 1992;56(2):185–187. doi:10.1016/0167-2789(92)90023-G.

45. Smith LA. Intrinsic limits on dimension calculations. Physics Letters A. 1988;133(6):283–288. doi:10.1016/0375-9601(88)90445-8.

46. Lajoie G, Lin KK, Shea-Brown E. Chaos and reliability in balanced spiking networks with temporal drive. Physical Review E. 2013;87(5):052901. doi:10.1103/PhysRevE.87.052901.

47. Benettin G, Galgani L, Giorgilli A, Strelcyn JM. Lyapunov Characteristic Exponents for smooth dynamical systems and for hamiltonian systems; A method for computing all of them. Part 2: Numerical application. Meccanica. 1980;15(1):21–30. doi:10.1007/BF02128237.

48. Ruelle D. An inequality for the entropy of differentiable maps. Bol Soc Bras de Mat. 1978;.

49. Ledrappier F, Young LS. The Metric Entropy of Diffeomorphisms: Part II: Relations between Entropy, Exponents and Dimension. Annals of Mathematics. 1985;122(3):540–574. doi:10.2307/1971329.

50. Ledrappier F, Young LS. Entropy formula for random transformations. Probability Theory and Related Fields. 1988;80(2):217–240. doi:10.1007/BF00356103.

51. Young LS. What Are SRB Measures, and Which Dynamical Systems Have Them? Journal of Statistical Physics. 2002;5-6(108):733–754. doi:10.1023/A:1019762724717.

52. Kaplan JL, Yorke JA. Preturbulence: A regime observed in a fluid flow model of Lorenz. Communications in Mathematical Physics. 1979;67:93–108. doi:10.1007/BF01221359.

53. Frederickson P, Kaplan JL, Yorke ED, Yorke JA. The Liapunov dimension of strange attractors. Journal of differential equations. 1983;49(2):185–207.

54. Alexander JC, Yorke JA. Fat baker's transformations. Ergodic Theory and Dynamical Systems. 1984;4(1):1–23. doi:10.1017/S0143385700002236.

55. Gao P, Ganguli S. On simplicity and complexity in the brave new world of large-scale neuroscience. Current Opinion in Neurobiology. 2015;32:148–155. doi:10.1016/j.conb.2015.04.003.

56. Cunningham JP, Yu BM. Dimensionality reduction for large-scale neural recordings. Nature Neuroscience. 2014;17(11):1500–1509. doi:10.1038/nn.3776.

57. Ruelle D. Large volume limit of the distribution of characteristic exponents in turbulence. Communications in Mathematical Physics. 1982;87(2):287–302. doi:10.1007/BF01218566.

58. Takeuchi KA, Ginelli F, Chaté H. Lyapunov Analysis Captures the Collective Dynamics of Large Chaotic Systems. Physical Review Letters. 2009;103(15):154103. doi:10.1103/PhysRevLett.103.154103.

59. Rajan K. Eigenvalue Spectra of Random Matrices for Neural Networks. Physical Review Letters. 2006;97(18). doi:10.1103/PhysRevLett.97.188104.

60. Massar M, Massar S. Mean-field theory of echo state networks. Physical Review E. 2013;87(4):042809. doi:10.1103/PhysRevE.87.042809.

61. Lin KK. Stimulus-Response Reliability of Biological Networks. In: Kloeden PE, Pötzsche C, editors. Nonautonomous Dynamical Systems in the Life Sciences. No. 2102 in Lecture Notes in Mathematics. Springer International Publishing; 2013. p. 135–161. Available from: http://link.springer.com/chapter/10.1007/978-3-319-03080-7_4.

62. Kifer Y. Ergodic Theory of Random Transformations. Springer Science & Business Media; 2012.

63. Baxendale PH. Stability and Equilibrium Properties of Stochastic Flows of Diffeomorphisms. In: Pinsky MA, Wihstutz V, editors. Diffusion Processes and Related Problems in Analysis, Volume II. No. 27 in Progress in Probability. Birkhäuser Boston; 1992. p. 3–35. Available from: http://link.springer.com/chapter/10.1007/978-1-4612-0389-6_1.

64. Le Jan Y. Equilibre statistique pour les produits de difféomorphismes aléatoires indépendants. Annales de l'IHP Probabilités et statistiques. 1987;23(1):111–120.

65. Amari SI. Learning Patterns and Pattern Sequences by Self-Organizing Nets of Threshold Elements. IEEE Transactions on Computers. 1972;C-21(11):1197–1206. doi:10.1109/T-C.1972.223477.

66. Parisi G. Asymmetric neural networks and the process of learning. Journal of Physics A: Mathematical and General. 1986;19(11):L675. doi:10.1088/0305-4470/19/11/005.

67. Doyon B, Cessac B, Quoy M, Samuelides M. Control of the transition to chaos in neural networks with random connectivity. International Journal of Bifurcation and Chaos. 1993;03(02):279–291. doi:10.1142/S0218127493000222.

68. Newman CM. The distribution of Lyapanov exponents: exact results for random matrices. Communications in mathematical physics. 1986;103(1):121–126.

69. Isopi M, Newman CM. The triangle law for Lyapunov exponents of large random matrices. Communications in mathematical physics. 1992;143(3):591–598.

70. Dressler U. Symmetry property of the Lyapunov spectra of a class of dissipative dynamical systems with viscous damping. Physical Review A. 1988;38(4):2103–2109. doi:10.1103/PhysRevA.38.2103.

71. Wojtkowski MP, Liverani C. Conformally Symplectic Dynamics and Symmetry of the Lyapunov Spectrum. Communications in Mathematical Physics. 1998;194(1):47–60. doi:10.1007/s002200050347.

72. Ostojic S. Two types of asynchronous activity in networks of excitatory and inhibitory spiking neurons. Nature Neuroscience. 2014;17(4):594–600. doi:10.1038/nn.3658.

73. Wainrib G, Touboul J. Topological and Dynamical Complexity of Random Neural Networks. Physical Review Letters. 2013;110(11):118101. doi:10.1103/PhysRevLett.110.118101.

74. Mastrogiuseppe F, Ostojic S. Intrinsically-generated fluctuating activity in excitatory-inhibitory networks. PLOS Computational Biology. 2017;13(4):e1005498. doi:10.1371/journal.pcbi.1005498.

75. García del Molino LC, Pakdaman K, Touboul J, Wainrib G. Synchronization in random balanced networks. Physical Review E. 2013;88(4):042824. doi:10.1103/PhysRevE.88.042824.

76. Cabana T, Touboul J. Large Deviations, Dynamics and Phase Transitions in Large Stochastic and Disordered Neural Networks. Journal of Statistical Physics. 2013;153(2):211–269. doi:10.1007/s10955-013-0818-5.

77. Ganguli S, Sompolinsky H. Compressed Sensing, Sparsity, and Dimensionality in Neuronal Information Processing and Data Analysis. Annual Review of Neuroscience. 2012;35(1):485–508. doi:10.1146/annurev-neuro-062111-150410.

78. Kuznetsov NV, Alexeeva TA, Leonov GA. Invariance of Lyapunov exponents and Lyapunov dimension for regular and irregular linearizations. Nonlinear Dynamics. 2016;85(1):195–201. doi:10.1007/s11071-016-2678-4.

79. Monasson R, Villamaina D. Estimating the principal components of correlation matrices from all their empirical eigenvectors. EPL (Europhysics Letters). 2015;112(5):50001. doi:10.1209/0295-5075/112/50001.

80. Rivkind A, Barak O. Local Dynamics in Trained Recurrent Neural Networks. Physical Review Letters. 2017;118(25):258101. doi:10.1103/PhysRevLett.118.258101.

81. Barak O, Sussillo D, Romo R, Tsodyks M, Abbott LF. From fixed points to chaos: Three models of delayed discrimination. Progress in Neurobiology. 2013;103:214–222.

82. Jaeger H. The "echo state" approach to analysing and training recurrent neural networks-with an erratum note. Bonn, Germany: German National Research Center for Information Technology GMD Technical Report. 2001;148:34.

83. Buehner M, Young P. A tighter bound for the echo state property. IEEE transactions on neural networks. 2006;17(3):820–824. doi:10.1109/TNN.2006.872357.

84. Jaeger H. Echo state network. Scholarpedia. 2007;2(9):2330. doi:10.4249/scholarpedia.2330.

85. Manjunath G, Jaeger H. Echo State Property Linked to an Input: Exploring a Fundamental Characteristic of Recurrent Neural Networks. Neural Computation. 2012;25(3):671–696.

86. Sommers HJ, Crisanti A, Sompolinsky H, Stein Y. Spectrum of Large Random Asymmetric Matrices. Physical Review Letters. 1988;60(19):1895–1898. doi:10.1103/PhysRevLett.60.1895.

87. Zhao L, II BB, Netoff T, Nykamp DQ. Synchronization from second order network connectivity statistics. Frontiers in Computational Neuroscience. 2011;5:28. doi:10.3389/fncom.2011.00028.

88. van Vreeswijk C, Sompolinsky H. Chaos in Neuronal Networks with Balanced Excitatory and Inhibitory Activity. Science. 1996;274(5293):1724 –1726. doi:10.1126/science.274.5293.1724.

89. van Vreeswijk C, Sompolinsky H. Chaotic Balanced State in a Model of Cortical Circuits. Neural Computation. 1998;10(6):1321–1371. doi:10.1162/089976698300017214.

90. Brunel N. Dynamics of Sparsely Connected Networks of Excitatory and Inhibitory Spiking Neurons. Journal of Computational Neuroscience. 2000;8(3):183–208. doi:10.1023/A:1008925309027.

91. Monteforte M, Wolf F. Dynamical Entropy Production in Spiking Neuron Networks in the Balanced State. Physical Review Letters. 2010;105(26):268104. doi:10.1103/PhysRevLett.105.268104.

92. Engelken R, Farkhooi F, Hansel D, van Vreeswijk C, Wolf F. A reanalysis of "Two types of asynchronous activity in networks of excitatory and inhibitory spiking neurons". F1000Research. 2016;5:2043. doi:10.12688/f1000research.9144.1.

93. Lajoie G, Thivierge JP, Shea-Brown E. Structured chaos shapes spike-response noise entropy in balanced neural networks. Frontiers in Computational Neuroscience. 2014;8:123. doi:10.3389/fncom.2014.00123.

94. Engelken R, Monteforte M, Wolf F. Input spike trains suppress chaos in balanced neural circuits; 2015.

95. Engelken R, Wolf F. Controlling chaos in balanced neural circuits with input spike trains; 2016.

96. Sussillo D, Barak O. Opening the Black Box: Low-Dimensional Dynamics in High-Dimensional Recurrent Neural Networks. Neural Computation. 2012;25(3):626–649.

97. Ginelli F, Poggi P, Turchi A, Chaté H, Livi R, Politi A. Characterizing Dynamics with Covariant Lyapunov Vectors. Physical Review Letters. 2007;99(13):130601. doi:10.1103/PhysRevLett.99.130601.

98. Kuptsov PV, Parlitz U. Theory and Computation of Covariant Lyapunov Vectors. Journal of Nonlinear Science. 2012;22(5):727–762. doi:10.1007/s00332-012-9126-5.

99. Wolfe CL, Samelson RM. An efficient method for recovering Lyapunov vectors from singular vectors. Tellus A. 2007;59(3):355–366. doi:10.1111/j.1600-0870.2007.00234.x.

100. Geist K, Parlitz U, Lauterborn W. Comparison of Different Methods for Computing Lyapunov Exponents. Progress of Theoretical Physics. 1990;83(5):875–893. doi:10.1143/PTP.83.875.

101. Kloeden PE, Platen E. Numerical Solution of Stochastic Differential Equations. Corrected edition ed. Berlin ; New York: Springer; 1992.

102. Bell RJ, Dean P. Atomic vibrations in vitreous silica. 1970;50(0):55–61. doi:10.1039/DF9705000055.

103. Bauer J, Chang TM, Skinner JL. Correlation length and inverse-participation-ratio exponents and multifractal structure for Anderson localization. Physical Review B. 1990;42(13):8121–8124. doi:10.1103/PhysRevB.42.8121.

104. Crisanti A. Products of Random Matrices: in Statistical Physics. Softcover reprint of the original 1st ed. 1993 ed. Berlin; New York: Springer-Verlag; 1993.

105. Crisanti A, Sompolinsky H. Dynamics of spin systems with randomly asymmetric bonds: Ising spins and Glauber dynamics. Physical Review A. 1988;37(12):4865–4874. doi:10.1103/PhysRevA.37.4865.

106. Götze F, Tikhomirov A. On the Asymptotic Spectrum of Products of Independent Random Matrices. arXiv:10122710 [math]. 2010;.

107. Bezanson J, Edelman A, Karpinski S, Shah V. Julia: A Fresh Approach to Numerical Computing. SIAM Review. 2017;59(1):65–98. doi:10.1137/141000671.

8 Dynamical models of cortical circuits

8.1 Summary

Cortical neurons operate within recurrent neuronal circuits. Dissecting their operation is key to understanding information processing in the cortex and requires transparent and adequate dynamical models of circuit function. Convergent evidence from experimental and theoretical studies indicates that strong feedback inhibition shapes the operating regime of cortical circuits. For circuits operating in inhibition-dominated regimes, mathematical and computational studies over the past several years achieved substantial advances in understanding response modulation and heterogeneity, emergent stimulus selectivity, inter-neuron correlations, and microstate dynamics. The latter indicate a surprisingly strong dependence of the collective circuit dynamics on the features of single neuron action potential generation. New approaches are needed to definitely characterize the cortical operating regime.

Citation

Fred Wolf, Rainer Engelken, Maximilian Puelma-Touzel, Juan Daniel Flórez Weidinger, and Andreas Neef. **"Dynamical Models of Cortical Circuits."** Current Opinion in Neurobiology 25 (April 2014): 228–36.

Original Contribution

RE prepared all figures. FW prepared an initial draft of the manuscript. All authors participated in manuscript writing. Simulations were performed by RE.

Available online at www.sciencedirect.com

ScienceDirect

Current Opinion in Neurobiology

Dynamical models of cortical circuits

Fred Wolf[1,2,3,4], Rainer Engelken[1,2,3,4], Maximilian Puelma-Touzel[1,2,3,4], Juan Daniel Flórez Weidinger[1,2,3,4] and Andreas Neef[1,2,3,4]

Cortical neurons operate within recurrent neuronal circuits. Dissecting their operation is key to understanding information processing in the cortex and requires transparent and adequate dynamical models of circuit function. Convergent evidence from experimental and theoretical studies indicates that strong feedback inhibition shapes the operating regime of cortical circuits. For circuits operating in inhibition-dominated regimes, mathematical and computational studies over the past several years achieved substantial advances in understanding response modulation and heterogeneity, emergent stimulus selectivity, inter-neuron correlations, and microstate dynamics. The latter indicate a surprisingly strong dependence of the collective circuit dynamics on the features of single neuron action potential generation. New approaches are needed to definitely characterize the cortical operating regime.

Addresses
[1] Max Planck Institute for Dynamics and Self-Organization, Göttingen, Germany
[2] Bernstein Center for Computational Neuroscience, Göttingen, Germany
[3] Bernstein Focus Neurotechnology, Göttingen, Germany
[4] Faculty of Physics, Göttingen University, Göttingen, Germany

Corresponding author: Wolf, Fred (fred@nld.ds.mpg.de)

Current Opinion in Neurobiology 2014, **25**:228–236

This review comes from a themed issue on **Theoretical and computational neuroscience**

Edited by **Adrienne Fairhall** and **Haim Sompolinsky**

For a complete overview see the Issue and the Editorial

Available online 20th March 2014

0959-4388

http://dx.doi.org/10.1016/j.conb.2014.01.017

Introduction

Cortical circuits are built of two main neuron classes — excitatory and inhibitory — that comprise about 80% and 20% of nerve cells respectively. An intricate network of synaptic connections links neurons within and across cortical layers. Long-ranging inputs drive and modulate activity in the local circuit, including afferent drive by specific thalamic nuclei and modulation by remote cortical cells [1,2]. Recurrent excitation in cortical circuits is believed to underlie the amplification of specific input patterns and the generation of persistent activity. In view of the large recurrently connected excitatory cell population, feedback inhibition appears indispensable for stabilizing recurrent cortical circuits. Recent functional and anatomical studies demonstrated that inhibitory connections in the local cortical circuit appear in general strong (see e.g. Ref. [3]) and dense [4–6]. This suggests that the inhibitory population as a whole can provide a dense 'blanket of inhibition' as a prerequisite for the utilization of recurrent excitation [7]. Over the past several years dynamical models of cortical circuits started to reveal unanticipated and counterintuitive roles of dominant feedback inhibition.

As any mathematically formalized model, models of cortical circuits have to strike a balance between idealization and detail. Current experimental approaches harnessing the ongoing progress in optophysiology, genetics and connectomics are beginning to picture cortical circuits in unprecedented detail. Substantial efforts in theoretical neuroscience are dedicated to laying the foundations for integrating and dissecting the emerging wealth of data. No amount of detail, however, can be expected to offset the need for idealization. Idealization — even counterfactual idealization, that is the neglect of known features — is required whenever the essential ingredients of a phenomenon need to be identified or when a qualitatively novel type of behavior demands conceptual advancement. For such challenges the ultimate aim is not realism but clarity, mathematical control, and the transparent penetration of complex phenomena. Recent work on the operating point of cortical circuits provides intriguing examples of paradoxical effects such as the suppression of activity by withdrawal of inhibition and excitation [8] or the emergence of response selectivity in random networks [9••]. The emerging understanding of such counterintuitive aspects of cortical operation promises to guide cortical circuit models to a mature balance of idealization and detail.

Balanced circuits, inhibition-stabilized networks (ISNs) and paradoxical responses

Dominant feedback inhibition plays a central role in virtually every dynamical model of cortical operation. Prime examples are models exhibiting *balanced states*, in which strong feed forward and recurrent excitation are balanced by equally strong recurrent and feedback

Figure 1

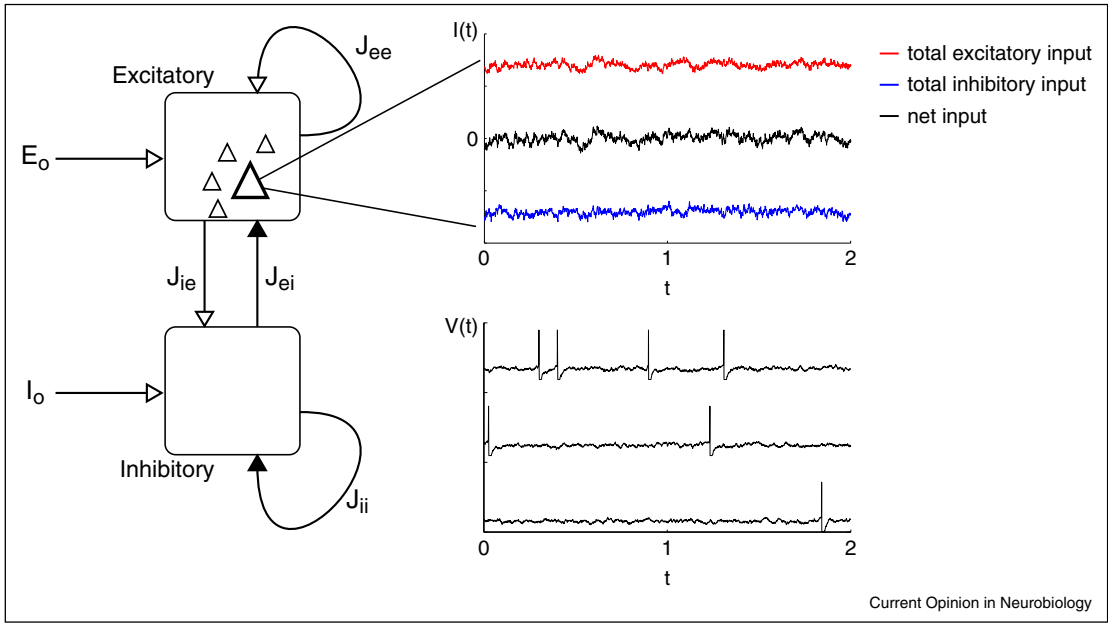

Balanced states robustly emerge in local circuits of inhibitory and excitatory neurons. Neurons in balanced networks are driven by residual input fluctuations that result from the near cancelation of excitatory and inhibitory inputs (upper right). The balance of excitatory and inhibitory inputs is a collective phenomenon and emerges from the recurrent interactions in the network. Balanced states were first found in sparse randomly connected networks. Recent work demonstrated the emergence of balanced states also in structured and more densely connected circuits and revealed that they actively suppress the occurrence of correlated activity. Cells in balanced networks robustly exhibit irregular and asynchronous activity patterns (lower left).

inhibition [10,11] (Fig. 1). Under such conditions spiking is driven by residual temporal fluctuations of net synaptic input and as a result is temporally irregular and only weakly correlated between cells. A related class of models are ISNs [8,12] (Fig. 2). ISNs are defined by recurrent excitation being so strong that runaway excitation cannot be prevented by any fixed amount of inhibition and stabilization can only be achieved if the activity of the inhibitory neuron population dynamically tracks every fluctuation in excitatory population activity. Balanced networks are in general ISNs but not all ISNs generate balanced states, strong input fluctuations and irregular asynchronous firing patterns. Above a threshold strength of recurrent excitation and inhibition, ISNs predict a paradoxical response to an additional external drive impinging on the inhibitory population (Fig. 2). One may naively expect that such a drive increases inhibition and reduces activity in the excitatory population by disynaptic inhibition. In a strongly coupled ISN, however, both activity levels drop leading to an effective 'withdrawal' of excitation and a paradoxical reduction of the level of feedback inhibition. Ozeki *et al.* recently found that this paradoxical response apparently underlies the phenomenon of surround suppression in cat V1 [8]. As the suppression of activity by a simultaneous reduction of excitation and inhibition in the local circuit seems hard to explain in any other way, this phenomenon represents an intriguing piece of evidence for an inhibition stabilized operating regime in which excitation and inhibition are strong and dynamically matched. While feedback inhibition also appears strong in rodent sensory cortex, a recent study reported evidence for the simpler scenario of increased inhibition as the basis of surround suppression in mouse visual cortex [13]. Furthermore optogenetic activation of interneurons in mouse visual cortex can generate a wide variety of effects but so far has not provided evidence for paradoxical responses [14,15]. Further work is needed to clarify the phenomenology and determine whether similar or distinct mechanisms mediate surround suppression in rodent, carnivore and primate visual cortex.

Independent lines of experimental and theoretical evidence further support a cortical operating regime of strong feedback inhibition and recurrent excitation. Experimentally, London *et al.* found that inducing an additional spike in a single excitatory neuron in rodent barrel cortex can trigger a substantial rate response in the local circuit that indicates an intrinsically unstable level of recurrent excitation [16]. Intracellular studies of layer IV neurons in mouse visual and auditory cortex provide direct evidence for the recruitment of strong, amplifying

Figure 2

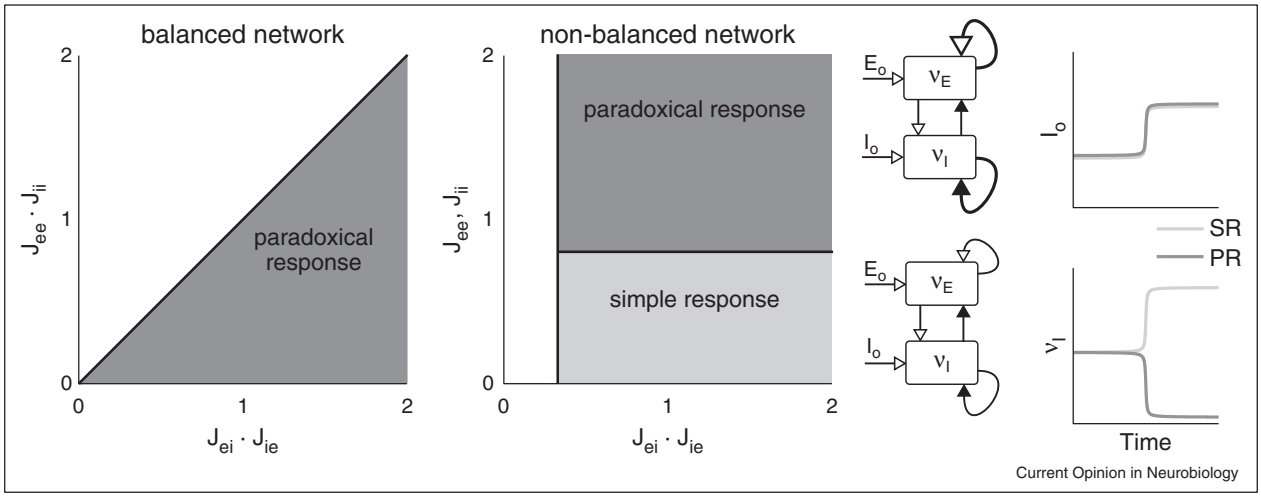

Inhibition-stabilized networks (ISNs) predict paradoxical responses beyond a threshold level of recurrent interactions. In ISNs recurrent excitation is so strong that runaway self-excitation can only be prevented if the inhibitory population tightly tracks fluctuations in the activity of the excitatory population. The schematic phase diagrams (left) indicates the occurrence of paradoxical responses in a section through the parameter space of a non-balanced and a balanced two population network, a special case of an ISN. The balanced network phase diagram also illustrates that parameter tuning is not required because balanced activity emerges from the network dynamics for an entire volume (grey) of parameter space. For strong recurrent interactions both the activity of the excitatory and the inhibitory population drop when the inhibitory population is subjected to an increased external drive (right, SR simple response, PR paradoxical response).

recurrent excitation [17–19] (discussed in Ref. [20]). In addition, theoretical studies that constructed comprehensive models for the contextual modulation of responses to grating stimuli in primate V1 ([21,22], see also Refs. [23,24]) are converging to a inhibition dominated local circuit structure. The same conclusion is supported by a study that tuned detailed recurrent circuit models to match the orientation tuning of subthreshold and spiking activity in pinwheel centers and orientation domains [25]. Finally, Persi *et al.* performed a comprehensive search for local circuit models that successfully reproduce contrast response functions in primate V1. They also conclude that cortical circuits without strong feedback inhibition are unable to match experimental observations [26].

Do visual cortical circuits operate in a balanced state?

In an attempt to extend the study of ISNs toward defining the operating regime of V1 circuits, Ahmadian *et al.* recently studied networks of model neurons with expansive nonlinear input–output relations [27•]. These networks, called stabilized supralinear networks (SSNs), exhibit supralinear responses for weak inputs and sublinear and non-monotonic responses for strong inputs (see also Ref. [26]). This crossover from supralinear to sublinear responses promises a novel theoretical account for a wide range of normalization phenomena found in V1 [28]. Classical models of cortical circuits in the balanced state are known to behave distinctly different. In these models, the condition of small average net input implies that the firing rates of the neuronal populations depend linearly on the external inputs. Ahmadian *et al.* therefore raised the question of whether the observed response non-linearity indicates that visual cortical networks are not operating in a balanced state. Two recent studies, however, show that response linearity is not a critical prediction of the balanced state [29••,30]. In these studies Mongillio, Hansel and coworkers for the first time presented a consistent treatment of balanced states in networks, in which synaptic inputs exhibit short-term plasticity such as synaptic depression and facilitation. Because of short-term plasticity the condition of small mean net input becomes nonlinear in the population firing rates and assumes a form that is similar to the equations that determine the firing rates in nonlinear rate models of the type used in [27•]. It is thus conceivable that a synaptic source of nonlinearity within a balanced network could result in similar normalization effects as predicted by a SSN. Further studies are needed to conclusively examine these alternative scenarios.

Feature selectivity and response heterogeneity in random circuits

Recently Hansel and van Vreesweijk showed that balanced states can lead to the emergence of sharp tuning for stimulus features even in randomly connected networks [9••]. They examined randomly wired networks of

Figure 3

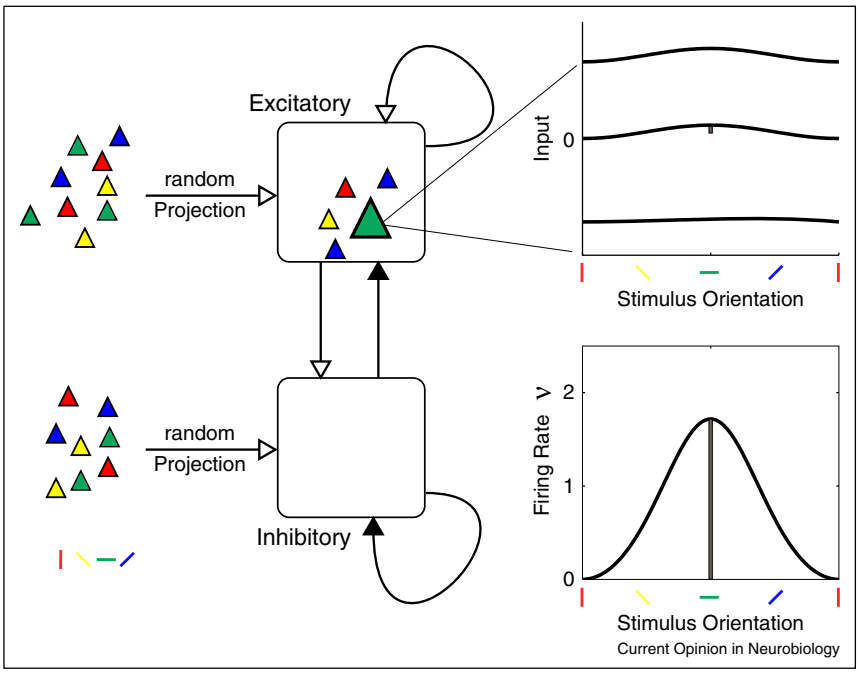

Randomly connected networks in the balanced state driven by a random projection from a population of orientation-tuned neurons can generate highly selective responses. The total excitatory input to each neuron in the network is only weakly tuned. The balance of mean excitation and inhibition emerging in the network, however, largely cancels the untuned mean input. As a result, the neurons input output function can generate highly selective orientation tuning.

neurons receiving weakly orientation tuned net input as a result of random wiring. The emergent balance in the network, however, cancels the mean input and adjusts the population activity such that output firing is tuned as sharply as observed in V1 (Fig. 3). This study constitutes an important contribution towards understanding the operation of rodent visual cortex. In all rodents examined so far orientation selective V1 neurons are not organized into an orientation map but are arranged in an interspersed layout (reviewed in Refs. [1,31] see also Ref. [32]). Locally neurons are preferentially but not exclusively connected to neurons of similar orientation preference and receive inputs from cells exhibiting the full complement of preferred orientations [33–35]. Thus mature mouse V1 can be viewed as composed of intermingled subcircuits that are partially but not completely segregated (reviewed in Ref. [1]). So mouse V1 is certainly not per se a random network. It remains, however, an open question whether or not the observed specificity contributes to response selectivity. Interestingly, mature-like oriented receptive fields are observed already at eye opening when the preferential connectivity is not yet established [36]. This is consistent with the finding of Hansel and van Vreeswijk that the specific connectivity is not a necessary prerequisite for the sharp orientation tuning. It is an important open question which neuronal operations are generated or enhanced by the selective excitatory connectivity in mouse visual cortex.

Balanced circuit models typically exhibit highly heterogeneous response properties that result from random variations in connectivity across neurons [10,11,37]. For instance, the balanced model for orientation tuning in rodent V1 [9••] exhibits substantial heterogeneity in orientation selectivity that is similar to the biologically observed heterogeneity in mouse visual cortex [38]. Balanced network models also robustly predict the most elementary kind of response heterogeneity: firing rate heterogeneity. Firing rate distributions have been examined in various cortical areas and appear to be generally broad and skewed toward low firing rates (reviewed in Ref. [39]). Roxin *et al.* recently presented a systematic analysis of firing rate distributions in balanced networks of neurons with expansive input–output relationships. Under a wide range of conditions these networks were found to robustly predict realistically broad firing rate distributions [40]. A slightly more complicated analysis can be performed to characterize the distribution of orientation selectivity in balanced

circuit models [37]. Such analyses will facilitate the quantitative comparison of balanced circuit predictions and population measurements. While the experimentally observed degree of response heterogeneity is consistent with generic predictions of balanced state models, biological response heterogeneity can in principle result from a wide range of sources. Dissecting the predicted response heterogeneity systematically should uncover more specific signatures of the distinct mechanisms.

Correlations and network structure

Correlations between the activities of different cortical neurons in a local circuit are on average relatively weak with correlation coefficients of 0.1 and below [41,42]. The classical models of balanced state networks are based on sparse random graphs in which the number of neurons in a population is much larger than the average number of synapses which is itself a large number. Numerical studies of balanced networks of spiking neurons, however, have for a long time indicated that a very sparse connectivity is not a strict requirement for the emergence of weakly correlated asynchronous states. Renart *et al.* recently extended the theoretical treatment of balanced networks to the case of dense connectivity, in which the number of connections per neuron scales proportional to the number of neurons in the population [43••]. They showed that even with dense connectivity correlations are weak and vanish in the large network limit. The basis for this robust suppression of interneuron correlations is the capability of the inhibitory and excitatory inputs to not only cancel on average but also to track each other dynamically, canceling a substantial fraction of common input fluctuations [43••,44]. This feature seems to be a general property of balanced circuit models but so far has been analytically derived only for idealized networks of binary neurons [43••].

Refined concepts for analyzing network generated patterns of correlations in spiking neuron networks have emerged over the past years. The transmission of input correlations into spike output correlations has been characterized for a diverse set of model neurons clarifying the dependence of correlation transmission on parameters of background input fluctuations, spike generation and synaptic characteristics [45–51]. Simple threshold neuron models apparently mimic correlation transmission in cortical neurons surprisingly well [48]. Using theses approaches recent studies have started to dissect self-consistent patterns of inter-neuron spike correlations in networks with random and structured connectivity [52–55]. These studies are building a coherent mathematical foundation for future analyses on how single neuron and synaptic dynamics together with the circuit's connectome shape the structure and strength of emergent correlations. Notably, they generally presuppose that the emergent states are statistically stationary. Litwin-Kumar and Doiron, however, discovered that introducing clustering motifs into balanced networks can lead to the emergence of slow firing rate fluctuations that deviate from a stationary process [56•]. It is thus an important open question how ubiquitous this phenomenon is and how structured or random a network needs to be to spontaneously generate slow rate fluctuations [72].

Chaotic dynamics, temporal-decorrelation and the bandwidth of neural population responses

Neuronal circuit models in the balanced state are nonlinear high dimensional dynamical systems. They are thus expected to evolve chaotically in time. The first balanced circuit models in fact exhibited an extremely strong form of chaotic dynamics in which trajectories starting from similar initial conditions diverged faster than exponential [11]. Recent analyses of balanced circuits of spiking neuron models have revealed that the strength and nature of deterministic chaos can qualitatively depend on the choice of single neuron model [57,58,59,60••,61••]. Balanced networks in which recurrent inhibition balances an external drive exhibit temporally irregular asynchronous spiking patterns. The generated sequences of spikes and subthreshold voltage fluctuations, however, can nevertheless be dynamically stable such that the network returns to a unique and invariant voltage trajectory and spike sequence after small perturbations [57,58,59,61••] (Fig. 4). This stable irregular spiking dynamics was first found in purely inhibitory networks of pulse-coupled leaky integrate-and-fire neurons (LIF), but appears to persist when synaptic currents decay sufficiently fast and when some amount of recurrent excitation is included [58,59]. By contrast, balanced networks of exactly the same structure but composed of units that explicitly model the process of spike initiation exhibit irregular asynchronous activity with chaotic dynamics such that perturbed trajectories exponentially separate [60••,62]. The single neuron instability underlying spike initiation that is neglected in simple threshold neurons such as the LIF can apparently substantially contribute to the divergence of network state trajectories. These advances in the microscopic characterization of spiking network dynamics have started to provide new avenues for an information theoretical characterization of the repertoire of activity patterns that large spiking circuits generate. Monteforte and Wolf, for instance, were able to calculate the total entropy of distinct spike sequences that a balanced random network of LIF neurons can generate from a characterization of the network's phase space [61••]. Studies of temporally driven balanced circuits (such as Refs. [62,63,73]) are needed to clarify the relationship of different types of chaotic dynamics and the representation of sensory information in patterns of network activity. Studies of network phase space organization have so far been performed mostly in networks of simple pulse coupled neurons. There are, however, no rigid limitations to generalizing

Figure 4

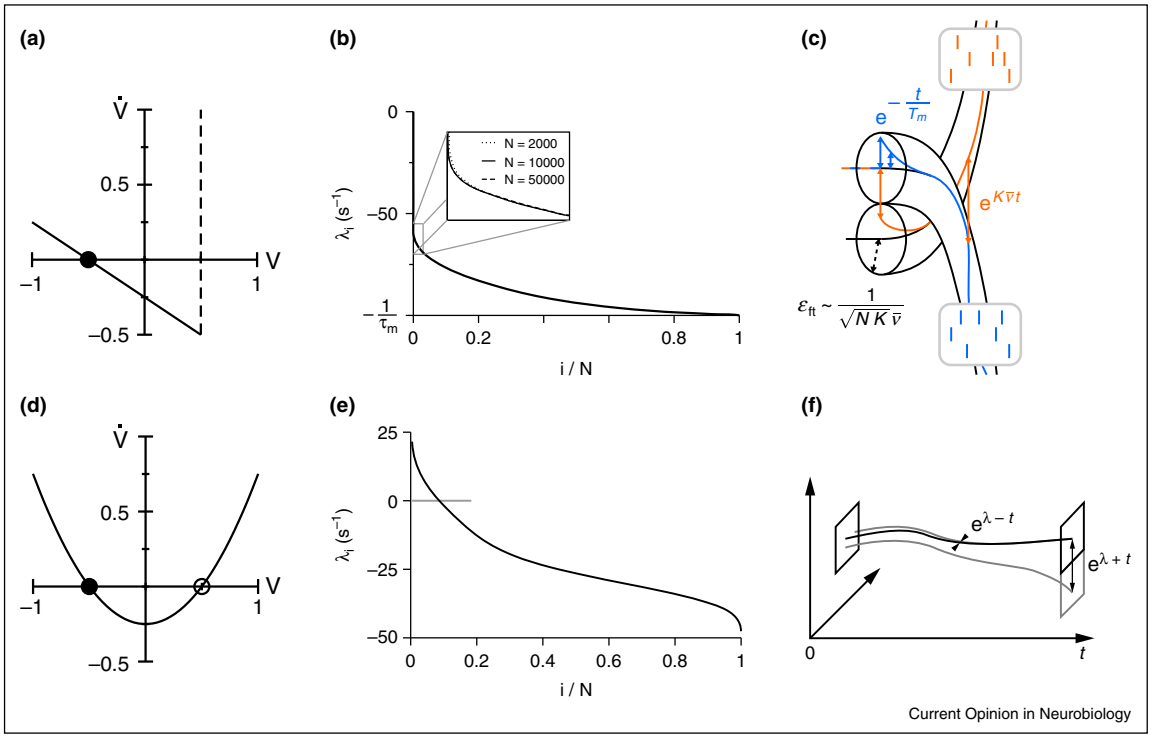

The nature of collective chaos in balanced networks is sensitive to single neuron dynamics. The left panels represent the single neuron membrane potential dynamics of the leaky integrate-and-fire neuron (a) and the quadratic integrate-and-fire neuron (d). The middle panels show spectra of Lyapunov exponents (LEs) that characterize the divergence/convergence of state trajectories in the phase space of otherwise identical balanced networks of these model neurons (b,e). Positive LEs demonstrate a chaotic dynamics in which trajectories exponentially diverge. Negative LEs characterize the decay of perturbations in particular directions in phase space as indicated in the lower right scheme (f). In the LIF network all LEs are negative demonstrating that the irregular firing sequences generated by the network are stable. The upper right scheme (c) summarizes the geometrical properties of the basins of attraction of the different stable irregular firing sequences exhibited by the network. *N* is the number of neurons in the network, and *K* is the mean number of synaptic connections (modifed from refs. 60,61).

the concepts and computational approaches to networks composed of more complex neuron models as long as they allow for an exact integration of the single neuron model between spike events.

A high speed of signal propagation is one basic advantage of asynchronous network states. In a large, asynchronously firing neuronal population a subset of cells is always close to threshold and thus ready to convey information rapidly. In balanced networks the speed of population responses is further increased by the strong net synaptic interactions [10,11]. Balanced networks are thus capable of rapid population responses even if the constituent neurons exhibit pronounced low pass characteristics. Recent experimental studies have started to address the bandwidth of spike encoding in fluctuation driven populations of real cortical neurons [64–68]. These studies consistently report that population responses are surprisingly rapid even in the absence of recurrent interactions. Even in response to very weak stimuli, populations of pyramidal cells can change their firing rate within less than a millisecond — at least an order of magnitude faster than expected from their membrane time constant [67]. Such rapid responses to weak stimuli have been theoretically predicted for simplified neuron models such as the leaky integrate-and-fire neuron, but seemed to be absent in biophysically more realistic models (see discussion in Ref. [67]). The biophysical basis of the high bandwidth of neural population encoding in the fluctuation driven regime is currently not understood and calls for a reinvestigation of the basic processes of action potential generation [69–71]. Further theoretical work is needed to disentangle the relative contributions of strong recurrent interactions and single neuron bandwidth to the processing speed of cortical circuits.

Conclusions

Many lines of current evidence indicate an inhibition dominated operating regime of cortical circuits in which recurrent excitation and feedback inhibition are strong and dynamically matched. Counter-intuitive theoretical

predictions such as the paradoxical response of ISNs [8,12] or the emergence of orientation selectivity from balanced random networks [9••] are contributing to our understanding cortical circuit operation. Theoretical studies over the past several years have strongly expanded the toolbox for a mathematically accurate and controlled dissection of cortical circuit models in balanced and inhibition-dominated network states. Together with the current development of powerful new approaches for the experimental interrogation of cortical networks this progress provides a strong basis for discerning the mode of operation of cortical networks with a balance of theory and experiment.

Acknowledgements

The authors thank Demian Battaglia, Theo Geisel, David Hansel, Guillaume Lajoie, Ken Miller, Michael Monteforte, Alfonso Renart, Eric Shea-Brown, Idan Segev, Shy Shoham, Haim Sompolinsky, and Carl van Vreeswijk for inspiring discussions. We acknowledge financial support by the German Federal Ministry of Education and Research (BMBF) via the Bernstein Center for Computational Neuroscience—Göttingen (01GQ1005B, 01GQ0430, 01GQ07113), the Bernstein Focus Neurotechnology—Göttingen (01GQ0811) and the Bernstein Focus Visual Learning (01GQ0921, 01GQ0922), the German Israel Research Foundation, the VolkswagenStiftung (ZN2632) and the Deutsche Forschungsgemeinschaft through CRC-889.

References and recommended reading

Papers of particular interest, published within the period of review, have been highlighted as:

- • of special interest
- •• of outstanding interest

1. Harris KD, Mrsic-Flogel TD: **Cortical connectivity and sensory coding**. *Nature* 2013, **503**:51-58.

2. Douglas RJ, Martin KAC: **Neuronal circuits of the neocortex**. *Annu Rev Neurosci* 2004, **27**:419-451.

3. Isaacson JS, Scanziani M: **How inhibition shapes cortical activity**. *Neuron* 2011, **72**:231-243.

4. Fino E, Yuste R: **Dense inhibitory connectivity in neocortex**. *Neuron* 2011, **69**:1188-1203.

5. Packer AM, Yuste R: **Dense, unspecific connectivity of neocortical parvalbumin-positive interneurons: a canonical microcircuit for inhibition?** *J Neurosci* 2011, **31**:13260-13271.

6. Hofer SB, Ko H, Pichler B, Vogelstein J, Ros H, Zeng H, Lein E, Lesica NA, Mrsic-Flogel TD: **Differential connectivity and response dynamics of excitatory and inhibitory neurons in visual cortex**. *Nat Neurosci* 2011, **14**:1045-1052.

7. Fino E, Packer AM, Yuste R: **The logic of inhibitory connectivity in the neocortex**. *Neuroscientist* 2012 http://dx.doi.org/10.1177/1073858412456743.

8. Ozeki H, Ozeki H, Finn IM, Finn IM, Schaffer ES, Schaffer ES, Miller KD, Miller KD, Ferster D, Ferster D: **Inhibitory stabilization of the cortical network underlies visual surround suppression**. *Neuron* 2009, **62**:578-592.

9. •• Hansel D, van Vreeswijk C: **The mechanism of orientation selectivity in primary visual cortex without a functional map**. *J Neurosci* 2012, **32**:4049-4064.
Balanced networks can generate sharp orientation tuning even if randomly wired. It shows that highly selective intracortical connectivity is not required for the generation of selective responses in rodent visual cortex.

10. Van Vreeswijk C, Sompolinsky H: **Chaos in neuronal networks with balanced excitatory and inhibitory activity**. *Science* 1996, **274**:1724-1726.

11. Vreeswijk CV, Sompolinsky H: **Chaotic balanced state in a model of cortical circuits**. *Neural Comput* 1998, **10**:1321-1371.

12. Tsodyks MV, Skaggs WE, Sejnowski TJ, McNaughton BL: **Paradoxical effects of external modulation of inhibitory interneurons**. *J Neurosci* 1997, **17**:4382-4388.

13. Adesnik H, Bruns W, Taniguchi H, Huang ZJ, Scanziani M: **A neural circuit for spatial summation in visual cortex**. *Nature* 2012, **490**:226-231.

14. Wilson NR, Runyan CA, Wang FL, Sur M: **Division and subtraction by distinct cortical inhibitory networks in vivo**. *Nature* 2012 http://dx.doi.org/10.1038/nature11347.

15. Lee S-H, Kwan AC, Zhang S, Phoumthipphavong V, Flannery JG, Masmanidis SC, Taniguchi H, Huang ZJ, Zhang F, Boyden ES *et al.*: **Activation of specific interneurons improves V1 feature selectivity and visual perception**. *Nature* 2012 http://dx.doi.org/10.1038/nature11312.

16. London M, Roth A, Beeren L, Häusser M, Latham PE: **Sensitivity to perturbations in vivo implies high noise and suggests rate coding in cortex**. *Nature* 2010, **466**:123-127.

17. Li L-Y, Li Y-T, Zhou M, Tao HW, Zhang LI: **Intracortical multiplication of thalamocortical signals in mouse auditory cortex**. *Nat Neurosci* 2013, **16**:1179-1181.

18. Li Y-T, Ibrahim LA, Liu B-H, Zhang LI, Tao HW: **Linear transformation of thalamocortical input by intracortical excitation**. *Nat Neurosci* 2013, **16**:1324-1330.

19. Lien AD, Scanziani M: **Tuned thalamic excitation is amplified by visual cortical circuits**. *Nat Neurosci* 2013, **16**:1315-1323.

20. Han Y, Mrsic-Flogel T: **A finely tuned cortical amplifier**. *Nat Neurosci* 2013, **16**:1166-1168.

21. Shushruth S, Mangapathy P, Ichida JM, Bressloff PC, Schwabe L, Angelucci A: **Strong recurrent networks compute the orientation tuning of surround modulation in the primate primary visual cortex**. *J Neurosci* 2012, **32**:308-321.

22. Piëch V, Li W, Reeke GN, Gilbert CD: **Network model of top-down influences on local gain and contextual interactions in visual cortex**. *Proc Natl Acad Sci U S A* 2013, **110**:E4108-E4117.

23. Henry CA, Joshi S, Xing D, Shapley RM, Hawken MJ: **Functional characterization of the extraclassical receptive field in macaque V1: contrast, orientation, and temporal dynamics**. *J Neurosci* 2013, **33**:6230-6242.

24. Rangan AV, Young L-S: **Emergent dynamics in a model of visual cortex**. *J Comput Neurosci* 2013, **35**:155-167.

25. Stimberg M, Wimmer K, Martin R, Schwabe L, Mariño J, Schummers J, Lyon DC, Sur M, Obermayer K: **The operating regime of local computations in primary visual cortex**. *Cereb Cortex* 2009, **19**:2166-2180.

26. Persi E, Hansel D, Nowak L, Barone P, van Vreeswijk C: **Power-law input–output transfer functions explain the contrast-response and tuning properties of neurons in visual cortex**. *PLoS Comput Biol* 2011:7.

27. • Ahmadian Y, Rubin DB, Miller KD: **Analysis of the stabilized supralinear network**. *Neural Comput* 2013, **25**:1994-2037.
Study of rate models that show a crossover from supralinear to sublinear responses with increasing input strength. This crossover offers a novel explanation for a broad set of normalization phenomena.

28. Carandini M, Heeger DJ: **Normalization as a canonical neural computation**. *Nat Rev Neurosci* 2012, **13**:51-62.

29. •• Mongillo G, Hansel D, van Vreeswijk C: **Bistability and spatiotemporal irregularity in neuronal networks with nonlinear synaptic transmission**. *Phys Rev Lett* 2012, **108**:158101.
The first self-consistent mean field theory of balanced networks with dynamic synapses, exhibiting synaptic depression and facilitation. Distinct from classical models of the balanced state this construction can support nonlinear effects such as multiple coexisting activity states.

30. Hansel D, Mato G: **Short-term plasticity explains irregular persistent activity in working memory tasks**. *J Neurosci* 2013, **33**:133-149.

31. Van Hooser SD: **Similarity and diversity in visual cortex: is there a unifying theory of cortical computation?** *Neuroscientist* 2007, **13**:639-656.

32. Keil W, Kaschube M, Schnabel M, Kisvarday ZF, Lowel S, Coppola DM, White LE, Wolf F: **Response to comment on 'universality in the evolution of orientation columns in the visual cortex.'**. *Science* 2012, **336**:413.

33. Jia H, Rochefort NL, Chen X, Konnerth A: **Dendritic organization of sensory input to cortical neurons in vivo**. *Nature* 2010, **464**:1307-1312.

34. Ko H, Hofer SB, Pichler B, Buchanan KA, Sjöström PJ, Mrsic-Flogel TD: **Functional specificity of local synaptic connections in neocortical networks**. *Nature* 2011, **473**:87-91.

35. Chen T-W, Wardill TJ, Sun Y, Pulver SR, Renninger SL, Baohan A, Schreiter ER, Kerr RA, Orger MB, Jayaraman V *et al.*: **Ultrasensitive fluorescent proteins for imaging neuronal activity**. *Nature* 2013, **499**:295-300.

36. Ko H, Cossell L, Baragli C, Antolík J, Clopath C, Hofer SB, Mrsic-Flogel TD: **The emergence of functional microcircuits in visual cortex**. *Nature* 2013, **496**:96-100.

37. Van Vreeswijk C, Sompolinsky H: **Course 9 irregular activity in large networks of neurons**. *Les Houches* 2005, **80**:341-406.

38. Niell CM, Stryker MP: **Highly selective receptive fields in mouse visual cortex**. *J Neurosci* 2008, **28**:7520-7536.

39. Barth AL, Poulet JFA: **Experimental evidence for sparse firing in the neocortex**. *Trends Neurosci* 2012, **35**:345-355.

40. Roxin A, Brunel N, Hansel D, Mongillo G, van Vreeswijk C: **On the distribution of firing rates in networks of cortical neurons**. *J Neurosci* 2011, **31**:16217-16226.

41. Cohen MR, Kohn A: **Measuring and interpreting neuronal correlations**. *Nature Neurosci* 2011, **14**:811-819.

42. Ecker AS, Berens P, Keliris GA, Bethge M, Logothetis NK, Tolias AS: **Decorrelated neuronal firing in cortical microcircuits**. *Science* 2010, **327**:584-587.

43. •• Renart A, La Rocha De J, Bartho P, Hollender L, Parga N, Reyes A, Harris KD: **The asynchronous state in cortical circuits**. *Science* 2010, **327**:587-590.

First analysis of balanced networks with dense connectivity. Demonstrates that asynchronous activity is actively generated in inhibition dominated circuits by dynamical tracking of activity levels in excitatory and inhibitory populations.

44. Hertz J: **Cross-correlations in high-conductance states of a model cortical network**. *Neural Comput* 2010, **22**:427-447.

45. Vilela R, Lindner B: **Comparative study of different integrate-and-fire neurons: spontaneous activity, dynamical response, and stimulus-induced correlation**. *Phys Rev E* 2009, **80**:1-12.

46. Ostojic S, Brunel N, Hakim V: **How connectivity, background activity, and synaptic properties shape the cross-correlation between spike trains**. *J Neurosci* 2009, **29**:10234-10253.

47. Burak Y, Lewallen S, Sompolinsky H: **Stimulus-dependent correlations in threshold-crossing spiking neurons**. *Neural Comput* 2009, **21**:2269-2308.

48. Tchumatchenko T, Malyshev A, Volgushev TG, Wolf MF: **Correlations and synchrony in threshold neuron models**. *Phys Rev Lett* 2010, **104**:58102.

49. Moreno-Bote R, Parga N: **Response of integrate-and-fire neurons to noisy inputs filtered by synapses with arbitrary timescales: firing rate and correlations**. *Neural Comput* 2010, **22**:1528-1572.

50. Litwin-Kumar A, Oswald A-MM, Urban NN, Doiron B: **Balanced synaptic input shapes the correlation between neural spike trains**. *PLoS Comput Biol* 2011, **7**:e1002305.

51. Rosenbaum R, Rubin JE, Doiron B: **Short-term synaptic depression and stochastic vesicle dynamics reduce and shape neuronal correlations**. *J Neurophysiol* 2013, **109**:475-484.

52. Pernice V, Staude B, Cardanobile S, Rotter S: **How structure determines correlations in neuronal networks**. *PLoS Comput Biol* 2011, **7**:e1002059.

53. Tetzlaff T, Helias M, Einevoll GT, Diesmann M: **Decorrelation of neural-network activity by inhibitory feedback**. *PLoS Comput Biol* 2012, **8**:e1002596.

54. Trousdale J, Hu Y, Shea-Brown E, Josić K: **Impact of network structure and cellular response on spike time correlations**. *PLoS Comput Biol* 2012, **8**:e1002408.

55. Hu Y, Trousdale J, Josić K, Shea-Brown E: **Motif statistics and spike correlations in neuronal networks**. *J Stat Mech* 2013 http://dx.doi.org/10.1088/1742-5468/2013/03/P03012.

56. • Litwin-Kumar A, Doiron B: **Slow dynamics and high variability in balanced cortical networks with clustered connections**. *Nat Neurosci* 2012 http://dx.doi.org/10.1038/nn.3220.

Integrating clustering motives into balanced state networks leads to the emergence of slow rate dynamics with different clusters switching between high and low activity levels.

57. Jahnke S, Memmesheimer R-M, Timme M: **Stable irregular dynamics in complex neural networks**. *Phys Rev Lett* 2008, **100**:1-4.

58. Zillmer R, Brunel N, Hansel D: **Very long transients, irregular firing, and chaotic dynamics in networks of randomly connected inhibitory integrate-and-fire neurons**. *Phys Rev E* 2009, **79**:1-13.

59. Jahnke S, Memmesheimer R-M, Timme M: **How chaotic is the balanced state?** *Front Comput Neurosci* 2009:3.

60. •• Monteforte M, Wolf F: **Dynamical entropy production in spiking neuron networks in the balanced state**. *Phys Rev Lett* 2010, **105**:1-4.

Demonstrates an intense chaotic dynamics in balanced networks of theta neurons. Chaos is extensive. A high entropy rate on the order of 1 bit spike and neuron is found.

61. •• Monteforte M, Wolf F: **Dynamic flux tubes form reservoirs of stability in neuronal circuits**. *Phys Rev X* 2012, **2**:041007.

Characterizes the geometry of phase space underlying complex stable spiking sequences in balanced networks exhibiting 'stable chaos'. The basins of attraction of complex spiking sequences are tubes diverging exponentially from each other leading to locally stable but globally unstable dynamics.

62. Lajoie G, Lin KK, Shea-Brown E: **Chaos and reliability in balanced spiking networks with temporal drive**. *Phys Rev E* 2013, **87**:052901.

63. Marre O, Yger P, Davison AP, Frégnac Y: **Reliable recall of spontaneous activity patterns in cortical networks**. *J Neurosci* 2009, **29**:14596-14606.

64. Köndgen H, Geisler C, Fusi S, Wang X-J, Lüscher H-R, Giugliano M: **The dynamical response properties of neocortical neurons to temporally modulated noisy inputs in vitro**. *Cereb Cortex* 2008, **18**:2086-2097.

65. Boucsein C, Tetzlaff T, Meier R, Aertsen A, Naundorf B: **Dynamical response properties of neocortical neuron ensembles: multiplicative versus additive noise**. *J Neurosci* 2009, **29**:1006-1010.

66. Higgs MH, Spain WJ: **Conditional bursting enhances resonant firing in neocortical layer 2–3 pyramidal neurons**. *J Neurosci* 2009, **29**:1285-1299.

67. Tchumatchenko T, Malyshev A, Wolf F, Volgushev M: **Ultrafast population encoding by cortical neurons**. *J Neurosci* 2011, **31**:12171-12179.

68. Ilin V, Malyshev A, Wolf F, Volgushev M: **Fast computations in cortical ensembles require rapid initiation of action potentials**. *J Neurosci* 2013, **33**:2281-2292.

69. Huang M, Volgushev M, Wolf F: **A small fraction of strongly cooperative sodium channels boosts neuronal encoding of high frequencies**. *PLoS ONE* 2012, **7**:e37629.

70. Brette R: **Sharpness of spike initiation in neurons explained by compartmentalization**. *PLoS Comput Biol* 2013, **9**:e1003338.

71. Wei W, Wolf F: **Spike onset dynamics and response speed in neuronal populations**. *Phys Rev Lett* 2011, **106**:88102.

72. Ostojic S: **Two types of asynchronous activity in networks of excitatory and inhibitory spiking neurons**. *Nat.Neuroscience* 2014 http://dx.doi.org/10.1038/nn.3658.

73. Lajoie G, Thivierge J-P, Shea-Brown E: *Structured chaos shapes spike-response noise entropy in balanced neural networks*. 2013arXiv:1311.7128.

9 Discussion

9.1 Summary of results

In this thesis, the chaotic dynamics of large networks of spiking neuron models and rate units have been studied using concepts from the ergodic theory of dynamical systems.

Information encoding, processing and transmission in neural circuits are intimately linked to the collective network dynamics. Therefore, a better understanding of the mechanisms that shape dynamically generated activity patterns in nervous systems is crucial. In this thesis, we studied how single-cell properties and streams of input spike trains influence chaoticity, dynamical entropy rate and attractor dimensionality in recurrent spiking neural networks.

The most striking effect of single-cell features on the collective dynamics we found in recurrent networks driven by streams of input spike trains: the collective state becomes much easier to control by spiking input when the neurons in the driven network had a rapid action potential (AP) onset dynamics. To our best knowledge this is the first time that for recurrent networks a clear link between spike onset dynamics and their role in the collective flow of information through neuronal circuits has been demonstrated. To achieve this, we first investigated the role of action potential initiation (AP) for information transmission in a feedforward circuit architecture and for the spontaneous recurrent activity with constant input. We showed that recurrent circuits composed of neurons with rapid AP onset have a surprisingly low attractor dimension. This is hidden from correlation-based dimensionality estimates. To study with high precision the dynamics of large spiking balanced circuits, we developed a novel efficient algorithm for calculating Lyapunov exponents in event-based numerically exact network simulations. Recently, the hypothesis was put forward that such spiking networks exhibit two qualitatively distinct irregular state for strong and very strong couplings and that the transition to this "heterogeneous state" is analogous to the classical chaotic instability of random rate networks [4]. In our reanalysis of such systems [3], we found no indication of a corresponding chaotic instability in the spiking network. Finally, for random firing-rate networks, we for the first time to our knowledge calculated entropy rate and attractor dimensionality. This opens a novel avenue to characterize the complex dynamics of rate networks and the geometric structure of their high-dimensional chaotic attractor.

Efficient algorithm for calculating Lyapunov exponents of large spiking networks
We first introduced a novel efficient method for numerically exact simulations of large sparse spike networks and the calculation of their Lyapunov exponents (**Chapter 3**). Our new algorithm reduces the computational cost from $\mathscr{O}(N)$ to $\mathscr{O}(\log(N))$ operations per network spike for a fixed number of synapses per neuron and Lyapunov exponents. We achieved this by changing the frame of reference of the neurons' phase-representation and by employing a data structure that avoids

iterating though all neurons at every network spike time to find the next spiking neuron. The proposed algorithm also generalizes to heterogeneous networks and arbitrary neuron models that can be solved analytically between spikes. This allows numerically exact simulations of large spiking networks ($N = 10^9$ neurons) and the characterization of their phase space structure. For example, calculating the largest Lyapunov exponent of a spiking neural network with one million neurons is sped up by more than four orders of magnitude.

High AP onset rapidness increases the information encoding rate In a feedforward architecture, we found that the AP onset rapidness limits the capability to encode high-frequency stimuli (**Chapter 4**). We confirmed with four independent methods that high-frequency signal components encoded in mean- and variance-modulations of a fluctuating input current are more reliably encoded into the outgoing spike train if the single neurons have a rapid action potential generation mechanism. We estimated the mutual information rate between a noisy stimulus and the outgoing spike train in the Gaussian channel approximation from the spectral coherence between input and output signal. The coherence was calculated by solving the time-dependent Fokker-Planck equation and confirmed in direct numerical simulations. We found that the information rate grows approximately logarithmically with AP onset rapidness: $I \propto \log(r)$. The reason for the logarithmic scaling is that the rapidness determines the cutoff frequency up to which the spectral coherence is proportional to f^{-1}. We confirmed the logarithmic scaling analytically using the high-frequency and high-rapidness responses of the single neurons.

Rapid AP onset reduces chaoticity and entropy rate in recurrent networks In recurrent networks, we characterized the role and relevance of AP onset for the collective network dynamics (**Chapter 4**). We calculated the Lyapunov spectrum in numerically exact event-based simulations of random networks using the novel efficient method mentioned above. We find that the largest Lyapunov exponent grows linearly with rapidness up to a peak value r_{peak}. For higher rapidness, the largest Lyapunov exponent decreases as $1/r$. Numerical simulations reveal the scaling of the peak rapidness $r_{\text{peak}} \propto \sqrt{K\bar{\nu}\tau_m/J_0}$. It occurs where the diffusion approximation breaks down and shot noise due to the finite connectivity K and nonvanishing coupling strength $J = J_0/\sqrt{K}$ becomes relevant. For smaller rapidness r, the largest Lyapunov exponent is independent of the connectivity K and the mean firing rate $\bar{\nu}$ and proportional to r.

The stabilization of the network dynamics for large r is accompanied by a decrease in dynamical entropy rate and attractor dimension. Intriguingly, the drastic decrease of attractor dimension is not detected by a conventional dimensionality estimate, based on the pairwise correlations of the activity. This implies that neuron states have strong statistical dependencies. To corroborate these results from idealized random (Erdős–Rényi) networks, we calculated for the first time, Lyapunov spectra in large networks with more realistic connectivity structure: we analyzed dynamical entropy rate of a multilayered cortical column network model and of large networks equipped with experimentally measured excitatory-excitatory motif frequencies. Our results demonstrate that the drastic reduction of chaos, dynamical entropy rate and attractor dimensionality by high AP onset rapidness observed in random networks also occurs in these more realistic network structures.

Input spike trains suppress chaos and lead to a transition to complete network state control In **Chapter 5**, we studied the effect of streams of input spike trains on the dynamics of balanced target circuits. To address this challenge, we developed an approach for balanced networks driven by external streams of spike trains and calculate their full Lyapunov spec-

tra, yielding the dynamical entropy rate and attractor dimensionality in efficient, numerically exact event-based simulations introduced in Chapter 3. To explore how features of input streams affect information transmission, we varied correlations, irregularity, coupling strength and spike rate of the input and action potential onset rapidness of the recurrent neurons.

We found that increasing the input rate or coupling strength aids in controlling the driven target circuit, reflected both in reduced trial-to-trial variability and in a decreasing dynamical entropy rate. For sufficiently strong input, we observe a transition to complete network state control. Surprisingly, this transition generally does not coincide with the transition from chaos to stability but occurs at larger values of external input strength than the transition from chaos to stability. Intriguingly, controllability of spiking activity is facilitated when neurons in the target circuit have a rapid action potential initiation.

Our study predicts that rapid AP initiation of target neurons decreases trial-to-trial variability and augments information flow. These results can also be used to develop testable predictions for emerging optogenetic approaches towards the causal interrogation of circuit function and activity control.

Reanalysis of "Two types of asynchronous activity in networks of excitatory and inhibitory spiking neurons" In **Chapter 6**, we reanalyzed a recent study that investigated networks of leaky integrate-and-fire neurons and suggested that they would exhibit a chaotic instability mathematically analogous to rate networks with matched topology and single unit characteristics for strong synaptic coupling [4]. We found expected hallmarks of a chaotic instability in the rate network. Close to the transition to chaos, we observed critical slowing down in response to small external perturbations. In contrast, in the spiking network rate deviations resulting from small input perturbations rapidly decayed. When approaching the alleged chaotic instability, the decay speeds up contrary to the critical slowing down exhibited in the rate network. We further found a quantitative mismatch between predictions of the mean-field theory and numerical simulations, for a variation of different network parameters, e.g. synaptic delay, fraction of inhibition and number of synapses per neuron K. In conclusion, our reanalysis demonstrates fundamental differences between the behavior of networks of pulse-coupled spiking LIF neurons and rate networks with matched topology and input-output function. In particular, contrary to the original study [4], we found no indication of a corresponding chaotic instability in the spiking network [3].

Entropy rate and attractor dimensionality of firing-rate network dynamics In **Chapter 7**, we calculated for the first time to our knowledge the full Lyapunov spectra of random firing-rate networks. The dynamics of such networks and their transition from a stable state for small synaptic couplings g to a chaotic state for strong coupling has been studied extensively. We found – as conjectured in the original publication [5] – extensive chaos. Thus, for sufficiently large network size N, the shape of the Lyapunov spectrum is invariant with respect to network size N and only depends on the coupling strength g. We found that the Kolmogorov-Sinai entropy scales $H \propto \log(g)$ and the relative attractor dimensionality D/N saturates exponentially $\propto (1 - a \cdot \exp(-c \cdot g))$, where $c > 0$ is the exponential rate by which the saturation value of approximately 10% of N is approached. Interestingly, the Lyapunov spectrum is point-symmetric around its negative mean. We derived an analytical expression for the mean Lyapunov exponent, both for continuous time and for discrete network dynamics. Our results show that for sufficiently large g and large time steps Δt the Jacobians commute. This suggests that in these cases the full Lyapunov spectrum can be calculated analytically. Larger time steps Δt generally lead to a more negative Lyapunov spec-

trum, which can be explained by less correlated subsequent Jacobians. We found that for large Δt, the Lyapunov spectrum follows approximately the Marchenko-Pastur distribution, for small g and small Δt the Wigner semicircle law and for large Δt and small g the triangle law [198–200].

Adding frozen Gaussian white noise to the dynamics reduced chaos, dynamical entropy rate and attractor dimensionality, but the mean exponent does not change. If the noise is much stronger than the recurrent coupling parameter g, all Lyapunov exponents approached $-\frac{1}{\tau}$, which is the negative inverse of the intrinsic single unit timescale.

9.2 Relation to previous work

In the following we relate our findings to previous computational, theoretical and experimental work. Our results regarding the role of AP onset rapidness for the information bandwidth in a feedforward architecture and chaos in recurrent circuits confirmed and extended earlier findings. For the first time to our knowledge, we linked these interesting mathematical findings to their relevance to cortical information processing: when driving recurrent networks by strong external spiking input, we found a suppression of chaos and a transition to complete network state control, which are both facilitated by rapid AP onset. We will discuss the relation to earlier theoretical findings and suggest experimental tests of our predictions. Lastly, we discuss our results on rate networks and describe how our approach to calculate the full Lyapunov spectrum of rate networks could be used as a toolkit from dynamical systems theory to analyze how different factors shape the complex rate activity and to quantify the reorganization of the collective network dynamics during learning.

Efficient exact large spiking networks simulations In Chapter 3 we introduced a novel efficient event-based algorithm for simulating the network dynamics and calculating the Lyapunov spectrum that reduces the computational cost from $\mathcal{O}(N)$ to $\mathcal{O}(\log(N))$ operations per network spike for a fixed number of Lyapunov exponents and synapses per neuron compared to earlier implementations [62, 125, 126, 201, 202]. This facilitates investigating the chaotic dynamics of simplified cortical microcircuit models (e.g. [203]), which usually require a supercomputer for simulations [204–207]. Efficient simulation of large networks might also be useful when gradually experimentally obtained wiring diagrams known as connectomes become available by novel circuit reconstruction methods [208, 209]. It also facilitates exploration of the scaling of e.g. the largest Lyapunov exponent or the average firing rate with network size N across many orders of magnitude (see Chapter 3 and 4). There are also limitations for our novel algorithm: it requires that the single neuron dynamics can be exactly solved between spike times, which excludes most multivariate neuron models (e.g. [210–214]) and networks driven by continuous time-varying input signals that prohibit event-based simulations.

AP onset rapidness & information bandwidth In our analysis of the role of action potential (AP) onset dynamics for the frequency response and information transmission in a feedforward architecture (Chapter 4), we found that the AP onset rapidness limits the high-frequency response. Our findings are in qualitative agreement with earlier studies which demonstrated this in different neuron models with variable AP onset rapidness. A limiting effect of AP onset rapidness on

high-frequency encoding was shown before in the exponential integrate-and-fire model [30, 186], a different generalization of the quadratic integrate-and-fire model [47] and in an analytical study of a piecewise linear integrate-and-fire model, called the rapid-τ-model [49].

Distinct from these earlier studies, we quantified the rapidness-dependence of the mutual information rate between a stimulus immersed in fluctuations and the outgoing spike train using a Gaussian channel approximation based on the spectral coherence (Chapter 4). We found that the mutual information rate increases logarithmically with increasing AP onset rapidness (both by solving the Fokker-Planck equation numerically and by an analytical approximation). This extends earlier numerical studies that calculated the mutual information rate in different integrate-and-fire type neuron models [46, 215–217], both by the direct method [218] and by using a Gaussian channel approximation. Our analytical approximation extends the previous studies which approximated the mutual information rate for a stochastic rate neuron that was modeled as *exponential-Poisson processes* [219, 220]. It is to our knowledge the first fully analytical estimation of the mutual information rate in a spiking neuron model. To solve the time-dependent Fokker-Planck equation, we extended a threshold integration method to piecewise Fokker-Planck equations and improved the numerical implementation with respect to memory consumption and speed (see also [221–224]).

AP onset rapidness & recurrent spiking network dynamics In our analysis of the role of AP onset rapidness for the recurrent network dynamics (Chapter 4) we confirmed the importance of AP onset for the recurrent chaotic dynamics in an independent reimplementation of the full Lyapunov spectrum of rapid theta neurons, which have a tunable AP onset rapidness (earlier work on rapid theta neurons can be found in [62]). This also allowed us to confirm that dynamical entropy rate and Kaplan-Yorke attractor dimensionality decay for increasing AP onset rapidness. In an extension of the earlier work in random Erdős–Rényi networks [62], we studied chaos and dynamical entropy rate in microscopically and macroscopically structured networks [203,225]. Both in a multilayered cortical column model with approximately 80000 neurons [203] and in mixed networks with realistic excitatory-excitatory second-order circuit motif frequencies [225], we confirmed that for high AP onset rapidness the entropy and dimensionality are drastically reduced. In a further extension to the earlier work [62], we calculated pairwise spike count correlations as a function of AP onset rapidness and bin size with high precision. This yielded a correlation-based dimensionality estimate which we found to be insensitive to AP onset rapidness. We concluded that the rapidness-dependent, microscopic phase space reorganization reflected in the Lyapunov spectrum and attractor dimensionality is not detected by the second order statistics. In addition to earlier work, the novel efficient algorithm (Chapter 3) allowed us to calculate the large N asymptotic form of the largest Lyapunov exponent as a function of AP onset rapidness. We further performed a systematic analysis of the scaling of the critical rapidness r_{crit}, at which the network dynamics turns stable; r_{peak}, where the largest Lyapunov exponent peaks as a function of rapidness; and the scaling of the largest Lyapunov exponent with network parameters. To assess the convergence within a single simulation, we introduced a novel single trial confidence and convergence estimator based on bootstrapping the finite-time Lyapunov exponents [226]. This allows estimating the degree of convergence on the fly during a simulation instead of comparing results across different runs with independent initial conditions and thus also reduces computational costs.

Moreover, using random matrix theory, we analytically calculated the mean Lyapunov exponent of the rapid theta network and studied its scaling with rapidness r and the number of synapses K.

We further analyzed the phase space structure of small networks and visualized the decreasing dimensionality for increasing rapidness using Poincaré sections. A single-cell parameter not

considered in this thesis is the synaptic time constant τ_s, which was shown to moderately influence chaoticity in earlier studies [62, 125, 126, 184, 227]. Moreover, we didn't consider synaptic delays, which were found to slightly reduce chaos in LIF networks with exponentially decaying synapses. A stronger reduction of chaos is observed, when the collective network state changes e.g. to oscillations or phase-locking [125].

In inhibitory LIF networks, earlier studies found an exotic phase space structure of *flux tubes* where the network state is insensitive to sufficiently small perturbations, while large perturbations grow exponentially [62,123,126,130]. For the first time, we also demonstrated the existence of flux tubes in networks where the single neuron dynamics have an active spike generation mechanism. We found the flux tube diameter to grow quadratically as a function of AP onset rapidness r closely above the critical rapidness r_{crit}, and visualized their cross-section, revealing a decreasing mean flux tube radius and curved flux tube boundaries when approaching the critical rapidness r_{crit} from above.

Evoked dynamics of balanced networks driven by streams of input spike trains
For nonautonomous network models, we extended earlier approaches in balanced theta neuron networks driven by white noise [162, 163] to an external input composed of streams of spike trains and a numerically exact simulation method. For input spike trains with sufficiently strong coupling and high rate, we for the first time to our knowledge found a suppression of chaos in spiking neural networks. A similar transition was previously found in networks of rate units [6–8], but not in spiking networks. Intriguingly, we found that suppression of network chaos occurs at a weaker input fluctuation strength than the transition to complete control of the network state. This is surprising, because earlier studies suggested that a negative largest Lyapunov exponent implies that trajectories formed by different initial conditions collapse in a random sink [161, 162, 165, 170]. While this holds in the limit of large time for random dynamical systems when certain non-degeneracy conditions are satisfied [168, 169], we find that on neurobiologically relevant time scales, streams of input spikes can suppress chaos without collapsing independent initial conditions onto a single globally attracting random sink. Thus, even if driven network dynamics are stable with respect to infinitesimal perturbations, reliability across trials with different initial conditions but frozen external input is not guaranteed. It was found earlier that reliable spikes exist even in the chaotic regime [162]. We can hence conclude more generally that the largest Lyapunov exponent alone is not a sufficient indicator of trial-to-trial reliability both in the chaotic and in the stable regime of spiking networks. This insight raises a new perspective on earlier studies, where negative Lyapunov exponents were often linked to reliability [147, 162, 170, 228–232]. A transition to complete network state control by time-varying input which we found in balanced spiking networks with streams of input spike trains was earlier reported in rate networks in the context of echo state networks for reservoir computing and termed *echo state property* [233–236]. For the first time to our knowledge we systematically examined the scaling of the chaoticity with various parameters of both external input and the recurrent network. We found that for increasing mean recurrent firing rate, recurrent coupling strength and membrane time constant, it becomes more difficult to suppress the recurrent chaos by the streams of input spike trains. Similarly, the critical external coupling $J^{\text{ext}}_{0\text{crit}}$ where the largest Lyapunov exponent becomes zero increases for stronger external spiking input. In contrast, the critical coupling strength decreases for higher firing rates of incoming spike trains and for more irregular input spike trains. In a low-noise limit of high input rates and low input coupling strength, we showed that the Lyapunov spectrum of the driven network approaches the Lyapunov spectrum of a network without spiking input. We further

extended the flux tube concept from constant [62, 126, 130] to time-dependent external input and analyzed the radius of the flux tubes as a function of external input coupling strength J_0^{ext} (Also see [237]). We hypothesized a growth of flux tube diameter for increasing external input variance. This was confirmed by direct numerical simulations (Chapter **5** and [237] for LIF neurons).

Relations to previous experimental results In agreement with experimental observations [44, 238, 239], we confirmed that AP onset rapidness limits the high-frequency encoding. Accordingly, we found that the mutual information rate between input and outgoing spike train of a neuron in a fluctuation-driven regime for fixed firing rates. While mutual information rates between stimulus and response have previously been measured experimentally [218, 240], the specific role of AP onset dynamics on information transmission has not directly been assessed.

More generally, our study contributes to the investigation of reliability of neuronal activity, which was extensively studied at the single neuron level in experiments [66–69]. Novel tools and bidirectional neural circuit interfaces for the first time allow experimentalists for selectively manipulating and monitoring the activity of vast numbers of neurons in the intact brain and even in behaving animals [175, 176, 241]. Previous experimental studies found that external drive reduces trial-to-trial spiking variability compared to the spontaneous activity state [242]. We found in our theoretical work that sufficiently variable external input is able to completely control the network state of a recurrent balanced target circuit. In the outlook section 9.3, we will discuss potential avenues to explore this experimentally.

Earlier studies investigated sensitivity of cortical circuits with respect to the addition of a single spike [128]. While the conclusions remain controversial, the experiments certainly reveal an important research direction: interrogating the neural code by perturbation experiments. In our analysis, we concluded that single neuron properties affect the sensitivity of circuits both to infinitesimal and finite size perturbations (Chapter 4) and that sufficiently strong time-varying input reduces the dynamic sensitivity of cortical circuits.

Reanalysis of the "heterogeneous balanced state" In our reanalysis of the "heterogeneous balanced state" [4], we added how firing rate, coefficient of variation of the interspike interval distributions and network synchrony scale with different system parameters, e.g. the synaptic delay time, the refractory period, the relative inhibitory strength and the number of synapses per neuron. Our results indicate that the mean-field theory, which is valid for the Poisson rate networks, quantitatively deviates from network simulations of spiking LIF neurons for slight variations of system parameters. This result contradicts the claim that "the Poisson network [...] exhibits an instability identical to that of the LIF network, at the same critical value of synaptic coupling" [4]. In addition to the earlier work [4], we also added an analysis of response of the network firing rate to small perturbations, where we found critical slowing down close to the phase transition in the firing-rate network but not in the corresponding circuit of leaky integrate-and-fire neurons. We thus corrected the original study, with respect to claim that the behavior of the spiking LIF networks is "mathematically analogous to the chaotic instability in rate networks" [4]. The mean-field theory of the original work assumes individual firing rates for each spiking neuron, *ad hoc*, which are claimed to rest at a fixed point below the critical coupling strength J_{crit} and to lose their stability above J_{crit}. Such a linear stability analysis is justified in the case of a rate network, where firing rates exist as dynamical variables. In contrast, in the LIF network, the dynamical variables are membrane potentials, which are driven to threshold due to the external input and are not at a fixed point. Therefore, a linearization around a stable fixed point is mathematically inappropri-

ate. The burstiness of single LIF neurons in the network for strong recurrent coupling is related to unphysiological, negative voltage excursions allowed by the linear V-$\dot{V}$-relationship of the LIF neuron model. If a physiological lower bound on the voltage is introduced reflecting e.g. the reversal potential of potassium channels, then the "heterogeneous" firing rate fluctuations caused by single-cell bursting vanish. Concomitantly, the coefficient of variation of the interspike interval distribution, which measures irregularity, becomes smaller than 1. More evidence in support of this explanation of the observed "heterogeneous activity" is that the phenomenon of a "heterogeneous state" does not occur in networks of quadratic integrate and fire neurons even for extremely strong synaptic couplings. While the reanalysis conclusively shows that there is no analogous relationship between the chaotic instability of rate networks and the behavior of the LIF network, the phenomenon of increasing firing rates for strong coupling in LIF networks itself is not fully understood. Temporally correlated fluctuations seem to be necessary for the increasing mean firing rate, but the role of the synaptic delay in this phenomenon is not clear. For a better analytical understanding, a self-consistent theory of spiking neurons which includes nontrivial autocorrelations appears needed. Until now, this was only achieved numerically [243, 244].

Chaos in firing-rate networks A seminal study showed that randomly connected rate units display a transition from an quiescent state to a highly heterogeneous, chaotic state with spontaneous rate fluctuations for sufficiently strong couplings [5]. Mechanisms underlying rate chaos have recently attracted a lot of attention in studies of network heterogeneity [131], bistability [187], external stimuli [6–8, 188] and the role of single unit transfer function [37] and slow synaptic dynamics [37, 92] for the collective network state (see also [3, 4, 8, 189–194]).

It is also increasingly appreciated that chaotic rate dynamics provide a substrate for complex nonlinear computations e.g. learning input-output relations [6, 35, 133, 245–248] and learning temporal sequences [249]. Intriguingly, transient rate chaos yields exponential expressivity in deep networks [250]. Our tools allow us to quantify the reorganization of the collective network dynamics during learning and to dissect the underlying mechanisms of different reservoir computing strategies.

A suppression of chaos by time-dependent input was studied earlier both with white noise input in discrete-time [6] and continuous-time networks [8] and with sinusoidal input [7]. Such a transition has relevance for information processing because the network loses its dependence on initial conditions, which might be a desirable feature, if the network should generate reliably controlled output trajectories for certain input patterns after learning [35, 249, 251]. The transition to complete network state control by an external stimulus and the associated independence from initial conditions was earlier studied in rate networks in the context of echo state networks for reservoir computing and termed *echo state property* [233–236].

Our approach provides a toolkit from dynamical systems theory to analyze how these different factors shape the complex rate dynamics. We compared the Lyapunov dimension with a dimensionality estimate based on principal component analysis (PCA), which is commonly used in neuroscience [7, 188, 195–197]. Generally, we find a quantitatively different but qualitatively similar scaling of the PCA-based dimensionality and the Lyapunov dimension: Both exponentially saturate with synaptic strength for g but they saturate at a different level and with distinct exponential rates. Crucially, Lyapunov exponents and thus also the Lyapunov dimension are invariant under diffeomorphisms on the phase space [252], while covariance-based dimensionality estimates are generally not invariant with respect to changes of variables and can be misleading if applied to limited data sets [253].

Furthermore, our approach also allows for interpolating from continuous-time to discrete dynamics. Discrete-time dynamics of rate networks has previously been studied in random diluted network topologies [189], on a ring topology [254] and with external white noise input [6]. One effect of temporal discretization is that subsequent Jacobians have lower correlation (see Chapter **7**), which facilitates their treatment with random matrix theory.

9.3 Outlook

We are only beginning to use ergodic theory to understand neural computation. By employing these concepts in large scale spiking and rate networks we have laid the foundation for further investigation. Until now computational ergodic theory of neural networks appears to be the only way to measure information theoretic quantities of large recurrent circuits. It is an important challenge to obtain a more comprehensive understanding of how different factors shape collective network dynamics and constrain information processing. In this final section, we propose several direct extensions of the work presented in this thesis followed by a discussion of two more general potential future research directions.

9.3.1 Extensions

Efficient numerically exact large network simulations Our novel efficient algorithm for large network simulations based on binary heaps and a change of the frame of reference of the neurons' phase-representation introduced in Chapter 3 could be further improved for large K by using one heap merge after every spike time instead of $K+1$ percolations through the binary heap. This would result in an expected speedup by $\mathscr{O}(K/\log(K))$. Especially for large excitatory networks, a Fibonacci heap might also be an efficient implementation [255], but for practical purposes, the asymptotic scaling of the computational complexity has an unfavorably large prefactor [256]. Therefore, other heap structure implementations might be faster in practice [257].

AP onset rapidness We propose four extensions to our analysis of the effect of action potential (AP) onset rapidness both for information transmission in a feedforward architecture and its role and relevance for recurrent circuit dynamics.

Firstly, we propose to investigate the effect of synaptic shot noise both on information transmission and on the recurrent network dynamics. The purpose of such an investigation would be to better understand the implications of strong synapses for information processing, as experiments indicate that few strong synapses – potentially at the tail of a lognormal weight distribution [84, 258–262] – are functionally particularly important [263]. In the analysis of the role of onset rapidness for the collective network dynamics, we found that for sufficiently high rapidness, the diffusion approximation breaks down and the effect of shot noise becomes significant. To obtain deeper understanding of the effect of synaptic shot noise, to start with, the single-cell characterization of the rapid theta model (Chapter 4) could be extended to include incoming shot noise instead of Gaussian white noise [264–266]. Besides the stationary voltage distribution under the influence of shot noise, also the impact of excitatory and inhibitory shot noise on the frequency response should be studied in more detail. Our preliminary results indicate that synaptic shot noise can amplify the high-frequency response both in the mean- and variance-channel especially for

high rapidness (Chapter 4, Supplementary figure 3). Analytical understanding of the effect of synaptic shot noise might also yield an analytical derivation of the scaling of the AP rapidness at which the largest Lyapunov exponent peaks. The stationary voltage distribution with synaptic shot noise would also further improve the analytical estimation of the mean Lyapunov exponent using the random matrix approach described in Chapter 4.

Secondly, also for the full Lyapunov spectrum or at least for the largest Lyapunov exponent, analytical expressions are desirable. As it is generally considered difficult to calculate the full Lyapunov spectrum [145], it might be advisable to first calculate the full Lyapunov spectrum of a model with simpler internal dynamics, e.g. the Gauss neuron [267–271] or the rapid-τ-model [49], using analytical methods [79, 200, 272–274]. Earlier results for leaky integrate-and-fire neurons might be useful to this end [126].

Thirdly, one should include temporally extended synaptic currents into the rapid theta model, to investigate the effect of synaptic dynamics on dynamical entropy rate and attractor dimensionality. Such an extension is not only indicated because depending on the synaptic dynamics can vary between millisecond for AMPA [185,275,276] and tens of millisecond timescales for NMDA [185, 277–279], but also because the synaptic dynamics affects chaoticity of spiking networks [62, 125, 126, 184, 227]. The rapid theta model dynamics between network spikes can still be analytically solved with exponentially decaying synaptic currents [280], yielding the *correlated rapid theta model*. The Lyapunov spectrum as a function of the two-dimensional parameter space spanned by AP onset rapidness r and synaptic timescale τ_s would be interesting to analyze. In the case of purely inhibitory random (Erdős–Rényi) networks of leaky integrate-and-fire neurons, increasing the synaptic time constant results in a transition from an asynchronous irregular state with a semi-definite negative Lyapunov spectrum – a state called *stable chaos* – to a slightly chaotic state for slow synaptic dynamics [62, 125, 126, 184, 227]. Therefore, for networks of *correlated rapid theta model neurons* in the balanced state, one might expect a semi-definite negative Lyapunov spectrum for high rapidness and short synaptic time constants and extensive chaos, as soon as either rapidness is reduced or the synaptic time constant τ_s is sufficiently large. In the limit of slow synaptic dynamics, the synaptic input current integrates over a long time and the network dynamics behave similar to a rate network in several quantitative comparisons, e.g. with respect to the firing rate distributions, the population autocorrelations and the synaptic current distribution in the large K-limit [92]. An interpolation from spiking to rate dynamics with increasing τ_s and a comparison of the associated Lyapunov spectra of rate with spectra of spiking networks should improve our understanding of chaos both in spiking and rate networks and of their relationship.

Fourthly, as biophysical properties of neurons are diverse, the effect of heterogeneity of AP onset rapidness should be studied. While rapid spike onset was discovered in in excitatory neurons [39–44,238,239], recent unpublished work also indicates rapid AP onset dynamics and high bandwidth in inhibitory neurons. As more data becomes available, the functional differential implications of AP onset rapidness in excitatory and inhibitory neurons should be investigated theoretically both in a feedforward architecture and in recurrent networks. For a feedforward architecture, we hypothesize that a small fraction of neurons with fast AP onset rapidness are enough to transmit a high-frequency signal.

Fifthly, to further corroborate and generalize the results from the rapid theta networks, one should also study the role of AP onset rapidness on the collective dynamics in other classes of neuron models. In a preliminary study of type II neurons, we found that similar to type I neurons high AP onset rapidness reduces chaos and dynamical entropy rate in spiking balanced networks. A similar result would be expected in conductance-based neuron models given the generality of

our findings in type I and type II neuron models.

Dynamics of balanced networks with input spike trains In addition to our analysis of spiking networks driven with input spike trains, we propose six extensions both towards experimental applications and a deeper theoretical understanding.

First, to make more predictions for experiments, beyond the general predictions from Chapter 5, answers to the following questions would be desirable: for concrete optogenetic experiments [176, 241, 281], what quantifiable predictions can be made? What fraction of neurons has to be externally driven to achieve complete network state control of a recurrent network, e.g. in cultured neuronal networks? Based on preliminary results, we hypothesize that it is not necessary to drive all recurrent neurons by a time-varying external input, because controlling a sufficient fraction of the network also controls the recurrent input to the other neurons. But additional factors need to be taken into account, e.g. stochastic synaptic transmission.

Second, a further challenge would be to investigate the response to a *partially non-frozen* input. In such a architecture, the relationship between trial-to-trial reliability and stimulus discriminability can be investigated: if only a fraction of the spiking input is the same across trials and the rest is different across trials, how much would the variability across trials of the driven network activity go down for strong input (see also [164])? What is the role of single neuron dynamics (AP onset rapidness and synaptic dynamics) in this case?

Third, the random dynamical systems approach to spiking neural networks could be extended to quantify the relative contribution of different sources of variability to *noise entropy* [65] (see also [163]). One way to investigate this would be to endow synapses with an intrinsic dynamical entropy rate. This approach would make it possible to quantify the relative contributions of dynamical entropy rate from unreliable synaptic release compared to the collective dynamical entropy rate.

Fourth, for a better understanding of the mathematical aspects of perturbed circuits, finding analytical conditions for complete network state control in spiking networks would be desirable. When is the network state of a spiking balanced network independent of initial conditions? Under which conditions does the Baxendale theorem still hold in shot noise driven systems [168]? In the thermodynamic limit, there is a diffusion across different initial conditions pulling trajectories apart arising from uncorrelated recurrent synaptic currents and at the same time a synchronizing effect across different initial conditions arising from the common external input and thereby self-consistently generated correlations. Our results indicate that there is a critical external input strength J_0^{ext}, at which the correlations induced by the external drive become so strong and consequently the diffusion across trials so weak that different initial states collapse onto one trajectory. Note that this it is a one way street, if the largest Lyapunov exponent is negative: once two network states are critically close together, they collapse. The large existing body of literature on chaos synchronization might provide further inspiration for appropriate analytical approaches [68, 177–183].

Fifth, in order to investigate the flow of information between different recurrent networks, one should extend our approach to two or more spiking neural networks that drive each other by streams of spike trains and calculate both the Lyapunov spectrum of the full system and the conditional Lyapunov spectrum of the driven subnetworks. This way indirect network state control via one or more intermediate networks could be investigated.

Finally, one remaining challenge is to make use of the networks' sensitivity to initial conditions for computation. One task where a sensitivity to initial conditions might be useful is discrimination or classification, e.g. in sensory processing: two signals, which are nearby in the *input space*

with respect to a certain metric are dynamically distinguished based on subtle differences. For example, the difference between the odor of a ripe and a slightly overripe fruit might activate a largely overlapping set of sensory neurons, but this nearby initial state could be pulled apart by the recurrent dynamics in subsequent processing stages [282–285]. Sensitivity to initial conditions in spiking neural networks thus might serve as a dynamical mechanism to pull nearby trajectories apart [286–288]. The challenging part would be to amplify useful informative differences, but not irrelevant ones by designing the phase space accordingly such that behaviorally relevant differences are being pulled apart while other differences of initial conditions are not. It is currently not clear how such a phase space structure could be learned in a spiking neural network. A second way would be to pull apart everything and have a readout which ignores irrelevant differences. Similar problems have been investigated in machine learning and it might be fruitful to join the efforts (see e.g. [250, 289]).

Experimentally testable predictions and proposals for experiments According to our analysis of information transmission in feedforward architectures, a reduced AP onset rapidness should also reduce the mutual information rate between input and outgoing spike train of a neuron in the fluctuation-driven regime for fixed firing rates. Depending on the experimental setup and on the number of spikes collected, the information rate in such an experiment should be calculated using the *direct method* [218, 290] or using a lower bound [240].

For recurrent circuits, we predict that the AP rapidness is a factor crucial for the recurrent dynamics. One scenario where this could potentially be tested experimentally is our prediction that high AP onset rapidness facilitates the complete control of the network state. If a reversible tool for manipulating the AP onset rapidness becomes available [175, 176, 241], our analysis would suggest that networks with high AP onset are more easily controlled by an external e.g. optogenetic or electrical stimulation. In other words, we predict that the trial-to-trial variability decreases when driving networks with high AP onset rapidness. This hypothesis could be tested in different scenarios: for bidirectional neural circuit interfaces [175, 176, 241], we predict that slowed down AP onset, which could be induced genetically or pharmacologically [44, 238, 239], leads to an increased trial-to-trial variability, when a frozen time-varying stimulus is driving the system repeatedly. Alternatively, it can also first be tested *in vitro* in networks of cultured neurons established experimental setups (e.g. [291–293]*).* One challenge would be to carefully design control experiments in order to isolate the effect and assert that changes of trial-to-trial variability can unambiguously be attributed to changes of AP onset rapidness and are not induced by other confounding variables.

More generally, our study contributes to the investigation of reliability of neuronal activity, which was extensively studied at the single neuron level in experiments [66–69]. Novel tools and bidirectional neural circuit interfaces now for the first time allow experimentalists to selectively manipulate and monitor the activity of large numbers of neurons even in behaving animals [175, 176, 241]. These technological advancements promote the perturbation of neural activity with millisecond and single-cell precision and allow new approaches to study trial-to-trial variability and controllability on a circuit level. Previous experimental studies found that external drive reduces trial-to-trial spiking variability compared to the spontaneous activity state [242]. We found in our theoretical work that sufficiently variable external input is able to completely control the network state of a recurrent balanced target circuit. Experimentally investigation of which stimulation methods and what spatiotemporal stimuli are best suited for manipulating and controlling recurrent cortical dynamics seems to be an appealing scientific question for future optogenetic

experiments both *in vivo* and *in vitro*. To fully harness the potential of such tools and approaches, it is vital, to make more specific experimentally testable and falsifiable predictions from models for the interaction of recurrent circuit dynamics and artificial perturbations. More specifically, the role of partially frozen input spike trains, input to only a part of a recurrent network, and the effect of including stochastic synaptic release should be further investigated (see also the outlook section 9.3). Another scenario where the role of stimulus statistics on trial-to-trial variability on the circuit level should be investigated are behavioral experiments with controlled stimulus statistics, e.g. perceptual decision-making in two-alternative forced choice tasks with random moving dot patterns [294]. In such an experiment, one could *freeze* the realization of the time-varying random dot pattern and study the response variability across presentation of the same stimulus as a function of stimulus statistics. Without overstretching the scope of application of our study, one might expect that spatiotemporally more structured stimuli reduce the trial-to-trial variability (see also [242]). In connection with perturbation experiments, one should investigate at what time during a trial both network dynamics and decision making are most susceptible to artificial perturbations and what kind of perturbation is most effective. These indicated links between emerging experimental paradigms and theoretical advances have to be deepened to foster progress towards the causal interrogation of circuit function.

Entropy and attractor dimensionality of firing-rate network dynamics Our study on entropy and attractor dimensionality of firing-rate networks opens a novel avenue to characterize their complex dynamics and the geometric structure of the corresponding high-dimensional chaotic attractor. This approach does not only promise a deeper understanding of the dynamics but also helps to harness its computational capacities, e.g. for plasticity and learning of stable trajectories. We propose several applications and extensions of our study.

First, our analysis of dimensionality and dynamical entropy rate in chaotic firing-rate networks should be extended to biologically more realistic asymmetric input-output transfer functions $\phi(h)$, e.g. threshold-power-law transfer functions. It was shown earlier that the existence of a transition to rate chaos and its critical properties strongly depend on the onset of the nonlinear transfer function $\phi(h)$ [37]. A similar significant role of the transfer function is expected both for the attractor dimensionality and the dynamical entropy rate.

Second, entropy and attractor dimensionality should be studied in different network topologies. One should e.g. investigate the role of excess bidirectional connections [295], other second order motifs [225] and strong self-coupling [187]. The analysis should also be extended to circuits in a balanced state, where large excitatory and inhibitory currents dynamically cancel each other. This has can be investigated both in spiking [33, 76, 77, 89, 123] and rate networks [4, 37, 92, 194] (but see also [3]).

Third, the link between chaos in spiking and rate networks should be studied using the full Lyapunov spectrum of spiking networks and rate networks. The link between firing-rate networks and spiking neural networks was recently studied by investigating networks in the limit of very slow synaptic dynamics. In this case the synaptic input current integrates over a long time window and the network dynamics is analogous to a rate network [92] with quantitatively similar activity fluctuations. An interpolation from spiking to rate dynamics with increasing τ_s and a comparison of the associated Lyapunov spectra of rate and spiking networks might improve our understanding of chaos both in spiking and rate networks.

Fourth, a recent work suggested an intriguing link between dynamical and topological complexity [190] of random neural networks, Briefly, this study found that the number of unstable

fixed points grows exponentially with system size closely beyond the transition to chaos. The link between this topological complexity and the dynamical complexity could be examined using the attractor dimensionality and dynamical entropy rate.

Fifth, it is also important to investigate how different features of a time-dependent external stimulus shape dimensionality and dynamical entropy rate [6, 7, 188, 189, 193]. (See also [162, 163] and Chapter 5 for driven spiking networks). Which features of the input statistics facilitate complete network state control and govern a transition from chaos to stability? How do spatial and temporal correlations in the input affect entropy rate and attractor dimensionality? Answering such questions does not only deepen our understanding of driven network dynamics, but can also help to harness the computational capabilities of cortical circuit models [35, 245–248, 296, 297]. This applies both to rate networks and to learning in spiking networks [133, 298–300].

Sixth, one should extend our work to study the change of network dynamics induced by learning. We will describe this in more detail in the final paragraph after discussing how Lyapunov vectors should be used to investigate the chaotic dynamics of rate and spiking networks.

9.3.2 Exploring stable and unstable manifolds using Lyapunov vectors and local Lyapunov exponents

Covariant Lyapunov vectors describe the local orientation of stable and unstable manifolds of a dynamical system. In contrast to the Gram-Schmidt vectors, which are the orthonormal basis evolved during the standard calculation of the Lyapunov spectrum [137, 138], the covariant Lyapunov vectors are as their name suggests covariant with the dynamics, thus $D_s \mathbf{v}_s^i = \gamma_i \mathbf{v}_{s+1}^i$ and invariant under time-reversal $\mathbf{v}_{s-}^i = \mathbf{v}_{s+}^{-i+N+1}$ with $\lambda_i^+ = -\lambda_{-i+N+1}^-$. Their time-averaged exponential expansion and contraction rates are the Lyapunov spectrum. Thus, they characterize how a small volume element evolves locally in time.

Although Lyapunov vectors were already introduced by Oseledets in 1968 [301] and more formally described by Ruelle as tangent directions of invariant manifolds in 1979 [302], they received little attention because there was no effective algorithm to determine them. Only recently, efficient methods have been introduced [139–141] (see also Chapter 2, 3 and 4).

Both for spiking and firing-rate networks, Lyapunov vectors and local Lyapunov exponents allow new approaches to fundamental questions. Six promising research directions are given in the following.

First, in small networks, one can visualize stable and unstable manifolds and study the emergence and spatial organization of chaos. This might help to foster a quantitative and analytical understanding of key factors at the single-cell level that shape network chaos. It might also help to find necessary conditions for a network topology such that network chaos can arise.

Second, in stable networks with a phase space consisting of flux tubes, the time-resolved phase space structure should be further investigated using Lyapunov vectors. Are their corresponding local Lyapunov exponents related to the distance to the flux tube boundary or to the next decorrelation event [126]? How do the local Lyapunov exponents along a stable trajectory change over time? In rapid theta networks with AP onset rapidness sufficiently high such that flux tubes exist, can positive local Lyapunov exponents be related to the granular dispersed regions of the flux tube cross sections observed when approaching the critical AP onset rapidness r_{crit}? How do local Lyapunov exponents change when the critical rapidness r_{crit} is approached? Are there longer episodes of positive local Lyapunov exponents or do they just grow in magnitude? (We would hypothesize the former, because increasing rapidness means that the fraction of neurons in the unstable convex

part of their phase decreases, but the single-cell instability is increasing (see Chapter 4).) Is there a systematic reorganization of Lyapunov vectors when approaching r_{crit}? How do the autocorrelations and cross-correlations of the local Lyapunov exponents change as a function of AP onset rapidness?

Third, also in the chaotic regime a time-resolved understanding of stability and chaos is desirable. The Lyapunov spectrum is defined in the asymptotic limit of long times, but cortical information processing takes place on short to intermediate timescales $\ll 50$ ms. To understand the relationship of transient dynamics and information processing, local Lyapunov exponents can be used to study when and where exactly nearby phases are pushed apart following microscopic perturbations. Are there specific activity sequences associated with local phase space expansion? One might expect that an incoming inhibitory perturbation pushes a neuron's phase apart once the spike-receiving neuron is in the convex segment of its unperturbed single neuron trajectory $V_i(t)$. In case of the rapid theta neuron this is expected once it is beyond the glue point V_G, where the derivative of the phase transition curve d becomes negative (See Chapter 4). Studying the spatiotemporal structure of local Lyapunov exponents can help us to obtain a better quantitative understanding of this mechanism in large circuits extending earlier work [62,126,162,201,202]. How are single-cell properties, e.g. indegree, outdegree, average firing rate, mean membrane potential related to their average contribution to the network chaos measured by e.g. their inverse participation ratio, which quantifies localization of chaos [62, 162, 201]? Do these properties in time correlate to network chaos contribution?

Fourth, as biophysical properties of cortical circuits are heterogeneous, the effect of heterogeneity e.g. with respect to AP onset rapidness, synaptic coupling strength, neuron types and external input should be investigated using Lyapunov vectors. This way, the role of various neuron (e.g. inhibitory) cell types in neural circuit computations can be investigated. If different neurons in a network model have distinct values of AP onset rapidness, are the unstable manifolds localized along the directions of neurons with low and intermediate AP onset rapidness which are expected to contribute more to the recurrent chaos? Are Lyapunov vectors in a multilayered network localized within the dynamics of the different layers? In a network with two or more unidirectionally connected subnetworks, are there Lyapunov vectors associated with unstable manifolds oriented along the projection? Can the corresponding local Lyapunov exponents be related to the information flow between the subnetworks? To what extent are the macroscopic directions of large variability in a driven target network across different initial conditions reflected in the orientation of unstable manifolds (see also [162])?

Finally, the relation between collective modes of activity and unstable manifolds should be investigated [303–307]? For various dissipative systems, it was shown using covariant Lyapunov vectors that the tangent space is split into two hyperbolically decoupled subspaces [305, 306]: one comprising a finite number of frequently entangled *physical* modes, which carry the physically relevant information of the trajectory, and a residual set of strongly decaying *spurious* modes. It was conjectured that the *physical* modes may constitute a local linear description of the *inertial manifold* at any point of the global attractor. Thus, covariant Lyapunov vectors are a promising approach to investigate collective degrees of freedom of neural circuits including their dimensionality, spatial organization and relation to information processing. This is especially of interest when the circuits have a nontrivial mesoscopic spatiotemporal rate dynamics, e.g. multistability or attractor networks [308]. Lyapunov exponents and covariant Lyapunov vectors characterize the network dynamics on the finest spatial scale. To examine dynamics on a mesoscopic scale, one promising approach is to use related tools that enable a smooth interpolation to a coarser

scale both temporally and spatially. Bred vectors, which are commonly used in weather prediction models [309], are a finite-time and finite-size perturbation analogue of the largest Lyapunov vector [310, 311]. Therefore, they promise to offer insights into the response of neural networks to mesoscopic perturbations.

9.3.3 Applications to plasticity and learning

In this thesis, we focused on the dynamics and neglected *plasticity* and *adaptation*, because these usually take place over longer timescales compared to the microscopic network dynamics. However, recent progress in the theoretical understanding of short-term synaptic plasticity (STP) and spike-time dependent plasticity and its role for spiking network dynamics raises questions about the interplay between network dynamics on the millisecond time-scale and adaptation and plasticity on longer timescales [36, 308, 312]. The tools presented in this thesis could be applied to study this interplay. For simple linear plasticity rules, e.g. the one proposed by Tsodyks and Markram [313], one should extend earlier studies of chaos in spiking networks to plastic networks. Instead of N dynamic variables, there are now $N \cdot (K+1)$ dynamic variables (all neurons and all synapses) and the corresponding number of Lyapunov exponents. In this way, one could study the collective activity modes of plastic networks with the concepts from computational ergodic theory. Concerning long-term plasticity, one aim could be to identify conditions for stabilization of the network connectivity despite chaotic network dynamics and a better understanding of the interplay between synaptic turnover with the chaotic network activity. Concerning short-term synaptic plasticity (STP), one could study the relation of microscopic dynamic stability and multistability in the balanced state originating from STP induced synaptic nonlinearities [308].

In rate networks, the Lyapunov spectrum could also be used to study the effects of dynamics and the phase space reorganization through learning. The complex chaotic dynamics of rate networks have been used as a reservoir for learning complex input-output relationships [35, 245–249, 296]. Earlier studies investigated the learning capabilities of rate networks by linearizing the rate dynamics e.g. around fixed points [248, 296]. Our approach could be extended to study the dynamics in the tangent space along a learned trajectory. For tracking the orientations of stable and unstable manifolds and the associated instantaneous exponential rates of expansion and contraction time, one should calculate the Lyapunov vectors and the local Lyapunov exponents [139–141]. How does the Lyapunov spectrum change from before to after learning for different task types? What does the Lyapunov spectra reveal about why some network topologies are better at learning than others? E.g. Is memory lifetime improved when the first Lyapunov exponents are close to zero (See also [247])? How is learning performance reflected in the Lyapunov spectrum? Is there some optimal chaotic reservoir to learn many/long patterns? How are transient stable periods reflected in the Lyapunov spectrum? Answering such questions would provide a deeper understanding of the reorganization of the phase space underlying different reservoir computing strategies.

The network topology – known as the connectome – is a crucial factor influencing the collective dynamics of neural networks and most learning algorithms, in fact, operate at this level [34–36]. Thus, to understand the effects of plasticity on the network dynamics, it is important to understand how different features of the network topology shape the dynamics. We showed that introducing both a more realistic microscopic second order motif structure and an experimentally inspired macroscopic structure with multiple layers with respective excitatory-inhibitory circuits has a rather mild effect on attractor dimensionality, dynamical entropy rate and chaoticity compared to the single-cell dynamics. But in general, more drastic changes to the network topology

can have a strong effect on the network dynamics and consequently also on entropy and dimensionality. For example, an embedded feedforward structure in a balanced network or increasing the symmetry of the adjacency matrix leads to less chaotic network dynamics. Also, interpolating from a random network to a regular lattice structure via a small-world network reduces entropy rate and chaoticity gradually. As an extension, one should investigate the dynamics of networks using the adjacency matrix obtained experimentally from circuit mapping and reconstruction as they become available (see e.g. [121]). As in most cases, we found that a more structured topology leads to a less chaotic network – except for small world networks – a similar decrease might be expected for reconstructed cortical network structures. We would still expect a strong effect of the AP onset rapidness as described before. A promising approach to studying the effect of different topologies on network chaos is to use a suitable high-dimensional optimization technique to minimize or maximize the largest Lyapunov exponent, the dynamical entropy rate or the attractor dimensionality. Note that the space of possible adjacency matrices grows quickly $\mathscr{O}\left(2^{\frac{N\cdot(N-1)}{N!}}\right)$. Therefore, a brute force method like simulated annealing is not suitable even for a moderate network size. This obviously becomes worse, if synaptic strengths are allowed to be heterogeneous. Instead, a suitable optimization scheme, e.g. genetic algorithms, might be useful. By analyzing the resulting optimized topologies, such an exploratory approach might give insights into how different microscopic, mesoscopic and macroscopic features of the network topology affect the network dynamics and the Lyapunov spectrum. Major effects are expected to arise due to changes of the collective network state, e.g. transition to population synchrony or regular periodic firing. The interesting challenge would be to detect and understand – e.g. by constrained optimization – more subtle effects by which features of the connectome interplay with biophysical properties of neurons to shape the coordinated activity of large neural circuits that process information in the brain.

References

[1] E. Dickinson: *The Complete Poems of Emily Dickinson with an Introduction By Her Niece Martha Dickinson Bianchi* (Little Brown and Company, 1929). 1

[2] A. K. Churchland and L. F. Abbott: "Conceptual and technical advances define a key moment for theoretical neuroscience." *Nature Neuroscience* **19**, 348–349 (2016). 1

[3] R. Engelken, F. Farkhooi, D. Hansel, C. van Vreeswijk, and F. Wolf: "A reanalysis of "Two types of asynchronous activity in networks of excitatory and inhibitory spiking neurons"." *F1000Research* **5**, 2043 (2016). 2, 13, 24, 117, 171, 173, 178, 183

[4] S. Ostojic: "Two types of asynchronous activity in networks of excitatory and inhibitory spiking neurons." *Nature Neuroscience* **17**, 594–600 (2014). 2, 13, 24, 117, 171, 173, 177, 178, 183

[5] H. Sompolinsky, A. Crisanti, and H. J. Sommers: "Chaos in Random Neural Networks." *Physical Review Letters* **61**, 259–262 (1988). 2, 4, 12, 24, 173, 178

[6] L. Molgedey, J. Schuchhardt, and H. Schuster: "Suppressing chaos in neural networks by noise." *Physical Review Letters* **69**, 3717–3719 (1992). 2, 23, 24, 176, 178, 179, 184

[7] K. Rajan, L. F. Abbott, and H. Sompolinsky: "Stimulus-dependent suppression of chaos in recurrent neural networks." *Physical Review E* **82**, 011903 (2010). 2, 23, 24, 176, 178, 184

[8] S. Goedeke, J. Schuecker, and M. Helias: "Noise dynamically suppresses chaos in neural networks." *arXiv:1603.01880 [nlin, q-bio]* ArXiv: 1603.01880 (2016). 2, 23, 24, 176, 178

[9] F. Wolf, R. Engelken, M. Puelma-Touzel, J. D. F. Weidinger, and A. Neef: "Dynamical models of cortical circuits." *Current Opinion in Neurobiology* **25**, 228–236 (2014). 2, 9, 23, 24

[10] A. Hodgkin and A. Huxley: "Action Potentials record from inside a nerve fiber." *Nature (Lond)* **144**, 710–711 (1939). 3

[11] A. L. Hodgkin and A. F. Huxley: "A quantitative description of membrane current and its application to conduction and excitation in nerve." *The Journal of Physiology* **117**, 500–544 (1952). 3, 4

[12] A. L. Hodgkin and A. F. Huxley: "Currents carried by sodium and potassium ions through the membrane of the giant axon of Loligo." *The Journal of Physiology* **116**, 449–472 (1952). 3

[13] A. L. Hodgkin and A. F. Huxley: "The components of membrane conductance in the giant axon of Loligo." *The Journal of Physiology* **116**, 473–496 (1952). 3

[14] A. L. Hodgkin and A. F. Huxley: "The dual effect of membrane potential on sodium conductance in the giant axon of Loligo." *The Journal of Physiology* **116**, 497–506 (1952). 3

[15] E. M. Izhikevich: *Dynamical Systems in Neuroscience: The Geometry of Excitability and Bursting* (The MIT Press, Cambridge, Mass.; London, 2010). ISBN 978-0-262-51420-0. 3

[16] K. L. Hedstrom, X. Xu, Y. Ogawa, R. Frischknecht, C. I. Seidenbecher, P. Shrager, and M. N. Rasband: "Neurofascin assembles a specialized extracellular matrix at the axon initial segment." *The Journal of Cell Biology* **178**, 875–886 (2007). 3

[17] A. Van Wart, J. S. Trimmer, and G. Matthews: "Polarized distribution of ion channels within microdomains of the axon initial segment." *The Journal of Comparative Neurology* **500**, 339–352 (2007). 3

[18] M. Royeck, M.-T. Horstmann, S. Remy, M. Reitze, Y. Yaari, and H. Beck: "Role of Axonal NaV1.6 Sodium Channels in Action Potential Initiation of CA1 Pyramidal Neurons." *Journal of Neurophysiology* **100**, 2361–2380 (2008). 3

[19] A. Lorincz and Z. Nusser: "Cell-Type-Dependent Molecular Composition of the Axon Initial Segment." *The Journal of Neuroscience* **28**, 14329–14340 (2008). 3

[20] A. Duflocq, B. Le Bras, E. Bullier, F. Couraud, and M. Davenne: "Nav1.1 is predominantly expressed in nodes of Ranvier and axon initial segments." *Molecular and Cellular Neuroscience* **39**, 180–192 (2008). 3

[21] T. Boiko, A. V. Wart, J. H. Caldwell, S. R. Levinson, J. S. Trimmer, and G. Matthews: "Functional Specialization of the Axon Initial Segment by Isoform-Specific Sodium Channel Targeting." *The Journal of Neuroscience* **23**, 2306–2313 (2003). 3

[22] W. Hu, C. Tian, T. Li, M. Yang, H. Hou, and Y. Shu: "Distinct contributions of Nav1.6 and Nav1.2 in action potential initiation and backpropagation." *Nature Neuroscience* **12**, 996–1002 (2009). 3

[23] C. Laing and G. J. Lord: *Stochastic Methods in Neuroscience* (OUP Oxford, 2010). ISBN 978-0-19-923507-0. 3

[24] I. Hepburn, W. Chen, S. Wils, and E. De Schutter: "STEPS: efficient simulation of stochastic reaction–diffusion models in realistic morphologies." *BMC Systems Biology* **6**, 36 (2012). 3

[25] M. L. Hines and N. T. Carnevale: "The NEURON Simulation Environment." *Neural Computation* **9**, 1179–1209 (1997). 3

[26] M. London and M. Häusser: "Dendritic Computation." *Annual Review of Neuroscience* **28**, 503–532 (2005). 4

[27] S. L. Smith, I. T. Smith, T. Branco, and M. Häusser: "Dendritic spikes enhance stimulus selectivity in cortical neurons in vivo." *Nature* **503**, 115–120 (2013). 4

[28] X.-J. Wang and G. Buzsáki: "Gamma Oscillation by Synaptic Inhibition in a Hippocampal Interneuronal Network Model." *The Journal of Neuroscience* **16**, 6402–6413 (1996). 4

[29] L. Lapicque: "Recherches quantitatives sur l'excitation electrique des nerfs traitee comme une polarization." *J Physiol Pathol Gen* **9**, 620–635 (1907). 4, 5

[30] N. Fourcaud-Trocmé, D. Hansel, C. van Vreeswijk, and N. Brunel: "How Spike Generation Mechanisms Determine the Neuronal Response to Fluctuating Inputs." *The Journal of Neuroscience* **23**, 11628–11640 (2003). 4, 5, 23, 175

[31] H. R. Wilson and J. D. Cowan: "Excitatory and Inhibitory Interactions in Localized Populations of Model Neurons." *Biophysical Journal* **12**, 1–24 (1972). 4

[32] A. Renart, J. d. l. Rocha, P. Bartho, L. Hollender, N. Parga, A. Reyes, and K. D. Harris: "The Asynchronous State in Cortical Circuits." *Science* **327**, 587–590 (2010). 4, 9

[33] C. van Vreeswijk and H. Sompolinsky: "Chaotic Balanced State in a Model of Cortical Circuits." *Neural Computation* **10**, 1321–1371 (1998). 4, 7, 8, 9, 10, 11, 23, 183

[34] E. L. Bienenstock, L. N. Cooper, and P. W. Munro: "Theory for the development of neuron selectivity: orientation specificity and binocular interaction in visual cortex." *The Journal of Neuroscience* **2**, 32–48 (1982). 4, 186

[35] D. Sussillo and L. F. Abbott: "Generating Coherent Patterns of Activity from Chaotic Neural Networks." *Neuron* **63**, 544–557 (2009). 4, 12, 178, 184, 186

[36] N. R. Tannenbaum and Y. Burak: "Shaping Neural Circuits by High Order Synaptic Interactions." *PLOS Comput Biol* **12**, e1005056 (2016). 4, 186

[37] J. Kadmon and H. Sompolinsky: "Transition to chaos in random neuronal networks." *Physical Review X* **5**. ArXiv: 1508.06486 (2015). 4, 9, 12, 24, 178, 183

[38] G. G. d. Polavieja, A. Harsch, I. Kleppe, H. P. C. Robinson, and M. Juusola: "Stimulus History Reliably Shapes Action Potential Waveforms of Cortical Neurons." *The Journal of Neuroscience* **25**, 5657–5665 (2005). 4

[39] H. Köndgen, C. Geisler, S. Fusi, X.-J. Wang, H.-R. Lüscher, and M. Giugliano: "The Dynamical Response Properties of Neocortical Neurons to Temporally Modulated Noisy Inputs In Vitro." *Cerebral Cortex* **18**, 2086–2097 (2008). 5, 180

[40] C. Boucsein, T. Tetzlaff, R. Meier, A. Aertsen, and B. Naundorf: "Dynamical Response Properties of Neocortical Neuron Ensembles: Multiplicative versus Additive Noise." *The Journal of Neuroscience* **29**, 1006–1010 (2009). 5, 180

[41] G. Silberberg, M. Bethge, H. Markram, K. Pawelzik, and M. Tsodyks: "Dynamics of Population Rate Codes in Ensembles of Neocortical Neurons." *Journal of Neurophysiology* **91**, 704–709 (2004). 5, 180

[42] M. H. Higgs and W. J. Spain: "Conditional Bursting Enhances Resonant Firing in Neocortical Layer 2–3 Pyramidal Neurons." *The Journal of Neuroscience* **29**, 1285–1299 (2009). 5, 180

[43] T. Tchumatchenko, A. Malyshev, F. Wolf, and M. Volgushev: "Ultrafast Population Encoding by Cortical Neurons." *The Journal of Neuroscience* **31**, 12171 –12179 (2011). 5, 180

[44] V. Ilin, A. Malyshev, F. Wolf, and M. Volgushev: "Fast Computations in Cortical Ensembles Require Rapid Initiation of Action Potentials." *The Journal of Neuroscience* **33**, 2281–2292 (2013). 5, 6, 23, 177, 180, 182

[45] N. Brunel and V. Hakim: "Fast Global Oscillations in Networks of Integrate-and-Fire Neurons with Low Firing Rates." *Neural Computation* **11**, 1621–1671 (1999). 5, 9

[46] B. Lindner and L. Schimansky-Geier: "Transmission of Noise Coded versus Additive Signals through a Neuronal Ensemble." *Physical Review Letters* **86**, 2934–2937 (2001). 5, 175

[47] B. Naundorf, T. Geisel, and F. Wolf: "Action Potential Onset Dynamics and the Response Speed of Neuronal Populations." *Journal of Computational Neuroscience* **18**, 297–309 (2005). 5, 23, 175

[48] B. Naundorf, F. Wolf, and M. Volgushev: "Unique features of action potential initiation in cortical neurons." *Nature* **440**, 1060–1063 (2006). 5, 6, 23

[49] W. Wei and F. Wolf: "Spike Onset Dynamics and Response Speed in Neuronal Populations." *Physical Review Letters* **106**, 088102 (2011). 5, 23, 175, 180

[50] E. Lazarov, M. Dannemeyer, B. Feulner, J. Enderlein, M. J. Gutnick, F. Wolf, and A. Neef: "Axonal spike initiation can be maintained with low axonal Na channel density, but temporal precision of spiking is lost." *arXiv:1711.03383 [q-bio]* ArXiv: 1711.03383 (2017). 6

[51] E. Lazarov, M. Dannemayer, A. Huss, M. Gutnick, F. Wolf, and A. Neef: "Functional and structural maturation of the axon initial segment in cultured hippocampal neurons." In preparation. 6

[52] P. Öz, M. Huang, and F. Wolf: "Action potential initiation in a multi-compartmental model with cooperatively gating Na channels in the axon initial segment." *Journal of Computational Neuroscience* **39**, 63–75 (2015). 6

[53] M. L. Molina, F. N. Barrera, A. M. Fernández, J. A. Poveda, M. L. Renart, J. A. Encinar, G. Riquelme, and J. M. González-Ros: "Clustering and Coupled Gating Modulate the Activity in KcsA, a Potassium Channel Model." *Journal of Biological Chemistry* **281**, 18837–18848 (2006). 6

[54] R. E. Dixon, C. Yuan, E. P. Cheng, M. F. Navedo, and L. F. Santana: "Ca2+ signaling amplification by oligomerization of L-type Cav1.2 channels." *Proceedings of the National Academy of Sciences* **109**, 1749–1754 (2012). 6

[55] A. I. Undrovinas, I. A. Fleidervish, and J. C. Makielski: "Inward sodium current at resting potentials in single cardiac myocytes induced by the ischemic metabolite lysophosphatidylcholine." *Circulation Research* **71**, 1231–1241 (1992). 6

[56] C. M. Moreno, R. E. Dixon, S. Tajada, C. Yuan, X. Opitz-Araya, M. D. Binder, and L. F. Santana: "Ca2+ entry into neurons is facilitated by cooperative gating of clustered CaV1.3 channels." *eLife* **5**, e15744 (2016). 6

[57] D. A. McCormick, Y. Shu, and Y. Yu: "Neurophysiology: Hodgkin and Huxley model — still standing?" *Nature* **445**, E1–E2 (2007). 6

[58] B. Naundorf, F. Wolf, and M. Volgushev: "Neurophysiology: Hodgkin and Huxley model — still standing? (Reply)." *Nature* **445**, E2–E3 (2007). 6, 23

[59] R. Brette: "Sharpness of Spike Initiation in Neurons Explained by Compartmentalization." *PLoS Computational Biology* **9** (2013). 6

[60] C. Zhang, F. Wolf, and A. Neef: "Hypothesis Tests of Neuronal Fast Population Encoding: A Multi-Compartment Approach." In preparation. 6

[61] G. Eyal, H. D. Mansvelder, C. P. J. d. Kock, and I. Segev: "Dendrites Impact the Encoding Capabilities of the Axon." *The Journal of Neuroscience* **34**, 8063–8071 (2014). 6

[62] M. Monteforte: *Chaotic Dynamics in Networks of Spiking Neurons in the Balanced State*. Ph.D. thesis, Georg-August-University, Göttingen (2011). 6, 51, 174, 175, 176, 177, 180, 185

[63] L. Squire, D. Berg, F. E. Bloom, S. d. Lac, A. Ghosh, and N. C. Spitzer, editors: *Fundamental Neuroscience, Fourth Edition* (Academic Press, Amsterdam ; Boston, 2012), 4 edition. ISBN 978-0-12-385870-2. 7

[64] G. L. Gerstein and B. Mandelbrot: "Random Walk Models for the Spike Activity of a Single Neuron." *Biophysical Journal* **4**, 41–68 (1964). 7

[65] A. Longtin: "Neuronal noise." *Scholarpedia* **8**, 1618 (2013). 7, 181

[66] W. H. Calvin and C. F. Stevens: "Synaptic noise and other sources of randomness in motoneuron interspike intervals." *Journal of Neurophysiology* **31**, 574–587 (1968). 7, 22, 177, 182

[67] H. L. Bryant and J. P. Segundo: "Spike initiation by transmembrane current: a white-noise analysis." *The Journal of Physiology* **260**, 279–314 (1976). 7, 22, 177, 182

[68] J. D. Hunter, J. G. Milton, P. J. Thomas, and J. D. Cowan: "Resonance Effect for Neural Spike Time Reliability." *Journal of Neurophysiology* **80**, 1427–1438 (1998). 7, 22, 23, 177, 181, 182

[69] Z. F. Mainen and T. J. Sejnowski: "Reliability of spike timing in neocortical neurons." *Science* **268**, 1503–1506 (1995). 7, 22, 177, 182

[70] G. R. Holt, W. R. Softky, C. Koch, and R. J. Douglas: "Comparison of discharge variability in vitro and in vivo in cat visual cortex neurons." *Journal of Neurophysiology* **75**, 1806–1814 (1996). 7

[71] T. Binzegger, R. J. Douglas, and K. A. C. Martin: "A Quantitative Map of the Circuit of Cat Primary Visual Cortex." *Journal of Neuroscience* **24**, 8441–8453 (2004). 7

[72] W. R. Softky and C. Koch: "Cortical Cells Should Fire Regularly, But Do Not." *Neural Computation* **4**, 643–646 (1992). 7

[73] W. R. Softky and C. Koch: "The highly irregular firing of cortical cells is inconsistent with temporal integration of random EPSPs." *The Journal of Neuroscience* **13**, 334–350 (1993). 7

[74] M. N. Shadlen and W. T. Newsome: "Noise, neural codes and cortical organization." *Current Opinion in Neurobiology* **4**, 569–579 (1994). 7

[75] M. N. Shadlen and W. T. Newsome: "The Variable Discharge of Cortical Neurons: Implications for Connectivity, Computation, and Information Coding." *The Journal of Neuroscience* **18**, 3870–3896 (1998). 7

[76] C. van Vreeswijk and H. Sompolinsky: "Chaos in Neuronal Networks with Balanced Excitatory and Inhibitory Activity." *Science* **274**, 1724 –1726 (1996). 7, 8, 9, 23, 183

[77] "Van Vreeswijk C, Sompolinsky H (2005) Irregular activity in large networks of neurons. Les Houches, Session LXXX, 2003 Methods and models in neurophysics. p. 341. - Open Access Library." 7, 183

[78] H. J. Hilhorst and M. Nijmeijer: "On the approach of the stationary state in Kauffman's random Boolean network." *Journal de Physique* **48**, 185–191 (1987). 8

[79] B. Derrida, E. Gardner, and A. Zippelius: "An Exactly Solvable Asymmetric Neural Network Model." *EPL (Europhysics Letters)* **4**, 167 (1987). 8, 180

[80] T. Tetzlaff, M. Helias, G. T. Einevoll, and M. Diesmann: "Decorrelation of Neural-Network Activity by Inhibitory Feedback." *PLOS Comput Biol* **8**, e1002596 (2012). 9

[81] A. S. Ecker, P. Berens, G. A. Keliris, M. Bethge, N. K. Logothetis, and A. S. Tolias: "Decorrelated Neuronal Firing in Cortical Microcircuits." *Science* **327**, 584–587 (2010). 9

[82] A. S. Ecker, P. Berens, R. J. Cotton, M. Subramaniyan, G. H. Denfield, C. R. Cadwell, S. M. Smirnakis, M. Bethge, and A. S. Tolias: "State Dependence of Noise Correlations in Macaque Primary Visual Cortex." *Neuron* **82**, 235–248 (2014). 9

[83] C. Holmgren, T. Harkany, B. Svennenfors, and Y. Zilberter: "Pyramidal cell communication within local networks in layer 2/3 of rat neocortex." *The Journal of Physiology* **551**, 139–153 (2003). 9

[84] S. Lefort, C. Tomm, J. C. Floyd Sarria, and C. C. H. Petersen: "The Excitatory Neuronal Network of the C2 Barrel Column in Mouse Primary Somatosensory Cortex." *Neuron* **61**, 301–316 (2009). 9, 179

[85] P. J. Sjöström, G. G. Turrigiano, and S. B. Nelson: "Rate, Timing, and Cooperativity Jointly Determine Cortical Synaptic Plasticity." *Neuron* **32**, 1149–1164 (2001). 9

[86] H. Markram, J. Lübke, M. Frotscher, A. Roth, and B. Sakmann: "Physiology and anatomy of synaptic connections between thick tufted pyramidal neurones in the developing rat neocortex." *The Journal of Physiology* **500**, 409–440 (1997). 9

[87] A. Mason, A. Nicoll, and K. Stratford: "Synaptic transmission between individual pyramidal neurons of the rat visual cortex in vitro." *The Journal of Neuroscience* **11**, 72–84 (1991). 9

[88] A. M. Thomson and C. Lamy: "Functional maps of neocortical local circuitry." *Frontiers in Neuroscience* **1**, 19–42 (2007). 9

[89] N. Brunel: "Dynamics of Sparsely Connected Networks of Excitatory and Inhibitory Spiking Neurons." *Journal of Computational Neuroscience* **8**, 183–208 (2000). 9, 183

[90] J. Hertz: "Cross-Correlations in High-Conductance States of a Model Cortical Network." *Neural Computation* **22**, 427–447 (2009). 9

[91] A. Kumar, S. Schrader, A. Aertsen, and S. Rotter: "The High-Conductance State of Cortical Networks." *Neural Computation* **20**, 1–43 (2007). 9

[92] O. Harish and D. Hansel: "Asynchronous Rate Chaos in Spiking Neuronal Circuits." *PLoS Comput Biol* **11**, e1004266 (2015). 9, 12, 24, 178, 180, 183

[93] A. Destexhe, M. Rudolph, and D. Paré: "The high-conductance state of neocortical neurons in vivo." *Nature Reviews Neuroscience* **4**, 739–751 (2003). 9

[94] Y. Shu, A. Hasenstaub, and D. A. McCormick: "Turning on and off recurrent balanced cortical activity." *Nature* **423**, 288–293 (2003). 9

[95] M. Wehr and A. M. Zador: "Balanced inhibition underlies tuning and sharpens spike timing in auditory cortex." *Nature* **426**, 442–446 (2003). 9

[96] B. Haider, A. Duque, A. R. Hasenstaub, and D. A. McCormick: "Neocortical Network Activity In Vivo Is Generated through a Dynamic Balance of Excitation and Inhibition." *The Journal of Neuroscience* **26**, 4535–4545 (2006). 9

[97] M. Xue, B. V. Atallah, and M. Scanziani: "Equalizing excitation-inhibition ratios across visual cortical neurons." *Nature* **511**, 596–600 (2014). 9

[98] H. Ozeki, I. M. Finn, E. S. Schaffer, K. D. Miller, and D. Ferster: "Inhibitory Stabilization of the Cortical Network Underlies Visual Surround Suppression." *Neuron* **62**, 578–592 (2009). 9

[99] M. V. Tsodyks, W. E. Skaggs, T. J. Sejnowski, and B. L. McNaughton: "Paradoxical Effects of External Modulation of Inhibitory Interneurons." *The Journal of Neuroscience* **17**, 4382–4388 (1997). 9

[100] D. B. Rubin, S. D. Van Hooser, and K. D. Miller: "The Stabilized Supralinear Network: A Unifying Circuit Motif Underlying Multi-Input Integration in Sensory Cortex." *Neuron* **85**, 402–417 (2015). 9

[101] K. D. Miller: "Canonical computations of cerebral cortex." *Current Opinion in Neurobiology* **37**, 75–84 (2016). 9

[102] W. E. Skaggs, B. L. McNaughton, M. A. Wilson, and C. A. Barnes: "Theta phase precession in hippocampal neuronal populations and the compression of temporal sequences." *Hippocampus* **6**, 149–172 (1996). 9

[103] M. Pecka, Y. Han, E. Sader, and T. D. Mrsic-Flogel: "Experience-Dependent Specialization of Receptive Field Surround for Selective Coding of Natural Scenes." *Neuron* **84**, 457–469 (2014). 10

[104] H. Adesnik, W. Bruns, H. Taniguchi, Z. J. Huang, and M. Scanziani: "A neural circuit for spatial summation in visual cortex." *Nature* **490**, 226–231 (2012). 10

[105] S.-H. Lee, A. C. Kwan, S. Zhang, V. Phoumthipphavong, J. G. Flannery, S. C. Masmanidis, H. Taniguchi, Z. J. Huang, F. Zhang, E. S. Boyden, K. Deisseroth, and Y. Dan: "Activation of specific interneurons improves V1 feature selectivity and visual perception." *Nature* **488**, 379–383 (2012). 10

[106] N. R. Wilson, C. A. Runyan, F. L. Wang, and M. Sur: "Division and subtraction by distinct cortical inhibitory networks in vivo." *Nature* **488**, 343–348 (2012). 10

[107] J. S. Isaacson and M. Scanziani: "How Inhibition Shapes Cortical Activity." *Neuron* **72**, 231–243 (2011). 10

[108] T. Dobzhansky: "Nothing in Biology Makes Sense Except in the Light of Evolution." *The American Biology Teacher* **75**, 87–91 (2013). 10

[109] P. T. d. Chardin: *The Phenomenon of Man* (Lulu Press, Inc, 2015). ISBN 978-1-329-69951-9. 10

[110] D. Attwell and S. B. Laughlin: "An energy budget for signaling in the grey matter of the brain." *Journal of Cerebral Blood Flow and Metabolism: Official Journal of the International Society of Cerebral Blood Flow and Metabolism* **21**, 1133–1145 (2001). 10

[111] B. W. Knight: "Dynamics of Encoding in a Population of Neurons." *The Journal of General Physiology* **59**, 734–766 (1972). 10

[112] D. Hansel and C. van Vreeswijk: "The Mechanism of Orientation Selectivity in Primary Visual Cortex Without a Functional Map." *The Journal of Neuroscience* **32**, 4049–4064 (2012). 10, 11

[113] C. Pehlevan and H. Sompolinsky: "Selectivity and Sparseness in Randomly Connected Balanced Networks." *PLOS ONE* **9**, e89992 (2014). 10, 11

[114] H. Ko, T. D. Mrsic-Flogel, and S. B. Hofer: "Emergence of Feature-Specific Connectivity in Cortical Microcircuits in the Absence of Visual Experience." *The Journal of Neuroscience* **34**, 9812–9816 (2014). 10

[115] H. Ko, L. Cossell, C. Baragli, J. Antolik, C. Clopath, S. B. Hofer, and T. D. Mrsic-Flogel: "The emergence of functional microcircuits in visual cortex." *Nature* **496**, 96–100 (2013). 10

[116] M. Boerlin, C. K. Machens, and S. Denève: "Predictive Coding of Dynamical Variables in Balanced Spiking Networks." *PLOS Comput Biol* **9**, e1003258 (2013). 10

[117] S. Denève and C. K. Machens: "Efficient codes and balanced networks." *Nature Neuroscience* **19**, 375–382 (2016). 10

[118] K. D. Miller: "The stabilized supralinear network: A unifying circuit motif underlying multi-input integration in sensory cortex." Workshop on "Dynamics of cortical and cortical-subcortical circuits", HHMI Janelia Farm, VA, USA (2013). 10

[119] R. Rosenbaum and B. Doiron: "Balanced Networks of Spiking Neurons with Spatially Dependent Recurrent Connections." *Physical Review X* **4**, 021039 (2014). 10

[120] B. Doiron, A. Litwin-Kumar, R. Rosenbaum, G. K. Ocker, and K. Josić: "The mechanics of state-dependent neural correlations." *Nature Neuroscience* **19**, 383–393 (2016). 10

[121] I. D. Landau, R. Egger, V. J. Dercksen, M. Oberlaender, and H. Sompolinsky: "The Impact of Structural Heterogeneity on Excitation-Inhibition Balance in Cortical Networks." *Neuron* **92**, 1106–1121 (2016). 11, 187

[122] F. Farkhooi and W. Stannat: "Complete Mean-Field Theory for Dynamics of Binary Recurrent Networks." *Physical Review Letters* **119**, 208301 (2017). 11

[123] M. Monteforte and F. Wolf: "Dynamical Entropy Production in Spiking Neuron Networks in the Balanced State." *Physical Review Letters* **105**, 268104 (2010). 11, 23, 176, 183

[124] S. Jahnke, R.-M. Memmesheimer, and M. Timme: "Stable Irregular Dynamics in Complex Neural Networks." *Physical Review Letters* **100**, 048102 (2008). 11, 23

[125] R. Zillmer, N. Brunel, and D. Hansel: "Very long transients, irregular firing, and chaotic dynamics in networks of randomly connected inhibitory integrate-and-fire neurons." *Physical Review E* **79**, 031909 (2009). 11, 23, 174, 176, 180

[126] M. Puelma Touzel: *Cellular dynamics and stable chaos in balanced networks*. Ph.D. thesis, Georg-August-University Göttingen (2016). 11, 12, 174, 176, 177, 180, 184, 185

[127] R. Shaw: "Strange Attractors, Chaotic Behavior, and Information Flow." *Zeitschrift Naturforschung Teil A* **36**, 80–112 (1981). 11, 16

[128] M. London, A. Roth, L. Beeren, M. Häusser, and P. E. Latham: "Sensitivity to perturbations in vivo implies high noise and suggests rate coding in cortex." *Nature* **466**, 123–127 (2010). 11, 177

[129] A. Politi and A. Torcini: "Stable Chaos." In M. Thiel, J. Kurths, M. C. Romano, G. Károlyi, and A. Moura, editors, *Nonlinear Dynamics and Chaos: Advances and Perspectives*, Understanding Complex Systems, pages 103–129 (Springer Berlin Heidelberg, 2010). ISBN 978-3-642-04628-5 978-3-642-04629-2. 11

[130] M. Monteforte and F. Wolf: "Dynamic Flux Tubes Form Reservoirs of Stability in Neuronal Circuits." *Physical Review X* **2**, 041007 (2012). 12, 176, 177

[131] J. Aljadeff, M. Stern, and T. Sharpee: "Transition to Chaos in Random Networks with Cell-Type-Specific Connectivity." *Physical Review Letters* **114**, 088101 (2015). 12, 24, 178

[132] O. Shriki, D. Hansel, and H. Sompolinsky: "Rate Models for Conductance-Based Cortical Neuronal Networks." *Neural Computation* **15**, 1809–1841 (2003). 12

[133] L. F. Abbott, B. DePasquale, and R.-M. Memmesheimer: "Building functional networks of spiking model neurons." *Nature Neuroscience* **19**, 350–355 (2016). 13, 178, 184

[134] K. Geist, U. Parlitz, and W. Lauterborn: "Comparison of Different Methods for Computing Lyapunov Exponents." *Progress of Theoretical Physics* **83**, 875–893 (1990). 13

[135] J. P. Eckmann and D. Ruelle: "Ergodic theory of chaos and strange attractors." *Reviews of Modern Physics* **57**, 617–656 (1985). 14, 16, 18

[136] V. Oseledets: "Oseledets theorem." *Scholarpedia* **3**, 1846 (2008). 14

[137] G. Benettin, L. Galgani, A. Giorgilli, and J.-M. Strelcyn: "Lyapunov characteristic exponents for smooth dynamical systems and for Hamiltonian systems - A method for computing all of them. I - Theory. II - Numerical application." *Meccanica* **15**, 9–30 (1980). 14, 15, 184

[138] G. Benettin, L. Galgani, A. Giorgilli, and J.-M. Strelcyn: "Lyapunov Characteristic Exponents for smooth dynamical systems and for hamiltonian systems; A method for computing all of them. Part 2: Numerical application." *Meccanica* **15**, 21–30 (1980). 14, 15, 184

[139] F. Ginelli, P. Poggi, A. Turchi, H. Chaté, R. Livi, and A. Politi: "Characterizing Dynamics with Covariant Lyapunov Vectors." *Physical Review Letters* **99**, 130601 (2007). 16, 184, 186

[140] C. L. Wolfe and R. M. Samelson: "An efficient method for recovering Lyapunov vectors from singular vectors." *Tellus A* **59**, 355–366 (2007). 16, 184, 186

[141] P. V. Kuptsov and U. Parlitz: "Theory and Computation of Covariant Lyapunov Vectors." *Journal of Nonlinear Science* **22**, 727–762 (2012). 16, 184, 186

[142] Y. G. Sinai: "Gibbs Measures in Ergodic Theory." *Russian Mathematical Surveys* **27**, 21–69 (1972). 16

[143] R. Bowen and D. Ruelle: "The Ergodic Theory of Axiom A Flows." In *The Theory of Chaotic Attractors*, pages 55–76 (Springer, New York, NY, 1975). ISBN 978-1-4419-2330-1 978-0-387-21830-4. DOI: 10.1007/978-0-387-21830-4_5. 16

[144] D. Ruelle: "An inequality for the entropy of differentiable maps." *Boletim da Sociedade Brasileira de Matemática - Bulletin/Brazilian Mathematical Society* **9**, 83–87 (1978). 16, 17

[145] A. Vulpiani, F. Cecconi, and M. Cencini: *Chaos: From Simple Models to Complex Systems* (World Scientific Pub Co Inc, Hackensack, NJ, 2009). ISBN 978-981-4277-65-5. 16, 17, 180

[146] Y. Sinai: "Kolmogorov-Sinai entropy." *Scholarpedia* **4**, 2034 (2009). 16

[147] L.-S. Young: "Mathematical theory of Lyapunov exponents." *Journal of Physics A: Mathematical and Theoretical* **46**, 254001 (2013). 16, 17, 19, 176

[148] H. Kantz and E. Olbrich: "Scalar observations from a class of high-dimensional chaotic systems: Limitations of the time delay embedding." *Chaos: An Interdisciplinary Journal of Nonlinear Science* **7**, 423–429 (1997). 17

[149] F. Ledrappier and L.-S. Young: "The Metric Entropy of Diffeomorphisms: Part I: Characterization of Measures Satisfying Pesin's Entropy Formula." *Annals of Mathematics* **122**, 509–539 (1985). 17

[150] C. Kuehn: *Multiple Time Scale Dynamics* (Springer, 2015). ISBN 978-3-319-12316-5. 17

[151] L.-S. Young: "What Are SRB Measures, and Which Dynamical Systems Have Them?" *Journal of Statistical Physics* **5-6**, 733–754 (2002). 17

[152] Prokofiev: "Minkowski–Bouligand dimension,Wikipedia Page Version ID: 725035554, Creative Commons Attribution-ShareAlike License." 18

[153] P. Grassberger and I. Procaccia: "Estimation of the Kolmogorov entropy from a chaotic signal." *Physical Review A* **28**, 2591–2593 (1983). 18

[154] P. Grassberger and I. Procaccia: "Characterization of Strange Attractors." *Physical Review Letters* **50**, 346–349 (1983). 18

[155] J. P. Eckmann and D. Ruelle: "Fundamental limitations for estimating dimensions and Lyapunov exponents in dynamical systems." *Physica D: Nonlinear Phenomena* **56**, 185–187 (1992). 18

[156] L. A. Smith: "Intrinsic limits on dimension calculations." *Physics Letters A* **133**, 283–288 (1988). 18

[157] J. L. Kaplan and J. A. Yorke: "Preturbulence: A regime observed in a fluid flow model of Lorenz." *Communications in Mathematical Physics* **67**, 93–108 (1979). 18

[158] J. C. Alexander and J. A. Yorke: "Fat baker's transformations." *Ergodic Theory and Dynamical Systems* **4**, 1–23 (1984). 18

[159] P. Frederickson, J. L. Kaplan, E. D. Yorke, and J. A. Yorke: "The Liapunov dimension of strange attractors." *Journal of differential equations* **49**, 185–207 (1983). 18

[160] F. Ledrappier: "Some relations between dimension and Lyapounov exponents." *Communications in Mathematical Physics* **81**, 229–238 (1981). 19

[161] K. K. Lin: "Stimulus-Response Reliability of Biological Networks." In P. E. Kloeden and C. Pötzsche, editors, *Nonautonomous Dynamical Systems in the Life Sciences*, number 2102 in Lecture Notes in Mathematics, pages 135–161 (Springer International Publishing, 2013). ISBN 978-3-319-03079-1 978-3-319-03080-7. 19, 176

[162] G. Lajoie, K. K. Lin, and E. Shea-Brown: "Chaos and reliability in balanced spiking networks with temporal drive." *Physical Review E* **87**, 052901 (2013). 19, 23, 176, 184, 185

[163] G. Lajoie, J.-P. Thivierge, and E. Shea-Brown: "Structured chaos shapes spike-response noise entropy in balanced neural networks." *Frontiers in Computational Neuroscience* **8**, 123 (2014). 19, 23, 176, 181, 184

[164] G. Lajoie, K. K. Lin, J.-P. Thivierge, and E. Shea-Brown: "Encoding in Balanced Networks: Revisiting Spike Patterns and Chaos in Stimulus-Driven Systems." *PLOS Computational Biology* **12**, e1005258 (2016). 19, 181

[165] G. Lajoie: *On driven neural assemblies: synchrony, chaos and entropy.* Ph.D. thesis, Dept. of Applied Mathematics, University of Washington (2013). 19, 176

[166] Y. Kifer: *Ergodic Theory of Random Transformations* (Springer Science & Business Media, 2012). ISBN 978-1-4684-9175-3. 19

[167] F. Ledrappier and L.-S. Young: "Entropy formula for random transformations." *Probability theory and related fields* **80**, 217–240 (1988). 20

[168] P. H. Baxendale: "Stability and Equilibrium Properties of Stochastic Flows of Diffeomorphisms." In M. A. Pinsky and V. Wihstutz, editors, *Diffusion Processes and Related Problems in Analysis, Volume II*, number 27 in Progress in Probability, pages 3–35 (Birkhäuser Boston, 1992). ISBN 978-1-4612-6739-3 978-1-4612-0389-6. 20, 176, 181

[169] Y. Le Jan: "Equilibre statistique pour les produits de difféomorphismes aléatoires indépendants." *Annales de l'I.H.P. Probabilités et statistiques* **23**, 111–120 (1987). 20, 176

[170] L.-S. Young: "Understanding Chaotic Dynamical Systems." *Communications on Pure and Applied Mathematics* **66**, 1439–1463 (2013). 20, 176

[171] K. D. Harris: "Neural signatures of cell assembly organization." *Nature Reviews Neuroscience* **6**, 399–407 (2005). 21

[172] D. G. Amaral, H. E. Scharfman, and P. Lavenex: "The dentate gyrus: fundamental neuroanatomical organization (dentate gyrus for dummies)." *Progress in brain research* **163**, 3–22 (2007). 22

[173] A. Treves, A. Tashiro, M. P. Witter, and E. I. Moser: "What is the mammalian dentate gyrus good for?" *Neuroscience* **154**, 1155–1172 (2008). 22

[174] J. M. Alonso and H. A. Swadlow: "Thalamus controls recurrent cortical dynamics." *Nature Neuroscience* **18**, 1703–1704 (2015). 22

[175] A. M. Packer, L. E. Russell, H. W. P. Dalgleish, and M. Häusser: "Simultaneous all-optical manipulation and recording of neural circuit activity with cellular resolution in vivo." *Nature Methods* **12**, 140–146 (2015). 22, 177, 182

[176] L. Grosenick, J. H. Marshel, and K. Deisseroth: "Closed-Loop and Activity-Guided Optogenetic Control." *Neuron* **86**, 106–139 (2015). 22, 177, 181, 182

[177] D. S. Goldobin and A. Pikovsky: "Antireliability of noise-driven neurons." *Physical Review E* **73**, 061906 (2006). 23, 181

[178] E. K. Kosmidis and K. Pakdaman: "An analysis of the reliability phenomenon in the FitzHugh-Nagumo model." *Journal of Computational Neuroscience* **14**, 5–22 (2003). 23, 181

[179] K. Pakdaman and D. Mestivier: "External noise synchronizes forced oscillators." *Physical Review E* **64**, 030901 (2001). 23, 181

[180] J.-n. Teramae and D. Tanaka: "Robustness of the Noise-Induced Phase Synchronization in a General Class of Limit Cycle Oscillators." *Physical Review Letters* **93**, 204103 (2004). 23, 181

[181] J. Ritt: "Evaluation of entrainment of a nonlinear neural oscillator to white noise." *Physical Review E* **68**, 041915 (2003). 23, 181

[182] C. Zhou and J. Kurths: "Noise-induced synchronization and coherence resonance of a Hodgkin–Huxley model of thermally sensitive neurons." *Chaos: An Interdisciplinary Journal of Nonlinear Science* **13**, 401–409 (2003). 23, 181

[183] A. Zador: "Impact of Synaptic Unreliability on the Information Transmitted by Spiking Neurons." *Journal of Neurophysiology* **79**, 1219–1229 (1998). 23, 181

[184] S. Jahnke, R.-M. Memmesheimer, M. Timme, S. Jahnke, R.-M. Memmesheimer, and M. Timme: "How chaotic is the balanced state?" *Frontiers in Computational Neuroscience* **3**, 13 (2009). 23, 176, 180

[185] N. Fourcaud and N. Brunel: "Dynamics of the Firing Probability of Noisy Integrate-and-Fire Neurons." *Neural Computation* **14**, 2057–2110 (2002). 23, 180

[186] N. Fourcaud-Trocmé and N. Brunel: "Dynamics of the Instantaneous Firing Rate in Response to Changes in Input Statistics." *Journal of Computational Neuroscience* **18**, 311–321 (2005). 23, 175

[187] M. Stern, H. Sompolinsky, and L. F. Abbott: "Dynamics of random neural networks with bistable units." *Physical Review E* **90**, 062710 (2014). 24, 178, 183

[188] K. Rajan, L. Abbott, and H. Sompolinsky: "Inferring Stimulus Selectivity from the Spatial Structure of Neural Network Dynamics." In J. D. Lafferty, C. K. I. Williams, J. Shawe-Taylor, R. S. Zemel, and A. Culotta, editors, *Advances in Neural Information Processing Systems 23*, pages 1975–1983 (Curran Associates, Inc., 2010). 24, 178, 184

[189] B. Doyon, B. Cessac, M. Quoy, and M. Samuelides: "Control of the transition to chaos in neural networks with random connectivity." *International Journal of Bifurcation and Chaos* **03**, 279–291 (1993). 24, 178, 179, 184

[190] G. Wainrib and J. Touboul: "Topological and Dynamical Complexity of Random Neural Networks." *Physical Review Letters* **110**, 118101 (2013). 24, 178, 183

[191] L. C. García del Molino, K. Pakdaman, J. Touboul, and G. Wainrib: "Synchronization in random balanced networks." *Physical Review E* **88**, 042824 (2013). 24, 178

[192] T. Cabana and J. Touboul: "Large Deviations, Dynamics and Phase Transitions in Large Stochastic and Disordered Neural Networks." *Journal of Statistical Physics* **153**, 211–269 (2013). 24, 178

[193] M. Massar and S. Massar: "Mean-field theory of echo state networks." *Physical Review E* **87**, 042809 (2013). 24, 178, 184

[194] F. Mastrogiuseppe and S. Ostojic: "Intrinsically-generated fluctuating activity in excitatory-inhibitory networks." *PLOS Computational Biology* **13**, e1005498 (2017). 24, 178, 183

[195] P. Gao and S. Ganguli: "On simplicity and complexity in the brave new world of large-scale neuroscience." *Current Opinion in Neurobiology* **32**, 148–155 (2015). 24, 178

[196] S. Ganguli and H. Sompolinsky: "Compressed Sensing, Sparsity, and Dimensionality in Neuronal Information Processing and Data Analysis." *Annual Review of Neuroscience* **35**, 485–508 (2012). 24, 178

[197] J. P. Cunningham and B. M. Yu: "Dimensionality reduction for large-scale neural recordings." *Nature Neuroscience* **17**, 1500–1509 (2014). 24, 178

[198] V. A. Marčenko and L. A. Pastur: "DISTRIBUTION OF EIGENVALUES FOR SOME SETS OF RANDOM MATRICES." *Mathematics of the USSR-Sbornik* **1**, 457 (1967). 174

[199] C. M. Newman: "The distribution of Lyapanov exponents: exact results for random matrices." *Communications in mathematical physics* **103**, 121–126 (1986). 174

[200] M. Isopi and C. M. Newman: "The triangle law for Lyapunov exponents of large random matrices." *Communications in mathematical physics* **143**, 591–598 (1992). 174, 180

[201] D. Festa: *Chaos Characterization of Pulse-Coupled Neural Networks in Balanced State*. Master's thesis, MPI DS / Università di Pisa, Göttingen/Pisa (2011). 174, 185

[202] J. Liedtke: *Geometry and organization of stable and unstable manifold in balanced networks*. Master's thesis, Georg-August-University, Göttingen (2013). 174, 185

[203] T. C. Potjans and M. Diesmann: "The Cell-Type Specific Cortical Microcircuit: Relating Structure and Activity in a Full-Scale Spiking Network Model." *Cerebral Cortex* (2012). 174, 175

[204] T. C. Potjans and M. Diesmann: "Multi-population Network Models of the Cortical Microcircuit." In *Advances in Cognitive Neurodynamics (III)*, pages 91–96 (Springer Netherlands, 2013). 174

[205] S. J. v. Albada, S. Kunkel, A. Morrison, and M. Diesmann: "Integrating Brain Structure and Dynamics on Supercomputers." In *Brain-Inspired Computing*, pages 22–32 (Springer International Publishing, 2013). 174

[206] S. J. v. Albada, M. Helias, and M. Diesmann: "Scalability of Asynchronous Networks Is Limited by One-to-One Mapping between Effective Connectivity and Correlations." *PLOS Computational Biology* **11**, e1004490 (2015). 174

[207] T. C. Potjans and M. Diesmann: "The Cell-Type Specific Cortical Microcircuit: Relating Structure and Activity in a Full-Scale Spiking Network Model." *Cerebral Cortex* **24**, 785–806 (2014). 174

[208] N. Kasthuri, K. J. Hayworth, D. R. Berger, R. L. Schalek, J. A. Conchello, S. Knowles-Barley, D. Lee, A. Vázquez-Reina, V. Kaynig, T. R. Jones, M. Roberts, J. L. Morgan, J. C. Tapia, H. S. Seung, W. G. Roncal, J. T. Vogelstein, R. Burns, D. L. Sussman, C. E. Priebe, H. Pfister, and J. W. Lichtman: "Saturated Reconstruction of a Volume of Neocortex." *Cell* **162**, 648–661 (2015). 174

[209] S. Mikula and W. Denk: "High-resolution whole-brain staining for electron microscopic circuit reconstruction." *Nature Methods* **12**, 541–546 (2015). 174

[210] E. M. Izhikevich: "Simple model of spiking neurons." *IEEE transactions on neural networks* **14**, 1569–1572 (2003). 174

[211] T. Tchumatchenko and C. Clopath: "Oscillations emerging from noise-driven steady state in networks with electrical synapses and subthreshold resonance." *Nature Communications* **5**, 5512 (2014). 174

[212] N. Brunel, V. Hakim, and M. J. E. Richardson: "Firing-rate resonance in a generalized integrate-and-fire neuron with subthreshold resonance." *Physical Review E* **67**, 051916 (2003). 174

[213] M. J. E. Richardson, N. Brunel, and V. Hakim: "From subthreshold to firing-rate resonance." *Journal of Neurophysiology* **89**, 2538–2554 (2003). 174

[214] M. P. Touzel and F. Wolf: "Complete Firing-Rate Response of Neurons with Complex Intrinsic Dynamics." *PLOS Computational Biology* **11**, e1004636 (2015). 174

[215] J.-H. Schleimer and M. Stemmler: "Coding of Information in Limit Cycle Oscillators." *Physical Review Letters* **103**, 248105 (2009). 175

[216] D. Bernardi and B. Lindner: "A frequency-resolved mutual information rate and its application to neural systems." *Journal of Neurophysiology* **113**, 1342–1357 (2015). 175

[217] B. Lindner: "Mechanisms of information filtering in neural systems." *IEEE Transactions on Molecular, Biological and Multi-Scale Communications* **PP**, 1–1 (2016). 175

[218] S. P. Strong, R. Koberle, R. R. de Ruyter van Steveninck, and W. Bialek: "Entropy and Information in Neural Spike Trains." *Physical Review Letters* **80**, 197–200 (1998). 175, 177, 182

[219] W. Bialek and A. Zee: "Coding and computation with neural spike trains." *Journal of Statistical Physics* **59**, 103–115 (1990). 175

[220] K. R. Rad and L. Paninski: "Information Rates and Optimal Decoding in Large Neural Populations." In J. Shawe-Taylor, R. S. Zemel, P. L. Bartlett, F. Pereira, and K. Q. Weinberger, editors, *Advances in Neural Information Processing Systems 24*, pages 846–854 (Curran Associates, Inc., 2011). 175

[221] M. J. E. Richardson: "Firing-rate response of linear and nonlinear integrate-and-fire neurons to modulated current-based and conductance-based synaptic drive." *Physical Review E* **76**, 021919 (2007). 175

[222] M. J. E. Richardson: "Spike-train spectra and network response functions for non-linear integrate-and-fire neurons." *Biological Cybernetics* **99**, 381–392 (2008). 175

[223] M. J. E. Richardson: "Dynamics of populations and networks of neurons with voltage-activated and calcium-activated currents." *Physical Review E* **80**, 021928 (2009). 175

[224] R. Rosenbaum: "A Diffusion Approximation and Numerical Methods for Adaptive Neuron Models with Stochastic Inputs." *Frontiers in Computational Neuroscience* page 39 (2016). 175

[225] L. Zhao, B. B. II, T. Netoff, and D. Q. Nykamp: "Synchronization from second order network connectivity statistics." *Frontiers in Computational Neuroscience* **5**, 28 (2011). 175, 183

[226] A. C. Davison: *Bootstrap Methods And Their Application* (Cambridge University Press, Cambridge ; New York, NY, USA, 1997). ISBN 978-0-521-57471-6. 175

[227] D. Angulo-Garcia and A. Torcini: "Stable chaos in fluctuation driven neural circuits." *Chaos, Solitons & Fractals* **69**, 233–245 (2014). 176, 180

[228] K. K. Lin, E. Shea-Brown, and L.-S. Young: "Reliability of Coupled Oscillators." *Journal of Nonlinear Science* **19**, 497–545 (2009). 176

[229] K. K. Lin, E. Shea-Brown, and L.-S. Young: "Spike-time reliability of layered neural oscillator networks." *Journal of Computational Neuroscience* **27**, 135–160 (2009). 176

[230] K. K. Lin, E. Shea-Brown, and L.-S. Young: "Reliability of layered neural oscillator networks." *Communications in Mathematical Sciences* **7**, 239–247 (2009). 176

[231] O. Marre, P. Yger, A. P. Davison, and Y. Frégnac: "Reliable Recall of Spontaneous Activity Patterns in Cortical Networks." *The Journal of Neuroscience* **29**, 14596–14606 (2009). 176

[232] K. K. Lin, E. Shea-Brown, and L.-S. Young: "Spike-time reliability of layered neural oscillator networks." In *AIP Conference Proceedings*, volume 1510, pages 207–209 (AIP Publishing, 2013). 176

[233] H. Jaeger: "The "echo state" approach to analysing and training recurrent neural networks-with an erratum note." *Bonn, Germany: German National Research Center for Information Technology GMD Technical Report* **148**, 34 (2001). 176, 178

[234] M. Buehner and P. Young: "A tighter bound for the echo state property." *IEEE transactions on neural networks* **17**, 820–824 (2006). 176, 178

[235] H. Jaeger: "Echo state network." *Scholarpedia* **2**, 2330 (2007). 176, 178

[236] G. Manjunath and H. Jaeger: "Echo State Property Linked to an Input: Exploring a Fundamental Characteristic of Recurrent Neural Networks." *Neural Computation* **25**, 671–696 (2012). 176, 178

[237] A. Schmidt: *Characterization of the phase space structure in driven neural networks in the balanced state*. Master's thesis, Georg-August-University, Göttingen (2016). 177

[238] E. Lazarov, M. Dannemayer, M. Gutnick, F. Wolf, and A. Neef: "Reduced Nav channel density in the axon initial segment slows down the action potential onset and impairs high-frequency encoding." In preparation. 177, 180, 182

[239] E. Lazarov, F. Wolf, M. Gutnick, and A. Neef: "The dynamic gain in cultured hippocampal neurons is modulated by membrane time constant and spike onset rapidness." In preparation. 177, 180, 182

[240] A. Borst and F. E. Theunissen: "Information theory and neural coding." *Nature Neuroscience* **2**, 947–957 (1999). 177, 182

[241] A. M. Packer, B. Roska, and M. Häusser: "Targeting neurons and photons for optogenetics." *Nature neuroscience* **16**, 805–815 (2013). 177, 181, 182

[242] M. M. Churchland, B. M. Yu, J. P. Cunningham, L. P. Sugrue, M. R. Cohen, G. S. Corrado, W. T. Newsome, A. M. Clark, P. Hosseini, B. B. Scott, D. C. Bradley, M. A. Smith, A. Kohn, J. A. Movshon, K. M. Armstrong, T. Moore, S. W. Chang, L. H. Snyder, S. G. Lisberger, N. J. Priebe, I. M. Finn, D. Ferster, S. I. Ryu, G. Santhanam, M. Sahani, and K. V. Shenoy: "Stimulus onset quenches neural variability: a widespread cortical phenomenon." *Nature Neuroscience* **13**, 369–378 (2010). 177, 182, 183

[243] S. Wieland, D. Bernardi, T. Schwalger, and B. Lindner: "Slow fluctuations in recurrent networks of spiking neurons." *Physical Review E* **92**, 040901 (2015). 178

[244] B. Dummer, S. Wieland, and B. Lindner: "Self-consistent determination of the spike-train power spectrum in a neural network with sparse connectivity." *Frontiers in Computational Neuroscience* **8**, 104 (2014). 178

[245] W. Maass, T. Natschläger, and H. Markram: "Real-Time Computing Without Stable States: A New Framework for Neural Computation Based on Perturbations." *Neural Computation* **14**, 2531–2560 (2002). 178, 184, 186

[246] O. Barak, D. Sussillo, R. Romo, M. Tsodyks, and L. F. Abbott: "From fixed points to chaos: Three models of delayed discrimination." *Progress in Neurobiology* **103**, 214–222 (2013). 178, 184, 186

[247] T. Toyoizumi and L. F. Abbott: "Beyond the edge of chaos: Amplification and temporal integration by recurrent networks in the chaotic regime." *Physical Review E* **84**, 051908 (2011). 178, 184, 186

[248] A. Rivkind and O. Barak: "Local Dynamics in Trained Recurrent Neural Networks." *Physical Review Letters* **118**, 258101 (2017). 178, 184, 186

[249] R. Laje and D. V. Buonomano: "Robust timing and motor patterns by taming chaos in recurrent neural networks." *Nature Neuroscience* **advance online publication** (2013). 178, 186

[250] M. Raghu, B. Poole, J. Kleinberg, S. Ganguli, and J. Sohl-Dickstein: "On the Expressive Power of Deep Neural Networks." In *PMLR*, pages 2847–2854 (2017). 178, 182

[251] H. Jaeger and H. Haas: "Harnessing Nonlinearity: Predicting Chaotic Systems and Saving Energy in Wireless Communication." *Science* **304**, 78–80 (2004). 178

[252] N. V. Kuznetsov, T. A. Alexeeva, and G. A. Leonov: "Invariance of Lyapunov exponents and Lyapunov dimension for regular and irregular linearizations." *Nonlinear Dynamics* **85**, 195–201 (2016). 178

[253] R. Monasson and D. Villamaina: "Estimating the principal components of correlation matrices from all their empirical eigenvectors." *EPL (Europhysics Letters)* **112**, 50001 (2015). 178

[254] M. Bauer and W. Martienssen: "Lyapunov exponents and dimensions of chaotic neural networks." *Journal of Physics A: Mathematical and General* **24**, 4557 (1991). 179

[255] M. L. Fredman and R. E. Tarjan: "Fibonacci heaps and their uses in improved network optimization algorithms." *Journal of the ACM (JACM)* **34**, 596–615 (1987). 179

[256] M. L. Fredman, R. Sedgewick, D. D. Sleator, and R. E. Tarjan: "The pairing heap: A new form of self-adjusting heap." *Algorithmica* **1**, 111–129 (1986). 179

[257] G. S. Brodal: "Worst-case efficient priority queues." *Proceedings of the Seventh Annual Acm-siam Symposium on Discrete Algorithms* pages 52–58 (1996). 179

[258] S. Song, P. J. Sjöström, M. Reigl, S. Nelson, and D. B. Chklovskii: "Highly Nonrandom Features of Synaptic Connectivity in Local Cortical Circuits." *PLoS Biol* **3**, e68 (2005). 179

[259] Y. Ikegaya, T. Sasaki, D. Ishikawa, N. Honma, K. Tao, N. Takahashi, G. Minamisawa, S. Ujita, and N. Matsuki: "Interpyramid Spike Transmission Stabilizes the Sparseness of Recurrent Network Activity." *Cerebral Cortex* **23**, 293–304 (2013). 179

[260] B. Barbour, N. Brunel, V. Hakim, and J.-P. Nadal: "What can we learn from synaptic weight distributions?" *Trends in Neurosciences* **30**, 622–629 (2007). 179

[261] L. Sarid, R. Bruno, B. Sakmann, I. Segev, and D. Feldmeyer: "Modeling a layer 4-to-layer 2/3 module of a single column in rat neocortex: Interweaving in vitro and in vivo experimental observations." *Proceedings of the National Academy of Sciences* **104**, 16353–16358 (2007). 179

[262] G. Buzsáki and K. Mizuseki: "The log-dynamic brain: how skewed distributions affect network operations." *Nature Reviews Neuroscience* **15**, 264–278 (2014). 179

[263] L. Cossell, M. F. Iacaruso, D. R. Muir, R. Houlton, E. N. Sader, H. Ko, S. B. Hofer, and T. D. Mrsic-Flogel: "Functional organization of excitatory synaptic strength in primary visual cortex." *Nature* **518**, 399–403 (2015). 179

[264] M. J. E. Richardson and R. Swarbrick: "Firing-Rate Response of a Neuron Receiving Excitatory and Inhibitory Synaptic Shot Noise." *Physical Review Letters* **105**, 178102 (2010). 179

[265] R. Iyer, V. Menon, M. Buice, C. Koch, and S. Mihalas: "The Influence of Synaptic Weight Distribution on Neuronal Population Dynamics." *PLoS Comput Biol* **9**, e1003248 (2013). 179

[266] F. Droste and B. Lindner: "Integrate-and-fire neurons driven by asymmetric dichotomous noise." *Biological Cybernetics* **108**, 825–843 (2014). 179

[267] T. Tchumatchenko, A. Malyshev, T. Geisel, M. Volgushev, and F. Wolf: "Correlations and Synchrony in Threshold Neuron Models." *Physical Review Letters* **104**, 058102 (2010). 180

[268] T. Tchumatchenko and F. Wolf: "Representation of Dynamical Stimuli in Populations of Threshold Neurons." *PLoS Comput Biol* **7**, e1002239 (2011). 180

[269] Y. Burak, S. Lewallen, and H. Sompolinsky: "Stimulus-Dependent Correlations in Threshold-Crossing Spiking Neurons." *Neural Computation* **21**, 2269–2308 (2009). 180

[270] P. Jung: "Stochastic resonance and optimal design of threshold detectors." *Physics Letters A* **207**, 93–104 (1995). 180

[271] P. Hiemeyer: *Mean field theory of firing rate heterogeneity in balanced neural networks: On silent neurons, the dark matter of the brain*. Master's thesis, Universität Regensburg//MPI DS, Göttingen (2009). 180

[272] A. Crisanti: *Products of Random Matrices: in Statistical Physics* (Springer-Verlag, Berlin; New York, 1993), softcover reprint of the original 1st ed. 1993 edition. ISBN 978-3-642-84944-2. 180

[273] R. Lima and M. Rahibe: "Exact Lyapunov exponent for infinite products of random matrices." *Journal of Physics A: Mathematical and General* **27**, 3427 (1994). 180

[274] A. Pikovsky and A. Politi: *Lyapunov Exponents: A Tool to Explore Complex Dynamics* (Cambridge University Press, Cambridge, 2016). ISBN 978-1-107-03042-8. 180

[275] S. Hestrin, P. Sah, and R. A. Nicoll: "Mechanisms generating the time course of dual component excitatory synaptic currents recorded in hippocampal slices." *Neuron* **5**, 247–253 (1990). 180

[276] N. Spruston, P. Jonas, and B. Sakmann: "Dendritic glutamate receptor channels in rat hippocampal CA3 and CA1 pyramidal neurons." *The Journal of Physiology* **482**, 325–352 (1995). 180

[277] G. Carmignoto and S. Vicini: "Activity-dependent decrease in NMDA receptor responses during development of the visual cortex." *Science* **258**, 1007–1011 (1992). 180

[278] H. Wang, G. G. Stradtman, X.-J. Wang, and W.-J. Gao: "A specialized NMDA receptor function in layer 5 recurrent microcircuitry of the adult rat prefrontal cortex." *Proceedings of the National Academy of Sciences* **105**, 16791–16796 (2008). 180

[279] T. Götz, U. Kraushaar, J. Geiger, J. Lübke, T. Berger, and P. Jonas: "Functional properties of AMPA and NMDA receptors expressed in identified types of basal ganglia neurons." *The Journal of Neuroscience: The Official Journal of the Society for Neuroscience* **17**, 204–215 (1997). 180

[280] A. Tonnelier, H. Belmabrouk, and D. Martinez: "Event-Driven Simulations of Nonlinear Integrate-and-Fire Neurons." *Neural Computation* **19**, 3226–3238 (2007). 180

[281] V. Emiliani, A. E. Cohen, K. Deisseroth, and M. Häusser: "All-Optical Interrogation of Neural Circuits." *The Journal of Neuroscience* **35**, 13917–13926 (2015). 181

[282] J. Chapuis and D. A. Wilson: "Bidirectional plasticity of cortical pattern recognition and behavioral sensory acuity." *Nature Neuroscience* **15**, 155–161 (2012). 182

[283] R. Huerta, T. Nowotny, M. García-Sanchez, H. D. I. Abarbanel, and M. I. Rabinovich: "Learning Classification in the Olfactory System of Insects." *Neural Computation* **16**, 1601–1640 (2004). 182

[284] R. Huerta and M. Rabinovich: "Reproducible Sequence Generation In Random Neural Ensembles." *Physical Review Letters* **93**, 238104 (2004). 182

[285] M. Puelma Touzel, M. Monteforte, and F. Wolf: "Olfactory bulb network dynamics as a pattern reservoir for adaptive cortical representations." *BMC Neuroscience* **14**, P422 (2013). 182

[286] P. Ashwin and M. Timme: "Nonlinear dynamics: When instability makes sense." *Nature* **436**, 36–37 (2005). 182

[287] M. Rabinovich, R. Huerta, and G. Laurent: "Transient Dynamics for Neural Processing." *Science* **321**, 48–50 (2008). 182

[288] M. Rabinovich, A. Volkovskii, P. Lecanda, R. Huerta, H. D. I. Abarbanel, and G. Laurent: "Dynamical Encoding by Networks of Competing Neuron Groups: Winnerless Competition." *Physical Review Letters* **87**, 068102 (2001). 182

[289] A. M. Saxe, J. L. McClelland, and S. Ganguli: "Exact solutions to the nonlinear dynamics of learning in deep linear neural networks." *arXiv:1312.6120 [cond-mat, q-bio, stat]* ArXiv: 1312.6120 (2013). 182

[290] I. Nemenman, F. Shafee, and W. Bialek: "Entropy and Inference, Revisited." In T. G. Dietterich, S. Becker, and Z. Ghahramani, editors, *Advances in Neural Information Processing Systems 14*, pages 471–478 (MIT Press, 2002). 182

[291] S. Paluch-Siegler, T. Mayblum, H. Dana, I. Brosh, I. Gefen, and S. Shoham: "All-optical bidirectional neural interfacing using hybrid multiphoton holographic optogenetic stimulation." *Neurophotonics* **2**, 031208–031208 (2015). 182

[292] N. Farah, A. Levinsky, I. Brosh, I. Kahn, and S. Shoham: "Holographic fiber bundle system for patterned optogenetic activation of large-scale neuronal networks." *Neurophotonics* **2**, 045002–045002 (2015). 182

[293] J. Barral and A. D. Reyes: "Synaptic scaling rule preserves excitatory-inhibitory balance and salient neuronal network dynamics." *Nature Neuroscience* **19**, 1690–1696 (2016). 182

[294] J. D. Roitman and M. N. Shadlen: "Response of Neurons in the Lateral Intraparietal Area during a Combined Visual Discrimination Reaction Time Task." *Journal of Neuroscience* **22**, 9475–9489 (2002). 183

[295] H. J. Sommers, A. Crisanti, H. Sompolinsky, and Y. Stein: "Spectrum of Large Random Asymmetric Matrices." *Physical Review Letters* **60**, 1895–1898 (1988). 183

[296] D. Sussillo and O. Barak: "Opening the Black Box: Low-Dimensional Dynamics in High-Dimensional Recurrent Neural Networks." *Neural Computation* **25**, 626–649 (2012). 184, 186

[297] R. Laje and D. V. Buonomano: "Robust timing and motor patterns by taming chaos in recurrent neural networks." *Nature Neuroscience* **16**, 925–933 (2013). 184

[298] B. DePasquale, M. M. Churchland, and L. F. Abbott: "Using Firing-Rate Dynamics to Train Recurrent Networks of Spiking Model Neurons." *arXiv:1601.07620 [q-bio]* ArXiv: 1601.07620 (2016). 184

[299] D. Thalmeier, M. Uhlmann, H. J. Kappen, and R.-M. Memmesheimer: "Learning universal computations with spikes." *PLOS Computational Biology* **12**, e1004895. ArXiv: 1505.07866 (2016). 184

[300] W. Nicola and C. Clopath: "Supervised learning in spiking neural networks with FORCE training." *Nature Communications* **8**, 2208 (2017). 184

[301] V. I. Oseledets: "A multiplicative ergodic theorem. Characteristic Ljapunov, exponents of dynamical systems." *Trudy Moskovskogo Matematicheskogo Obshchestva* **19**, 179–210 (1968). 184

[302] D. Ruelle: "Ergodic theory of differentiable dynamical systems." *Publications Mathématiques de l'Institut des Hautes Études Scientifiques* **50**, 27–58 (1979). 184

[303] H. Chaté and P. Manneville: "Emergence of Effective Low-Dimensional Dynamics in the Macroscopic Behaviour of Coupled Map Lattices." *EPL (Europhysics Letters)* **17**, 291 (1992). 185

[304] K. A. Takeuchi, F. Ginelli, and H. Chaté: "Lyapunov Analysis Captures the Collective Dynamics of Large Chaotic Systems." *Physical Review Letters* **103**, 154103 (2009). 185

[305] H.-l. Yang, K. A. Takeuchi, F. Ginelli, H. Chaté, and G. Radons: "Hyperbolicity and the Effective Dimension of Spatially Extended Dissipative Systems." *Physical Review Letters* **102**, 074102 (2009). 185

[306] K. A. Takeuchi, H.-l. Yang, F. Ginelli, G. Radons, and H. Chaté: "Hyperbolic decoupling of tangent space and effective dimension of dissipative systems." *Physical Review E* **84**, 046214 (2011). 185

[307] K. A. Takeuchi and H. Chaté: "Collective Lyapunov modes." *Journal of Physics A: Mathematical and Theoretical* **46**, 254007 (2013). 185

[308] G. Mongillo, D. Hansel, and C. van Vreeswijk: "Bistability and Spatiotemporal Irregularity in Neuronal Networks with Nonlinear Synaptic Transmission." *Physical Review Letters* **108**, 158101 (2012). 185, 186

[309] T. N. Palmer: "Predicting uncertainty in forecasts of weather and climate." *Reports on Progress in Physics* **63**, 71 (2000). 186

[310] Z. Toth and E. Kalnay: "Ensemble Forecasting at NMC: The Generation of Perturbations." *Bulletin of the American Meteorological Society* **74**, 2317–2330 (1993). 186

[311] N. Balci, A. L. Mazzucato, J. M. Restrepo, and G. R. Sell: "Ensemble Dynamics and Bred Vectors." *Monthly Weather Review* **140**, 2308–2334 (2012). 186

[312] B. Babadi and L. F. Abbott: "Pairwise Analysis Can Account for Network Structures Arising from Spike-Timing Dependent Plasticity." *PLOS Comput Biol* **9**, e1002906 (2013). 186

[313] M. Tsodyks, K. Pawelzik, and H. Markram: "Neural Networks with Dynamic Synapses." *Neural Computation* **10**, 821–835 (1998). 186

Affidavit

I hereby declare that I prepared this dissertation entitled “Chaotic Neural Circuit Dynamics” on my own and with no other sources and aids than quoted.

Göttingen, 31th December 2016

Rainer Engelken

Acknowledgments

I am full of gratitude towards all the people that made this work possible.

First of all, I want to thank my supervisor Fred Wolf for guidance though this endeavor, always asking deeper, always encouraging me to go beyond the beaten paths to explore new and uncharted territory, for teaching me how to combine scientific rigor with creativity and for both scientific and personal support.

I want to thank Theo Geisel for creating the strange attractor *Max Planck Institute for Dynamics and Self-Organization*, *Department of Nonlinear Dynamics.* The combination of positive liberty and almost unlimited support in a vibrant atmosphere is invaluable.

I am grateful to Farzad Farkhooi, David Hansel and Carl van Vreeswijk for many instructive conversations on mean-field theory, synchrony, correlations and more.

Further, I want to thank Srdjan Ostojic for many intense and respectful scientific discussions.

This thesis profited from the cooperative spirit of many people in the theoretical neurophysics group and its environment, in particular launching assistance by Michael Monteforte and scientific exchange with Joscha Liedtke, Max Puelma Touzel, Manuel Schottdorf, Alexander Schmidt, Agostina Palmigiano, Guillaume Lajoie, Markus Helmer, Frank Stollmeier, Juan Daniel Flórez Weidinger, Andreas Neef, Chenfei Zhang, Enno Fischer, Luis G. R. T. Lopez and others.

Furthermore, I am grateful for discussion on frequency-response and mutual information with Jan Hendrik Schleimer, Benjamin Lindner, Davide Bernardi, Tatjana Tchumatchenko, Tilo Schwalger, David Hofmann and Magnus Richardson; I enjoyed the discussion on rate chaos with Jonathan Kadmon, Sven Goedeke, Haim Sompolinsky, David Hansel, Andrea Crisanti, Yashar Ahmadian, Larry Abbott, Marc Timme and Merav Stern. I am indebted to Haim Sompolinsky, Surya Ganguli, Ann Kennedy for supervising my project in Woods Hole. I want to thank Farzad Farkhooi, Alfonso Renart, Carl van Vreeswijk, David Hansel and Ken Miller for discussions on how to keep a balanced state (even after a cup of coffee) and how to go beyond it.

I greatly appreciate the administrative support by Victoria Nowak, Tobias Niemann, Regina Wunderlich, Ayse Bolik, Zrinka Gattin, the GGNB team and the MPI DS staff. I am grateful to Yorck-Fabian Beensen, Marcus Schwamberger, Barbara Guichemer, Hecke Schrobsdorff and Denny Fliegner for keeping the IT infrastructure and specially the high performance cluster running and for their tolerance when Julia occasionally kicked over the traces.

I want to thank Max P. T., Fred, Joscha, Sven, Alex, Andreas, David, Guillaume, Chepe, Cosima, Eva, Emma, Manuel, Farzad, Max V., Norma, Roberta, Dominika, Tūreiti and Youngmin for proofreading. I acknowledge financial support by honest taxpayers redistributed via ES Villigst.

Three cheers for the free libre open source community (GNU/Linux, Python, Julia, Inkscape, git, vim and more)! Particularly Tim Holy, Christopher Rackauckas, Scott P. Jones from the Julia community for advice and Duane Nykamp for sharing his SONET code. Thanks for fruitful input by Tobias Stöber and his team. Thanks to Alexandra Elbakyan for sharing so much knowledge. I appreciated the generous input from Petra, Uwe et al. and occasional Fassberg rides by friendly GöVB drivers. Thanks to Ed Snowden and the pope Francis for keeping the spirits up.

I am very grateful to those who sustained me through joy and sorrow, especially my family and my friends Cornelia, Dankrad, Norma, Wilhelm, Nora, Johannes, Sophie, Martin, Sarah, Patrick, Johanna, Felix, Julia and Henning.

Finally and most especially I would like to thank Cosima TT. Mattner for her support, tolerance and love during the last years.

List of Symbols

$\bar{\nu}$	The network-averaged firing rate.
χ	The synchrony measure.
η	The ratio of inter-population excitatory coupling.
λ_i	The i-th Lyapunov exponent.
$\mathbf{D}$	The single spike Jacobian.
ω	The constant phase velocity of a neuron.
ϕ	The phase of a neuron.
τ_{m}	The membrane time constant.
ε	The ratio of inter-population excitatory coupling.
cv	The coefficient of variation.
D	The attractor dimension.
D_ϕ	The phase-distance between trajectories.
h	The dynamical entropy rate.
I_0	The strength of the constant external currents.
I_T	The rheobase current.
J_0	The strength of the synaptic coupling.
K	The average number of synapses per neuron.
N	The number of neurons in the networks.
N_E	The number of excitatory neurons.
N_I	The number of inhibitory neurons.
P	The ratio of inter-population excitatory coupling.
r	The action potential onset rapidness.
V	The membrane potential (voltage) of a neuron.
$Z(\phi)$	The phase-response curve.
AP	Abbreviation for action potential.
LIF	The leaky integrate and fire model.